Target Identification for and Optimization of Two Novel Series of Rho-mediated Gene Transcription Inhibitors with Anti-Fibrotic Properties

by

Dylan J. Kahl

A dissertation submitted in partial fulfillment
of the requirements for the degree of
Doctor of Philosophy
(Medicinal Chemistry)
in the University of Michigan
2019

Doctoral Committee:

Research Professor, Scott D. Larsen, Co-Chair
Professor, Richard R. Neubig, Michigan State University, Co-Chair
Assistant Professor, Brent R. Martin
Professor, Henry I. Mosberg

Dylan J. Kahl

djkahl@med.umich.edu

ORCID iD: 0000-0002-0304-336X

Dedication

To my grandma: without your impression, my passion for medicine would not be as deep-rooted as it is.

Acknowledgements

The first person that deserves acknowledgement is my-soon-to-be wife Hayley. I could not have made it to the finish line (nor would I have wanted to) without your continued support, motivation and love; you mean the world to me, and I can't wait to spend the rest of my life with you. Next, I would like to thank my mother Dawn, my grandfather Sam, and my late grandmother Gladys for teaching me how important confidence and a diligent work ethic are in life, and I cannot thank you enough for your nurture and always being there for me. Thank you to my father Dale and my not-so-evil-step-mother Nan for ingraining in me the importance of "good food"; my passion for food and cooking is another element that inspired my initial interest in chemistry. Also, a big thank you to my soon-to-be-mother-and-father-in-law Renée and Larry; I cannot thank you two enough for raising such an amazing daughter, and for supporting her decision to move across the country to this frozen tundra with me. Also, thank you to my step-sister Monica and my soon-to-be-brothers-and-sister-in-law Harrison, Julian, and Lawren for showing me what it's like to have siblings even though I am an only child.

Next, thank you to my godparents John and Lynda; your constant integration of science into my life provided the exposure I needed for science to be an important part of my life. I also want to thank my adopted grandmother Vicki and her family for providing an example of how to treat people in the world, regardless if they treat you with the consideration they deserve. I need to thank my best friends Dylan and Kendall as well as Efren, Eric, and Patrick for illuminating to me that true friendship will always last, no matter the distance. The last "person" that needs thanks in my personal life is one of my best friends, Wyatt; you will always be a special part of my memory.

A huge thank you to Scott Larsen for being an incredible mentor; your instruction related to Medicinal Chemistry, scientific communication, and scientific scholarship throughout my four-and-a-half years at Michigan has been exactly what I needed to approach the next chapter in my life confidently. Also, thank you so much for your genuine support of my decision to pursue an alternative career path; your advice really helped crystalize my decision. Another big thank you needs to go to the late Edward Skibo. I will never forget the patience you had laying a great foundation in Medicinal Chemistry; you are missed. I also want to thank my co-mentor Rick Neubig for allowing me to work on this fantastic project; your mentorship has helped me gain a fuller comprehension of the biological component of drug development. Also, thank you to the other members of my dissertation committee, Hank Mosberg and Brent Martin, for your advice and suggestions.

A special thank you to Mike Wilson and Kim Hutchings for your guidance at the lab bench; I had some pretty hairy moments there, but I made it out alive and (probably) unharmed because of you two. Thank you to current and former members of the VMCC, Walajapet Rajeswaran, Susan Hagan, Hollis Showalter, Andy White, Xinmin Gan, Pil Lee, Brandt Huddle, Helen Waldschmidt, Jake Hitchens, Rachel Rowlands, and Shiyuan Zhang. A special shout out to Jeffery Zwicker for your friendship and mentorship during the past four-and-a-half years. Also, thank you Larisa Yeomans in the NMR core for helping me set up experiments at my beck and call. Last, I want to thank all the talented people who helped progress this project. Thank you, Erika Lisabeth, Jessica Bell, Andrew Haak, Jeffrey Leipprandt, Tom Dexheimer, Pil Lee, Sarah Hayes, David Fox, Dinesh Khanna, Pei-Suen Tsou, Phillip L. Campbell, and all the members at the PK core for your hard work.

Thank you to everyone (especially Kim Hutchings, Jeff Zwicker and Larisa Yeomans) for putting up with my antics during my tenure at Michigan.

Table of Contents

List of Figures

List of Tables

List of Schemes

List of Abbreviations

ADME - Absorption, distribution, metabolism, excretion

AUC – Area under the curve

αSMA – Alpha-smooth muscle actin

CCG - Center for Chemical Genomics (University of Michigan)

CNMR - Carbon nuclear magnetic resonance spectroscopy

cPr - Cyclopropyl

CTGF - Connective tissue growth factor

DMSO - Dimethyl sulfoxide

ECM – Extracellular matrix

EMT - Epithelial-to-mesenchymal transition

EndoMT - Endothelial-to-mesenchymal transition

FGF - Fibroblast growth factor

FMT - Fibroblast-to-myofibroblast

HNMR - Proton nuclear magnetic resonance spectroscopy

HPLC - High-performance liquid chromatography

HTS – High-throughput screen

IC_{50} - Half maximal inhibitory concentration

IL - Interleukin

IPF - Idiopathic pulmonary fibrosis

LC - Liquid chromatography

LPA - Lysophosphatidic acid

MLM - Mouse liver microsome

MMP - Matrix metalloproteinase

MRTF - Myocardin-related transcription factor

MS - Mass spectrometry

MW - Molecular weight

NMR - Nuclear magnetic resonance spectroscopy

PD – Pharmacodynamic

PDB - Protein Data Bank

PDGF – Platelet-derived growth factor

PK - Pharmacokinetic

ROCK - Rho-associated coiled-coil containing protein kinase

ROS - Reactive oxygen species

SAR - Structure-activity relationship

SBDD - Structure-based drug design

SEM - Standard error of the mean

SILAC - Stable isotope labeling of amino acids in cell culture

SRE – Serum response element

SRE L – Serum response element luciferase

SRF - Serum response factor

SSc – Scleroderma

TGF-β - Transforming growth factor- β

TNF - Tumor necrosis factors

Abstract:

Wound healing is characterized by the excessive deposition of extracellular matrix (ECM) components. Fibrosis is a devastating result of the improper regulation of the wound healing process, and it contributes to ~45% of deaths in the developed world. A major hallmark of fibrosis is the fibroblast-to-myofibroblast transition. Myofibroblasts have an increased production of ECM components and impart contractile forces that cause architectural distortion to the surrounding tissue. These forces recruit signal transduction by various extracellular signaling pathways, including transforming growth factor β (TGF-β), lysophosphatidic acid (LPA), endothelin, and connective tissue growth factor (CTGF), ultimately activating the Rho family of GTPases and their downstream kinase, Rho-associated coiled-coil containing protein kinase (ROCK). This signaling leads to myocardin-related transcription factor (MRTF)/serum response factor (SRF)-mediate gene transcription of SRF-associated cytoskeletal genes, ultimately causing fibroblast differentiation into myofibroblast cells. Since Rho/MRTF/SRF-mediated signaling is known to regulate pro-fibrotic gene expression arising from multiple extracellular signaling pathways, inhibition of this common pathway is hypothesized to be a particularly effective way to treat/prevent fibrosis.

In 2007, two distinct series—a 5-aryl-1,3,4-oxadiazol-2-ylthiopropionic acid (58150-) and a bis-amide (222740-) series—of novel inhibitors of Rho/MRTF/SRF-mediated gene expression were identified by the Neubig lab through a phenotypic high-throughput screening campaign. Both series have produced inhibitors that show promising results in multiple *in vitro* and *in vivo* models of fibrosis. Due to the phenotypic nature of the assay, the target(s) for both series are unknown. Recently, potential biological targets for both series have been identified through

proteomics studies using immobilized agarose resin high affinity pull-down probes. Target validation efforts for both series were conducted in a collaborative effort between the Neubig, Larsen, and Martin labs; and, the successful identification of pirin as a biological target for the 222740-series is reported. Additionally, through structure-based drug design (SBDD) efforts using pirin co-crystal structures, the cellular potency for the series was improved about ten-fold, and additional novel bis-amide scaffolds were discovered.

Also, despite the inability to validate a target for the 58150-series, the cellular activity from hit-to-lead was rapidly improved by over 5 orders of magnitude (180 nM to 1 pM). The levels of cellular potency and depth of SAR, coupled with the relatively low molecular weight (<400 g/mol) of the series, suggests that binding to the unknown molecular target may occur through a novel covalent mechanism. In support of this hypothesis, modifications made to the scaffold that would presumably reduce covalent reactivity produced inhibitors with significantly diminished activities. Nevertheless, the series has no observable cytotoxicity up to 100 µM. As a result, two highly potent and orally bioavailable anti-fibrotic agents for the 58150-series were developed that dose-dependently reduce CTGF gene expression *in vitro* and significantly and dose-dependently diminish the development of bleomycin-induced dermal fibrosis in mice *in vivo*.

Chapter 1: Introduction

Fibrosis is characterized by the excessive deposition of extracellular matrix (ECM) components in organs and tissues[1-4], and ~45% of deaths in the developed world can be attributed to fibroproliferative diseases (e.g. cardiac, cirrhosis, scleroderma, pulmonary, renal etc.).[1,4,5] Despite this surprising statistic, pathological fibrosis remains a highly neglected health issue worldwide; the only FDA-approved antifibrotic-specific agents in the U.S. today are pirfenidone and Nintedanib for the treatment of idiopathic pulmonary fibrosis (IPF).[6,7] The build-up of collagen-rich scar tissue and the architectural distortion caused by scar retraction in organs contribute to the high mortality rate of diseases linked to fibrosis.[8] However, even though many of the basic molecular and cellular mechanisms for the development of fibrosis are well-understood, significant gaps of knowledge exist regarding how pathological fibrosis initiates and progresses as well as many pertinent details regarding the mechanisms that regulate fibrosis.[9,10] Discerning the regulation of overlapping inflammatory, immunological (innate and adaptive), and fibrotic responses that underlie fibrosis presents a major difficulty in understanding the pathophysiology of the disease. Because of redundant, overlapping pathways associated with these responses, the drug discovery and development landscape for therapeutic agents for diseases associated with pathological fibrosis remains convoluted.

Fibrosis pathology overview:

The biological intent of wound repair is to reestablish tissue homeostasis and integrity after an insult.[11] The capability of the wound healing process to proceed properly depends on factors such as injury severity and how the inflammatory and redox status of the injury develop over time.[11,12] Wound repair or scarring, which can be classified as the excessive accumulation

of collagen, actin, and fibronectin in epithelial tissue, is initiated when tissue damage occurs, causing an intricate cascade of cellular and molecular responses.[1,3,4] The wound healing process generally consists of initiation, effector cell activation, stem-cell differentiation (e.g. epithelial-to-mesenchymal transition (EMT), fibroblast-to-myofibroblast (FMT) transition, etc.), extracellular matrix (ECM) elaboration, and dynamic deposition/resorption of ECM components (Figure 1).[1]

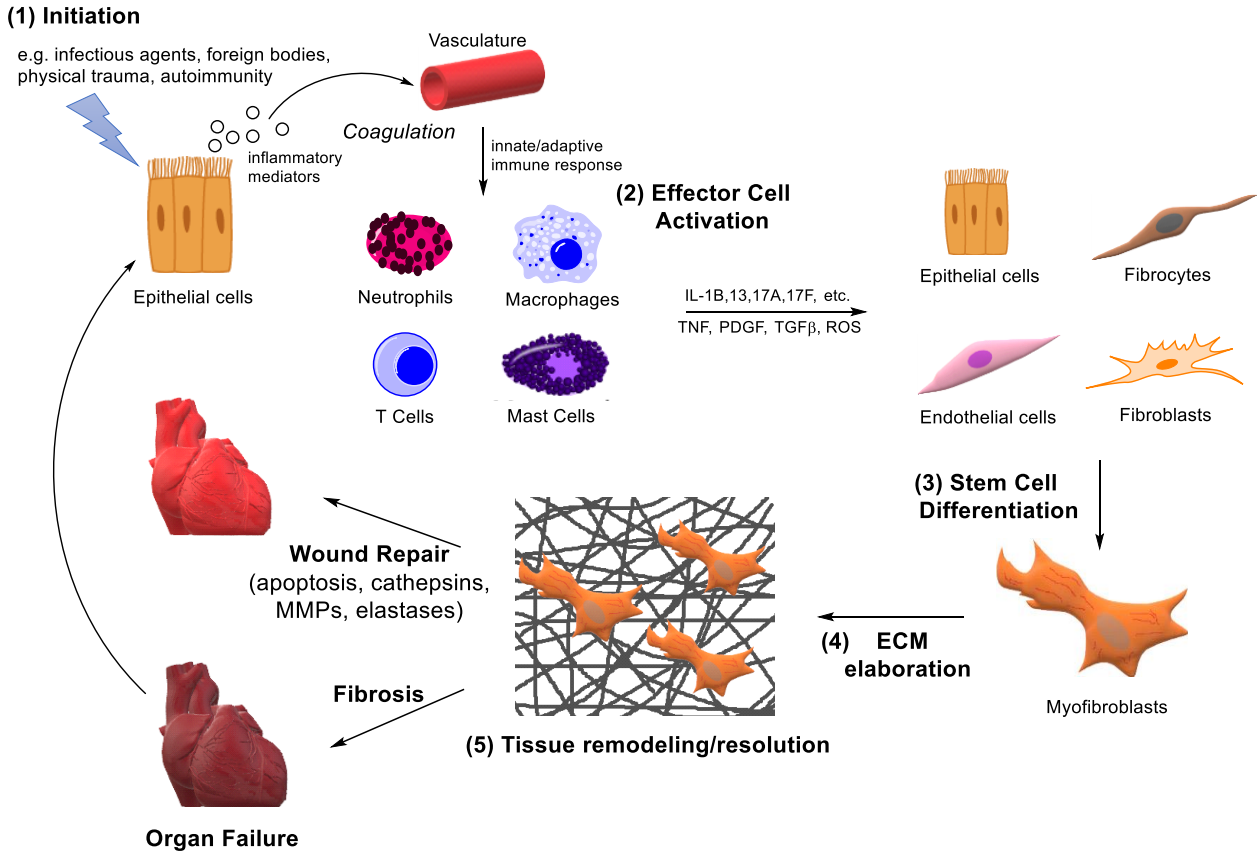

Figure 1: General schematic of wound healing and fibrosis

General schematic of healing, resulting in either proper wound repair (degradation of extracellular matrix (ECM) components via appropriate regulation of collagenous and noncollagenous connective tissue components (e.g. elastases, cathepsins, matrix metalloproteinases (MMPs), etc.) or fibrosis (continual deposition and inefficient clearance and resorption of ECM components). **(1)** Initiation leads to **(2)** effector cell (e.g. macrophage, neutrophil, T helper cell, etc.) recruitment and activation. These inflammatory and immunity cells release pro-fibrotic cytokines (e.g. transcription growth factor (TGF)-β, tumor necrosis factors (TNFs), etc.) and produce reactive oxygen species (ROS), leading to the recruitment, proliferation, and activation of cell types (e.g. epithelial cells, fibroblasts, etc.) capable of **(3)** differentiating to

myofibroblasts. **(4 & 5)** Myofibroblasts remodel the microenvironment by increasing mechanical stress and tension, which is accomplished by their increased sequestration of ECM components (e.g. αSMA). Apoptosis of immune cells, well-orchestrated degradation and resorption of ECM by mainly MMPs, and regeneration of epithelial cells leads to proper wound repair; however, in a pathological fibrotic state, immune cells, fibroblasts, and myofibroblasts persist, and ECM components are over-produced and not resolved, eventually leading to the architectural disruption that can cause organ failure.

When tissue injury occurs (e.g. physical, chemical, autoimmunity, etc.), pro-inflammatory mediators (e.g. histamine, interleukins (ILs), tumor necrosis factors (TNFs), etc.; see Table 1) are released during the coagulation cascade, leading to the recruitment of innate and adaptive immune cells (e.g. macrophages, mast cells, neutrophils, T helper cells, etc.).[12] Recruited innate immune cells (e.g. neutrophils and macrophages) scavenge tissue debris and dead cells, and kill damaged cells and invading pathogens through both reactive oxygen species (ROS) and pro-inflammatory chemokines and cytokines, which in turn amplifies inflammatory reactions and leads to the recruitment of additional immune cells.[11-13] When the inflammatory phase is perpetuated, fibrogenesis is exacerbated, ultimately leading to excessive and prolonged scar formation and fibrosis.[11,13]

Interestingly, clotting not only reduces blood loss and pathogen invasion, but the resulting fibrin-containing clot acts as preliminary ECM scaffolding and provides mechanical provision for cellular attachment and proliferation.[11,13] The stimulation and proliferation of immune cells leads to the release of various pro-fibrotic cytokines (e.g. transcription growth factor (TGF)-β, platelet derived growth factor (PDGF), TNFs, ROSs, IL-1B,13,17A, etc.; see Table 1) that provide a signal for migration, activation, and proliferation of fibrogenic cell types (e.g. fibroblasts, epithelial cells, fibrocytes, endothelial cells, etc.).[11-13] Also of importance, innate immune cells secrete enzymes (elastases, cathepsins, matrix metalloproteinases (MMPs); see Table 1) that can specifically cleave collagenous and non-collagenous connective tissue components; a crucial process for ECM homeostasis during the fibrotic response.[11,13]

The unifying hallmark of fibrosis is the differentiation of pluripotent stem cells (e.g. fibroblast-to-myofibroblast differentiation, epithelial- or endothelial-to-mesenchymal transition (EMT or EndoMT, respectively), etc.) and, ultimately, the excessive deposition of ECM components by myofibroblasts.[14] EMT or EndoMT are processes epithelial (tissue) or endothelial (blood vessel) cell types, respectively, undergo to become mesenchymal stem cells that can differentiate into various cell types, including fibroblasts.[8,14] During this process, cells lose polarity and cell-cell adhesion capabilities and gain migratory and invasive properties. Both resident and migratory fibroblasts are key components for the production of excessive ECM. In particular, fibroblasts differentiate into a myofibroblast phenotype—as defined by the assembly of F-actin—that has an increased production of ECM components, such as α-smooth muscle actin (α-SMA), fibronectin, and collagen (Figure 2).[9,14]

The ECM elaboration and contractile forces imparted by myofibroblasts produce the architectural distortion observed in tissue fibrosis.[15-17] The contractile forces imparted by myofibroblasts further perpetuate the fibrotic process through the release of additional pro-fibrotic cytokines by inflammatory, immune, and fibrotic cell types, circularly tilting the balance towards producing superfluous ECM.[18] In a normal circumstance, ECM elaboration eventually terminates, immune cells undergo apoptosis, excess ECM components are sufficiently degraded, and epithelial and endothelial cells regenerate, but when the fibrotic response is prolonged, excessive scarring, cellular dysfunction, and, ultimately, organ failure can occur. [1,3]

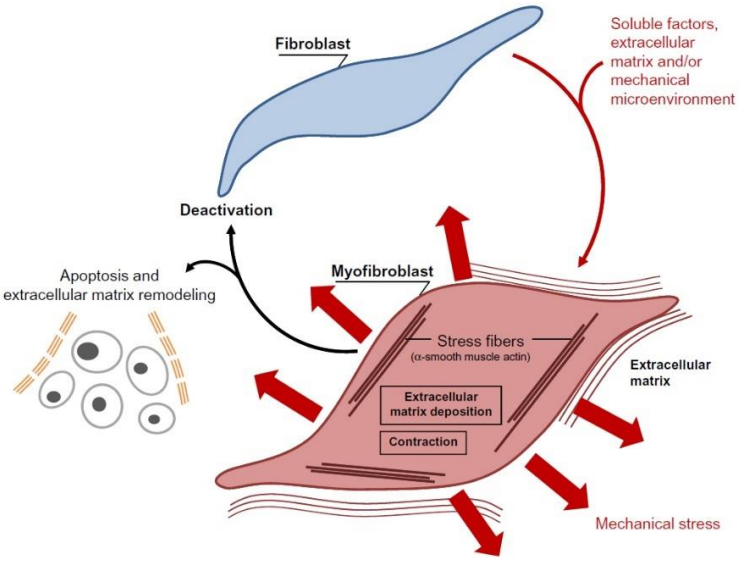

Figure 2: Fibroblast to myofibroblast differentiation and fibroblast resolution

Fibroblast differentiation into myofibroblasts is stimulated mainly by TGF-β and mechanical stress imparted by damaged ECM at the site of injury. Myofibroblasts secrete excessive amounts of various stress fibers (e.g. αSMA) that they utilize to impart contractile forces at the site of injury to properly close the wound. Eventually, pro-fibrotic input signals are suppressed and myofibroblasts either undergo apoptosis or resolve back to fibroblasts, at which point various enzymes can effectively remodel ECM and, ultimately, the surrounding tissue.

Image derived from Darby et al (2014)[19]

Immunological mechanisms that regulate fibrosis:

During injury, damaged or slain cells release danger signals (e.g. histamine, ILs, TNFs, etc.; see Table 1) and crystallized endogenous molecules (e.g. cholesterol, uric acid, etc.) that activate the inflammasome.[20-22] There are multiple subsets of inflammasome receptors, stemming from pattern recognition receptors (PPRs) (e.g. Toll-like receptors (TLRs), nucleotide-binding oligomerization domain and leucine-rich repeat-containing receptors (NLRs), AIM2-like receptors (ALRs) etc.), stimulated during the fibrotic response, and their primary function is to activate the inflammatory response by promoting the maturation and secretion of pro-inflammatory cytokines (e.g. IL-1β, IL-18).[23-26] These cytokines promote a highly inflammatory-specific form of programmed cell death—pyroptosis.[27]

At the same time, neutrophils, monocytes, and mast cells—members of the innate immune response—are heavily recruited to the affected area by platelet degranulation products (e.g. PDGF, TGF-β1, IL-1, etc.) secreted during the inflammatory response by neighboring cells within the site of injury (Figure 3).[28-30] Neutrophils clean-up the area via phagocytosis, removing damaged matrix materials as well as infectious and noninfectious foreign material.[31] During the fibrotic process, neutrophils also release granules containing various proteases (e.g. elastases, cathepsins, etc.) capable of cleaving damaged ECM and ROSs that further prolong the innate immune response and pyroptosis as well as promote fibrogenesis.[28,29,32]

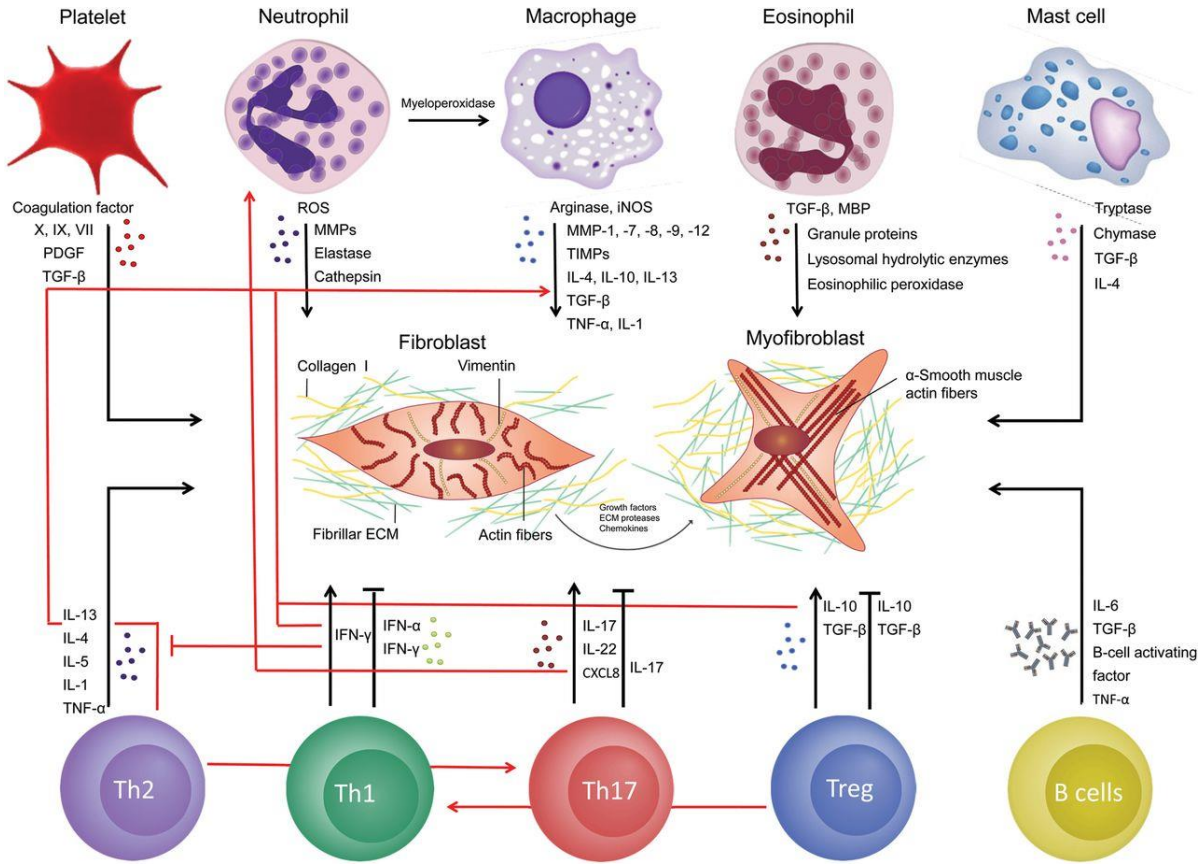

Figure 3: Inflammatory and immune response in wound healing/fibrosis:
Important inflammatory and immune cells that release pro- and anti-fibrotic cytokines, chemokines, and enzymes that regulate the fibrotic process. The roles for many of these mediators are listed in Table 1.
Image derived from Van Linthout et al (2014)[33]

Likewise, macrophages manage the initial reconstruction of the wound microenvironment by 1) engulfing and digesting cellular debris and foreign materials 2)

secreting enzymes that regulate ECM degradation, such as matrix metalloproteinases (MMPs) and tissue inhibitor of metalloproteinases (TIMPs), and 3) release multiple cytokines vital for fibrogenesis (Figure 4).[34-37] Particularly, M1 macrophages release pro-inflammatory chemokines and cytokines, such as ROS, TNF-α, and IL-1β, while M2 macrophages release pro-fibrotic cytokines, such as IL-4, IL-10, IL-13, PDGF, VEGF, IGF-1, and TGF-β1, to regulate angiogenesis and epithelium, endothelium, and fibroblast proliferation.[34,36] Ultimately, macrophages offer the appropriate components to support cellular proliferation, propagate the immune response, and regulate ECM homeostasis.[36]

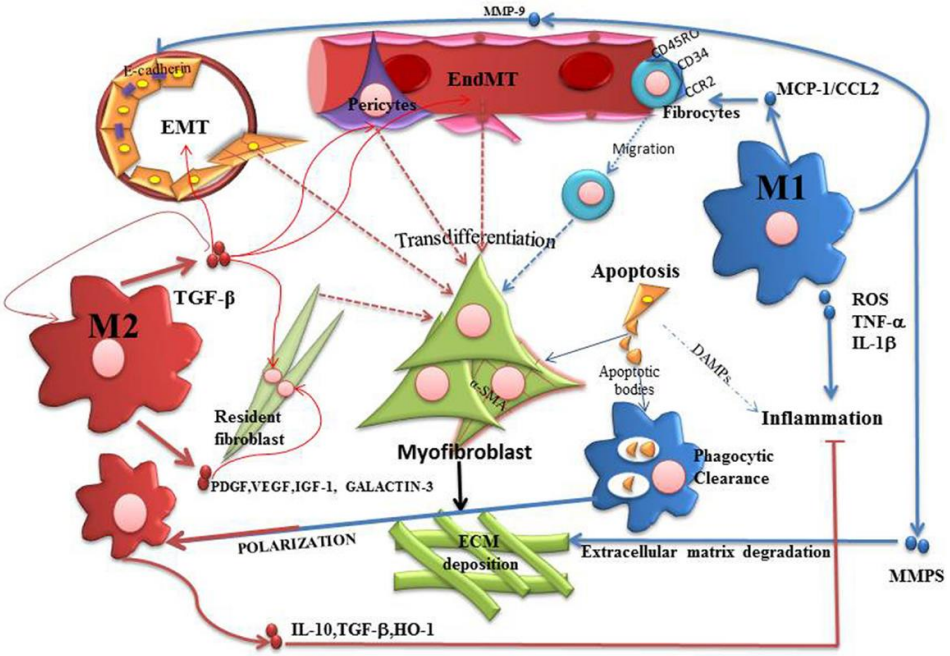

Figure 4: Role of the macrophage in wound healing:

Macrophages regulate multiple faucets of the fibrotic process. M1 macrophages mainly impart pro-inflammatory mediators and propagate ECM clearance mechanisms. M2 macrophages mainly secrete mediators that promote ECM expression and cell differentiation. An appropriate balance of M1 and M2 macrophages at various stages of the fibrotic process is essential for the regulation of the fibrotic response.

Image derived from Braga et al (2015)[34]

MMPs are metal-dependent extracellular endopeptidases that degrade ECM components such as collagens, proteoglycans, laminins, and fibronectin.[38,39] MMPs are also capable of modulating various cell types by activating latent cytokines, stimulating both pro- and

anti-fibrotic effects.[38-41] The balance between MMPs and their endogenous inhibitors—TIMPs—is extremely important for ECM homeostasis.[38,40-42] During the fibrotic process, MMPs are mainly produced by macrophages, but other cell types, such as mast cells, T cells, neutrophils, etc., also play a role regulating MMP and TIMP biosynthesis and activity.[40,41,43] For instance, MMP biosynthesis can be suppressed without affecting TIMP production via IL-4 and IFN-γ released by lymphocytes.[44,45]

Mast cells also release enzymes and cytokines essential for ECM homeostasis. Mast cells release histamine, proteoglycans, lipid mediators, chymases, tryptases, and carboxypeptidases via degranulation, and they synthesize and release other cytokines, such as leukotrienes, prostaglandins, interleukins (e.g. IL-3-6, -10, -13), TNF-α, TGF-β, monocyte chemoattractant protein-1 (CCL2), fibroblast growth factor (FGF), and PDGF, just to name a few (Figure 5).[46-48] Particular to the fibrotic response, the proteases chymase and tryptase can affect ECM homeostasis, and they also help modulate connective tissue cells.[49-51] For example, these proteases stimulate epithelial cell and fibroblast proliferation, fibroblast migration, and myofibroblast differentiation.[50,52] As for their ability to aid in ECM homeostasis, both proteases can activate latent MMPs, TGF-β, and IL-1β, and tryptase can restrain type I collagen and fibronectin production by fibroblasts.[49-52]

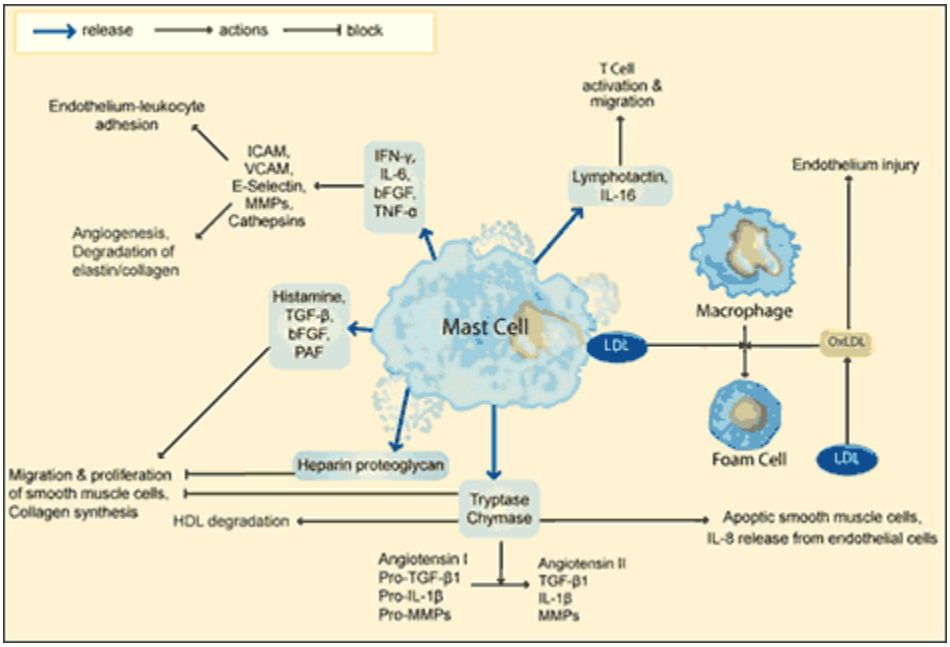

Figure 5: Role of the mast cell in wound healing:

Mast cells are important drivers of the fibrotic response. Along with various pro-inflammatory and pro-fibrotic cytokines, mast cells release two important proteases—chymase and tryptase. These two enzymes are responsible for activating latent cytokines (e.g. TGF- β and IL-1β) and MMPs vital to ECM homeostasis.

Image derived from Bot et al (2015)[53]

As can be seen in Figure 3, there are many other immunological cell types that affect the fibrotic response, but the final type discussed here will be T cells (Figure 3 & 6). They release cytokines such as interleukins, interferons, and TNFs that regulate the adaptive immune and inflammatory responses and contribute to the management of the fibrotic process.[11,54,55] In particular, Th1 differentiation is promoted by IL-12, and Th1 cells secrete pro-inflammatory cytokines, such as IFN-γ and IL-2; and Th2 differentiation is driven by IL-4, and Th2 cells produce IL-4, IL-10, and IL-13, which are anti-inflammatory cytokines that can influence a pro-fibrotic environment for cell types that drive the fibrotic process (e.g. fibroblasts and myofibroblasts).[11,54] A disproportion between Th1/Th2/Th17 cells has been shown to drive inflammation (Th1 dominant) in early stages of fibrotic diseases and pathological fibrosis (Th2/Th17 dominant) in later stages.[11]

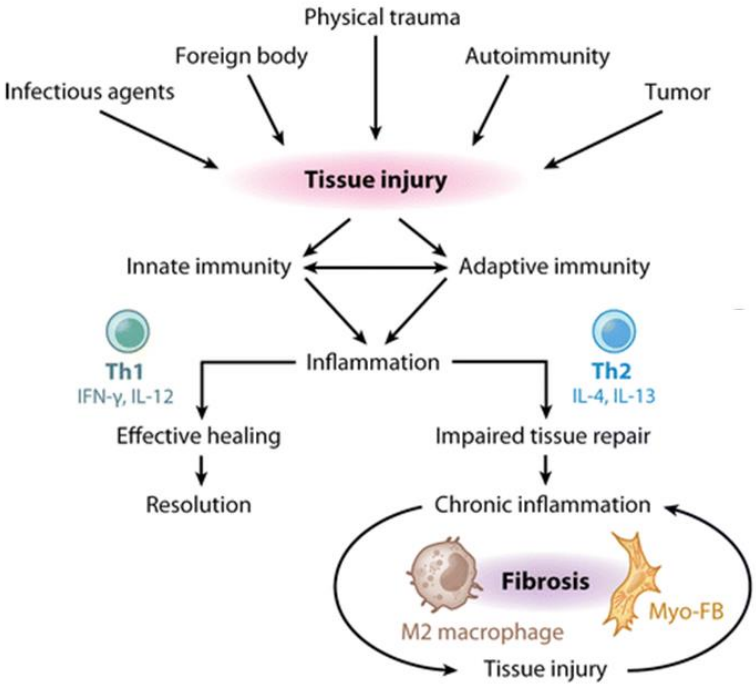

Figure 6: Balance between innate and adaptive immune responses in wound healing/fibrosis: This balance is critical for proper regulation of the fibrotic process. In general, Th1 cells release cytokines that promote resolution of the fibrotic response, while Th2 cells release cytokines that drive chronic inflammation and myofibroblast differentiation.
Image derived from Wick et al (2013)[11]

Fibrotic mechanisms that regulate fibrosis:

Cytokines released during the inflammatory response markedly recruit pro-fibrotic cells to the site of injury where they differentiate, propagate, and produce/deposit excessive ECM to repair the wound.[4,5,11,28-30,32,56-58] The most important cytokine for the fibrotic process may be TGF-β. TGF-β is responsible for stimulating almost all processes of the fibrotic response, including the recruitment, proliferation, and differentiation of multiple pro-inflammatory and pro-fibrotic cell types as well as ECM production and deposition by fibroblasts and myofibroblasts (Figure 7A & B).[59-61]

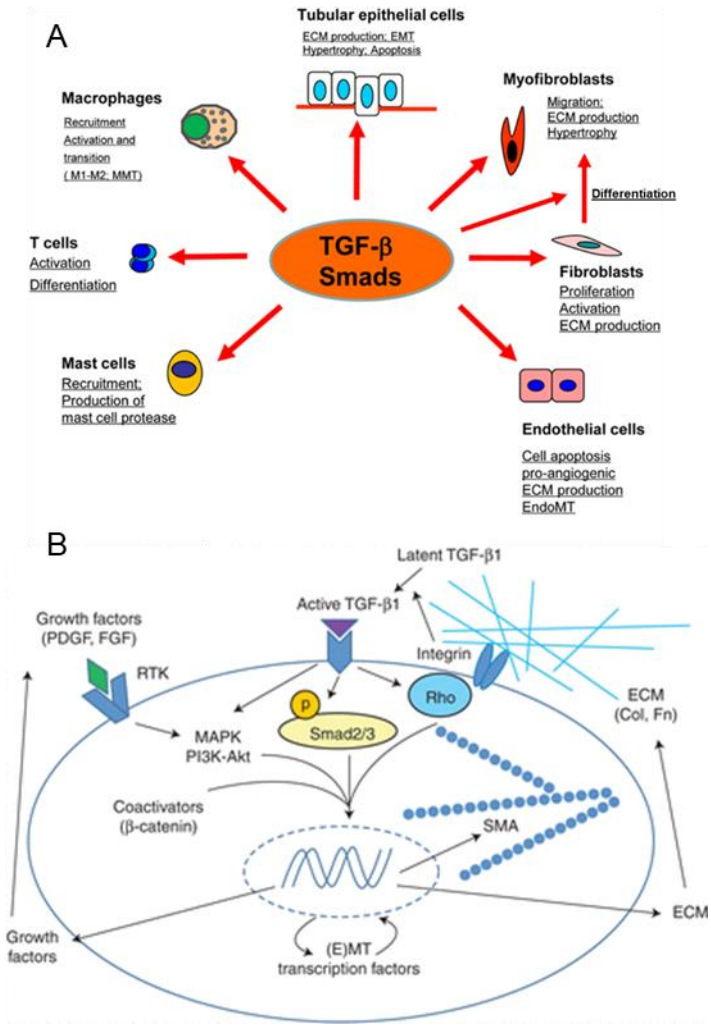

Figure 7: TGF-β and Smad signaling in wound healing/fibrosis:

(A) TGF-β, acting through Smad signaling pathways, regulates multiple actions by various cell types important for the fibrotic response. (B) TGF-β/Smad2/3 signaling pathways activate multiple processes vital for mesenchymal stem cells, fibroblasts, and myofibroblasts, including differentiation, expression and release of growth factors, and secretion and deposition of αSMA and other important ECM components.

Images derived from (A) Meng et al (2015)[62] (B) Kim et al (2018)[60]

The main goal of pro-fibrotic cells during the fibrotic process is to locally increase mechanical stress at the site of injury through the production of excessive ECM components (e.g. αSMA, collagen, fibronectin, etc.) to properly close and heal the wound; myofibroblasts are essential to accomplish this goal.[1,19,63] Myofibroblasts are specialized for this role in that they express excess αSMA, are contractile (via integrins and cadherins), produce and secrete ECM components at a greater rate than other pro-fibrotic cells, and are resistant to apoptosis.[63-65]

Myofibroblast contractile forces are imparted by the mechano-sensory capabilities of highly expressed integrins and cadherins on the cell surface (Figure 8).[17,66] Myofibroblasts also constitutively express high amounts of chemokines, cytokines, and cell surface receptors that perpetuate the fibrotic process.[67] These characteristics facilitate ECM fiber manipulation, wound contraction, and propagation of fibrosis at the site of injury.[17,63-66]

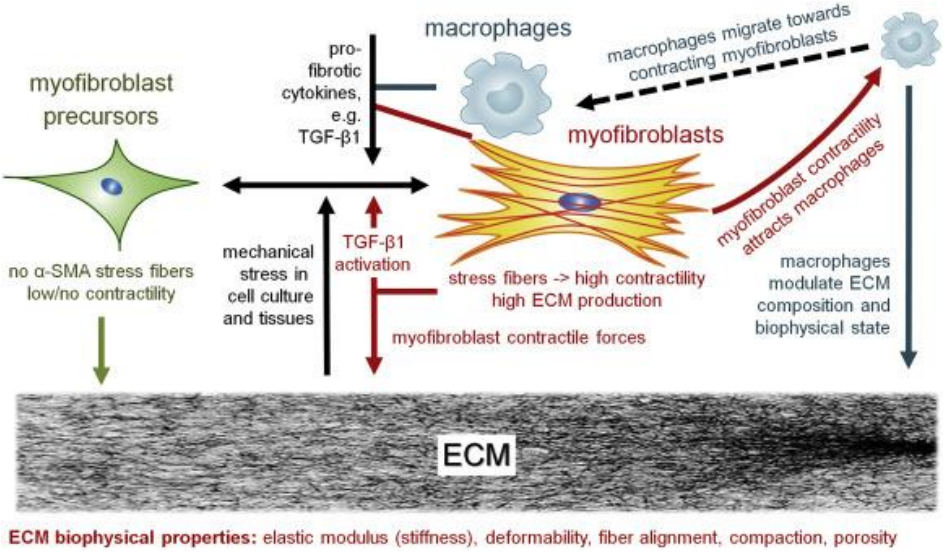

Figure 8: Role of myofibroblasts in wound healing/fibrosis:

Myofibroblasts impart contractile forces on the microenvironment. This is accomplished by coordination between various cadherins and integrins with, among other ECM components, αSMA. The stiffness, deformability, and fiber alignment and compaction coupled with the contractions coordinated by myofibroblasts provides a suitable environment for proper wound closure.

Image derived from Pakshir et al (2018)[63]

Myofibroblasts are not typically found in healthy human tissue; rather they derive from multiple cell types, such as epithelial cells, endothelial cells, fibroblasts, multipotent monocytes, pericytes, and fibrocytes.[68] There are three well-described processes central to myofibroblast production: epithelial-to-mesenchymal transition (EMT)[69], endothelial-to-mesenchymal transition (EndoMT)[70], and fibroblast-to-myofibroblast transition (FMT).[71] EMT and EndoMT are similar in that both processes convert polarized, adhered tissue and blood vessel cells, respectively, to migratory, invasive, and apoptotic-resistant mesenchymal cells (Figure 9).[72] These cells are characterized by their expression of, among many other cytokines, αSMA, fibronectin, N-

cadherin, and β-catenin.[69-71] The main effector of both the EMT and EndoEMT is TGFβ, but other mediators (e.g. type I collagen, MMP2, ROSs) stimulate these processes as well.[69-71,73]

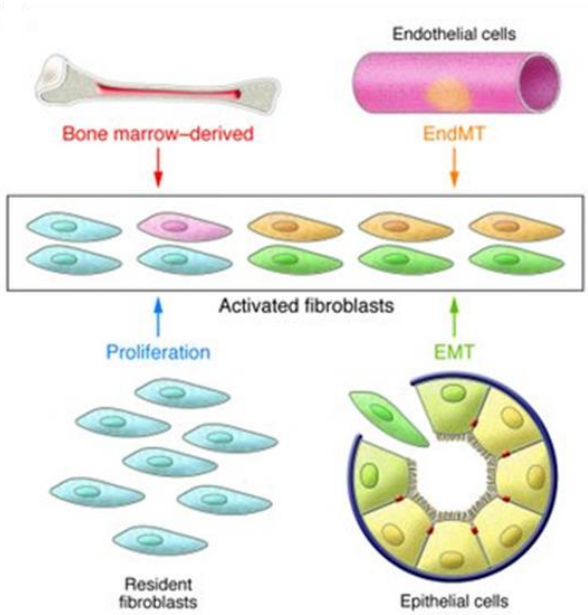

Figure 9: Processes for the differentiation into activated fibroblasts:
Various cell types undergo different processes to differentiate into an activated fibroblast phenotype. For instance, (1) resident fibroblasts proliferate and become activated to release cytokines and ECM components at the site of injury; (2) mesenchymal stem cells (e.g. fibrocytes and pericytes) can differentiate to an activated fibroblast phenotype; (3) epithelial cells undergo epithelial-to-mesenchymal (EMT) transition to form activated fibroblast by breaking away and migrating from the basement membrane; (4) endothelial cells from proximal blood vessels migrate to the site of injury and differentiate to fibroblasts through the endothelial-to-mesenchymal transition (EndoMT).
Image derived from Kalluri et al (2010)[72]

Mesenchymal stem cells, which can differentiate into fibroblasts, join resident fibroblasts at the site of injury after EMT and EndoMT.[74] Fibroblasts are pivotal to the wound healing process. Not only do they produce and secrete structural proteins (e.g. collagen and elastin), adhesive proteins (e.g. laminin and fibronectin), and ground substance (e.g. glycosaminoglycans and glycoproteins, which correspondingly help immune cells migrate into connective tissue), but they also support various fibrotic processes, such as inflammation, innate immunity, blood clotting, angiogenesis, and ECM maintenance and reabsorption.[19,67,75] For example, fibroblasts release lysyl oxidase (Lox), which strengthens collagen fibers by cross-

linking them, MMPs, and TIMPs to aid in ECM homeostasis.[75,76] Moreover, fibroblasts synthesize and secrete cytokines (e.g. TGFβ1, IL-1β, IL-33, etc.), chemokines (e.g. CXC and CCL2), and ROSs that propagate the immune and inflammatory responses (Figure 3).[11,75]

Arguably, fibroblasts' most crucial role in the fibrotic process is their capability to differentiate into myofibroblasts.[66,71,75] Along with the mechanical tension created by the site of injury and ECM components secreted by fibroblasts, TGF-β is the main promoter of the FMT.[75,77] When constrained, fibroblasts undergo a transition into a proto-myofibroblast phenotype, which begins to take on myofibroblastic characteristics, such as focal adhesion sites and production of αSMA, fibronectin, and ED-A fibronectin—an ED-A splice variant (Figure 10).[17,66,75] In the presence of mechanical stress, TGF-β, and ED-A fibronectin, proto-myofibroblasts fully differentiate to myofibroblasts.[17] Among others, Wnt[78], Notch[79], Hedgehog[80,81], and Rho[82,83] signaling pathways play crucial roles in myofibroblast differentiation from progenitor cells, including fibroblasts and mesenchymal stem cells derived from epithelium, endothelium, pericytes, multipotent monocytes, and fibrocytes.

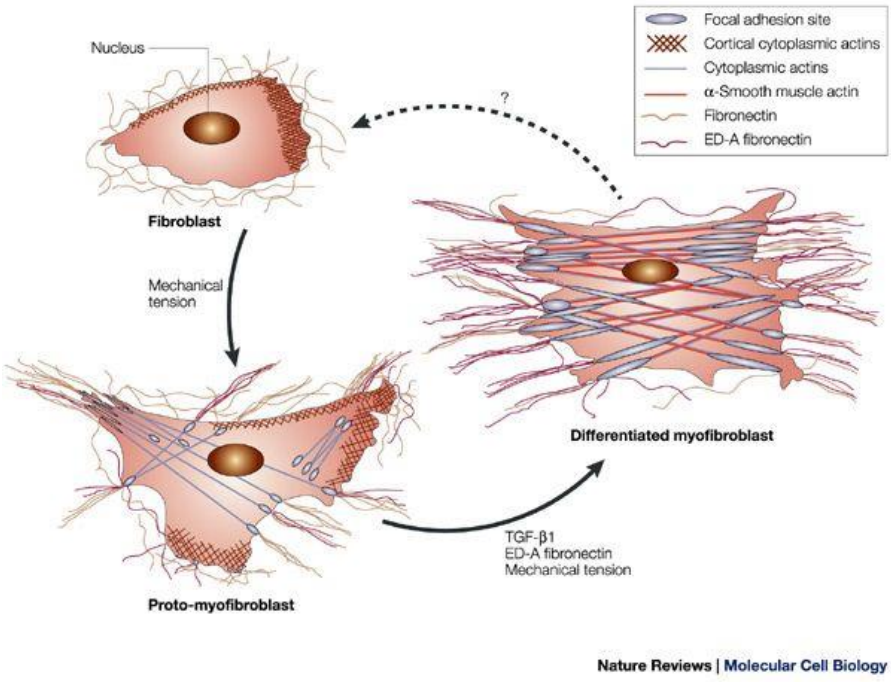

Figure 10: Fibroblast-to-myofibroblast transition:

The transition of fibroblasts into myofibroblasts is a two-step process. First, fibroblasts begin transitioning into a proto-myofibroblast phenotype when mechanical tension created by ECM increases. The proto-myofibroblast phenotype produces various cadherins and integrins and synthesizes and secretes ECM components, such as αSMA. Increased levels of mechanical tension, TGF-β, and ED-A fibronectin drives the FMT to completion. Myofibroblasts secrete excessive amounts of ECM components and focal adhesion sites (through integrins and cadherins), at which point they can utilize their contractibility to close the wound. Myofibroblasts can dedifferentiate back to fibroblasts after pro-fibrotic signaling tapers down.

Image derived from Tomasek et al (2002)[17]

Clearance mechanisms that regulate fibrosis:

There are multiple mechanisms central to resolving the fibrotic process. Effective resolution is dependent on, most importantly, removing myofibroblasts from repaired tissue and, secondly, resolving excess ECM.[84,85] As discussed previously, ECM degradation and resolution are tightly controlled by MMPs and TIMPs, and once myofibroblasts are removed, ECM synthesis is significantly reduced, and these enzymes can effectively clear excessive ECM.[38,41,84,85] There are three coordinated mechanisms involved in removing myofibroblasts: dedifferentiation, apoptosis, and senescence.

Myofibroblast dedifferentiation leads to the restoration of progenitor cells (e.g. epithelium, endothelium, fibroblasts, etc.) that myofibroblasts originate from.[86] The exact mechanisms by which myofibroblasts dedifferentiate are not well-understood, but one study suggests that inhibition of TGF-β and MAPK-signaling networks together induces marked myofibroblast dedifferentiation.[87] However, several other factors have been linked to myofibroblast dedifferentiation as well.[84]

Yet, myofibroblasts are mainly eliminated from post-fibrotic tissue through apoptosis.[84] Interestingly, evidence suggests that distinct sub-populations of macrophages play a critical role in signaling apoptosis of myofibroblasts (Figure 11).[36,84,88,89] In models of both toxic liver injury and bleomycin-induced lung fibrosis, depletion of macrophages during fibrotic recovery delayed the resolution of fibrosis.[88,90] Intuitively, this role would make sense since macrophages are a

main source of MMPs that specifically degrade ECM, and they clear cellular debris, collagen, and apoptotic cells via phagocytosis, and both mechanisms are known to impede the pro-fibrotic effects of myofibroblasts.[36]

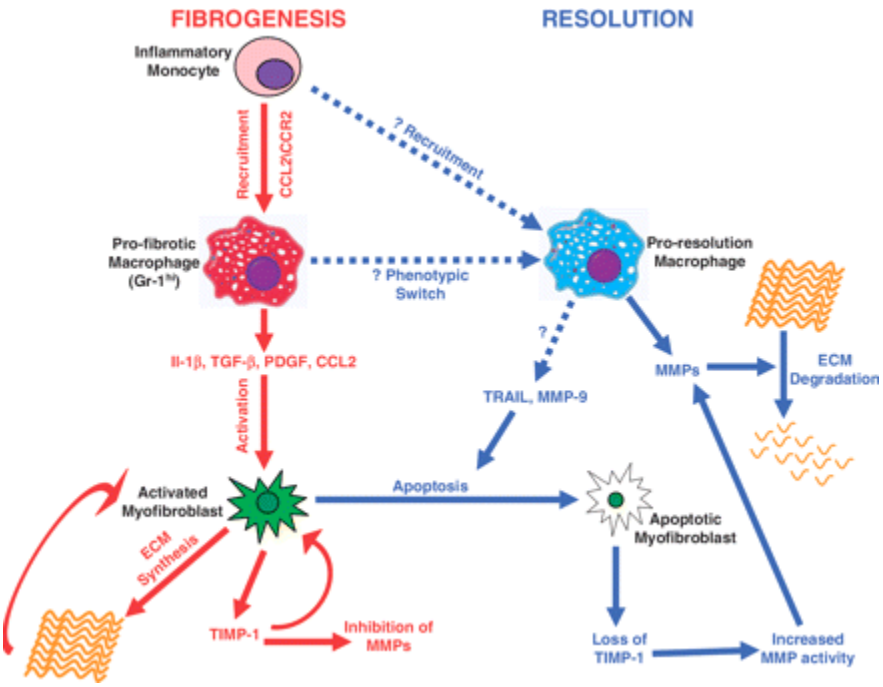

Figure 11: Resolution of the fibrotic process:

Resolution of the fibrotic process is mainly accomplished through apoptosis of myofibroblasts. Specialized macrophages may be responsible for releasing chemokines and enzymes critical for either promoting or resolving the fibrotic response. As a result of this, some macrophages may play a critical role in resolving fibrosis by activating myofibroblast apoptotic signaling pathways.

Image derived from Ramachandran et al (2012)[91]

Replicative senescence intrinsically limits the amount of cellular divisions a cell can undergo[92], and it is thought to limit the development of fibrosis during wound repair by restricting myofibroblasts' life-span.[84] Studies suggest that myofibroblast senesce during normal wound repair, allowing them to take on a gene expression profile that reduces expression of genes encoding ECM components, increases ECM-degrading enzyme production, and increases gene products predicted to augment myofibroblast clearance by immune cells.[93,94] However, senescence may be a double-edged sword in myofibroblast elimination during a pathological

state of fibrosis as prolonged myofibroblast senescence encourages resistance to apoptosis, which, as mentioned above, is the main route of myofibroblast clearance.[84,93,94]

Table 1: Some main effectors of the fibrotic response:

Mediator	Mainly produced or secreted by	Main fibrotic signaling pathway	Main function related to fibrosis	Reference
Ang-II	Macrophages, myofibroblasts	STAT, ERK/Smad2,3	Enhances TGFβ-mediated tissue remodeling	Murphy et al [95]
αSMA	Myofibroblasts	N/A	Expressed in excess by myofibroblasts to drive the fibrotic process; drives myofibroblast contractility vital for wound healing; expression driven by TGF- β/Smad2/3 signaling pathway	Talele et al [96]
CCL2	Monocytes, macrophages	STAT3, Rho, MAPK, NF-κB	Potent chemotaxis cytokine that recruits monocytes, T cells, and fibrocytes; up-regulates TGF-β expression, promoting fibroblast collagen synthesis; induces F-actin nuclearization, polymerization, and migration	Sahin et al [57] and Deng et al [97]
chymase	Mast cells	N/A	Serine protease that activates latent TGF-β and MMP-9 and inactivates various TIMPs; accelerates tissue inflammation and fibrosis by converting Ang-I to Ang-II; mainly produces pro-fibrotic effects	Beghdadi et al [49] and Masubuchi et al [51]
Collagen	Fibroblasts, myofibroblasts	N/A	Multiple types; the main structural protein of the extracellular space in connective tissues; basement membrane ECM composed mainly of collagen type IV; collagen type I promotes TGF-β signaling and fibroblast and mesenchymal stem cell differentiation into myofibroblasts	Wynn [5]
CTGF	Fibroblasts, endothelium	ERK, PKC/MAPK, PI3K	Plays roles in angiogenesis and fibrosis; interacts with various receptors, extracellular ligands, and ECM proteins; synergistic with TGF-β to promote pathological fibrosis; TGF-β1 induces CTGF in fibroblasts; activates myofibroblast differentiation and activation	Lipson et al [98]
Endothelin-1	Fibroblasts, endothelium	rac/Rho, PI3K/Akt, ERK	Promotes cellular differentiation to myofibroblasts; enhances collagen expression in fibroblasts; increases myofibroblast survival	Rodríguez-Pascual et al [99]
FGF	Mast cells, epithelium, fibroblasts	RAS-MAPK, PI3K-AKT, STAT	Diverse family of growth factors that require heparins or heparan sulfate for receptor binding, meaning proximity to ECM and fibroblasts that secrete ECM is required for activity; stimulates angiogenesis; stimulates proliferation, migration, and differentiation of epithelial cells and fibroblasts; chemotactic effects on tissue remodeling; inhibits EMT and antagonizes TGF-β-mediated effects	Kim et al [100] and Maddaluno et al [101]
Fibronectin	Fibroblasts, macrophages	PI3K/Akt, STAT3, MAPK, TGF- β	Adhesive proteins that connect cells to ECM via integrins transmembrane proteins; essential for collagen assembly into ECM and blood clotting; regulates active TGF-β concentrations; protects tissue from TGF-β hyperstimulation; degraded by MMPs	To et al [102]
histamine	Mast cells, damaged cells	G protein-coupled histamine	Stimulates vasodilation; recruits immune and inflammatory cells; increases cytokine production and secretion	Panula et al [103]

		receptors		
iNOS	Neutrophils, T cells, macrophages	N/A	Inducible form from a family of enzymes that produce NO from L-arginine after binding calmodulin; stimulated by IL-1, TNF-α, and IFN-γ.	Iwakiri [104]
IFN-γ	Th1 cells, macrophages	STAT1, ERK, NF-κB	Mainly exerts antifibrotic effects; downregulates TGF-β1 expression; promotes Th1 development and antagonizes Th2 development; activates iNOS; promotes leukocyte migration; antagonizes TGF-β-induced ECM synthesis mechanisms	Segel et al [105]
IL-1β	M1 macrophages, fibroblasts	Interleukin receptors, NF-κB	Potent pro-inflammatory cytokine; induces production of PDGF and TGFβ	Borthwick [106]
IL-3	T cells, mast cells	Interleukin receptors, various	Pro-inflammatory cytokine that upregulates IL-33 production, influences Th17-mediated inflammation and Th2-driven fibrosis, and facilitates myofibroblast pro-fibrotic activity	Van Linthout et al [33]
IL-4	Th2 cells, mast cells	PI3K/Akt, STAT, Ras	Suppresses MMP biosynthesis by macrophages; drives Th2 development and antagonizes Th1 development	Wick et al [11]
IL-5	Th2 cells, mast cells	STAT, MAPK, PI3K, NF-κB	Aids in recruitment, differentiation and activation of eosinophils, which may attenuate rather than drive fibrosis	Borthwick et al [56]
IL-6	T cells, macrophages, fibroblasts, mast cells	STAT3, PI3K/Akt/MAPK	Shifts wound healing to a chronic inflammatory state; well-known roles in inflammation, cellular differentiation, and fibrosis; increases MMP-1 and TIMP-1 expression as well as collagen synthesis	Agarwal et al [107]
IL-10	Macrophages, Th2 cells, Tregs, mast cells	STAT3, PI3K, NF-κB, MAPK	Inhibits synthesis of pro-inflammatory cytokines such as IFN-γ, IL-2, IL-3, and TNFα made by Th1 cells and macrophages; affects expression of MMP9, iNOS, INF-γ; effects of IL-10 are anti-fibrotic	Sziksz et al [58]
IL-12	Macrophages, neutrophils	STAT4	Drives Th1 differentiation from naïve T cells; stimulates IFN-γ and TNF-α production from T cells	Huaux et al [108]
IL-13	Mast cells, Th2 cells, epithelium, macrophages	STAT, ERK, TGF- β/Smad	Participates in TGF-β production and activation; stimulates proliferation, differentiation, and collagen synthesis of/by fibroblasts	Passalacqua et al [109]
IL-17	Th17 cells	NF-κB, MAPK	Stimulates interleukin-6 (IL-6) secretion in fibroblasts; increases IL-1 production; increases fibroblast proliferation; promotes collagen synthesis; attenuates myofibroblast transdifferentiation in pathological fibrotic states	Park et al [110]
IL-18	Macrophages, epithelium, T cells	MAPK, NF-κB	Stimulates natural killer (NK) cells and certain T cells to release IFN-γ; various pro-fibrotic characteristics such as increased proliferation, migration, and collagen synthesis by fibroblasts	Borthwick [106]
IL-33	Fibroblasts, epithelium, macrophages	MAPK, NF-κB	Production can be induced by inflammation mechanical stress; implicated in both inflammatory and fibrotic processes (drives production of type 2 cytokines)	Borthwick [106]
LPA	Not clear, although possibly platelets	Ras/MAPK, Rho, NF-κB	Produced from lysophosphatidylcholine (LPC) by autotaxin; encourages cell proliferation, angiogenesis, cell survival, and migration/invasion; produced in response to TNF-mediated inflammation to increase	Rancoule et al [111]

			wound repair; may play a role in collagen production	
MMP-1	fibroblasts, macrophages, epithelium, endothelium	N/A	Breaks down types I-III collagens; may promote epithelial cell proliferation and migration, and inhibits oxidant production and apoptosis; promotes regeneration of epithelial cells	Craig et al [40] and Giannandrea et al [41]
MMP-2	epithelium, macrophages, endothelium, fibroblasts, fibrocytes	TGF-β, Wnt/β-catenin	Cleaves basement membrane proteins and type IV and denatured collagens; latent MMP-2 is activated by MT-MMPs and TIMP-2 on the surfaces of fibroblasts and macrophages; promotes EMT by activating latent TGF-β	Craig et al [40] and Giannandrea et al [41]
MMP-3	Epithelium, fibroblasts, endothelium, macrophages, monocytes	TGF-β, Wnt/β-catenin	Latent form activated by tryptase; cleaves type IV collagen and basement membrane proteins; promotes EMT; activates latent TGF-β	Craig et al [40] and Giannandrea et al [41]
MMP-7	Epithelium, fibrocytes	N/A	Cleaves syndecan-1, allowing neutrophil infiltration; promotes fibroblast proliferation by cleaving latent heparin-binding epidermal growth factor (EGF)-like growth factor (HB-EGF) and epithelial cell regeneration by cleaving E-cadherin	Craig et al [40] and Giannandrea et al [41]
MMP-8	Neutrophils, monocytes, macrophages, epithelium, fibroblasts, fibrocytes, T-cells, mesenchymal stem cells	N/A	Stored in neutrophil granules and released upon activation; regulated by TGF-β1, TNF-α, and IL-1β; breaks down types I-III collagens; influences multiple processes by modulating cellular inflammation, cytokine inactivation, and fibroblast activation	Craig et al [40] and Giannandrea et al [41]
MMP-9	leukocytes, fibroblasts, epithelium, endothelium	N/A	Latent form stored in neutrophil granules (activated by interacting protease cascade including plasmin and MMP-3); stimulates collagen contraction when interacting with TGF-ß1, involved in removing fibrinogen matrix; recruits neutrophils and endothelial stem cells; activates latent TGF-ß1 and IL-1β; promotes EMT	Craig et al [40] and Giannandrea et al [41]
MMP-12	Macrophages	N/A	degrades soluble and insoluble elastin; influences fibroblast activation and collagen production; suppresses expression of other anti-fibrotic MMPs	Craig et al [40] and Giannandrea et al [41]
MMP-13	Fibroblasts	N/A	Breaks down types I-III collagens; regulated by TGF-β, IL-1β, IL-6, and TNF-α; activated by MMP-2 and MT1-MMP (MMP-14); cleaves and inactivate CCL2; processes many other cytokines	Craig et al [40] and Giannandrea et al [41]
MMP-19	Monocytes, macrophages, fibroblasts, endothelium	N/A	Induces prostaglandin G/H synthase 2 (PTGS2), which generates PGE2 (anti-fibrotic cytokine)	Craig et al [40] and Giannandrea et al [41]
NO	Neutrophils, macrophages	MAPK, NF-κB	In an oxidative environment, high levels of NO can interact with superoxide ($^{\bullet}O^{-2}$) to produce peroxynitrite, leading to cell toxicity. NO engages in various pro-inflammatory and pro-fibrotic activities such as oxidative burst and increased production of pro-fibrotic cytokines.	Iwakiri [104]
PDGF	platelets, endothelium,	VEGF, FAK, PI3K/AKT	Induces type I collagen expression; acts on mesenchyme and fibroblasts to induce	Klinkhammer et al [112]

	smooth muscle cells, and macrophages		proliferation, differentiation, and ECM production	
PGE2	N/A	Wnt/β-catenin, PI3K/Akt	Suppresses fibrosis by inhibiting fibroblast migration, proliferation, collagen synthesis and differentiation into myofibroblasts	Bozyk et al [113]
ROS	Neutrophils, M1 macrophages, endothelium	TGF- β/SMAD	Examples include: hydroxyl radical ($^{\bullet}OH$), hydrogen peroxide (H_2O_2), superoxide radical ($^{\bullet}O^{-2}$), and ultimately oxygen (O_2); increases TGF-β1 activation and production; involved in various feed-forward and feedback mechanisms important for the inflammatory and fibrotic responses	Richter et al [114]
TIMPs	Myofibroblasts, macrophages	N/A	Family (TIMP1-4) of enzymes that bind to and inhibit MMP binding site; activated by MMP-2 & -9; each TIMP inhibits most MMPs, but MT-MMPs are mainly inhibited by TIMP-2 & -3 and TIMP-1 coordinates to pro–MMP-9, preventing its activation	Arpino et al [42]
TLRs	macrophages, T cells, epithelium, endothelium, fibroblasts	MAPK, ERK, NF-κB, PI3K-AKT	The main member of the PRRs involved in fibrosis; signal the presence of various pathogen-associated molecular patterns (PAMPs) and damage-associated molecular patterns (DAMPs) to innate and adaptive immune cells as well as pro-fibrotic cells; main initiators of the fibrotic process	Huebener et al [23]
TGF-β	Platelets, macrophages, mast cells, fibroblasts, T cells, myofibroblasts	SMAD-2/3 axis	Main fibrotic effector; drives migration, proliferation, and differentiation of fibroblasts; stimulates αSMA, fibronectin, pro-fibrotic cytokine production; regulates the expression of ROS-producing enzymes	Kim et al [60]
tryptase	Mast cells	N/A	Pro-fibrotic serine protease that activates fibroblast proliferation and collagen synthesis; cleaves latent MMP-3; activates IL-6 release in eosinophils by MAPK and AP-1 pathways	Levi-Schaffer et al [50]
TNF-α	M1 macrophages, neutrophils, mast cells, fibroblasts	MAPK, NF-κB, ERK, Smad	Has both pro-fibrotic and antifibrotic effects depending on state of macrophages and micro-environment; activates fibroblasts and overproduction of ECM; activates expression of fibrogenic cytokines; stimulates macrophage phagocytosis	Distler et al [115]
VEGF	Epithelium, macrophages, fibroblasts	VEGF	Promotes angiogenesis; could play a role in vascular damage signaling that promotes fibroblast activation	Barratt et al [116]

Angiotensin (Ang), α-smooth muscle actin (αSMA), C-C motif chemokine ligand 2 (CCL2), connective tissue growth factor (CTGF), fibroblast growth factor (FGF), inducible nitric oxide synthase (iNOS), interferon-γ (IFN-γ), interleukin (IL), matrix metalloproteinase (MMP), nitric oxide (NO), platelet-derived growth factor (PDGF), reactive oxygen species (ROS), tissue inhibitor of metalloproteinase (TIMP), Toll-like receptor (TLR), transforming growth factor-β (TGF-β), tumor necrosis factor- α (TNF-α), vascular endothelial growth factor (VEGF)

Fibrotic signaling pathways:

There are multiple overlapping signaling pathways that regulate various components of the wound healing process. Figure 12 represents many important fibrotic signaling pathways (e.g. Wnt, TGFβ/Smad, VEGF, TNF, PI3K/AKT, mTOR, etc.)[117]. While it is difficult to encompass all the signaling components central to fibrosis in a single figure, there are many reviews that describe important fibrotic signaling pathways in depth.[118-122]

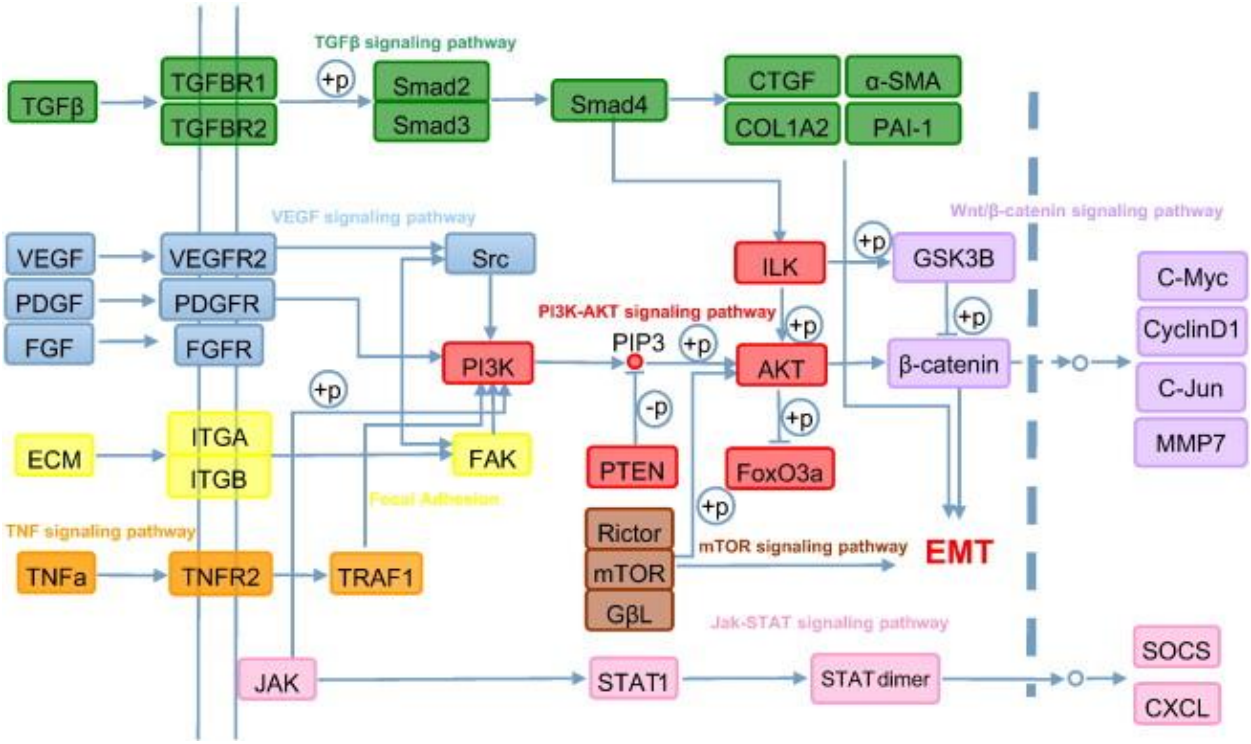

Figure 12: Some notable signaling pathways in fibrosis:

TGFβ/Smad promotes production of genes encoding for ECM components (e.g. collagen-1A2 (COL-1A2) and αSMA) and cytokines that drive myofibroblast differentiation (e.g. CTGF), EMT and blood clotting (e.g. plasminogen activator inhibitor-1 (PAI-1)); VEGF[116]/PDGF[123]/FGF[100]-signaling feeds into various pathways that are important for the fibrotic response, such as phosphoinositide 3-kinase (PI3K)[124], proto-oncogene tyrosine-protein kinase Src (Src)[125], protein kinase B (Akt)[126]/mechanistic target of rapamycin (mTOR)[127]; signaling mediated by focal adhesion (e.g. focal adhesion kinase (FAK)) also feeds into PI3K/Akt pathways, and it is important for cell migration and myofibroblast activation[128]; Wnt/β-catenin signaling not only plays a central role in organ development, but it is also a critical mediator of the fibrotic response[129]; signaling through tumor necrosis factor-α (TNF-α)[115] and janus kinases (JAK)/Signal Transducer and Activator of Transcription (STAT)[130] are suggested to have mostly anti-fibrotic effects; Rho-signaling is important for actin assembly, which transduces multiple components of the fibrotic process.[119]

Image derived from Yan et al (2014)[117]

Therapeutic agents and strategies for fibrotic diseases:

Even though many complexities of the fibrotic process are generally well understood, including many of the mechanisms that are critical for driving pathological fibrosis, the therapeutic landscape for treating fibrotic diseases remains in its infancy. Despite the tremendous number of biological processes and targets identified as being potential strategies for treating fibrotic diseases, there are currently only two agents specifically approved in the U.S. for treating pathological forms of fibrosis—Nintedanib and pirfenidone (Figure 13)—albeit they are generally only mildly successful.[131-134] The lack of successful fibrotic treatments stems from the difficulty of precisely modulating the numerous multifaceted biological processes that take place during the fibrotic response (many of which are described in the sections above).[12,135]

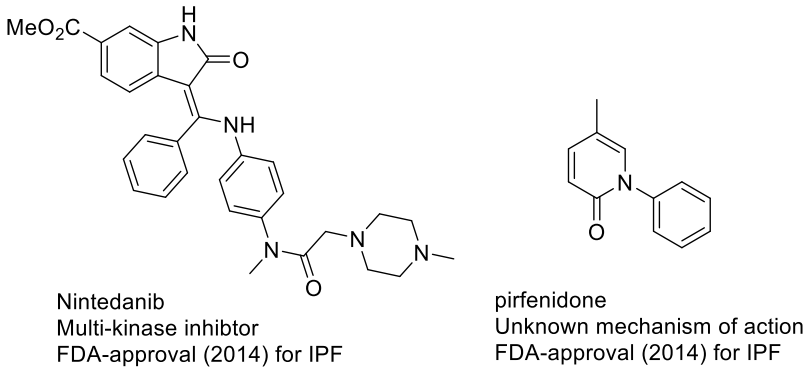

Figure 13: FDA approved anti-fibrotic agents:
Nintedanib and pirfenidone—two FDA approved therapeutic agents approved for idiopathic pulmonary fibrosis (IPF)—are mildly successful therapies used to treat fibrotic diseases.

Many unsuccessful anti-fibrotic drug development efforts attempt to modulate pro- or anti-fibrotic signaling pathways by affecting easily accessible extracellular targets.[12,135] However, this type of therapeutic approach has generally been problematic because precisely regulating the complicated cross-talk that takes place between fibrotic signaling pathways is very challenging. Also, many efforts focus on modulating targets that are not only activated during the fibrotic response but are also critical for normal cellular functions, which can lead to

undesirable side effects that limit therapeutic effectiveness.[12,135,136] For example, while TGF- β signaling is central to all fibrotic diseases, TGF-β targeted therapies (e.g. antibodies, peptides, receptor decoys, small-molecules, etc.) for fibrotic diseases have failed to gain FDA approval[12,135]; unfortunately, not only is TGF-β signaling critical for normal biological functions, there are other pro-fibrotic factors in advanced fibrotic diseases that can overcome TGF-β inhibition and drive pro-fibrotic signaling pathways.[137] Despite the lack of success, alternative approaches to targeting TGF-β are still being pursued.[12,137]

Even successful therapies are promiscuous and guilty of attempting to control pro-fibrotic signaling pathways by modulating up-stream targets.[12,134,138] For example, Nintedanib inhibits multiple pro-fibrotic kinase receptor signaling activities (e.g. VEGFR, PDGFR, and FGFR; Figure 14)[134,138], and while such pathways may be essential and highly upregulated during pathological fibrosis, they also control various processes that not only may help resolve the fibrotic response but are also central to normal cellular functions.[4,12,134] Unfortunately, Nintedanib's promiscuity has significantly limited its clinical success, producing undesirable off-target effects that restricts its therapeutic utility.[12,134]

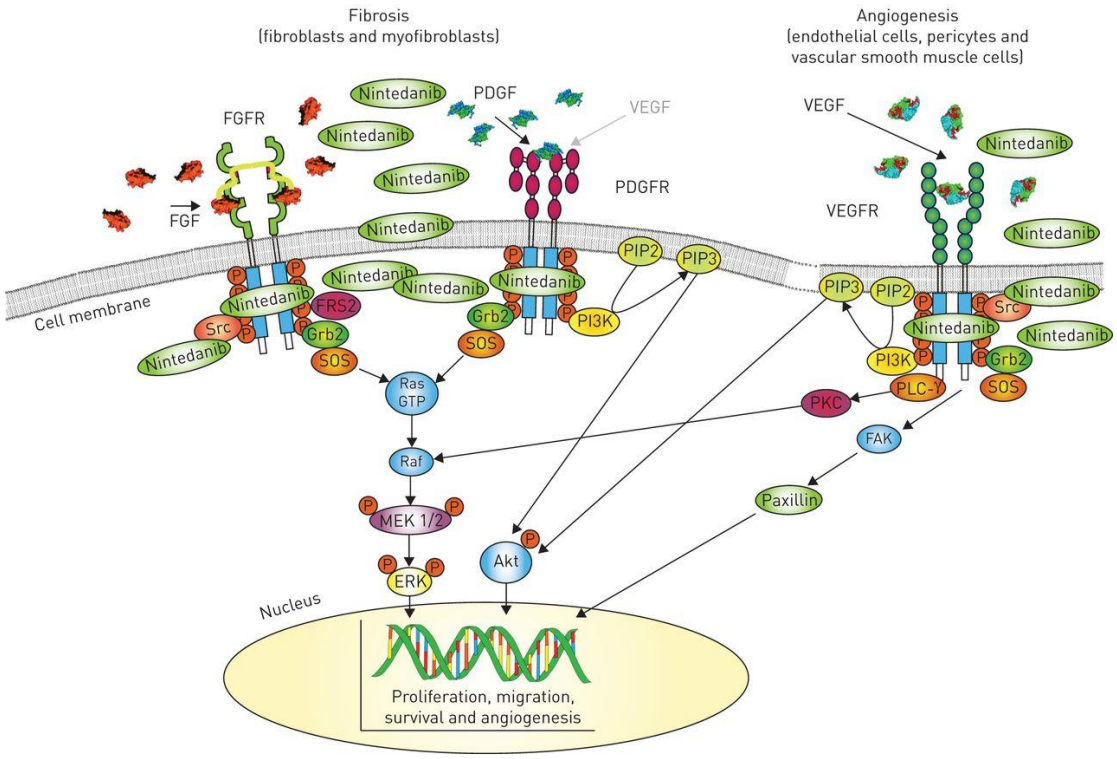

Figure 14: Nintedanib's mechanism of action:

Nintedanib potently inhibits kinase activity for FGFR, PDGFR, and VEGFR by binding to their intracellular ATP binding pockets. This inhibition blocks various downstream fibrotic and angiogenic signaling pathways, such as Akt, Src, FAK, ERK, vital for the fibrotic response.

Image derived from Wollin et al (2015)[138]

As for the success of Nintedanib and pirfenidone in the clinic, they are currently only capable of slowing disease progression by matters of months in IPF patients, and pirfenidone is generally only prescribed to bridge the time between diagnosis and lung transplantation—which remains the only intervention method with proven long-term benefit.[12,132,136] A critical reason that these two drugs lack long-term success is because the resolution of fibrosis requires more than simply preventing fibrosis; it also requires restoring organ function, which presents a major hurdle in designing therapeutic agents for fibrotic diseases.[84,136] However, promising research with stem cell therapies is being conducted that will hopefully enhance tissue repair in patients diagnosed with fibrotic diseases.[136,139]

Based on recent reports for therapeutic strategies for fibrotic diseases[84,85,122,131,133,135-137,140,141], the crucial next step is to develop a therapy that can halt fibrotic disease progression.

However, as a result of the multilayered etiology of fibrotic disorders, this has posed a challenge. Still, the common belief to accomplish this is to design a therapy that selectively targets a mechanism specific to the fibrotic process.[140-142] Ideally, the mechanism would be regulated by a biological target that is far-downstream within a fibrotic-dependent signaling pathway that is highly suppressed or upregulated during pathological fibrosis; for instance, modulating a biological target that directly regulates myofibroblast differentiation or controls the excessive expression of ECM.

Many approaches are being conducted to determine the feasibility of therapeutic strategies with down-stream targets.[140-142] For instance, microRNAs (miRNAs) have emerged as a potential therapeutic target.[141,142] miRNA are short non-coding nucleic acid polymers that can silence mRNA and regulate post-transcriptional gene expression.[143] Multiple miRNAs have been shown to either be overexpressed or downregulated during fibrotic disease progression, and these alterations can change a multitude of fibrotic processes, such as TGF-β-mediated signaling and the expression of ECM components.[141,142] For example, inhibition of miR-21 with anti-miR-21 in mice results in recovery of heart function[144], and synthetic overexpression of miR-29 in mice with cardiac disease post-myocardial infarction (MI) reduces collagen production and fibrosis.[145] Overall, miR-based therapy has provided strong preclinical indications that it may be an effective therapeutic strategy for various fibrotic diseases.[141,142]

Alternatively, peroxisome proliferator-activated receptor (PPAR) agonists have recently received attention for their anti-fibrotic capabilities.[141] There are three subtypes of PPARs (PPARα, PPARβ/δ, and PPARγ), and they are nuclear transcription factors that homodimerize with retinoid-X receptors to affect gene transcription.[146] Traditionally in the clinic, PPAR agonists (e.g. thiazolidinediones (TZDs)) are primarily used to enhance insulin sensitivity to promote glucose uptake in diabetes patients, but PPAR agonists have long been known to have anti-inflammatory properties, and, recently, more studies are revealing their anti-fibrotic properties.[147] For instance, rosiglitazone—a PPARγ agonist—prevented radiation induced pulmonary

fibrosis[148], and it reduced inflammation and collagen deposition in a bleomycin-induced model of dermal fibrosis.[149] Unfortunately, many undesirable side effects (e.g. weight gain, edema, bone density loss, etc.) have been established throughout the years with PPAR agonists, which has limited their use and effectiveness in the clinic.[147] While it is unknown if attempts to circumvent these side effects by using dual-, pan-, or mixed- agonists will improve PPARs utility as antifibrotic agents in the clinic, the results published over the past few years regarding their activity is a step in the right direction regarding designing anti-fibrotic agents that modulate intranuclear biological targets.[141]

Recently, the Neubig lab discovered two novel series of small-molecule inhibitors that may modulate down-stream biological targets within signaling pathways that are linked to fibrotic processes (discussed in more detail in the next few sections). Based on promising results, both series of inhibitors might represent another anti-fibrotic strategy capable of targeting down-stream biological targets, potentially bridging the gap between only slowing fibrotic disease progression to halting it altogether.

Rho/MRTF/SRF-regulated gene transcription and fibrosis:

As mentioned, various overlapping biochemical pathways in a variety of cell types are triggered during the fibrotic process; however, Rho-signaling is central to the FMT. Soluble profibrotic mediators, such as TGF-β, endothelin, fibronectin, connective tissue growth factor (CTGF), lysophosphatidic acid (LPA), etc., induce the FMT through Rho-signaling (Figure 15).[14,121] The Rho family of GTPases and their downstream kinase, Rho-associated kinase (ROCK), are known to coordinate with myocardin-related transcription factor (MRTF) and serum resonse factor (SRF) to play a vital role in myofibroblast differentiation and contraction.[121,150-156]

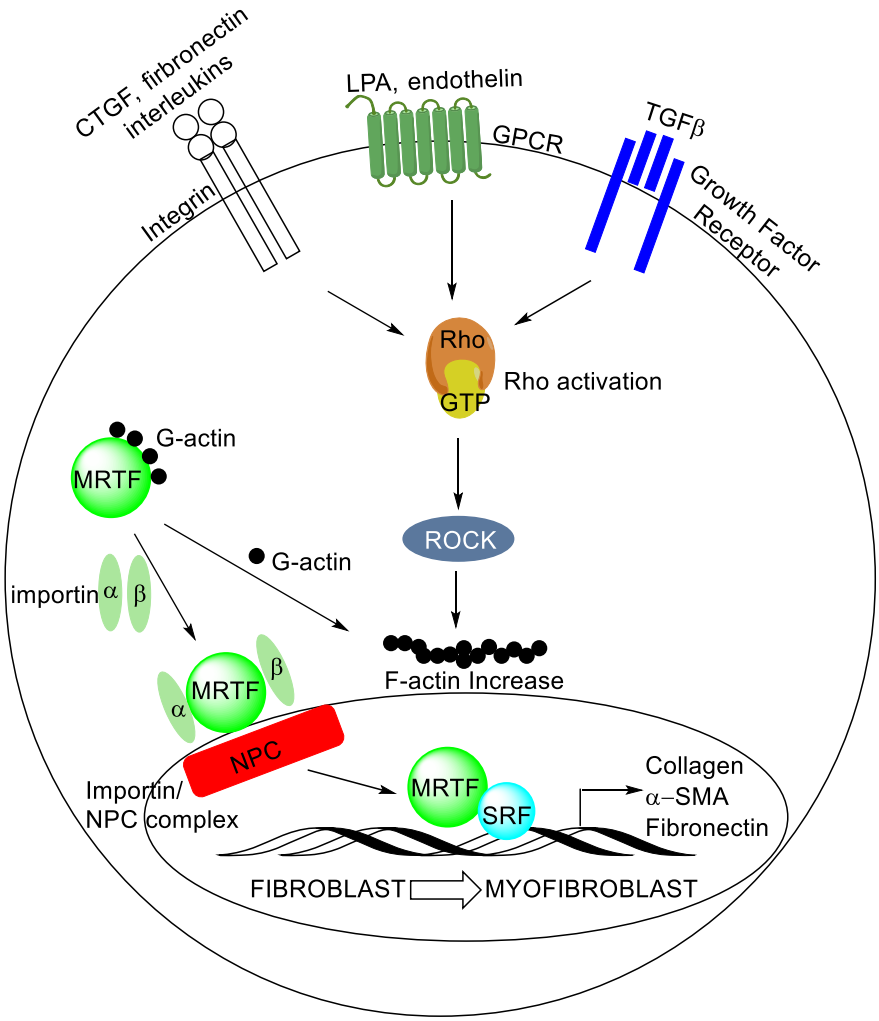

Figure 15: The role of Rho/MRTF/SRF-signaling in the fibrotic process:

The fibroblast-to-myofibroblast transition is tightly regulated by Rho/MRTF/SRF signaling. Both soluble and mechanical stimuli promote MRTF nuclear translocation in fibroblasts. In the resting state, actin is not polymerized, and MRTF is bound to G-actin and sequestered into the cytoplasm. When stress fibers form in response to these stimuli, G-actin polymerizes into F-actin and MRTF is released. This allows MRTF to translocate into the nucleus via binding to importins followed by MRTF/importin/nuclear pore complex (NPC) formation. The MRTF/SRF coactivator complex increases ECM and pro-fibrotic gene expression, contributing to the FMT.

Rho/ROCK-signaling has been shown to participate in both soluble mediator and stiff matrix-induced FMT. [121,157] Inhibition of the Rho/ROCK-signaling pathway blocks myofibroblast differentiation through the disruption of stress fiber formation *in vitro* and reduces the severity of fibrosis *in vivo*.[152] In addition to interrupting stress fiber formation, modulating Rho/ROCK alters

the gene expression profile of (myo)fibroblasts.[121,153] A crucial link between simultaneous induction of stress fiber formation and altered gene expression during myofibroblast differentiation has been identified as MRTF.[153] MRTF functions in coordination with SRF as a transcriptional coactivator that modulates the expression of myofibroblast genes, including smooth muscle aortic alpha-actin (ACTA2), connective tissue growth factor (CTGF), and collagen type I alpha 2 (COL1A2).[14,150,153] The inhibition of MRTF/SRF-mediated gene transcription has been shown to mitigate myofibroblast differentiation and ECM synthesis in colonic fibroblasts and human skin fibroblasts from patients with scleroderma.[158,159] Rho/MRTF/SRF-signaling is known to regulate pro-fibrotic genes from multiple extracellular signaling pathways[156,160-162], and therefore inhibition of this critical signaling pathway might be a general way to effectively treat/prevent pathological fibrosis (Figure 16).

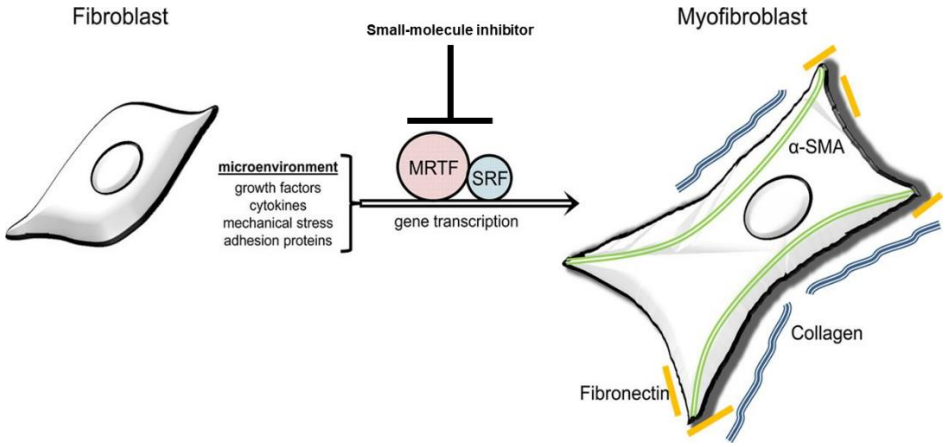

Figure 16: Alternative route for treating fibrosis:

Inhibition of MRTF/SRF signaling, which is important for the fibroblast-to-myofibroblast transition, could provide an alternative route to treating fibrotic diseases.

Image derived from Tsou et al (2014)[121]

Novel inhibitors of Rho/MRTF/SRF-regulated gene transcription:

The Neubig and Larsen labs identified Rho/MRTF/SRF-mediated gene transcription inhibitors using a high-throughput phenotypic screen utilizing a modified SRE.L reporter assay in HEK293T cells.[163] Two series of inhibitors have been developed from this assay—the series

developed from CCG-1423 was identified from a 2,000 compound screen and that from CCG-58146 was identified from an 80,000 compound screen (Figure 17).

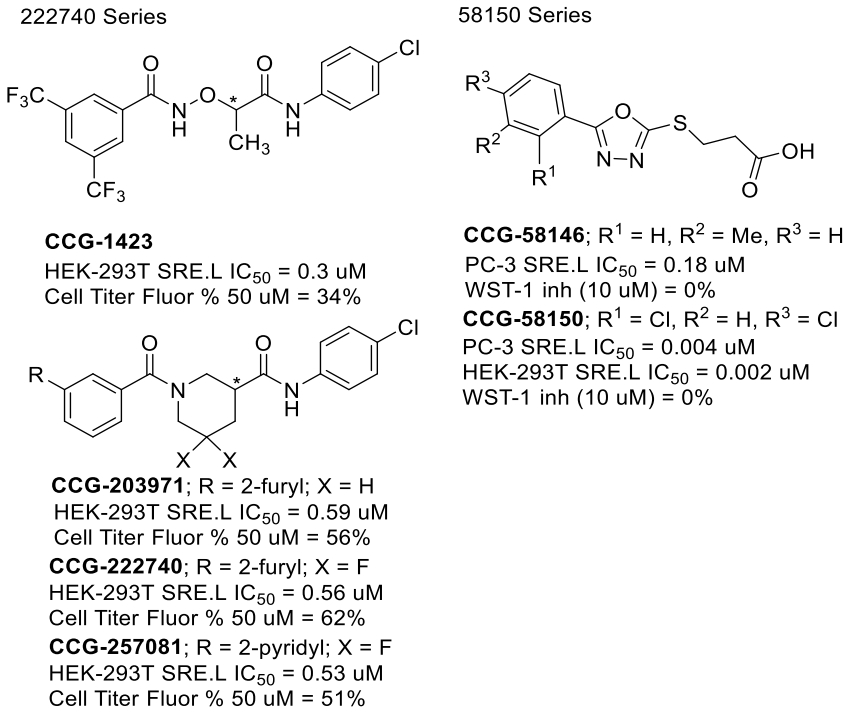

Figure 17: Hits and leads from the 222740- and 58150-series:
Structures, potency, and cell-toxicity of two distinct series of Rho/MRTF/SRF-mediated gene transcription inhibitors.

CCG-1423 has been an important probe compound for Rho/MRTF/SRF-regulated gene transcription.[10,157,158,163-166] However, due to undesirable cytotoxicity and PK properties, the series was optimized to CCG-203971[167], CCG-222740, and CCG-257081[168] (Figure 17). This bis-amide series has provided promising *in vitro* and *in vivo* results in multiple fibrotic models. For instance, CCG-203971 repressed TGF-β-induced α-SMA and COL1A1 transcription and protein expression dose dependently in low-passage colonic myofibroblasts (CCD-18co cells), and transcriptionally repressed key effector molecules within the RhoA/MRTF-A pathway itself.[158] Additionally, CCG-203971 increased susceptibility of healthy fibroblasts and fibroblasts derived from idiopathic pulmonary fibrosis (IPF) patients to undergo apoptosis, blocked TGF-β1-induced myofibroblast differentiation, and inhibited TGF-β1-induced expression of fibronectin.[169]

In another study, CCG-203971 inhibited the expression of CTGF, α-SMA, and COL1A1 in both fibroblasts derived from scleroderma patients and in LPA stimulated fibroblasts.[159] In various murine models[159,163,166-173], CCG-203971 is capable of reducing lung collagen content, promoting myofibroblast apoptosis[169], and preventing bleomycin-induced skin thickening and collagen deposition.[159]

The novel and highly potent 1,3,4-oxadiazole thioether inhibitors CCG-58146 and CCG-58150 were identified in the larger screen. The series was originally identified as a potential inhibitor of cancer metastasis; however, this direction was deprioritized due to the series' potent anti-fibrotic activities. For instance, CCG-58150 not only inhibits expression of the MRTF/SRF reporter SRE.L in both HEK-293T and PC-3 cells (Figure 17 & 18A), but it also blocks CTGF expression of mRNA in LPA-stimulated fibroblasts (Figure 18B) and abrogates RhoC dependent PC-3 migration at sub-nM concentrations with similar potency (Figure 18C). The extremely high potency of CCG-58150 may be attributable to a covalent mechanism (discussed in Chapter 2), and the binding is apparently highly selective since it displays 0% WST-1 inhibition at 100 μM. *In vivo*, CCG-58150 has shown promising results in the prevention of bleomycin-induced skin fibrosis (Figure 19).

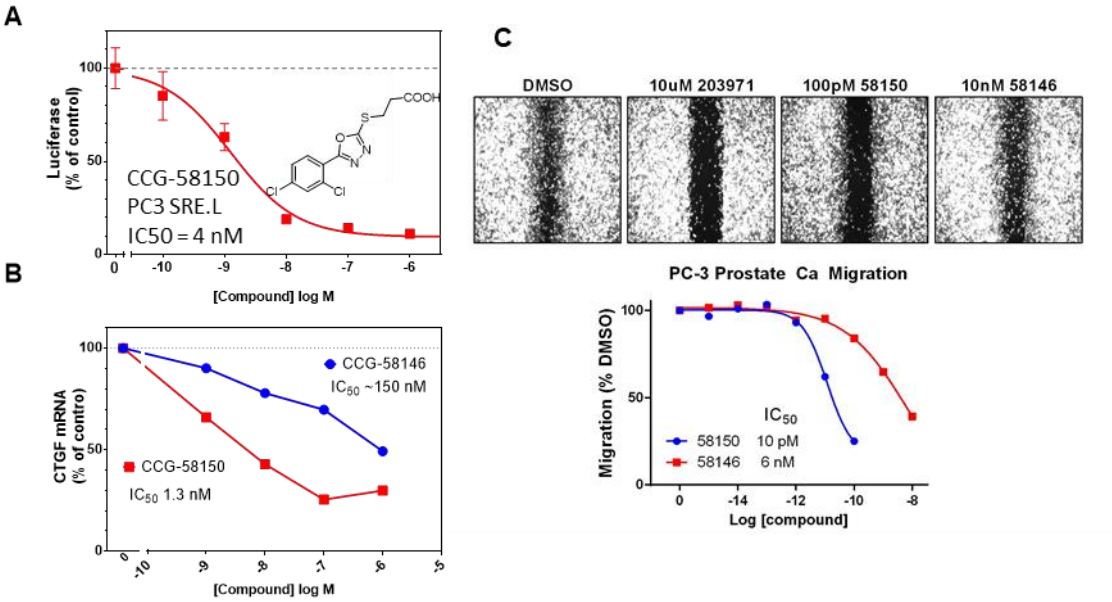

Figure 18: Potent *in vitro* activities for CCG-58150:

A) SRE-Luciferase activity in PC-3 cells with transfected with constitutively active Gα12 to stimulate Rho is inhibited by CCG-58150. B) Endogenous CTGF mRNA in NIH-3T3 cells was stimulated with LPA (10 uM for 30 minutes) in the presence of various concentrations of CCG-58146 (*blue*) and CCG-58150 (*red*). C) (*top*) Migration of PC-3 prostate cancer cells in scratch assays has previously been shown to be RhoC-dependent. (*bottom*) CCG-58150 (*blue*) blocks migration at pM concentrations and CCG-58146 blocks migration at nM concentrations (*red*).

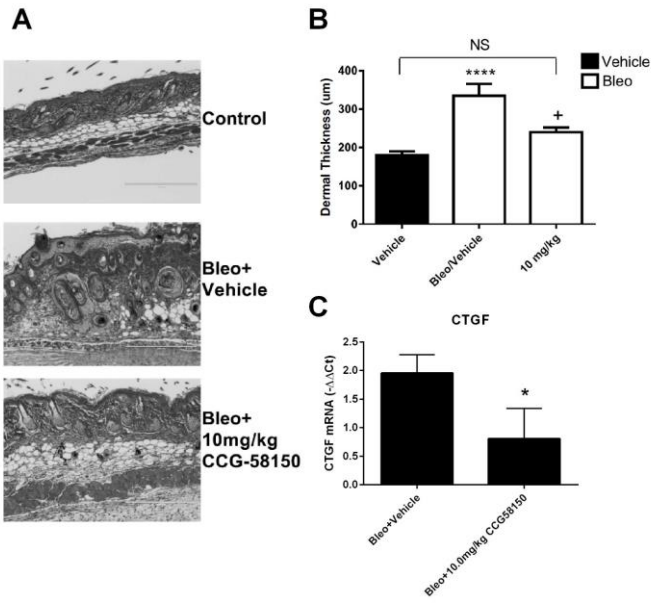

Figure 19: Potent *in vivo* activities for CCG-58150 in fibrotic mice:

Skin fibrosis was induced by daily bleomycin injections for two weeks. A group treated with CCG-58150 (10 mg/kg p.o daily) showed: A & B) reduced skin thickness and C) decreased expression of the MRTF target gene CTGF. Skin thickness n=9-10 per group. CTGF n=5 due to limited tissue. ****, $p<0.001$ vs Vehicle, + or *, $p<0.05$ vs Bleo, Student's t test.

The Neubig lab has shown that inhibiting Rho/MRTF/SRF-mediated gene transcription decreases myofibroblast differentiation and ECM synthesis.[158,159] The likelihood of generating a therapeutically important class of anti-fibrotic compounds from either series is highly probable due to the fundamental role that serum-regulated gene transcription has in cell survival, proliferation, and migration for fibrotic diseases.[174] However, to increase the likelihood of this success, target identification campaigns to reveal the biological target(s) for both series were undertaken.

Project Goals:

Until recently, the major focus of the 222740 series has been to improve SRE.L activity and ADMET properties, while the emphasis on the 58150 series has been to explore the SAR around the aromatic ring. To better understand the mechanism of action for each series, additional target identification efforts by designing and synthesizing chemical probes for each series were planned. If successful, these target identification campaigns would potentially provide a more effective route to generate optimized therapeutic agents as well as provide a better understanding of on-target vs. off-target effects for each series. The recent efforts to identify the biological target(s) for both series are discussed in Chapter 2.

Regardless of whether these efforts were successful, another goal of the project was to determine the potential anti-fibrotic capabilities of both series by developing pre-clinical candidates that could be tested in relevant murine models of fibrosis. This goal required improvements in cellular potencies, pharmacokinetic (PK) profiles, and proof-of-concept validation in various *in vitro* models of fibrosis. Recent advancements toward this goal for the 58150- and 222740-series are discussed in Chapters 3 and 4, respectively. Also, with these

goals in mind, Chapter 5 discusses some potential next steps that can be taken to progress the project.

Chapter 2: Probe Design and Development/Target Identification

Brief Target Identification Introduction:

There are many approaches to identifying unknown biological targets for small-molecule inhibitors, such as immobilized resin[175,176], photo-affinity[177,178], and fluorescent[179] probes; however, target identification campaigns are frequently multifaceted, time-consuming, and expensive to complete.[180-184] The first step is often designing and synthesizing a chemical probe that retains the observed phenotypic biological activity.[175,180,183] This can be challenging for many reasons, such as (1) attaching appendages to the small-molecule's scaffolding can change or eliminate relevant biological activity (2) many small-molecule series that require target ID campaigns are identified in phenotypic assays, making it difficult to verify relevant activity of the probe-mimics or the probe itself (3) the probe design process can be slow in general since multiple iterations of probe mimics (and their syntheses) may be required to confirm the biological activities relevant to biological target engagement.[175,183]

After a probe is produced, the proper pull-down experiments need to be designed and conducted.[175,178,180,183] Often, the probe alone does not suffice for accurate identification of the biological target(s). For instance, various controls, such as a competitor (e.g. active analog within the series), a structurally related "inactive" probe, or the solid phased capped without compound, can be used to compare protein fragmentation patterns after quantitative proteomic analysis.[175,178,183] Such control experiments help tease out proteins that non-specifically bind to the probe as a whole rather than the portion of the probe containing the small-molecule. Moreover, various target identification approaches, such as stable isotope labeling of amino

acids in cell culture (SILAC)[185], drug affinity responsive target stability (DARTS)[186], and differential radial capillary action of ligand assay (DRaCALA)[187], can enhance the accuracy of the proteomic analysis.[188] The pull-down experiment may require an even more intricate design if the small-molecule/probe only interacts weakly with relevant macromolecule(s), the biological target is in low cellular abundance, or the biological target is unstable or susceptible to post-translational modifications.[180,183,188]

Once the proper probe and isolation experiments are designed and conducted, the resulting batches of macromolecules collected can be proteolytically cleaved (e.g. trypsin), producing fragments of amino acids that can be analyzed for characteristic (and ideally unique) sequences by mass spectrometry.[183] The ensuing quantitative proteomic analysis of these amino acid fragments can be used to generate a list of protein candidates.[183,189] After a reasonable list is generated, the next step is to validate the biological target(s).[181-183,190] Generally, the candidate list can be narrowed down by searching the literature for macromolecules with relevant biological activities; however, validating even just one potential biological target can be time-consuming and expensive. For instance, even if a protein candidate is found to physically interact with analogs from a series of small-molecules, confirming a biological target typically also requires connecting the identified target to the phenotypic assay (*in vitro*) and the disease state (*in vivo*).[181-183,190]

All considered, it is very important to establish valid reasons for pursuing a target identification campaign. The exciting *in vitro* and *in vivo* biological activity of the 58150- and 222740-series (discussed in the Chapter 1) convinced us to pursue a target ID campaign for both series.

CCG-58150 Series Target Identification Efforts:

Parts of this subsection have been included in a submitted manuscript entitled "5-Aryl-1,3,4-oxadiazol-2-ylthioalkanoic Acids: A Highly Potent New Class of Inhibitors of Rho-Mediated Gene Transcription as Potential Antifibrotic Agents for Scleroderma" by Kahl et al.

58150 Series Probe Design Rationale:

The early SAR trends (*vide infra*) suggested the 58150 series exhibits a covalent mechanism of action with the biological target that transduces the series' biological activity; we imagined our probe design would benefit from this proposed mechanism of action. The proposed covalent reactivity is implied from both the nM-pM potency and clear activity cliffs observed upon minor alterations to various regions of the chemical scaffolding. In our preliminary SAR investigation, the importance of the phenyl-substituted oxadiazole ring and the carboxylic acid system was highlighted with commercially available compounds (Figure 20). Pyridyl (**A1** and **A2**) and furanyl (**A3**) substituted oxadiazole analogs completely lost all activity compared to hit **58146**. Attempts to replace the oxadiazole core with other heterocycles (**A4-A6**) were similarly unsuccessful. Replacement of the carboxylic acid with an acetal isostere (**A7**) led to a similar loss in activity. Based on these strongly negative results, we concluded that the 5-aryl-1,3,4-oxadiazole ring was required for potent activity, and replacing the carboxylic acid functionality may be difficult.

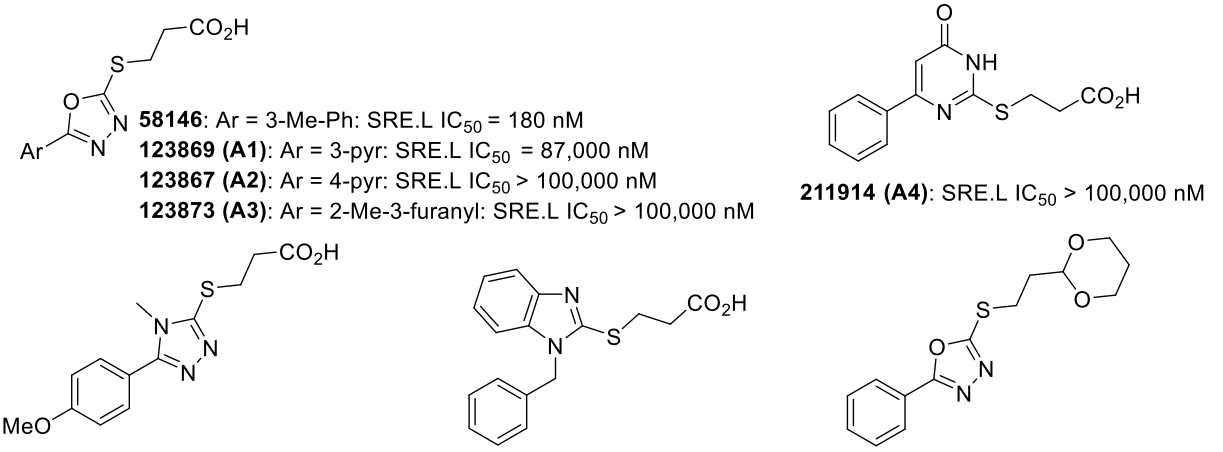

Figure 20: Preliminary SAR of 58150-series heterocycle and carboxylic acid.
SRE.L activity in PC-3 cells (mean of n = 3, SEM < 10%).

Next, using a general Topliss approach, we systematically investigated prototype electron donating (methoxy), withdrawing (chloro) and alkyl (methyl) groups at each of the three aryl positions (Table 2, **A8**-**A16**). Remarkably, this revealed an over 250-fold span of potency over just these first 9 analogs; SRE.L IC_{50}s ranged from 6300 nM (**A15**) to 25 nM (**A14**). Within this small initial group were several clear activity cliffs, including 2-Cl **A14** (25 nM) vs 3-Cl **A12** (1500 nM) and 4-Me **A9** (34 nM) vs 3-Me **58146** (180 nM) vs 2-Me **A15** (6300 nM). We were then interested to see if the individual optimum substitutions would be synergistic. From the data in Table 2, among the four substitutions investigated at each position, Cl is optimum at R^1, Me at R^2, and Me and OMe at R^3. Various dual combinations of these were attempted (**58150-A18**), giving compounds with single digit nM SRE.L IC_{50}s. Also, despite these significant improvements in SRE.L activity, all analogs tested were unable to affect cell proliferation/viability up to 100 µM as measured by WST-1, highlighting the series lack of cytotoxicity at high concentrations.

The phenotypic SRE.L assay was originally designed as a HTS for cancer therapeutics using PC-3 cells.[163] However, to improve the throughput of the transfection, the cell line was switched to HEK-293T cells. To ensure equivalency in SRE.L potency from one cell line to the

other, various analogs were tested in both assay conditions (e.g. **58150**, **232120** (Table 3), **232964** (Chapter 3), etc.). Notable differences in activity were not observed between the two transfected cell lines, so the assay was eventually switched to HEK-293T cells.

The activity was further improved with trisubstituted analogs (**A19**-**A21**) that combined the best R^1, R^3-disubstitution analogs (**58150** & **A17**) with the best R^2/R^4 substituent (Me). This resulted in the first sub-nanomolar analogs in the series, with SRE.L potency as high as IC_{50} = 20 pM (**A19**). These extremely tight and potent SAR trends suggest that these inhibitors likely interact with a very well-defined binding site on the unknown molecular target.

Table 2: Systematic SAR investigation of aryl ring:

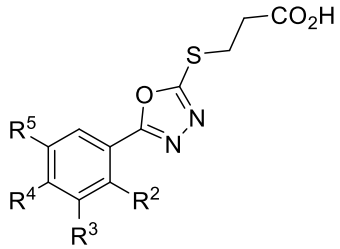

CCG-	Entry	R^2	R^3	R^4	R^5	SRE.L IC_{50} (nM)[a, b]
123859	**A8**	H	H	H	H	3,500
123852	**A9**	H	H	Cl	H	340
123862	**A10**	H	H	Me	H	34
123855	**A11**	H	H	OMe	H	160
123851	**A12**	H	Cl	H	H	1,500
58146	**-**	H	Me	H	H	180
211911	**A13**	H	OMe	H	H	3,600
232700	**A14**	Cl	H	H	H	25
232841	**A15**	Me	H	H	H	6,300
232740	**A16**	OMe	H	H	H	3,100
58150	**-**	Cl	H	Cl	H	2 (4[c])
232001	**A17**	Cl	H	Me	H	1.5
215220	**A18**	Cl	H	OMe	H	2.6
258043	**A19**	Cl	Me	Me	H	0.02[c]
258041	**A20**	Cl	H	Me	Me	0.23[c]
258021	**A21**	Cl	H	Cl	Me	0.32[c]

[a]Inhibition of Gα12-stimulated SRE.L activity (mean of n = 3, SEM < 10%) in PC3 cells unless otherwise noted. [b]Cell viability and proliferation assay with WST-1 < 5% inhibition up to 100 μM inhibitor (mean of n = 3, SEM < 10%). [c]SRE.L assay performed in HEK293T cells (mean of n = 3, SEM < 10%).

Replacing the carboxylic acid functionality with neutral methyl amide (**A23**) was unsuccessful (Table 3); however, ethyl ester **A22** maintained activity, likely due to hydrolysis by non-specific esterases in the biological conditions of the assay. Unfortunately, the t-butyl ester homolog was not tested to further confirm this hypothesis. To determine the optimal carbon chain length between the oxadiazole and carboxylic acid, analogs bearing linkers from one to seven methylenes were synthesized (**A25**-**A30**). Considering drug-like properties, we deemed the optimal carbon chain length to be three (**232120**). Interestingly, activity was completely lost when there was only one carbon separating the oxadiazole and carboxylic acid (**A25**). Amazingly, while hydroxamic acid replacement was unsuccessful (**A26**), isosteric replacement of the carboxylic acid with a tetrazole (**A24**) led to an unexpected improvement in activity; this recent data warrants further follow up (discussed in Chapter 5). These steep SAR trends are evidence for the importance of the carboxylic acid group and its position relative to the oxadiazole ring.

Table 3: Carboxylic acid sidechain SAR:

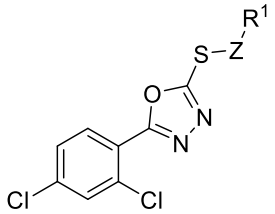

CCG	Entry	Z	R^1	SRE.L IC_{50} (nM)[a, b]	MLM $T_{1/2}$ (min)[d]
58150	-	$(CH_2)_2$	CO_2H	4 (2[c])	>60
215161	**A22**	$(CH_2)_2$	CO_2Et	2.6	-
232661	**A23**	$(CH_2)_2$	$CONHCH_3$	>100,000	-
257447	**A24**	$(CH_2)_2$	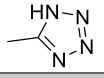	0.009[c]	-
215027	**A25**	CH_2	CO_2H	>100,000	-
232120	-	$(CH_2)_3$	CO_2H	1.8 (0.84[c])	>60
257445	**A26**	$(CH_2)_3$	CONHOH	465[c]	-
232503	**A27**	$(CH_2)_4$	CO_2H	43	-
232923	**A28**	$(CH_2)_5$	CO_2H	0.63	-
232962	**A29**	$(CH_2)_6$	CO_2H	72	-
232963	**A30**	$(CH_2)_7$	CO_2H	24	-

[a]Inhibition of Gα12-stimulated SRE.L (mean of n = 3, SEM < 10%) in PC3 cells. [b]Cell viability and proliferation assay with WST-1 < 5% inhibition up to 100 μM inhibitor (mean of n = 3, SEM < 10%) up to 100 μM inhibitor. [c]SRE.L assay performed in HEK293T cells (mean of n = 3, SEM < 10%). [d]Half-life in mouse liver microsomes.

Based on (1) our unsuccessful attempts to replace the oxadiazole core with similar heterocycles (Figure 20) (2) the steep SAR of the series with regard to both aryl substitution and alkanoic acid chain length (Tables 2 & 3) and (3) the extraordinary activity achieved (sub-nanomolar) with such low molecular weight compounds (further discussed in depth in Chapter 3), we hypothesized that the oxadiazole thioether core might be engaging with a binding site nucleophile covalently as illustrated in Figure 21. Therefore, analogs structurally similar to **58150** but predicted to be much less capable of reacting with nucleophiles were synthesized and tested (Figure 21). In support of the covalent hypothesis, an almost complete loss in activity occurred upon replacement of the S with O or CH_2 (**A31**, **A32**), migration of the S away from the heterocyclic core (**A33**), or alteration (**A34**) of the core heterocycle.

Interestingly, activity was maintained when the system was made more susceptible to nucleophilic attack with sulfone **A36**; however, this trend was not observed with all analogs that attempted to increase the oxadiazole core electrophilicity (**A35**), possibly because of an inability to engage with the biological target (e.g. rapid elimination of reactive compound by cellular milieu or incapable of forming the proper intermediate for target engagement). Additionally, the result for sulfone **A36** suggests our series may get activated within the cell, either by the biological target itself or a separate protein altogether, to impart the potent inhibition of Rho/MRTF/SRF signaling.

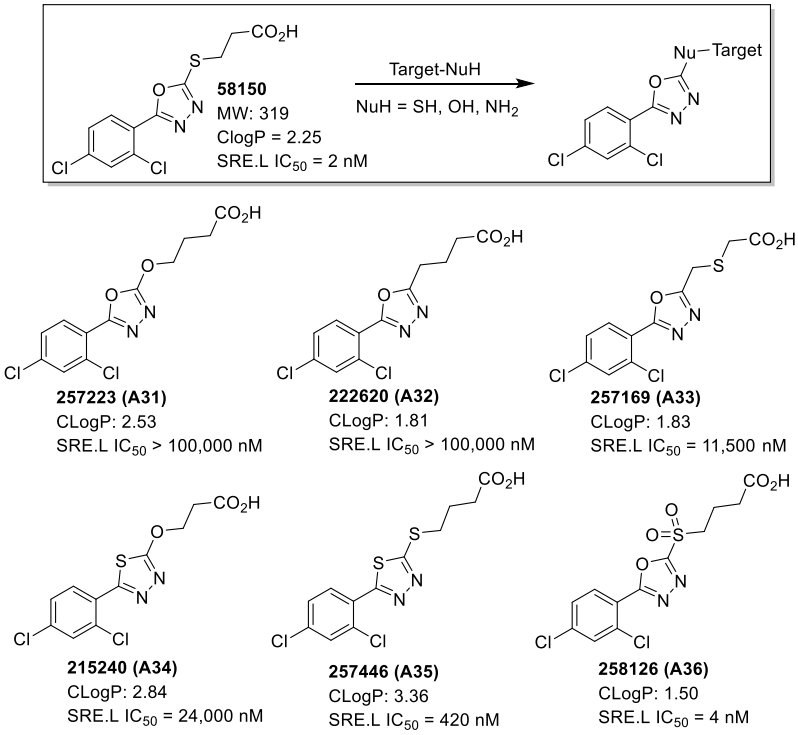

Figure 21: Hypothetical electrophilic reactivity of 58150-series

Hypothetical reaction of **58150** with a target nucleophile and SRE.L activity of analogs designed to modulate susceptibility of the oxadiazole ring system to nucleophilic attack.

If this covalent mechanism is ultimately proven, this would be the first example of an oxadiazole-thioether heterocyclic system being susceptible to covalent modification by a biological target. There are, however, reports in the literature that suggest the oxadiazole thioether core is chemically reactive under various conditions.[191-193] It is possible that our analogs are getting oxidized prior, or subsequent, to binding to the target, forming an activated metabolite, like **A36**. Indeed, the 5-thioalkyl-1,3,4-oxadiazole core is susceptible to oxidation and nucleophilic displacement in our hands (Scheme 1) in a manner that is comparable to the proposed mechanism in Figure 21, lending additional support to our covalent hypothesis.[192,194] Future directions to validate this hypothesis are discussed in Chapter 5.

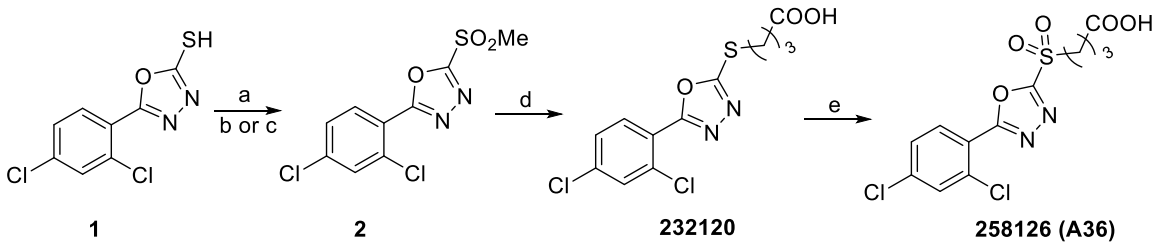

Scheme 1: Reaction exemplifying chemical reactivity of oxadiazole core:

Reagents and conditions: (a) MeI, Et_3N, THF, 25 °C, 2 hr (b) $(NH_4)_6Mo_7O_{24}$, H_2O_2, EtOH, 25 °C, 2 hr (c) mCPBA, DCM, 25 °C, 2 hr (d) 4-mercaptobutanoic acid, K_2CO_3, acetone, 25 °C, 1 hr, (e) mCPBA, DCM, 25 °C, 2 hr.

Generally, the chances for success of a target identification campaign are assumed to increase the higher the affinity of the small-molecule to the biological target, which is understandable because high-affinity complexes can be preserved under extensive washing conditions, reducing the amount of non-specific binding proteins in quantitative proteomic analysis.[176,183] However, this implied affinity can be misleading since the assumption is generally based on cellular activities, and cellular activity does not necessarily translate to high-affinity complexes between the ligand and the biological target that affords the activity.[183]

Probes with covalent handles can enhance confidence that the probe will strongly engage with the biological target of interest in a pulldown experiment.[176,177,188] For instance, the photolyzable diazirine functionality is the golden standard in covalent handles (Figure 22).[177,195] This functional group is exceptional in that it is (1) stable to ambient light (in both acidic and basic conditions) (2) compact (isosteric in size to methyl) (3) easily accessed synthetically through various alkyl ketones and (4) the alkyl carbene intermediate formed upon photo-activation (355 nm) is highly selective for N—H, S—H, and O—H, and, when insertion into the desired biological target cannot occur, this intermediate is rapidly quenched by solvent or internal rearrangement to a stable side-product.[177]

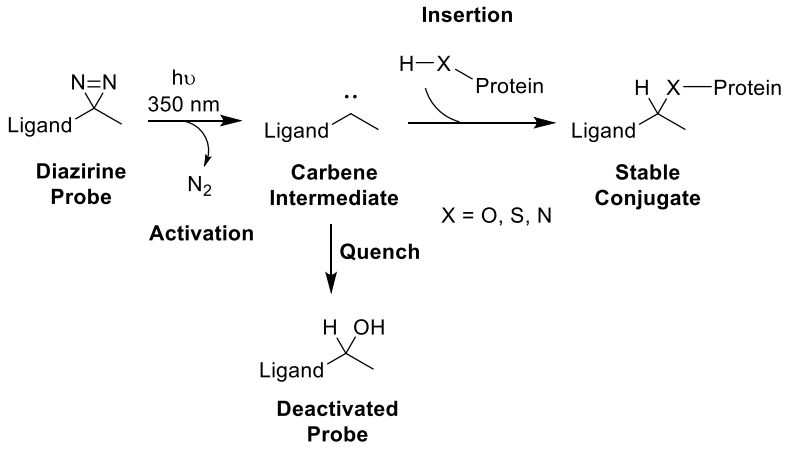

Figure 22: Pull-down strategy using diazirine functional group:

Reactivity of the diazirine photoprobe enhances probe pulldown success through carbene intermediate formation and rapid reaction with proximal proteins or solvent.

Since we had strong evidence that our series had an imbedded covalent handle that was likely important for activity, we decided to utilize this in our immobilized resin affinity probe design (Figure 23). Also, based on the tight SAR, we assumed we would be able to develop a structurally very similar inactive control probe.

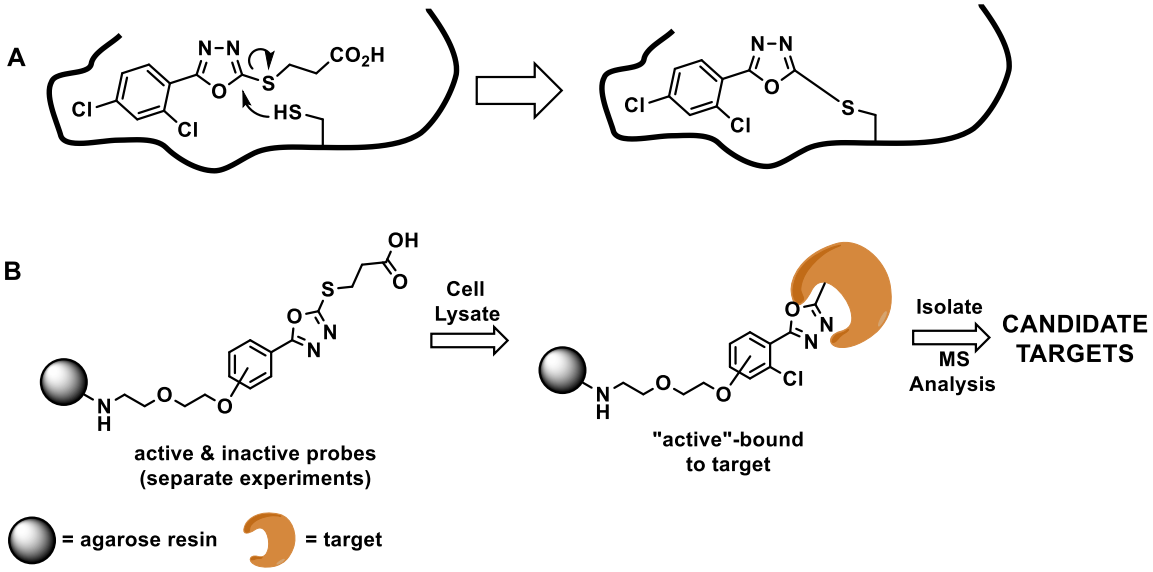

Figure 23: 58150-series probe design:

A) The proposed covalent mechanism of CCG-58150 to its biological target. B) The “active” and “inactive” resin-bound affinity probes synthesized can be incubated with cell lysates, and then isolated, trypsin digested, and proteomic analysis can be performed.

First, a “methoxy scan” to probe suitable positions to fasten the PEG-amine linker for attachment to the immobilization resin was performed (Figure 24); the SAR generated from the methoxy scan analogs further exemplified the tight SAR of the series. Appendages replacing the carboxylic acid functional group (**A37**) or those directly attached to the aliphatic linker (**A38**-**A40**) eliminated SRE L activity. Critical activity cliffs to design the appropriate active and inactive control probes appeared with alterations around the aromatic ring. In general, substitution at the *para*-position was preferred (**A43** vs **A41** & **A42**) and, consistent with our previous SAR trends, di-substitution at the *para* and *ortho* positions provided the best activity profile. For example, **A44** was up to ten-fold more active than closely related homologs **A45** & **A46** and ten-thousand-fold more active than **A47**.

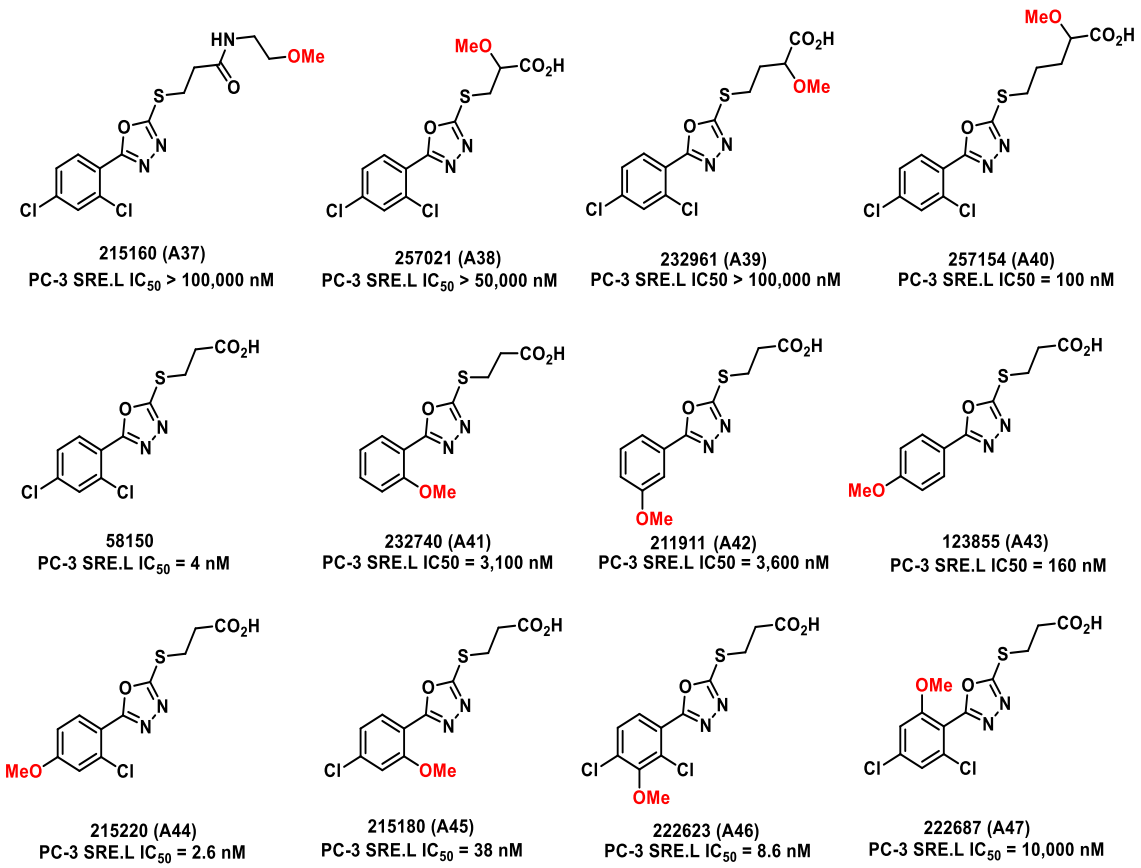

Figure 24: Methoxy-scan for 58150-series:

Methoxy-scan of the 58150-scaffold to identify “active” and “inactive” positions for agarose resin tethering.

Clearly, **A44**-**A46** exhibited the most attractive substitution pattern to further assess a pendant more similar in size to the PEG-amine linker. Therefore, "PEG-mimics" **A48**-**A50** were synthesized to validate tolerance for the steric bulk required for immobilized probes (Figure 25). **A48** retained most of **215220**'s activity, and closely related analog **A50** was ~1000-fold fold less active than **A48**. These results provided rationale to attach the PEG-amine linker for immobilized resin to the *para*-position for the active probe (similar to **A48**) and the *ortho*-position for the inactive control probe (similar to **A50**).

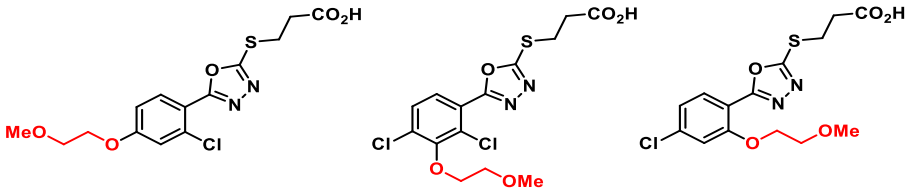

Figure 25: PEG mimic scan for 58150 series:
CCG-58150-scaffold methoxy-ethoxy-scan of potent methoxy-scan positions

Synthesis of Key 5-aryl-1,3,4-oxadiazol-2-ylthioalkanoic acids for Probe Design:

The general synthesis of 5-aryl-1,3,4-oxadiazol-2-ylthioalkanoic acids and related homologs is summarized in Scheme 2. Aryl bromide **3** was subjected to standard lithiation/carboxylation conditions followed by an acidic workup to produce the subsequent aryl benzoic acid. Various aromatic benzoic acids (**4**) were converted to their respective methyl esters under standard Fischer esterification conditions, and then converted to the corresponding hydrazides (**5**) by refluxing in MeOH with excess hydrazine hydrate. Refluxing **5** and carbon disulfide in EtOH under basic conditions, followed by acidic workup, generated 2-mercapto-5-aryl-1,3,4-oxadiazoles (**1, 6**). S-alkylation with either methyl, ethyl, or t-butyl Ω-bromoalkanoates and 5-(2-chloroethyl)-1H-tetrazole provided the thioether esters (**7**, **8**, and **215161**) and tetrazole **257447**. Hydrolysis of the esters was accomplished with either trifluoroacetic acid (t-butyl esters) or sodium hydroxide (methyl esters) to give final carboxylic acids **9**. The tert-butyl esters became the preferred precursor when n = 2 because basic hydrolysis of the methyl ester

intermediates resulted in competing retro-Michael elimination to regenerate the 1, 3, 4-oxadiazole-2-thiols (**1, 6**). Amide **232661** was prepared by conversion of **9** to the corresponding acid chloride with oxalyl chloride in DMF/DCM at room temperature, followed by addition of methylamine. Carboxylic acid **9** was also easily converted to hydroxylamine **257445** by reacting the mix anhydride intermediate generated from ethyl chloroformate with freshly prepared hydroxylamine hydrochloride.[196]

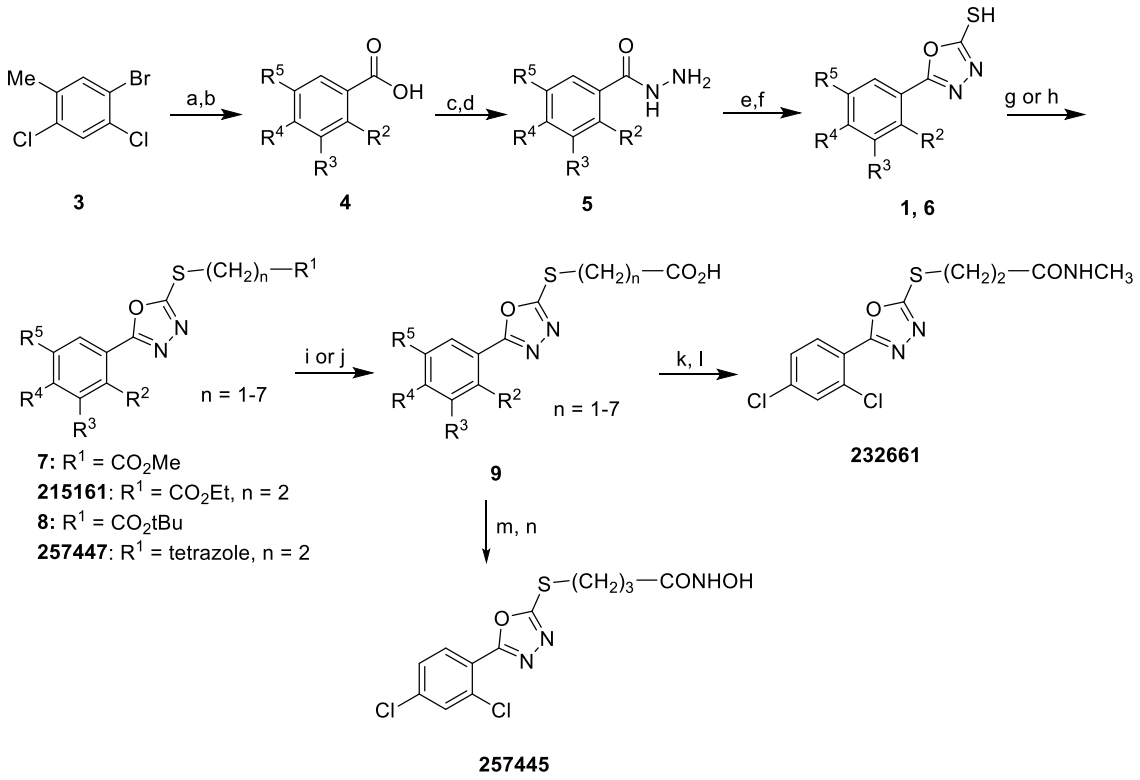

Scheme 2: General scheme for synthesis of 5-aryl-1,3,4-oxadiazol-2-ylthioalkanoic acids and related analogs

Reagents and conditions: (a) n-BuLi, THF, -78 °C 5 min, then $CO_{2\,(s)}$ (b) 1N HCl workup (c) H_2SO_4/MeOH, 85 °C, 6 hr (d) H_4N_2•H_2O, 85 °C, 14 hr (e) KOH/H_2O/EtOH, CS_2, 95 °C, 16 hr (f) 1N HCl workup (g) acetone, K_2CO_3, Br-$(CH_2)_n$-CO_2R', 25 °C, 5-24 hr (h) Acetone, K_2CO_3, 5-(2-chloroethyl)-1H-tetrazole, 60 °C, 48 hr (i) DCM, TFA, 25 °C, 3 hr (j) 1M NaOH, THF, 25 °C, 16 hr (k) oxalyl chloride, DMF, DCM, 25 °C, 2 hr (l) $MeNH_2$ in EtOH, 25 °C, 16 hr (m) NMM, $ClCO_2Et$, 0 °C, 10 min (n) MeOH, NH_2OH•HCl, 25 °C, 45 min.

The syntheses of 4-((5-(2,4-dichlorophenyl)-1,3,4-oxadiazol-2-yl)oxy)butanoic acid (**257223**), 2-(((5-(2,4-dichlorophenyl)-1,3,4-oxadiazol-2-yl)methyl)thio)acetic acid (**257169**), and

3-((5-(2,4-dichlorophenyl-1,3,4-thiadiazol-2-yl)oxy)propanoic acid (**215240**) are depicted in Scheme 3. **5a** was used as a common starting material for key intermediates **10**[194], **11**[197], **1**, and **12**[198]. As reported by Yan et al.[194], intermediate **10** was produced through the cyclization/rearrangement of **5a** with propylene oxide. O-alkylation with t-butyl 4-bromobutyrate followed by acidic hydrolysis with trifluoroacetic acid provided carboxylic acid **257223**. Alternatively, per Sun et al.[197], subjecting **5a** to bromoacetic acid and $POCl_3$ afforded intermediate **11**. Basic S-alkylation with potassium carbonate and 2-mercaptoacetic acid produced carboxylic acid **257169**.

As described previously (Scheme 2), 2, 4-dichloro-1,3,4-oxadiazole-2-thiol (**1**) was synthesized with refluxing **5a** and carbon disulfide under basic conditions, followed by acidic workup. **1** was converted to the thiadiazole ether **215240** by subjection to acrylic acid and trimethylamine in refluxing THF. These reaction conditions were originally attempted to produce carboxylic acids (**9**) through a Michael reaction (Scheme 4), however the conditions unexpectedly produced **215240** (Scheme 5). This transformation further exemplifies the reactivity of the 1, 3, 4-oxadiazole core to proximal nucleophiles, and provides support for the covalent hypothesis proposed for these inhibitors. Subjecting **1** to the general basic S_N2 conditions with methyl 4-bromobutanoate followed by basic hydrolysis and mCPBA oxidation afforded **258126**. Thiadiazole intermediate **12** was synthesized with a modified cyclization procedure that utilized fuming sulfuric acid.[198] *O*-alkylation with methyl 4-bromobutyrate followed by basic hydrolysis provided carboxylic acid **257446**.

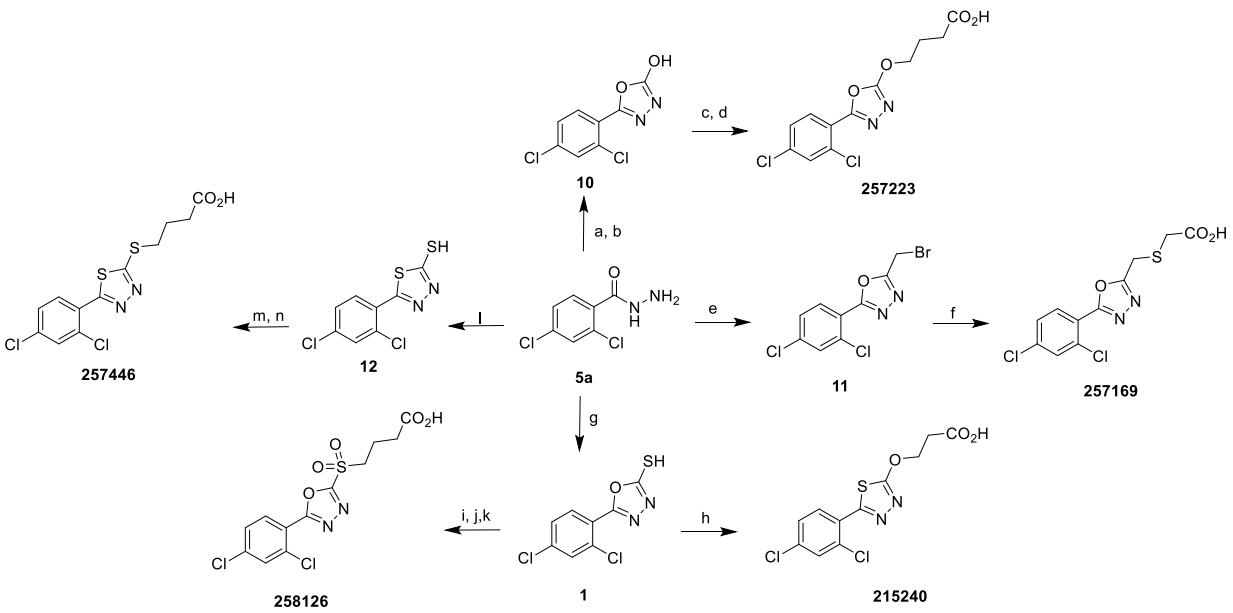

Scheme 3: Synthetic routes for alternate core and linker analogs:

Reagents and conditions: (a) K_3PO_4, CS_2, H_2O, 106 °C, 2 hr. (b) propylene oxide, 25 °C, 16 hr (c) DMF, K_2CO_3, Br-$(CH_2)_3$-CO_2OtBu, 90 °C, 1 hr (d) DCM, TFA, 25 °C, 1 hr (e) $POCl_3$, bromoacetic acid, 106 °C, 16 hr (f) 2-mercaptoacetic acid, Acetone, K_2CO_3, 25 °C, 2 hr (g) KOH/H_2O/EtOH, CS_2, 95 °C, 16 hr (h) acrylic acid, Et_3N, THF, 70 °C, 16 hr (i) Acetone, K_2CO_3, Br-$(CH_2)_3$-CO_2Me, 25 °C, 5 hr (j) 1M NaOH/THF, 25 °C, 1 hr (k) mCPBA, DCM, 25 °C, 4 hr (l) KOH/H_2O/EtOH, CS_2, 25 °C, 3 hr, then fuming H_2SO_4, 25 °C, 2 hr (m) K_2CO_3, Br-$(CH_2)_3$-CO_2Me, DMF, 90 °C, 1 hr (n) 1M NaOH/THF, 25 °C, 1 hr.

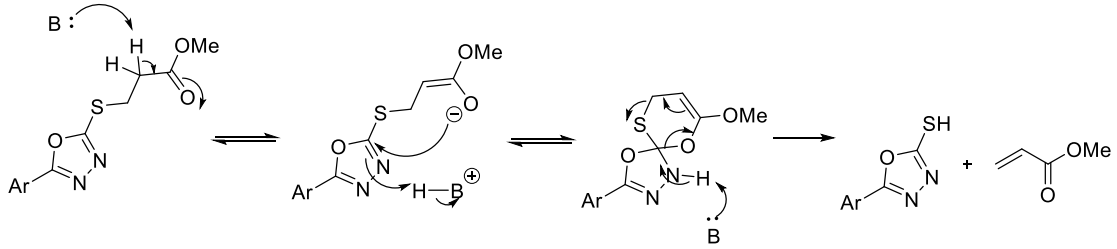

Scheme 4: Proposed retro-Michael mechanism under basic saponification conditions

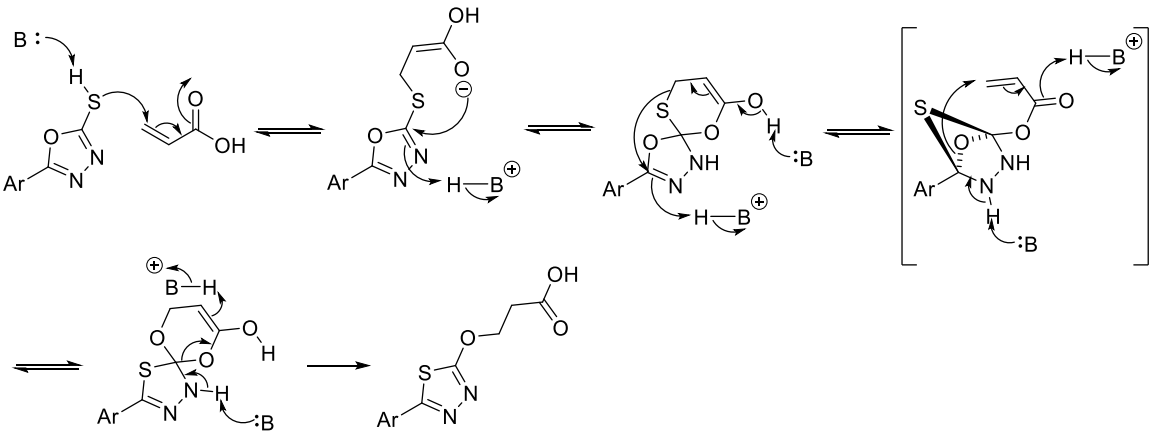

Scheme 5: Proposed mechanism for formation of 215240

Propanoic acid **257021** was challenging to synthesize (Scheme 6); however, since all pathways attempting to install the alkyl chain with nucleophilic displacement with thiol **1** were unsuccessful, the synthesis was eventually accomplished utilizing an Ümplong route. Unsuccessful routes included: (1) nucleophilic displacement of various epoxides, all of which attempts formed rearrangement product **10** (2) nucleophilic displacement of alkyl bromide **14** followed by reduction of the resulting ketone **15** with various reducing reagents, including $NaBH_4$, $NaBH(OAc)_3$, and $NaBH_3CN$ (3) Michael conditions using **17**.

Alternatively, affixing the alkyl chain with the nucleophilic thiol **21** and converting the 1,3,4-oxadiazole core into the electrophile **2** resulted in generation of **257021**.[199] Michael reaction between benzyl mercaptan and Michael acceptor **19** using a weak base produced methyl ester intermediate **20**. Hydrolysis of methyl ester **20** followed by Birch Reduction and acidic workup afforded thiol **21**. The synthesis of **257021** concluded nicely with displacement of methyl sulfone **2** with thiol **21** in mildly basic conditions.

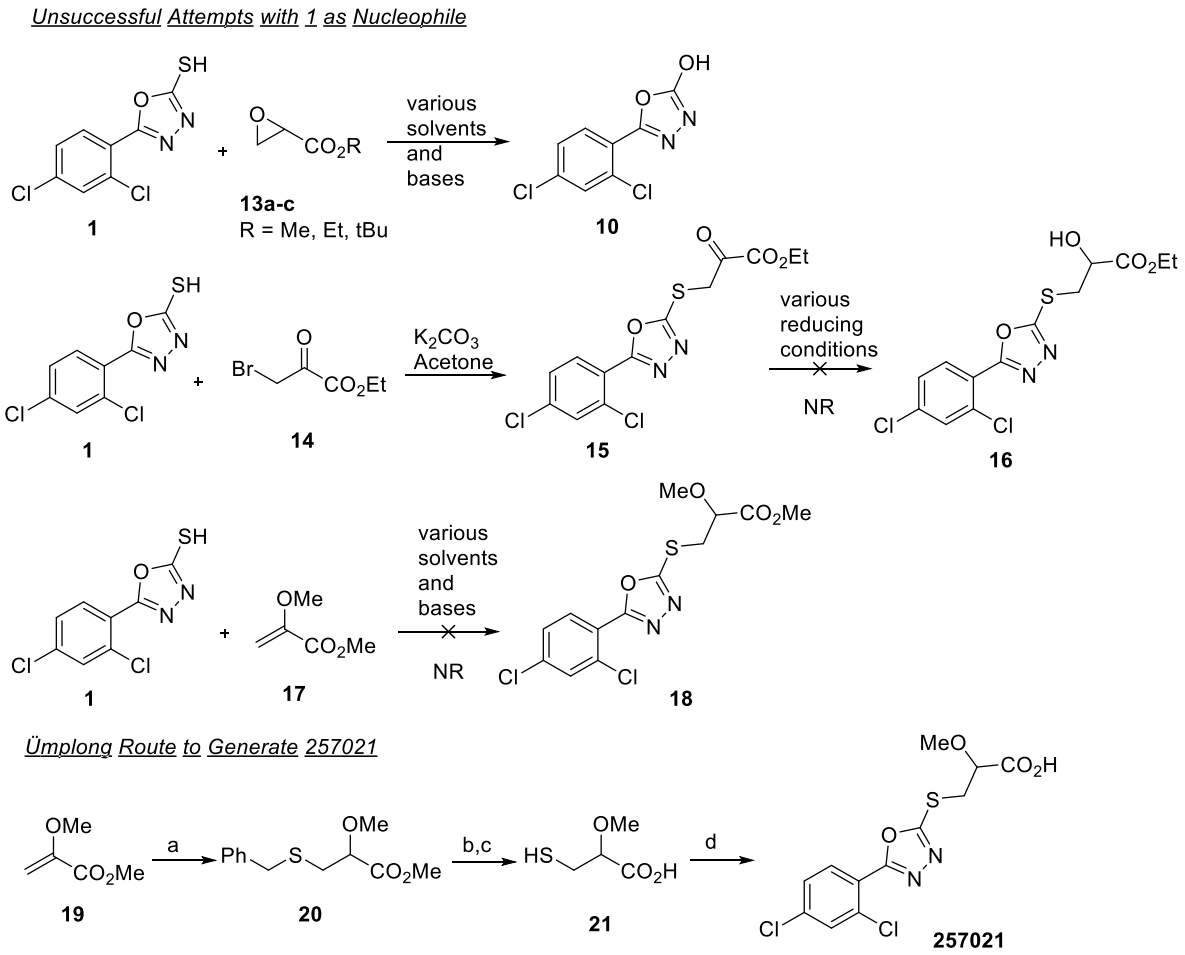

Scheme 6: Attempts to access 257021:

Reagents and conditions: (a) 1M TBAF in THF, BnSH, 25 °C, 2 hr (b) H_2O, MeOH, K_2CO_3, 25 °C, 16 hr (c) $Na_{(o)}$, $NH_{3\,(liq)}$, -30 °C, 25 min then HCl workup (d) Acetone, K_2CO_3, **2**, 25 °C, 2 hr.

The synthesis for **232961** proceeded smoother (Scheme 7). Starting from lactone **22**, electrophilic intermediate **23** was accessed through silver (II) oxide-mediate methylation followed by a one-pot ring opening, iodination, and esterification with TMSI and MeOH. Reacting thiol **1** with electrophile **23** easily produced butanoic acid **232961** with our typical S_N2 conditions followed by basic hydrolysis.

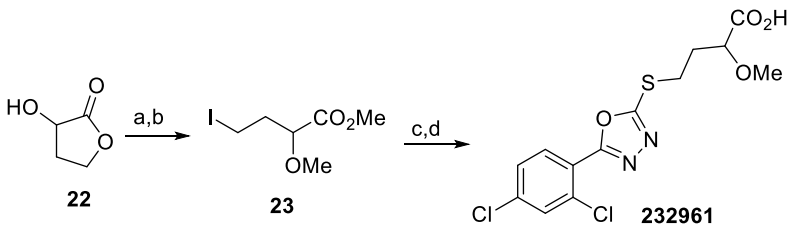

Scheme 7: Synthesis of 232961

Reagents and conditions: (a) DCM, MeI, Ag_2O, 70 °C, 1 hr (b) DCM, MeOH, TMSI, -10 °C, 1 hr then 25 °C, 3 hr (c) Acetone, K_2CO_3, **1**, 25 °C, 4 hr (d) 1M NaOH/THF, 25 °C 1 hr.

257222 (Scheme 8) was synthesized utilizing similar chemistry as displayed in Scheme 7. One-pot ring opening, iodination, and acetylation of tetrahydrofuran **24** was accomplished with acetyl chloride and sodium iodide to produce electrophile **25**.[200] This intermediate was subjected to our standard S_N2 conditions with thiol **1**, generating methyl ester **26**. Pentatonic acid **257222** was produced by deacetylation with weak base, silver (II) oxide-mediated methylation with methyl iodide, followed by basic hydrolysis.

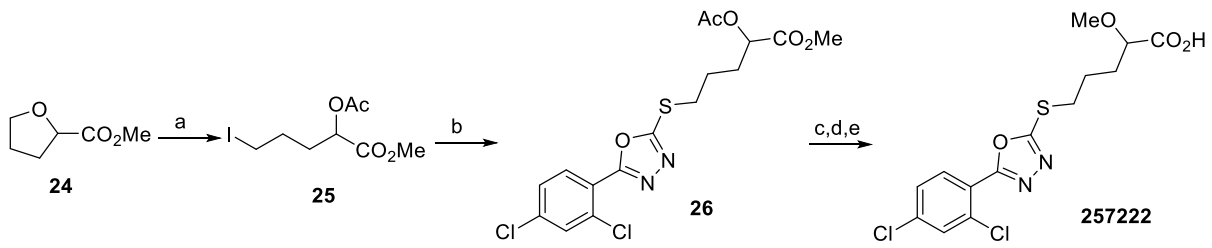

Scheme 8: Synthesis of 257222

Reagents and conditions: (a) MeCN, CH_3COCl, NaI, 25 °C 24 hr (b) Acetone, K_2CO_3, **1**, 25 °C, 1 hr (c) MeOH, K_2CO_3, 25 °C, 30 min (d) DCM, Ag_2O, MeI, 70 °C, 1 hr (e) 1M NaOH/THF, 25 °C 1 hr.

The ethoxymethoxy functional groups of probe mimic analogs **257156**-**232964** (Figure 25) were installed at the beginning of their syntheses (Scheme 9). **27** was converted to benzoic acid **30a** by TES protection of the phenol, lithiation/carboxylation followed by acidic workup[201], and then alkylation with 1-bromo-2-methoxyethane and strong base. These alkylation conditions were also used to produce **30b**. However, likely due to steric or electronic contributions of the 2-position, alternative basic alkylation conditions in DMF were required for the generation of **30c**.

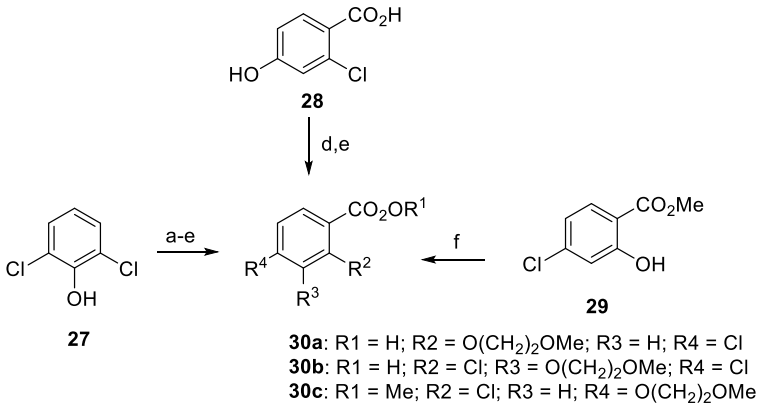

Scheme 9: Synthesis of 30a-c

Reagents and conditions: (a) TESCl, Et_3N, THF, 50 °C, 24 hr (b) sBuLi, cHex, THF, -78 °C, 45 min (c) $CO_{2\ (s)}$, then HCl workup (d) KOH, EtOH, K_2CO_3, $Br(CH_2)_2OMe$, 95 °C, 24 hr (e) HCl workup (f) DMF, K_2CO_3, $Br(CH_2)_2OMe$, 25 °C, 5 hr

Synthesis of Active and Inactive Immobilized Agarose Resin Probes:

Both “active” (**A52**) and “inactive” (**A53**) PEG-amine linker analogs for immobilized probe development were synthesized (Scheme 10). Esterification followed by *O*-akylation of phenols **4a** & **4b** using either propargyl benzenesulfonate or benzyl bromide, respectively, provided esters **4a’** & **4b’** that were converted to the 5-aryl-2-mercapto-1,3,4-oxadiazoles **6a** & **6b** as previously described.[202-205] *S*-alkylation with *t*-butyl-3-bromobutanoate followed by reductive and Lewis acid-mediated deprotection of the resulting propargyl esters generated **8a** & **A51**. The TFA salt form of the PEG-amine linker analogs **A52** & **A53** were obtained by *O*-alkylation followed by acidic hydrolysis. The final probes were produced by the Neubig lab with NHS-agarose beads using solid phase amine coupling chemistry followed by blocking of residual reactive groups with ethanolamine (Experimental section).

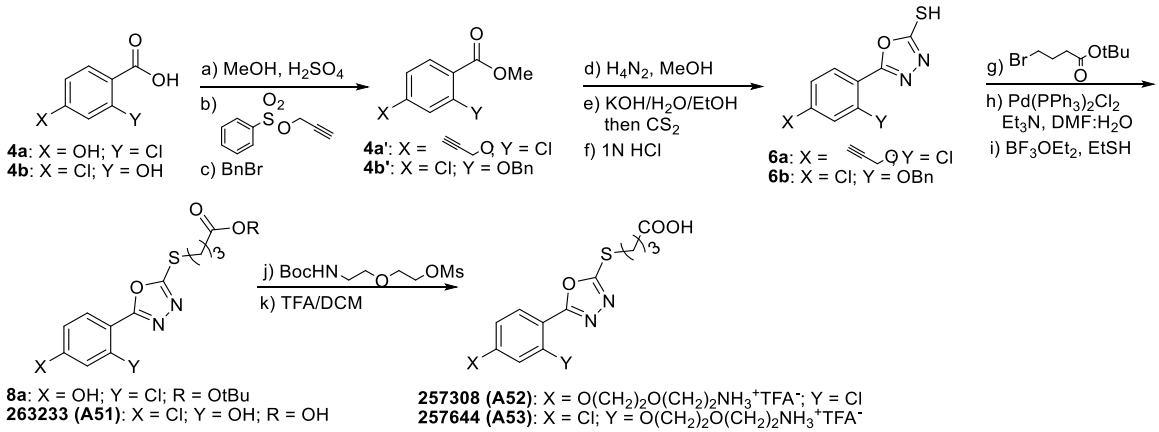

Scheme 10: Synthetic routes to produce 58150-series active and inactive probes

Biological Target Pull-down and Proteomic Analysis:

Through the experimental design shown in Figure 26, a list of protein candidates was systematically generated using our active and inactive immobilized affinity resin probes. HEK293T cell lysate were treated with “active” (**A52**) and “inactive” (**A53**) immobilized probes at 10 µM. The immobilized probes were washed with PBS to remove non-specifically bound membranes and proteins. The Martin lab generated protein fragments for relevant biological targets by trypsin digestion of the beads directly, removed the remaining beads by centrifugation, and then the resulting supernatants were subjected to mass spectroscopic analysis. This analysis consisted of evaluating various fragment batches using spectral counting to identify proteins enriched in the active bead samples compared to the inactive bead samples. Protein candidates that had an active/inactive enrichment ratio ≥ 2 and relatively high unique peptide counts were considered as potential biological targets (Table 4). Efforts to validate the top candidate are discussed in the next subsection.

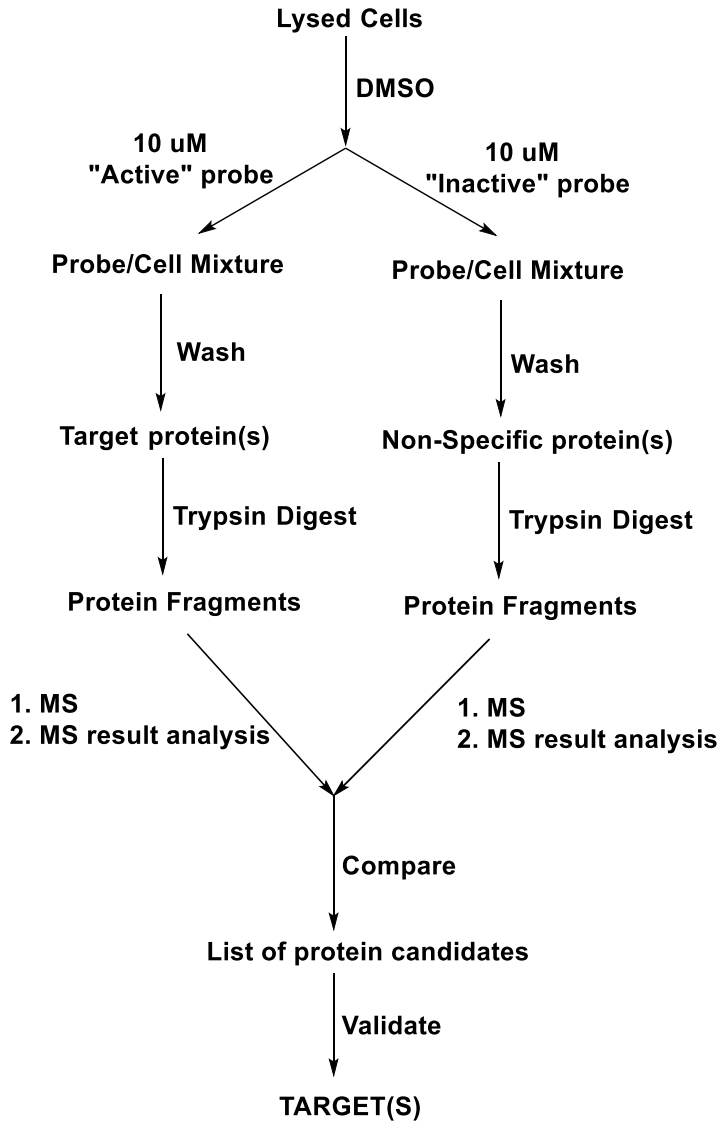

Figure 26: Target identification methodology performed for the 58150 series "active" and "inactive" agarose resin affinity probes.

In separate experiments, the "active" (**A52**) and "inactive" (**A53**) probes were subjected to cell lysate in DMSO and applied to a spin column. These mixtures were incubated at room temperature for 1 hour and then the samples were washed with PBS to remove membranes and non-specific proteins. The sample beads from each experiment were subjected to trypsin digestion, and the resulting protein fragments were analyzed on a Waters mass spectrometer. The average abundance of peptide fragments for each protein candidate were compared between "active" and "inactive" probe experiments, producing the enrichment ratio, to help consolidate interesting protein candidates. An extensive literature search for relevant biology on candidates with an enrichment ratio greater than 2 was performed. Validation efforts for the proteins of interest were attempted to identify potential biological targets.

Table 4: Top 20 protein candidates after proteomic analysis

Protein	Peptide Count	Unique Peptide Count	Enrichment Ratio
Deoxycytidylate deaminase	2	1	30.6
Testican-2	2	1	26.1
dCTPase	37	32	12.9
Genome polyprotein	4	1	8.5
Phosphoglycerate mutase 1	2	1	7.5
Insulin-like growth factor 2 mRNA-binding protein 3	4	1	6.6
RNA-binding protein EWS	4	1	5.9
UBX domain-containing protein 1	6	1	5.4
Heterogeneous nuclear ribonucleoproteins A2/B1	3	1	5.3
Transmembrane protein 263	4	4	5.1
Desmoglein-1	6	3	4.3
Selenoprotein H	4	3	4.2
Junction plakoglobin	3	1	4.0
Histone H1.4	5	2	3.9
40S ribosomal protein S4, Y isoform 1	12	1	3.9
Oxygen-dependent coproporphyrinogen-III oxidase, mitochondrial	20	12	3.8
Tyrosine-protein phosphatase non-receptor type 11	22	14	3.8
Cleavage and polyadenylation specificity factor subunit 5	1	1	3.4
Cyclin-dependent kinase 20	5	1	3.2
Fibroblast growth factor receptor 2	9	1	3.1

Peptide counts refer to the number of peptides identified for a given protein, while unique peptide count refers to the number of peptides identified that are completely unique for a given protein. The enrichment ratio is the raw mean ratio between peptides identified in the active vs. inactive samples.

Biological Target Validation Efforts:

From these results, dCTP pyrophosphatase 1 (dCTPase, DCTPP1, or XTP3TPA) (n = 4) was identified as the top candidate protein target for the 58150-series. This protein had an enrichment ratio of 12.9, and 32 of the 37 peptides identified for dCTPase from the proteomics studies were unique for the macromolecule. dCTPase is an all-α-nucleoside triphosphate (NTP) pyrophosphatase that catalyzes the Mg^{2+}-mediated hydrolysis of non-canonical and canonical deoxynucleoside triphosphates (dNTPs) to the respective deoxynucleoside monophosphates (dNMPs).[206] Interestingly, dCTPase has a higher affinity towards 5-modified non-canonical dNTPs over canonical dNTPs and rNTPs, ultimately leading to decreased intracellular levels of non-canonical dNTPs.[206,207] In short, dCTPase is responsible for regulating the global dNTP pool, and it also plays an epigenetic "housekeeping" role. dCTPase has been found to be strongly associated with cancer. In particular, dCTPase accumulates in the nucleus of multiple carcinomas[208] and plays a role in gastric and breast cancer stemness.[207,209]

Dr. Erika Lisabeth in the Neubig lab took several steps attempting to validate dCTPase as a target for this series. First, she showed that knocking down dCTPase led to a decrease in the production of LPA-stimulated CTGF mRNA in primary dermal fibroblast cells (Figure 27A). Interestingly, the knockdown did not affect TGFβ-stimulated CTGF mRNA production. In a similar experiment, **58150** and **232964**—a potent inhibitor discussed in more detail in Chapter 3—inhibited LPA-stimulated CTGF mRNA expression but did not affect TGFβ-stimulated CTGF expression (Figure 27B & 27C), a result that correlates to the dCTPase knock-down study (Figure 27A). Taken together, these data (1) suggested dCTPase might play a role within our SRE L. assay and (2) demonstrated that knocking down dCTPase has selectivity for inhibiting only LPA-induced and not TGFβ-stimulated CTGF expression like our series.

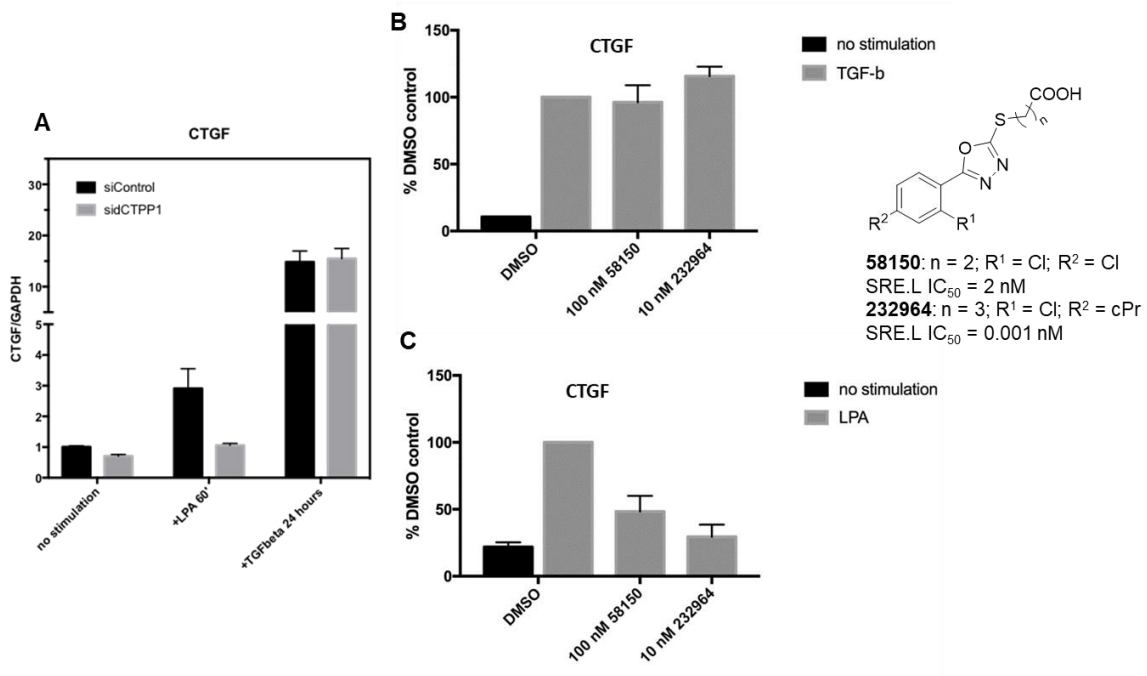

Figure 27: Comparison between siRNA dCTPase activity and 58150-series inhibitors in primary dermal fibroblast cells:

A) siRNA dCTPase leads to decreased production of LPA-stimulated CTGF mRNA, but not TGFβ-stimulated CTGF mRNA production. B & C) **58150** (B) and **232964** (C) decreased LPA-stimulated CTGF mRNA expression but did not affect TGFβ-stimulated CTGF mRNA expression.

Additionally, an attempt to validate this target by synthesizing and testing a literature dCTPase inhibitor was made.[210] In our SRE L. assay, the resynthesized literature inhibitor **31** displayed only weak activity (HEK293T SRE L. IC_{50} = 3,100 nM, n = 3; Figure 28). While the literature inhibitor did not display the same SRE.L potency as our inhibitors, the presence of activity indicates that dCTPase may play some role within our assay. *If dCTPase is a target for the 58150-series*, since it is not known whether the literature inhibitor binds covalently to dCTPase[210], my hypothesis is that the literature inhibitor might not interact with dCTPase for long enough to elicit the potency we observe for our inhibitors. This could be a result of poor membrane permeability, rapid efflux, or cellular metabolism of the inhibitor within the time course of the assay.

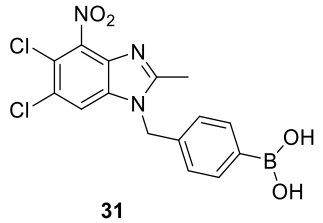

31
Literature dCTPase Inhibitor
Literature Malachite Green IC_{50} = 46 nM
HEK 293T SRE.L IC_{50} = 3,100 nM

Figure 28: Biological activity for a literature dCTPase inhibitor

This data, along with the qPCR results (Figure 27), gave us confidence to test our inhibitors in the reported dCTPase Malachite Green assay to determine if our compounds directly inhibit purified dCTPase (Figure 29A). A Malachite Green assay is a test for the colorimetric detection of inorganic phosphate[211]—a by-product of dCTPases catalytic reaction. Unfortunately, **58150** and **232964** displayed minimal inhibition (IC_{50} ~ 30 µM and 15 µM, respectively) in this assay. Isothermal titration calorimetry (ITC)—a method to test the extent that a ligand affects the melting temperature in a dose dependent manner of a protein to obtain a K_d[212]—was also used to directly test our inhibitors' binding affinity with dCTPase (Figure 29B & 29C). Unfortunately, minimal binding was observed for **232964** in these experiments as well (K_d ~ 15 uM). While the lack of direct physical binding in these assays does not support dCTPase being a biological target for this series, perhaps these conditions don't impart the correct biochemical conditions for our series to interact with dCTPase (discussed further below).

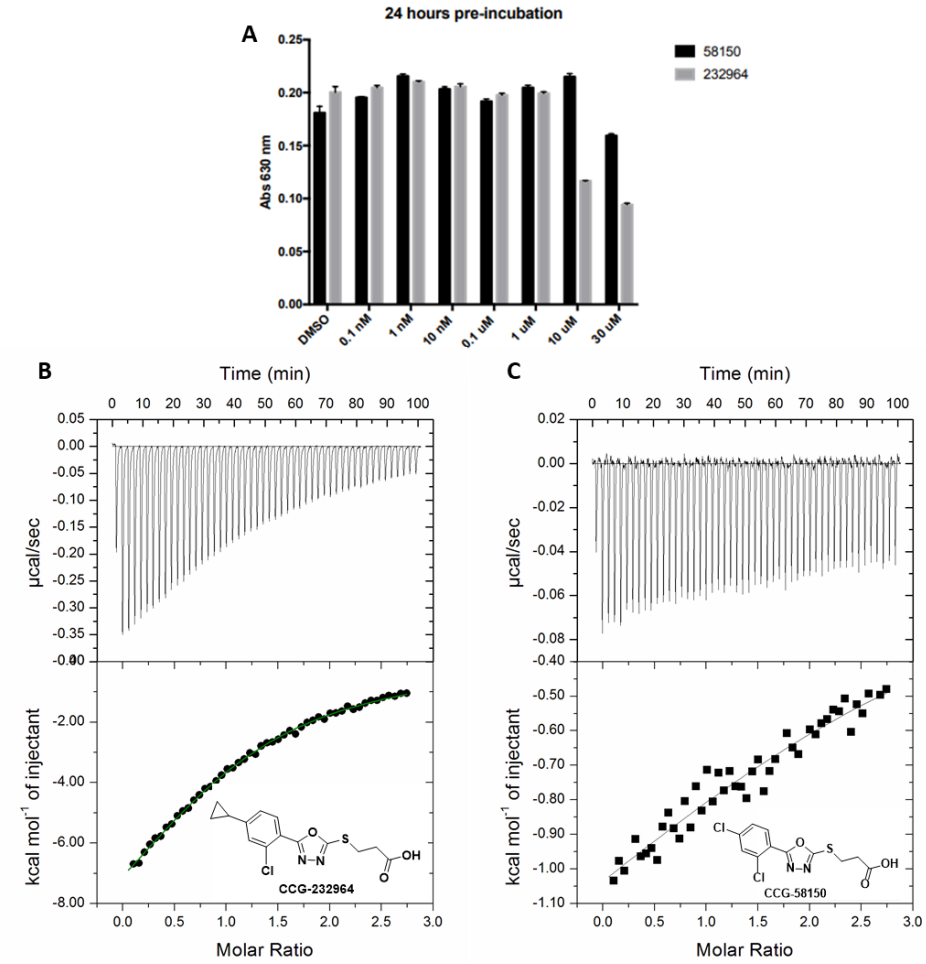

Figure 29: Direct binding assay with dCTPase and 58150-series analogs:
(A) Using the Malachite Green assay, dose-dependent inhibition of dCTPase with 58150 and 232964 after 24-hrs preincubation provided minimal activity; 2-hrs preincubation produced similar results. (B & C) Change in enthalpy during ITC assay for **232964** & **58150**, respectively, to dCTPase resulted in minimal binding affinity for **232964** (K_d ~ 15 uM) and insignificant affinity for **58150**.

The final experiment the Neubig lab performed to attempt to validate this target is a global DNA methylation assay (Figure 30). As stated previously, dCTPase plays an important role cleaning up non-canonical dNTPs, mainly methylated dNTPs. Short interspersed nuclear elements (SINEs) and long interspersed nuclear elements (LINEs) repeats contribute to more than 35% of the total genomic DNA mass.[213] Specifically, LINE-1 repeats make up roughly 17% of the human genome, making LINE-1 promoter a widely used surrogated marker that positively correlates with global DNA methylation levels.[214] In a preliminary study, the Dr. Lisabeth showed

that **58150** and **232964** may increase LINE-1 methylation in a dose-dependent manner in primary human dermal fibroblasts compared to untreated cells after 72-hour inhibitor pre-incubation (Figure 30A). Also, these same inhibitors affected LINE-1 methylation in scleroderma cells (Figure 30B).

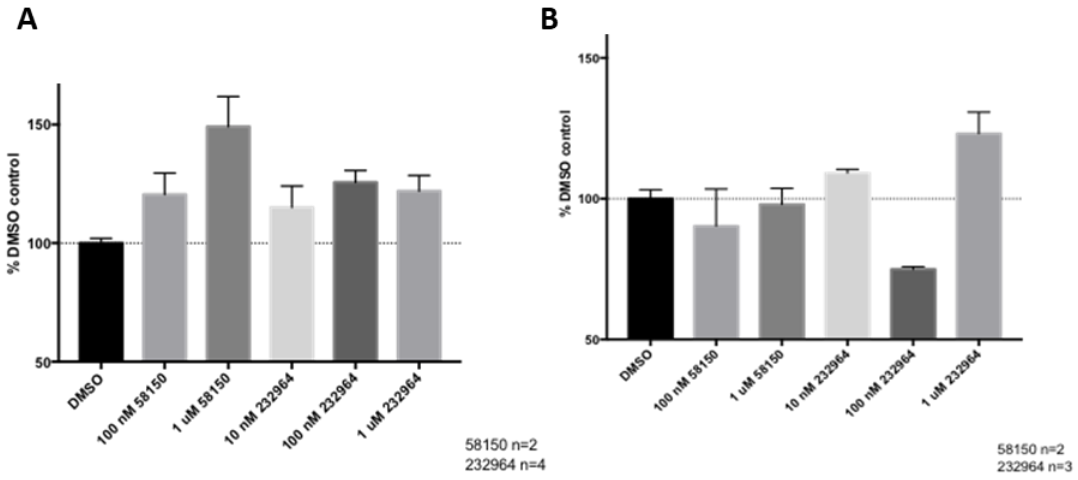

Figure 30: Global LINE-1 DNA methylation for primary human dermal fibroblasts and scleroderma cells after 72-hour inhibitor pre-incubation:

A) Shows that there is a general dose dependent increase in global DNA methylation for both **58150** and **232964** in primary human dermal fibroblasts. B) Shows that scleroderma cells are affected by **58150** and **232964**.

Interpreting these inconclusive methylation results is complicated. In fact, global DNA methylation patterns in fibrotic diseases are difficult to interpret altogether. The literature suggests that different fibrotic diseases have varying degrees of either increased or decreased levels of global DNA methylation.[215] As a result, a distinct connection between upregulation or downregulation in global DNA methylation and fibrotic diseases has not been reported to date. The take away from these results is that our inhibitors *might* affect global DNA methylation in both primary dermal fibroblast and scleroderma cells, and, since dCTPase has been shown to regulate global DNA methylation[207], this affect may be due to inhibition of dCTPase.

However, based on the totality of the results, it is *unlikely* that dCTPase is the biological target that imparts the potent SRE.L inhibition by the 58150 series. However, I would like to describe three *hypothetical* scenarios that might help explain the conflicting data between the

correlation amid the qPCR results and the lack of a physical interaction between dCTPase and **58150** and **232964**. I think regardless of whether dCTPase is a relevant biological target for this series, it is valuable to discuss these scenarios because they still might be applicable to this series' unknown mechanism of action. I will use dCTPase to discuss these scenarios, but another potential biological target can be exchanged with dCTPase.

First, dCTPase may undergo post-translational modifications in cells that cannot be recreated with the biochemical techniques used. As discussed, the literature suggests that dCTPase plays an important role in the epigenetic regulation of cells, particularly global methylation of DNA. Epigenetic regulators commonly undergo post-translational modifications in order to perform their specific functions.[216] If dCTPase undergoes post-translational modification in cells, then it may be difficult to recreate the "active" state of dCTPase required for our inhibitors biochemically.

The second possible scenario is that our inhibitors are modified in cells, ultimately activating them for covalent interaction with dCTPase. Of note, to test this hypothesis, a sulfone derivative (**258126**, Figure 21) was synthesized and tested in both the SRE L. assay and the Malachite Green assay. Unfortunately, despite this inhibitor being equipotent to 58150 in the SRE.L assay (Figure 21), it only had minimal activity in the Malachite green assay (data not shown). The activity of **258126** in the SRE.L assay is a strongly supportive result that chemical modifications to our series within cells may be required for potent biological activity. Yet, the lack of binding in the Malachite Green assay could be due to several reasons, such as the sulfone not being stable to the assay conditions or the inhibitor not being incubated long enough with dCTPase to bind properly.

The last hypothesis I present here is our inhibitors could be slow-binding ligands for dCTPase. This hypothesis would help explain the extremely tight and deep SAR we observe for this series. One could imagine that the inhibitors rapidly bind in a low-affinity enzyme-inhibitor complex that undergoes a slow relaxation to a very tight or covalently bound complex.[217-219] This

hypothesis also explains the weak biochemical binding vs the strong activity in cells. For instance, in cells, the enzyme has the time and necessary post-translational machinery to undergo the proper relaxation required to elicit the observed biological activity, but, biochemically, these mechanisms do not exist, so only the weakly bound low-affinity enzyme-inhibitor complex is achieved.

Until very recently, progress towards target identification for the 58150-series was at a full stop due to the exciting results obtained for the 222740-series target ID studies (discussed in the next subsection). While it is unfortunate that a target has not been determined yet for this series, there are still many possible target identification studies that can be performed using either our high-affinity agarose resin or propargyl click probes (Discussed in Chapter 5). The implied cellular activity profile for these probes (or probe mimics) suggests they are ideal to do further target identification studies with. If this series of inhibitors has a complicated mechanism of action, more complex target identification experimentation may provide a better path to identify the target.

CCG-222740 Series Target Identification Efforts:

Most of this subchapter has been included in a submitted manuscript entitled "Identification of Pirin as a Molecular Target of the CCG-1423/CCG-203971 Series of Anti-Fibrotic and Anti-Metastatic Compounds" by Lisabeth et al.

As mentioned in Chapter 1, subsequent chemical modification and structure-activity relationship (SAR) studies for CCG-1423 yielded the nipecotic acid derivatives CCG-100602 and CCG-203971[167,170], which removed the labile and potentially reactive N-alkoxybenzamide functionality of CCG-1423 (Figure 31). These analogs provided improved tolerability *in vitro* and *in vivo* as exemplified by their capability to reduce bleomycin-induced skin and lung fibrosis[,159,169] and melanoma lung metastasis[171] in two separate preclinical murine models. Further improvements to the series resulted in CCG-222740 and CCG-232601, which prevented

ocular fibrosis and skin fibrosis *in vivo.*[168,173] Recent optimization for metabolic stability yielded CCG-257081, which has improved pharmacokinetic properties and was shown to be orally active in a bleomycin-induced fibrosis murine model (Figure 32).[168]

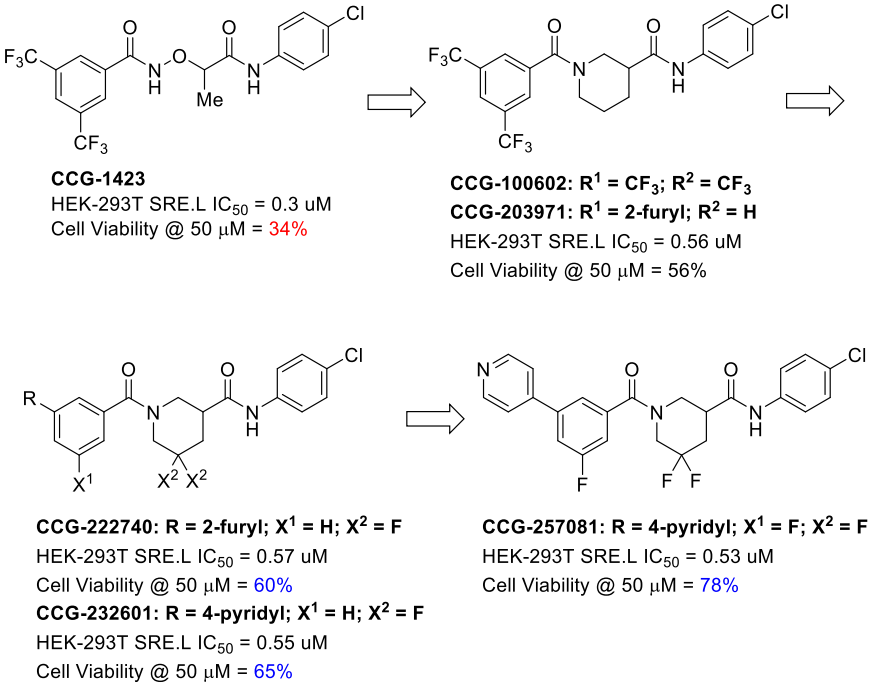

Figure 31: The drug development progression for the CCG-222740 series

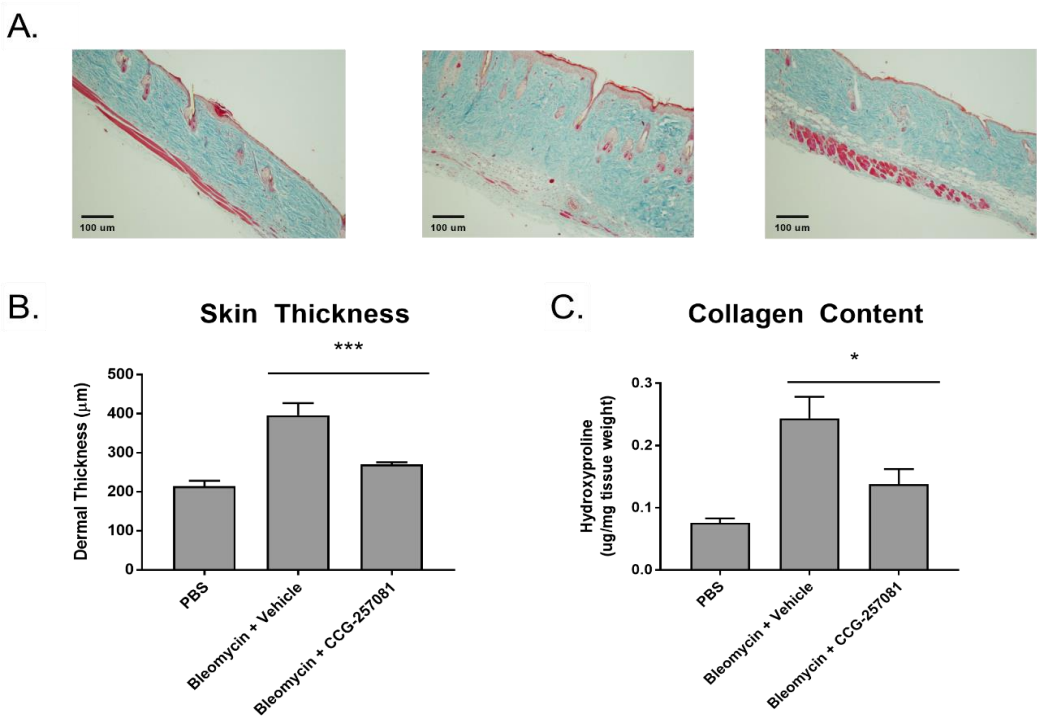

Figure 32: CCG-257081 prevents bleomycin induced fibrosis:

Mice treated with 50 mg/kg PO qd CCG-257081 had significantly reduced skin thickness as compared to vehicle control. (A) Masson's trichrome stained skin sections from vehicle treated mice (left panel) bleomycin treated mice (middle panel) and bleomycin+CCG-257081 treated mice (right panel). N=7 (B) Quantification of (A) by measuring the maximal distance between the epidermal-dermal junction and the dermal-subcutaneous fat junction ***p<0.001 using One-way ANOVA. (C) Quantification of collagen using hydroxyproline measurements *p<0.05 using One-way ANOVA.

Previous Target Identification Attempts:

Due to the phenotypic nature of the HTS, the identification of biological targets for the 222740-series has been elusive. Previous target ID efforts using CCG-1423 (Figure 31) have generated a couple possible biological targets; however, CCG-1423's promiscuity (as evidenced by poor cellular viability) has marred the reliability that the targets identified as being the ones responsible for the series' biological activity.

First, it has been reported that CCG-1423 can interact with the N-terminal nuclear localization sequence (NLS) in the RPEL domain of MRTF-A, blocking MRTF-A nuclear translocation by inhibition of the interaction between MRTF-A and importin α1/β1[220]; however,

attempts by the Neubig lab to tie this interaction into biologically relevant pathways have been unsuccessful (data not shown). Alternatively, microarray analysis of gene transcription changes in PC3 cells treated with CCG-1423 had significant overlap with effects of Latrunculin B—an actin polymerization inhibitor—as well as effects on cell cycle, ER stress, and metastasis gene networks, suggesting shared biological targets between these two inhibitors.[221]

Lundquist et al. showed that CCG-1423 binds directly to MICAL-2—an atypical actin-regulatory protein that mediates SRF/MRTF-A-dependent gene transcription via serum.[222] MICAL-2 is proposed to function by inducing redox-dependent depolymerization of nuclear actin, ultimately decreasing nuclear G-actin and increasing MRTF-A in the nucleus.[222] The major issue with this study is that CCG-1423 is one of the most cytotoxic and, thus, highest "off-target" liable analogs from our series. For instance, the significant decrease in MICAL-2 enzymatic activity of CCG-100594—an analogous compound to CCG-1423 that lacks the liable N-O functionality—is evidence that Lundquist et al.'s target ID results may be due to the off-target liability of CCG-1423.

Hayashi et al. took an immobilization probe approach where they non-specifically and covalently attached CCG-1423 to Sepharose using a photolizable cross-linker.[220,223] They pulled down flag tagged MRTF-A, but, again, besides questionable coupling techniques for immobilization resin attachment, using CCG-1423 significantly decreases the reliability of their findings. Previous target ID efforts in our lab using an acetophenone photo-probe with a propargyl Click handle on the CCG-203971 scaffold were inconclusive (Figure 33).[224] However, we were hopeful that utilizing a more potent and less promiscuous scaffold would be a more viable approach to identifying the biological target(s) for this series.

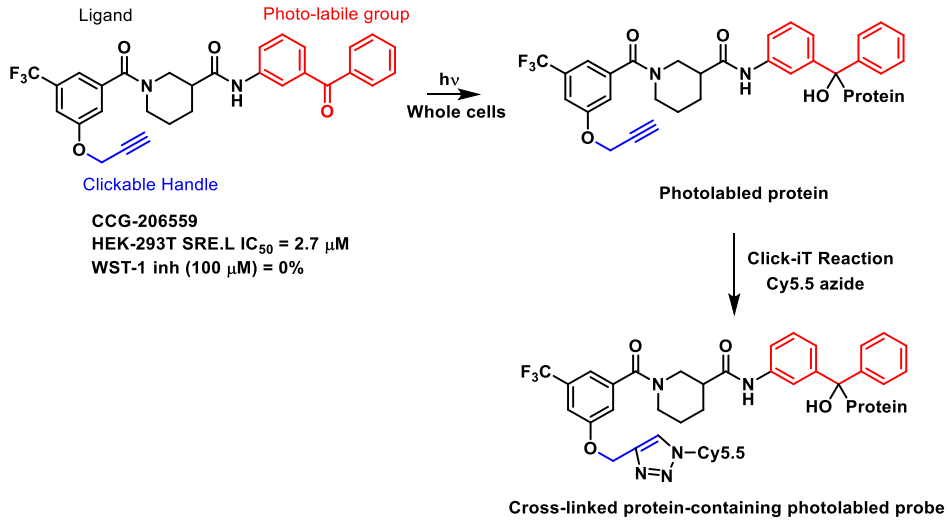

Figure 33: Tag-free photoprobe approach in whole cells previously attempted in our lab: Multiple benzophenone, azide, and acetylene substitutions were tested for potency, but CCG-206559 provided the best potency/cytotoxicity profile. This probe was irradiated with hv at 350 nm in the presence of HEK293T cells, and, after purification, the Click Reaction was performed using InvitrogenTM Click-iT(R) Reaction Buffer Kit to attach Cy5.5 dye for visualization. In the presence of 20 µg proteins, a faint band at 24 kDa in PC3 cells was observed. No further attempts to identify this band have been made.

Despite multiple potential molecular targets for the series, there has been no robust biophysical evidence presented to conclusively designate the biological target that affords the biologically activity associated with this series. However, because identifying the target would help us develop these exciting antifibrotic agents, we undertook an unbiased mass spectrometry-based target identification approach using an immobilized agarose resin affinity probe based on the less promiscuous CCG-222740 scaffold.

222740 Series Probe Design Rationale

To develop an affinity matrix for target enrichment, CGG-222740 was used as the starting chemical scaffold, mostly because of its improved cellular potency and superior inhibition of TGFβ-induced ACTA2 gene expression as compared to CCG-203971.[168] To identify the optimal linker placement, we performed a methoxy scan followed by an ethoxymethoxy scan on each aryl ring (Table 5, **A54**-**A58**). Taking into consideration the flat SAR, retained potency, efficacy, and availability of starting material, we chose to attach the PEG linker at the 5-position

of the 3-furyl phenyl ring. Since attaching either small (**A54**) or large (**A59**) functional groups at the 3-position did not markedly reduce activity, we were confident that attaching the probe linker (**A62**, Table 5) at that position would allow for the probe (**32**, Figure 34) to maintain acceptable binding affinity to the biological target(s).

Table 5: Exemplary probe development SAR

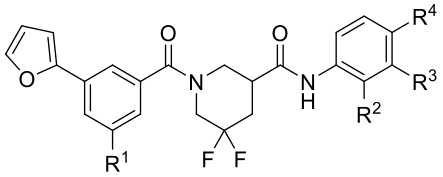

CCG-	Entry	R^1	R^2	R^3	R^4	SRE.L IC_{50} (uM)[a]	Max Efficacy
222740	-	H	H	H	Cl	0.4	100
258524	**A54**	OMe	H	H	Cl	2	100
258165	**A55**	H	OMe	H	Cl	0.83	100
258166	**A56**	H	H	OMe	Cl	1.1	100
258704	**A57**	H	H	Cl	OMe	0.58	88
258705	**A58**	H	H	H	OMe	5.6	100
258662	**A59**	$O(CH_2)_2OMe$	H	H	Cl	2.3	90
258742	**A60**	H	$O(CH_2)_2OMe$	H	Cl	2.5	68
258724	**A61**	H	H	$O(CH_2)_2OMe$	Cl	1.6	99
262545	**A62**	$O(CH_2)_2OC(CH_2)_2NH_2$•HCl	H	H	Cl	ND	ND

[a]SRE.L assay performed in HEK293T cells (mean of n = 3, SEM < 10%).

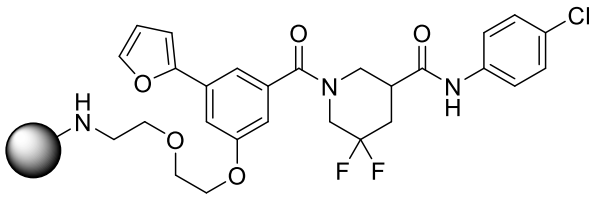

32

Figure 34: Immobilized agarose resin affinity probe for 222740-series

Synthesis of Probe Mimic Analogs and Probe for CCG-222740 Series:

The synthesis to generate probe mimics with the methoxy- and ethoxymethoxy-containing aryl rings on the right side of the piperidine core started from either the commercially available carboxylic acid **33** or methyl ester **34**, which was synthesized as previously described (Scheme 11).[168] Commercially available carboxylic acid **33** was subjected to standard HATU

amide coupling conditions with commercially available anilines. The final mimic analogs **36** were generated after acid mediated Boc-deprotection and subsequent amide coupling with HATU. Alternatively, the analogs were built from the left-hand side first to assemble ethoxymethoxy analog **258724**; this more convergent route would have been preferred from the beginning of the synthesis for these analogs, but an efficient route to generate intermediate ester **37** was not discovered until most of these probe mimic analogs were generated.

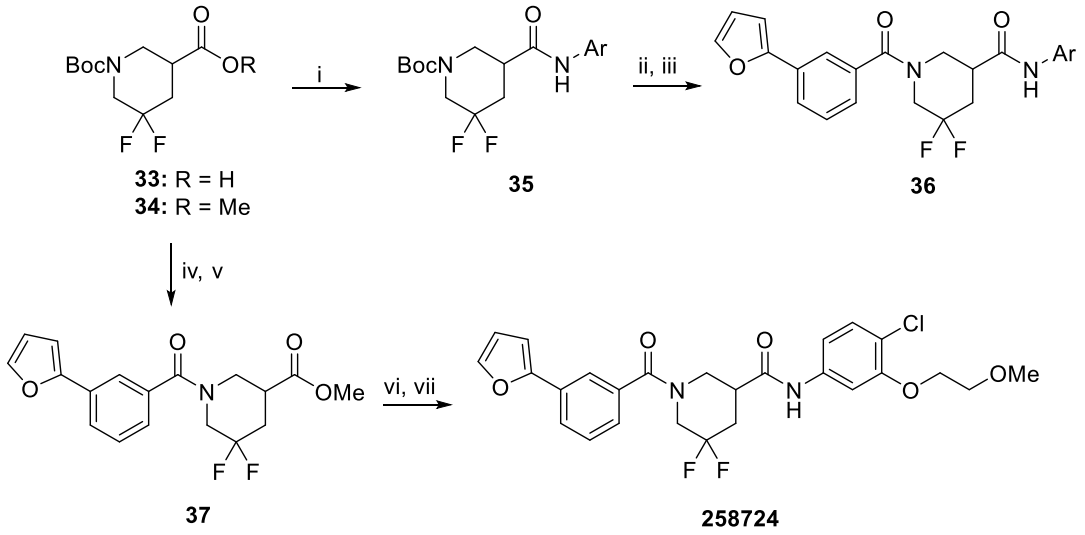

Scheme 11: Synthesis of probe mimic analogs with methoxy or ethoxymethoxy functional groups on the right side of the piperidine core

Conditions: (i) HATU, aniline, DIPEA, DMF, rt (ii) 4M HCl in dioxanes, rt; (iii) HATU, 3-(furan-2-yl)benzoic acid, DIPEA, DMF, rt (iv) 4M HCl in dioxanes, rt (v) HATU, 3-(furan-2-yl)benzoic acid, DIPEA, DMF, rt (vi) 1M NaOH, THF, rt (vii) HATU, 4-chloro-3-(2-methoxyethoxy)aniline, HCl, DIPEA, DMF, rt.

Incorporating the methoxy and ethoxymethoxy functionalities to the aryl ring on the left side of the piperidine core was not as simple as the analogs with these functionalities on the right-hand side, as they required a couple of extra steps to synthesize the necessary starting materials (Scheme 12). Intermediates **39-41** were generated according to previously described chemistry.[225-227]

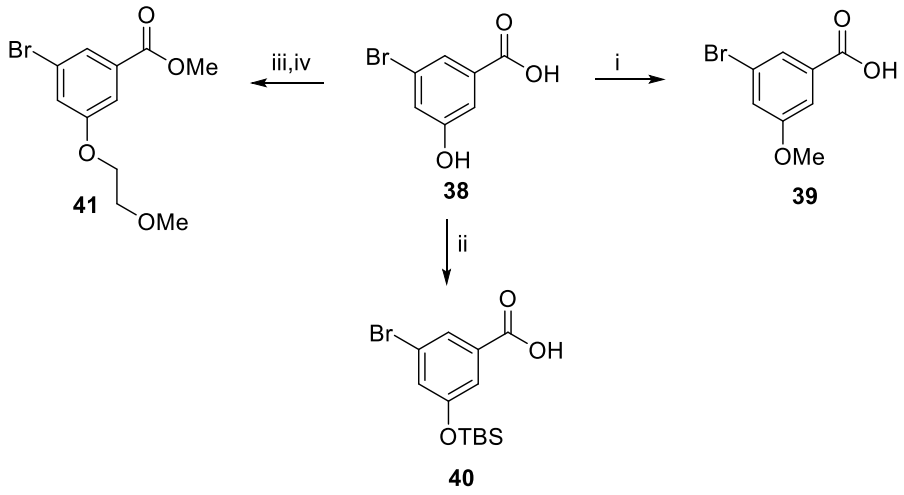

Scheme 12: Synthesis of 39, 40, and 41

Conditions: (i) Cs_2CO_3, MeI, DMF, rt[225] (ii) TBS-Cl, imidazole, DMF, rt[226] (iii) H_2SO_4, MeOH, reflux (iv) $BrCH_2CH_2OMe$, K_2CO_3, DMF, 90 °C[227].

Although probably unnecessary, unprotected benzoic acids **39** & **41** were esterified, and then methyl esters **42a-c** were subjected to Suzuki cross coupling chemistry with furan-2-ylboronic acid, producing benzoic acid intermediates **43a-c** (Scheme 13). Since the TBS protecting group of intermediate **42b** was hydrolyzed during the cross-coupling reaction, this provided a handle to install the PEG amine linker, and the availability of this late-stage intermediate is one of the reasons why the 3-position was later selected for PEG linker attachment. To install the linker, benzoic acid intermediate **43b** was esterified, freshly prepared 2-(2-((t-butoxycarbonyl)amino)ethoxy)ethyl methanesulfonate [228] was coupled to phenol **44** in basic alkylation conditions, and then benzoic acid intermediate **46** was generated through saponification of methyl ester **45**.

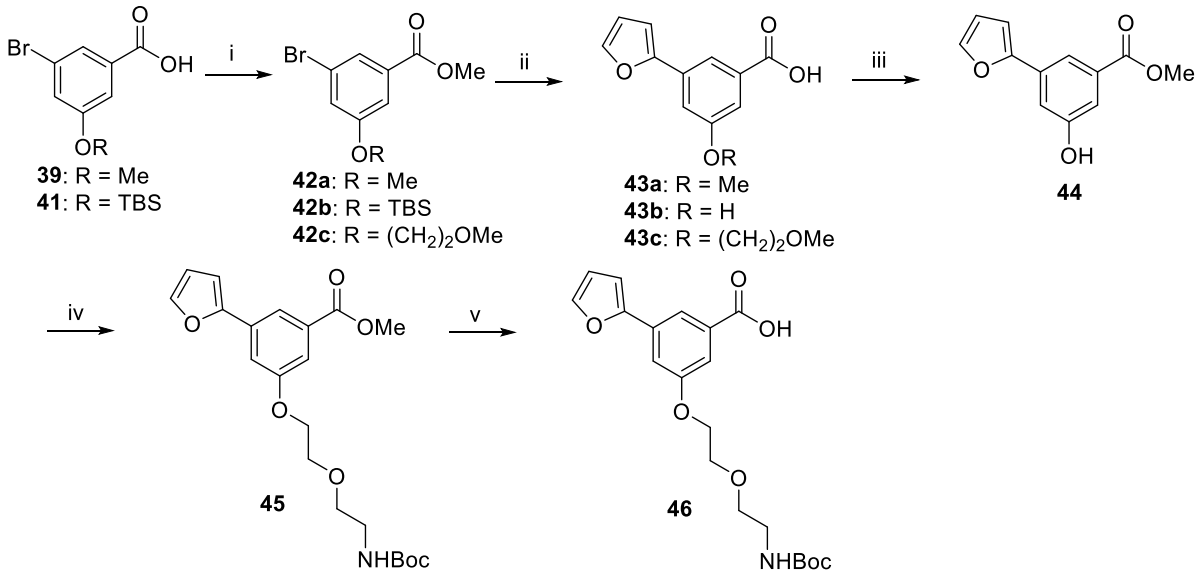

Scheme 13: Synthesis of 46

Conditions: (i) H_2SO_4, MeOH, reflux (ii) furan-2-ylboronic acid, Na_2CO_3, $Pd(PPh_3)_4$, H_2O, DME, 100 °C (iii) H_2SO_4, MeOH, reflux (iv) $BocHN(CH_2)_2O(CH_2)_2OMs$, Cs_2CO_3, DMF, 75 °C (v) 1M NaOH, THF, rt.

Assembly of probe **32** began with basic hydrolysis of methyl ester **34** followed by HATU-mediated amide coupling with 4-chloroaniline to produce carbamate **35a** (Scheme 14). Acid-mediated Boc deprotection generated HCl amine salt **47**, which was subjected to HATU-mediated amide coupling conditions with the required benzoic acid intermediates **43a**, **43c**, and **46** to produce methoxy probe mimic **258524**, ethoxymethoy probe mimic **258662**, and Boc protected PEG-linker intermediate **48**. After acidic hydrolysis, **262545** was generated and linked to NHS-agarose beads using solid phase amine coupling chemistry followed by blocking of residual reactive groups with ethanolamine to produce **32**, which was subsequently used as our immobilized affinity pull-down probe.

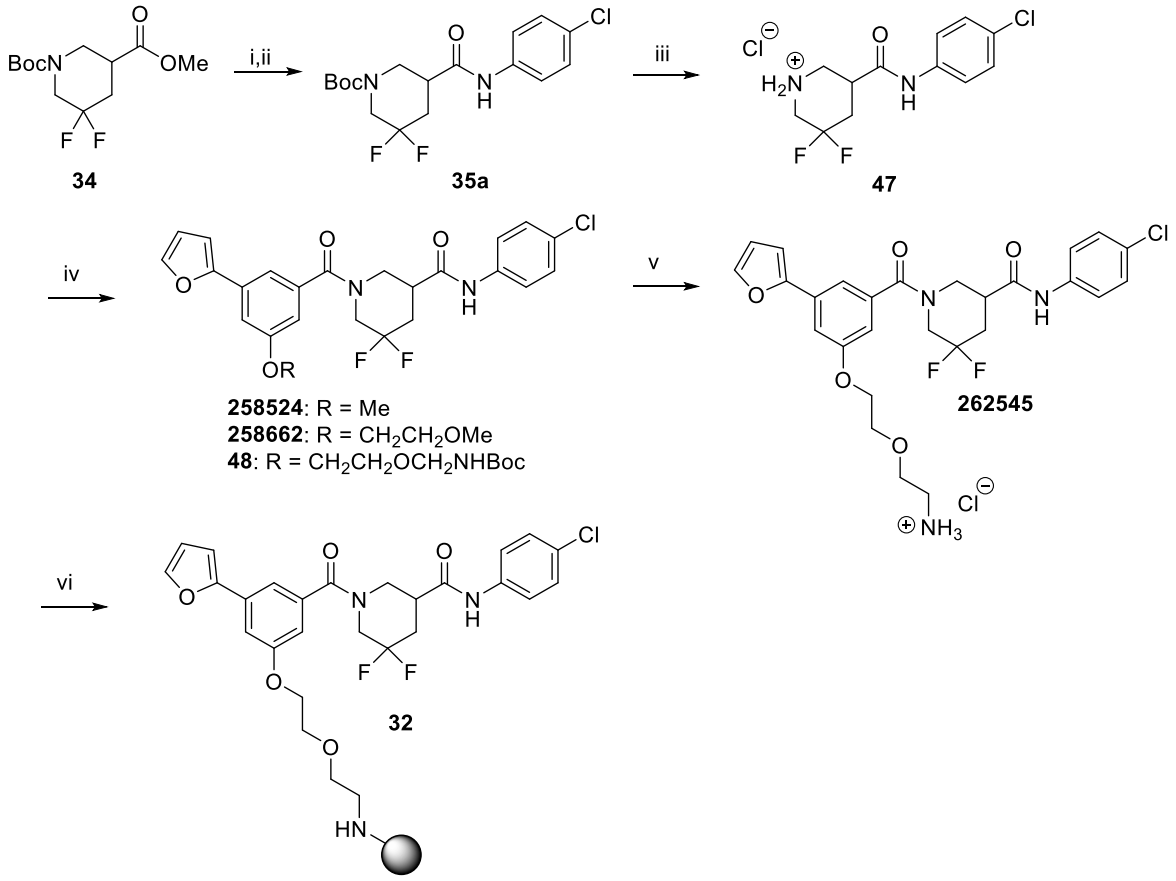

Scheme 14: Synthesis of 222740-series immobilized probe

Conditions: (i) 1M NaOH, THF, rt (ii) HATU, 4-chloroaniline, DIPEA, DMF, rt (iii) 4M HCl in Dioxanes, rt (iv) HATU, **43a**, **43c**, & **46**, DIPEA, DMF, rt (v) 4M HCl in Dioxanes, rt (vi) NHS-activated agarose resin, DMSO, PBS, followed by ethanolamine.

Pirin Identified as A Potential Target of CCG-222740

The agarose-bound probe (**32**) was mixed with whole cell lysates from HEK-293T cells containing DMSO (unblocked) or 30 µM CCG-222740 (blocked). Beads were then washed several times with cold PBS (adapted from[229]). Pulldown mixtures were analyzed after trypsin digestion and subsequent proteomic analysis (see Experimental). Comparison between the normalized peptide abundance in the DMSO control lysates and the CCG-222740 treated cell lysates revealed one protein—pirin—that stood out with 5-fold greater peptide abundance in the DMSO control lysates and a p-value of 1.3 e^{-13} (Table 6). Of note, the p-value is a statistical measure of the significance between active/blocked lysate calculation.

Table 6: List of putative targets for 222740-series

Accession	Description	Peptide count	Unique peptides	Normalized Unblocked/ Blocked Beads	p-value
PIR_HUMAN	**Pirin**	**4**	**3**	**4.98**	**1.32E-13**
RBM4B_HUMAN;E9PLB0;E9PM61;U3KQD5	RNA-binding protein 4B	14	1	2.87	5.41E-04
CKAP4_HUMAN	Cytoskeleton-associated protein 4	2	1	2.85	1.28E-04
WAPL_HUMAN;Q8WVX6	Wings apart-like protein homolog	6	3	2.69	2.44E-05
SNX4_HUMAN	Sorting nexin-4	3	2	2.65	2.18E-02
RU1C_HUMAN;A0A0A0MRR7	U1 small nuclear ribonucleoprotein C	5	5	2.51	1.88E-04
PRPS1_HUMAN;B1ALA9	Ribose-phosphate pyrophosphokinase 1	3	1	2.46	4.68E-03
B4DWR3;PFD3_HUMAN	B4DWR3_HUMAN Prefoldin subunit 3	3	2	2.22	2.81E-02
HSP72_HUMAN	Heat shock-related 70 kDa protein 2	19	3	2.22	1.57E-03
CRIPT_HUMAN	Cysteine-rich PDZ-binding protein	2	1	2.21	1.80E-05
HSP76_HUMAN	Heat shock 70 kDa protein 6	12	1	2.20	4.77E-05
CNBP_HUMAN	Cellular nucleic acid-binding protein	15	12	2.18	3.59E-06
PLSL_HUMAN	Plastin-2	4	1	2.14	1.10E-05
RL38_HUMAN;J3KSP2;J3KT73;J3QL01	60S ribosomal protein L38	6	3	2.09	6.98E-06
K7EKX7;A0A087WT12;A0A087X2I2;A0A0A0MTT1;GPX4_HUMAN	K7EKX7_HUMAN Glutathione peroxidase (Fragment)	6	4	2.08	1.09E-04
SYDC_HUMAN;H7C278	Aspartate--tRNA ligase, cytoplasmic	4	3	2.07	1.07E-05
XPO2_HUMAN	Exportin-2	10	5	2.06	1.49E-03
ZN706_HUMAN	Zinc finger protein 706	2	2	2.05	1.71E-06
GSTP1_HUMAN;A0A087X2E9;A8MX94	Glutathione S-transferase P	12	11	2.00	5.49E-04

Peptide counts refer to the number of peptides identified for a given protein, while unique peptide count refers to the number of peptides identified that are completely unique for a given protein. Normalized unblocked/blocked beads is the raw mean ratio between peptides identified in unblocked vs. blocked samples.

Pirin is a well-conserved protein originally identified in a yeast two-hybrid screen with the transcription factor NF-1.[230] Pirin has also been implicated in NF-κB signaling through its interaction with Bcl3—a NF-κB co-activator—and through direct interaction with a p65/p65 homodimer.[231-233] Pirin is expressed ubiquitously, and basal expression is, in part, regulated through Nrf2-regulated gene transcription.[234] Pirin acts as a redox-sensing transcription factor regulator within the nucleus.[230] It has been suggested that pirin is important for cell migration [233,235-237] as well as the epithelial-mesenchymal transition (EMT).[238,239]

Two drug discovery campaigns have previously been described for pirin. The first report used fluorescently labeled pirin to identify small molecules in an immobilized compound library that directly bound to pirin; however, the cellular effects of the identified compound, TPhA (Figure 35), were only modest.[233] A second study identified CCT251236 while screening for inhibitors of the Heat Shock Factor 1 (HSF1) transcription pathway.[240] Their target identification efforts yielded pirin as the target of CCT251236, which has efficacy in an ovarian cancer model *in vivo* and inhibits melanoma migration *in vitro.*[240] This interesting biological activity and the

structural similarities between CCT251236 and the CCG-222740 series (e.g. the central bis-amide core flanked by substituted-aryl functionalities) provided an initial level of confidence to pursue pirin as a biological target for CCG-222740.

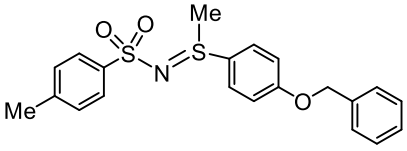

TPhA
Chemical Array Screen K_D = 600 nM
HEK-293T SRE.L IC_{50} > 50 μM

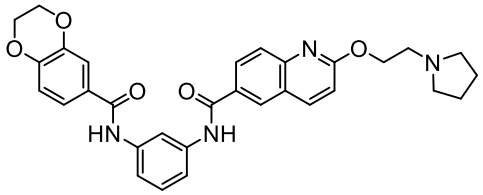

CCT251236
HSP72 induction inhibition (ELISA) IC_{50} = 3.3 nM
Pirin SPR K_D = 31 nM
HEK-293T SRE.L IC_{50} < 10 nM

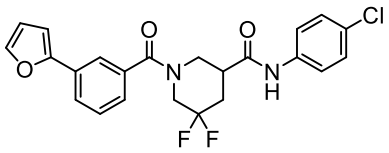

CCG-222740
HEK-293T SRE.L IC_{50} = 0.57 μM

Figure 35: Pirin inhibitors and their activities

First, the Neubig lab tested whether the literature pirin inhibitors, TPhA and CCT251236, could inhibit the Gα12-mediated SRE.L assay. While the weak pirin inhibitor TPhA was considered inactive in the SRE.L assay, CCT251236 had a remarkable effect on SRE.L activity, with an IC_{50} of 3.3 nM (Figure 36A), without affecting luciferase catalytic activity directly (Figure 37). This pharmacologically validates pirin in the same Gα12 driven SRE.L Luciferase assay that we discovered and developed our series of compounds. Moreover, CCT251236 has nM potency in the reported cell-based Heat shock protein (HSP)72 phenotypic assay and binds to pirin *in vitro* with a K_D of 44 nM as measured by SPR[240], so it is not surprising that CCT251236 has such a high level of activity in our SRE.L assay.

In an attempt to further validate pirin's importance in the SRE.L assay, pirin was overexpressed in HEK293T cells with a SRE.L Luciferase reporter. Pirin alone was capable of modestly increasing SRE.L driven luciferase expression, suggesting that pirin can enhance MRTF/SRF transcription (Figure 36B). Moreover, to determine whether reduction of pirin

through siRNA could suppress MRTF-A-dependent SRE.L Luciferase, primary human dermal fibroblasts were treated with a Dharmacon smartpool siRNA targeting pirin. MRTF-A-driven SRE.L Luciferase was significantly reduced when pirin mRNA levels were decreased. This suggests that pirin modulates gene transcription at the MRTF-A level of regulation (Figure 36 C and D). Taken together, these results support interplay between pirin and MRTF- and SRF-driven luciferase transcription.

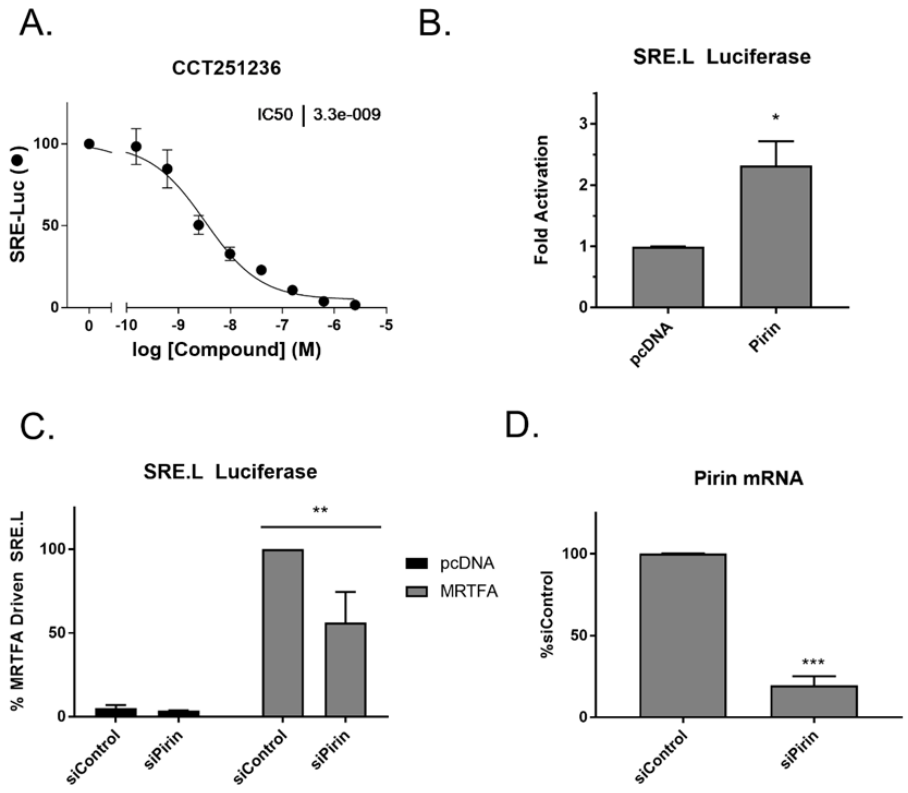

Figure 36: Pirin interacts with the MRTF/SRF pathway:

(A) CCT251236 inhibits Q231L Gα12 activated SRE.L Luciferase in HEK293T cells; n=4 (B) Overexpression of C-terminally V5 tagged pirin induces SRE.L Luciferase signal in HEK293T cells. Results are expressed as the mean ± SEM. ***p< 0.05 using Student's t-test; n=3 (C) Knockdown of pirin also reduces MRTF-A driven SRE.L Luciferase in primary dermal fibroblasts. Results are expressed as the mean ±SEM **p<0.01 using 2-way ANOVA; n=3 (D) Validation of pirin knockdown using qPCR. Results are expressed as the mean ± SEM ***p<0.001 using Student's t-test; n=3.

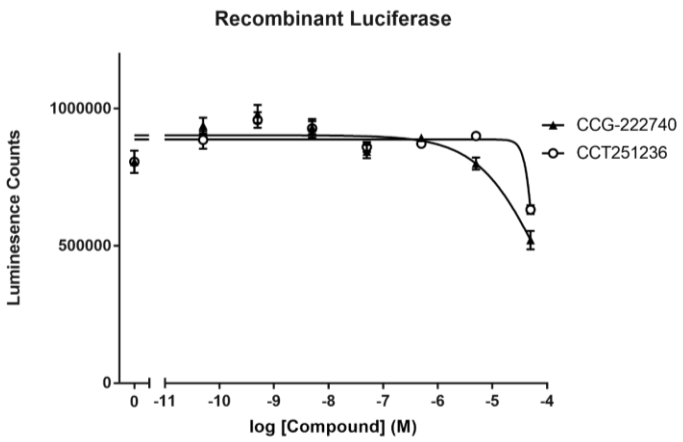

Figure 37: CCG-222740 and CCT251236 have minimal effects on recombinant luciferase activity. Recombinant firefly luciferase was incubated with varying concentrations of CCG-222740 or CCT251236. Neither inhibited luciferase activity with 100% efficacy, and CCG-222740 both have an $IC_{50}>10^{-4}$ M. n=2.

The Neubig lab also took a bioinformatics approach to compare a gene expression signature of CCG-1423 target genes with 12,922 MSigDB or in-house gene sets (see Erika et al). Only 347 (2.7%) of the gene sets showed a statistically significant correlation with the CCG-1423 regulated genes at the Bonferroni-corrected p-value ($p < 3.87x10^{-6}$). A siPirin gene set was the most significantly enriched ($p = 4.44x10^{-72}$), with an overlap of 44 genes with the CCG-1423 signature (Figure 38A). By comparison, the overlap between the Neubig lab's in-house MRTF signature and the CCG-1423 gene signature was only 8 genes (data not shown). Therefore, the bioinformatics analysis, comparing the CCG-1423 microarray dataset and the siPirin microarray dataset, was very encouraging and consistent with the idea that pirin may be a direct target of our series.

While these results strongly correlate pirin to the SRE.L assay, we still required biophysical evidence that the 222740-series interacted with pirin. Therefore, recombinant pirin was purified to test whether CCG-222740 and CCG-257081 engaged with pirin *in vitro*. As a comparison, a structurally related inhibitor that was nearly inactive in our Gα12 induced SRE.L assay was also tested (Figure 38B and C). Purified, recombinant pirin was used in isothermal titration calorimetery (ITC) experiments to determine the K_D of our compounds. CCG-222740

and CCG-257081 bound to pirin with a K_D of 4.3 µM and 8.5 µM, respectively. The change in enthalpy for the 'inactive' compound "**5**" (Figure 38C only)—an inactive analog from the 222740 series—was much less than either CCG-222740 or CCG-257081; it did not provide a reliable fit for binding analysis. Although this is a small set of compounds, it is encouraging to note that two of our lead inhibitors appear to bind to pirin while an inactive compound shows minimal binding to pirin *in vitro (*Figure 38C).

Furthermore, to understand how our small molecules bind to pirin, we solved high-resolution x-ray co-crystal structures of pirin in complex with CCG-222740 and CCG-257081 (1.7 Å and 1.5 Å, respectively) (Figure 38D). The two compounds bind very similarly, both analogs co-crystallized in the *R*-confirmation with the 4-chloroaniline projecting deep into the hydrophobic pocket and the furan/pyridine rings jutting out into solvent (Figure 38D and E). There are no direct contacts between the compound and the iron; the interaction is mostly mediated by hydrogen bonds with Fe-ligated waters (Figure 38E). When these compound-bound pirin co-crystal structures are compared to both the inactive (Fe^{2+} bound) and the active (Fe^{3+} bound) forms described in the literature, a high level of similarity exists. Overall, there is a RMSD between 257081-bound pirin and the literature reported Fe^{2+} bound pirin of 0.251 Å and between 257081-bound pirin and the literature reported Fe^{3+} bound pirin of 0.582 Å.[232]

Of note, the RMSD is a measure that provides a comparison between protein structures[241], so since there is a greater overall distance between Fe^{3+} bound pirin and 257081-bound pirin vs. Fe^{2+} bound pirin and 257081-bound pirin, these results suggest our inhibitors may inhibit pirin activation by binding to the Fe^{2+} state. In summary, a direct interaction between pirin and the CCG-222740 series of compounds was confirmed with the co-crystal structures, and they may highlight how our series bind to pirin to block Rho-mediated gene transcription.

The exact mechanism of how small-molecules affect pirin activity is unknown, but these results indicate the possibility that our series stabilizes either an oxidized or reduced form of pirin, affecting the ability of pirin to bind to co-activators or transcription factors. Of note, it has

been shown that only Fe^{3+} bound pirin binds to p65, whereas Fe^{2+} bound does not.[232] Also, CCG-1423 has been shown to displace MRTF-A and SRF from the ACTA2 promoter[242], which suggests that compound binding to pirin may disrupt a pirin/MRTF-A/SRF/DNA complex. Future work will address these and other questions, including exploring the implications of pirin modulation on global measures of gene transcription.

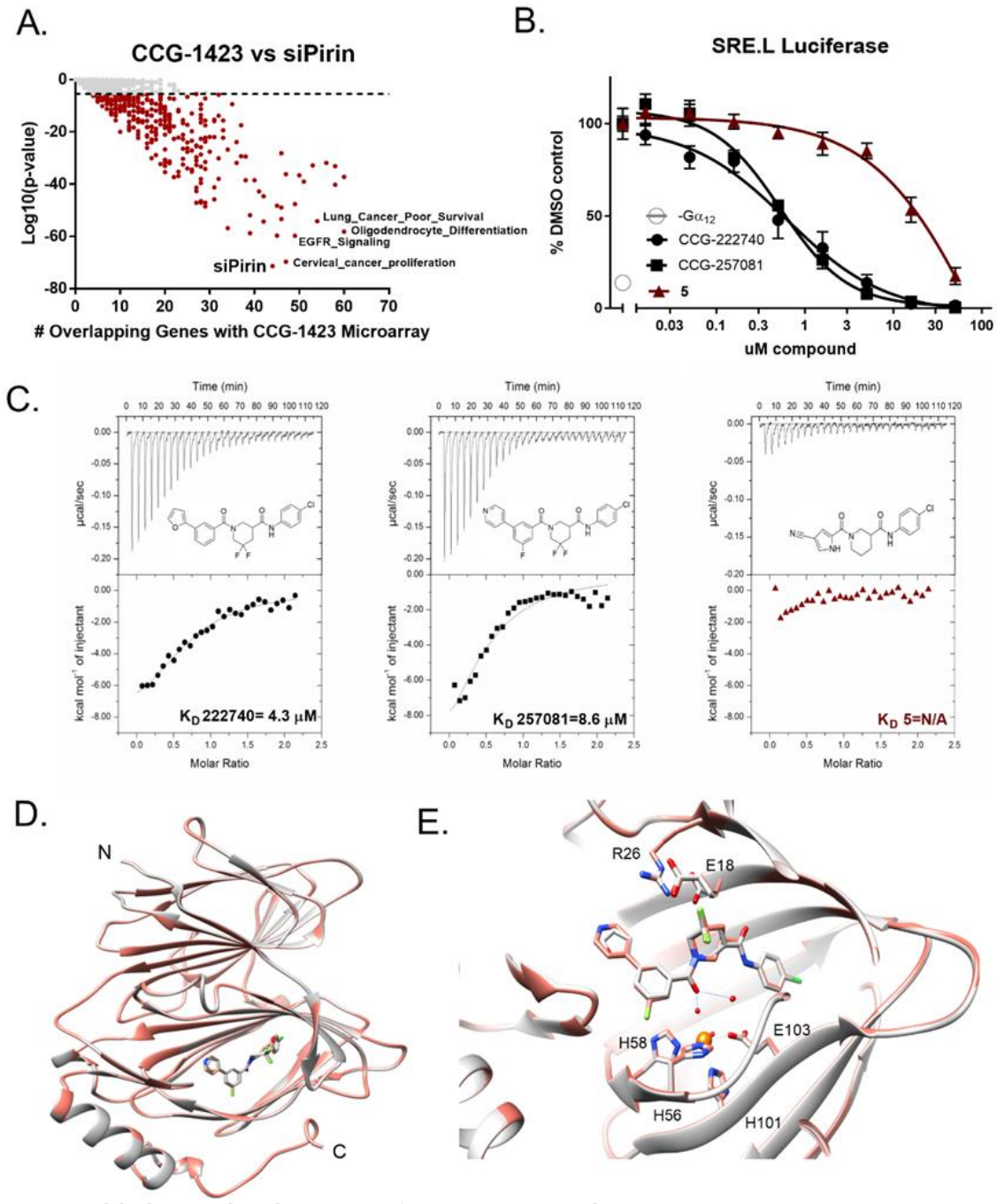

Figure 38: Pirin is a molecular target of CCG-222740 and CCG-257081

(A) Differential gene expression (based on fold change) was calculated for Pirin knockdown (GSE 17551) and CCG-1423 treatment (GSE 30188) and found to have high significance and an overlap of 44 genes in their datasets. (B) HEK293T cells co-transfected with Q231L $G\alpha_{12}$ and a SRE.L Luciferase reporter were treated with CCG-222740, CCG-257081 or CCG-258531 (C) Isotherm generated by ITC shows that CCG-257081 (black) has a greater enthalpy change upon binding to pirin, as compared to CCG-258531 (red), indicative of better binding to recombinant pirin. (D) Crystal structure overlap of pirin bound to CCG-222740 (gray) and CCG-257081 (salmon). (E) Detailed view of the compound binding pocket with

overlaid CCG-222740 (gray) and CCG-257081 (salmon) pirin-bound structures. Also indicated is the metal ion (orange) as well as coordinating residues and water molecules (dashed lines), and hydrogen bonds (solid lines).

The CCG-203971/CCG-222740 series is known to inhibit pro-fibrotic signaling, and a large body of literature exists that suggests this is through MRTF/SRF.[159,173,243,244] However, CCT251236 was used to pharmacologically verify that pirin is involved in TGF-β dependent gene expression. Human primary dermal fibroblasts were activated with TGF-β for 24 hours with or without CCG-222740 or CCG-257081 as well as CCT251236. All three compounds significantly reduced TGF-β induced ACTA2 expression (Figure 39A). ACTA2 is the gene for α-SMA, which is a marker of myofibroblast transition, and a direct target of MRTF/SRF-mediated transcription[244]. In addition, these compounds were tested against CTGF expression (CCN2). CTGF is a pro-fibrotic mediator that is also, in part, regulated by MRTF/SRF.[245] Although not as potent, a decrease in CTGF mRNA levels was also observed after treatment with all three compounds (Figure 39B).

To further confirm that pirin is involved in TGF-β-mediated gene expression, pirin expression was reduced through pirin siRNA. Knockdown of pirin led to a 50% decrease in TGF-β induced ACTA2 and CTGF mRNA, further verifying the role of pirin in TGF-β mediated gene expression (Figure 39C and 39D). Pirin mRNA levels were reduced 80% in primary dermal fibroblasts after siRNA treatment (data not shown) and protein amounts were reduced approximately 50% (Figure 39E and 39F).

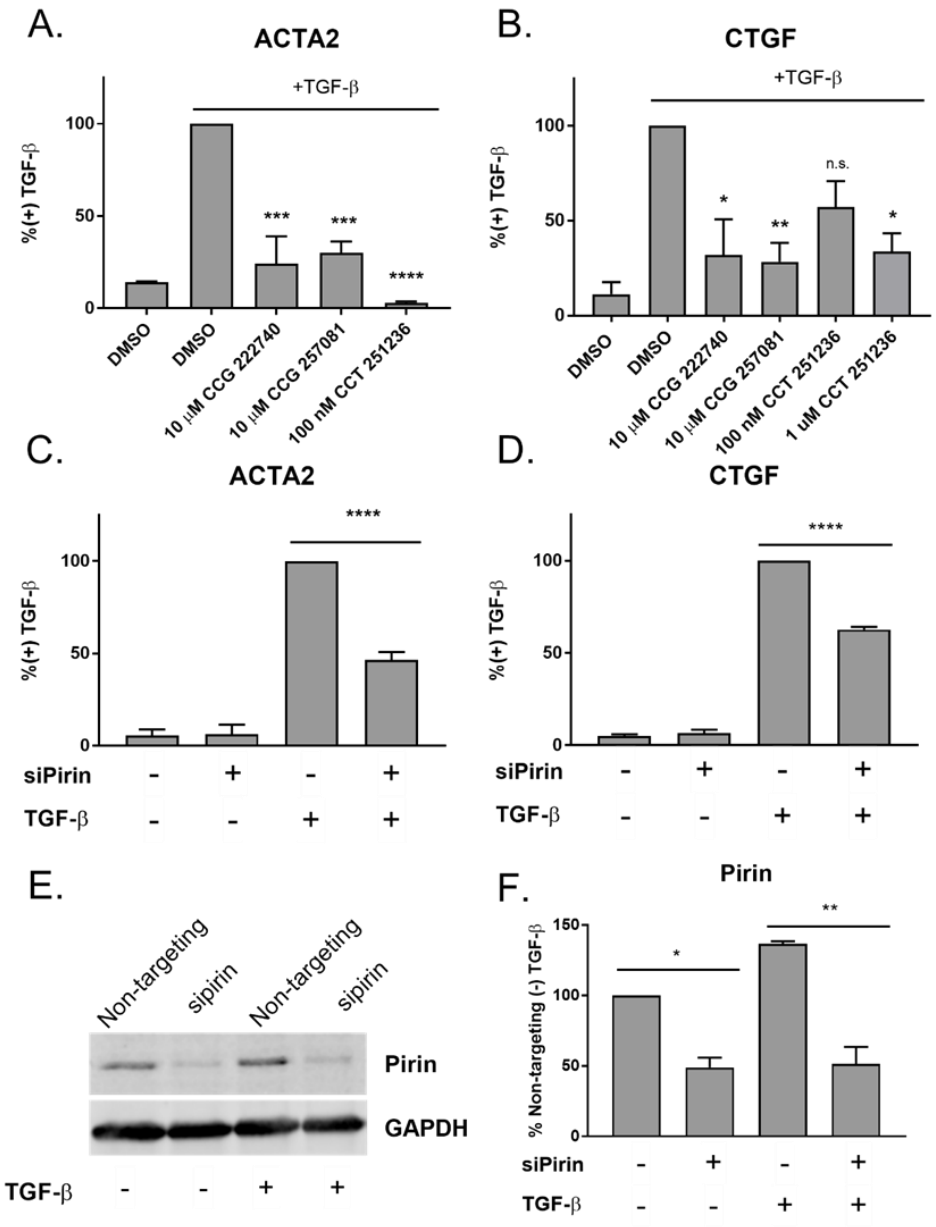

Figure 39: Inhibition or ablation of pirin reduces TGF-β dependent gene expression

(A) Primary dermal fibroblasts from healthy donors were treated with TGF-β and either vehicle control, CCG compounds, or CCT251236. Levels of ACTA2 were measured by qPCR. Results are expressed as the mean ± SEM. ***p< 0.001, ****p<0.0001 using One-way ANOVA; n=3 (B). Similarly, CTGF mRNA levels were measured after treatment with TGF-β and pirin inhibitors. Results are expressed as the mean ± SEM. *p<0.05, **p<0.01 using One-way ANOVA; n=3. (C) Pirin knockdown reduces TGF-β stimulated ACTA2 in human primary dermal fibroblasts. Results are expressed as the mean ± SEM ****p<0.0001 using One-way ANOVA; n=3. Non-targeting siRNA was used in siPirin (-) conditions. (D) Pirin knockdown reduces TGF-β stimulated CTGF. Primary dermal fibroblasts were treated similarly to C. The results are expressed as the mean ± SEM of ****p=0.0001; n=3. (E) Western blot of pirin protein after siRNA

treatment. The results are expressed as the mean ± SEM of two independent experiments (*p<0.05, **p<0.01, using One-way ANOVA). (F) Quantification of E.

Further work will yield insights into the biology of pirin and how it relates to the MRTF/SRF signaling pathway and pro-fibrotic mechanisms. Pirin has been implicated in melanoma cell migration, progression, and senescence[233,235,246], but has not been explored in terms of fibrotic disease. This is the first report implicating pirin in a pro-fibrotic signaling pathway, so dissecting the exact role of pirin in TGF-β mechanisms will be an important question to address in the future. Also, while pirin is clearly a target for the 222740-series of compounds, these results do not prove that pirin is the target that elicits the series' antifibrotic activity. Additional experiments to tie pirin and our series are currently underway, and validation efforts for other proteins identified from our pull-down studies may be performed to identify other relevant biological targets. Moreover, additional target identification designs and experiments that could produce alternative lists of protein candidates are discussed in Chapter 5.

Chapter 3: 58150 Series Further SAR Development and Anti-Fibrotic Properties

Parts of Chapter 3 are included in a submitted manuscript entitled "5-Aryl-1,3,4-oxadiazol-2-ylthioalkanoic Acids: A Highly Potent New Class of Inhibitors of Rho-Mediated Gene Transcription as Potential Antifibrotic Agents for Scleroderma" by Kahl et al.

SAR Development—pM Activity:

As discussed in Chapter 2, there is strong evidence that the 58150-series of Rho/MRTF/SRF-mediated gene transcription inhibitors proceed through a covalent mechanism with the unknown biological target. In summary, this evidence includes: the (1) requirement of the oxadiazole core (2) complete loss of potency with analogs predicted to be much less capable of reacting with a binding site nucleophile (3) steep SAR for alkanoic acid chain and (4) tight SAR for the substituents surrounding the phenyl ring. Also, all analogs tested were unable to affect cell proliferation/viability up to 100 μM as measured by WST-1, highlighting the series lack of cytotoxicity at high concentrations despite extremely potent cellular activity. In this chapter, I will focus on the development of highly potent compounds guided by cellular SRE.L activity, and the attempts to improve the *in vivo* pharmacokinetic (PK) profile for pre-clinical testing in murine models of fibrosis.

In Chapter 2, a general Topliss approach to probe the SAR surrounding the aromatic ring of the 58150 series is briefly discussed; additional aromatic ring SAR for the propanoic acid scaffold is shown in Table 7. *Ortho*-Cl (**A14**) is clearly preferred over any other substitution introduced at the R_2 position, *meta*-Me (**58146**) for R_3, and *para*-Me (**A10**) for R_4. Out of these positions, substitution at the *para* position appears to be the most well-tolerated regardless of the size or electronics of the substituent. Generally, size doesn't appear to contribute as heavily

as electronic effects at the *ortho* (e.g. **A14** vs. **A15** & **A16**), *meta* (**58146** vs. **A12** & **A13**), or *para* (**A10** vs. **A9** & **A11**) positions; although, size can play a role (e.g. **A63** vs. **A14**), which is further expounded in Table 8. Generally, improvements in activity from combining the top substitution patterns are additive, with the biggest exceptions of this being the 2,6-dihalo analogs **A66** & **A67**. Interestingly, even combining substitutions that weren't noteworthy mono-substituents (e.g. **A45** vs. **A16** or **A68** vs. **A15** & **A11**) led to significant improvements in activity.

At the *para* position, an additive activity boost is achieved by combining *ortho*-Cl with any type of substituent at the *para*-position (**58150**-**A70**). Moreover, a clear size correlation with the *ortho*-Cl/R^4 substitution pattern is present: bulky *para* substituents improve SRE.L activity regardless of electronic effects (**A69** < **58150** < **A44** = **A17** < **A70**). This size dependence is consistent with the fact that the *para* position is the most well-tolerated mono-substitution position. Lastly, an amazing additive effect is observed when each of the best aryl mono-substituents (*ortho*-Cl (**A14**), *meta*-Me (**58146**), *para*-Me (**A10**)) is combined into one analog (**A19**), achieving 20 pM SRE.L activity. Of note, the 2, 3, 4-trisubstitution pattern (**A19**) improves SRE.L activity ten-fold more than 2, 4, 5-trisubstitution (**A20** and **A21**), indicating a clear preference for 3-Me over 5-Me.

Table 7: Sub-nM potent propanoic acid analogs

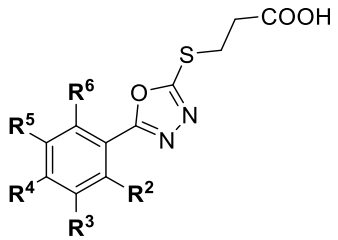

CCG-	Entry	R_2	R_3	R_4	R_5	R_6	SRE.L IC_{50} (nM) [a, b]
123859	**A8**	H	H	H	H	H	3,500
262529	**A63**	F	H	H	H	H	4,200[c]
232700	**A14**	Cl	H	H	H	H	25
232841	**A15**	Me	H	H	H	H	6,300
232740	**A16**	OMe	H	H	H	H	3,100
262528	**A64**	CF_3	H	H	H	H	1,850[c]

123851	**A12**	H	Cl	H	H	H	1,500
123853	**A65**	H	Br	H	H	H	6,400
58146	**-**	H	Me	H	H	H	180
211911	**A13**	H	OMe	H	H	H	3,600
123852	**A9**	H	H	Cl	H	H	340
123862	**A10**	H	H	Me	H	H	34
123855	**A11**	H	H	OMe	H	H	160
262530	**A66**	Cl	H	H	H	Cl	5,400[c]
262527	**A67**	F	H	H	H	F	12,250[c]
215180	**A45**	OMe	H	Cl	H	H	38
215201	**A68**	Me	H	OMe	H	H	23
58150	**-**	Cl	H	Cl	H	H	4.0
232002	**A69**	Cl	H	F	H	H	25[c]
215220	**A44**	Cl	H	OMe	H	H	2.6
232001	**A17**	Cl	H	Me	H	H	1.5[c]
259068	**A70**	Cl	H	cPr	H	H	0.09[c]
258043	**A19**	Cl	Me	Me	H	H	0.02[c]
258041	**A20**	Cl	H	Me	Me	H	0.23[c]
258021	**A21**	Cl	H	Cl	Me	H	0.32[c]

Italicized CCG numbers were either purchased or synthesized by Kim Hutchings. [a]Inhibition of Gα12-stimulated SRE.L activity (mean of n = 3, SEM < 10%) in PC3 cells unless otherwise noted. [b]Cell viability and proliferation assay with WST-1 < 5% inhibition up to 100 μM inhibitor (mean of n = 3, SEM < 10%). [c]SRE.L assay performed in HEK293T cells (mean of n = 3, SEM < 10%).

As mentioned in Chapter 2, the preferred alkanoic acid chain length separating the S of the thioether and the carboxylic acid functionality is 3 carbons (butanoic acid, Table 3). Therefore, additional butanoic acid 5-Aryl-1,3,4-oxadiazol-2-ylthioalkanoic acid derivatives were made to further investigate the aliphatic SAR of the phenyl ring (Table 8). The preference for *para*-Me over *para*-Cl carried over from the propanoic acid analogs for both mono- and 2, 4-di-substituted butanoic acid analogs (**A71** vs. **A72** and **232120** vs. **A73**, respectively). Generally, bulkier *para*-aliphatic substituents are preferred (**A73** < **A75** ≈ **232964** ≈ **A79** ≈ **A82** < **A81** ≈ **A83**), which is consistent with the size trend outlined in Table 7. Interestingly, unsaturated substituents are less active than *para*-aliphatic comparators (e.g. **A74** vs. **A75** & **A78** vs. **A79**), and a clear size limit exists, as can be seen with the decrease in activity for **A84**; but even these less active *para* substituents are still fairly well-tolerated.

Again, the *para* position appeared to be preferred over both *meta* and *ortho* positions for bulky aliphatic substituents, as a scan of the 3-, 4-, and 5-positions with cyclopropyl (cPr)

resulted in a strong preference for R^2/R^4-disubstitution (e.g. **232964** vs. **A76** & **A77**). Moreover, *ortho*-Cl does not appear to be required for small or large *para*-aliphatic analogs to maintain potency (e.g. **A72** vs. **A73** & **A80** vs. **A79**, respectively), suggesting bulky alkyl substitution at the *para* position may be required for pM activity but *ortho*-Cl is not. However, from a metabolic standpoint, having the Cl's presence in the phenyl ring is beneficial, so 2-Cl substitution is incorporated in most analogs.

Para-alkoxy analogs that explore both size and electronic effects display a similar trend as *para*-alkyl analogs. Importantly, activity is maintained between alkoxy propanoic acid (**A18**; Table 2) and butanoic acid (**A85**) analogs. Also, pM activity is present for *para*-ethoxy (**A86**) and *para*-isopropoxy (**A89**) derivatives, but a sharp decrease in activity occurs with larger *para*-alkoxy analogs (e.g. **A90**). Since a clear limit in pM potent activity was not established with *para*-alkyl substituents (e.g. **A83**), the decrease in activity for bulky para-alkoxy analogs may be a result of both size and electronic effects. Scanning the *ortho*- and *meta*-positions with a bulky alkoxy substituent—propargyl—revealed an amazing result: *meta* substitution (**A92**) was ~ten-fold more potent than *para* substitution (**A88**), and *six-orders in magnitude* more potent than *ortho* substitution (**A91**). Not only does this indicate a clear disfavor of large substitution at the *ortho* position, but the activity difference for these analogs can be utilized as active and inactive propargyl Click probes for target identification studies (discussed more in Chapter 5).

Another surprising result from the butanoic acid SAR is the difference in trisubstituted analog activity compared to that for the propanoic acid derivatives. For the propanoic acids, *ortho*-Cl, 3-*meta*-Me, *para*-Me substitution (**A19**) was preferred and consistent with mono-substituted analogs (**A14**, **58146**, & **A10**). However, this substitution pattern is clearly disfavored for the butanoic acid derivatives (**A94**), and activity was reduced for the *ortho*-Cl, 5-*meta*-Me, *para*-Me substitution (**A93**) butanoic acid analog compared to the comparator propanoic acid derivative (**A20**). This SAR implies the that a different binding pose is adopted within the unknown biological target for both propanoic and butanoic acid analogs, as altering the carbon

chain length by just one methylene significantly affects activity that is usually controlled by aryl substituents.

The final surprising trend from these SAR studies is the activity achieved with phenolic derivative **A95**. In the mono-substituted propanoic acid derivatives, Cl was the only substituent that had nM levels of activity at the *ortho* position, and Cl was special in that the activity cliff at the *ortho* position didn't appear to be controlled by size or electronics. However, *ortho*-OH substitution is clearly also special since **A95** achieves pM activity. Other phenolic analogs were made but have not been tested yet.

Mouse liver microsome (MLM) analysis for metabolic stability for the butanoic acid analogs was predictable. In general, the 58150 series has an acceptable metabolic stability profile, with both propanoic (**58150**) acid and butanoic (**232120**) acid derivatives having stability greater than 60 mins. Additionally, alkyl substitution on the phenyl ring significantly diminished MLM stability (**A73**, **232964**, and **A86**). This result suggests that while we may be able to achieve potent SRE.L activity with alkyl substitution, this substitution may also be problematic for the series' in vivo PK profile. Efforts to improve metabolic activity while maintaining pM potent inhibition are discussed later in this chapter.

Table 8: Sub-pM potent butanoic acid analogs

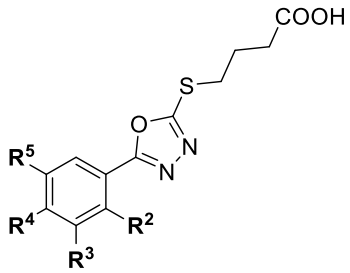

CCG-	Entry	R_2	R_3	R_4	R_5	SRE.L IC_{50} (nM) [a, b]	MLM $T_{1/2}$ (min) [c]
232943	**A71**	H	H	Cl	H	8.6	-
232924	**A72**	H	H	Me	H	0.29	-
232120	**-**	Cl	H	Cl	H	1.8	>60
232922	**A73**	Cl	H	Me	H	0.1	28
262544	**A74**	Cl	H	Vinyl	H	0.71	-

259166	**A75**	Cl	H	Et	H	0.0004	-
259066	**A76**	Cl	cPr	H	H	0.019	-
232964	**-**	Cl	H	cPr	H	0.001	47
259067	**A77**	Cl	H	H	cPr	20	-
259164	**A78**	Cl	H	isopropenyl	H	0.009	-
259165	**A79**	Cl	H	iPr	H	0.0007	-
262458	**A80**	H	H	iPr	H	0.0007	-
259001	**A81**	Cl	H	Pr	H	<0.0001	-
259002	**A82**	Cl	H	n-Bu	H	0.003	-
259003	**A83**	Cl	H	s-Bu	H	0.0001	-
257423	**A84**	Cl	H	Ph	H	7	-
262827	**A85**	Cl	H	OMe	H	2	-
262687	**A86**	Cl	H	OEt	H	0.007	19
262688	**A87**	Cl	H	OPr	H	0.15	-
257274	**A88**	Cl	H	$OCH_2C{\equiv}C$	H	0.02	-
262691	**A89**	Cl	H	OiPr	H	0.007	>60
262689	**A90**	Cl	H	OBu	H	1.2	-
257291	**A91**	$OCH_2C{\equiv}C$	H	Cl	H	7,600	-
257631	**A92**	Cl	$OCH_2C{\equiv}C$	H	H	0.005	-
258042	**A93**	Cl	H	Me	Me	0.4	-
258044	**A94**	Cl	Me	Me	H	4,300	-
257422	**A95**	OH	H	Cl	H	0.002	-
263234	**A96**	Cl	OH	H	H	ND	-
263233	**A51**	Cl	H	OH	H	ND	-

[a]Inhibition of Gα12-stimulated SRE.L (mean of n = 3, SEM < 10%) in HEK293T cells. [b]Cell viability and proliferation assay with WST-1 < 5% inhibition up to 100 μM inhibitor (mean of n = 3, SEM < 10%) up to 100 μM inhibitor. [c]Half-life in mouse liver microsomes.

Synthesis of pM Potent 5-aryl-1,3,4-oxadiazol-2-ylthioalkanoic Acids:

Many analogs from the previous section were synthesized by the route depicted in Scheme 15, which is simplified from Scheme 2 in Chapter 2. Of note, the synthetic route depicting the synthesis for **258021** is also shown in Scheme 2.

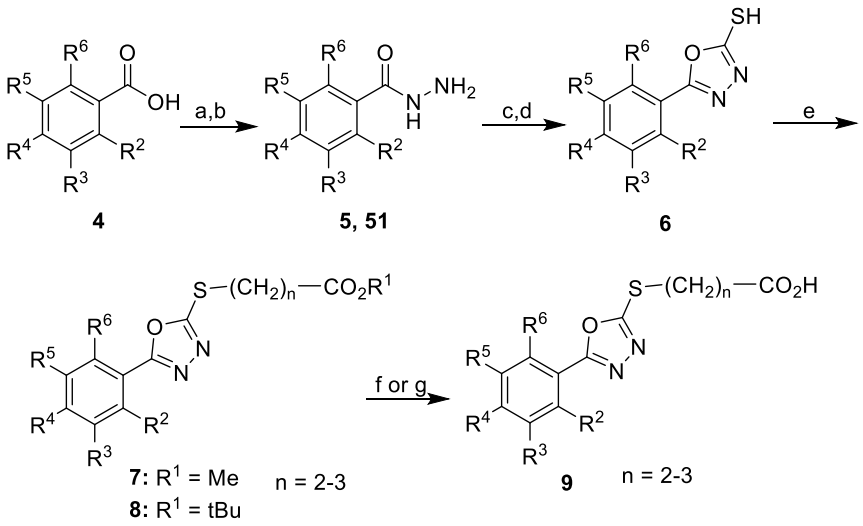

Scheme 15: General synthesis of 5-aryl-1,3,4-oxadiazol-2-ylthioalkanoic acids

Reagents and conditions: (a) H_2SO_4/MeOH, 85 °C 6 hr.; (b) H_2NNH_2, 85 °C 14 hr.; (c) KOH/H_2O/EtOH, CS_2, 95 °C 16 hr., (d) 1N HCl workup; (e) acetone, K_2CO_3, Br-$(CH_2)_n$-CO_2R', 25 °C, 5-24 hr; (f) DCM, TFA, 25 °C 3 hr; (g) 1M NaOH, THF, 25 °C 16 hr.

Alternative routes were required to generate various benzoate ester or hydrazide starting materials (Schemes 16-18). For example, aryl hydrazide **50** was not produced through the typical esterification route depicted in Scheme 15 because the methyl ester was inaccessible using standard Fisher Esterification conditions, so the more reactive acyl chloride **49** was used instead (Scheme 16)

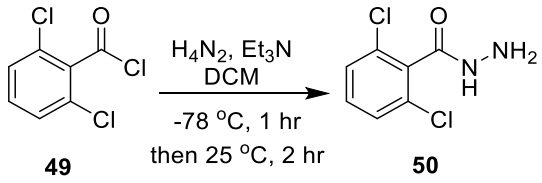

Scheme 16: Synthesis of hydrazide intermediate 50

Bulky alkyl and alkoxy derivatives were synthesized as shown in Scheme 17. Routes to obtain vinyl and isopropyl methyl esters **53a** & **53e** were performed as previously described.[247,248] Suzuki coupling of commercially available **51a-c** with cyclopropyl boronic acid afforded cycloalkyl methyl esters **53b-d**. Alkyl methyl esters **53e-h** were synthesized by alkylating **4k** with two equivalents of LDA and the respective alkyl halide, followed by esterification. 4-Ph methyl ester **53i** was produced using published Suzuki cross-coupling

conditions.[249] 4-alkoxy aryl derivatives **53j-m** were formed by *O*-alkylation of commercially available phenol **52** using cesium carbonate and the respective alkyl halide in DMF. Reduction of vinyl intermediate **53a** with 2-nitrobenzene-1-sulfonyl chloride and hydrazine hydrate afforded ethyl intermediate **53a'**. Using chemistry analogous to Scheme 15, these aryl methyl esters were converted to respective hydrazides, 5-aryl-2-mercapto-1,3,4-oxadiazoles, thioethers, and final carboxylic acids (Table 8).

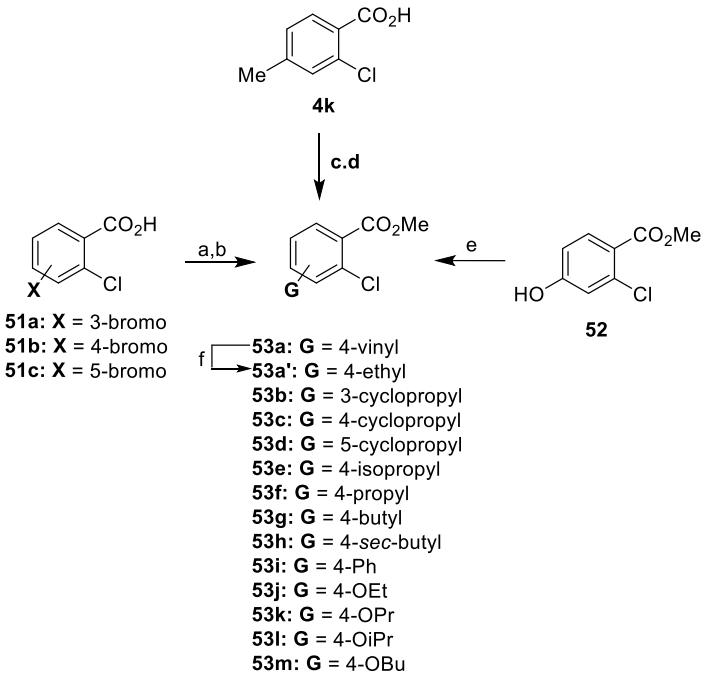

Scheme 17: Synthesis of 53a-53m and 53a'

Reagents and conditions: (a) MeOH, H_2SO_4, 85 °C, 16 hr (b) Pd(II)OAc_2Cl_2, K_3PO_4, $P(Cy)_3$, cyclopropyl boronic acid, toluene, H_2O, 100 °C, 3 hr (c) LDA (2 eq.), THF, 0 °C, 10 min, then alkyl halide, 0 °C, 1 hr (d) MeOH, H_2SO_4, 85 °C, 16 hr (e) alkyl halide, Cs_2CO_3, DMF, 75 °C, 1 hr (f) 2-nitrobenzene-1-sulfonyl chloride, H_2N_4, MeCN, 0 °C to 25 °C, 16 hr.

Similar to chemistry discussed in Scheme 10, *O*-propargyl aryl methyl ester starting materials **4a'** and **55a,b** were accessed by alkylating the respective phenolic methyl esters with propargyl benzenesulfonate and K_2CO_3 in refluxing acetone (Scheme 18). Moreover, phenolic 5-aryl-1,3,4-oxadiazol-2-ylthioalkanoic acids **257422-263233** were synthesized through late stage deprotection as described in Scheme 10 in Chapter 2.

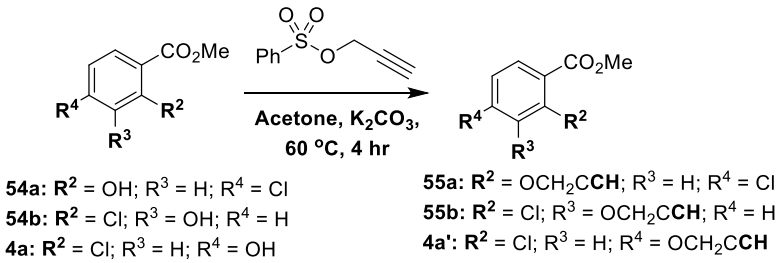

54a: R^2 = OH; R^3 = H; R^4 = Cl
54b: R^2 = Cl; R^3 = OH; R^4 = H
4a: R^2 = Cl; R^3 = H; R^4 = OH

55a: R^2 = $OCH_2C\mathbf{CH}$; R^3 = H; R^4 = Cl
55b: R^2 = Cl; R^3 = $OCH_2C\mathbf{CH}$; R^4 = H
4a': R^2 = Cl; R^3 = H; R^4 = $OCH_2C\mathbf{CH}$

Scheme 18: Synthetic route to produce aryl O-propargyl methyl ester starting materials

In Vivo PK Evaluation of CCG-58150, CCG-232120, and CCG-232964:

Full IV and PO PK analyses were performed on representative analogs **58150**, **232120**, and **232964** (Table 4). Propionic acid **58150** demonstrated good oral bioavailability (67%) and a moderate half-life (2 hr). Rather surprisingly, the corresponding butanoic acid **232120**, despite apparently similar metabolic stability *in vitro*, had inferior *in vivo* PK, with lower oral bioavailability and a clearance rate 3-fold higher than **58150**. Butanoic acid **232964** also had a higher *in vivo* clearance rate, suggesting that the longer alkanoic acid moiety was a primary site of metabolism.

Table 9: Physical and Pharmacokinetic Parameters for Selected Rho/MRTF/SRF Inhibitors

CCG-	SRE. L IC_{50} (nM)	Solubility (uM)[a]	MLM T½ (min)[b]	Route, Dose (mg/kg)	T ½ (hr)	AUC (hr*ng/mL)	Cl (mL/min/kg)	Cmax (ng/mL)	F %
58150	4	682	>60	IV, 15	2.0	47350	5.3	88550	-
				PO, 30	2.0	63170	-	34050	67
232120	1.8	841	>60	IV, 10	1.4	10716	15.5	35650	-
				PO, 20	1.2	11140	-	23150	52
232964	0.0012	>1000[b]	47	IV, 3	1.7	3255	15.4	8140	-
				PO, 3	1.6	361	-	397	11
				PO, 10	1.8	1826	-	1433	17
				PO, 30	2.2	9496	-	10053	29

[a]Thermodynamic solubility analysis was performed by Analiza Inc. using quantitative nitrogen detection. (www.analiza.com). [b]Equilibrium solubility in PBS at 25 °C. [c]Half-life in mouse liver microsomes. PK parameters were estimated using non-compartmental analysis with Phoenix/WINONLIN.

In Vivo Metabolic Identification of CCG-232964:

With the objective of reducing the metabolic susceptibility of **232964** *in vivo* while maintaining SRE.L potency, an *in vivo* metabolic identification study was performed (Figure 40).

The study confirmed that the major routes of oxidation were occurring at the *para*-cyclopropyl substituent and the alkyl carbon chain linking the oxadiazole thioether to the carboxylic acid, and minor amounts of oxidation were occurring on the aromatic ring. Not surprisingly, we also observed conjugation of the carboxylic acid.

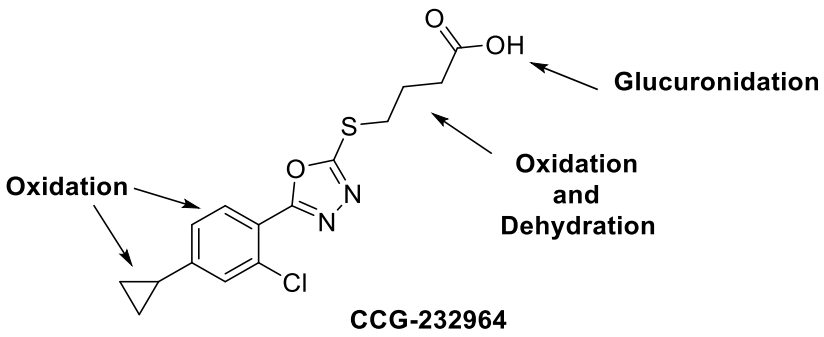

Figure 40: Major sites of metabolism for CCG-232964 *in vivo*

SAR Development—Improving In Vivo PK Profile:

In an attempt to improve metabolic stability and maintain SRE.L activity, fluorinated analogs (Table 10) structurally similar to the pM potent alkyl and alkoxy analogs (Table 8) were designed. We were initially very optimistic about this design since big, hydrophobic aryl substituents produced analogs with sub-pM activity. The trend between SRE.L activity and increasing halogen substituent size is recapitulated (e.g. **232120** and **A97**); but, unfortunately, a complete analysis regarding halogen size and activity cannot be discussed since *para*-F analog **A98** was not tested. Regardless, the *para* position is clearly still preferred for fluorinated analogs (**A100** < **A101** < **A102**), with **A102** achieving an improvement in activity (single digit pM) comparable to improvements observed for bulky alkyl analogs (Table 8). While every fluoro-containing, mono-substituted *para* analog tested (**A103**-**A108**) was well-tolerated regardless of size, no mono-fluoro- or 2-Cl/4-fluoro-containing (**A109-A112**) analog achieved the same level of activity as bulky aliphatic comparators (Table 8). In all, the SAR in Table 10 exemplifies how (1) minute changes to aryl substituents cause huge deviations in activity (2) fluoroalkyl and

fluroalkoxy substituents at R^4 maintain the maximum MLM stability of Cl, and (3) 2-Cl is superior to 2-H.

Table 10: SAR of fluorinated analogs designed to attempt to improve PK profile of aromatic ring

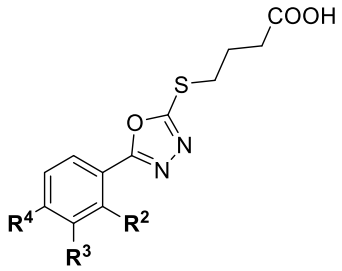

CCG-	Entry	R_2	R_3	R_4	SRE.L IC_{50} (nM)[a, b]	MLM (min)[c]
232120	**-**	Cl	H	Cl	1.8	>60
257389	**A97**	Cl	H	Br	0.002	-
263236	**A98**	Cl	H	F	-	-
262526	**A99**	F	H	H	350	-
232922	**A73**	Cl	H	Me	0.1	28
262525	**A100**	CF_3	H	H	10,000	-
263104	**A101**	Cl	CF_3	H	330	-
257390	**A102**	Cl	H	CF_3	0.0004	>60
263094	**A103**	H	H	CF_3	46	-
263101	**A104**	H	H	CHF_2	160	-
263107	**A105**	H	H	$OCHF_2$	130	-
263103	**A106**	H	H	OCF_3	78	
263100	**A107**	H	H	OCH_2CF_3	240	-
263106	**A108**	H	H	$CF(CH_3)_2$	9.5	-
263105	**A109**	Cl	H	$CF(CH_3)_2$	0.5	-
263097	**A110**	Cl	H	OCF_3	3.6	-
262687	**A86**	Cl	H	OCH_2CH_3	0.0007	19
263095	**A111**	Cl	H	OCH_2CF_3	0.8	>60
263235	**A112**	Cl	OCH_2CF_3	H	-	-

[a]Inhibition of Gα12-stimulated SRE.L (mean of n = 3, SEM < 10%) in HEK293T cells. [b]Cell viability and proliferation assay with WST-1 < 5% inhibition up to 100 μM inhibitor (mean of n = 3, SEM < 10%) up to 100 μM inhibitor. [c]Half-life in mouse liver microsomes.

Next, being guided by the SRE.L activity and MLM stability of **232964**, we considered improving the metabolic stability of the series through bulky cyclic substituents at the *para*-position (Table 11). These analogs exemplified that not all substituents with hydrophobic steric bulk afford pM potency (e.g. **A115**-**A118**); there is clearly a size limit to the *para*-substituent, as already exemplified in Table 8. Moreover, an attempt to create a pro-drug (**A113**) led to a

significant reduction in SRE.L activity, so among the analogs in Tables 10 and 11, **232964** appeared to be optimal.

Table 11: SAR of cyclic analogs designed to attempt to improve PK profile of aromatic ring

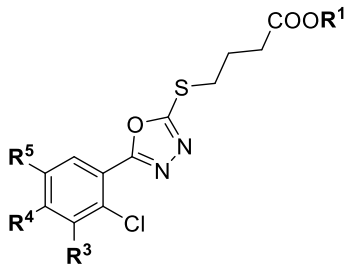

CCG-	Entry	R_3	R_4	R_5	R_1	SRE.L IC_{50} (nM)[a, b]	MLM (min)[c]
232964	**-**	H	cPr	H	H	0.001	>60
263086	**A113**	H	cPr	H	Me	3	ND
262762	**A114**	H	OcPr	H	H	1.3	>60
262690	**A115**	H	OCH_2cPr	H	H	0.11	ND
263096	**A116**	H	*O*-oxetanyl	H	H	370	>60
263098	**A117**	H	*O*-oxetanylmethyl	H	H	35	ND
263099	**A118**	H	*O*-1-methyl oxetanylmethyl	H	H	42	ND

[a]Inhibition of Gα12-stimulated SRE.L (mean of n = 3, SEM < 10%) in HEK293T cells. [b]Cell viability and proliferation assay with WST-1 < 5% inhibition up to 100 μM inhibitor (mean of n = 3, SEM < 10%) up to 100 μM inhibitor. [c]Half-life in mouse liver microsomes.

We then turned our efforts to improving the stability of the propylene linker, which the metabolic ID studies indicated was a major site for metabolism (Figure 40). Our hypothesis was that by substituting (Table 12) or cyclizing (Table 13) the alkyl chain, we could further improve *in vivo* PK stability. However, we were concerned about these analogs maintaining SRE.L activity because, during probe development for target identification (Chapter 2), the chain length SAR was very tight, and we observed complete loss in activity with any appendage attached to the alkyl chain (**A38**-**A119**; Table 12). Not surprisingly, this trend continued with additional attempts to block oxidation α (**A120** & **A121**) or β (**A122**) to the carboxylic acid. These results convinced us that blocking metabolism by attaching appendages to the alkyl chain could not be accomplished without losing SRE.L activity.

Table 12: SAR of substituted linker analogs designed to attempt to improve PK profile of alkyl chain

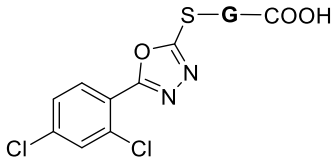

CCG-	Entry	G	SRE.L IC_{50} (nM)[a, b]
58150	**-**	$(CH_2)_2$	2
232120	**-**	$(CH_2)_3$	0.84
257021	**A38**	CH_2CHOMe	>100,000
232961	**A39**	$(CH_2)_2CHOMe$	>100,000
257222	**A119**	$(CH_2)_3CHOMe$	100
257154	**A120**	$(CH_2)_3CHOH$	200[c]
262707	**A121**	$(CH_2)_2C(CH_3)_2$	4,500
262705	**A122**	$CH_2C(cPro)CH_2$	4,500

[a]Inhibition of Gα12-stimulated SRE.L (mean of n = 3, SEM < 10%) in HEK293T cells unless otherwise noted. [b]Cell viability and proliferation assay with WST-1 < 5% inhibition up to 100 μM inhibitor (mean of n = 3, SEM < 10%) up to 100 μM inhibitor. [c]Inhibition of Gα12-stimulated SRE.L (mean of n = 3, SEM < 10%) in PC3 cells.

Alternatively, *cis*-cyclobutyl (**A123**) and *cis*-cyclopentyl (**A125**) chains were well-tolerated in the SRE. L assay, almost being equipotent to the straight chain linker (**232120**). Also, a large difference in SRE.L activity between *cis* and *trans* conformers is present (**A123** vs. **A124** and **A125** vs. **A126**), indicating that a certain sidechain conformation is critical for target binding. More evidence for this hypothesis is that, apart from **A125**, both *cis* and *trans* 5- and 6-membered ring derivatives (**A126**-**A128**) were completely inactive. Additionally, while **A125** maintained good potency, it was four-orders in magnitude more potent than the *trans* conformer **A126**. While a ten-fold improvement in the SRE.L activity was achieved through the combination of the 4-cPr (**232964**) with the *cis*-cyclobutyl linker (**A129**), this same improvement in activity did not translate for the same design with 4-CF_3 (**A131**). Regardless, we were satisfied with the acceptable activity for both **A123** and **A129**, and the preservation between the difference in *cis*/*trans* activity for this subset of analogs.

Table 13: SAR of representative cyclic linker analogs designed to attempt to improve PK profile of alkyl chain

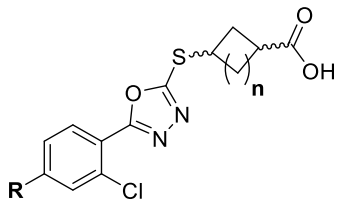

CCG-	Entry	R	n	stereochem	SRE.L IC_{50} (nM)[a, b]	MLM (min)[c]
232120	**-**	Cl	0	N/A	0.84	>60
262588	**A123**	Cl	1	cis	6.4	>60
262587	**A124**	Cl	1	trans	550	ND
263108	**A125**	Cl	2	cis	15	ND
263091	**A126**	Cl	2	trans	>100,000	ND
263092	**A127**	Cl	3	cis	>100,000	ND
263093	**A128**	Cl	3	trans	>100,000	ND
232964	**-**	cPr	0	N/A	0.001	47
263087	**A129**	cPr	1	cis	0.46	>60
263088	**A130**	cPr	1	trans	2.6	ND
263089	**A131**	CF_3	1	cis	42	ND
263090	**A132**	CF_3	1	trans	1000	ND

[a]Inhibition of Gα12-stimulated SRE.L (mean of n = 3, SEM < 10%) in HEK293T cells unless otherwise noted. [b]Cell viability and proliferation assay with WST-1 < 5% inhibition up to 100 μM inhibitor (mean of n = 3, SEM < 10%) up to 100 μM inhibitor. [c]Half-life in mouse liver microsomes.

Synthesis of 5-aryl-1,3,4-oxadiazol-2-ylthioalkanoic Acids with Improved In Vivo PK:

Many 5-aryl-1,3,4-oxadiazol-2-ylthioalkanoic acids discussed in this subsection were synthesized as shown in Scheme 15; however, alternative routes for some analogs were required (Scheme 19-21). For instance, 4-(1-fluoro)-isopropyl methyl esters **57a,b** were synthesized from **56a,b** by Grignard reaction with acetone followed by fluorination of the tertiary alcohol with DAST (Scheme 19). Also, trifluoromethoxy benzoic acid **59** was produced from aryl halide **58** using lithiation/carboxylation chemistry.

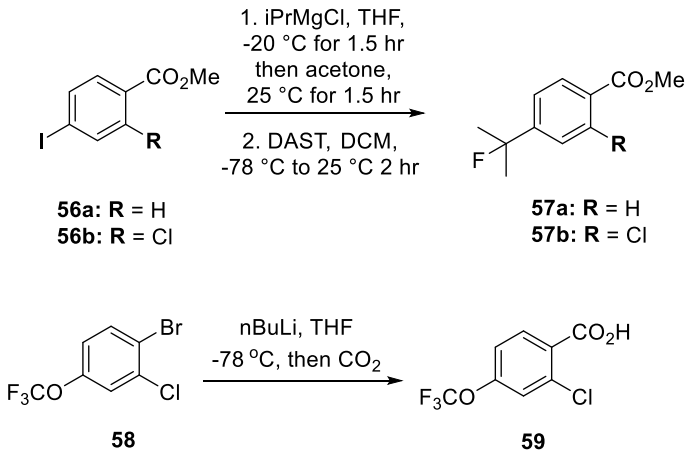

Scheme 19: Synthesis of 57a,b and 59

4-alkoxy aryl intermediates were formed by *O*-alkylation of respective phenolic compounds using various alkylating agents, bases, solvents, and temperatures (Scheme 20). The alkylation conditions that worked well with the alkoxy derivatives displayed in Scheme 17 were attempted for all intermediates shown in Scheme 20; however, the only successful coupling with these conditions for these analogs was using cyclopropylmethoxy intermediate **8a**. The remaining intermediates mainly didn't react under these conditions, but alternative routes were found. For example, the syntheses for 1-trifluorethoxy aryl methyl esters **62a,b** and *O*-oxetanyl methyl ester **62c** were accomplished with their respective alkyl halides and Cs_2CO_3 in DMSO. Surprisingly, 1-bromocyclopropane did not react in alkylation conditions with DMF, and it appeared to decompose per HPLC, but carboxylic acid intermediate **63** was eventually formed from phenolic aryl methyl ester **52** in DMA at 155 °C using Cs_2CO_3 as the base. Finally, *O*-oxytanylmethyl and *O*-1-methyloxetanylmethyl methyl ester intermediates **65a,b** were generated from the respective freshly prepared oxetanylmethyl methanesulfonate alkylating agents (**64a,b**) in DMF with K_2CO_3 as the base.[250]

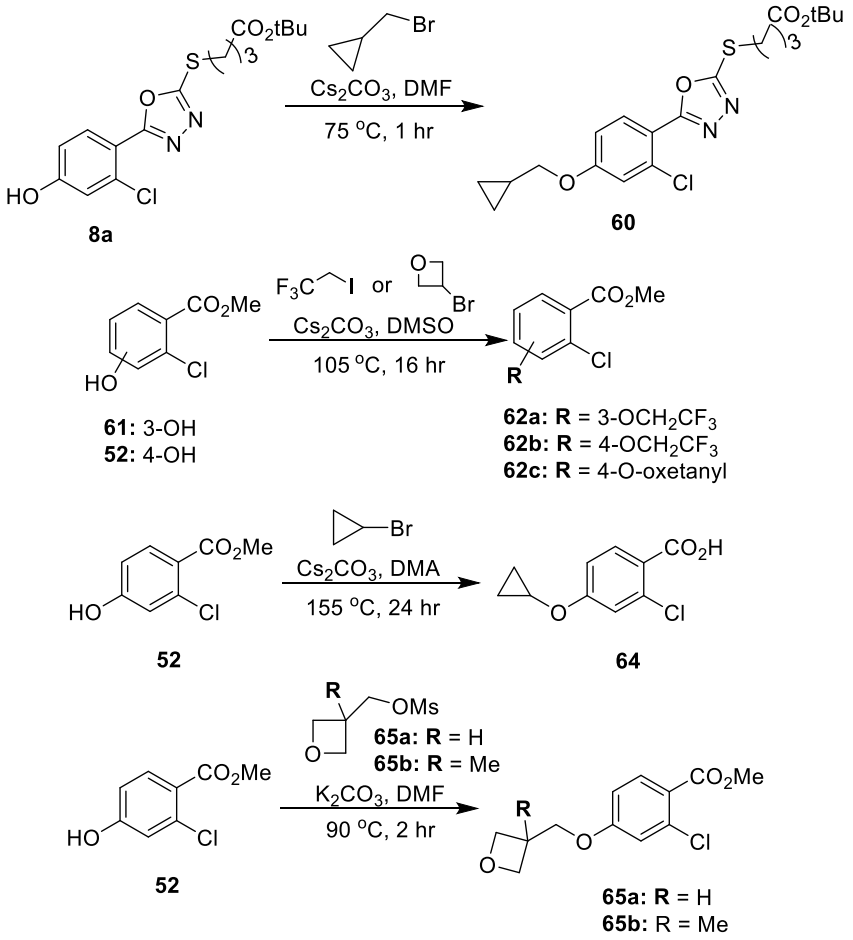

Scheme 20: Synthesis of intermediates 60-65a,b

The *cis* and *trans* cyclobutane, cyclopentane, and cyclohexane analogs were synthesized by base-catalyzed alkylation of **1**, **66a,b** with the appropriate cycloalklyl chloride or mesylate (**67a,b**) [251] (Scheme 21). The resulting esters were hydrolyzed under basic conditions without epimerization to afford cyclobutylalkonic acid analogs.

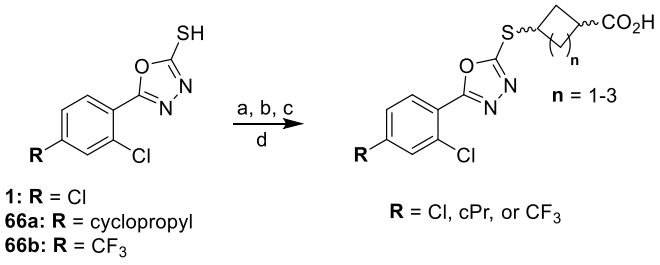

Scheme 21: Synthesis of cyclobutane, cyclopentane, and cyclohexane analogs

Reagents and conditions: (a) *cis*/*trans*-methyl 3-chlorocyclobutanecarboxylate, Cs_2CO_3, NaI, DMSO, 100 °C, 40 hr (b) *cis*/*trans*-methyl 3-((methylsulfonyl)oxy)cyclopentanecarboxylate (**67a**), NaH, THF, 50 °C, 16

hr (c) *cis*/*trans*-ethyl 4-((methylsulfonyl)oxy)cyclohexanecarboxylate (**67b**), Cs_2CO_3, DMSO, 100 °C, 72 hr (d) 1M NaOH, THF, 25 °C, 1-24 hr.

In Vivo PK Evaluation of CCG-262588:

To determine how much cyclizing the alkyl chain improves *in vivo* PK profile for the series, we compared 2,4-dichloro-*cis*-cyclobuytyl analog **A123** with homologous acyclic butanoic acid **232120** (Table 14). The PK profile of **A123** was significantly improved, having 2-fold better *in vivo* half-life and nearly 5-fold better plasma exposure than acyclic **232120**. Unfortunately, even though **A123** had an estimated 10-fold better exposure than **232964** (Table 9), this was not enough to overcome the vastly superior (over 1000-fold) potency of **232964**. Assuming 2-cPr-4-chloro-*cis*-cyclobuytyl analog **A129** would have a similar, if not worse, PK profile than **A123** (based on comparison of the *in vivo* PK profiles of **232120** and **232964** (Table 9)), we elected to not obtain *in vivo* PK for **A129**. Also, by the time **A129** was synthesized and tested, we had already obtained a large amount of *in vivo* PK data for **232964**, and gram quantities of **232964** were already made for *in vivo* testing, so we decided to advance **58150** and **232964** into *in vitro* and *in vivo* models of efficacy.

Table 14: Pharmacokinetic parameters of 232120 vs. 262588 in plasma following PO administration

CCG-	Entry	SRE. L IC_{50} (nM)	MLM T½ (min)[a]	Route, Dose (mg/kg)	$T_{1/2}$ (hr)	AUCINF (hr*ng/mL)	Cl (mL/min/kg)	Cmax (ng/mL)
232120	**-**	1.8	>60	PO, 20	1.2	11140	30	23150
262588	**A123**	6.4	>60	PO, 20	2.6	50146	6.7	13600

[a]Half-life during incubation with mouse liver microsomes.

Inhibition of LPA Induced CTGF Expression In Vitro by CCG-58150 and CCG-232964:

To assess effects on pro-fibrotic gene expression, primary human dermal fibroblasts were pre-treated with **58150** or **232964** for 48 or 72 hours (Figure 41). After the pre-incubation, cells were stimulated with LPA—a direct activator or the Rho pathway through Gα12/13[252]—for 1 hour. Interestingly, after 48 hours, neither **58150** nor **232964** had any significant effect on

CTGF gene expression; however, after 72 hours, both inhibitors dose-dependently reduced CTGF gene expression, with **232964** being ~100x more potent than **58150**.

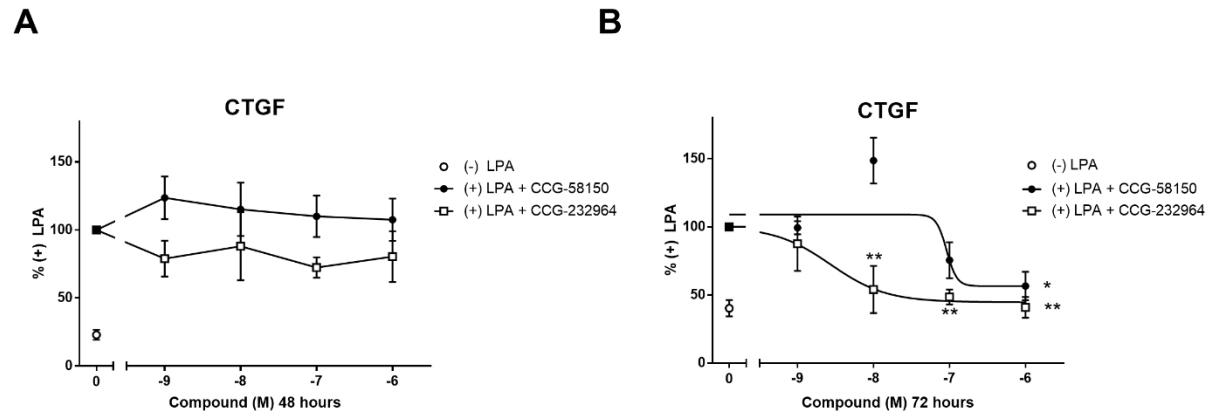

Figure 41: CCG-58150 and CCG-232964 Inhibit LPA induced CTGF gene expression

Primary dermal fibroblasts from healthy donors were pre-treated with varying concentrations of CCG-58150 and CCG-232964 for 48 hours (A) or 72 hours (B) and stimulated with 1 μM LPA for 1 hour. CTGF mRNA levels were measured by qPCR. Results are expressed as the mean ± SEM. *p<0.05, **p<0.01 vs DMSO control using One-way ANOVA; n>3.

Murine Bleomycin Prevention Study with CCG-58150 and CCG-232964:

We selected a mouse model of dermal fibrosis that entails inhibition of dermal thickening induced by bleomycin as our preliminary measure of *in vivo* efficacy of **58150** and **232964**. This model has been well-described in the literature[159,253,254] and entails daily intracutaneous injections of bleomycin with concurrent treatment by drug or vehicle for 14 days. At the end of the dosing period, the mice are sacrificed and sections of skin at the injection site are excised and analyzed for dermal thickness and hydroxyproline—a major component of collagen and an accepted biomarker for collagen content.[255]

Based on the high C_{max} achieved in the mouse PK study for **58150** (30 mg/kg PO dosing (107 μM) relative to the SRE.L IC_{50} (4 nM)), we selected three lower doses for **58150** (0.1, 1 and 10 mg/kg/day) by oral gavage during bleomycin treatment. **58150** was able to dose-dependently reduce both measures of bleomycin-induced fibrotic effects (dermal thickness and

hydroxyproline content), having significant effects at 10 mg/kg vs bleomycin/vehicle control (Figure 42A and 42B). In a subsequent study, two doses were selected for the more potent but less bioavailable compound **232964** (3 and 10 mg/kg PO). The lower dose was calculated based on the single dose oral PK data (Table 9) to achieve comparable plasma AUC: SRE.L IC_{50} ratio as the efficacious 10 mg/kg dose of **58150**. At the conclusion of this study, **232964** significantly reduced bleomycin-induced dermal fibrosis at both doses, indicating that it is at least 3-fold more potent than **58150** *in vivo* (Figure 42C-E). The ability of **232964** to prevent dermal skin thickening and maintain hydroxyproline levels at nearly baseline-control levels highlights the antifibrotic potential of this novel series.

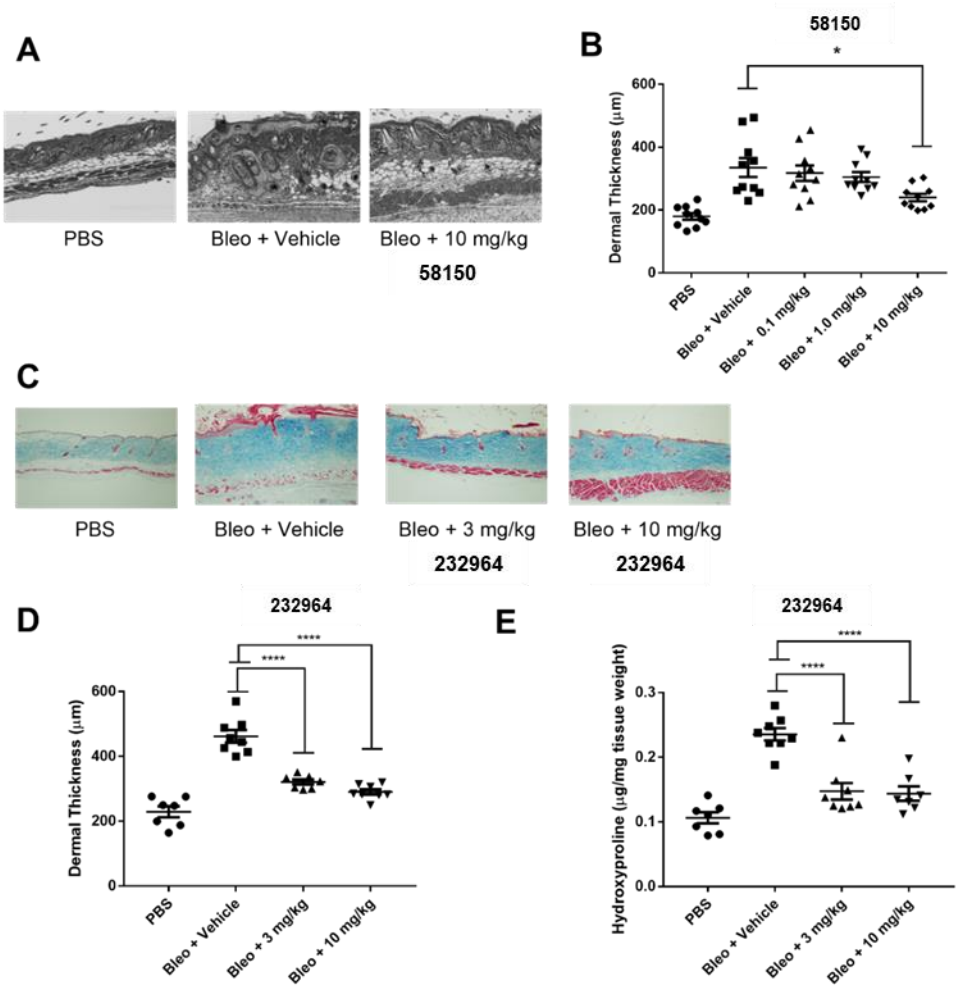

Figure 42: 5-Aryl-1,3,4-oxadiazol-2-ylthioalkanoic acids prevent bleomycin-induced dermal fibrosis

Mice treated with inhibitors displayed significantly reduced skin thickness and collagen content as compared to vehicle control (A) Masson's trichrome stained skin sections from PBS (left panel), Bleomycin + Vehicle control (middle panel), and Bleomycin +10 mg/kg **58150** (right panel). N=10 per group (B) Quantification of A, by measuring the distance between the subcutaneous fat and the epidermis. *, $p<0.05$ by using One-way ANOVA (C) Masson's trichrome stained skin sections for PBS (left panel), Bleomycin+Vehicle (middle left panel), Bleomycin +3 mg/kg **232964** (middle right panel) or Bleomcyin +10 mg/kg **232964** (right panel). N=7 per group (D) Quantification of C. ****, $p<0.0001$, using One-way ANOVA. (E) Quantification of collagen content by hydroxyproline measurement. ****, $p<0.0001$, using One-way ANOVA.

Conclusion:

A novel and highly potent series of inhibitors of Rho/MRTF/SRF-mediated gene transcription was developed. The hit—CCG-58146—was discovered during our previously reported phenotypic HTS utilizing a SRE.L expression readout. We systematically explored modifications to the heterocyclic core, the aromatic ring at C-5, and the alkanoic acid sidechain. During this process we observed extremely tight SAR and multiple activity cliffs. We ultimately achieved an astonishing 150,000-fold improvement in SRE.L activity while progressing from hit **58146** (IC_{50} = 180 nM) to lead **232964** (IC_{50} = 0.0012 nM). This is likely the result of both an extremely well-defined binding site on the currently unknown molecular target as well as the hypothesized availability of a covalent mode of binding. Selected inhibitors **58150** and **232964** were able to reduce expression of the pro-fibrotic gene CTGF in LPA-stimulated fibroblasts. In improving the series' activity, we were also able to generate inhibitors with acceptable PK profiles for *in vivo* studies. The potent and dose-dependent anti-fibrotic effects displayed by both **58150** and **232964** provide an introduction to orally efficacious 5-aryl-1,3,4-oxadiazol-2-ylthioalkanoic acid Rho/MRTF/SRF-mediate gene transcription inhibitors for potentially treating fibrotic diseases. Prior to further development of these inhibitors as anti-fibrotic agents, identification of the biological target(s) as well as clarification of the novel covalent mechanism of action should be accomplished (Discussed in Chapter 5).

Chapter 4: 222740 Series Structure-Based Drug Design with Pirin

Co-Crystal Structure Comparison:

Since we had strong evidence that pirin is a biological target for the 222740-series (Chapter 2), we attempted to improve SRE.L activity using a structure-based drug design (SBDD) approach utilizing the pirin co-crystal structures for CCT251236, CCG-222740 (Figure 38D,E, 1.7 Å), & CCG-257081 (Figure 43, 1.5 Å). Unfortunately, the natural ligand that modulates pirin's biological activity is currently unknown. Therefore, since the evidence suggests pirin may adopt multiple binding orientations to accomplish its biological activity[223,240,256,257], we hoped that improvements to SRE.L activity for the 222740-series would be achieved by designing inhibitors that bound to pirin in a similar manner as CCT251236.

Secondarily, we hoped that our SBDD efforts would help validate pirin as a target for the 222740-series. Prior to obtaining the co-crystal structures for CCG-222740 and CCG-257081, we reasoned that if the SAR trends reported by Cheeseman et al could be mimicked by SRE.L SAR trends for 222740-series analogs that combined certain aspects of the CCT251236 scaffold, then we would have more evidence that pirin is a biological target for the 222740-series. However, since we did not have a reliable binding assay to directly determine exactly how structural changes affect binding to pirin, we knew we would have to take pharmacodynamic properties (e.g. solubility, ClogP, etc.) into consideration during our design, complicating the SBDD analysis. Cheeseman et al do report a SPR binding assay for pirin, and the Neubig lab has been attempting to set this assay up, but no reliable, high-throughput data has been produced to date. So, all SBDD efforts discussed in this chapter were heavily guided by cellular SRE.L activities.

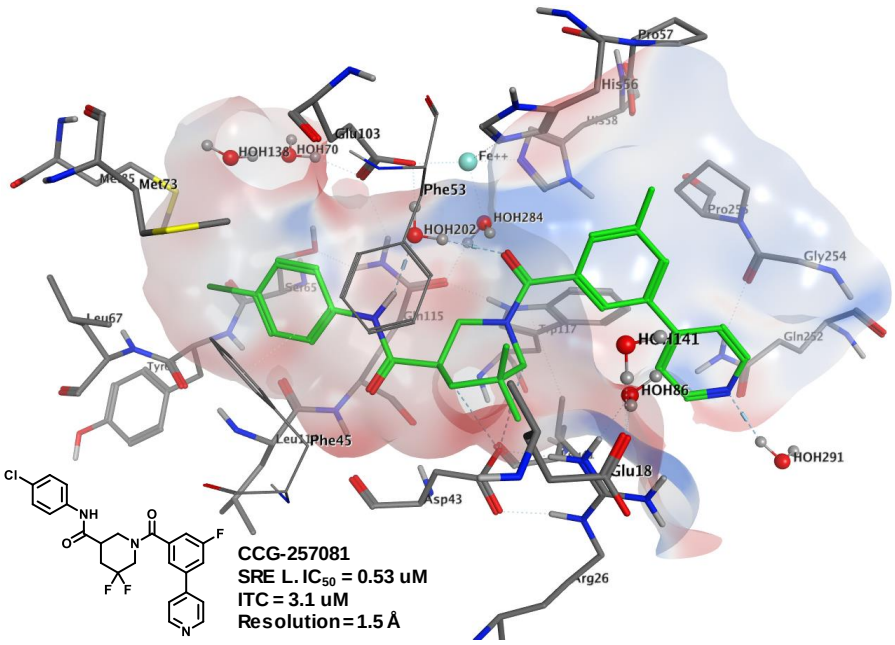

Figure 43: Co-crystal structure of CCG-257081:

Co-crystal structure of CCG-257081 (green) bound to pirin in the R-conformation (1.5 Å). Blue shading indicates H-bond donating regions and red shading indicates H-bond accepting regions. White regions indicate non-polar residues.

Likely due to their structural similarities, the CCG-222740 series (e.g. CCG-257081) and CCT251236 bind to pirin very similarly to each other (Figure 44). Obvious similarities in the binding poses are: (1) the aromatic rings of both series occupy similar space deep within pirin's lipophilic pocket and (2) both series have comparable H-bonding interactions between the water molecule bound to pirin's Fe core and each inhibitor's bis-amide core. Interestingly, CCT251236 establishes two additional H-bonding interactions with Asp43 and Glu18 in a highly ordered orientation, perhaps accounting for its high binding affinity (Kd, ~20 nM). Also, in the CCT251236 co-crystal structure, Glu18 is significantly shifted to engage in a H-bonding interaction with the amide N-H of the inhibitor; CCG-222740 or CCG-257081 cannot engage in this type of H-bonding interaction because they lack amide N-H's in this region. Also, CCT251236 may have higher affinity to pirin than our series because of a potentially critical π-π stacking interaction between CCT251236's phenyl core and Phe 45 & 53 (Figures 43 & 44). Of note, the pyrrolidine appendage on CCT-251238 was implemented by Cheeseman et al to

improve the poor solubility of the series, and it is projecting into solvent and presumably does not interact with pirin; hence, this moiety is not resolved in the co-crystal structure.

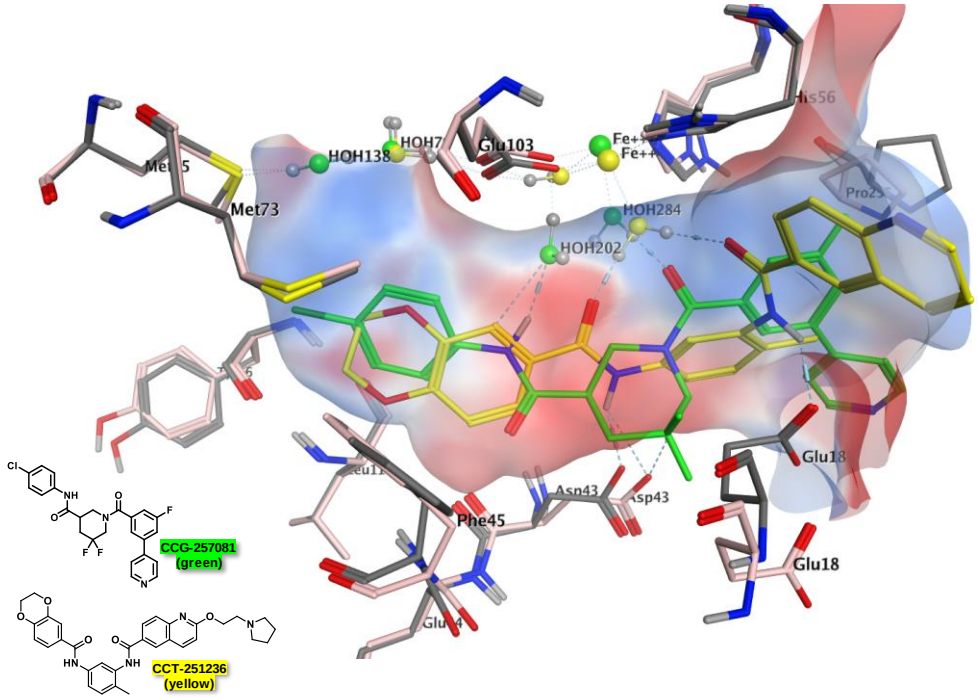

Figure 44: Overlay of the CCG-257081 and CCT251236 co-crystal structures

Overlay of the CCG-257081 (green) and CCT251236 (yellow; PDB 5JCT) co-crystal structures. Residues belonging to the CCG-257081 co-crystal structure are displayed in pink, while the residues for the CCT251236 co-crystal structure are shown in grey. Blue shading indicates H-bond donating regions and red shading indicates H-bond accepting regions. White regions indicate non-polar residues.

CCG-222740/CCT251236 Hybrid Analogs:

First, we attempted to integrate the CCG-222740 series scaffold with key pharmacophores reported by Cheeseman et al that afforded CCT251236's tight binding with pirin (Figure 45).[240] These key pharmacophores consisted of: (1) the aromatic core (green) (2) the presence of two, secondary amides (pink) (3) the aromatic dioxane pendant (blue). Of note, all analogs tested for this series are compared to the activity of **222740** because of the high level of variability in SRE.L activity between experimental batches. Hybrid analog **263154** integrated CCT251236's aryl bis amide core with **222740**'s flanking aryl pendants, and it had roughly the same SRE.L activity as **222740**. We were not surprised **263154** did not acquire the

same level of activity as CCT251236 because Cheeseman et al reported very tight SAR around the dioxane aryl functionality of CCT251236; however, this result did further suggest that even if the bis-amide core of CCT251236 is critical for tight binding, the pendants flanking the core may be equally as important. Interestingly, all attempts to synthesize a hybrid analog lacking the methyl group within the aryl core were unsuccessful (not shown), and these failed syntheses suggest that the amide α to the methyl group is highly susceptible to hydrolysis, even when in weak base, without the methyl present.

Switching the orientation of one of the amides did not improve activity (**A133** vs **A134**), and removal of the aromatic methyl with this bis-amide configuration (**A135** & **A136**), which produced analogs no longer susceptible to hydrolysis, also did not lead to an improvement in activity. However, the 100-fold difference in activity between **A135** and **A134** indicates a clear conformational preference for the methyl imbedded within the aryl core. These results not only suggest that, with the correct aromatic pendants, alternative amide orientations might provide high levels of affinity to pirin, but this activity is likely dependent on how the bis-amide and the flanking aryl pendants are oriented, which is likely directed by the methyl within the aryl core. However, since the goal of these analogs was to investigate the SAR of CCT251236's bis-amide core, we looked to explore the effects of the aryl dioxane pendant.

Cheeseman et al reported an interesting SAR trend with the CCT251236 scaffold: when the dioxarine ring system was replaced with mono- or di-methoxy pendants or migrated from the 3,4-position, the ligand lost all affinity for pirin. We were able to recapitulate this result with **222740**'s central bis-amide core. While less potent than **222740**, dioxirane rings attached to either aryl ring (e.g. **A137** & **A138**) were significantly more active than homologous di-methoxy analogs (**A139** & **A140**), mirroring the SAR trend reported by Cheeseman et al. While we were excited by this SAR trend, the lack of activity comparable to CCT251236 for this initial set of hybrid compounds suggests there are additional interactions needed to improve the SRE.L activity for the **222740** series to the range of potency achieved by CCT251236. While we

wanted the published SAR for CCT251236 to guide our improvements in SRE.L activity for the 222740-series, we wanted to remain within the limits of novel IP, so we focused our design on docking analogs from the **222740** series into the CCT251236 co-crystal structure 5JCT (*vide infra*).

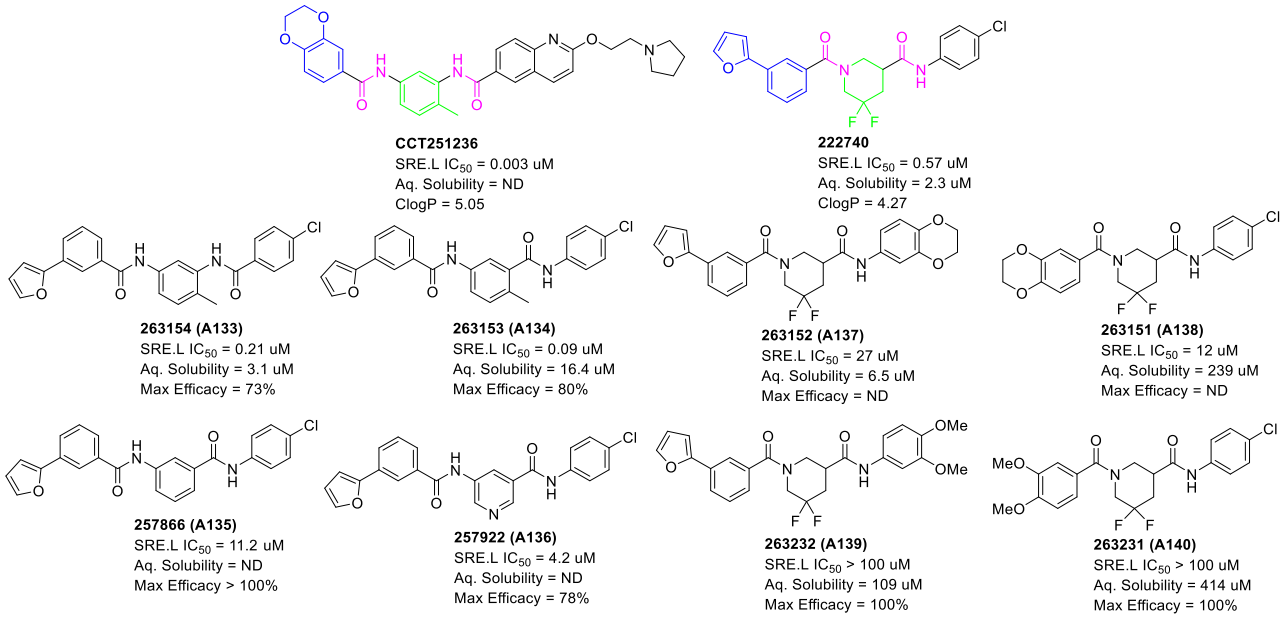

Figure 45: CCT251236/CCG-222740 hybrid analogs and activity in HEK-293T cells

Hybrid Analog Synthesis:

The synthetic route for many **222740** analogs was accomplished using the three routes depicted in Scheme 22. Starting from the piperidine carboxylic acid **33** or ester **34**, a series of HATU-mediated amide couplings and deprotections were used to produce bis-amide analogs. For example, similar to Route 1 in Scheme 11, the scaffolding is built from right to left in Route 1 (Scheme 22), introducing the aniline coupling partner first and the furan-2-yl benzoic acid last; the same right-to-left construction is depicted in Route 2 but 4-chloroaniline is kept constant and the benzoic acid piece is derivatized; analogs were also assembled from left to right, as shown in Route 3, generating a late stage carboxylic acid intermediate that was subjected to HATU-mediated amide coupling conditions to quickly produce bis-amide analogs. The preferred amide

coupling conditions consisted of HATU, DIPEA, and DMF at room temperature, and reactions were generally left overnight.

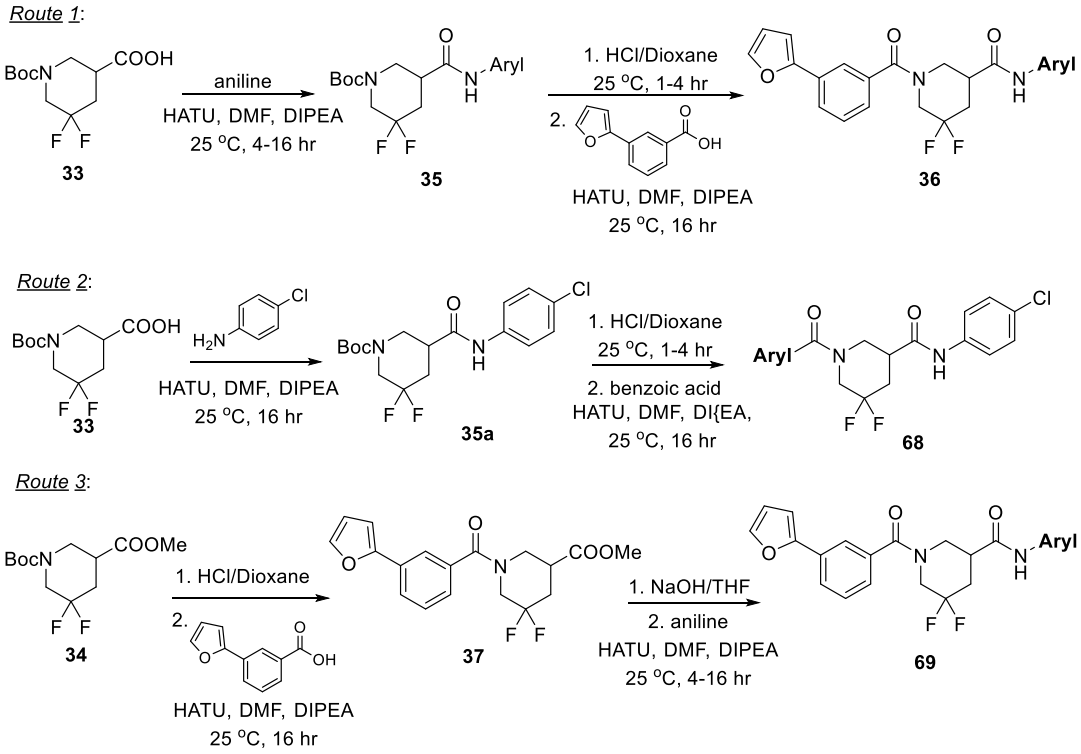

Scheme 22: Three general routes used to produce 222740 analogs

A similar sequence of amide couplings and deprotections afforded bis-amides with aromatic cores (Scheme 23). Depending on the available starting materials, the bis-amides were assembled starting from either the left or the right side of the core. In order to accelerate the syntheses for analogs **257866** & **257922**, amide couplings were done at 150 °C for 1 hr (Scheme 24).

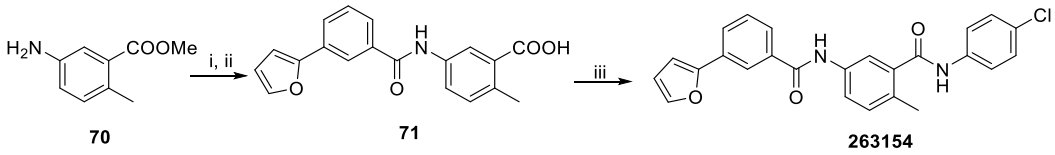

Scheme 23: Synthesis of 263154

(i) 3-(furan-2-yl))benzoic acid, HATU, DIPEA, DMF, 25 °C, 16 hr (ii) 1M NaOH, THF, 45 °C, 1 hr (iii) 4-chloroaniline, HATU, DIPEA, DMF, 25 °C, 16 hr.

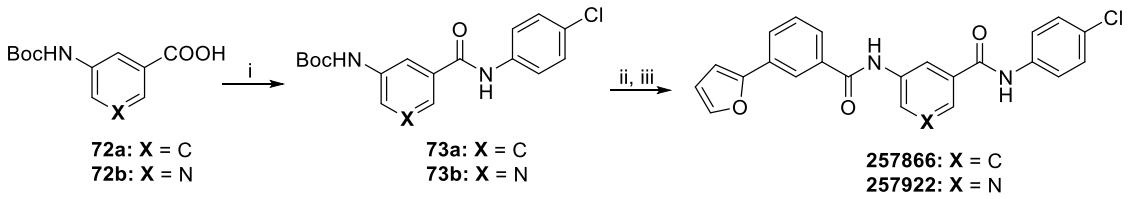

72a: X = C
72b: X = N

73a: X = C
73b: X = N

257866: X = C
257922: X = N

Scheme 24: Synthesis of 257866 and 257922

(i) 4-chloroaniline, HATU, DIPEA, DMF, 25 °C, 1 hr, then 150 °C, 15 min (ii) 4M HCl in dioxanes, 25 °C, 3 hr (iii) 3-(furan-2-yl))benzoic acid, HATU, DIPEA, DMF, 25 °C, 1 hr, then 150 °C, 2 hr.

Docking Studies and SBDD with 5JCT Co-Crystal Structure:

Docking studies were performed by Pil Lee using Molecular Operating Environment (MOE) docking software. We first wanted to find analogs from the 222740 series that mimicked certain interactions CCT251236 made with pirin. In an initial study keeping pirin's residues static, 12 structurally distinct analogs from the 222740-series with varying SRE.L activities were docked into the 5JCT co-crystal structure published by the Cheeseman group (Figure 46). Structural differences across the selected 222740 analogs included: small and large appendages on each aryl ring (**A141**-**A143**, **A57**, **A145**), an unsaturated bis-amide core (**A144**), and indole-containing aryl pendants that had diverse activities (**A146**-**A150**) (Figure 46). We hoped that we would see a trend in the binding modes for active vs. inactive analogs that we could utilize for our SBDD.

Of note, propargyl analogs **A141**-**A143** were originally made in parallel to the ethoxymethoxy probe mimics discussed in Chapter 2. The original rationale to make these analogs was to make propargyl Click probes with a range of SRE.L activity for target identification studies. While these analogs did not achieve significant differences in activity, they had large pendants that maintained activity compared to **222740**, and so we were interested in using them for docking to see how these analogs interacted with pirin.

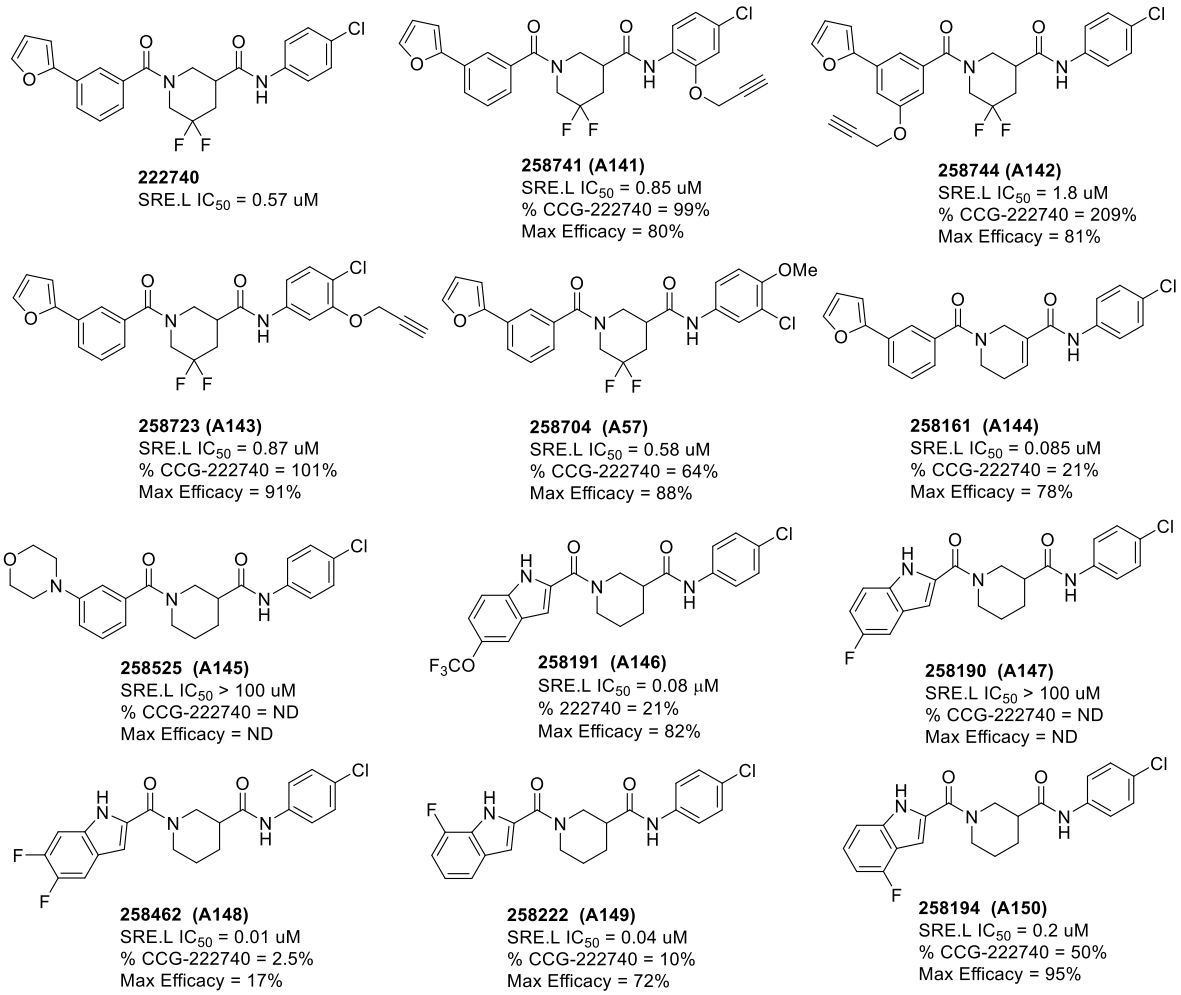

Figure 46: The first set of structurally diverse analogs with varying SRE.L activities docked into a co-crystal structure (PDB 5JCT) of CCT251236 and pirin.

Unfortunately, compared to the co-crystal structures for CCG-222740 and CCG-257081, many of the docked analogs had completely flipped binding modes amongst the 5 highest scoring poses generated. This phenomenon complicated the analysis of which structural changes were important in the next SBDD analogs because we couldn't be certain that changes in SRE.L activity were due to flipped binding modes or not. It should be noted again that the 222740-series, especially analogs containing indole pendants, is notorious for poor solubility and having somewhat inconsistent SRE.L IC_{50}s and maximum efficacies across experimental batches, so the percent of CCG-222740 IC_{50} for each plate is reported.

Despite the flipped binding mode complication, one of the more potent indoles (CCG-258222, Figure 47) consistently docked in a conformation that provided us with a scaffold that could be manipulated to potentially modulate SRE.L activity with structural alterations. The docking poses for this analog consistently projected the indole ring into pirin's hydrophobic pocket, and the docking suggested the indole N—H and Asp43 could engage in a H-bonding interaction. In fact, we were looking for analogs that could achieve such an interaction since we deduced it may be critical for ligand affinity since the bis-amide/central core of CCT251236 was highly coordinated with Asp43, Glu18, and the water bound to the Fe core.

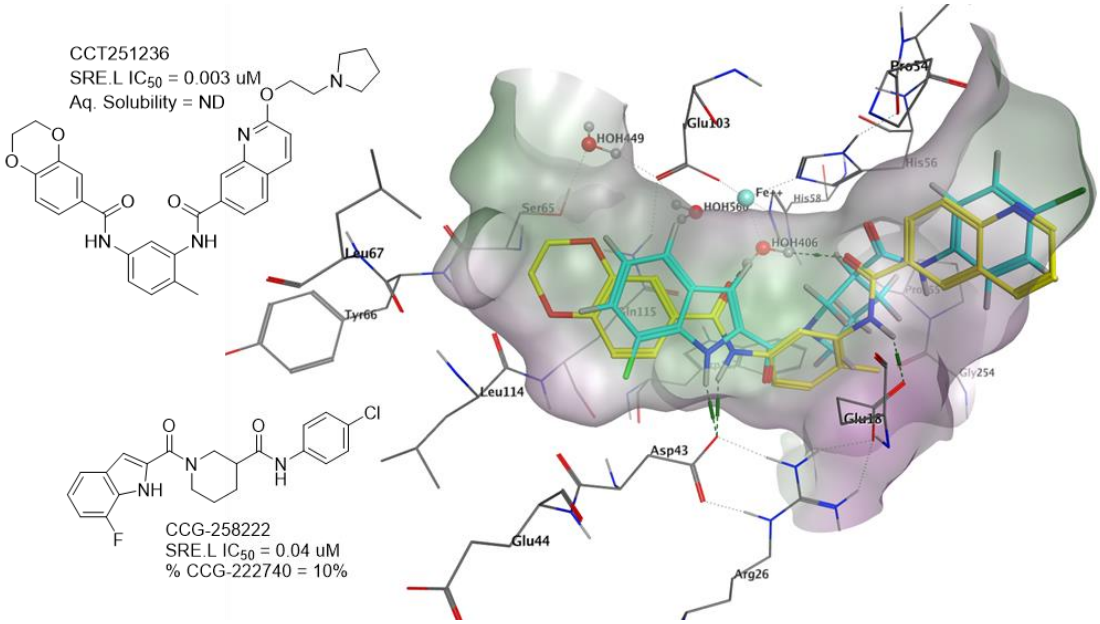

Figure 47: CCG-258222 docked into CCT251236 co-crystal structure (PDB 5JCT)
Key interactions between CCT251236 and pirin appear to be between Asp43, Glu18, and HOH406—Fe, with hydrophobic interactions in the pocket with the aromatic dioxane ring system. CCG-258222 is predicted to be capable of engaging with Asp43 and HOH406.

From this round of docking, ~15 analogs were designed, synthesized, and tested in the SRE.L assay. The goal of these analogs was to not only generate ligands with higher affinity for pirin, but to provide additional evidence that SRE.L activity for the 222740-series occurs through pirin; however, the latter would only be possible with a direct binding assay to correlate with SRE.L. N-1 methyl indole analog **A151** displayed almost a ten-fold reduction in SRE.L activity

compared to **A150** (Table 15), suggesting, as the docking model predicted, the indole nitrogen might be important for pirin binding (Figure 47). Despite this activity difference, this result would be more revealing towards the series working through pirin if these analogs were to be tested in a direct binding assay. Alternatively, the activity difference between the closely related homologs **A153-A155** suggests (1) the hydrophobic pocket can accommodate larger aliphatic groups, albeit these analogs maintained roughly equipotent activity compared to **222740** and (2) 4,5-dioxane (**A155**) is the preferred substitution pattern. However, electronic effects may also play a role since the 4,5-difluoro substituted indole analog **A152** completely lost SRE.L activity.

Investigations to see how other changes to indole-containing analogs would affect activity were also made. Both 5,6-difluoro- and 5-trifluoromethoxy indole substituted bis-amide analogs were used to accomplish this investigation, but since activities were similar between both types of indole substitution, only 5-trifluoromethoxy indole-containing analogs are shown in Table 16. Attempts to improve solubility (in a similar manner as Cheeseman et al utilized for CCT251236) of the indole-containing compounds with **A157** led to significant reductions in SRE.L activities. Attempts to improve solubility with pyridyl substitution was similarly unsuccessful (**A158** & **A159**). Also, while enantiomers **A160** & **A161** did have significant differences in activity, the activity preference for the *R*-conformation is not supported by our docking results because **A149** docked mainly in the *S*-conformation (Figure 47). These enantiomers were docked into the 5JCT co-crystal structure, but no noteworthy differences in binding were observed (not shown)

The analysis of this initial docking study is limited by the lack of a direct binding assay since we cannot be certain whether differences in activity are a result of physicochemical properties or interaction with pirin. Regardless, small changes in activity amongst the analogs designed from this docking model were important for our considerations of potential binding modes the 222740-series could adopt within pirin. Disappointed we didn't observe significant improvements in activity, we moved away from the indole-containing analogs.

Table 15: SAR of analogs from the docking studies with CCT co-crystal structure

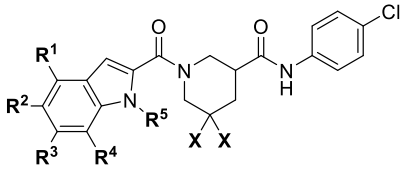

CCG-	Entry	SRE.L IC_{50} (μM)[a]	% 222740 (%)	Max Efficacy (%)	Aq. Solubility (μM)[b]	R^1	R^2	R^3	R^4	R^5	X
258222	**A149**	0.04	10	72	4	H	H	H	F	H	H
257941	**A150**	0.05	13	65	40	H	H	F	H	H	F
263415	**A151**	0.39	70	ND	76	H	H	F	H	Me	F
258462	**A148**	0.01	2.5	17	<2.1	H	F	F	H	H	H
263412	**A152**	>100	ND	ND	112	F	F	H	H	H	F
263481	**A153**	3	304	ND	29	H	H			H	F
263414	**A154**	2	419	80	5	H			H	H	F
263413	**A155**	0.26	73	ND	28			H	H	H	F

[a]Inhibition of Gα12-stimulated SRE.L (mean of n = 3, SEM < 10%) in HEK293T cells unless otherwise noted. [b]Thermodynamic solubility analysis was performed by Analiza Inc. using quantitative nitrogen detection. (www.analiza.com).

Table 16: SAR of 5-trifluoromethoxy indole analogs from the docking studies with CCT co-crystal structure

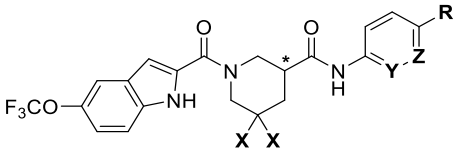

CCG-	Entry	SRE.L IC_{50} (μM)[a]	% 222740 (%)	Max Efficacy (%)	Aq. Solubility (μM)[b]	*	X	Y	Z	R
258191	**A156**	0.08	21	82	8.2	*rac*	H	H	H	Cl
263680	**A157**	37	18,000	100	151	*rac*	F	C	C	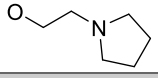
263681	**A158**	0.56	329	100	26	*rac*	F	C	N	Cl
263740	**A159**	2.8	1,670	100	97	*rac*	F	N	C	Cl
263658	**A160**	23	11,500	100	ND	S	H	C	C	Cl
263687	**A161**	0.2	100	100	ND	R	H	C	C	Cl

[a]Inhibition of Gα12-stimulated SRE.L (mean of n = 3, SEM < 10%) in HEK293T cells unless otherwise noted. [b]Thermodynamic solubility analysis was performed by Analiza Inc. using quantitative nitrogen detection. (www.analiza.com).

In an attempt to engage with Asp43 & Glu18, various 5- and 6-membered cycloalkyl bis-amide analogs that could mimic CCT251236's bis-amide core were designed and docked into the 5JCT co-crystal structure using MOE (Figure 48, PR-VC-21-4 shown as example). We were happy to see that the model predicted many of the designed analogs could bind in a similar orientation as CCT251236. Importantly, with various docked analogs, *both* carbonyl groups of the bis-amide system appeared to engage with the water molecule bound to the Fe core, and (sometimes) both N-H groups could engage with the potentially key residues Asp43 & Glu18. Of note, the docking model predicted a flipped binding mode for various designed analogs where the furanyl functionality projected deeper into the hydrophobic pocket than the dioxane ring of CCT251236 (exemplified in Figure 48). Therefore, we thought that if our designed inhibitors could engage with pirin as the docking model suggested, perhaps we could produce a new chemotype of potent pirin ligands.

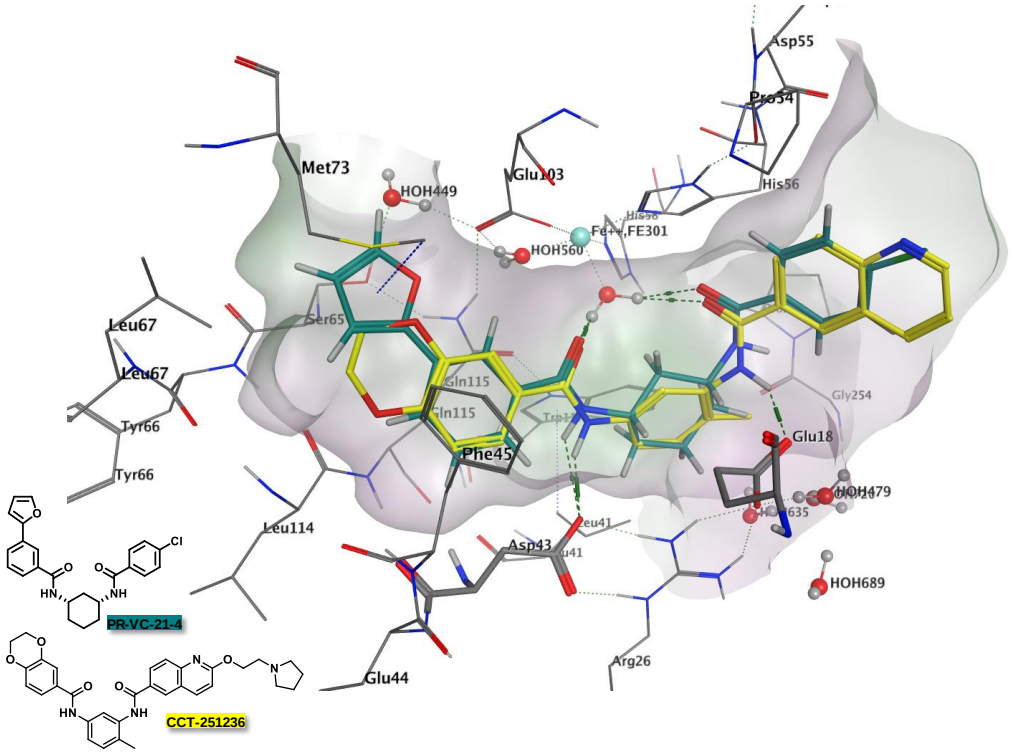

Figure 48: Overlay of an exemplary docking analog and CCT251236 in the co-crystal structure (PDB 5JCT)

Overlay of an exemplary docking analog— PR-VC-21-4 (seafoam)—and CCT251236 (yellow) in the co-crystal structure (PDB 5JCT). Green shading indicates hydrophobic regions and pink shading indicates hydrophilic regions.

Based on these docking results, ~20 five- and six-membered cycloalkyl bis-amide analogs were synthesized (Table 17). Despite many analogs from this subset maintaining activity comparable to **222740**, the results were disappointing since none of these analogs had similar SRE.L activity comparable to CCT251236. Additionally, the analog that was the most potent and structurally most similar to CCT251236 (**A163**, 0.06 µM) had very poor efficacy, likely due to its meager solubility (this analog had very poor solubility, even in DMSO).

Table 17: SAR of representative five- and six-membered ring bis-amide analogs that were designed to attempt to improve affinity for pirin

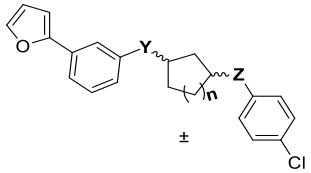

CCG-	Entry	Y	Z	n	Stereochem.	SRE.L IC_{50} (µM)[a]	% 222740 (%)	Max Efficacy (%)	Sol (µM)[b]
263875	**A162**			1	cis	5.8	2,900	100	656
263880	**A163**			2	cis	0.06	30	21	54
263872	**A164**			1	cis	0.47	235	96	93
263876	**A165**			2	cis	0.86	430	100	299
263877	**A166**			1	trans	1.1	550	36	1391
263879	**A167**			2	trans	13	6,500	100	213
263873	**A168**			1	trans	0.35	175	96	13
263878	**A169**			2	trans	1.1	550	100	<1
257942	**A170**			1	cis	0.37	93	100	-
257865	**A171**			2	cis	10	809	100	-

258452	**A172**			1	trans	20	5000	44	-
257863	**A173**			2	trans	4	333	90	-

[a]Inhibition of Gα12-stimulated SRE.L (mean of n = 3, SEM < 10%) in HEK293T cells unless otherwise noted. [b]Thermodynamic solubility analysis was performed by Analiza Inc. using quantitative nitrogen detection. (www.analiza.com).

To circumvent the likely solubility issue of **A163**, I designed and synthesized multiple **A163** analogs containing a pyrrolidine solubilizing group (the solubilizing group that provided Cheeseman et al with the best activity profile for CCT251236) to various locations of the **A163** scaffold (Figure 49). Again, unable to breach even single-digit μM SRE.L activity, the results for these analogs were also disappointing; attaching the solubilizing group to either side of the **A163** bis-amide core (**A174** & **A175**) resulted in an over 200-fold loss of activity vs **222740.** Likewise, an analog that replaced the central bis-amide core of CCT251236 with **A163**'s core (**A176**) was still over 100-fold less active than CCG-222740.

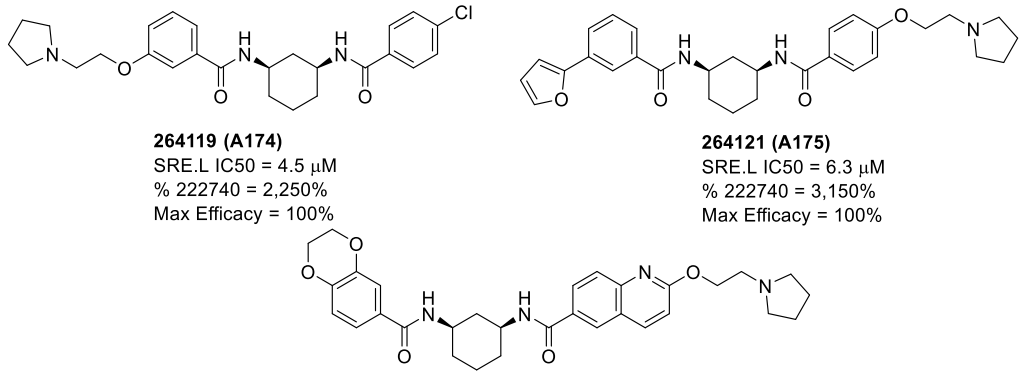

264119 (A174)
SRE.L IC50 = 4.5 μM
% 222740 = 2,250%
Max Efficacy = 100%

264121 (A175)
SRE.L IC50 = 6.3 μM
% 222740 = 3,150%
Max Efficacy = 100%

264120 (A176)
SRE.L IC50 = 2.6 μM
% 222740 = 1,300%
Max Efficacy = 100%

Figure 49: 263880 derived analogs attempting to improve solubility

One potential explanation for these negative results is that pirin may not be able to adopt the conformation, as the docking model suggests (Figure 48), required by either 5- or 6-membered cycloalkyl bis-amide cores to fit the 2-furyl or 4-Cl-aniline aryl functional groups into the hydrophobic pocket. As evidence of this hypothesis, the docking model predicts flipped

binding poses that can accommodate less favorable interactions with pirin (not shown); notably, the highly coordinated H-bonding network is not established by these flipped binding modes. This suggests that if the aryl functional groups cannot fit into the hydrophobic pocket in the best docking poses, the analog will likely not achieve CCT251236 levels of affinity to pirin because the H-bonding network cannot be adopted. Moreover, in support of pirin's selectivity of aromatic pendants that can fit in its hydrophobic pocket, the SAR results reported by Cheeseman et al suggests very tight SAR with small structural changes to CCT251236's pendants located in the hydrophobic pocket.

However, evidence against this explanation is that even when the same CCT251236 pendants were incorporated into the saturated 6-membered ring core (**A176**), activity significantly decreased. Therefore, another possible explanation for these disappointing results is that the bulkier 5- and 6-membered ring systems might prevent the inhibitors from entering the somewhat narrow bridge leading towards pirin's hydrophobic pocket. CCT251236 likely easily slides into this bridge region because of the flatness of the bis-amide core. So, flattening out the 5- or 6-membered ring systems through unsaturation could potentially circumvent this issue. Interestingly, this explanation is consistent with multiple analogs Kim Hutchings made earlier in the project (not shown), which achieved noticeable improvements in activity after flattening out the piperdine core. Nevertheless, efforts were not made to flatten out the 5- and 6-bis-amide core because: (1) flattening out the core makes the analogs more like CCT251236, eliminating the novelty of this design (2) facile synthetic routes weren't found (3) flatter cores would be expected to have worse metabolic stability than the piperidine (4) at the time we got these results, we were following an alternative SAR trend (discussed in the next subsection). However, it would be interesting to know if flattening the ring would afford tighter pirin binding.

Lastly, based on cellular activities alone, we cannot be certain that these analogs do not strongly interact with pirin; perhaps these analogs are incapable of crossing the plasma and/or

nuclear membranes. Pirin SPR data would help us determine whether the 5- or 6-membered ring bis-amide core is a good strategy for designing novel and potent pirin ligands.

Synthesis of Analogs from Docking SBDD:

Propargyloxy aniline (**75a,b**) and benzoic acid (**76**) intermediates were made using the same chemistry with propargyl benzenesulfonate and potassium carbonate to install the propargyl functionality to the respective phenols (Schemes 25 and 26). Protection of nucleophilic functionalities was required to block undesirable side-reactions in refluxing acetone. Deprotection of these functionalities afforded intermediates that could be subjected to chemistry shown in Scheme 22 to produce bis-amide analogs **258741**-**258704** (Figure 46).

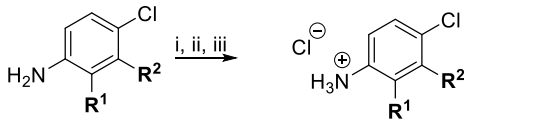

74a: R^1 = OH; R^2 = H
74b: R^1 = H; R^2 = OH

75a: R^1 = propargyloxy; R^2 = H
75b: R^1 = H; R^2 = propargyloxy

Scheme 25: Synthesis of 75a,b

(i) Boc_2O, THF, 70 °C, 4 hr (ii) propargyl benzenesulfonate, K_2CO_3, acetone, 65 °C, 3 hr (iii) 4M HCl in dioxanes, 25 °C, 4 hr.

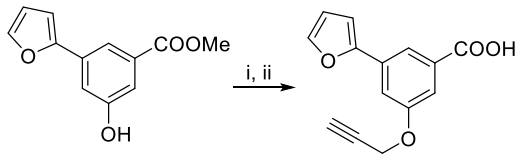

44 **76**

Scheme 26: Synthesis of 76

(i) propargyl benzenesulfonate, K_2CO_3, acetone, 65 °C, 3 hr (ii) 1M NaOH, THF, 25 °C, 2 hr

Unsaturation was easily installed into the piperidine core through chemistry described previously (**78**).[258] 3-(furan-2-yl))benzoic acid was converted to acyl chloride **77** using oxalyl chloride. These two coupling partners were subjected to triethylamine in DCM to produce α,β-unsaturated carboxylic acid intermediate **79** (Scheme 27), which could then be subjected to amide coupling chemistry similar to that shown in Scheme 20, Route 3.

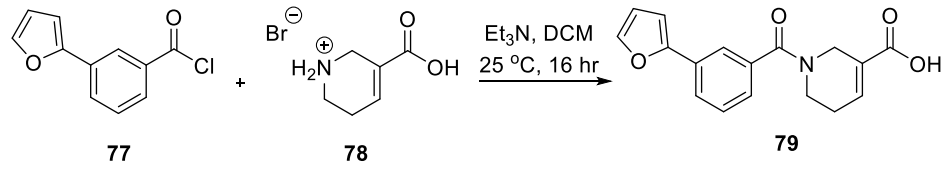

77 78 79

Scheme 27: Synthesis of 79

Dioxinoindole carboxylic acid intermediates **82a-c** were produced from 3,4-dioxinamine **81a** using previously described chemistry (Scheme 28).[259] First, the diazonium chloride salt was produced and reacted with ethyl 2-methylacetoacetate, forming the subsequent hydrazone intermediate that was cyclized to the respective 4,5- and 5,6-ethylenedioxyindoles in base. The ethyl esters were easily saponified to the carboxy-indole intermediates **82a,b**. Adapting this chemistry with 2,3-dioxinamine **81b** regioselectively afforded carboxy-indole intermediate **82c**. Similarly, 6,7-difluoroindole intermediate **84** was synthesized via hydrazone formation and acid-mediated ring closure starting from hydrazine **83** using previously described chemistry (Scheme 29).[260]

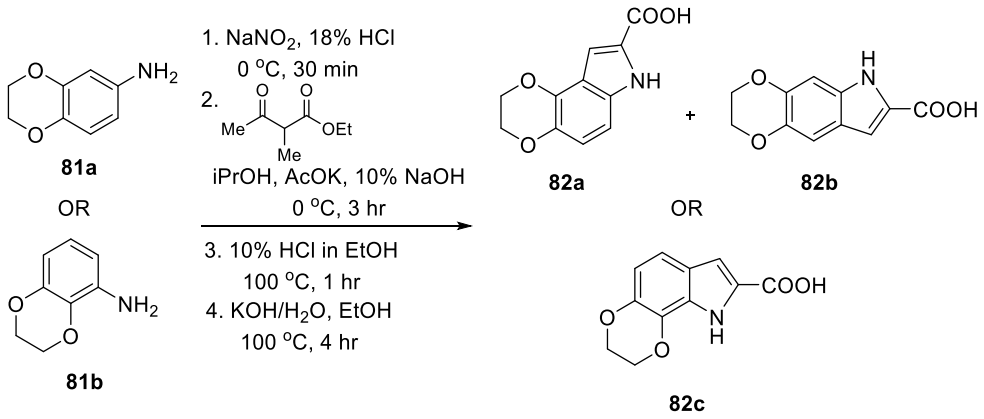

81a 81b 82a 82b 82c

Scheme 28: Synthesis of dioxinoindole carboxylic acid intermediates 82a-c

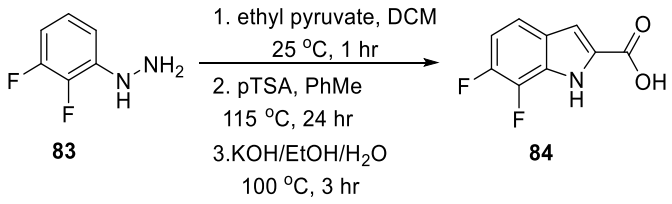

83 84

Scheme 29: Synthesis of 84

Many of the indole-containing bis-amide analogs were formed using HATU-mediated amide coupling adapted from synthetic Route 2 in Scheme 22; however, other analogs were

converted to acyl chlorides from the respective carboxy-indole intermediates, and then subjected to triethylamine and HCl amine salt **47** to produce indole-containing analogs. (Scheme 30). This acyl chloride route was adapted from chemistry Kim Hutchings developed to synthesize many indole-containing analogs from the 222740-series; however, the HATU-mediated amide coupling conditions in DMF were found to be more effective since the indoles at any stage of the acyl halide route had poor solubility in DCM.

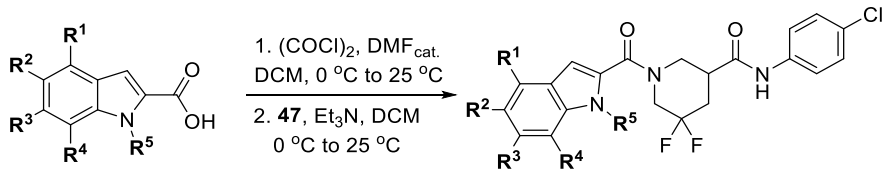

Scheme 30: Alternative route to produce indole-containing analogs

263681 & **263740** were synthesized by a modified Route 3 from Scheme 22 starting from 5-(trifluoromethoxy)-1H-indole-2-carboxylic acid instead of 3-(furan-2-yl)benzoic acid (not shown). **263658** & **263687** were also synthesized by modified Route 2 in Scheme 22 using *R*- or *S*-5-(trifluoromethoxy)-1H-indole-2-carboxylic acid instead of 3-(furan-2-yl)benzoic acid (not shown); these reactions occurred without racemization.

Various 5- and 6-membered ring 3-amino carbamates were used to produce bis-amide analogs displayed in Scheme 31. The variability in the synthetic routes for these homologous analogs is a result of starting material availability. The HATU-mediated amide coupling chemistry used for piperidine analogs translated well to generate these bis-amide analogs without racemization. Since these reactions occurred without racemization, I was able to synthesize the trans-6-membered ring analog **86d** starting from the cis/trans 3-amino carbamate **85d** followed by chromatographic separation; diastereomer assignment was done by comparing the HNMR/CNMR chemical shifts to carbamate intermediate **86b**, which was produced from pure cis-3-amino carbamate **85b**.

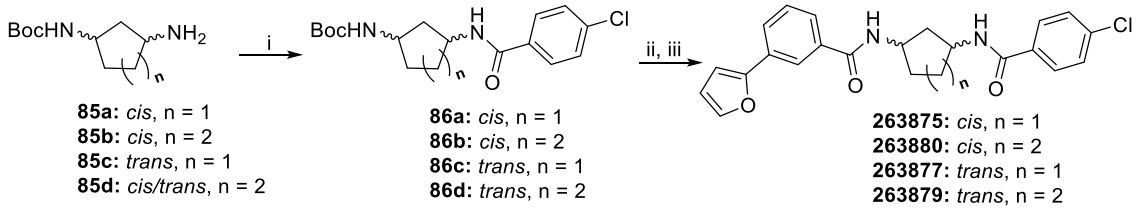

85a: *cis*, n = 1
85b: *cis*, n = 2
85c: *trans*, n = 1
85d: *cis/trans*, n = 2

86a: *cis*, n = 1
86b: *cis*, n = 2
86c: *trans*, n = 1
86d: *trans*, n = 2

263875: *cis*, n = 1
263880: *cis*, n = 2
263877: *trans*, n = 1
263879: *trans*, n = 2

Scheme 31: Synthesis of 263875, 263880, 263877, and 263879

(i) 4-chlorobenzoic acid, HATU, DIPEA, DMF, 25 °C, 16 hr (ii) 4M HCl in dioxanes, 25 °C, 2 hr (iii) 3-(furan-2-yl))benzoic acid, HATU, DIPEA, DMF, 25 °C, 16 hr.

Cis-3-carboxylic acid intermediate **89** was produced from the cis/trans mixture of di-carboxylic acid starting material **87** (Scheme 32). This was accomplished using previously described chemistry to produce *cis*-oxabicyclo-2,4-dione intermediate **88**.[261] This intermediate was easily coupled to 4-chloroaniline to produce pure *cis*-cyclopentanecarboxylic acid intermediate **89**. HATU-mediated amide coupling of 3-(furan-2-yl)aniline, HCl to **89** completed the synthesis of **263872**.

Having produced pure *cis*-cyclopentanecarboxylic acid intermediate **89**, trans-cyclopentanecarboxylic acid was generated from the *cis*/*trans* mixture starting material **90a** (Scheme 33). Of note, not only were *cis* and *trans* cyclopentanecarboxylic acid intermediates generated from **90a**, *cis* and *trans* di-4-chloroaniline substituted bis-amide analogs (not shown) were also produced. Fortunately, all four products were easily separable by column chromatography, and the NMR spectra for both *cis* and *trans* cyclopentane carboxylic acid intermediates synthesized were compared to the NMR spectra for *cis*-cyclopentane carboxylic acid intermediate **89**. *Trans*-cyclopentanecarboxylic acid intermediate **91a** was subjected to HATU-mediated amide coupling conditions with 3-(furan-2-yl)aniline, HCl to produce *trans*-bis-amide analog **263873**.

Trans-cyclohexane bis-amide analog **91b** was produced starting from *trans*-dicyclohexanecarboxylic starting material **90b** in a similar sequence as was used to generate **263878** (Scheme 33). On the other hand, the synthesis for *cis*-cyclohexane bis-amide analog **263876** began from carboxylic acid **92**, which had a methyl ester protected carboxylic acid

(Scheme 33). This route would have obviously been preferred for all bis-amide analogs with this amide orientation, but available starting materials led to a wide-array of synthetic routes for these analogs.

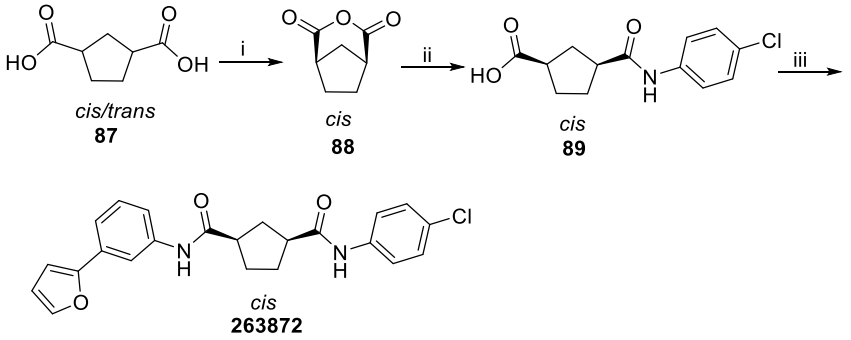

Scheme 32: Synthesis of 263872

(i) Ac_2O, MW, 150 °C, 30 min (ii) 4-chloroaniline, DMF, 25 °C, 16 hr (iii) 3-(furan-2-yl)aniline, HCl, HATU, DIPEA, DMF, 25 °C, 16 hr.

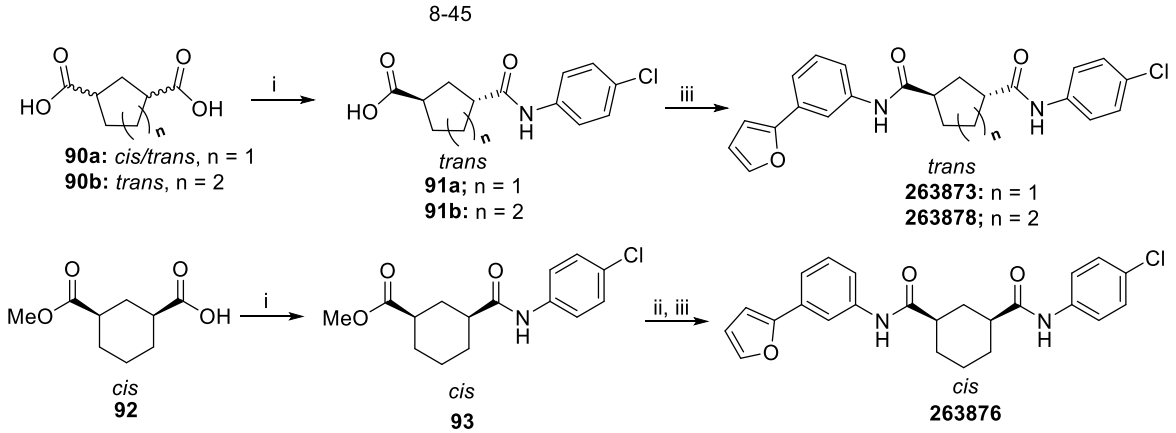

Scheme 33: Synthesis of 263876

(i) 4-chloroaniline, HATU, DIPEA, DMF, 25 °C, 16 hr (ii) 1M NaOH, THF, 25 °C, 1 hr (iii) 3-(furan-2-yl)aniline, HCl, HATU, DIPEA, DMF, 25 °C, 16 hr.

Fortunately, the starting materials to produce bis-amide analogs shown in Scheme 32 were available in their pure *cis* or *trans* isoforms (**94a-c** and **96**), and all analogs could be easily produced with chemistry similar to what has been previously described. (Schemes 34 & 35).

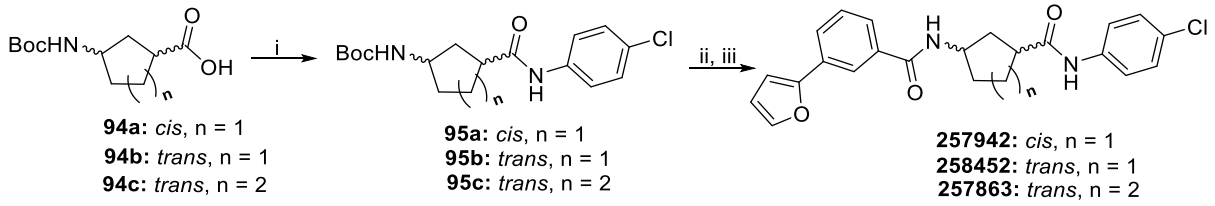

94a: *cis*, n = 1
94b: *trans*, n = 1
94c: *trans*, n = 2

95a: *cis*, n = 1
95b: *trans*, n = 1
95c: *trans*, n = 2

257942: *cis*, n = 1
258452: *trans*, n = 1
257863: *trans*, n = 2

Scheme 34: Synthesis of 257942, 258452, and 257863

(i) 4-chloroaniline, HATU, DIPEA, DMF, 25 °C, 16 hr (ii) 4M HCl in dioxanes, 25 °C, 2 hr (iii) 3-(furan-2-yl)benzoic acid, HATU, DIPEA, DMF, 25 °C, 16 hr.

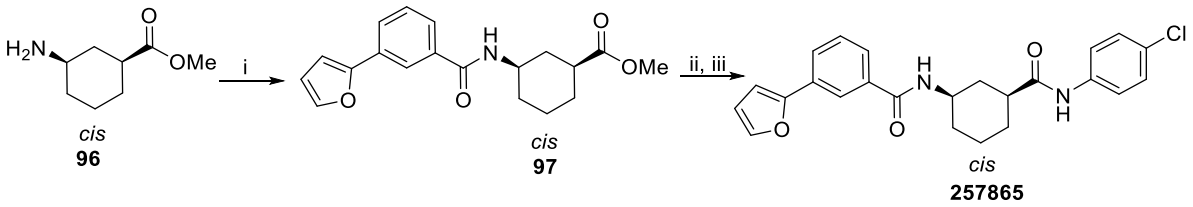

cis
96

cis
97

cis
257865

Scheme 35: Synthesis of 257865

(i) 3-(furan-2-yl)benzoic acid, HATU, DIPEA, DMF, 25 °C, 16 hr (ii) 1M NaOH, THF, 25 °C, 1 hr (iii) 4-chloroaniline, HATU, DIPEA, DMF, 25 °C, 16 hr.

Analogs **264119-264121** were produced from the *cis*-cyclohexyl 3-amino carbamate core, albeit this starting material was manipulated from either side of the core as to install the pyrrolidine functionality in the final step (Scheme 36-38). The installation of the pyrrolidine functionality began from phenolic starting materials **98** and **101**. These intermediates were subjected to HATU-mediated coupling conditions with the respective *cis*-cyclohexyl 3-amino carbamate cores to afford analogs **264119** and **264121**. Also, since I synthesized CCT251236 as previously described by Cheeseman et al, I had the required intermediates in stock to easily produce analog **264120**.

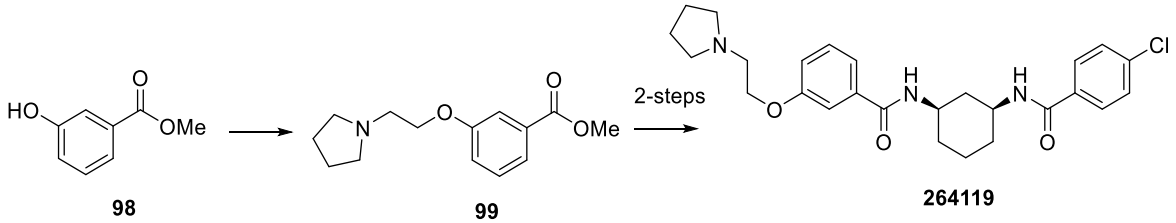

98

99

264119

Scheme 36: Synthesis of 264119

(i) 1-(2-chloroethyl)pyrrolidine, K_2CO_3, DMF, 100 °C, 4 hr (ii) 1M NaOH, THF 25 °C, 5 hr followed by HCl workup (iii) **86b**', HATU, NMM, DMF, 25 °C, 16 hr.

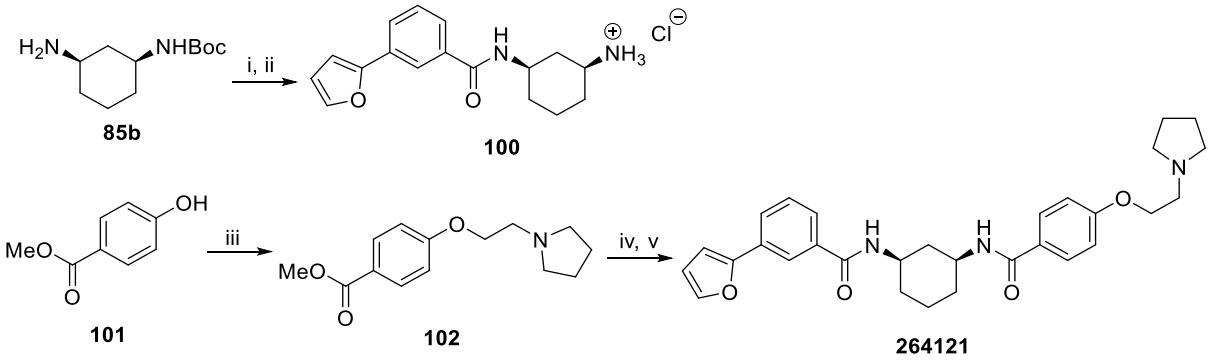

Scheme 37: Synthesis of 264121

(i) 3-(furan-2-yl)benzoic acid, HATU, DIPEA, DMF, 25 °C, 16 hr (ii) 4M HCl in dioxane, 25 °C, 2 hr (iii) 1-(2-chloroethyl)pyrrolidine, K_2CO_3, DMF, 100 °C, 4 hr (iv) 1M NaOH, THF 25 °C, 5 hr followed by HCl workup (v) **100**, HATU, NMM, DMF, 25 °C, 16 hr.

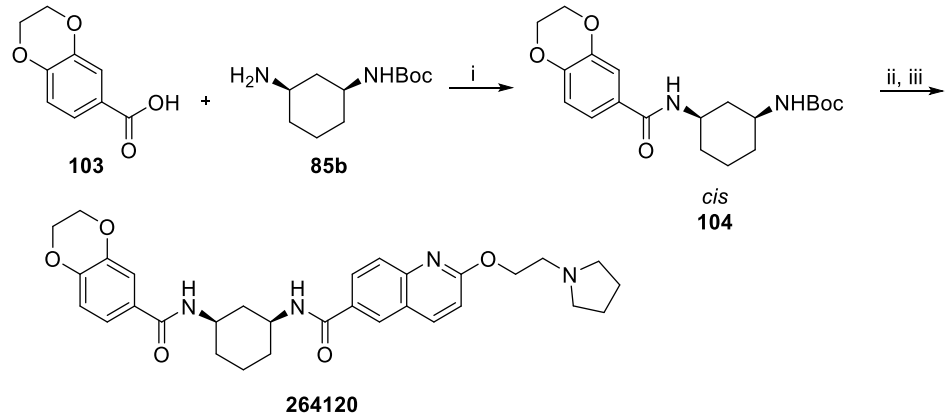

Scheme 38: Synthesis of 264120

(i) HATU, DIPEA, DMF, 25 °C, 16 hr (ii) 4M HCl in dioxane, 25 °C, 2 hr (iii) 2-(2-(pyrrolidin-1-yl)ethoxy)quinoline-6-carboxylic acid, HCl, HATU, NMM, DMF, 25 °C, 16 hr.

Probing Pirin's Hydrophobic Pocket with CCG-257081-like Analogs:

We turned our attention to make more subtle changes to the series, and, using the 257081 co-crystal structure of pirin, designed CCG-257081-derived analogs with appendages that could reach deeper into the fairly open hydrophobic pocket (Table 18). First, seeing that there were water molecules (HOH70 and HOH138) that could potentially get knocked out of pirin's pocket (Figure 43), I designed and synthesized phenolic (**A177**) and hydroxymethyl (**A178**) analogs. Unfortunatley, these analogs did not provide the activity we hoped for, suggesting these changes likely did not displace or engage with the waters within the pocket.

However, 3-Cl (**264059**) and 3,4-Cl (**A179**) aniline analogs provided a noticeble improvement in SRE.L activity over 4-Cl **222740**. Satisfyingly, the tight SAR within pirin's hydrophobic pocket observed in the Cheeseman paper [240] was evident with the 2-Cl aniline derivative (**A180**). These chlorophenyl analogs provided the first distinct and consistant SAR cliff from our SBDD efforts.

Intruigued by these results, I synthesized various analogs with hydrophobic 3-substituents. We observed a change in activity from small (**A181**) to bulky (**A184**-**A186**) substituents, ultimately achieving approximately five-fold improved potency compared to CCG-222740 with 3-cPr and 3-CF_3 analogs **A184** and **A185**. Also, this improvement persisted regardless of electronic effects (**264059** vs. **A184**-**A186**). Again, with longer rigid substituents, we tried to engage with or knock-out the water molecules deep within the hydrophobic pocket; this time, acetylene (**A187**) and nitrile (**A188**) substituents were used. While **A187** maintained the befificial effects of 3-substitution, **A188** was not able to, likely suggesting the nitrile has a desolvation penalty that limits any potential engagement with the water molecules within the hydrophobic pocket.

Table 18: SAR of analogs designed to attempt to reach deeper into pirin's the hydrophobic pocket.

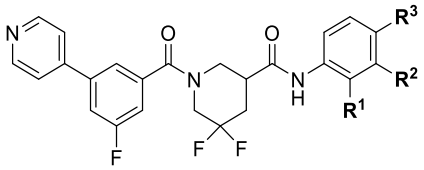

CCG-	Entry	R^1	R^2	R^3	SRE.L IC_{50} (μM)[a]	% 222740 (%)	Max Efficacy (%)	Aq. Solubility (μM)[b]
257081	**-**	H	H	Cl	~0.2	ND	100	9.8
263482	**A177**	H	OH	Cl	16	ND	ND	14
263741	**A178**	H	CH_2OH	Cl	0.64	320	100	ND
264059	**-**	H	Cl	H	0.08	40	100	ND
264060	**A179**	H	Cl	Cl	0.1	50	100	ND
264327	**A180**	Cl	H	H	7.5	1,320	100	ND
264321	**A181**	H	Me	H	1.4	246	100	ND
264322	**A182**	H	Et	H	0.38	67	100	ND
264323	**A183**	H	iPr	H	0.33	58	100	ND
264324	**A184**	H	cPr	H	0.15	26	100	ND
264325	**A185**	H	CF_3	H	0.12	21	100	ND

264326	**A186**	H	OCF_3	H	0.29	51	100	ND
264605	**A187**	H	CCH	H	0.29	47	85	ND
264604	**A188**	H	CN	H	1.1	177	100	ND

[a]Inhibition of Gα12-stimulated SRE.L (mean of n = 3, SEM < 10%) in HEK293T cells unless otherwise noted. [b]Thermodynamic solubility analysis was performed by Analiza Inc. using quantitative nitrogen detection. (www.analiza.com).

We docked many of these 3-substituated analogs into the CCG-257081 co-crystal structure to determine how these more potent analog might be engaging with pirin (CCG-264059 shown as example in Figure 50). Interestingly, the docking results for CCG-264059 suggest that the 3-Cl substituent actually doesn't project deeper into the hydrophobic pocket, rather it positions the aromatic ring so that the 3-Cl group is butting up against the wall of the hydrophobic pocket, potentially improving affinity thorugh hydrophobic interations with pirin. Of note, the docking model does not predict this alteration significantly affecting the interaction between the bis-amide core and HOH202/284. We hypothesized that if this docking model is accurate, we might be able to engage deeper into the pocket occuped by HOH138 and HOH70 by adding a hydrophobic or hydrophilic substituent to the 5-position of the aniline ring. Therefore, we refocused our efforts to producing 3, 5-disubstitued analogs to attempt to further improve SRE.L activity (Table 19).

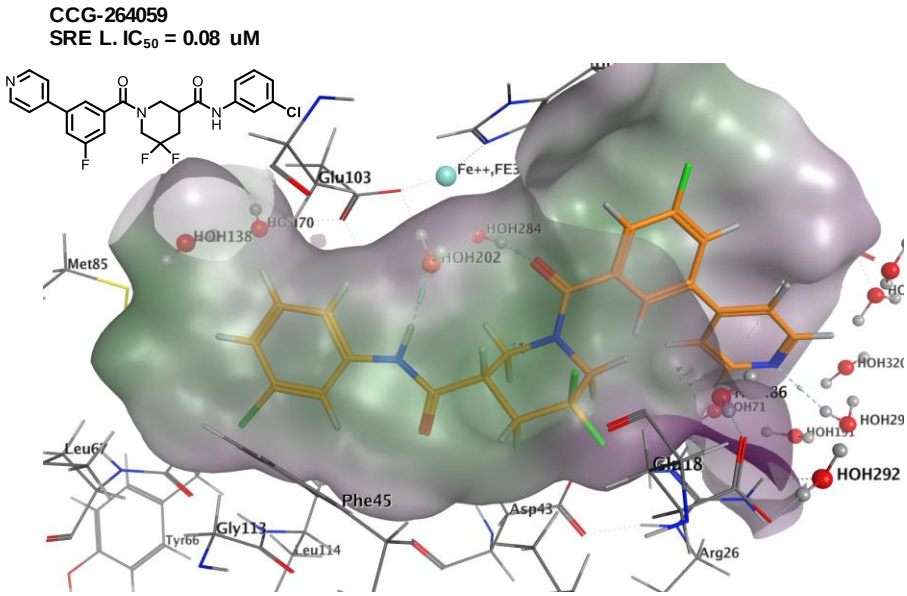

Figure 50: CCG-264059 docked into the CCG-257081 co-crystal structure

Green shading indicates hydrophobic regions and pink shading indicates hydrophilic regions.

Many 3,5-disubsituted analogs had improved activity compared to CCG-222740 control (Table 19); however, none of the analogs achieved better activity than the 3-substituted analogs discussed above (Table 18). Still, there were observable SAR trends for this set of analogs. **A189** was equipotent to CCG-222740, yet the bulkier Br substituted analog **A190** was almost 10-fold less potent. Also, unlike the 3-substituted analogs, 5-alkyl or alkoxy (**A191** & **A192**) and 5-fluoro alkyl (**A193**-**A195**) substitution maintained or improved activity compared to **222740**, indicating that perhaps large hydrophobic substituents can fill the pocket to improve affinity. Moreover, while hydroxyl analogs **A196** & **A197** do not appear capable of engaging with the waters within the hydrophobic pocket, nitrile **A198** may be able to do so. Sadly, none of the mono- or di-substituted analogs (Table 18 and 19) produced activity comparable to CCT251236; nevertheless, the improvements in activity based on this structure-guided design provide additional evidence for pirin being a target that drives the SRE.L activity of the 222740 series.

Table 19: 3,5-disubstituted SAR

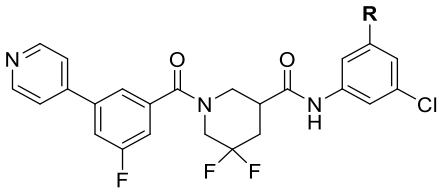

CCG-	Entry	R	SRE.L IC_{50} (μM)[a]	% 222740 (%)	Max Efficacy (%)
264059	**-**	H	0.08	40	100
265067	**A189**	Cl	1.4	100	100
265068	**A190**	Br	10	757	75
265069	**A191**	Me	0.9	67	100
265070	**A192**	OMe	1.6	123	100
265172	**A193**	F	0.4	31	95
265173	**A194**	CF_3	0.5	39	100
265174	**A195**	OCF_3	0.6	42	100
265071	**A196**	OH	3.2	242	100
265072	**A197**	CH_2OH	4.8	362	100
265171	**A198**	CN	0.5	39	85

[a]Inhibition of Gα12-stimulated SRE.L (mean of n = 3, SEM < 10%) in HEK293T cells unless otherwise noted.

In an attempt to understand how solubilizing groups would affect SRE.L activity for **264059** & **A179**, we attempted to attach a pyrrolidine solubilizing group to the scaffold at a location that wouldn't affect pirin binding (Table 20). We selected the 3-position of the benzamide (R^1) based on previous SAR trends. While a pyrrolidine solubilizing group reduced SRE.L activity ten-fold for **A199** and **A200** compared to **222740**, the solubilizing group was better tolerated with the **A179** scaffold (**A201** and **A202**) to maintain equipotency to **222740**. While this is about a 5-fold loss in activity compared to **A179** itself, this result suggests attaching a solubilizing group to this scaffold may be an amenable way to improve PK properties for the series.

Table 20: SRE.L activity for 264059 and A179 derived analogs with solubilizing groups

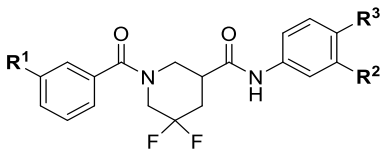

CCG-	Entry	R^1	R^2	R^3	SRE.L	%	Max

					IC_{50} (μM)	222740 (%)	Max Efficacy (%)
264465	**A199**	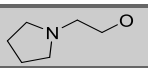	Cl	H	7.4	1299	90
264466	**A200**	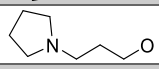	Cl	H	6.1	1070	85
264468	**A201**	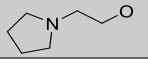	Cl	Cl	0.63	111	85
264469	**A202**	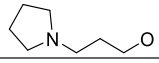	Cl	Cl	0.98	172	95

[a]Inhibition of Gα12-stimulated SRE.L (mean of n = 3, SEM < 10%) in HEK293T cells unless otherwise noted.

Next, analogs were designed in an attempt to eliminate the structural alert associated with the aniline functional group (upon hydrolysis, anilines can lead to renal toxicity through various mechanisms[262-266]) (Table 21). Inserting nitrogen into an aniline ring is known to significantly mitigate toxic effects by reducing binding affinity to CYP1A2 and stabilizing the reactive nitrenium ion that forms after metabolic activation.[266-269] We thought if these analogs maintained SRE.L activity, this design could provide a more suitable candidate for future clinical studies.

Unfortunately, again, the analogs in this subset generally maintained or lost activity compared to **222740**. Benzylic analogs **A203** & **A204** and pyrazolo analog **A205** were designed to probe how deep substituents could penetrate pirin's hydrophobic pocket and to remove the potentially cytotoxic aniline altogether, but they were not tolerated. Swapping the 3-Cl aniline ring with 3-Cl pyridyl rings were generally not tolerated either (**A206-A208**); **A209** was the exception, having SRE.L activity comparable to **264059**. We docked this subset of analogs into CCG-257081 co-crystal structure to attempt to explain these SAR trends (not shown); however, no obvious differences in binding modes explained these results.

Table 21: Alternative 3-Cl substituted heterocycle SAR

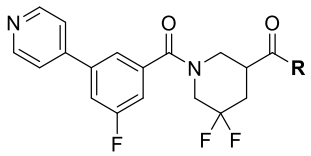

CCG-	Entry	R	SRE.L	%	Max

			IC_{50} (μM)	control (%)	Efficacy (%)
264059	**-**	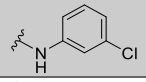	0.08	40	100
264058	**A203**	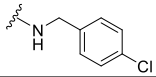	2.2	1,100	100
264642	**A204**	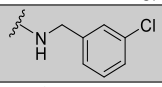	3.9	629	100
264641	**A205**	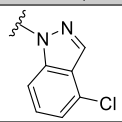	15	2,419	95
264606	**A206**	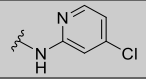	0.99	157	95
264607	**A207**	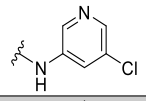	2.1	339	100
264608	**A208**	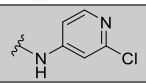	2.8	419	100
264609	**A209**	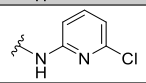	0.37	60	100

[a]Inhibition of Gα12-stimulated SRE.L (mean of n = 3, SEM < 10%) in HEK293T cells unless otherwise noted.

As a follow-up to a previous result from an analog Kim Hutchings made (**A210**), I synthesized analogs that implemented the 3-Cl & 3,4-diCl aniline with 2-F substitution instead of 3-F substitution on the aryl ring on the left side of the bis-amide core (Table 22); bromo aryl intermediates from this batch of analogs were tested as well. We were happy to see that the majority of the analogs in this batch maintained activity comparable to **264059** & **A179**, helping validate that 3-Cl & 3,4-Cl substitution is preferred as long as small structural changes are made to the left-handed aryl ring.

Table 22: 2-fluoro, 5-pyridyl substituted bis-amide SAR

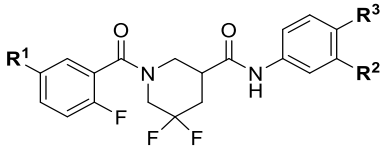

CCG	Entry	R^1	R^2	R^3	SRE.L IC_{50} (μM)	% control (%)	Max Efficacy (%)
257622	**A210**	4-Pyr	H	Cl	0.59	369	100
264464	**A211**	Br	Cl	H	0.86	151	95

264470	**A212**	4-Pyr	Cl	H	0.1	18	90
264467	**A213**	Br	Cl	Cl	0.13	23	100
264471	**A214**	4-Pyr	Cl	Cl	0.14	25	100

[a]Inhibition of Gα12-stimulated SRE.L (mean of n = 3, SEM < 10%) in HEK293T cells unless otherwise noted.

The final SAR trend discussed in this subsection is an investigation of alternative piperidine ring systems. Early in the investigations for the series, **A144** (Figure 46) had an almost ten-fold improvement in activity compared to **222740** just from adding unsaturation to the piperidine ring. Considering how the flatness of the aromatic central bis-amide core of CCT251236 might affect its affinity for pirin (discussed above), we designed analogs that would modulate the orientation of the bis-amide core and provide us with novel IP. Interestingly, the 3-Cl aniline substituent that was beneficial for the fully saturated piperidine analog **264059** was not advantageous for **A215**'s activity (Figure 51), which also implies an ability to adopt a different binding mode. Furthermore, adding a methyl α to the amide attached to the aniline (**A216**) supported the hypothesis that a flatter core is preferred since this methyl group makes the piperdine core bulkier and **A216** was 6-fold less potent than **222740**. Internal amide **A217** also supports the "flat-core" hypothesis, having a ~7-fold improvement in SRE.L activity compared to **222740**. Unfortunately, 3-Cl aniline internal amide analog **A218** did not inhibit SRE.L activity at the same level as **A217**, but this result can be easily rationalized since **A218** may adopt a completely different conformation within pirin that doesn't accommodate the 3-Cl aniline as well.

Of note, these internal amide analogs were originally designed to attempt to engage with the water-mediated iron core of pirin in a different way than **222740**. And while the docking model suggests the internal amide doesn't interact with the water molecules bound to the Fe core (Figure 52), the SRE.L activity does suggest this analog is capable of modulating pirin more effectively than most other analogs in the 222740-series. The Neubig lab attempted to obtain a co-crystal structure with **A217** to better understand this improvement in activity; but,

even though crystals were produced, **A217** did not co-crystalize with pirin during the soak. The Neubig lab is currently attempting alternative crystallization techniques to obtain a co-crystal structure with this novel analog.

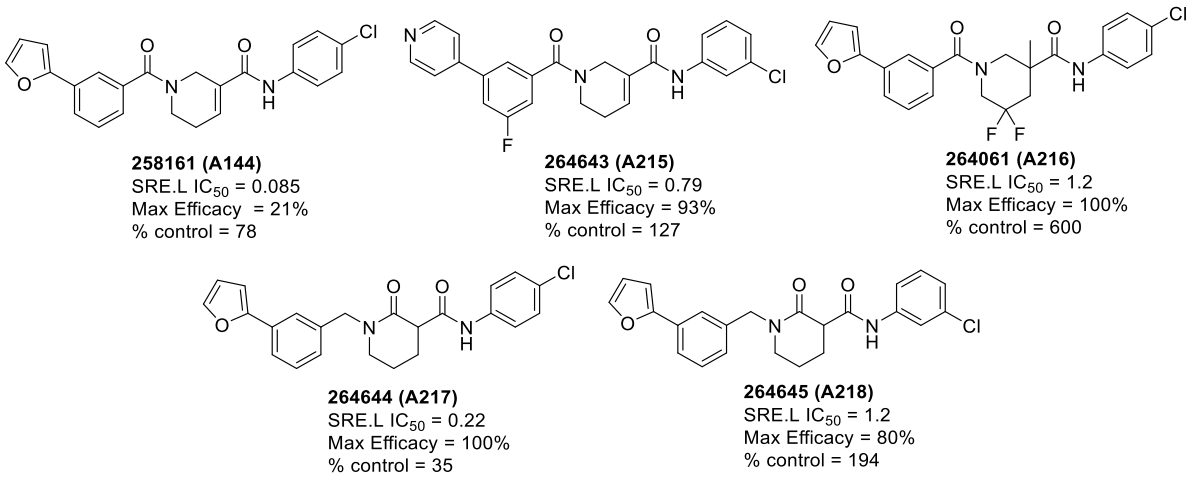

Figure 51: Alternative piperidine ring system SAR

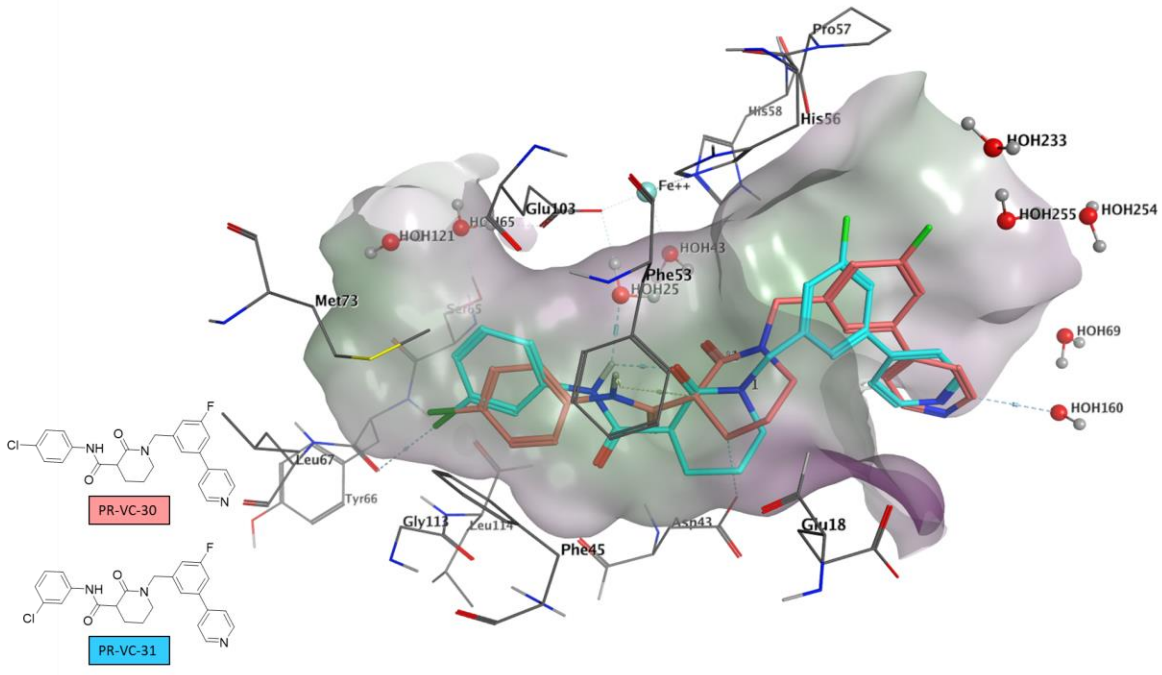

Figure 52: Docking models for A217/A218 analogs

Docking models for **A217/A218** analogs (PR-VC-30 and 31) do not indicate the internal amide carbonyl group can interact with the water molecules ligated to the Fe core.

Synthesis of CCG-257081-derived SBDD Analogs:

Since I was previously able to use propargyl functional groups as a protecting group, I knew this would be an amenable strategy to produce analog **263482** (Scheme 39). Therefore, using intermediate **75b'**, **105** was formed from HATU-mediated amide coupling conditions. This intermediate was subjected to acid-mediated hydrolysis to free up the amine that was subsequently coupled to 3-fluoro-5-(pyridin-4-yl)benzoic acid in HATU-mediated amide coupling conditions to produce **258723**. Using Pd-mediated reduction conditions, the propargyl functionality was removed, producing phenolic analog **263482**.

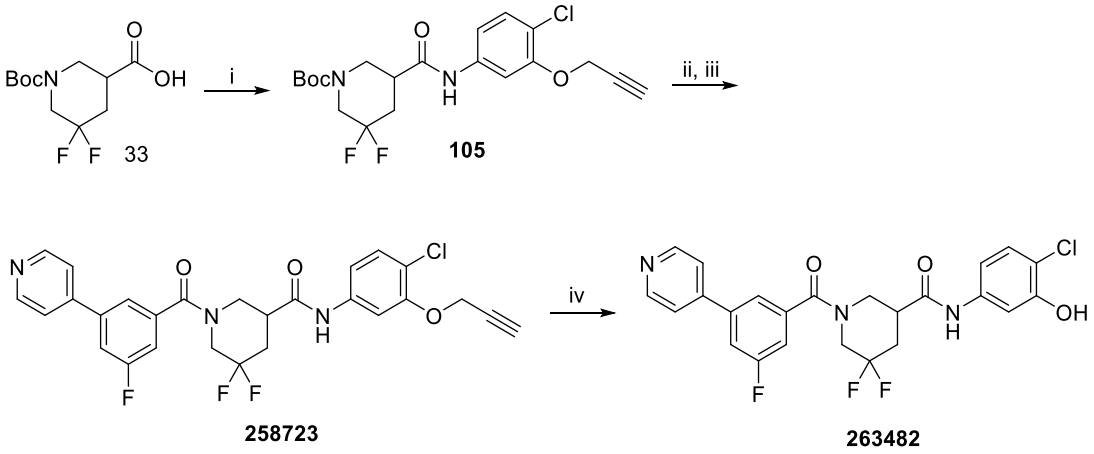

Scheme 39: Synthesis of 263482

(i) **75b'**, HATU, DIPEA, DMF, 25 °C, 16 hr (ii) HCl in dioxanes, 25 °C, 2 hr (iii) 3-fluoro-5-(pyridin-4-yl)benzoic acid, HATU, NMM, DMF, 25 °C, 16 hr (iv) $Pd(PPh_3)_2Cl_2$, Et_3N, DMF, H_2O, 85 °C, 1 hr.

Methyl alcohol analog **263741** was generated from (5-amino-2-chlorophenyl)methanol (**106**, Scheme 40), which was synthesized as previously described.[270] **106** was easily converted to carbamate intermediate **107** by TBDPS protection followed by HATU-mediated amide coupling with the subsequent aniline and **33**. Bis-amide intermediate **108** was produced after another round of deprotection/amide coupling. This intermediate was subjected to TBAF to remove the TBDPS protecting group, producing bis-amide analog **263741**.

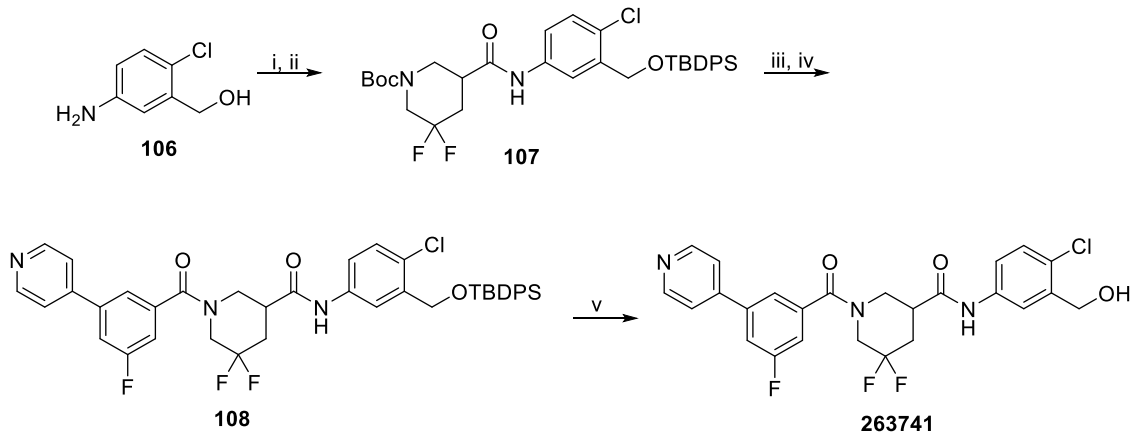

Scheme 40: Synthesis of 263741

(i) TBDPSCl, ImH, DMF, 0 °C to 25 °C, 24 hr (ii) **33**, HATU, NMM, DMF, 25 °C, 16 hr (iii) 4M HCl in dioxanes, 25 °C, 2 hr (iv) 3-fluoro-5-(pyridin-4-yl)benzoic acid, HATU, NMM, DMF, 25 °C, 16 hr (v) 1M TBAF in THF, 25 °C, 1 hr.

Most of the **257081**-derived bis-amide analogs were produced using either Route 1 or 2 depicted in Scheme 41. Analogs were either generated from the common carboxylic acid intermediate **109** or they were derivatized at the beginning of the synthesis from **33**, and subsequently added to the pyridyl-containing benzoic acid. Generally, Route 1 was attempted first, but many of the anilines were very weak nucleophiles, and, to preserve **109**, the chemistry was worked out on **33**.

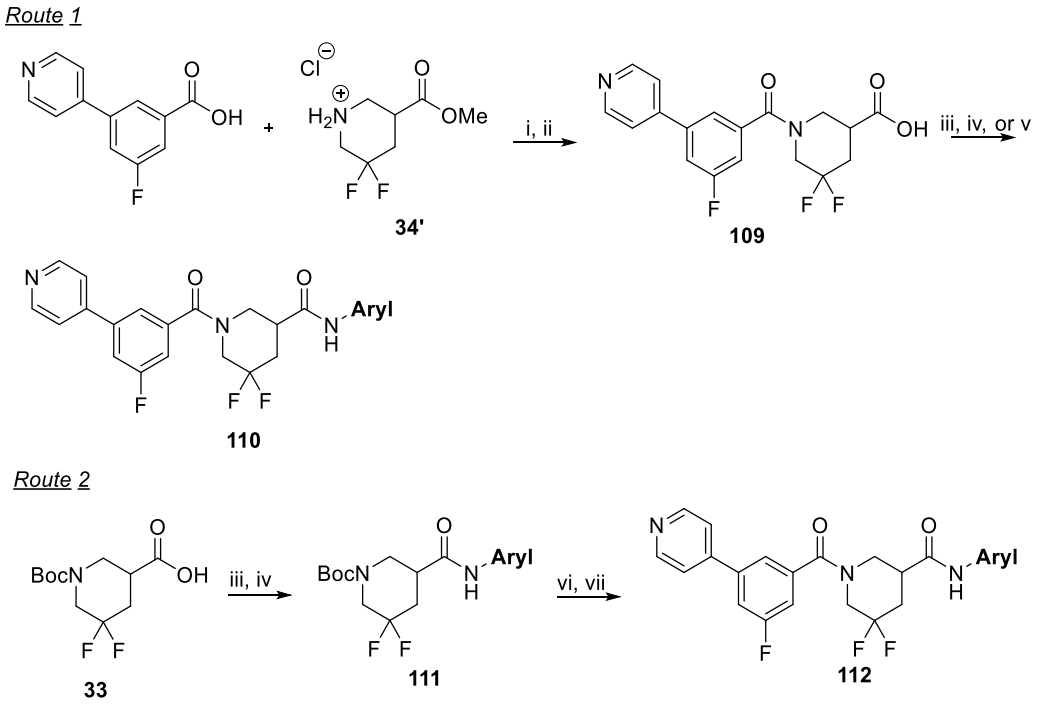

Scheme 41: General routes to synthesis 257081-derived bis-amide analogs

(i) HATU, NMM, DMF, 25 °C, 16 hr (ii) 1M NaOH, THF, 25 °C, 1 hr then HCl workup (iii) aniline or aryl amine, HATU, NMM, DMF, 25 °C, 16 hr (iv) aniline or aryl amine, HATU, NMM, DMF, 85 °C, 16 hr (v) 3-chloro-5-fluoroaniline, EDC•HCl, DMAP, DIPEA, DMF, 85 °C, 16 hr (vi) 4M HCl in dioxanes, 25 °C, 2 hr (vii) 3-fluoro-5-(pyridin-4-yl)benzoic acid, HATU, DIPEA, 25 °C, 16 hr.

Similar to Schemes 36 and 37, pyrrolidine analogs **264465-264468** were produced from benzoic acid intermediate **99** or **113** (Scheme 42). The final amide coupling was accomplished using either HCl amine salt **114** or **115**.

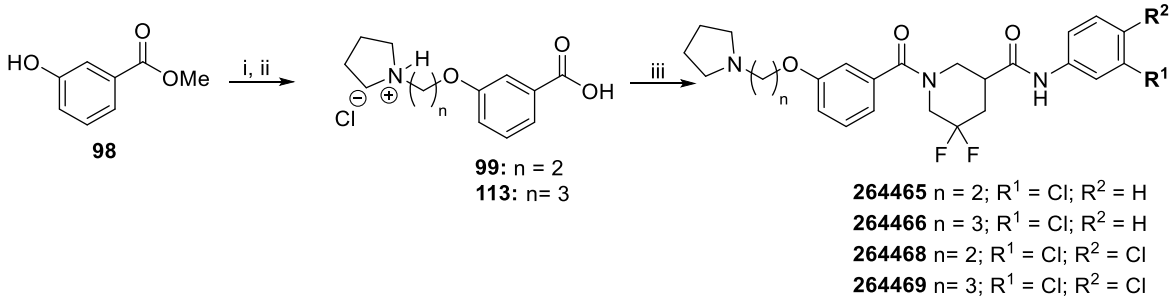

Scheme 42: Synthesis of 264465, 264466, 264468, and 264469

(i) 1-(3-chloropropyl)pyrrolidine, K_2CO_3, DMF, 100 °C, 6 hr (ii) 1M NaOH, THF 25 °C, 2 hr followed by HCl workup (iii) **114** or **115**, HATU, DIPEA, DMF, 25 °C, 16 hr

Pyridyl analogs **264470** and **264471** were assembled with late stage Suzuki-cross coupling chemistry from **264464** and **264467** using 4-pyridyl boronic acid and Tetrakis (Scheme 43).

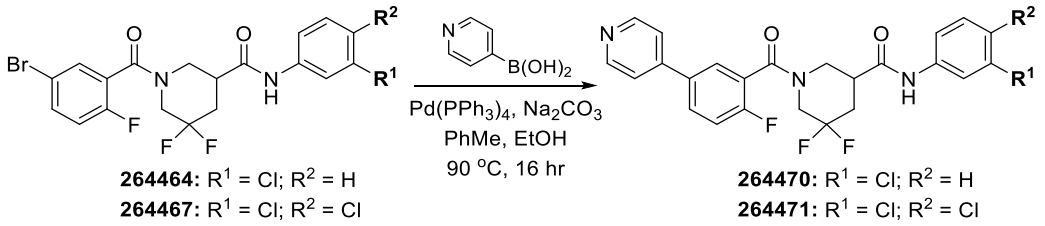

Scheme 43: Synthesis of 264470 and 264471

Using chemistry similar to Scheme 27, α,β-unsaturated carboxylic acid intermediate **116** was generated from **78** and the acyl chloride generated from 3-fluoro-5-(pyridin-4-yl)benzoic acid (Scheme 44). Simple HATU-mediated amide coupling afforded analog **264643**.

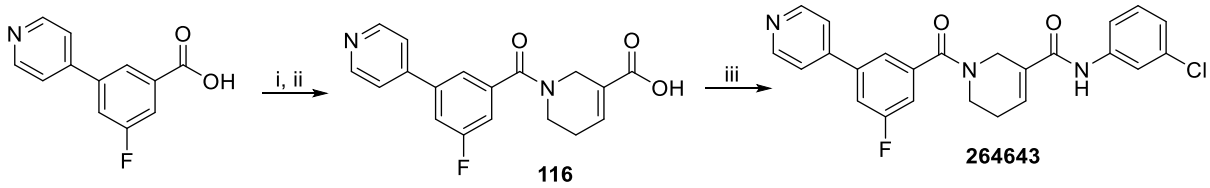

Scheme 44: Synthesis of 264643

(i) $(COCl)_2$ DMF (cat.), DCM, 0 °C to 25 °C, 1 hr (ii) **78**, Et_3N, DCM, 25 °C, 16 hr (iii) 3-chloroaniline, HATU, NMM, DMF, 25 °C, 16 hr.

α-methyl carboxylic acid intermediate **117** was produced using methyl ester piperidine **34** (Scheme 45). Strong base easily removed the proton α to the ester, and this anion was quenched with MeI, producing the desired intermediate that was hydrolyzed to intermediate **117**.

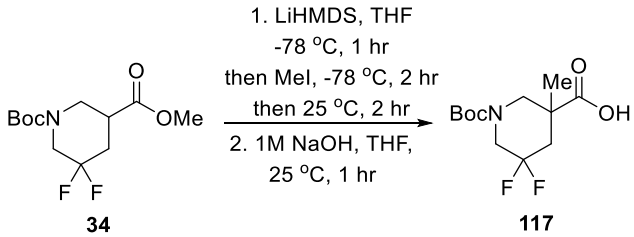

Scheme 45: Synthesis of 117

Intermediate **119** was synthesized adapting previously described chemistry (Scheme 46).[271] This chemistry consisted of alkylation of piperidin-2-one using 3-bromobenzyl bromide followed by benzylcarboxylation α to the amide using LiHMDS and benzyl chloroformate. Suzuki-cross coupling using furan-2-yl boronic acid and Tetrakis not only installed the furan functionality, but it also reduced the benzyl group, freeing up the carboxylic acid. Carboxylic acid intermediate **120** was then subjected to HATU-mediated amide coupling with either 3- or 4-chloroaniline.

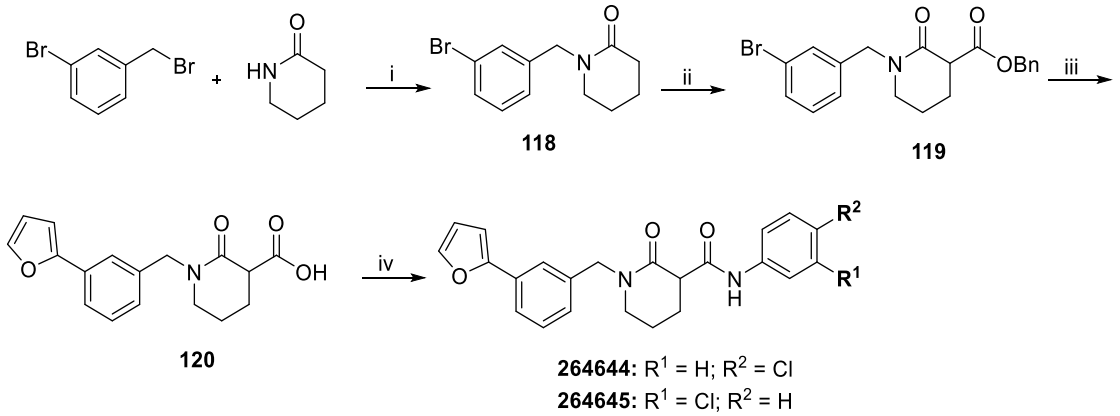

Scheme 46: Synthesis of 264644 and 264645

(i) NaH, THF, 0 °C, 2 hr then 25 °C, 4 hr (ii) LiHMDS, THF, -78 °C, 1 hr (iii) furan-2-yl boronic acid, $Pd(PPh_3)_4$, Na_2CO_3, DME, H_2O, 100 °C, 16 hr (iv) 3- or 4-chloroaniline, HATU, DIPEA, DMF, 25 °C, 16 hr.

While there was no precedent to synthesize α,β-unsaturated methyl esters similar to **123**, amide coupling using amine **122** and acyl chloride **121** in triethylamine was attempted (Scheme 47). Unfortunately, this reaction produced multiple products, and none of the products isolated resembled **123**. This result using these simple amide-coupling conditions caused us to give up on an analog with this type of piperidine core.

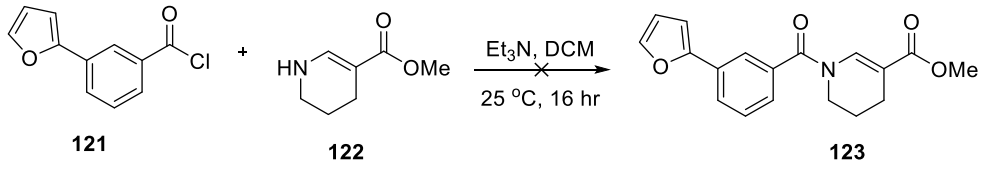

Scheme 47: Attempt to produce alternative piperidine core 123

I also tried to synthesize analogs that removed the external amide functionality (Scheme 48). We assumed we could (1) improve PK properties of the series by removing this amide, which is susceptible to hydrolysis in biological conditions, and (2) potentially improve the fit into pirin's hydrophobic pocket by installing an indazole functionality. While I was eventually able to generate mesyl intermediate **125** via selective reduction of the carboxylic acid **33** with BH_3•THF followed by treatment with mesyl chloride and triethylamine, I struggled to synthesize the desired carbamate intermediate **126a,b** using 4-chloro-1H-indazole. I eventually worked out chemistry to obtain both **126a,b**, but I only produced 9 mg each product, and I couldn't distinguish either analog by NMR. Since these analogs were high risk anyways, we abandoned attempting to generate analogs with this scaffold.

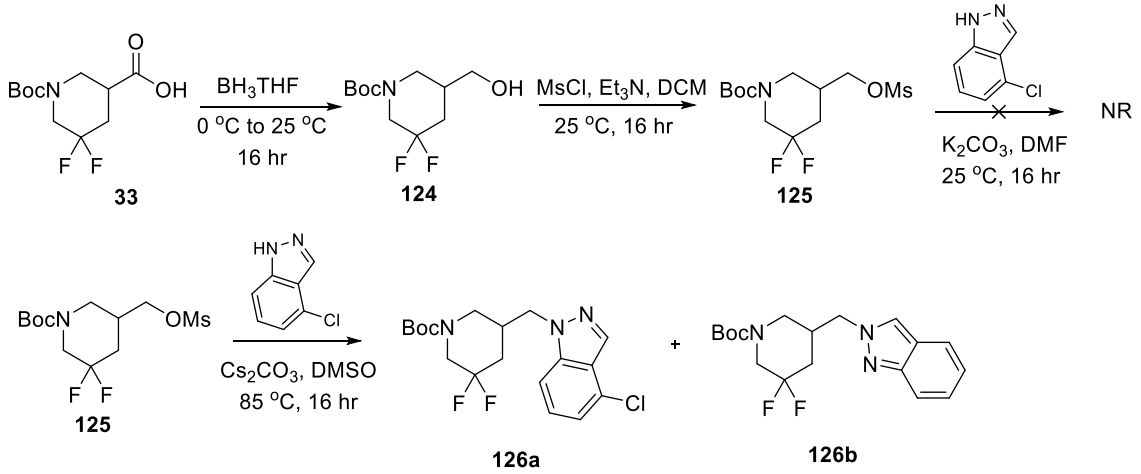

Scheme 48: Attempts to produce indazole intermediate 126a,b

Another interesting analog design that I could not work the chemistry out for was the removal of the amide and the implementation of an indolinone in place of the aniline (Scheme 49); this analog was designed with the same rationale as for the indazole just described. Even though I was able to generate a late stage mesyl intermediate (**128**) by selectively reducing the carboxylic acid of **109** followed by mesylation with mesyl chloride and triethylamine, I did not find coupling conditions that afforded installation of indolin-2-one. Therefore, this analog was also abandoned.

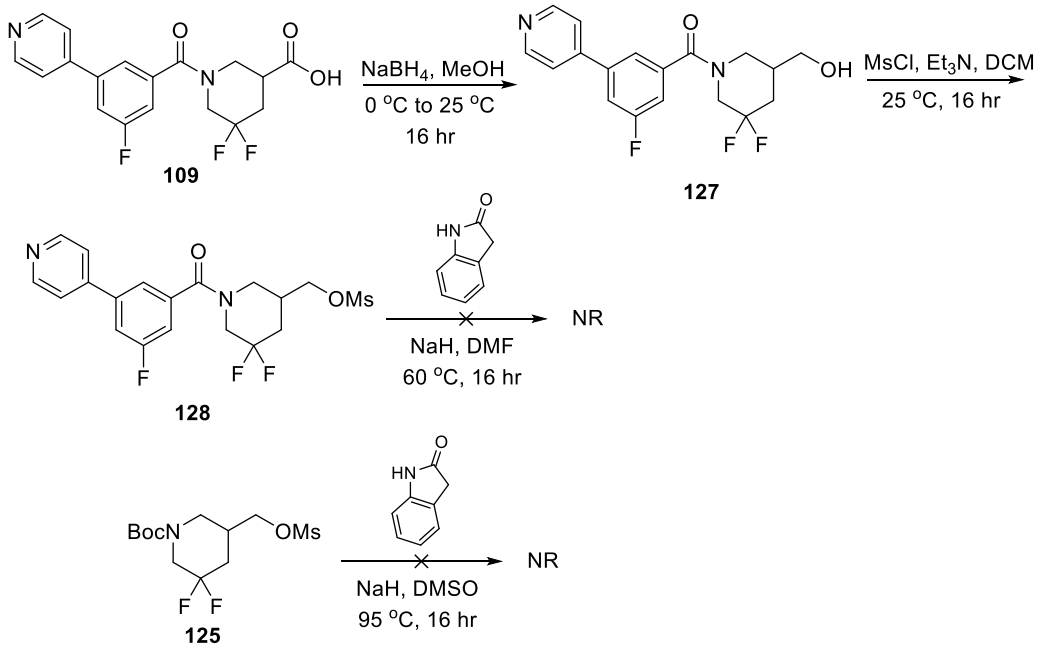

Scheme 49: Attempts to produce an indoline-containing analog

Virtual Screen with CCG-222740 Scaffold:

In a final effort to remove the potentially toxic 4-chloroaniline group, we performed a virtual screen using the co-crystal structure with pirin and CCG-257081. To design non-aniline analogs of CCG-257081, Pil Lee performed a virtual screening of a combi-library created computationally in MOE. This virtual screening library was developed using the CCG-257081-scaffolding shown in Table 23 paired with Sigma Aldrich's amine library of 9997 amines. In MOE, keeping the pirin structure static, a virtual combi-library of 6710 bis-amide analogs that incorporated commercially available amines was generated. This set of compounds was further parsed to 301 non-aniline derivatives by only keeping analogs with molecular weight less than 550 g/mol. 122 compounds were selected from this set based on the novelty, removing analogs with pendants with predictable metabolic liability or cytotoxicity. Subsequently, these virtual analogs were subjected to flexible docking with an induced fit using the co-crystal structure for CCG-257081. Finally, several compounds were selected for synthesis based on docking score, docking pose with additional interactions within pirin, and synthetic feasibility.

As an example, the docking result for **265188 (A220)** is shown in Figure 53. This analog was able to maintain similar interactions with the ligated water molecules as CCG-257081, but the docking results suggest the aromatic pendant can fit much deeper into pirin's hydrophobic pocket. From this virtual screen, 13 analogs were produced (Table 23). These analogs remain to be tested in the SRE.L assay.

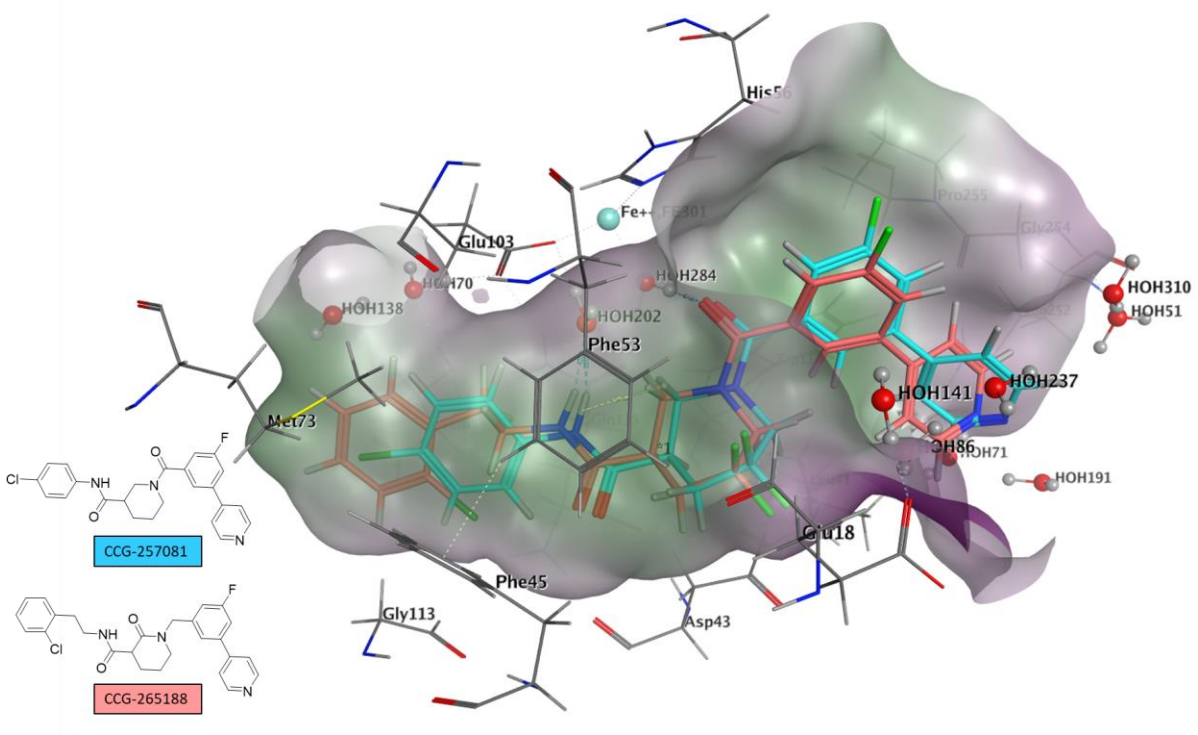

Figure 53: Docking for 265188

The best docking pose for 265188—an analog generated in a virtual screen using the CCG-257081 scaffold.

Table 23: Virtual screen analogs

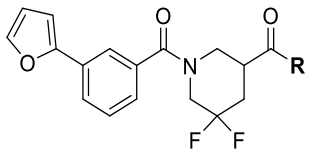

CCG-	Entry	R	SRE.L IC_{50} (μM)
265187	**A219**	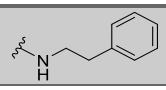	ND

265188	**A220**	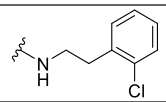	ND
265189	**A221**	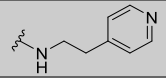	ND
265190	**A222**	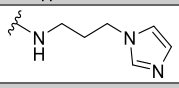	ND
265191	**A223**	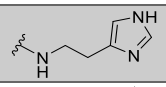	ND
265192	**A224**	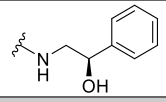	ND
265193	**A225**	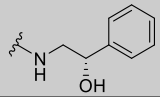	ND
265194	**A226**	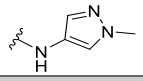	ND
265195	**A227**	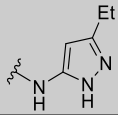	ND
265196	**A228**	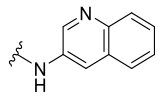	ND
265197	**A229**	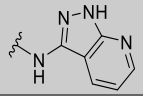	ND
265198	**A230**	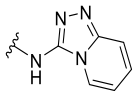	ND
265199	**A231**	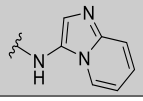	ND

Synthesis of Virtual Screen Analogs:

The virtual screen analogs were easily synthesized with HATU-mediated amide couplings of intermediate **37'** and the various primary amines ordered from Sigma Aldrich (Scheme 50).

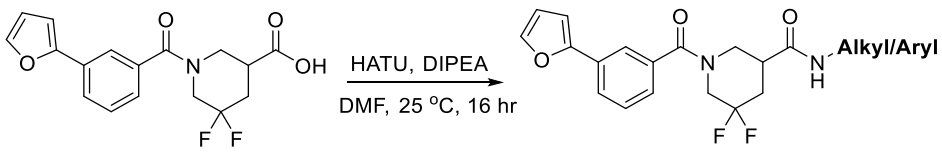

37' **126**

Scheme 50: Synthetic route used to quickly produce virtual screen analogs

Conclusion:

Using pirin co-crystal structures with CCT251236, CCG-222740, and CCG-257081, we designed 222740-series analogs with modified aryl pendants that we hoped would engage more deeply into pirin's hydrophobic pocket as well as analogs with alternative central bis-amide cores that we hoped would interact with the waters ligated to the Fe core of pirin in a similar manner as CCT251236. Through these efforts, the SRE.L activity for the 222740-series improved by about 10-fold, and certain designs removed structural alerts while retaining this improvement in activity. Notably, certain efficacious analogs like **A217** may provide novel scaffolding, with an internal bis-amide core, that can lead to analogs with an improved PK profile. Also, the improvement in activity for pyridyl analog **A209** provides confidence that the aniline structural alert can be removed by insertion of a nitrogen into the 4-Cl aryl ring.

Furthermore, if a direct binding assay for pirin is established, the analogs developed during this project may provide a launching pad to produce more potent pirin inhibitors from the 222740-series. While the SRE.L activities may not suggest significant improvements in affinity for pirin, a binding assay would confirm or disprove this result, which would ultimately help any future drug design for this series since it would confirm if the design or PK/PD an issue. Also, since this series already has such exciting biological activity, many of the new analogs reported here should be tested for any improvement in PK properties. Regardless if the SRE.L activity of the series can be improved further with the 222740-series scaffold, many of the reported analogs have a chance to have an improve *in vivo* PK profile, which could lead to a significant improvement in efficacy in anti-fibrotic models.

Chapter 5: Future Directions

Overview:

Many goals have been accomplished since the outset of this project: (1) chemical probes capable of pulling down protein candidates were designed and synthesized, leading to the identification of potential targets for both the 58150- and 222740-series of Rho/MRTF/SRF-mediated gene transcription inhibitors (Chapter 2) (2) hit-to-lead development of extremely potent 58150-series analogs produced inhibitors capable of significantly and dose-dependently preventing fibrosis in a murine model of bleomycin-induced fibrosis (Chapter 3) and (3) SAR exploration of the 222740-series provides an introduction to key pharmacophores necessary for engagement to pirin (Chapter 4).

Despite these advancements, several critical questions remain unanswered. For instance, while a potential list of candidate proteins for the 58150-series was generated using the immobilized pull-down probes, target validation efforts have been unsuccessful. Also, while target validation efforts for the 222740-series make it clear that pirin is a target for the series, it is still not clear whether the series works through other biological targets to afford its activity. Potential options to circumvent these issues are discussed in the next few sections.

Additionally, while much of the SAR was well-defined for the 58150-series, there are a few trends that should be followed-up. There are also several gaps in the SBDD SAR for the 222740-series that, if explored further, could lead to inhibitors with better affinity for pirin. Suggestions for follow-up analogs for both series are discussed in the sections below.

58150-Series Target Identification using Click Probes:

The most critical question that remains unanswered for the 58150-series is: does the oxadiazole core react covalently with the biological target that affords activity? While the SAR discussed in Chapter 2 clearly supports this hypothesis, there is no direct evidence for it. The ideal way to determine if the series acts covalently is to identify the target for the series. Another route to identify the biological target of the 58150-series is to use the previously developed propargyl Click probes **A88** and **A91** instead of the immobilized affinity probes (Figure 54). The major advantage of the propargyl probes is they can be incubated with whole cells instead of cell lysates. Additionally, this methodology would ensure the potential intracellular activation of the oxadiazole core could take place prior to target engagement. Since it is unknown whether the biological target for the series is stable to lysate conditions or whether the core needs to be activated for covalent reactivity, this route could provide a better way assure the probes are interacting with the biological target(s) in a similar manner as they are in the SRE.L assay.

Additionally, the SRE.L activity ascertained from the propargyl Click probes is more definitive than that for the immobilized affinity resin probes. Since we only inferred the SRE.L activity of the immobilized affinity probes from ethoxymethoxy mimics, we cannot be certain whether the “active” probe used for the pulldown inhibits SRE.L activity, and, therefore, interacts with the biological target. Moreover, there is a 250,000-fold difference in activity between the structurally similar “active” (**A88**) and “inactive” (**A91**) propargyl probes, which should further improve the accuracy of the proteomic analysis used to produce the list of protein candidates.

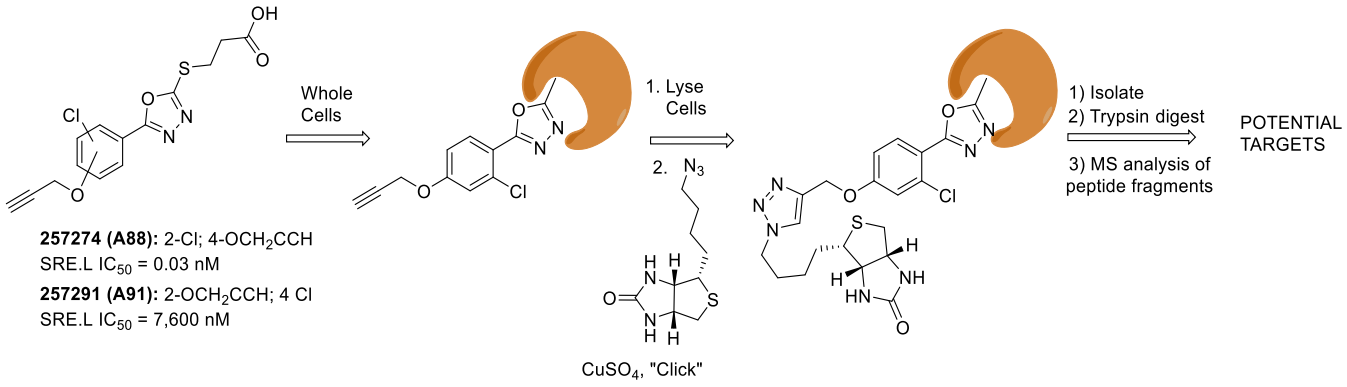

Figure 54: Alternative target identification route for the 58150-series using propargyl Click probes instead of immobilized agarose resin probes

The Martin and Neubig labs are currently performing pulldown experiments with these propargyl Click probes to generate a new list of candidate targets. However, if the list of candidate targets generated from the pulldown experiments using the propargyl probes does not contain biological targets that can be validated, stable isotope labeling by amino acids in cell culture (SILAC) enrichment experiments may further improve the pulldown experiment. SILAC would be a helpful technique to use if the biological target for the 58150-series is in low cellular abundance.[181] The technique utilizes the mass difference between "heavy" ^{12}C or ^{15}N isotopically enriched cells and "light" normal cells to improve the accuracy of the proteomic analysis; the difference in mass of the amino acid fragments from these cells can be compared to determine whether amino acid fragments for a particular protein are real or artifactual.[181]

222740-Series Target Identification using Photo-Labeled Click Probes:

As discussed in Chapter 3, we have strong evidence that pirin is a biological target for the 222740-series; however, we are less certain whether the series works through other biological targets to afford the observed biological activity. Since we are not sure if the series interacts strongly with another potential biological target, a diazirine photoprobe could be used to increase the likelihood that the biological target of interest will be pulled down (Figure 55). This methodology is particularly useful when (1) affinity to the molecular target or (2) the cellular abundance of the target is low.[173,188] Moreover, as discussed in the previous subsection,

propargyl Click probes could be included in the 222740-series probe design to help ensure the probe interacts with any biological targets that are potentially unstable to lysate conditions.

Since I have already designed synthetic routes to incorporate the propargyl handle into the 222740-scaffold (Chapter 2), the new design would require installation of the diazirine functionality. As I also mentioned in Chapter 2, many routes to produce diazirine-containing probes are reported in the literature. Additionally, since the SAR developed for the PEG-mimic analogs (Chapter 2) suggests attachment of large aliphatic substituents is tolerated at various locations on the scaffold, I would assume attaching the propargyl functionality to multiple positions on the aryl functionalities would maintain SRE.L activity. Nevertheless, a suggested photo-Click probe is shown in Figure 55. Since alternative substitution of the 4-Cl aniline ring tends to affect SRE.L activity more than alterations made on the other aryl pendant, the 4-Cl aniline pendant seems more important for activity, and, therefore, I would install the diazirine functionality to the 4-position of the aniline ring. Since the propargyl handle should be partially exposed so it can react with azide during the Click reaction, the placement of the propargyl handle to the 3-aryl position of the 5-furyl substituted aryl pendant. Of note, difluoro-substitution does not significantly affect SRE.L activity (it mainly improves metabolic stability), so this functionality can be eliminated from the probe design. All considered, this probe design route might be an amenable option to determine whether other biologically relevant targets for the 222740-series.

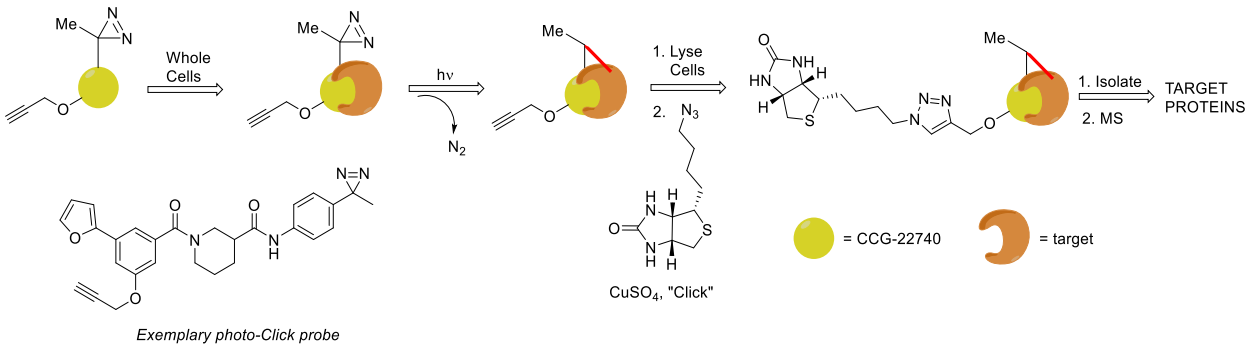

Figure 55: Alternative target identification route for the 222740-series using propargyl Click probes with a photo-affinity handle

58150-Series SAR Gaps:

Certain gaps in the SAR for the 58150-series were mentioned in Chapter 3. First, the approximate 100-fold increase in activity observed for tetrazole (**A24**) (Figure 56) should be followed-up by directly comparing **58150** and **A24**'s ability to inhibit LPA-stimulated CTGF gene expression as described in Chapter 3. This analog was synthesized a while ago, and the preliminary n = 1 data suggested the tetrazole reduced SRE.L activity. However, recently, the n = 3 data revealed that the tetrazole significantly improves SRE.L activity. This is the only carboxylic acid isostere that has better activity than the carboxylic acid functionality, and, since carboxylic acids are notorious for poor *in vivo* PK, the tetrazole could potentially be used to improve the *in vivo* PK profile of the series. Yet, prior to making additional tetrazole-containing analogs, the potent activity of tetrazole **A24** should followed up by testing it in the LPA-stimulated CTGF qPCR assay. If this analog is of equal or greater potency than **232964** in this qPCR assay, then it would be important to follow-up this result with *in vivo* PK analysis, as additional analogs containing the tetrazole could lead to novel intellectual property.

Considering the totality of the SAR obtained for the 58150-series discussed in Chapters 2 and 3, proposed tetrazole-containing analogs that might maintain pM potency and improve the *in vivo* PK profile of the series are shown in Figure 56. Analogs containing either 4-Cl or 4-cPr should be combined with analogs containing either the ethyl, propyl or cyclobutyl as the chain (**127-129**). Since there was significant variation between the activity and *in vivo* PK profile for carboxylic acid homologs, it is important that these follow-up analogs have multiple chain lengths and types. I would expect proposed analog **128** will afford the best activity profile; however, it is difficult to predict whether the unknown biological target can accommodate the 3-C chain length with the tetrazole functional group.

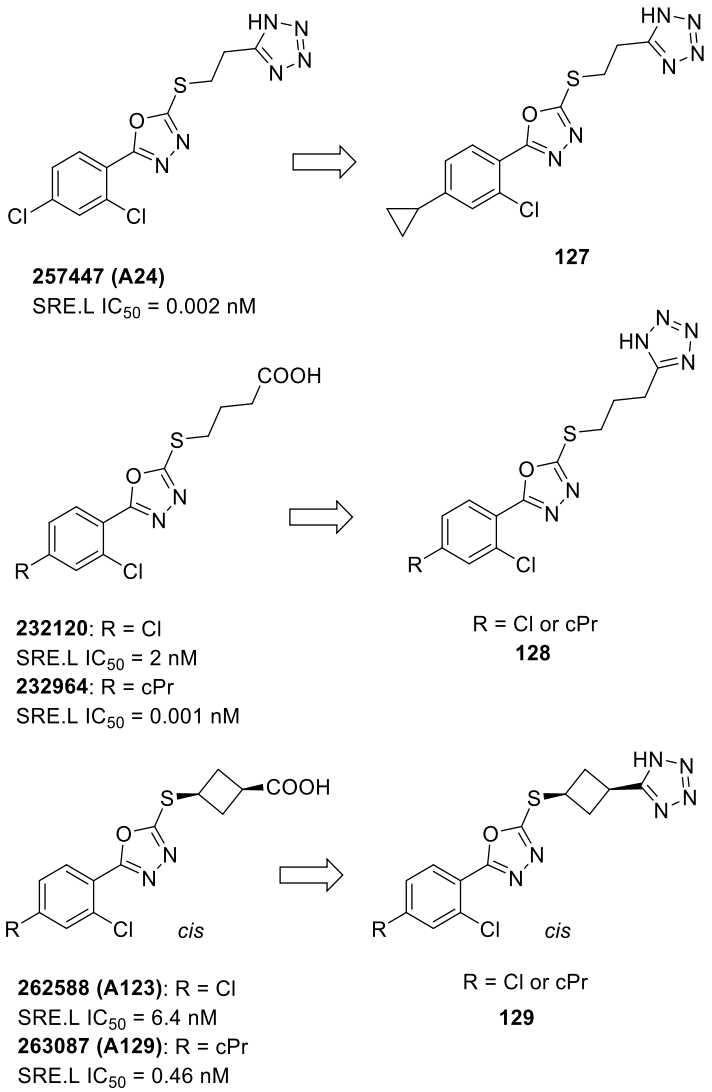

Figure 56: Proposed follow-up analogs replacing carboxylic acid with tetrazole isostere

The other gap in the SAR that should be followed-up is the surprising result for phenol analog **A95**. The 2-OH substitution was the only other functionality in the 2-position that maintained or improved upon the activity of 2-Cl substitution. Analogs **A96** and **A51** (Table 8, Chapter 3)—derivatives containing 3- and 4-OH—should be tested before follow-up analogs are made, but some proposed analogs are shown in Figure 57. It would be interesting to see if pM potent activity comparable to **232964** would be maintained with 2-OH,4-cPr substitution. If it was maintained, then an analog with the cyclobutyl chain with this substitution pattern should be made as well.

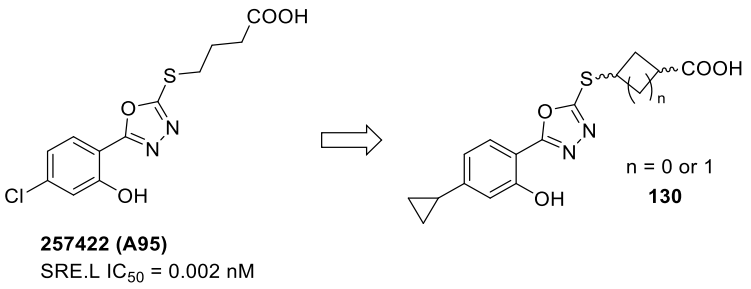

Figure 57: Proposed follow-up analogs investigating the effects of incorporating 2-OH into the 58150-series scaffold

222740-Series SBDD Follow-up Analogs:

Even though the 222740-series SBDD efforts did not produce analogs with comparable activity to CCT251236, many promising SAR trends were uncovered. First, it appears that activity can be improved by incorporating small, hydrophobic substituents in the aniline aryl functionality. This result is promising for future design in that once an optimum bis-amide core is discovered, the activity and PK profile of the series could be fine-tuned by incorporating such small substituents. Furthermore, as mentioned in Chapter 4, since the 4-Cl aniline has a high liability for cytotoxicity, this could be eliminated by swapping out the Cl for a metabolically stable, small, hydrophobic substituent (e.g. cPr or CF_3).

Second, progress towards finding a better bis-amide core system was made. For example, internal bis-amide **A217** had a three-fold improvement in activity compared to **222740**. This result suggests the piperidine core can be altered to potentially produce a core with better activity. As mentioned, an attempt was made to co-crystalize **A217** with pirin, but the inhibitor did not soak into the crystals. If a co-crystal structure containing **A217** was obtained, it may reveal an alternative mode of binding that can be utilized to produce improved analogs. Since we don't have a co-crystal structure, it is difficult to propose additional analogs following-up on the internal bis-amide core result, but, based on docking and the SAR for the series (Figure 53), incorporating small, hydrophobic substituents into the aryl aniline would be a good place to start (Figure 58). Additionally, if **A217** adopts a flipped binding mode compared to CCG-222740,

analogs with alternative aryl groups in the 3-position of the aryl ring on the left side of the bis-amide core could produce analogs with higher affinity for pirin. (Figure 58).

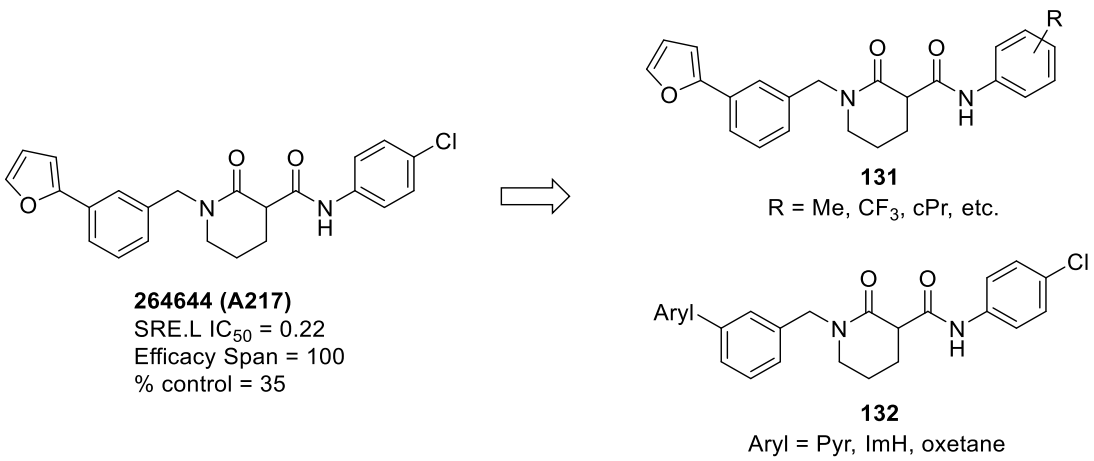

Figure 58: Proposed follow-up analogs that explore substituents surrounding the aryl functionalities flanking the internal bis-amide core of 264644

The last result that could be followed-up on depends on how potent the virtual screen analogs discussed in Chapter 4 are compared to **222740**. If the docking model is any indication, these analogs could bind significantly better to pirin than **222740**. Analogs from this batch that have significantly better activity than **222740** could be co-crystallized with pirin or at least followed up on with SAR to confirm/modify the docking pose. Depending how the analogs bind, these co-crystal structures can be used to design additional analogs.

Conclusion:

Throughout this project, significant advances towards the development of both the 58150- and 222740-series of Rho/MRTF/SRF-mediated gene transcription inhibitors as anti-fibrotic agents were made. The single greatest accomplishment achieved from this project is the development of the 58150-series to pM potent inhibitors capable of dose-dependently and significantly preventing fibrosis in mice with bleomycin-induced fibrosis. These exciting results justify additional research, such as (1) identifying the biological target (2) determining if the series proceeds through a covalent mechanism of action, which could lead to the application of

a novel irreversible moiety for drug discovery in general and (3) developing pM potent inhibitors with an improved PK profile.

Another noteworthy accomplishment achieved during this project is the development of an immobilized affinity probe capable of pulling down a biological target for the 222740-series. While pirin may not be the only target that affords the series' phenotypic activity, there is strong circumstantial evidence that pirin is a molecular target for the series (e.g. co-crystal structures with 222740-series analogs, siRNA pirin knocked down fibrotic gene expression, etc.). Therefore, in any subsequent pre-clinical studies with the 222740-series, inhibition of pirin should be considered as a mechanism of action that affords therapeutic efficacy for the series.

In all, this research represents a significant advance to introducing novel anti-fibrotic agents to the drug development landscape. This research has helped launch FibrosIX, and future research can potentially help bring a new anti-fibrotic therapeutic to the clinic.

Experimentals:

SRE.L Luciferase Assay:

For luciferase assays using PC3 cells, 20,000 cells/well were plated in a 96- well plate in 10% FBS+DMEM. The next day, cells were transfected with 56 ng of SRE.L Luciferase reporter and 2 ng/well of either Gα12 Q231L or pcDNA using Lipofectamine 2000 (Life Technologies) and Opti-MEM (Gibco). After 4 h of transfection, media was changed to 0.5% FBS+DMEM and cells were treated with compounds or DMSO control overnight. The next day, viability was measured using WST-1 (Roche) and absorbance was read at 450 nm. After viability was measured, cells were lysed, and luciferase was measured using the Luciferase Assay System (Promega).

For luciferase assays in 293T cells, see Hutchings et al.[168]

58150-Series Target ID Agarose Pulldown Materials and Methods:

NHS-agarose linking

10 mM solutions of 'active' compound (CCG-257308 (**A52**)) and 'inactive' compound (CCG-257644 (**A53**)) were made in 100% DMSO and diluted to 600 µM in PBS. 80 mg of dry NHS-activated agarose (Thermo-Fisher Cat# 26197) was mixed with 2 mL of either active or inactive compound and PBS solution and rotated for 2 hours at room temperature. Beads were washed twice with PBS and the remaining NHS sites were blocked with 1 mL of 1 M ethanolamine. Beads were washed again with PBS and resuspended in 2 mL of PBS + 0.05% Na Azide.

Cell lysate preparation

HEK293T cells were passaged in DMEM (Gibco, cat#11995065) containing 10% fetal bovine serum (FBS) and 1% penicillin/streptomycin (Gibco) at 37 °C in 5% CO_2. Cells were grown in

15 cm plates and lysed in PBS with protease inhibitors (Roche, cat #11836145001) and sonicated. The lysates were spun at 20,000 rpm for 45 mins at 4 °C and the supernatant was snap frozen with liquid nitrogen and stored at -80 °C.

Agarose bead pulldown

Supernatants were separated into two groups, each approximately 2 mg/mL total protein concentration. One group of cell lysate received 10 µM CCG-58150, and the other received DMSO control for 30 minutes on ice. Technical duplicates were incubated on ice for 30' and then 750 µL of each sample was applied to a spin column (Pierce, cat #69705) loaded with prepared active (**A52**) or inactive (**A53**) agarose resin. Lysates and beads were incubated at room temperature with rotation for 1 hour, and immediately washed 3 times with 1 mL chilled PBS. Beads were collected and snap frozen and sent on dry ice for liquid chromatography-mass spectrometry proteomics analysis.

222740-Series Target ID Agarose Pulldown Materials and Methods:

NHS-agarose linking

A 10 mM solution of CCG-262545 (**A62**) was made in 100% DMSO and diluted to 600 µM in PBS. 160 mg of dry NHS-activated agarose (Thermo-Fisher Cat# 26197) was mixed with 2 mL of compound and PBS solution and rotated for 2 hours at room temperature. Beads were washed twice with PBS and the remaining NHS sites were blocked with 1 mL of 1 M ethanolamine. Beads were washed again with PBS and resuspended in 2 mL of PBS + 0.05% NaN_3.

Cell lysate preparation

HEK293T cells were passaged in DMEM (Gibco, cat#11995065) containing 10% fetal bovine serum (FBS) and 1% penicillin/streptomycin (Gibco) at 37 °C in 5% CO_2. Cells were grown in 15 cm plates and lysed in PBS with protease inhibitors (Roche, cat #11836145001) and sonicated. The lysates were spun at 20,000 rpm for 45 mins at 4 °C and the supernatant was snap frozen with liquid nitrogen and stored at -80 °C.

Agarose bead pulldown

Supernatants were separated into two groups, each approximately 1 mg/mL total protein concentration. One group received 30 µM CCG-222740, and the other received DMSO control. Technical duplicates were incubated on ice for 30 mins and then 750 µL of each sample was applied to a spin column (Pierce, cat #69705) loaded with prepared agarose resin. Lysates and beads were incubated at room temperature with rotation for 1 hour, and immediately washed 3 times with 1 mL chilled PBS. Beads were collected and snap frozen and sent on dry ice for liquid chromatography-mass spectrometry proteomics analysis.

Mass Spectrometry and Proteomic Materials and Methods:

Mass spectrometry

Proteomics Sample Preparation. Reagents were obtained from Fisher unless otherwise noted. On-bead digests were performed by resuspending each sample in 200 µL of phosphate-buffered saline (PBS) containing 6M urea. To each sample, dithiothreitol (DTT) was added to a final concentration of 5 mM and allowed to sit at room temperature for 30 minutes. Iodoacetamide (Sigma) was then added to a final concentration of 30 mM and incubated in the dark at room temperature for 30 minutes. Samples were diluted to a final concentration of 1.2 M urea and digested overnight with Trypsin-LysC mix (Promega). Following digestion, samples were centrifuged at 1000 rpm for 1 minute (Eppendorf Centrifuge 5424) and the supernatant was collected. To remove any remaining beads, supernatants were filtered through polypropylene Micro Bio-Spin Columns (BioRad) by centrifugation at 5000 rpm with two 200 µL washes with PBS. These washes were combined and desalted with Waters Oasis HLB Prime µElution Plate according to the manufacturer's protocol. Samples were then dried on a Savant SPD1010 SpeedVac Concentrator.

Liquid chromatography-mass spectrometry

Desalted, dried peptides were resuspended in LC-MS grade water with 3% acetonitrile and 0.1% formic acid. Three LC-MS injections (technical replicates) were made for each biological

replicate. LC-MS analysis was performed using a Waters nanoAcquity UPLC system fitted with a 5 µm Symmetry C18 trap column (180 µm x 20 mm) and a 1.8 µm HSS T3 analytical column (75 µm x 250 mm). Tryptic peptides were loaded onto the trap column for a 10 minute wash, followed by analytical separation over a 110 minute gradient (3% acetonitrile to 40% acetonitrile over 92 minutes) at a flow rate of 0.5 µL / min. Eluting peptides were introduced into the Synapt-G2S HDMS traveling wave ion mobility quadrupole time-of-flight mass spectrometer (Waters) by electrospray ionization using a pre-cut uncoated 10 µm ID SilicaTip nanospray emitter (New Objective). The Synapt-G2S auxiliary pump was used to deliver the lock mass compounds [Glu1]-Fibrinopeptide B (100 fmol / µL; Waters) at 400 nL / min through the reference sprayer of the nanoLockSpray source. The nanoESI source was set to 70°C with a 3 kV applied potential. Data-independent acquisition was performed in positive mode. The quadrupole mass analyzer was set to transmit all precursor ions (50-2000 m/z) through to the TOF mass analyzer. Precursor ions traveled through the quadrupole mass analyzer and were then separated in the traveling wave device using the manufacturer recommended constant wave height of 40 V and variable wave velocity of 1000-600 m/s. Low and elevated-energy scans were alternated every 0.5 seconds (0.05 s interscan delay) to acquire sequential precursor and product ion data. Collision energy was applied after ion mobility separation in the transfer cell. In the low-energy mode, data were collected at constant collision energy (CE) of 4 eV across all 200 drift bins (TOF scans). In high-energy mode, collision energy ramping was applied as follows: 0 eV for bins 1-19; 16.4-58.5 eV for bins 20 – 119; and 58.9 – 63.9 eV for bins 120 – 200. Wave velocities in the trap and transfer cell were set to 311 m / s and 380 m / s, respectively, with wave heights of 4 V. In the trap cell, the N_2 gas flow rate was 2.0 mL / min. In the ion mobility cell, the He_2 and N_2 flow rates were set to 180 and 90 mL / min, respectively. The mass spectrometer was operated in Resolution mode (V-mode), with a typical resolving power of at least 20,000 FWHM. Data were mass corrected post-acquisition by comparison to the doubly-

charged monoisotopic peak of [Glu1]-Fibrinopeptide B (m/z = 785.843), which was sampled every 30 seconds during acquisition.

Proteomics data analysis

Raw data were analyzed with ProteinLynx Global SERVER version 3.0.2 (PLGS, Waters Corporation), searching against the Uniprot database of the human proteome. The following criteria were applied to perform the search: (i) trypsin as digestion enzyme, (ii) one missed cleavage allowed, (iii) carbamidomethyl cysteine as a fixed modification and methionine oxidation as a variable modification, (iv) a minimum of two identified fragment ions per peptide and a minimum of five fragments per protein, and (v) at least two identified peptides per protein. The global protein false discovery rate (FDR) was set at 1% using a reversed sequence database. Any identified peptides with calculated mass error greater than 10 ppm were not considered. Protein abundance fold differences and p-values between active / blocked lysate were calculated based on label-free peptide abundances using only unique peptides.

Gene Expression Analysis:

Differential gene expression (based on fold change) was calculated for Pirin knockdown (GSE 17551) and CCG-1423 treatment (GSE 30188). The top 100 downregulated genes were used to create gene signatures from the Pirin microarray dataset and the CCG-1423 microarray dataset. The C1-C6 and H gene set collections were dowloaded from MSigDB (accessed 09/2017). The hypergeometric distribution between the CCG-1423 gene set and all other gene sets was calculated in R to identify statistically significant gene set overlaps. The pirin target gene set has the most significant overlap with the CCG-1423 dataset.

Protein Purification:

Pirin protein purification protocol was adapted from [272]. Using site-directed mutagenesis, a stop codon was introduced in front of the streptavidin tag and confirmed by sequencing. Pirin plasmid was transformed into BL21 DE3 One Shot cells (Novagen). A single colony was grown in 50 mL LB with 100 ug/mL ampicillin overnight at 37 °C with shaking and transferred to 1 L LB

containing 100 µg/mL ampicillin the next day. Cells were grown until the OD600 reached 0.5 and then cells were induced with 0.7 mM IPTG for 5 hours at 37 °C. Cells were lysed in 50 mL of 20 mM Tris-HCl pH 8.0, 150 mM NaCl with protease and phosphatase inhibitors (Roche) using sonication. Lysates were spun down at 12,000 rpm for 40 mins at 4 °C and the supernatent was loaded onto a pre-equilibrated Ni^{2+} column (equilibrated with 50 mL of 20 mM Tris-HCl pH 8.0, 500 mM NaCl, 10 mM Imidazole). The column was washed with equilibration buffer including 40 mM Imidazole and eluted with equilibration buffer with 150 mM Imidizaole. The elution was then further purified on a Superdex 200 Prep Grade column (GE) in 20 mM Tris pH 8.0, 150 mM NaCl and analyzed by SDS-PAGE.

Isothermal Titration Calorimetry:

Thermodynamic measurements were performed with a VP-ITC Microcalorimeter (MicroCal). Purified and concentrated pirin (100 µM) was loaded into the injection syringe in gel filtration buffer with addition of DMSO (0.1%). The compounds were also dissolved in matched gel filtration buffer at 10 µM and loaded into the cell. Both protein and compounds were degassed for 5 minutes under vacuum. The first injection of protein was 0.8 µL, all subsequent injections were 10 µL, duration 1.5 or 20 seconds, with spacing of 120 or 240 seconds and 29 injections total. A DMSO control experiment was subtracted from each experiment, and data were analyzed by a one-site binding model in VP Viewer 200, using the plotting software ORIGIN 7 (Origin Lab Corp).

Protein Crystallization:

Pirin was crystallized by concentrating to 56 mg/mL and setting up hanging drop trays in 24 well trays (Hampton Research). Hanging drops were set up with 1 µL of protein and 1 µL of reservoir solution (0.1 M Hepes, pH 7.5, 8% Ethylene Glycol, 20% PEG 8000)8 Crystals grew in less than 1 week at 25 °C and then were soaked in 250 µM CCG-257081 or CCG-222740. The diffraction data were collected at the Life Sciences Collaborative Access Team beamline 21-ID-D and 21-ID-G at the Advanced Photon Source, Argonne National Laboratory. Data were

processed using the HKL2000 package, and iterative model building and refinement were carried out using Coot9 and Phenix10, to yield the final refined structures whose statistics are detailed in Supplemental Table II. Structure figures were generated using UCSF Chimera.

Cell Culture:

Human primary dermal fibroblasts were grown in DMEM (Gibco) containing 10% fetal bovine serum (FBS) and 1% penicillin/streptomycin (Gibco) at 37 °C in 5% CO_2. All fibroblasts were grown in 6-well (for siRNA studies) or 96-well plates (for compound studies). For compound studies, the cells were stimulated with TGF-β (10 ng/mL, R&D cat #240-B-002) and co-treated with compounds for 24 hours before lysis.

siRNA-mediated gene silencing:

ON-TARGET plus SMART pools were commercially synthesized by Dharmacon against human pirin (GE, cat # L-012613-00-0005) or non-targeting pool control (GE, cat# D-001810-10-05) and were used according to the manufacturer's recommendations. Briefly, normal primary dermal fibroblasts (2 x 105) were plated in 6-well culture plates with DMEM containing 10% FBS and 1% 100 units/mL antibiotics/antimycotics. The next day, 25 nmol/L siRNA smart pools were transfected using DharmaFECT 1 (GE, cat# T-2001-01) dissolved in Opti-MEM media. After 24 hours of transfection, the media on the cells was changed to DMEM containing 10% FBS and 1% 100 units/mL antibiotics/antimycotics and were kept for an additional 24 hours before changing the media to 0.5% FBS+DMEM and treating with the stimulus.

RT-PCR:

10,000 cells were plated in each well of a 96 well plate for 24 hours before changing the media to DMEM containing 0.5% FBS and concurrently adding TGFβ as well as compound or DMSO control. The cells were lysed in iScript RT-qPCR lysis buffer (Biorad, cat #170-8898), and the iTaq Universal SYBR Green One Step Kit was used (BioRad, cat #172-5151) following the manufacturer’s instructions. 1 uL of template lysate was added to the RT-qPCR master mix. Alternatively, RNA was isolated using the RNeasy Kit (Qiagen) following the manufacturer's

protocol. RNA (1 µg) was used as a template for synthesizing complementary DNA utilizing the High Capacity cDNA Reverse Transcription Kit (Thermo Fisher Scientific). SYBR green qPCR (Thermo Fisher Scientific) was performed using a Stratagene Mx3000P (Agilent Technologies) and Ct values were analyzed relative to GAPDH expression. Primer sequences used were as follows: GAPDH: 5′-GAAGGTGAAGGTCGGAGTCA-3′, 3′-CTGGGGAAGTAACTGGAGTT-5′; CTGF: 5′-CAGAGTGGAGCGCCTGTT-3′, 3′-CTGCAGGAGGCGTTGTCA-5′; ACTA2: 5′-AGCCCAGCCAAGCACTG-3′, -3′-GAGACATTCCGGCCGAAAC-5′ and PIRIN: 5′-GTGGAGCCTCAGTACCAGGA-3′, 3′-AAATGTGAGCGTGTGGTTGG-5′

Western blotting:

Cells were lysed with RIPA buffer containing 10 mM Tris-HCl, 1 mM EDTA, 1% Triton X-100, 0.1% SDS, 140 mM NaCl, protease inhibitor cocktail (Roche, cat# 11873580001). Cell lysates were sonicated for 10 min and centrifuged to pellet insoluble material. The supernatant was transferred to labeled Eppendorf tubes and protein concentrations were quantitated using a BCA protein assay (Pierce BCA Protein Assay, Thermo Scientific). Protein lysates (40 µg) were then run on 10% polyacrylamide gels and transferred to PVDF membranes and blocked in LI-COR buffer for one hour. Membranes were incubated in 1:1000 diluted primary antibodies pirin (Thermo Fisher Scientific, cat # PA5-51441) and GAPDH (Santa Cruz, cat # SC-365062) overnight at 4 °C and were incubated in 1:5000 diluted secondary antibodies for one hour at 25 °C the next day. Blots were visualized using a LI-COR Odyssey Fc and quantified using Image Studio software.

GST-MRTF-A Actin Pulldown:

GST-MRTFA 10-142 plasmid (in pGEX-4T-2 vector) was transformed into BL21 DE3 One Shot cells (Novagen). A single colony was grown in 50 mL LB with 100 ug/mL ampicillin overnight at 37 °C with shaking and transferred to 1 L LB containing 100 ug/mL ampicillin the next day. Cells were grown until the OD600 reached 0.5 and then cells were induced overnight at 25 °C. Cell pellets were resuspended in 50 mL of 50 mM Tris pH 8.0, 300 mM NaCl, 1% Triton-X, 1

mM DTT, 1 mM EDTA and protease inhibitors (Roche). Pellets were sonicated, and lysate was centrifuged at 33,000 rpm for 20 mins at 4 °C. Soluble lysate was bound to Glutathione beads overnight and washed with 25 mL lysis buffer without Triton-X and eluted with lysis buffer including 40 mM reduced glutathione. Actin lysate was collected from 2 confluent plates of NIH-3T3 cells that were lysed in 50 mM Tris-HCl pH 8.0, 100 mM NaCl, 3 mM $MgCl_2$, 0.2 mM EGTA, 0.2 mM ATP, 1 mM DTT, 0.5% Triton-X and protease inhibitors.

qPCR for LPA-stimulated Expression of CTGF:

LPA stimulation

Primary dermal fibroblasts isolated from healthy donors were cultured in DMEM containing 10% FBS and 1% Pen/Strep. Prior to LPA stimulation, cells were seeded in 0.5% FBS containing DMEM and pre-treated with compounds or DMSO control for 48 or 72 h. After the pre-treatment, LPA (1-Oleoyl Lysophosphatidic Acid, Cayman Chemical, Cat #10010093) was added at a final concentration of 10 µM for 1 h in DMEM containing 0.5% FBS and 1% Pen/Strep. After LPA stimulation, cells were lysed in iScript RT-qPCR lysis buffer (Biorad, Hercules CA, Cat #170-8898). Cells used for experiments were passaged no more than 8 times.

qPCR

For qPCR analysis, the iTaq Universal SYBR Green One Step Kit was used (BioRad, Hercules, CA Cat #172-5151) following the manufacturer's instructions. 1 µL of template lysate was added to the RT-qPCR master mix. Primers used were: CTGF Forward 5'-CAGAGTGGAGCGCCTGTT -3', CTGF Reverse 5'- TTGTCCGCGAGGTGAGAC-3', GAPDH forward 5' GAAGGTGAAGGTCGGAGTCA and GAPDH reverse 5'-TTGAGGTCAATGAAGGGGTC-3'. Fold differences were calculated using the ΔΔCt method with GAPDH as a reference. PCR products were analyzed on a 1% agarose gel.

Metabolic Stability in Mouse Liver Microsomes:

The metabolic stability was assessed using CD-1 mouse liver microsomes. One micromolar of each compound was incubated with 0.5 mg/mL microsomes and 1.7 mM cofactor NADPH in 0.1

M phosphate buffer (pH = 7.4) containing 3.3 mM MgCl2 at 37 °C. The DMSO concentration was less than 0.1% in the final incubation system. At 0, 5, 10, 15, 30, 45, and 60 min of incubation, 40 µL of reaction mixture were taken out, and the reaction is quenched by adding 3-fold excess of cold acetonitrile containing 100 ng/mL of internal standard for quantification. The collected fractions were centrifuged at 15000 rpm for 10 min to collect the supernatant for LC−MS/ MS analysis, from which the amount of compound remaining was determined. The natural log of the amount of compound remaining was plotted against time to determine the disappearance rate and the half-life of tested compounds.

Pharmacokinetic Studies in Mice:

All animal experiments in this study were approved by the University of Michigan Committee on Use and Care of Animals and Unit for Laboratory Animal Medicine. The abbreviated pharmacokinetics for 8j, 8q, and 19f were determined in female CD-1 mice following intravenous (iv) and/or orally (po). Compound was dissolved in the vehicle containing 15% (v/v) DMSO, 15% (v/v) PEG-400, and 70% (v/v) PBS. Four blood samples (50 µL) were collected over 7 h (at 0.5h, 2h, 4h, and 7h), centrifuged at 3500 rpm for 10 min, and plasma was frozen at -80˚C for later analysis. Plasma concentrations of the compounds were determined by the LC−MS/MS method developed and validated for this study. The LC−MS/MS method consisted of a Shimadzu HPLC system, and chromatographic separation of tested compound which was achieved using a Waters Xbridge-C18 column (5 cm × 2.1 mm, 3.5 µm). An AB Sciex QTrap 4500 mass spectrometer equipped with an electrospray ionization source (ABI-Sciex, Toronto, Canada) in the positive-ion multiple reaction monitoring (MRM) mode was used for detection. All pharmacokinetic parameters were calculated by non-compartmental methods using WinNonlin, version 3.2 (Pharsight Corporation, Mountain View, CA, USA).

Bleomycin skin fibrosis for CCG-257081:

Twenty-Four C57BL/6J mice were ordered from Jackson labs for delivery at 15-16 weeks of age. Mice were preconditioned with supplemental chow for two weeks prior to start of

experiment. Mice were randomized by weight into three groups (vehicle, CCG-257081, PBS). Each group consisted of two cages with four mice per cage. Drug stock solutions were aliquoted and stored at 4 °C for the duration of the study. Aliquots were warmed to 37 °C and briefly vortexed prior to filling the gavage syringes. Vehicle and CCG-257081 groups received daily bleomycin injections (0.1 mL, ID) each afternoon in a defined area of shaved dorsal skin. PBS control group received daily injections (0.1 mL, ID) of PBS in the afternoon. Mice were anesthetized with ketamine/xylazine for ID injections. CCG-257081 (50 mg/kg) and the vehicle (20% DMSO/50% PEG-400/30% PBS) were administered (PO) in the morning by the University of Michigan's Unit for Laboratory Animal Medicine In-Vivo Animal Core. Mice were weighed daily to determine gavage dosage volume. Mice were euthanized after fourteen days of treatment by CO_2 inhalation/thoracotomy. Skin from the defined area was excised for biochemical and histological analysis. A portion of the skin was fixed in neutral buffered formalin (10%), washed in 70% ethanol, and paraffin-embedded for Masson's trichrome histological staining. Another portion of the skin was snap frozen for hydroxyproline measurement.

Histological analysis

Fixed skin was paraffin embedded and sectioned at the University of Michigan Comprehensive Cancer Center Histology Core. Skin sections were stained with Masson's trichrome (Sigma-Aldrich). Stained sections were analyzed with an Olympus BX51\DP72 microscope. Dermal thickness was determined by measuring the maximal distance between the epidermal-dermal junction and the dermal-subcutaneous fat junction. Three measurements were averaged from each skin section. The measurement was performed using the measurement tool in the cellSens imaging software package (Olympus).

Hydroxyproline assay

Skin sections were weighed and hydrolyzed in 6M HCl at 120 °C for three hours. Hydrolyzed skin supernatant and hydroxyproline standards (Sigma-Aldrich) were transferred to a microplate and dried at 60oC. Samples and standards were oxidized with Chloramine T oxidation buffer for

5 minutes at room temperature. 4-(Dimethylamino) benzaldehyde was added to the wells and incubated at 60 °C until the standard was well-defined (approximately 90 minutes). Absorbance was measured at 560 nm using a Synergy HT microplate reader (BioTek Instruments). Hydroxyproline values were normalized to tissue weight.

Bleomycin-Induced Antifibrotic Effects in Mice—CCG-58150:

During intradermal injections and gavage of test substance mice were anesthetized using isoflurane. The back was shaved and the injection site (~1cm_2) cleaned with three alternating passes of chlorhexidine and warm, sterile saline or water. The periphery of the injection site was circled using a sharpie marker as a visual aid. Bleomycin was dissolved in sterile PBS at a concentration of 1mg/ml, sterile filtered, and frozen in aliquots appropriately sized for the daily injections prior to the start of the dosing period. 100µl of bleomycin or PBS (Vehicle 1) was administered to anesthetized mice by intradermal injection using a 0.5cc TB syringe with a 27G needle. Following bleomycin or vehicle administration, test substance (CCG-58150) or Vehicle 2 (20% DMSO/30% PEG/50% PBS) was administered by oral gavage at 10µL/gram of body weight. Mice received daily clinical observations, injections of vehicle/bleomycin and oral vehicle/test substance for 14 days. Mice were weighed weekly and were euthanized on Day 15. The bleomycin injection site was visually assessed, and apparent fibrosis was graded as Not Detectable (0), Mild Fibrosis (1), Moderate Fibrosis (2) or Severe Fibrosis (3), based on the appearance of lesion. A terminal blood sample was collected for determination of serum chemistry values. The liver was collected and fixed in neutral buffered formalin, slides prepared and stained with Hematoxolin and eosin (H&E). The skin at the injection site was excised to contain a few mm of normal skin around the perimeter of the fibrotic skin. A small section (~5x2mm) of the fibrotic skin was collected using a scalpel, placed in a microfuge tube, snap frozen in liquid nitrogen, and stored at -80°C for future evaluation by the sponsor. The remaining tissue was pinned flat and fixed in 10% buffered formalin at room temperature. After fixation for at least 24 h, the skin was cut into 1-2mm wide strips and embedded in paraffin with the tissue

cross section facing up and all strips oriented in the same direction in the cassette. Slides were prepared and stained with H & E and Masson's trichrome. All slides and frozen tissue were sent to the Sponsor at study completion.

Bleomycin-Induced Antifibrotic Effects in Mice—CCG-232964:

C57BL/6J mice were ordered from Jackson labs for delivery at 15-16 weeks of age. Mice were preconditioned with supplemental chow for two weeks prior to start of experiment. Mice were randomized by weight into four groups (vehicle, CCG-232964 (3 mg/kg), CCG-232964 (10 mg/kg), PBS). Each group consisted of two cages with four mice per cage. Drug stock solutions were aliquoted and stored at 4 °C for the duration of the study. Aliquots were warmed to 37 °C and briefly vortexed prior to filling the gavage syringes. Vehicle and CCG-232964 groups received daily bleomycin injections (0.1mL, ID) each afternoon in a defined area of shaved dorsal skin. PBS control group received daily injections (0.1mL, ID) of PBS in the afternoon. Mice were anesthetized with ketamine/xylazine for ID injections. CCG-232964 (3 or 10 mg/kg) and the vehicle (20% DMSO/50% PEG-400/30% PBS) were administered (po) in the morning by the University of Michigan's Unit for Laboratory Animal Medicine In-Vivo Animal Core. Mice were weighed daily to determine gavage dosage volume. Mice were euthanized after fourteen days of treatment by CO_2 inhalation/thoracotomy. Skin from the defined area was excised for biochemical and histological analysis. A portion of the skin was fixed in neutral buffered formalin (10%), washed in 70% ethanol, and paraffin embedded for Masson's trichrome histological staining. Another portion of the skin was snap frozen for hydroxyproline measurement.

Fixed skin was paraffin embedded and sectioned at the University of Michigan Comprehensive Cancer Center Histology Core. Skin sections were stained with Masson's trichrome (Sigma-Aldrich). Stained sections were analyzed with an Olympus BX51\DP72 microscope. Dermal thickness was determined by measuring the maximal distance between the epidermal-dermal junction and the dermal-subcutaneous fat junction. Three measurements were averaged from

each skin section. The measurement was performed using the measurement tool in the cellSens imaging software package (Olympus).

Skin sections were weighed and hydrolyzed in 6M HCl at 120 °C for three h. Hydrolyzed skin supernatant and hydroxyproline standards (Sigma-Aldrich) were transferred to a microplate and dried at 60 °C. Samples and standards were oxidized with Chloramine T oxidation buffer for 5 minutes at room temperature. 4-(Dimethylamino) benzaldehyde was added to the wells and incubated at 60 °C until the standard was well defined. Absorbance was measured at 560 nm using a Synergy HT microplate reader (BioTek Instruments). Hydroxyproline values were normalized to tissue weight.

Docking With Pirin Co-Crystal Structures:

The protein structures were prepared to correct the common errors associated with the crystallographic data by capping the terminal residues, completing residues with missing atoms, and selecting appropriate alternate locations for atoms with fractional occupancies. Hydrogens were added and optimized for optimal hydrogen bond network, charges were calculated, and the tethered energy minimization was performed to relieve bad crystallographic contacts or other bad geometries. Co-crystallized ligand atoms defined the binding site. The ligand molecules were drawn in ChemDraw Professional 16.0.1.4 (77) and saved as sdf file. The chiral compounds were saved with the chiral center specified. The Amber10:EHT was used for the force field in the docking. We mostly used the rigid docking since the rigid docking of the ligand in 5jct.pdb reproduced the crystal structure of the bound ligand with the root mean square deviation (rmsd) of 0.3 A.

Virtual Screen Using 222740-Scaffold in CCG-222740 Co-Crystal Structure:

To design non-aniline analogs of CCG-257081, we performed a virtual screening of the combi-library created computationally. The chemical structures of a list of 9997 commercially available amines were obtained from Sigma Aldrich's website. A virtual combi-library of 6710 compounds was created by replacing the 4-chloro anilines in the CCG-257081 with the commercially

available amines in MOE. Out of this library, a set of 301 non-aniline compounds was saved after applying molecular weight less than 550 and by removing 68 aniline compounds. 122 compounds were selected based on the novelty of chemical structures and subsequently were subjected to the flexible docking with the induced fit option in the binding pocket of the X-ray crystal structure of Pirin complexed with CCG-257081. Finally, several compounds were selected for synthesis based on the docking scores, docking poses with additional interactions with the enzyme, and the synthetic feasibility.

General Chemistry Info:

All reagents were used without further purification as received from commercial sources unless noted otherwise. ^{1}H NMR and ^{13}C NMR spectra were taken in DMSO-d_6, MeOD-d_4, or $CDCl_3$ at room temperature on Varian Inova 400 MHz or Varian Inova 500 MHz instruments. Reported chemical shifts for the ^{1}H NMR and ^{13}C NMR spectra were recorded in parts per million (ppm) on the δ scale from an internal standard of residual tetramethylsilane (0 ppm). Mass spectrometry data were obtained on either a Micromass LCT or Agilent Q-TOF. An Agilent 1100 series HPLC with an Agilent Zorbax Eclipse Plus−C18 column (3.5 µM, 4.6 x 100 mm) was used to determine purity of biologically tested compounds. All tested compounds were determined to be >95% pure using a 6-minute gradient of 10-90% acetonitrile in water followed by a 2-minute hold at 90% acetonitrile at a flow rate of 1 mL/min with detection at 254 nm. Purification was accomplished using silica gel 40-63µm 60Å for column chromatography. Purification of some final compounds required Waters semipreparative HPLC with a Vydac protein and peptide C18 reverse phase column, using a linear gradient of 0% solvent B (0.1% TFA in acetonitrile) in solvent A (0.1% TFA in water) to 100% solvent B in solvent A at a rate 1% per minute and monitoring UV absorbance at 230 nm.

General Methods:

Method A: General Procedure for Fisher Esterification of Carbocyclic Acids

The appropriate acid (1.0 eq) was dissolved in MeOH (2-4 mL/1 mmol), and 98% sulfuric acid (1 eq) was added. The mixture was heated to reflux 4-16 h. The reaction solution was cooled to room temperature and concentrated in vacuo. The resulting crude residue was dissolved in a sat. $NaHCO_3$ (aq) solution and extracted with DCM. The combined organic layers were washed with brine, dried over $MgSO_4$ and concentrated to afford the desired ester. Yields: 50%-100%

Method B: General Procedure for *O*-Alkylation Using Propargyl Benzenesulfonate:

In a round-bottomed flask the starting phenol (1.0 eq) was dissolved in acetone (2-30 mL) and placed under inert atmosphere. K_2CO_3 (1.3 eq) and prop-2-yn-benzenesulfonate (1.5 eq) were added and the reaction proceeded at reflux (60 °C) for 3 hr under inert atmosphere. Acetone was evaporated in vacuo and the residue was taken up in water (2-30 mL). The product was extracted with EtOAc (3 x 30 mL), washed with brine, dried with $MgSO_4$, and the solvent evaporated. The oil was subjected to silica gel chromatography eluting with 15% EtOAc: 85% Hex. The fractions containing product were concentrated in vacuo to produce white powder. Yields: 76-92%.

Method C: General Procedure for Hydrazine Coupling of Aryl Methyl Carboxylates

In a round-bottomed flask, the starting aryl ester (1.0 eq) was dissolved in MeOH (2-4 mL/mmol), and hydrazine hydrate (10 eq) was added. The solution was heated to reflux (85 °C) for overnight. The reaction was cooled to 25 °C and concentrated in vacuo. The residue was taken up in DCM, partitioned between water, and the product was extracted with DCM (3 x 20 mL). The combined organic layers were washed with brine, dried with $MgSO_4$, and concentrated in vacuo to obtain white crystals. Yields: 70-100%

Method D: General Procedure for 1, 3, 4-oxadiazole-thiol Cyclization of Aryl Hydrazides

In a round-bottomed flask, the appropriate aryl hydrazide (1eq) was dissolved in a 0.1 M solution of KOH (1 eq) in EtOH (2-4 mL/mol)/H_2O (10 eq) and placed under nitrogen. Carbon disulfide (1 eq) was added and the reaction was heated to reflux (95 °C) overnight. Upon completion, most of the EtOH was evaporated in vacuo and the residue was cooled to 0 °C. The

product was acidified to pH 1 with 1 N HCl, and the subsequent white precipitate was filtered and dried under vacuum. Yields: 50-90%

Method E: General Procedure for Alkyl Halide Coupling of 1,3,4-Oxadiazole-2-Thiols

The starting thiol (1 eq), acetone (2-4 mL/1 mmol), and potassium carbonate (1.3 eq) were combined in a round-bottomed flask. The alkyl halide (1.3 eq mmol) was added to the solution and the reaction was stirred under nitrogen at 25 °C overnight. The crude mixture was concentrated in vacuo, and the residue was partitioned between DCM and water. The product was extracted with DCM (3 x 15 mL), washed with brine (30 mL), dried with $MgSO_4$, and concentrated in vacuo. The oil was subjected to silica gel chromatography eluting with 30-80% EtOAc: Hex. The fractions containing product were concentrated; and, after sitting overnight, some of the subsequent oils produced white solid. Yields: 50-95%

Method F: General Procedure for Acidic Ester Hydrolysis of t-Butyl Esters

In a round-bottomed flask the appropriate t-butyl ester (1 eq) was dissolved in DCM (2-4 mL/1 mmol). Trifluoroacetic acid (25 eq) was added and reaction was stirred under nitrogen at 25 °C for 3 h. The crude mixture was concentrated in vacuo and then dissolved in a minimal amount of EtOAc. The product was triturated out with Hex, and the subsequent white precipitate was filtered and dried under vacuum. Yields: 20-90%

Method G: General Procedure for Basic Ester Hydrolysis of Methyl Esters

In a round-bottomed flask, the starting methyl ester (1 eq) was dissolved in THF (1-2 mL/1 mmol). 1 M NaOH (1-2 mL/1 mmol) was added to the solution and the reaction was stirred at 25 °C for 3 h. The THF was evaporated in vacuo, and then the aqueous layer was acidified with 1 N HCl (7 mL). The product was extracted with EtOAc (3 x 15 mL), washed with brine (3 x 10 mL), dried with $MgSO_4$, and concentrated in vacuo. The residue was dissolved in minimal EtOAc and the product was triturated with Hex, producing a white precipitate that was filtered and dried under vacuum. Yields: 50-90%

Method H: General Procedure for Suzuki Cross Coupling (222740-Series):

In a round bottomed flask, aryl halide (1 eq), furan-2-ylboronic acid (1.2 eq), Tetrakis® (0.05 eq), and Na_2CO_3 (2.5 eq) were dissolved in DME (2-10 mL) and H_2O (2-10 mL). The solution was degassed, and then heated at 100 °C for 16 hr under Ar_2. The solution was filtered through a pad of Celite® to remove particulates. The filtrate was acidified with 1N HCl (15 mL), and the product was extracted with EtOAc (3 x 15 mL), washed with brine (1 x 15 mL), dried with $MgSO_4$, and concentrated in vacuo. The subsequent oil was subjected to silica gel chromatography eluting with 5% MeOH: 95% DCM. The fractions containing product were concentrated in vacuo. Yields: 30-88%

Method I: General Procedure for Amide Coupling Using HATU:

In a round bottomed flask, the carboxylic acid (1 eq) was dissolved in DMF (2-10 mL), and HATU (1.5 eq), desired aniline (1.1 eq), and DIPEA (3-4 eq) were added, respectively. The reaction was stirred at 25 °C for 16 hr, and then quenched with brine (10 mL). The product was extracted with EtOAc (3 x 15 mL), dried with $MgSO_4$, and concentrated in vacuo. The subsequent oil was subjected to silica gel chromatography eluting with 15% EtOAc: 85% Hex. The fractions containing product were concentrated in vacuo. Yields: 15-100%

Method J: General Procedure for Boc-Deprotection:

In a round-bottomed flask or scintillation vial, the Boc-amine (1 eq) was dissolved in 4 M HCl/Dioxanes (1.5-10 mL) and the reaction was stirred at 25 °C for 1 hr. The solvents were evaporated in vacuo, and the subsequent solid was taken into the next step without further purification. Yields: quant.

Method K: General Procedure for Suzuki Cross Coupling (58150-Series)

The appropriate aryl bromide (1 eq) was dissolved in toluene (2-4 mL/1 mmol) and degassed under inert atmosphere. H_2O (10 eq), potassium phosphate dibasic (3.5 eq), cyclopropyl boronic acid (1.2 eq), tricyclohexylphosphine (0.1 eq), and palladium (II) acetate (0.15 eq) were added. The mixture was heated at reflux (100 °C) for 3 hr under N_2. The mixture was cooled to 25 °C and H_2O was added. The product was extracted with EtOAc (3 x 15 mL), washed with brine (2 x

15 mL), dried with $MgSO_4$, and concentrated in vacuo. The yellow residue was subjected to silica gel chromatography eluting with 2.5% EtOAc: 97.5% Hex. Yields: 70-95%

Method L: General Procedure for *O*-Alkylation:

In a round-bottomed flask, the respective phenol (1 eq) was dissolved in 1-3 mL DMF. The respective alkyl halide (1.3 eq) along with Cs_2CO_3 (5 eq) were added and the reaction was stirred at 75 °C for 1 hr. The reaction was diluted with 10 mL brine and extracted with EtOAc (3x 10 mL). The organic layers were combined, dried with $MgSO_4$, and evaporated. The subsequent oil was subjected to silica gel chromatography eluting with 15% EtOAc: 75% Hex. The fractions containing product were concentrated in vacuo to produce colorless oil. Yields: 84-98%

Method M: General Procedure for Acyl Chloride Formation:

In a flame dried round bottomed flask or scintillation vial, the benzoic acid (1 eq) was dissolved in DCM (1-4 mL) and DMF (5-30 µL) was added. The solution was cooled to 0 °C and $(COCl)_2$ (1.1 eq) was added dropwise. The solution was stirred at 0 °C for 10 min and then at 25 °C for 1 hr. The reaction was concentrated in vacuo and the remaining $(COCl)_2$ was azeotroped with DCM (2 x 10 mL) to produce solid that was taken into next reaction without further purification.

Method N: General Procedure for Amide Coupling using Acyl Halide:

The respective amine or aniline (1 eq) was dissolved in DCM (1-5 mL) and Et_3N (4-6 eq) was added. The reaction was cooled to 0 °C and the respective acyl chloride in a solution of DCM was added dropwise. The reaction was stirred at 25 °C for 16 hr and then acidified with 1N HCl (7 mL). The product was extracted with DCM (3 x 15 mL), washed with brine (3 x 15 mL), dried with $MgSO_4$, and concentrated in vacuo. The oil was subjected to silica gel chromatography. The fractions containing product were concentrated to produce solid.

58150-Series Target Identification Analog Procedures (Chapter 2):

methyl-2,2-dimethoxypropanoate. methyl-2-oxopropanoate (1.77 mL, 19.6 mmol), p-toluenesulfonic acid (1.86 g, 9.8 mmol), trimethylorthoformate (2.6 mL, 23.5 mmol), and methanol (3.96 mL) were combined in a 50 mL round-bottomed flask and stirred under nitrogen

at 55 °C for 24 hr. The reaction was cooled to 0 °C and 30% sodium methoxide was added portion-wise. The crude mixture was concentrated in vacuo and dried under vacuum. The product was distilled at 50 °C/ 30 mm Hg as colorless oil. Yield=60%. ^{1}H NMR (401 MHz, $CDCl_3$-*d*) δ ppm 3.75 (s, 3H) 3.22 (s, 6H) 1.46 (s, 3H).

methyl-2-methoxyacrylate. In a 50 mL round-bottomed flask methyl-2,2-dimethoxypropanoate (1.74 g, 11.74 mmol), p-toluenesulfonic acid (0.067 g, 0.357 mmol), and hydroquinone (0.052 g, 0.470 mmol) were combined. The mixture was heated at 150 °C under ambient pressure while distilling MeOH byproduct. After about 4 mL of MeOH was collected (~5hr) the reaction mixture was cooled to 25 °C. The product was then distilled at 60 °C/ 30 mm Hg as colorless oil. Yield=64%. ^{1}H NMR (401 MHz, $CDCl_3$-*d*) δ ppm 5.37 (d, J = 2.7 Hz, 1H) 4.64 (d, J = 2.7 Hz, 1H) 3.82 (s, 3H) 3.29 (s, 3H).

methyl 3-(benzylthio)-2-methoxypropanoate. In a 50 mL round-bottomed flask methyl 2-methoxyacrylate (0.71 g, 6.14 mmol) was dissolved in THF (5 mL) and cooled to 0 °C. benzylmercaptan (0.76g, 6.14 mmol, 0.72 mL) dissolved in 1 M TBAF (in THF) (5.0 mL, 5.0 mmol) was added and the mixture was stirred under nitrogen at 25 °C for 2 hr. The reaction was quenched with water (20 mL) and the product was extracted with EtOAc (3x 15 mL). The organic layer was washed with brine, dried with magnesium sulfate, and evaporated, providing yellow oil. The residue was subjected to silica gel chromatography eluting with 10% EtOAc: 90% Hex. The fractions containing product were concentrated in vacuo to produce colorless oil. Yield=42.4%. ^{1}H NMR (500 MHz, $CDCl_3$-*d*) δ ppm 7.34-7.24 (m, 5H) 3.90 (m, 1H) 3.79 (s, 2H) 3.76 (s, 3H) 3.42 (s, 3H) 2.82-2.69 (m, 2H); TOF ES+ MS: (M+H) 241.1; HPLC Ret: 8.80 min.

3-(benzylthio)-2-methoxypropionic acid. In a 100 mL round-bottomed flask methyl 3-(benzylthio)-2-methoxypropanoate (0.63 g, 2.60 mmol) was dissolved in H_2O:MeOH (2:10 mL). Potassium carbonate (0.61 g, 4.43 mmol) was added and the reaction was stirred at 25 °C for 16 h. The reaction was quenched with sat. NH_4Cl (10 mL) and then acidified to pH ~ 1 with 1N

HCl (12 mL). The product was extracted with EtOAc (3x 20 mL). The organic layer was washed with brine, dried with magnesium sulfate, and evaporated, providing colorless oil. Yield=92%. ^{1}H NMR (500 MHz, $CDCl_3$-*d*) δ ppm 7.36-7.22 (m, 5H) 3.94 (m, 1H) 3.81 (s, 2H) 3.47 (s, 3H) 2.90-2.73 (m, 2H); HPLC Ret: 5.86 min.

3-mercapto-2-methoxypropionic acid. In a 100 mL round-bottomed three neck flask 3-(benzylthio)-2-methoxypropanoic acid (0.54 g, 2.40 mmol) was dissolved in liquid ammonia (12 mL) at -30 °C under inert atmosphere. Sodium metal (0.221 g, 9.40 mmol) was added portion-wise, turning the solution deep blue. The reaction was stirred under inert atmosphere at -30 °C for 30 min. The ammonia was removed with a constant flow of N_2 at -10 °C, causing the reaction to go from deep blue to clear. The reaction was quenched with H_2O (10 mL) and then acidified to pH ~ 2 with 1N HCl (20 mL). The product was extracted with EtOAc (3x 50 mL). The organic layer was dried with magnesium sulfate and then evaporated, providing colorless oil. Yield=84%. ^{1}H NMR (400 MHz, $CDCl_3$-*d*) δ ppm 9.49 (br. s. 1H) 4.01 (m, 1H) 3.53 (s, 3H) 2.98-2.90 (m, 2H) 1.78 (t, J = 8.5 Hz, 1H).

***tert*-butyl oxirane-2-carboxylate:** mCPBA (4.85 g, 28.1 mmol) and *tert*-butyl acrylate (3.0 g, 23.41 mmol) were dissolved in DCM (100 mL) and heated at 55 °C for 48 hr. The reaction was concentrated *in vacuo* and the residue was partitioned between EtOAc (30 mL) and water (30 mL). The product was extracted with EtOAc (3x 30 mL), washed with saturated sodium carbonate (3x 30 mL) and brine (3x 30 mL), dried with magnesium sulfate, and concentrated *in vacuo*. The product was dried on under vacuum while allowing any remaining *m*-chlorobenzoic acid to crystalize. The colorless oil was filtered through a cotton-plugged pipette. Yield=81%. ^{1}H NMR (401 MHz, $CDCl_3$-*d*) δ ppm 3.32 (dd, J = 4.0, 2.5 Hz, 1H) 2.90 (qd, J = 6.5, 3.3 Hz, 2H) 1.50 (s, 9H).

3-methoxydihydrofuran-2(3H)-one. 3-hydroxydihydrofuran-2(3H)-one (2.0 g, 1.5 mL, 19.59 mmol) was dissolved in 20 mL DCM. Silver oxide (18.16 g, 78.0 mmol) and iodomethane (27.8

g, 12.25 mL, 196.0 mmol) were added and the reaction was heated to reflux (70 °C) for 1 hr. The mixture was cooled and filtered through a pad of celite. The solvent was evaporated to dryness *in vacuo* to produce yellow oil. Yield=94%. ^{1}H NMR (500 MHz, $CDCl_3$-*d*) δ ppm 4.47-4.18 (m, 2H) 4.05 (t, J = 7.7 Hz, 1H) 3.57 (s, 3H) 2.60-2.18 (m, 2H).

methyl 4-iodo-2-methoxybutanoate. 3-methoxydihydrofuran-2(3H)-one (1.0 g, 8.61 mmol) was dissolved in 30 mL DCM and placed under inert atmosphere. MeOH (0.276 g, 0.35 mL, 8.61 mmol) was added and the reaction was cooled to -10 °C. Iodotrimethylsilane (1.90 g, 1.29 mL, 9.47 mmol) was added dropwise over a time of 15 min, after which the solution was stirred at -10 °C for 1 hr. The reaction was warmed up to 25 °C and stirred for 3 hr. The solution was washed with sat. $NaHCO_3$ (20 mL), 10% $Na_2S_2O_3$ (20 mL), and brine (20 mL). The organic layer was dried with $MgSO_4$ and concentrated *in vacuo* to produce yellow oil. Yield=68%. ^{1}H NMR (500 MHz, $CDCl_3$-*d*) δ ppm 4.45-4.24 (m, 2H) 4.02 (t, J = 7.7 Hz, 1H) 3.76 (s, 3H) 3.56 (s, 3H) 2.36-2.18 (m, 2H).

Methyl-2-acetoxy-5-iodopentanoate. Methyl tetrahydrofuran-2-carboxylate (1.1g, 8.45 mmol, 1.0 mL) and sodium iodide (2.5g, 16.9 mmol) were dissolved in 10 mL acetonitrile and cooled to 0 °C. Acetyl chloride (1.33g, 16.9 mmol, 1.2 mL) was added dropwise and the reaction took place at 25 °C for 24 hours. The reaction was quenched with concentrated sodium bicarbonate (30 mL). The product was extracted with Et_2O (3x 15 mL) and the organic layers were combined, washed with 10% sodium thiosulfate (15 mL) and brine (15 mL). The solvent was dried with $MgSO_4$and concentrated to dryness, producing yellow oil. Yield=99%. ^{1}H NMR (500 MHz, $CDCl_3$-*d*) δ ppm 5.02 (tq, J = 5.0, 2.9, 2.3 Hz, 1H) 3.76 (s, 3H) 3.20 (q, J = 7.0 Hz, 2H) 2.15 (s, 3H) 2.00-1.89 (m, 4H).

t-butyl (2-(2-hydroxyethoxy)ethyl)carbamate. In a 100-mL round bottomed flask, 2-(2-aminoethoxy)ethanol (2 g, 19.02 mmol) was dissolved in a H_2O (20 mL) and dioxane (10 mL) solution. Potassium hydroxide (1.2 g, 20.9 mmol) was dissolved and the solution was cooled to

0 °C. Boc anhydride (4.6 g, 20.9 mmol) was slowly added and the reaction was stirred at 0 °C for 1 hr, after which the solution was warmed to room temperature and stirred for 4 hr. The product was extracted with DCM (3 x 30 mL), washed with brine, dried with $MgSO_4$, and the solvent evaporated. The oil was subjected to silica gel chromatography eluting with 70% EtOAc: 30% Hex. The fractions containing product were concentrated in vacuo to produce pale yellow oil. Yield=86%. ^{1}H NMR (500 MHz, $CDCl_3$-*d*) δ ppm 5.13 (br. s, 1H) 3.74 (t, J = 5.5 Hz, 2H) 3.59-3.55 (m, 4H) 3.33 (q, J = 5.5 Hz, 2H) 1.45 (s, 9H).

2-(2-((t-butoxycarbonyl)amino)ethoxy)ethyl methanesulfonate. t-butyl (2-(2-hydroxyethoxy)ethyl)carbamate (1.06 g, 5.16 mmol, 1.0 mL), trimethylamine (1.05 g, 10.33 mmol, 1.44 mL), methanesulfonyl chloride (0.77 g, 6.71 mmol, 0.52 mL), and THF (20 mL) were combined and stirred at 25 °C for 3 hr. The trimethylamine hydrochloride salt was filtered through a pad of Celite and the filtrate was concentrated in vacuo. The subsequent oil was subjected to silica gel chromatography eluting with 50% EtOAc: 50% Hex. The fractions containing product were concentrated in vacuo to produce pale yellow oil. Yield=96%. ^{1}H NMR (500 MHz, $CDCl_3$-*d*) δ ppm 4.92 (br. s, 1H) 4.37 (t, J = 5.2 Hz, 2H) 3.73 (t, J = 5.2 Hz, 2H) 3.56 (t, J = 5.2 Hz, 2H) 3.33 (q, J = 5.5 Hz, 2H) 3.07 (s, 3H) 1.45 (s, 9H).

(2,6-dichlorophenoxy)triethylsilane. In a 250 mL round-bottomed flask, 2,6-dichlorophenol (5 g, 30.7 mmol) was dissolved in tetrahydrofuran (150 mL), and triethylamine (6.38 mL, 46 mmol) was added. Chlorotriethylsilane (7.72 mL, 46 mmol) was added dropwise prior to heating under nitrogen at 50 °C for 28 hr. Once the solution was cooled to room temperature it was washed thrice with both 10% citric acid (3x 50 mL) and saturated sodium carbonate (3 x 50 mL). The organic layer was washed with brine, dried with $MgSO_4$, and concentrated *in vacuo*. The product was isolated as colorless oil from a silica plug eluting with hexanes. Yield=84%. ^{1}H NMR (401 MHz, $CDCl_3$-*d*) δ ppm 7.28-7.20 (m, 2H) 6.82 (t, J = 8.1 Hz, 1H) 1.04-0.88 (m, 9H) 0.82 (q, J = 7.7 Hz, 6H); HPLC Ret: 10.11 min.

(2-chlorophenoxy)triisopropylsilane. In a 250 mL round-bottomed flask, 2-chlorophenol (5 g, 38.9 mmol, 3.96 mL) was dissolved in DMF (15 mL). Imidazole (2.65 g, 38.9 mmol) and triisopropylsilane chloride (7.5 g, 38.9 mmol, 8.24 mL) were added and the reaction was stirred at 25 °C for 24 hr. The reaction was diluted with 20 mL H_2O and the product was extracted with DCM (3 x 40 mL). The organic layers were combined and washed with brine, dried with $MgSO_4$, and concentrated *in vacuo*. The resulting oil was subjected to a silica plug eluting with hexanes, producing colorless oil. Yield=89%. ^{1}H NMR (500 MHz, $CDCl_3$-*d*) δ ppm 7.33 (td, J = 8.0, 1.5 Hz, 1H) 7.09 (td, J = 8.3, 1.6 Hz, 1H) 6.93-6.81 (m, 2H) 1.38-1.24 (m, 3H) 1.12 (d, J = 7.5 Hz, 21H); HPLC Ret: 9.35 min.

2,4-dichloro-3-hydroxybenzoic acid. (2,6-dichlorophenoxy)triethylsilane (2.3 g, 8.30 mmol) was added to an oven dried 100 mL round-bottomed flask charged with a stir bar containing tetrahydrofuran (12 mL). The solution was placed under nitrogen, cooled to -78 °C, and *sec*-butyllithium in cyclohexane (1.4 M, 6.52 mL) was added dropwise. The reaction proceeded for 45 min at -78 °C, and then was quickly poured over dry ice (7.3 g, 166 mmol) in a 150 mL beaker. Once the crude mixture warmed to 25 °C, 1N HCl (10.3 mL, 10.29 mmol) was added and stirred for 10 min. The product was extracted with EtOAc (3x 20 mL), washed with brine (3x 10 mL), dried over $MgSO_4$, and concentrated in vacuo. The crude extract was dissolved in EtOAC (20 mL) and a base wash with sodium bicarbonate (3x 10 mL) was performed. The subsequent aqueous layer was acidified to pH 3 with 1N HCl (25 mL) and the product was extracted with EtOAc (3x 20 mL). The organic layer was dried over $MgSO_4$ and, upon evaporation; the product was isolated as a fine white powder. Yield=20%. ^{1}H NMR (401 MHz, DMSO-d_6) δ ppm 13.41 (br. s., 1H) 10.38 (s, 1H) 7.83 (s, 1H) 7.44 (d, J = 8.4 Hz, 1H) 7.23 (d, J = 8.4 Hz, 1H).

2-chloro-3-hydroxybenzoic acid. (2-chlorophenoxy)triisopropylsilane (2.8 g, 9.83 mmol) was added to an oven dried 100 mL round-bottomed flask charged with a stir bar containing

tetrahydrofuran (12 mL). The solution was placed under nitrogen, cooled to -78 °C, and *sec*-butyllithium in cyclohexane (1.3 M, 9.1 mL) was added dropwise. The reaction proceeded for 1 hr at -78 °C, and then was quickly poured over fresh dry ice. Once the crude mixture warmed to 25 °C, 1N HCl (15 mL) was added and stirred for 10 min. The product was extracted with Et_2O (3x 50 mL), washed with brine, dried over $MgSO_4$, and concentrated in vacuo. The oil was dissolved in 1M TBAF in THF (9.83 mmol, 9.8 mL) the reaction was stirred at 25 °C for 2 hr. The solvent was evaporated in vacuo and the product (TBAF salt form) was crystalized with toluene to produce white platelets. Yield=42%. ^{1}H NMR (500 MHz, DMSO-d_6) δ ppm 10.60 (br. s., 1H) 6.86 (t, J = 7.7 Hz, 1H) 6.73 (q, J = 8.0 Hz, 1H) 6.56 (dd, J = 7.4, 1.6 Hz, 1H) 3.20-3.13 (m, 8H) 1.56 (t, 6.1 Hz, 8H) 1.30 (h, 7.4 Hz, 8H) 0.93 (t, 7.3 Hz, 12H); HPLC Ret: 3.93 min.

methyl 4-chloro-2-hydroxybenzoate. Method A starting from 4-chloro-2-hydroxybenzoic acid (2.0 g, 11.59 mmol) gave 3 methyl 4-chloro-2-hydroxybenzoate as yellow oil (1.21 g, 56%); ^{1}H NMR (500 MHz, $CDCl_3$-*d*) δ ppm 7.78 (dd, J = 8.6, 1.0 Hz, 1H) 6.96 (dd, J = 2.0, 1.0 Hz, 1H) 6.93-6.84 (m, 1H) 3.94 (s, 3H); TOF ES+ MS: (M+H) 187.4; HPLC Ret: 7.63 min.

methyl 2-chloro-4-hydroxybenzoate. Method A starting from 2-chloro-4-hydroxybenzoic acid (1.0 g, 6.08 mmol) gave methyl 2-chloro-4-hydroxybenzoate as tan powder (1.14 g, quant); HPLC Ret: 5.72 min.

methyl 2-chloro-3-hydroxybenzoate. Method A starting from 2-chloro-3-hydroxybenzoic acid (0.7 g, 4.06 mmol) gave methyl 2-chloro-3-hydroxybenzoate as colorless oil (0.4 g, 53%); ^{1}H NMR (500 MHz, $CDCl_3$-*d*) δ ppm 7.45 (dd, J = 7.6, 1.7 Hz, 1H) 7.28-7.16 (m, 2H) 3.93 (s, 3H); HPLC Ret: 5.42 min.

2,4-dichloro-3-(2-methoxyethoxy)benzoic acid. In a 50 mL round-bottomed flask 2,4-dichloro-3-hydroxybenzoic acid (0.25 g, 1.21 mmol) was dissolved in EtOH (3 mL) and placed under nitrogen. A 0.11 M solution of KOH (0.156 g, 2.78 mmol) in EtOH (1.5 mL) and 1-bromo-2-methyoxyethane (0.147 mL, 1.57 mmol) were added to the solution. The reaction was heated

to reflux (95 °C) for 24 hr. To drive the reaction to completion, another batch of 0.1 M KOH in EtOH (1 mL, 0.1 g) was added and heated to reflux (95 °C) for 2 hr. The crude mixture was concentrated in vacuo, diluted with H_2O (10 mL), and acidified to pH 1 with 1N HCl (2.5 mL). The product was extracted with EtOAc (3 x 10 mL), washed with brine (3 x 10 mL), dried with $MgSO_4$, and concentrated *in vacuo* to obtain light brown oil. Yield=94%. ^{1}H NMR (401 MHz, DMSO-d_6) δ ppm 13.55 (s, 1H) 7.62-7.50 (m, 2H) 4.13 (t, J = 4.0 Hz, 2H) 3.71 (t, J = 4.0 Hz, 2H) 3.17 (s, 3H); TOF ES- MS: (M-H) 264.9; HPLC Ret: 3.76 min.

methyl 4-chloro-2-(2-methoxyethoxy)benzoate. methyl 4-chloro-2-hydroxybenzoate (1.2 g, 6.43 mmol) was dissolved in 20 mL DMF. K_2CO_3 (1.78 g, 12.86 mmol) and 1-bromo-2-methoxyethane (1.16 g, 0.81 mL, 8.36 mmol) were added and the mixture was stirred at 90 °C for 4 hr. DMF was removed *in vacuo* and residue was partitioned between H_2O (15 mL) and DCM (15 mL). The product was extracted with DCM (3x 15 mL), washed with brine (20 mL), dried with $MgSO_4$, and concentrated *in vacuo*. The crude oil was subjected to silica gel chromatography eluting with 20% EtOAc: 80% Hex. The fractions containing product were concentrated to produce faint yellow/colorless oil. Yield=95%. ^{1}H NMR (500 MHz, $CDCl_3$-*d*) δ ppm 7.76 (dd, J = 8.0, 4.9 Hz, 1H) 7.02-6.93 (m, 2H) 4.17 (t, J = 5.0 Hz, 2H) 3.87 (s, 3H) 3.80 (t, J = 5.0 Hz, 2H) 3.47 (s, 3H); TOF ES+ MS: (M+H) 245.0; HPLC Ret: 6.75 min.

2-chloro-4-(2-methoxyethoxy)benzoic acid. In a 250 mL round-bottomed flask 2-chloro-4-hydroxybenzoic acid (3.5 g, 20.28 mmol) was dissolved in EtOH (40 mL) and placed under nitrogen. A 0.11 M solution of KOH (2.62 g, 46.6 mmol) in EtOH (25 mL) and 1-bromo-2-methyoxyethane (2.5 mL, 26.5 mmol) were added to the solution. The reaction was heated to reflux (95 °C) for 24 hr. A second batch of 0.1 M KOH in EtOH (2 g, 40.0 mmol, 20 mL) was added and heated to reflux (95 °C) for 2 hr. The crude mixture was concentrated in vacuo, diluted with H_2O (175 mL), and acidified on ice to pH 1 with 1N HCl (20 mL). The tan precipitate that formed was filtered and dried under vacuum. Yield=66%. ^{1}H NMR (401 MHz, MeOD-d_4) δ

ppm 7.90 (d, 7.2 Hz, 1H) 7.06 (s, 1H) 6.95 (d, 7.2 Hz, 1H) 4.17 (t, 6.3 Hz, 2H) 3.74 (t, 6.3 Hz, 2H) 3.41 (s, 3H); TOF ES- MS: (M-H) 229.9; HPLC Ret: 5.33 min.

methyl 2-chloro-4-(prop-2-yn-1-yloxy)benzoate. Method B starting from methyl 2-chloro-4-hydroxybenzoate (1.8 g, 9.8 mmol) gave methyl 2-chloro-4-(prop-2-yn-1-yloxy)benzoate as white solid (1.98 g, 90%); ^{1}H NMR (400 MHz, $CDCl_3$-*d*) δ ppm 7.89 (d, J = 8.8 Hz, 1H) 7.06 (d, J = 2.5 Hz, 1H) 6.91 (dd, J = 8.8, 2.5 Hz, 1H) 4.73 (d, J = 2.4 Hz, 2H) 3.90 (s, 3H) 2.58 (t, J = 2.4 Hz, 1H); TOF ES+ MS: (M+H) 224.9; HPLC Ret: 6.99 min.

methyl 4-chloro-2-(prop-2-yn-1-yloxy)benzoate. Method B starting from methyl 4-chloro-2-hydroxybenzoate (2.0 g, 10.6 mmol) gave methyl 4-chloro-2-(prop-2-yn-1-yloxy)benzoate as yellow oil (2.26 g, 92%); ^{1}H NMR (500 MHz, $CDCl_3$-*d*) δ ppm 7.78 (d, J = 8.3, 1H) 7.13 (d, J = 1.8 Hz, 1H) 7.03 (dd, J = 8.4, 1.9 Hz, 1H) 4.79 (d, J = 2.3 Hz, 2H) 3.88 (s, 3H) 2.58 (t, J = 2.3 Hz, 1H); TOF ES+ MS: (M+Na) 247.0; HPLC Ret: 6.92 min.

methyl 2-chloro-3-(prop-2-yn-1-yloxy)benzoate. Method B starting from methyl 2-chloro-3-hydroxybenzoate (0.37 g, 2.0 mmol) gave methyl 2-chloro-3-(prop-2-yn-1-yloxy)benzoate as yellow oil (0.34 g, 76%); ^{1}H NMR (500 MHz, $CDCl_3$-*d*) δ ppm 7.40 (dd, J = 7.7, 1.6 Hz, 1H) 7.29 (t, 8.3 Hz, 1H) 7.23 (dd, J = 8.3, 1.5 Hz, 1H) 4.81 (d, J = 2.4 Hz, 2H) 3.93 (s, 3H) 2.55 (t, J = 2.4 Hz, 1H); TOF ES+ MS: (M+H) 225.0; HPLC Ret: 6.74 min.

methyl 2-(benzyloxy)-4-chlorobenzoate. Methyl 4-chloro-2-hydroxybenzoate (1.0 g, 5.36 mmol) was dissolved in 15 mL DMF. K_2CO_3 (1.48 g, 10.72 mmol) and benzyl bromide (1.10 g, 6.43 mmol, 0.77 mL) were added and the mixture was stirred at 90 ^{o}C for 4 hr. DMF was removed in vacuo and the resulting oil was diluted with 20 mL H_2O and extracted with DCM (3x 20 mL). The organic layers were combined, washed with brine, dried with $MgSO_4$, and evaporated. The subsequent oil was subjected to silica gel chromatography eluting with 10% EtOAc: 90% Hex. The fractions containing product were concentrated in vacuo to produce colorless oil. Yield=86%. ^{1}H NMR (500 MHz, $CDCl_3$-*d*) δ ppm 7.78 (d, J = 8.3, 1H) 7.52-7.45 (m,

2H) 7.43-7.36 (m, 2H) 7.32 (t, J = 7.4 Hz, 1H) 7.03-6.94 (m, 2H) 5.15 (s, 2H) 3.88 (s, 3H); TOF ES+ MS: (M+Na) 298.9; HPLC Ret: 8.17 min.

2,4-dichloro-3-(2-methoxyethoxy)benzohydrazide. Method A followed by Method C starting from 2,4-dichloro-3-(2-methoxyethoxy)benzoic acid (0.3 g, 1.4 mmol) gave 2,4-dichloro-3-(2-methoxyethoxy)benzohydrazide as tan solid (0.22 g, 70%); ^{1}H NMR (401 MHz, DMSO-d_6) δ ppm 10.61 (s, 1H) 7.59-7.46 (m, 2H) 4.51 (br. s., 2H) 4.12 (t, J = 4.7 Hz, 2H) 3.70 (t, J = 4.0 Hz, 2H) 3.32 (s, 3H); HPLC Ret: 4.27 min.

2-chloro-4-(2-methoxyethoxy)benzohydrazide. (DJK-1-8). Method A followed by Method C starting from 2-chloro-4-(2-methoxyethoxy)benzoic acid (3 g, 13.01 mmol) gave 2-chloro-4-(2-methoxyethoxy)benzohydrazide as tan solid (3.2 g, 67%); ^{1}H NMR (401 MHz, DMSO-d_6) δ ppm 9.44 (s, 1H) 7.32 (d, 7.2 Hz, 1H) 7.06 (s, 1H) 6.94 (d, J = 7.2 Hz, 1H) 4.44 (br. s., 2H) 4.15 (t, 6.4 Hz, 2H) 3.64 (t, 6.3 Hz, 2H) 3.31 (s, 3H); TOF ES+ MS: (M+H) 245.0; HPLC Ret: 3.74 min.

4-chloro-2-(2-methoxyethoxy)benzohydrazide. (DJK-1-70). Method C starting from methyl 4-chloro-2-(2-methoxyethoxy)benzoate (1.0 g, 4.1 mmol) gave 4-chloro-2-(2-methoxyethoxy)benzohydrazide as white solid (0.86 g, 86%); ^{1}H NMR (401 MHz, $CDCl_3$-d) δ ppm 9.17 (br. s., 1H) 8.12 (d, J = 8.4 Hz, 1H) 7.09 (dd, J = 8.5, 1.9 Hz, 2H) 6.96 (d, J = 1.9 Hz, 1H) 4.28-4.21 (m, 2H) 4.16 (br. s., 2H) 3.84-3.76 (m, 2H) 3.50 (s, 3H); TOF ES+ MS: (M+H) 245.0; HPLC Ret: 4.48 min.

2-chloro-4-(prop-2-yn-1-yloxy)benzohydrazide. Method C starting from methyl 2-chloro-4-(prop-2-yn-1-yloxy)benzoate (2.0 g, 8.8 mmol) gave 2-chloro-4-(prop-2-yn-1-yloxy)benzohydrazide as yellow solid (1.48 g, 75%); ^{1}H NMR (400 MHz, $CDCl_3$-d) δ ppm 7.77 (br. s., 1H) 7.64 (d, 8.7 Hz, 1H) 7.00 (d, J = 2.5 Hz, 1H) 6.92 (dd, J = 8.7, 2.5 Hz, 1H) 4.72 (d, J = 2.4 Hz, 2H) 4.16 (br. s., 2H) 2.59 (t, J = 2.4 Hz, 1H); TOF ES+ MS: (M+H) 224.9; HPLC Ret: 4.28 min.

4-chloro-2-(prop-2-yn-1-yloxy)benzohydrazide. Method C starting from methyl 4-chloro-2-(prop-2-yn-1-yloxy)benzoate (2.0 g, 8.9 mmol) gave 4-chloro-2-(prop-2-yn-1-yloxy)benzohydrazide as yellow solid (0.6 g, 32%); ^{1}H NMR (400 MHz, $CDCl_3$-*d*) δ ppm 8.71 (d, 8.5 Hz, 1H) 8.14 (d, J = 2.5 Hz, 1H) 7.12 (dd, J = 8.5, 2.6 Hz, 1H) 4.84 (d, J = 2.5 Hz, 2H) 4.19 (br. s., 2H) 2.66 (t, J = 2.8 Hz, 1H); TOF ES+ MS: (M+H) 225.0; HPLC Ret: 4.38 min.

2-chloro-3-(prop-2-yn-1-yloxy)benzohydrazide. Method C starting from methyl 2-chloro-3-(prop-2-yn-1-yloxy)benzoate (0.34 g, 1.5 mmol) gave 2-chloro-3-(prop-2-yn-1-yloxy)benzohydrazide as white solid (0.26 g, 76%); ^{1}H NMR (500 MHz, DMSO-d_6) δ ppm 9.52 (br. s., 1H) 7.35 (dd, J = 8.4, 7.5 Hz, 1H) 7.26 (dd, 8.4, 1.4 Hz, 1H) 6.97 (dd, J = 8.4, 1.4 Hz, 1H) 4.95 (d, J = 2.4 Hz, 2H) 4.47 (br. s., 2H) 3.63 (t, J = 2.4 Hz, 1H); TOF ES+ MS: (M+H) 225.0; HPLC Ret: 6.39 min.

methyl 2-(benzyloxy)-4-chlorobenzoate. Method C starting from methyl 2-(benzyloxy)-4-chlorobenzoate (1.2 g, 4.3 mmol) gave 2-(benzyloxy)-4-chlorobenzohydrazide as white solid (1.19 g, 99%); ^{1}H NMR (500 MHz, DMSO-d_6) δ ppm 9.22 (s, 1H) 7.62 (d, J = 8.2 Hz, 1H) 7.50-7.43 (m, 2H) 7.45-7.36 (m, 2H) 7.37-7.30 (m, 1H) 7.27 (d, J = 1.9 Hz, 1H) 7.08 (dd, J = 8.3, 1.9 Hz, 1H) 5.26 (s, 2H); TOF ES+ MS: (M+Na) 277.0; HPLC Ret: 5.76 min.

5-(2,4-dichloro-3-(2-methoxyethoxy)phenyl)-1,3,4-oxadiazole-2-thiol. Method D starting from 2,4-dichloro-3-(2-methoxyethoxy)benzohydrazide (0.22 g, 0.79 mmol) gave 5-(2,4-dichloro-3-(2-methoxyethoxy)phenyl)-1,3,4-oxadiazole-2-thiol as yellow solid (0.09 g, 35%); ^{1}H NMR (400 MHz, CDCl-*d*) δ ppm 7.70 (dd, 2H) 4.19 (t, J = 6.3 Hz, 2H) 3.73 (t, J = 6.3 Hz, 2H) 3.39 (s, 3H); TOF ES- MS: (M-H) 320.9; HPLC Ret: 6.68 min.

5-(2-chloro-4-(2-methoxyethoxy)phenyl)-1,3,4-oxadiazole-2-thiol. Method D starting from 2-chloro-4-(2-methoxyethoxy)benzohydrazide (2.0 g, 8.2 mmol) gave 5-(2-chloro-4-(2-methoxyethoxy)phenyl)-1,3,4-oxadiazole-2-thiol as yellow solid (1.92 g, 82%); ^{1}H NMR (401 MHz, $CDCl_3$-*d*) δ ppm 7.88 (d, J = 8.8 Hz, 1H) 6.88 (s, 1H) 6.80 (d, J = 8.8 Hz, 1H) 4.07 (t, J =

9.0 Hz, 2H) 3.70 (t, J = 9.0 Hz, 2H) 3.39 (s, 3H); ^{13}C NMR (401 MHz, $CDCl_3$-*d*) δ ppm 167.09, 160.77, 132.03, 131.66, 131.55, 125.23, 116.20, 113.40, 70.59, 67.71, 59.20; TOF ES- MS: (M-H) 284.9; HPLC Ret: 6.24 min.

5-(4-chloro-2-(2-methoxyethoxy)phenyl)-1,3,4-oxadiazole-2-thiol. Method D starting from 4-chloro-2-(2-methoxyethoxy)benzohydrazide (0.86 g, 3.5 mmol) gave 5-(4-chloro-2-(2-methoxyethoxy)phenyl)-1,3,4-oxadiazole-2-thiol as white solid (0.81 g, 80%); ^{1}H NMR (500 MHz, $CDCl_3$-*d*) δ ppm 11.38 (br. s., 1H) 7.78-7.74 (m, 1H) 7.09-7.05 (m, 2H) 4.36-4.28 (m, 2H) 3.88 (t, J = 4.8 Hz, 2H) 3.51 (s, 3H); TOF ES+ MS: (M+H) 287.0; HPLC Ret: 6.50 min.

5-(2-chloro-4-(prop-2-yn-1-yloxy)phenyl)-1,3,4-oxadiazole-2-thiol. Method D starting from 2-chloro-4-(prop-2-yn-1-yloxy)benzohydrazide (1.5 g, 6.6 mmol) gave 5-(2-chloro-4-(prop-2-yn-1-yloxy)phenyl)-1,3,4-oxadiazole-2-thiol as yellow solid (1.45 g, 83%); ^{1}H NMR (500 MHz, DMSO-d_6) δ ppm 7.92 (d, 8.8 Hz, 1H) 7.40 (d, J = 2.5 Hz, 1H) 7.24 (dd, J = 8.9, 2.6 Hz, 1H) 5.03 (d, J = 2.4 Hz, 2H) 2.71 (t, J = 2.4 Hz, 1H); TOF ES$^+$ MS: (M+H) 266.9; HPLC Ret: 6.58 min.

5-(2-chloro-4-(prop-2-yn-1-yloxy)phenyl)-1,3,4-oxadiazole-2-thiol. Method D starting from 4-chloro-2-(prop-2-yn-1-yloxy)benzohydrazide (0.64 g, 2.9 mmol) gave 5-(4-chloro-2-(prop-2-yn-1-yloxy)phenyl)-1,3,4-oxadiazole-2-thiol as yellow solid (0.75 g, 99%); ^{1}H NMR (400 MHz, DMSO-d_6) δ ppm 7.76 (d, 8.4 Hz, 1H) 7.41 (d, J = 1.8 Hz, 1H) 7.21 (dd, J = 8.4, 1.8 Hz, 1H) 5.03 (d, J = 2.3 Hz, 2H) 3.68 (t, J = 2.3 Hz, 1H); TOF ES$^+$ MS: (M+H) 267.0; HPLC Ret: 6.62 min.

5-(2-chloro-3-(prop-2-yn-1-yloxy)phenyl)-1,3,4-oxadiazole-2-thiol. Method D starting from 2-chloro-3-(prop-2-yn-1-yloxy)benzohydrazide (0.26 g, 1.15 mmol) gave 5-(2-chloro-3-(prop-2-yn-1-yloxy)phenyl)-1,3,4-oxadiazole-2-thiol as yellow solid (0.3 g, 98%); ^{1}H NMR (400 MHz, DMSO-d_6) δ ppm 7.51-7.22 (m, 3H) 5.02 (d, J = 2.4 Hz, 2H) 3.68 (t, J = 2.4 Hz, 1H); HPLC Ret: 6.39 min.

5-(2-(benzyloxy)-4-chlorophenyl)-1,3,4-oxadiazol-2-thiol. Method D starting from methyl 2-(benzyloxy)-4-chlorobenzoate (1.2 g, 4.34 mmol) gave 5-(2-(benzyloxy)-4-chlorophenyl)-1,3,4-oxadiazol-2-thiol as white solid (1.3 g, 93%); ^{1}H NMR (400 MHz, DMSO-d_6) δ ppm 12.41 (br. s., 1H) 7.77 (d, J = 8.4 Hz, 1H) 7.52 (d, J = 1.9 Hz, 1H) 7.47-7.27 (m, 5H) 7.20 (dd, J = 8.4, 1.9 Hz, 1H) 5.33 (s, 2H); TOF ES+ MS: (M+Na) 341.0; HPLC Ret: 7.64 min.

5-(2,4-dichlorophenyl)-1,3,4-oxadiazol-2-ol. In a 50 mL round bottomed flask 2,4-dichlorobenzohydrazide (0.5g, 2.44 mmol), K_3PO_4 (0.52, 2.44 mmol), and CS_2 (0.19g, 0.15 mL, 2.44 mmol) were stirred in 10 mL of H_2O for 10 min at 25 °C. The reaction was then stirred at reflux (106 °C) for 2 hr and then cooled to 25 °C. propylene oxide (0.14 g, 2.44 mmol, 0.17 mL) was added and the reaction was stirred at 25 °C for 16 hr. The product was extracted with EtOAc (3x 15 mL), washed with brine, dried with $MgSO_4$. and the solvent was evaporated. The residue was subjected to silica gel chromatography eluting with 20% EtOAc: 80% Hex. The fractions containing product were concentrated in vacuo to produce white solid. Yield=23% (2 steps). ^{1}H NMR (500 MHz, $CDCl_3$-d) δ ppm 9.18 (br. s., 1H) 7.83-7.73 (m, 1H) 7.57-7.55 (m, 1H) 7.41-7.38 (m, 1H); TOF ES+ MS: (M+H) 228.9; HPLC Ret: 6.39 min.

5-(2, 4-dichlorophenyl)-1,3,4-thiadiazole-2-thiol. 2, 4-dichlorobenzohydrazide (0.5 g, 2.44 mmol) was dissolved in a 0.1 M solution of KOH (0.27 g, 4.88 mmol) in EtOH/H_2O (10 mL/0.44 mL, 24.4 mmol mmol) and placed under nitrogen. Carbon disulfide (0.44 g, 7.32 mmol 0.44 mL) was added and the reaction was stirred at 25 °C for 3 hr. The solid that formed was filtered and dried in vacuo. The solid was subjected to fuming sulfuric acid (3 mL) and stirred under N_2 for 2 hr. Upon completion the reaction was diluted with 30 mL H_2O and the subsequent solid was filtered and dried in vacuo. Yellow solid. Yield=40.5%. ^{1}H NMR (500 MHz, DMSO-d_6) δ ppm 9.35 (br. s., 1H) 7.93 (d, J = 8.5 Hz, 1H) 7.71 (d, J = 8.4 Hz, 1H) 7.51 (dd, J = 8.4, 2.1 Hz, 1H); TOF ES- MS: (M-H) 262.9; HPLC Ret: 7.45 min.

2-(bromomethyl)-5-(2,4-dichlorophenyl)-1,3,4-oxadiazole. In a 100 mL round bottomed flask 2,4-dichlorobenzohydrazide (0.5 g, 2.44 mmol) and bromoacetic acid (0.34 g, 2.44 mmol) were combined under inert atmosphere. The reagents were dissolved in $POCl_3$ (5.0 mL) and stirred at reflux (106 °C) for 16 hr. The reaction was cooled to room temperature and poured over ice water (5 mL). The solution was neutralized to pH ~ 9 with $NaHCO_3$ (20% → sat) causing a yellow precipitate to form. The product was extracted with EtOAc (3x 25 mL), washed with brine, dried with $MgSO_4$, and the solvents were evaporated producing brown oil. The impurities were triturated out with EtOAc:Hex (tan solid) and the mother liquor was evaporated to provide the desired product as white/tan solid. Yield=49%. ^{1}H NMR (500 MHz, $CDCl_3$-*d*) δ ppm 7.97 (d, J = 8.3, 1H) 7.60 (s, 1H) 7.42 (dd, J = 8.3, 2.2 Hz, 1H) 4.62 (s, 2H); TOF ES+ MS: (M+MeOH+Na) 359.9; HPLC Ret: 7.42 min.

2-(2-chloro-4-cyclopropylphenyl)-5-(chloromethyl)-1,3,4-oxadiazole. In a 25 mL round bottomed flask 2-chloro-4-cyclopropylbenzohydrazide (0.15 g, 0.1 mmol) and chloroacetic acid (0.07 g, 0.71 mmol) were combined under inert atmosphere. The reagents were dissolved in $POCl_3$ (1.5 mL) and stirred at reflux (106 °C) for 6 hr. The reaction was cooled to room temperature and poured over ice water (5 mL). The product was extracted with EtOAc (3x 20 mL), washed with brine, dried with $MgSO_4$, and the solvents were evaporated producing brown oil. The impurities were crystalized with EtOAc:Hex to provide white solid. Yield=56%. ^{1}H NMR (500 MHz, DMSO-d_6) δ ppm 7.36 (dd, J = 8.3, 1.5 Hz, 1H) 7.25 (s, 1H) 7.13 (dd, J = 8.3, 1.6 Hz, 1H) 4.18 (s, 2H) 1.09-0.98 (m, 2H) 0.79-0.74 (m, 2H); HPLC Ret: 7.52 min.

2-(2,4-dichlorophenyl)-5-(methylthio)-1,3,4-oxadiazole. 5-(2,4-dichlorophenyl)-1,3,4-oxadiazole-2-thiol (0.25 g, 1.01 mmol) was dissolved in 5 mL THF. Triethylamine (0.12 g, 0.17 mL, 1.21 mmol) and iodomethane (0.16 g, 0.07 mL, 1.11 mmol) were added and the mixture was stirred at 25 °C for 2 hr. The reaction was quenched with 5 mL H_2O. The product was extracted with EtOAc (3x, 15 mL), washed with brine (20 mL), dried with $MgSO_4$, and

concentrated *in vacuo*. The residue was dissolved in minimal EtOAc and the product was triturated with Hex, producing a white precipitate that was filtered and dried under vacuum. Yield=81%. ^{1}H NMR (401 MHz, $CDCl_3$-*d*) δ ppm 7.91 (d, J = 8.5 Hz, 1H) 7.57 (d, J = 2.1 Hz, 1H) 7.39 (dd, J = 8.5, 2.1 Hz, 1H) 2.79 (s, 3H); TOF ES+ MS: (M+H) 260.9; HPLC Ret: 7.57 min.

2-(2,4-dichlorophenyl)-5-(methylsulfonyl)-1,3,4-oxadiazole.

Method 1: 2-(2,4-dichlorophenyl)-5-(methylthio)-1,3,4-oxadiazole (0.215 g, 0.823 mmol) was dissolved in 5 mL EtOH and cooled to 0 °C. Ammonium molybdate tetrahydrate (0.20 g, 0.165 mmol) and hydrogen peroxide (0.28 g, 0.25 mL, 2.47 mmol) were added and stirred at 25 °C for 2 hr. The reaction was quenched with 10% sodium thiosulfate (10 mL). The product was extracted with EtOAc (3x, 15 mL), washed with brine (20 mL), dried with $MgSO_4$, and concentrated *in vacuo*. The yellow residue was subjected to silica gel chromatography eluting with 20% EtOAc: 80% Hex. The fractions containing product were concentrated *in vacuo* to produce white solid. Yield=54%. ^{1}H NMR (401 MHz, $CDCl_3$-*d*) δ ppm 8.02 (d, J = 8.5 Hz 1H) 7.64 (d, J = 2.0 Hz 1H) 7.47 (dd, J = 8.5, 2.0 Hz, 1H) 3.55 (s, 3H); TOF ES+ MS: (M+H) 292.9; HPLC Ret: 6.96 min.

Method 2: 2-(2,4-dichlorophenyl)-5-(methylthio)-1,3,4-oxadiazole (0.3 g, 1.15 mmol) was dissolved in 5 mL DCM. mCPBA (0.57 g, 2.30 mmol) was added and the reaction was stirred at 25 °C for 2 hr. The solvent was evaporated, and the yellow residue was subjected to silica gel chromatography eluting with 20% EtOAc: 80% Hex. The fractions containing product were concentrated *in vacuo* to produce white solid. Yield=64%.

***tert*-butyl-3-((5-(2,4-dichloro-3-(2-methoxyethoxy)phenyl)-1,3,4-oxadiazol-2-yl)thio)propanoate.** Method E starting from 5-(2,4-dichloro-3-(2-methoxyethoxy)phenyl)-1,3,4-oxadiazole-2-thiol (0.9 g, 0.28 mmol) and t-butyl-3-bromopropanoate (0.07 g, 0.34 mmol) gave tert-butyl-3-((5-(2,4-dichloro-3-(2-methoxyethoxy)phenyl)-1,3,4-oxadiazol-2-yl)thio)propanoate as colorless oil (0.09 g, 64%); ^{1}H NMR (401 MHz, $CDCl_3$-*d*) δ ppm 7.65 (d, J = 8.6 Hz, 1H) 7.43

(d, J = 8.5 Hz, 1H) 4.31-4.21 (m, 2H) 3.87-3.79 (m, 2H) 3.51 (t, J = 6.8 Hz, 2H) 3.49 (s, 3H) 2.86 (t, J = 6.8 Hz, 2H) 1.47 (s, 9H); TOF ES+ MS: (M+H) 249.0; HPLC Ret: 8.51 min.

***tert*-butyl-3-((5-(2-chloro-4-(2-methoxyethoxy)phenyl)-1,3,4-oxadiazol-2-yl)thio)propanoate.** Method E starting from 5-(2-chloro-4-(2-methoxyethoxy)phenyl)-1,3,4-oxadiazole-2-thiol (1.0 g, 3.5 mmol) and t-butyl-3-bromopropanoate (0.9 g, 4.2 mmol) gave tert-butyl-3-((5-(2-chloro-4-(2-methoxyethoxy)phenyl)-1,3,4-oxadiazol-2-yl)thio)propanoate as colorless oil (0.78 g, 54%); ^{1}H NMR (401 MHz, $CDCl_3$-*d*) δ ppm 7.86 (d, J = 8.8 Hz, 1H) 7.08 (d, J = 2.5 Hz, 1H) 6.95 (dd, J = 8.8, 2.5 Hz, 1H) 4.21-4.07 (m, 2H) 3.81-3.72 (m, 2H) 3.50 (t, J = 6.8 Hz, 2H) 3.47 (s, 3H) 2.86 (t, J = 6.8 Hz, 2H) 1.47 (s, 9H); ^{13}C NMR (401 MHz, $CDCl_3$-*d*) δ ppm 172.47, 163.73, 161.81, 133.31, 132.57, 117.03, 114.94, 114.88, 81.02, 70.48, 68.27, 61.14, 58.59, 35.29, 28.74, 25.56, 21.16, 14.78; HPLC Ret: 8.09 min.

tert-butyl 3-((5-(4-chloro-2-(2-methoxyethoxy)phenyl)-1,3,4-oxadiazol-2-yl)thio)propanoate. Method E starting from 5-(4-chloro-2-(2-methoxyethoxy)phenyl)-1,3,4-oxadiazole-2-thiol (0.2 g, 0.7 mmol) and t-butyl-3-bromopropanoate (0.18 g, 0.84 mmol) gave tert-butyl 3-((5-(4-chloro-2-(2-methoxyethoxy)phenyl)-1,3,4-oxadiazol-2-yl)thio)propanoate as colorless oil (0.24 g, 83%); ^{1}H NMR (500 MHz, $CDCl_3$-*d*) δ ppm 7.94-7.74 (m, 1H) 7.09-7.03 (m, 2H) 4.23 (t, J = 3.5 Hz, 2H) 3.82 (t, J = 3.5 Hz, 2H) 3.49 (t, J = 6.8 Hz, 2H) 3.47 (s, 3H) 2.85 (t, J = 6.8 Hz, 2H) 1.47 (s, 9H); TOF ES+ MS: (M+H) 415.1; HPLC Ret: 8.28 min.

methyl 4-((5-(2-chloro-4-(2-methoxyethoxy)phenyl)-1,3,4-oxadiazol-2-yl)thio)butanoate. Method E starting from 5-(2-chloro-4-(2-methoxyethoxy)phenyl)-1,3,4-oxadiazole-2-thiol (0.25 g, 0.87 mmol) and methyl 4-bromobutanoate (0.19 g, 1.1 mmol) gave methyl 4-((5-(2-chloro-4-(2-methoxyethoxy)phenyl)-1,3,4-oxadiazol-2-yl)thio)butanoate as colorless oil (0.22 g, 64%); ^{1}H NMR (500 MHz, $CDCl_3$-*d*) δ ppm 7.88 (d, J = 7.4 Hz, 1H) 7.09 (d, J = 4.0 Hz, 1H) 6.96 (dd, J = 7.1, 2.8 Hz, 1H) 4.19 (t, J = 9.3 Hz, 2H) 3.78 (t, J = 9.3 Hz, 2H) 3.70 (s, 3H) 3.47 (s, 3H) 3.36 (t,

J = 7.2 Hz, 2H) 2.54 (t, J = 7.3 Hz, 3H) 2.20 (p, J = 7.0 Hz, 2H); TOF ES+ MS: (M+H) 386.9; HPLC Ret: 7.01 min.

t-butyl-4-((5-(2-chloro-4-(prop-2-yn-1-yloxy)phenyl)-1,3,4-oxadiazol-2-yl)thio)butanoate. Method E starting from 5-(2-chloro-4-(prop-2-yn-1-yloxy)phenyl)-1,3,4-oxadiazole-2-thiol (0.5 g, 1.9 mmol) and t-butyl-4-bromobutanoate (0.46 g, 2.06 mmol) gave t-butyl-4-((5-(2-chloro-4-(prop-2-yn-1-yloxy)phenyl)-1,3,4-oxadiazol-2-yl)thio)butanoate as colorless oil (0.44 g, 58%); ^{1}H NMR (500 MHz, $CDCl_3$-*d*) δ ppm 7.90 (d, 8.8 Hz, 1H) 7.14 (d, J = 2.5 Hz, 1H) 7.00 (dd, J = 8.8, 2.6 Hz, 1H) 4.76 (d, J = 2.4 Hz, 2H) 3.34 (t, J = 7.2 Hz, 2H) 2.59 (t, J = 2.4 Hz, 1H) 2.43 (t, J = 7.2 Hz, 2H) 2.15 (p, J = 7.2 Hz, 2H) 1.45 (s, 9H); TOF ES^+ MS: (M+H) 409.9; HPLC Ret: 8.35 min.

t-butyl-4-((5-(4-chloro-2-(prop-2-yn-1-yloxy)phenyl)-1,3,4-oxadiazol-2-yl)thio)butanoate. Method E starting from 5-(4-chloro-2-(prop-2-yn-1-yloxy)phenyl)-1,3,4-oxadiazole-2-thiol (0.2 g, 0.75 mmol) and t-butyl-4-bromobutanoate (0.2 g, 0.9 mmol) gave t-butyl-4-((5-(4-chloro-2-(prop-2-yn-1-yloxy)phenyl)-1,3,4-oxadiazol-2-yl)thio)butanoate as yellow oil (0.17 g, 56%); ^{1}H NMR (500 MHz, $CDCl_3$-*d*) δ ppm 7.87 (d, 8.4 Hz, 1H) 7.20 (d, J = 1.8 Hz, 1H) 7.11 (dd, J = 8.4, 1.9 Hz, 1H) 4.85 (d, J = 2.4 Hz, 2H) 3.33 (t, J = 7.2 Hz, 2H) 2.60 (t, J = 2.4 Hz, 1H) 2.42 (t, J = 7.2 Hz, 2H) 2.14 (p, J = 7.2 Hz, 2H) 1.45 (s, 9H); TOF ES^+ MS: (M+H) 408.1; HPLC Ret: 8.36 min.

methyl 4-((5-(2-chloro-3-(prop-2-yn-1-yloxy)phenyl)-1,3,4-oxadiazol-2-yl)thio)butanoate. Method E starting from 5-(2-chloro-3-(prop-2-yn-1-yloxy)phenyl)-1,3,4-oxadiazole-2-thiol (0.3 g, 1.13 mmol) and methyl 4-bromobutanoate (0.27 g, 1.46 mmol) gave methyl 4-((5-(2-chloro-3-(prop-2-yn-1-yloxy)phenyl)-1,3,4-oxadiazol-2-yl)thio)butanoate as white solid (0.21 g, 50%); ^{1}H NMR (500 MHz, $CDCl_3$-*d*) δ ppm 7.58 (d, 8.4 Hz, 1H) 7.37 (d, J = 1.9 Hz, 1H) 7.27 (dd, J = 8.4, 1.9 Hz, 1H) 4.84 (d, J = 2.4 Hz, 2H) 3.69 (s, 3H) 3.36 (t, J = 7.2 Hz, 2H) 2.60 (t, J = 2.4 Hz, 1H) 2.55 (t, J = 7.2 Hz, 2H) 2.22 (p, J = 7.2 Hz, 2H); TOF ES^+ MS: (M+H) 367.1; HPLC Ret: 7.09 min.

t-butyl-4-((5-(2-(benzyloxy)-4-chlorophenyl)-1,3,4-oxadiazol-2-yl)thio)butanoate. Method E starting from 5-(2-(benzyloxy)-4-chlorophenyl)-1,3,4-oxadiazol-2-thiol (1.0 g, 3.1 mmol) and t-butyl-4-bromobutanoate (0.9 g, 4.1 mmol) gave t-butyl-4-((5-(2-(benzyloxy)-4-chlorophenyl)-1,3,4-oxadiazol-2-yl)thio)butanoate as colorless oil (1.06 g, 73%); ^{1}H NMR (500 MHz, $CDCl_3$-*d*) δ ppm 7.89 (d, J = 8.3 Hz, 1H) 7.54-7.47 (m, 2H) 7.41 (t, J = 7.5 Hz, 2H) 7.40-7.29 (m, 1H) 7.12-7.04 (m, 2H) 5.21 (s, 2H) 3.27 (t, J = 7.1 Hz, 2H) 2.38 (t, J = 7.2 Hz, 2H) 2.08 (p, J = 7.4 Hz, 2H) 1.45 (s, 9H); TOF ES+ MS: (M+H) 461.1; HPLC Ret: 9.49 min.

methyl 4-((5-(2,4-dichlorophenyl)-1,3,4-oxadiazol-2-yl)thio)-2-methoxybutanoate. Method E starting from 5-(2,4-dichlorophenyl)-1,3,4-oxadiazol-2-thiol (0.2 g, 0.81 mmol) and methyl 4-iodo-2-methoxy)butanoate (0.25 g, 0.97 mmol) gave methyl 4-((5-(2,4-dichlorophenyl)-1,3,4-oxadiazol-2-yl)thio)-2-methoxybutanoate as colorless oil (0.21 g, 67%); ^{1}H NMR (500 MHz, $CDCl_3$-*d*) δ ppm 7.91 (d, J = 8.5, 1H) 7.57 (d, J = 2.0 Hz, 1H) 7.39 (dd, J = 8.5, 2.1 Hz, 1H) 3.97 (dd, J = 8.7, 4.0 Hz, 1H) 3.78 (s, 3H) 3.44 (s, 3H) 2.42-2.21 (m, 2H); ^{13}C NMR (500 MHz, $CDCl_3$-*d*) δ ppm 172.21, 164.89, 163.39, 138.03, 133.72, 131.54, 131.17, 127.60, 121.39, 78.33, 58.40, 52.13, 32.32, 28.37; TOF ES+ MS: (M+H) 377.0; HPLC Ret: 7.87 min.

methyl 2-acetoxy-5-((5-(2,4-dichlorophenyl)-1,3,4-oxadiazol-2-yl)thio)pentanoate Method E starting from 5-(2,4-dichlorophenyl)-1,3,4-oxadiazol-2-thiol (0.5 g, 2.0 mmol) and methyl 2-acetoxy-5-iodopentanoate (0.73 g, 2.4 mmol) gave methyl 2-acetoxy-5-((5-(2,4-dichlorophenyl)-1,3,4-oxadiazol-2-yl)thio)pentanoate as colorless oil (0.78 g, 92%); ^{1}H NMR (500 MHz, $CDCl_3$-*d*) δ ppm 7.91 (d, J = 8.5, 1H) 7.57 (s, 1H) 7.40 (dd, J = 8.5, 2.3 Hz, 1H) 5.06 (dd, J = 4.5, 1.9 Hz, 1H) 3.76 (s, 3H) 3.34 (dt, J = 8.8, 5.7 Hz, 2H) 3.15 (s, 3H) 2.11-1.96 (m, 4H) ; TOF ES+ MS: (M+H) 418.9; HPLC Ret: 7.96 min.

methyl 5-((5-(2,4-dichlorophenyl)-1,3,4-oxadiazol-2-yl)thio)-2-hydroxypentanoate. methyl 2-acetoxy-5-((5-(2,4-dichlorophenyl)-1,3,4-oxadiazol-2-yl)thio)pentanoate (0.78 g, 1.86 mmol) was dissolved in MeOH (8 mL) and K_2CO_3 (0.26 g, 1.86 mmol) was added. The reaction was

stirred at 25 °C for 30 min upon which the MeOH was removed in vacuo. The product was extracted with EtOAc (3x 15 mL) and the organic layers were combined, washed with brine, dried with $MgSO_4$, and evaporated. The residue was subjected to silica gel chromatography eluting with 30% EtOAc: 70% Hex. The fractions containing product were concentrated in vacuo to produce white oil. Yield=49%. ^{1}H NMR (500 MHz, $CDCl_3$-*d*) δ ppm 7.91 (d, J = 8.4 Hz, 1H) 7.57 (s, 1H) 7.39 (dd, J = 8.4, 2.1 Hz, 1H) 4.26 (ddd, J = 7.9, 5.0, 3.1 Hz, 1H) 3.80 (s, 3H) 3.36 (t, J = 6.7 Hz, 2H) 2.11-1.94 (m, 4H); TOF ES+ MS: (M+H) 398.9; HPLC Ret: 7.03 min.

methyl 5-((5-(2,4-dichlorophenyl)-1,3,4-oxadiazol-2-yl)thio)-2-methoxypentanoate. In a 15 mL pressure vessel methyl 5-((5-(2,4-dichlorophenyl)-1,3,4-oxadiazol-2-yl)thio)-2-hydroxypentanoate (0.2 g, 0.53 mmol) was dissolved in DCM (5.0 mL). Ag_2O (0.5 g, 2.12 mmol) and MeI (0.75 g, 5.3 mmol, 0.33 mL) were added and the reaction was stirred at 60 °C for 18 hr. The solids were filtered through a pad of Celite and the mother liquor was evaporated. The residue was subjected to silica gel chromatography eluting with 20% EtOAc: 80% Hex. The fractions containing product were concentrated in vacuo to produce yellow oil. Yield=39%. ^{1}H NMR (500 MHz, $CDCl_3$-*d*) δ ppm 7.91 (d, J = 8.5 Hz, 1H) 7.57 (d, J = 2.1 Hz, 1H) 7.39 (dd, J = 8.5 , 2.1 Hz, 1H) 3.82 (ddd, J = 7.4, 4.2, 2.1 Hz, 1H) 3.77 (s, 3H) 3.40 (s, 3H) 3.34 (t, J = 7.0 Hz, 2H) 2.10-1.81 (m, 4H); TOF ES+ MS: (M+H) 390.9; HPLC Ret: 7.96 min.

***tert*-butyl-3-((5-(2,4-dichlorophenyl)-1,3,4-oxadiazol-2-yl)thio)2-hydroxypropanoate.** In a 50 mL round-bottomed flask, 5-(2,4-dichlorophenyl)-1,3,4-oxadiazole-2-thiol (0.5 g, 2.023 mmol) was dissolved in THF (10 mL) and combined with 1 M TBAF in THF (3.0 mL, 3.04 mmol) and *tert*-butyl oxirane-2-carboxylate (2.8 g, 20.23 mmol). The mixture was stirred under nitrogen at 25 °C for 36 hr and, upon completion, concentrated in vacuo. The residue was subjected to silica gel chromatography eluting with 25% EtOAc: 75% Hex. The fractions containing product were concentrated in vacuo to produce faint yellow oil, which crystallized upon standing.

Yield=38%. ^{1}H NMR (401 MHz, DMSO-d_6) δ ppm 7.99 (d, 1H) 7.91 (s, 1H) 7.66 (d, 1H) 5.99 (d, 1H) 4.33 (t, 1H) 3.67-3.48 (m, 2H) 1.40 (s, 9H); HPLC Ret: 7.90 min.

2-(((5-(2,4-dichlorophenyl)-1,3,4-oxadiazol-2-yl)methyl)thio)acetic acid. (CCG-257169). 2-mercaptoacetic acid (0.13 g, 1.36 mmol, 0.10 mL) was dissolved in acetone (5 mL) and K_2CO_3 (0.19 g, 1.36 mmol) and 2-(bromomethyl)-5-(2,4-dichlorophenyl)-1,3,4-oxadiazole (0.35 g, 1.14 mmol) were added. The reaction was stirred at 25 °C for 24 hr and the solvent was removed in vacuo. The residue was taken up in H_2O (2 mL) and acidified to pH ~ 1 with 1 N HCl (3 mL). The product was extracted with DCM (3x 15 mL), washed with brine, dried with $MgSO_4$, and the solvent was evaporated in vacuo. The residue was subjected to silica gel chromatography eluting with 5% MeOH: 95% DCM: 0.01% AcOH. The fractions containing product were concentrated and the residue was triturated with DCM. The product was filtered producing white crystals. Yield=20%. ^{1}H NMR (400 MHz, DMSO-d_6) δ ppm 12.73 (br. s., 1 H) 7.96 (d, J = 8.4, 1H) 7.89 (d, J = 2.1, 1H) 7.65 (dd, J = 8.5, 2.1 Hz, 1H) 4.62 (s, 2H) 3.46 (s, 2H); ^{13}C NMR (400 MHz, DMSO-d_6) δ ppm 171.17, 165.24, 162.28, 137.57, 133.27, 132.91, 131.20, 128.81, 121.93, 33.93, 24.95; TOF ES+ MS: (M+H) 318.9; HPLC Ret: 6.13 min.

3-(((5-(2-chloro-4-cyclopropylphenyl)-1,3,4-oxadiazol-2-yl)methyl)thio)propanoic acid. (CCG-259013). 3-mercaptopropionic acid (0.024 g, 0.22 mmol, 0.02 mL) was dissolved in acetone (1.5 mL) and K_2CO_3 (0.031 g, 0.22 mmol) and 2-(2-chloro-4-cyclopropylphenyl)-5-(chloromethyl)-1,3,4-oxadiazole (0.05 g, 0.19 mmol) were added. The reaction was stirred at 25 °C for 24 hr and the solvent was removed in vacuo. The residue was taken up in H_2O (2 mL) and acidified to pH ~ 1 with 1 N HCl (3 mL). The product was extracted with EtOAc (3x 15 mL), washed with brine, dried with $MgSO_4$, and the solvent was evaporated in vacuo. The residue was subjected to silica gel chromatography eluting with 2% to 5% MeOH DCM: 0.01% AcOH. The fractions containing product were concentrated and the product was crystalized from EtOAc/Hex producing white powder. Yield=20%. ^{1}H NMR (500 MHz, MeOD) δ ppm 7.50 (d, J =

8.0 Hz, 1H) 7.19 (d, J = 1.7 Hz, 1H) 7.08 (dd, J = 8.0, 1.7 Hz, 1H) 3.33 (s, 2H) 2.93 (t, J = 7.1 Hz, 2H) 2.69 (t, J = 7.1 Hz, 2H) 1.95-1.88 (m, 1H) 1.10-0.98 (m, 2H) 0.79-0.69 (m, 2H); ^{13}C NMR (500 MHz, MeOD) δ ppm 174.25, 169.98, 167.21, 149.21, 131.22, 130.31, 129.13, 126.70, 123.59, 33.78, 32.73, 27.06, 14.54, 9.18; TOF ES+ MS: (M+H_2O) 357.1; HPLC Ret: 5.21 min.

tert-butyl 4-((5-(2,4-dichlorophenyl)-1,3,4-oxadiazol-2-yl)oxy)butanoate. 5-(2,4-dichlorophenyl)-1,3,4-oxadiazol-2-ol (0.06 g, 0.251 mmol) was dissolved in DMF (2 mL). K_2CO_3 (0.045 g, 0.33 mmol) and tert-butyl 4-bromobutanoate (0.07 g, 0.33 mmol, 0.06 mL) were added and the reaction was stirred at 90 °C for 1 hr. The solvent was removed in vacuo and the residue was partitioned between H_2O (10 mL) and DCM (10 mL). The product was extracted with DCM (3x 10 mL), washed with brine, dried with $MgSO_4$, and evaporated. The oil was subjected to silica gel chromatography eluting with 10% EtOAc: 90% Hex. The fractions containing product were concentrated in vacuo to produce white solid. Yield=62%. ^{1}H NMR (500 MHz, $CDCl_3$-*d*) δ ppm 7.75 (d, J = 8.5, 1H) 7.54 (d, J = 2.1 Hz, 1H) 7.37 (dd, J = 8.5, 2.1 Hz, 1H) 3.88 (t, J = 6.8 Hz, 2H) 2.36 (t, J = 7.3 Hz, 2H) 2.10 (p, J = 7.1 Hz, 2H) 1.45 (s, 9H); TOF ES+ MS: (M+Na) 396.9; HPLC Ret: 8.72 min.

methyl 4-((5-(2,4-dichlorophenyl)-1,3,4-thiadiazol-2-yl)thio)butanoate. Potassium carbonate (0.17 g, 1.24 mmol) and methyl 4-bromobutryate (0.22 g, 1.24 mmol, 0.17 mL) were added to 5-(2,4-dichlorophenyl)-1,3,4-thiadiazole-2-thiol (0.25 g, 0.95 mmol) dissolved in DMF (5 mL). The mixture was stirred at 90 °C for 1 hr. The DMF was evaporated, the oil was diluted with H_2O, and product was extracted with DCM (3 x 15 mL). The organic layers were combined, washed with brine, and evaporated. The oil was subjected to silica gel chromatography eluting with 20% EtOAc: 80% Hex. The fractions containing product were concentrated to produce white solid. Yield=35%. ^{1}H NMR (500 MHz, $CDCl_3$-*d*) δ ppm 7.80 (d, J = 8.4 Hz, 1H) 7.48 (d, J = 2.0 Hz, 1H) 7.31 (dd, J = 8.4, 2.1 Hz, 1H) 4.38 (t, J = 6.3 Hz, 2H) 3.68 (s, 3H) 2.50 (t, J = 7.4 Hz, 2H) 2.11 (p, J = 7.3 Hz, 2H); TOF ES+ MS: (M+Na) 387.0; HPLC Ret: 8.67 min.

t-butyl-4-((5-(2-chloro-4-hydroxyphenyl)-1,3,4-oxadiazol-2-yl)thio)butanoate. t-butyl-4-((5-(2-chloro-4-(prop-2-yn-1-yloxy)phenyl)-1,3,4-oxadiazol-2-yl)thio)butanoate (0.1 g, 0.25 mmol) was dissolved in 2:1 DMF/H_2O solution. Bis(triphenylphosphine)palladium(II) chloride (0.01 g, 0.015 mmol) and trimethylamine (0.2 g, 1.96 mmol, 0.27 mL) were added and the reaction was stirred under nitrogen at 80 °C for 5 hr. The reaction was quenched with H_2O (5 mL) and acidified to pH ~ 1 with 1N HCl (2 mL). The product was extracted with EtOAc (3 x 15 mL), and the resulting organic layer was washed with brine (20 mL), dried with $MgSO_4$, and evaporated. The oil was subjected to silica gel chromatography eluting with 40% EtOAc: 60% Hex. The fractions containing product were concentrated in vacuo to produce yellow solid. Similar analogs were made in an analogous fashion. Yield=52%. ^{1}H NMR (500 MHz, $CDCl_3$-*d*) δ ppm 7.80 (d, 8.6 Hz, 1H) 7.07 (d, J = 2.5 Hz, 1H) 6.89 (dd, J = 8.6, 2.5 Hz, 1H) 3.33 (t, J = 2.4 Hz, 1H) 2.43 (t, J = 7.2 Hz, 2H) 2.15 (p, J = 7.2 Hz, 2H) 1.46 (s, 9H); TOF ES$^+$ MS: (M+Na) 393.0; HPLC Ret: 7.37 min.

methyl 4-((5-(2-chloro-3-hydroxyphenyl)-1,3,4-oxadiazol-2-yl)thio)butanoate. *note: methyl 4-((5-(2-chloro-3-(prop-2-yn-1-yloxy)phenyl)-1,3,4-oxadiazol-2-yl)thio)butanoate used as starting material; silica gel chromatography eluting with 35% EtOAc to 50% EtOAc: 65% Hex to 50% Hex: 0.01% AcOH. White solid. Yield=41%; ^{1}H NMR (500 MHz, $CDCl_3$-*d*) δ ppm 7.37 (dt, 7.8, 1.2 Hz, 1H) 7.30 (t, J = 8.1 Hz, 1H) 7.15 (dd, J = 8.2, 1.4 Hz, 1H) 3.67 (s, 3H) 3.37 (t, J = 7.2 Hz, 2H) 2.54 (t, J = 7.2 Hz, 2H) 2.16 (p, J = 7.2 Hz, 2H); TOF ES$^+$ MS: (M+H) 329.0; HPLC Ret: 6.02 min.

4-((5-(4-chloro-2-hydroxyphenyl)-1,3,4-oxadiazol-2-yl)thio)butanoic acid (CCG-257422). tert-butyl 4-((5-(2-(benzyloxy)-4-chlorophenyl)-1,3,4-oxadiazol-2-yl)thio)butanoate (0.085 g, 0.195 mmol) was dissolved in 0.5 mL ethane thiol. Boron trifluoride etherate (0.183 g, 1.289 mmol, 0.06 mL) was added and the reaction was stirred at 25 ^{o}C for 1 hr. The reaction was quenched with 5 mL H_2O and the product was extracted with Et_2O (3 x 20 mL). The organic

layers were combined, washed with brine, dried with $MgSO_4$, and evaporated, producing a white powder. Yield=98%. ^{1}H NMR (500 MHz, DMSO-d_6) δ ppm 12.18 (br. s., 1H) 8.03 (d, J = 1.9 Hz, 1H) 7.90 (d, J = 8.4 Hz, 1H) 7.78 (dd, J = 8.4, 1.9 Hz, 1H) 3.33 (t, J = 2.4 Hz, 1H) 2.39 (t, J = 7.3 Hz, 2H) 2.00 (p, J = 7.3 Hz, 2H); HPLC Ret: 6.90 min.

tert-butyl 4-((5-(4-(2-(2-((tert-butoxycarbonyl)amino)ethoxy)ethoxy)-2-chlorophenyl)-1,3,4-oxadiazol-2-yl)thio)butanoate. tert-butyl 4-((5-(2-chloro-4-hydroxyphenyl)-1,3,4-oxadiazol-2-yl)thio)butanoate (0.047 g, 0.13mmol) was dissolved in 1 mL DMF. Freshly prepared 2-(2-((tert-butoxycarbonyl)amino)ethoxy)ethyl methanesulfonate (0.033 g, 0.12 mmol) along with Cs_2CO_3 (0.19 g, 0.58 mmol) were added and the reaction was stirred at 75 ^{o}C for 1.5 hr. The DMF was evaporated and the resulting oil was diluted with 10 mL H_2O and extracted with DCM (3 x 10 mL). The organic layers were combined, washed with brine, dried with $MgSO_4$, and evaporated. The subsequent oil was subjected to silica gel chromatography eluting with 60% EtOAc: 40% Hex. The fractions containing product were concentrated in vacuo to produce pale yellow oil. Similar compounds were made in an analogous fashion. Yield=93%. ^{1}H NMR (400 MHz, $CDCl_3$-*d*) δ ppm 7.88 (d, 8.8 Hz, 1H) 7.08 (d, J = 2.5 Hz, 1H) 6.94 (dd, J = 8.8, 2.5 Hz, 1H) 4.94 (br. s, 1H) 4.16 (t, J = 5.2 Hz, 2H) 3.84 (t, J = 5.6 Hz, 2H) 3.62 (t, J = 5.2 Hz, 2H) 3.37-3.32 (m, 4H) 2.43 (t, J = 7.2 Hz, 2H) 2.16 (p, J = 7.2 Hz, 2H) 1.45 (s, 18H); TOF ES$^+$ MS: (M+H) 557.9; HPLC Ret: 8.58 min.

4-((5-(2-(2-(2-((tert-butoxycarbonyl)amino)ethoxy)ethoxy)-4-chlorophenyl)-1,3,4-oxadiazol-2-yl)thio)butanoate. *note: 4-((5-(4-chloro-2-hydroxyphenyl)-1,3,4-oxadiazol-2-yl)thio)butanoic acid (0.06 g, 0.19 mmol) used as starting material; reaction done at 90 ^{o}C for 3 hr; silica gel chromatography eluting with 40% EtOAc: 60% Hex. Colorless oil. Yield=77%; ^{1}H NMR (500 MHz, $CDCl_3$-*d*) δ ppm 7.83 (d, 8.5 Hz, 1H) 7.73 (d, J = 1.3 Hz, 1H) 7.54 (dd, J = 8.5, 2.0 Hz, 1H) 5.30 (br. s, 1H) 4.25 (t, J = 5.6 Hz, 2H) 3.66 (t, J = 5.2 Hz, 2H) 3.54 (t, J = 5.2 Hz, 2H) 3.40-3.31 (m, 4H) 2.57 (t, J = 7.1 Hz, 2H) 2.22 (p, J = 7.2 Hz, 2H) 1.44 (s, 9H); HPLC Ret: 8.38 min.

2-((2-(1H-tetrazol-5-yl)ethyl)thio)-5-(2,4-dichlorophenyl)-1,3,4-oxadiazole. (CCG-257447). 5-(2,4-dichlorophenyl)-1,3,4-oxadiazole-2-thiol (0.2 g, 0.81 mmol), potassium carbonate (0.145 g, 1.05 mmol), and 5-(2-chloroethyl)-1H-tetrazole (0.14 g, 1.05 mmol) were dissolved in acetone (5 mL). The mixture was stirred at 60 °C for 2 days. The acetone was removed in vacuo and the remaining oil was diluted in 5 mL H_2O, acidified to pH ~ 1 with 1N HCl, and extracted with EtOAc (3 x 15 mL). The organic layers were combined, washed with brine, dried with $MgSO_4$, and evaporated in vacuo. The solid obtained was subjected to silica gel chromatography eluting with 1% MeOH: 99% DCM. The fractions containing product were concentrated *in vacuo* to produce white solid. Yield=38%. ^{1}H NMR (500 MHz, DMSO-d_6) δ ppm 8.00 (d, J = 8.5 Hz, 1H) 7.92(d, J = 2.1 Hz, 1H) 7.67 (dd, J = 8.5, 2.2 Hz, 1H) 3.74 (t, J = 7.0 Hz, 2H) 3.50 (t, J = 7.0 Hz, 2H) 3.40 (br. s., 1H); ^{13}C NMR (500 MHz, $CDCl_3$-*d*) δ ppm 164.47, 163.05, 137.61, 133.17, 132.75, 131.21, 128.65, 121.61, 30.10, 23.94; TOF ES- MS: (M+H) 342.9; HPLC Ret: 6.32 min; 96% pure.

3-((5-(2,4-dichloro-3-(2-methoxyethoxy)phenyl)-1,3,4-oxadiazol-2-yl)thio)propanoic acid (CCG-224500). Method F starting from tert-butyl-3-((5-(2,4-dichloro-3-(2-methoxyethoxy)phenyl)-1,3,4-oxadiazol-2-yl)thio)propanoate (0.08 g, 0.18 mmol) gave 3-((5-(2,4-dichloro-3-(2-methoxyethoxy)phenyl)-1,3,4-oxadiazol-2-yl)thio)propanoic acid as white crystals (0.09 g, 64%); ^{1}H NMR (401 MHz, $CDCl_3$-*d*) δ ppm 7.65 (d, J = 8.0 Hz, 1H) 7.43 (d, J = 8.0 Hz, 1H) 4.25 (t, J = 4.0 Hz, 2H) 3.83 (t J = 4.0 Hz, 2H) 3.55 (t, J = 8.0 Hz, 2H) 3.48 (s, 3H) 3.05 (t, J = 8.0 Hz, 2H); TOF ES+ MS: (M+H) 393.24; HPLC Ret: 6.32 min; 97.5% pure.

3-((5-(2-chloro-4-(2-methoxyethoxy)phenyl)-1,3,4-oxadiazol-2-yl)thio)propanoic acid (CCG-224480). Method F starting from tert-butyl-3-((5-(2-chloro-4-(2-methoxyethoxy)phenyl)-1,3,4-oxadiazol-2-yl)thio)propanoate (0.3 g, 0.72 mmol) gave 3-((5-(2-chloro-4-(2-methoxyethoxy)phenyl)-1,3,4-oxadiazol-2-yl)thio)propanoic acid as white crystals (0.22 g, 85%); ^{1}H NMR (401 MHz, $CDCl_3$-*d*) δ ppm 7.86 (d, J = 8.0 Hz, 1H) 7.08 (d, J = 4.0 Hz, 1H) 6.94 (dd, J

= 8.0, 4.0 Hz, 1H) 4.18 (t, J = 4.0 Hz, 2H) 3.78 (t, J = 4.0 Hz, 2H) 3.53 (t, J = 8.0 Hz, 2H) 3.46 (s, 3H) 3.02 (t, J = 8.0 Hz, 2H); ^{13}C NMR (401 MHz, $CDCl_3$-*d*) δ ppm 175.92, 163.91, 161.44, 134.12, 131.96, 116.98, 115.22, 113.87, 70.59, 67.82, 59.25, 33.92, 27.02, 14.17; TOF ES+ MS: (M+H) 359.0; HPLC Ret: 5.85 min; 92.7% pure.

3-((5-(4-chloro-2-(2-methoxyethoxy)phenyl)-1,3,4-oxadiazol-2-yl)thio)propanoic acid. (CCG-232942). Method F starting from tert-butyl-3-((5-(4-chloro-2-(2-methoxyethoxy)phenyl)-1,3,4-oxadiazol-2-yl)thio)propanoate (0.24 g, 0.58 mmol) gave 3-((5-(4-chloro-2-(2-methoxyethoxy)phenyl)-1,3,4-oxadiazol-2-yl)thio)propanoic acid as white powder (0.15 g, 69%); ^{1}H NMR (500 MHz, $CDCl_3$-*d*) δ ppm 7.87-7.82 (m, 1H) 7.07-7.05 (m, 2H) 4.24 (t, J = 5.0 Hz, 2H) 3.83 (t, J = 5.0 Hz, 2H) 3.52 (t, J = 6.8 Hz, 2H) 3.46 (s, 3H) 3.00 (t, J = 6.8 Hz, 2H); ^{13}C NMR (500 MHz, $CDCl_3$-*d*) δ ppm 175.48, 163.84, 157.38, 138.88, 131.01, 121.49, 113.97, 111.65, 70.62, 68.93, 59.39, 34.02, 27.06, 14.17; TOF ES+ MS: (M+H) 359.0; HPLC Ret: 6.148 min; 98% pure.

4-((5-(2-chloro-4-(2-methoxyethoxy)phenyl)-1,3,4-oxadiazol-2-yl)thio)butanoic acid (CCG-257156). Method G starting from methyl 4-((5-(2-chloro-4-(2-methoxyethoxy)phenyl)-1,3,4-oxadiazol-2-yl)thio)butanoate (0.22 g, 0.56 mmol) gave 4-((5-(2-chloro-4-(2-methoxyethoxy)phenyl)-1,3,4-oxadiazol-2-yl)thio)butanoic acid as white powder (0.14 g, 65%); ^{1}H NMR (500 MHz, $CDCl_3$-*d*) δ ppm 8.25 (br. s., 1H) 7.87 (d, J = 8.8 Hz, 1H) 7.08 (d, J = 2.1 Hz, 1H) 6.95 (dd, J = 8.5, 2.0 Hz, 1H) 4.21-4.15 (m, 2H) 3.81-3.75 (m, 2H) 3.46 (s, 3H) 3.37 (t, J = 7.2 Hz, 2H) 2.58 (t, J = 7.1 Hz, 2H) 2.21 (p, J = 7.2 Hz, 2H); TOF ES+ MS: (M+H) 373.0; HPLC Ret: 6.03 min; 97 % pure.

4-((5-(2-chloro-4-(prop-2-yn-1-yloxy)phenyl)-1,3,4-oxadiazol-2-yl)thio)butanoic acid. (CCG-257274). Method F starting from t-butyl-4-((5-(2-chloro-4-(prop-2-yn-1-yloxy)phenyl)-1,3,4-oxadiazol-2-yl)thio)butanoate (0.15 g, 0.37 mmol) gave 4-((5-(2-chloro-4-(prop-2-yn-1-yloxy)phenyl)-1,3,4-oxadiazol-2-yl)thio)butanoic acid as white powder (0.12 g, 97%); ^{1}H NMR

(500 MHz, $CDCl_3$-*d*) δ ppm 9.99 (br. s., 1H) 7.90 (d, 8.8 Hz, 1H) 7.14 (d, J = 2.5 Hz, 1H) 7.00 (dd, J = 8.8, 2.6 Hz, 1H) 4.76 (d, J = 2.4 Hz, 2H) 3.37 (t, J = 7.1 Hz, 2H) 2.59 (m, 3H) 2.22 (p, J = 7.1 Hz, 2H); ^{13}C NMR (500 MHz, $CDCl_3$-*d*) δ ppm 177.81, 164.17, 164.04, 160.00, 134.12, 131.97, 117.44, 116.06, 114.05, 76.70, 56.19, 32.24, 31.59, 24.34; TOF ES^+ MS: (M+H) 353.0; HPLC Ret: 6.35 min; 98% pure.

4-((5-(4-chloro-2-(prop-2-yn-1-yloxy)phenyl)-1,3,4-oxadiazol-2-yl)thio)butanoic acid. (CCG-257291). Method F starting from t-butyl-4-((5-(4-chloro-2-(prop-2-yn-1-yloxy)phenyl)-1,3,4-oxadiazol-2-yl)thio)butanoate (0.1 g, 0.25 mmol) gave 4-((5-(4-chloro-2-(prop-2-yn-1-yloxy)phenyl)-1,3,4-oxadiazol-2-yl)thio)butanoic acid as yellow solid (0.08 g, 89%); ^{1}H NMR (500 MHz, $CDCl_3$-*d*) δ ppm 9.36 (br. s., 1H) 7.84 (d, 8.3 Hz, 1H) 7.22 (d, J = 1.3 Hz, 1H) 7.12 (dd, J = 8.4, 1.4 Hz, 1H) 4.86 (d, J = 2.3 Hz, 2H) 3.38 (t, J = 7.1 Hz, 2H) 2.61-2.59 (m, 3H) 2.20 (p, J = 7.1 Hz, 2H); ^{13}C NMR (500 MHz, $CDCl_3$-*d*) δ ppm 177.78, 164.37, 163.40, 156.00, 139.21, 130.98, 122.17, 114.42, 111.34, 77.34, 56.71, 32.18, 31.54, 24.28; TOF ES^+ MS: (M+H) 353.0; HPLC Ret: 6.40 min; 95% pure.

4-((5-(2-chloro-3-(prop-2-yn-1-yloxy)phenyl)-1,3,4-oxadiazol-2-yl)thio)butanoic acid. **(CCG-257631).** Method G starting from methyl 4-((5-(2-chloro-3-(prop-2-yn-1-yloxy)phenyl)-1,3,4-oxadiazol-2-yl)thio)butanoate (0.05 g, 0.14 mmol) gave 4-((5-(2-chloro-3-(prop-2-yn-1-yloxy)phenyl)-1,3,4-oxadiazol-2-yl)thio)butanoic acid as white solid (0.048 g, 100%); ^{1}H NMR (500 MHz, $CDCl_3$-*d*) δ ppm 7.58 (dd, 7.8, 1.4 Hz, 1H) 7.37 (t, J = 8.1 Hz, 1H) 7.28 (dd, J = 8.1, 1.4 Hz, 1H) 4.85 (d, J = 2.4 Hz, 2H) 3.39 (t, J = 7.1 Hz, 2H) 2.61-2.59 (m, 3H) 2.23 (p, J = 7.1 Hz, 2H); ^{13}C NMR (500 MHz, $CDCl_3$-*d*) δ ppm 177.65, 164.78, 164.08, 154.11, 134.23, 127.46, 124.48, 123.7, 116.87, 77.44, 57.17, 32.21, 31.59, 24.33; TOF ES^+ MS: (M+H) 353.0; HPLC Ret: 6.20 min; 95% pure.

4-((5-(2,4-dichlorophenyl)-1,3,4-oxadiazol-2-yl)thio)-2-methoxybutanoic acid (CCG-232961). Method G starting from methyl 4-((5-(2,4-dichlorophenyl)-1,3,4-oxadiazol-2-yl)thio)-2-

methoxybutanoate (0.2 g, 0.33 mmol) gave 4-((5-(2,4-dichlorophenyl)-1,3,4-oxadiazol-2-yl)thio)-2-methoxybutanoic acid as white powder (0.11 g, 55%); ^{1}H NMR (500 MHz, $CDCl_3$-*d*) δ ppm 8.77 (br. s., 1H) 7.91 (d, J = 8.5 Hz, 1H) 7.57 (d, J = 1.7 Hz, 1H) 7.39 (dd, J = 8.5, 1.7 Hz, 1H) 4.02 (ddd, J = 8.7, 4.0, 1.3 Hz, 1H) 3.50 (s, 3H) 3.47-3.42 (m, 2H) 2.49-2.28 (m, 2H); ^{13}C NMR (500 MHz, $CDCl_3$-*d*) δ ppm 175.86, 164.92, 163.44, 138.14, 133.75, 131.60, 131.19, 127.63, 121.26, 78.06, 58.60, 31.98, 28.20, 14.11; TOF ES+ MS: (M+H) 363.0; HPLC Ret: 6.78 min; 99% pure.

5-((5-(2,4-dichlorophenyl)-1,3,4-oxadiazol-2-yl)thio)-2-methoxypentanoic acid. (CCG-257222). Method G starting from methyl 5-((5-(2,4-dichlorophenyl)-1,3,4-oxadiazol-2-yl)thio)-2-methoxypentanoate (0.08 g, 0.20 mmol) gave 5-((5-(2,4-dichlorophenyl)-1,3,4-oxadiazol-2-yl)thio)-2-methoxypentanoic acid as white oil (0.07 g, 88%);. ^{1}H NMR (500 MHz, $CDCl_3$-*d*) δ ppm 9.27 (br. s., 1H) 7.91 (d, J = 8.4, 1H) 7.57 (d, J = 2.3 1H) 7.39 (dd, J = 8.4, 2.3 Hz, 1H) 3.87 (dt, J = 7.5, 4.2 Hz, 1H) 3.46 (s, 3H) 3.36 (t, J = 7.4 Hz, 2H) 2.13-1.95 (m, 4H); ^{13}C NMR (500 MHz, $CDCl_3$-*d*) δ ppm 177.25, 165.21, 163.33, 138.06, 131.58, 131.17, 127.61, 121.37, 79.43, 58.45, 32.14, 31.10, 25.12, 20.75; TOF ES+ MS: (M+H) 376.9; HPLC Ret: 6.93 min; 95% pure.

4-((5-(2,4-dichlorophenyl)-1,3,4-thiadiazol-2-yl)thio)butanoic acid. **(CCG-257446).** Method G starting from methyl 4-((5-(2,4-dichlorophenyl)-1,3,4-thiadiazol-2-yl)thio)butanoate (0.12 g, 0.73 mmol) gave 4-((5-(2,4-dichlorophenyl)-1,3,4-thiadiazol-2-yl)thio)butanoic acid as white solid (0.08 g, 73%);. ^{1}H NMR (500 MHz, $CDCl_3$-*d*) δ ppm 8.25 (d, J = 8.6 Hz, 1H) 7.54 (d, J = 2.1 Hz, 1H) 7.40 (dd, J = 8.6, 2.1 Hz, 1H) 3.48 (t, J = 7.1 Hz, 2H) 2.60 (t, J = 7.1 Hz, 2H) 2.21 (p, J = 7.1 Hz, 2H); ^{13}C NMR (500 MHz, $CDCl_3$-*d*) δ ppm 167.02, 162.72, 137.16, 132.90, 131.51, 130.32, 127.92, 127.38, 32.93, 32.27, 24.29; TOF ES+ MS: (M+Na) 372.9; HPLC Ret: 7.49 min; 97% pure.

4-((5-(4-(2-(2-(aminoethoxy)ethoxy)-2-chlorophenyl)-1,3,4-oxadiazol-2-yl)thio)butanoic acid. (CCG-257308). Method F starting from tert-butyl 4-((5-(4-(2-(2-((tert-butoxycarbonyl)amino)ethoxy)ethoxy)-2-chlorophenyl)-1,3,4-oxadiazol-2-yl)thio)butanoate (0.06 g, 0.11 mmol) gave 4-((5-(4-(2-(2-(aminoethoxy)ethoxy)-2-chlorophenyl)-1,3,4-oxadiazol-2-yl)thio)butanoic acid as white oil (0.054 g, 99%); ^{1}H NMR (500 MHz, DMSO-d_6) δ ppm 8.99 (br. s., 1H) 7.81 (br. s., 3H) 7.71 (d, 8.8 Hz, 1H) 7.21 (d, J = 2.5 Hz, 1H) 7.06 (dd, J = 8.8, 2.5 Hz, 1H) 4.19 (t, J = 5.3 Hz, 2H) 3.74 (t, J = 5.4 Hz, 2H) 3.60 (t, J = 5.3 Hz, 2H) 3.24 (t, J = 7.2 Hz, 2H) 2.94 (t, J = 5.6 Hz, 2H) 2.32 (t, J = 7.3 Hz, 2H) 1.93 (p, J = 7.3 Hz, 2H); ^{19}F NMR (500 MHz, DMSO-d_6) δ ppm 74.30; ^{13}C NMR (500 MHz, $CDCl_3$-d) δ ppm 174.09, 164.11, 163.67, 161.71, 133.36, 132.68, 117.12, 115.03, 114.93, 69.00, 68.37, 67.25, 39.01, 32.64, 31.96, 25.01; TOF ES$^+$ MS: (M+H) 403.9; HPLC Ret: 4.62 min; 95% pure.

4-((5-(2-(2-(2-((tert-butoxycarbonyl)amino)ethoxy)ethoxy)-4-chlorophenyl)-1,3,4-oxadiazol-2-yl)thio)butanoic acid. Method F starting from tert-butyl 4-((5-(2-(2-(2-((tert-butoxycarbonyl)amino)ethoxy)ethoxy)-4-chlorophenyl)-1,3,4-oxadiazol-2-yl)thio)butanoate (0.07 g, 0.14 mmol) gave 4-((5-(2-(2-(2-((tert-butoxycarbonyl)amino)ethoxy)ethoxy)-4-chlorophenyl)-1,3,4-oxadiazol-2-yl)thio)butanoic acid as yellow oil (0.07 g, quant); ^{1}H NMR (500 MHz, DMSO-d_6) δ ppm 7.87 (br. s., 3H) 7.80 (d, 8.4 Hz, 1H) 7.73 (d, J = 1.9 Hz, 1H) 7.55 (dd, J = 8.5, 1.9 Hz, 1H) 5.18-5.09 (m, 3H) 4.29 (t, J = 5.3 Hz, 2H) 3.81-3.70 (m, 4H) 3.35 (t, J = 6.7 Hz, 2H) 3.29 (br. s., 2H) 2.55 (t, J = 6.9 Hz, 2H) 2.20 (p, J = 7.0 Hz, 2H); ^{13}C NMR (500 MHz, $CDCl_3$-d) δ ppm 172.87, 165.53, 163.51, 134.08, 133.72, 131.60, 130.67, 126.48, 121.27, 77.20, 69.41, 66.16, 63.18, 40.00, 32.61, 31.50, 24.68; HPLC Ret: 5.64 min.

5-((5-(2,4-dichlorophenyl)-1,3,4-oxadiazol-2-yl)thio)-2-hydroxypentanoic acid (CCG-257154). In a 50 mL round bottomed flask methyl 5-((5-(2,4-dichlorophenyl)-1,3,4-oxadiazol-2-yl)thio)-2-hydroxypentanoate (0.34 g, 0.90 mmol) was dissolved in THF (4 mL) and cooled to 0 °C under an inert atmosphere. 60% NaH in mineral oil (0.043 g, 1.10 mmol) and MeI (0.13 g,

0.90 mmol, 0.056 mL) were added and the reaction was stirred at 0 °C for 30 min. The solvent was evaporated, and the residue was acidified with 1N HCl (5 mL). The product was extracted with EtOAc (3x 15 mL), washed with brine, dried with $MgSO_4$, and concentrated in vacuo. The product was dissolved in a minimal amount of EtOAc and triturated with hexane to provide white solid. Yield=44.3%. ^{1}H NMR (400 MHz, $CDCl_3$-*d*) δ ppm 7.88 (d, J = 8.5, 1H) 7.55 (d, J = 2.0. 1H) 7.39 (dd, J = 8.5, 2.1 Hz, 1H) 4.36 (dd, J = 7.8, 3.0 Hz, 1H) 3.35 (t, J = 6.8 Hz, 2H) 2.15-1.98 (m, 4H); ^{13}C NMR (400 MHz, $CDCl_3$-*d*) δ ppm 177.32**,** 165.69, 163.29, 138.25, 133.72, 131.62, 131.29, 127.61, 121.02, 69.67, 32.49, 31.91, 25.12; TOF ES+ MS: (M+H) 384.9; HPLC Ret: 6.27 min; 95% pure.

3-((5-(2,4-dichlorophenyl)-1,3,4-oxadiazol-2-yl)thio)-2-methoxypropanoic acid. (**CCG-257021**). 2-(2,4-dichlorophenyl)-5-(methylsulfonyl)-1,3,4-oxadiazole (0.25 g, 0.853 mmol) was dissolved in 10 mL acetone. K_2CO_3 (0.141 g, 1.02 mmol) and 3-mercapto-2-methoxypropanoic acid (0.139 g, 1.02 mmol) were added and the mixture was stirred at 25 °C for 2 hr. The acetone was removed *in vacuo* and the remaining residue was partitioned between water (5 mL) and DCM (5 mL). The aqueous was acidified to pH ~ 1 with 1N HCl (15 mL) and the product was extracted with EtOAc (3x 15 mL). The organic layers were washed with brine (20 mL), dried with $MgSO_4$, and concentrated *in vacuo*. The residue was dissolved in minimal EtOAc and the product was triturated with Hex, producing a white precipitate that was filtered and dried under vacuum. Yield=64%. ^{1}H NMR (500 MHz, $CDCl_3$-*d*) δ ppm 7.92 (d, J = 8.5Hz, 1H) 7.58 (d, J = 3.0 Hz, 1H) 7.40 (dd, J = 8.5, 3.0 Hz, 1H) 4.28 (td, J = 7.7, 3.8 Hz, 1H) 3.88-3.83 (m, 2H) 3.56 (s, 3H); TOF ES+ MS: (M+H) 350.9; HPLC Ret: 6.65 min; 95.1 % pure.

4-((5-(2,4-dichlorophenyl)-1,3,4-oxadiazol-2-yl)thio)-N-hydroxybutanamide. (CCG-257445). 4-((5-(2,4-dichlorophenyl)-1,3,4-oxadiazol-2-yl)thio)butanoic acid (0.1 g, 0.3 mmol) was dissolved in 3 mL Et_2O and cooled to 0 °C. Ethyl chloroformate (0.04g, 0.36 mmol, 0.035 mL)) and N-methylmorpholine (0.04 g, 0.39 mmol, 0.043 mL) were added and the reaction was

stirred at 0 °C for 10 min. The salt was filtered and the filtrate was added to a round bottomed flask containing freshly prepared hydroxylamine (0.042 g, 0.6 mmol) in MeOH (4 mL). The reaction was stirred at 25 °C for 45 min. The solvent was evaporated and the solid obtained was subjected to silica gel chromatography eluting with 10% MeOh: 90% DCM. The fractions containing product were concentrated *in vacuo* to produce white solid. Yield=25%. ^{1}H NMR (500 MHz, DMSO-d_6) δ ppm 10.45 (br. s., 1H) 8.74 (s, 1H) 8.00 (d, J = 8.4 Hz, 1H) 7.92 (d, J = 2.1 Hz, 1H) 7.66 (dd, J = 8.4, 2.2 Hz, 1H) 3.36-3-30 (m, 2H) 2.14 (t, J = 7.3 Hz, 2H) 2.01 (p, J = 7.3 Hz, 2H); ^{13}C NMR (500 MHz, $CDCl_3$-*d*) δ ppm 179.71, 168.50, 164.98, 162.95, 137.98, 132.77, 131.17, 128.64, 121.70, 32.12, 31.29, 25.63; TOF ES- MS: (M-H) 246.9; HPLC Ret: 5.73 min; 95% pure.

4-((5-(2,4-dichlorophenyl)-1,3,4-oxadiazol-2-yl)sulfonyl)butanoic acid (CCG-258126). 4-((5-(2,4-dichlorophenyl)-1,3,4-oxadiazol-2-yl)thio)butanoic acid (0.05 g, 0.15 mmol) was dissolved in 1 mL DCM. 70% mCPBA (0.08 g, 0.33 mmol) was added and the reaction was stirred at 25 °C for 4 hr. The solvent was evaporated, and the yellow residue was subjected to silica gel chromatography eluting with 5% MeOH: 95% DCM. The fractions containing product were concentrated *in vacuo* to produce white solid. The solid was crystalized with EtOAc/Hex to produce white powder. Yield=58%. ^{1}H NMR (500 MHz, DMSO-d_6) δ ppm 12.31 (br. s, 1H) 8.10 (d, J = 8.5 Hz, 1H) 8.00 (J = 2.0 Hz, 1H) 7.74 (dd, J = 8.5, 2.1 Hz, 1H) 3.83 (t, J = 7.3 Hz, 2H) 2.43 (t, J = 7.3 Hz, 2H) 2.01 (p, J = 7.5 Hz, 2H); ^{13}C NMR (500 MHz, DMSO-d_6) δ ppm 173.73, 164.02, 161.87, 138.74, 133.93, 133.60, 131.45, 128.83, 120.84, 54.32, 31.71, 17.93; TOF E-MS: (M-H) 364.98; HPLC Ret: 6.56 min; 99% pure.

<u>222740-Series Target Identification Analog Procedures (Chapter 2):</u>

1-tert-butyl 3-methyl 5-oxopiperidine-1,3-dicarboxylate. In a flame dried 50-mL round bottomed flask, $(COCl)_2$ (0.71 g, 0.49 mL, 5.6 mmol) was dissolved in DCM (15 mL) and cooled to -78 °C. DMSO (0.87 g, 0.79 mL, 11.2 mmol) was added and the solution was stirred for 15

min. 1-tert-butyl 3-methyl 5-hydroxypiperidine-1,3-dicarboxylate (1.0 g, 3.86 mmol) dissolved in DCM (5 mL) was added dropwise and the reaction was stirred at -78 °C for 15 min. Et_3N (1.76 g, 2.42 mL, 17.4 mmol) was added, the reaction stirred at -78 °C for 30 min, and then at 25 °C for 2 hr. The reaction was quenched with sat. $NaHCO_3$ (20 mL). The product was extracted with DCM (3 x 20 mL), washed with brine (3 x 15 mL), dried with $MgSO_4$, and concentrated in vacuo. The oil was subjected to silica gel chromatography eluting with 25% EtOAc: 75% Hex. The fractions containing product were concentrated to produce yellow solid. Yield=85%. ^{1}H NMR (500 MHz, $CDCl_3$-*d*) δ ppm 4.01 (s, 2H) 3.88-3.77 (m, 2H) 3.73 (s, 3H) 3.07 (p, 6.1 Hz, 1H) 2.74 (dd, 16.9, 7.4 Hz, 1H) 2.63 (dd, 16.9, 5.8 Hz, 1H) 1.46 (s, 9H); QTOF ES+ MS: (M+MeOH+Na) 312.14.

1-tert-butyl 3-methyl 5,5-difluoropiperidine-1,3-dicarboxylate. In a flame dried 50-mL round bottomed flask, 1-tert-butyl 3-methyl 5-oxopiperidine-1,3-dicarboxylate (0.84 g, 3.28 mmol) was dissolved in DCM (15 mL) and cooled to -78 °C. DAST (1.06 g, 0.87 mL, 6.56 mmol) was added and the solution was stirred for 1 hr, and then at 25 °C for 1 hr. The reaction was quenched with sat. $NaHCO_3$ (20 mL). The product was extracted with DCM (3 x 20 mL), washed with brine (3 x 15 mL), dried with $MgSO_4$, and concentrated in vacuo. The oil was subjected to silica gel chromatography eluting with 15% EtOAc: 85% Hex. The fractions containing product were concentrated to produce yellow solid. Yield=83%. ^{1}H NMR (500 MHz, $CDCl_3$-*d*) δ ppm 4.49-4.22 (m, 2H) 3.72 (s, 3H) 3.09-2.90 (m, 2H) 2.85-2.75 (m, 2H) 2.00 (dtd, 31.5, 13.0, 4.8 Hz, 1H) 1.47 (s, 9H); QTOF ES+ MS: (M+Na) 302.12.

1-(tert-butoxycarbonyl)-5,5-difluoropiperidine-3-carboxylic acid. In a 25 mL round-bottomed flask 1-tert-butyl 3-methyl 5,5-difluoropiperidine-1,3-dicarboxylate (0.32 g, 1.15 mmol) was dissolved in THF (3.0 mL). 1 M NaOH (3.0 mL) was added to the solution and the reaction was stirred at 25 °C for 1 hr. The THF was evaporated *in vacuo* and then the solution was acidified with 1 N HCl (7 mL). The product was extracted with EtOAc (3x 20 mL), washed with

brine (3x 15 mL), dried with $MgSO_4$, and concentrated in vacuo. The residue was crystalized with EtOAc/Hex, producing a white precipitate that was filtered and dried under vacuum. Yield=79%. QTOF ES- MS: (M-H) 264.10.

methyl 3-bromo-5-methoxybenzoate. In a 50 mL round bottomed flask, 3-bromo-5-hydroxybenzoic acid (0.5 g, 2.3 mmol) was dissolved in DMF (10 mL). Cs_2CO_3 (2.25 g, 6.91 mmol) and (after 10 mins stirring) MeI (0.82 g, 0.36 mL, 5.76 mmol) were added. The reaction took place at 25 °C for 16 hr. The product was extracted with EtOAc (3 x 20 mL), washed with brine (2 x 15 mL), and concentrated in vacuo to afford brown oil. Yield = 97%. ^{1}H NMR (500 MHz, $CDCl_3$-*d*) δ ppm 7.76 (t, 1.5 Hz, 1H) 7.49 (dd, J = 2.5, 1.3 Hz, 1H) 7.24 (t, J = 2.1 Hz, 1H) 3.94 (s, 3H) 3.84 (s, 3H); QTOF ES+ MS: (M+H) 246.98; HPLC Ret: 7.64 min.

methyl 3-bromo-5-((tert-butyldimethylsilyl)oxy)benzoate. Methyl 3-bromo-5-hydroxybenzoate (0.47 g, 2.03 mmol) was dissolved in DMF (5.0 mL), and then ImH (0.18 g, 2.64 mmol) and TBS-Cl (0.34 g, 2.24 mmol) were added. The reaction was stirred at 25 ^{o}C for 16 hr. The reaction was partitioned between H_2O and 1:1 EtOAc/Hex, and the product was extracted with 1:1 EtOAc/Hex (3 x 20 mL). The organic layers were combined, washed with brine (3x 10 mL), dried with $MgSO_4$, and concentrated *in vacuo* to produce orange oil. ^{1}H NMR (500 MHz, $CDCl_3$-*d*) δ ppm 7.77 (t, J = 1.4 Hz, 1H) 7.42 (dd, J = 2.3, 1.1 Hz, 1H) 7.18 (dd, J = 4.2, 0.7 Hz, 1H) 3.91 (s, 3H) 0.99 (s, 9H) 0.23 (s, 6H); ^{13}C NMR (126 MHz, $CDCl_3$-*d*) δ ppm 165.58, 156.45, 132.67, 127.72, 125.56, 122.39, 119.88, 52.37, 25.53, 18.13, -4.51; QTOF ES- MS: (M+H) 347.05.

methyl 3-bromo-5-(2-methoxyethoxy)benzoate. 3-bromo-5-hydroxybenzoic acid (1.0 g, 4.61 mmol) was dissolved in 20 mL MeOH. Sulfuric acid (0.59 g, 0.3 mL, 5.99 mmol) was added dropwise and the reaction mixture was heated at reflux (95 °C) for 16 hr. MeOH was removed *in vacuo* and the residue was diluted in 15 mL H_2O. The product was extracted with EtOAc (3x 15

mL), washed with brine (2 x 10 mL), dried with $MgSO_4$, and concentrated *in vacuo*. The resulting oil was triturated with EtOAc/Hex to produce pale orange powder. The freshly synthesized methyl 3-bromo-5-hydroxybenzoate (0.2 g, 0.87 mmol) was dissolved in DMF (4.0 mL), and then K_2CO_3 (0.24 g, 1.73 mmol) and 1-bromo-2-methoxyethane (0.16 g, 1.13 mmol, 0.11 mL) were added. The reaction was stirred at 90 ^oC for 1 hr. After the reaction cooled to 25 ^oC, brine was added, and the product was extracted with DCM (3 x 20 mL). The organic layers were combined, washed with brine (2 x 10 mL), dried with $MgSO_4$, and concentrated *in vacuo*. The subsequent oil was subjected to silica gel chromatography eluting with 100% EtOAc. The fractions containing product were concentrated *in vacuo* to produce orange oil. Yield = 85%. ^1H NMR (500 MHz, $CDCl_3$-*d*) δ ppm 7.75 (t, J = 1.4 Hz, 1H) 7.51 (dd, J = 2.5, 1.3 Hz, 1H) 7.29 (dd, J = 2.5, 1.3 Hz, 1H) 4.14 (t, J = 4.5 Hz, 2H) 3.90 (s, 3H) 3.76 (t, J = 4.5 Hz, 2H) 3.44 (s, 3H); ^{13}C NMR (126 MHz, $CDCl_3$-*d*) δ ppm 165.51, 159.37, 132.62, 125.06, 122.78, 122.61, 114.01, 70.66, 67.86, 59.18, 52.39; QTOF ES- MS: (M+H) 289.01; HPLC Ret: 7.37 min.

3-(furan-2-yl)-5-methoxybenzoic acid. Method H starting from methyl 3-bromo-5-methoxybenzoate (0.55 g, 2.24 mmol) gave 3-(furan-2-yl)-5-methoxybenzoic acid as white solid (0.28 g, 58%); ^1H NMR (500 MHz, DMSO-d_6) δ ppm 13.22 (br. s, 1H) 7.88 (t, 1.5 Hz, 1H) 7.80 (d, J = 1.7 Hz, 1H) 7.49 (dd, J = 1.6 Hz, 1H) 7.38 (d, J = 1.4 Hz, 1H) 7.11 (d, J = 3.4 Hz, 1H) 6.64 (dd, J = 3.4, 1.8 Hz, 1H) 3.88 (s, 3H); ^{13}C NMR (126 MHz, DMSO-d_6) δ ppm 167.29, 160.17, 152.38, 143.82, 133.37, 132.28, 124.39, 114.29, 113.53, 112.63, 107.54, 55.92; QTOF ES- MS: (M-H) 217.11; HPLC Ret: 6.35 min.

3-(furan-2-yl)-5-(2-methoxyethoxy)benzoic acid. Method H starting from methyl 3-bromo-5-(2-methoxyethoxy)benzoate (0.2 g, 0.69 mmol) gave 3-(furan-2-yl)-5-(2-methoxyethoxy)benzoic acid as white solid (0.18 g, 98%); ^1H NMR (500 MHz, DMSO-d_6) δ ppm 13.20 (br. s, 1H) 7.87 (t, 1.4 Hz, 1H) 7.80 (d, J = 1.8 Hz, 1H) 7.52 (t, J = 2.0 Hz, 1H) 7.42 (t, J = 2.2 Hz, 1H) 7.12 (d, J = 3.4 Hz, 1H) 6.63 (dd, J = 3.4, 1.8 Hz, 1H) 4.23 (t, J = 4.5 Hz, 2H) 3.71 (t, J = 4.5 Hz, 2H) 3.34

(s, 3H); ^{13}C NMR (126 MHz, DMSO-d_6) δ ppm 167.27, 159.41, 152.36, 143.82, 133.37, 132.30, 124.49, 122.10, 114.18, 112.63, 107.57, 70.73, 67.79, 58.61; QTOF ES- MS: (M-H) 261.08; HPLC Ret: 6.17 min.

3-(furan-2-yl)-5-hydroxybenzoic acid. Method H starting from methyl 3-bromo-5-((tert-butyldimethylsilyl)oxy)benzoate (0.59 g, 1.71 mmol) gave 3-(furan-2-yl)-5-hydroxybenzoic acid as white solid (0.26 g, 74%); ^{1}H NMR (500 MHz, DMSO-d_6) δ ppm 13.00 (br. s, 1H) 9.97 (s, 1H) 7.80-7.71 (m, 2H) 7.38-7.27 (m, 2H) 7.00 (d, J = 3.4 Hz, 1H) 6.61 (dd, J = 3.5, 1.8 Hz, 1H); ^{13}C NMR (126 MHz, DMSO-d_6) δ ppm 167.46, 158.32, 152.63, 143.62, 133.21, 132.17, 122.69, 115.74, 114.64, 112.58, 107.00; QTOF ES- MS: (M-H) 203.03; HPLC Ret: 5.42 min.

methyl 3-(furan-2-yl)-5-(prop-2-yn-1-yloxy)benzoate. Method A followed by Method B starting from 3-(furan-2-yl)-5-hydroxybenzoic acid (0.15 g, 0.74 mmol) gave methyl 3-(furan-2-yl)-5-(prop-2-yn-1-yloxy)benzoate as white solid (0.05 g, 81% over 2 steps); HPLC Ret: 7.60 min.

methyl 3-(2-(2-((tert-butoxycarbonyl)amino)ethoxy)ethoxy)-5-(furan-2-yl)benzoate. Methyl 3-(furan-2-yl)-5-hydroxybenzoate (0.05 g, 0.23 mmol) was dissolved in 1 mL DMF. Freshly prepared 2-(2-((tert-butoxycarbonyl)amino)ethoxy)ethyl methanesulfonate (0.06 g, 0.21 mmol) along with Cs_2CO_3 (0.1 g, 0.31 mmol) were added, and the reaction was stirred at 75 ^{o}C for 2 hr. The reaction was diluted with 10 mL brine and extracted with DCM (3 x 15 mL). The organic layers were combined, dried with $MgSO_4$, and evaporated. The subsequent oil was subjected to silica gel chromatography eluting with 30% EtOAc: 70% Hex. The fractions containing product were concentrated *in vacuo* to produce pale yellow oil. Yield=86%. ^{1}H NMR (500 MHz, $CDCl_3$-d) δ ppm 7.94 (t, 1.4 Hz, 1H) 7.51-7.42 (m, 2H) 6.72 (d, J = 3.3 Hz, 1H) 6.48 (dd, J = 3.4, 1.8 Hz, 1H) 5.00 (br. s, 1H) 4.22 (t, J = 5.7 Hz, 2H) 3.93 (s, 3H) 3.85 (t, J = 5.5 Hz, 2H) 3.62 (t, J = 5.3 Hz, 2H) 3.36 (q, J = 5.7 Hz, 2H) 1.43 (s, 9H); ^{13}C NMR (126 MHz, DMSO-d_6) δ ppm 166.62, 159.06, 152.73, 142.49, 132.30, 131.85, 125.18, 122.88, 117.89, 114.85, 113.61, 111.79,

106.19, 70.47, 69.42, 67.72, 52.24, 40.35, 28.36; TOF ES^+ MS: (M+H) 406.2; HPLC Ret: 7.89 min.

3-(furan-2-yl)-5-(prop-2-yn-1-yloxy)benzoic acid. (DJK-4-85). Method G starting from methyl 3-(furan-2-yl)-5-(prop-2-yn-1-yloxy)benzoate (0.05 g, 0.21 mmol) gave 3-(furan-2-yl)-5-(prop-2-yn-1-yloxy)benzoic acid as yellow solid (0.05 g, quant); ^{1}H NMR (500 MHz, DMSO-d_6) δ ppm 13.19 (br. s, 1H) 7.87 (t, J = 1.4 Hz, 1H) 7.80 (dd, J = 1.9, 0.7 Hz, 1H) 7.54 (dd, J = 2.5, 1.5 Hz, 1H) 7.43 (dd, J = 2.6, 1.3 Hz, 1H) 7.11 (dd, J = 3.4, 0.8 Hz, 1H) 6.63 (dd, J = 3.4, 1.8 Hz, 1H) 4.94 (d, J = 2.4 Hz, 2H) 3.36 (t, J = 2.4 Hz, 1H); HPLC Ret: 6.50 min.

3-(2-(2-((tert-butoxycarbonyl)amino)ethoxy)ethoxy)-5-(furan-2-yl)benzoic acid. Method G starting from methyl 3-(2-(2-((tert-butoxycarbonyl)amino)ethoxy)ethoxy)-5-(furan-2-yl)benzoate (0.07 g, 0.18 mmol) gave 3-(2-(2-((tert-butoxycarbonyl)amino)ethoxy)ethoxy)-5-(furan-2-yl)benzoic acid as white solid (0.07 g, 96%); ^{1}H NMR (500 MHz, $CDCl_3$-*d*) δ ppm 11.17 (br. s, 1H) 8.00 (s, 1H) 7.55-7.46 (m, 3H) 6.73 (d, J = 3.4 Hz, 1H) 6.51-6.45 (m, 1H) 5.04 (br. s, 1H) 4.22 (t, J = 4.6 Hz, 2H) 3.85 (t, J = 4.5 Hz, 2H) 3.64 (t, J = 4.6 Hz, 2H) 3.41-3.32 (m, 2H) 1.44 (s, 9H); ^{13}C NMR (126 MHz, $CDCl_3$-*d*) δ ppm 170.94, 159.10, 152.60, 142.56, 132.42, 131.17, 125.71, 123.58, 118.47, 115.56, 113.96, 111.81, 106.30, 70.47, 69.44, 67.72, 40.35, 28.38; TOF ES+ MS: (M+H) 391; HPLC Ret: 6.80 min.

tert-butyl (4-chloro-3-hydroxyphenyl)carbamate. In a 100 mL round bottomed flask 5-amino-2-chlorophenol (0.5 g, 3.5 mmol) was dissolved in THF (15 mL), and Boc_2O (0.84 g, 3.8 mmol) was added. The reaction was stirred at 70 ^{o}C for 4 hr, and then diluted with Et_2O (70 mL). The product was washed with 10% citric acid (2 x 30 mL) and brine (3 x 20 mL), dried with $MgSO_4$, and concentrated in vacuo to afford orange oil. Analogous compounds were synthesized with this procedure. Yield=100%. ^{1}H NMR (500 MHz, $CDCl_3$-*d*) δ ppm 7.19 (s, 1H) 7.13 (d, J = 2.5

Hz, 1H) 6.87 (dd, J = 8.7, 2.5 Hz, 1H) 6.44 (s, 1H) 5.52 (s, 1H) 1.52 (s, 9H); QTOF ES+ MS: (M+Na) 266.06; HPLC Ret: 6.69 min.

tert-butyl (4-chloro-2-hydroxyphenyl)carbamate. Brown solid. Yield=95%. ^{1}H NMR (500 MHz, $CDCl_3$-*d*) δ ppm 8.42 (s, 1H) 7.00-6.91 (m, 2H) 6.83 (dd, J = 8.5, 2.3 Hz, 1H) 6.57 (s, 1H) 1.53 (s, 9H); QTOF ES+ MS: (M+Na) 266.06; HPLC Ret: 7.40 min.

tert-butyl (4-chloro-3-(prop-2-yn-1-yloxy)phenyl)carbamate. Method B starting from tert-butyl (4-chloro-3-hydroxyphenyl)carbamate (0.30 g, 1.23 mmol) gave tert-butyl (4-chloro-3-(prop-2-yn-1-yloxy)phenyl)carbamate as white solid (0.12 g, 35%); ^{1}H NMR (500 MHz, $CDCl_3$-*d*) δ ppm 7.32 (d, J = 2.3, 1H) 6.84 (dd, J = 8.6, 2.3 Hz, 1H) 6.48 (s, 1H) 4.77 (d, J = 2.4 Hz, 2H) 2.55 (t, J = 2.4 Hz, 1H) 1.52 (s, 9H); TOF ES+ MS: (M+Na) 304.07.

tert-butyl (4-chloro-2-(prop-2-yn-1-yloxy)phenyl)carbamate. Method B starting from tert-butyl (4-chloro-2-hydroxyphenyl)carbamate (0.3 g, 1.23 mmol) gave tert-butyl (4-chloro-2-(prop-2-yn-1-yloxy)phenyl)carbamate as white solid (0.28 g, 81%); ^{1}H NMR (500 MHz, $CDCl_3$-*d*) δ ppm 8.05 (d, J = 8.6, 1H) 6.99-6.91 (m, 3H) 4.74 (d, J = 2.4 Hz, 2H) 2.58 (t, J = 2.4 Hz, 1H) 1.52 (s, 9H); TOF ES+ MS: (M+Na) 304.07; HPLC Ret: 8.30 min.

tert-butyl (4-chloro-3-(2-methoxyethoxy)phenyl)carbamate. tert-butyl (4-chloro-3-hydroxyphenyl)carbamate (0.3 g, 1.23 mmol) was dissolved in DMF (6.0 mL) and K_2CO_3 (0.34 g, 2.46 mmol) and 1-bromo-2-methoxyethane (0.22 g, 1.60 mmol, 0.16 mL) were added. The reaction was stirred at 90 ^{o}C for 1 hr. After the reaction cooled to 25 ^{o}C brine was added and the product was extracted with DCM (3 x 20 mL). The organic layers were combined, washed with brine (3x 10 mL), dried with $MgSO_4$, and concentrated *in vacuo*. The subsequent oil was subjected to silica gel chromatography eluting with 15% EtOAc: 85% Hex. The fractions containing product were concentrated in vacuo to produce white solid. Similar compounds were made in an analogous fashion. Yield = 44%. ^{1}H NMR (500 MHz, $CDCl_3$-*d*) δ ppm 7.31 (s, 1H)

7.22 (d, J = 8.6 Hz, 1H) 6.70 (dd, J = 8.6, 2.4 Hz, 1H) 6.46 (s, 1H) 4.19 (t, J = 4.5 Hz, 2H) 3.80 (t, J = 4.5 Hz, 2H) 3.48 (s, 3H) 1.51 (s, 9H); QTOF ES+ MS: (M+Na) 324.10.

tert-butyl (4-chloro-2-(2-methoxyethoxy)phenyl)carbamate. Red oil. Yield = 43.3%. ^{1}H NMR (500 MHz, $CDCl_3$-*d*) δ ppm 8.04 (s, 1H) 7.28 (s, 1H) 6.95 (dd, J = 8.7, 2.3 Hz, 1H) 6.88 (s, 1H) 4.14 (t, J = 4.5 Hz, 2H) 3.73 (t, J = 4.5 Hz, 2H) 3.46 (s, 3H) 1.52 (s, 9H); QTOF ES+ MS: (M+Na) 324.10.

tert-butyl 5-((4-chlorophenyl)carbamoyl)-3,3-difluoropiperidine-1-carboxylate. Method I starting from 1-(tert-butoxycarbonyl)-5,5-difluoropiperidine-3-carboxylic acid (0.05 g, 0.19 mmol) and 4-chloroaniline (0.04 g, 0.19 mmol) gave tert-butyl 5-((4-chlorophenyl)carbamoyl)-3,3-difluoropiperidine-1-carboxylate as white solid (0.05 g, 64%); ^{1}H NMR (500 MHz, $CDCl_3$-*d*) δ ppm 8.16 (br.s, 1H) 7.51 (d, J = 8.7 Hz, 1H) 7.29 (d, J = 8.6, 2H) 4.05 (br. s, 2H) 3.41-3.30 (m, 2H) 2.80-2.75 (m, 1H) 2.51-2.30 (m, 2H) 1.48 (s, 9H); QTOF ES+ MS: (M+Na) 397.11; HPLC Ret: 8.06 min.

tert-butyl 5-((4-chloro-2-methoxyphenyl)carbamoyl)-3,3-difluoropiperidine-1-carboxylate. Method I starting from 1-(tert-butoxycarbonyl)-5,5-difluoropiperidine-3-carboxylic acid (0.05 g, 0.19 mmol) and 4-chloro-2-methoxyaniline (0.05 g, 0.19 mmol) gave tert-butyl 5-((4-chloro-2-methoxyphenyl)carbamoyl)-3,3-difluoropiperidine-1-carboxylate as yellow solid (0.06 g, 84%); ^{1}H NMR (500 MHz, $CDCl_3$-*d*) δ ppm 9.61 (br.s, 1H) 7.87 (d, J = 8.6 Hz, 1H) 7.12 (d, J = 2.3 Hz, 1H) 6.97 (dd, J = 8.5, 2.3 Hz, 1H) 4.12 (br. s, 2H) 3.85 (s, 3H) 3.76 (s, 2H) 3.10-3.02 (m, 1H) 2.35-2.10 (m, 2H) 1.42 (s, 9H); QTOF ES+ MS: (M+H) 405.14; HPLC Ret: 8.17 min.

tert-butyl 5-((4-chloro-3-methoxyphenyl)carbamoyl)-3,3-difluoropiperidine-1-carboxylate. Method I starting from 1-(tert-butoxycarbonyl)-5,5-difluoropiperidine-3-carboxylic acid (0.05 g, 0.19 mmol) and 4-chloro-3-methoxyaniline (0.05 g, 0.19 mmol) gave tert-butyl 5-((4-chloro-3-methoxyphenyl)carbamoyl)-3,3-difluoropiperidine-1-carboxylate as white solid (0.05 g, 63%); ^{1}H

NMR (500 MHz, $CDCl_3$-*d*) δ ppm 10.35 (br.s, 1H) 7.51 (d, J = 2.3 Hz, 1H) 7.34 (d, J = 8.6 Hz, 1H) 7.17 (dd, J = 8.7, 2.2 Hz, 1H) 4.14 (br. s, 2H) 3.81 (s, 3H) 3.32 (s, 2H) 2.85-2.80 (m, 1H) 2.35-2.10 (m, 2H) 1.42 (s, 9H); QTOF ES+ MS: (M+H) 405.14; HPLC Ret: 7.95 min.

tert-butyl 5-((3-chloro-4-methoxyphenyl)carbamoyl)-3,3-difluoropiperidine-1-carboxylate. Method I starting from 1-(tert-butoxycarbonyl)-5,5-difluoropiperidine-3-carboxylic acid (0.05 g, 0.19 mmol) and 3-chloro-4-methoxyaniline (0.05 g, 0.19 mmol) gave tert-butyl 5-((3-chloro-4-methoxyphenyl)carbamoyl)-3,3-difluoropiperidine-1-carboxylate as white solid (0.07 g, 88%); ^{1}H NMR (500 MHz, $CDCl_3$-*d*) δ ppm 7.92 (br.s, 1H) 7.64 (br. s, 1H) 7.38 (dd, J = 8.8, 1H) 6.88 (d, J = 8.8 Hz, 1H) 4.04 (br. s, 2H) 3.88 (s, 3H) 3.40-3.32 (m, 2H) 2.79-2.73 (m, 1H) 2.48-2.28 (m, 2H) 1.48 (s, 9H); QTOF ES+ MS: (M+Na) 427.12; HPLC Ret: 7.82 min.

tert-butyl 3,3-difluoro-5-((4-methoxyphenyl)carbamoyl)piperidine-1-carboxylate. Method I starting from 1-(tert-butoxycarbonyl)-5,5-difluoropiperidine-3-carboxylic acid (0.05 g, 0.19 mmol) and 4-methoxyaniline (0.02 g, 0.19 mmol) gave tert-butyl 3,3-difluoro-5-((4-methoxyphenyl)carbamoyl)piperidine-1-carboxylate as white solid (0.07 g, 95%); ^{1}H NMR (500 MHz, $CDCl_3$-*d*) δ ppm 7.70 (br. s, 1H) 7.43 (d, J = 8.0, 2H) 6.86 (d, J = 8.1 Hz, 2H) 4.10 (br. s, 2H) 3.79 (s, 3H) 3.29-3.19 (m, 2H) 2.78-2.74 (m, 1H) 2.47-2.29 (m, 2H) 1.48 (s, 9H); QTOF ES+ MS: (M+Na) 393.16; HPLC Ret: 7.39 min.

tert-butyl 5-((4-chloro-2-(prop-2-yn-1-yloxy)phenyl)carbamoyl)-3,3-difluoropiperidine-1-carboxylate. Method J followed by Method I starting from tert-butyl (4-chloro-2-(prop-2-yn-1-yloxy)phenyl)carbamate (0.06 g, 0.19 mmol) and 1-(tert-butoxycarbonyl)-5,5-difluoropiperidine-3-carboxylic acid (0.05 g, 0.19 mmol) gave tert-butyl 5-((4-chloro-2-(prop-2-yn-1-yloxy)phenyl)carbamoyl)-3,3-difluoropiperidine-1-carboxylate as white solid (0.06 g, 71%); ^{1}H NMR (500 MHz, $CDCl_3$-*d*) δ ppm 8.28 (d, J = 8.7 Hz, 1H) 7.83 (s, 1H) 7.05-6.99 (m, 2H) 4.80 (d,

J = 2.3 Hz, 2H) 4.45-4.29 (m, 2H) 3.11-2.85 (m, 2H) 2.82-2.72 (m, 1H) 2.63 (d, J = 2.6 Hz, 1H) 2.48-2.15 (m, 2H) 1.49 (s, 9H); QTOF ES+ MS: (M+H) 429.14; HPLC Ret: 8.14 min.

tert-butyl 5-((4-chloro-2-(2-methoxyethoxy)phenyl)carbamoyl)-3,3-difluoropiperidine-1-carboxylate. Method J followed by Method I starting from tert-butyl (4-chloro-2-(2-methoxyethoxy)aniline (0.06 g, 0.19 mmol) and 1-(tert-butoxycarbonyl)-5,5-difluoropiperidine-3-carboxylic acid (0.05 g, 0.19 mmol) gave tert-butyl 5-((4-chloro-2-(2-methoxyethoxy)phenyl)carbamoyl)-3,3-difluoropiperidine-1-carboxylate as white solid (0.06 g, 73%); ^{1}H NMR (500 MHz, $CDCl_3$-*d*) δ ppm 8.48 (br. s, 1H) 8.28 (d, J = 8.7 Hz, 1H) 7.03-6.94 (m, 2H) 4.48-4.30 (m, 2H) 4.14 (t, J = 4.5 Hz, 2H) 3.74 (t, J = 4.5 Hz, 2H) 3.48 (s, 3H) 3.02-2.75 (m, 4H) 2.42-2.18 (m, 2H) 1.48 (s, 9H); QTOF ES+ MS: (M+H) 449.17; HPLC Ret: 8.23 min.

methyl 5,5-difluoro-1-(3-(furan-2-yl)benzoyl)piperidine-3-carboxylate. Method J followed by Method I starting from 1-tert-butyl 3-methyl 5,5-difluoropiperidine-1,3-dicarboxylate (0.12 g, 0.44 mmol) and 3-(furan-2-yl)benzoic acid (0.08 g, 0.44 mmol) gave methyl 5,5-difluoro-1-(3-(furan-2-yl)benzoyl)piperidine-3-carboxylate as yellow oil (0.13 g, 84%); ^{1}H NMR (500 MHz, $CDCl_3$-*d*) δ ppm 7.79-7.70 (m, 2H) 7.51-7.41 (m, 2H) 7.33-7.23 (m, 1H) 6.71 (d, J = 3.4 Hz, 1H) 6.49 (dd, J = 3.4, 1.8 Hz, 1H) 4.97 (br. s, 1H) 3.74 (br. s, 3H) 3.32-3.15 (m, 2H) 3.08-2.88 (m, 2H) 2.65-2.51 (m, 2H); QTOF ES+ MS: (M+H) 350.12; HPLC Ret: 7.02 min.

5,5-difluoro-1-(3-(furan-2-yl)benzoyl)piperidine-3-carboxylic acid. Method G starting from methyl 5,5-difluoro-1-(3-(furan-2-yl)benzoyl)piperidine-3-carboxylate (0.13 g, 0.36 mmol) gave 5,5-difluoro-1-(3-(furan-2-yl)benzoyl)piperidine-3-carboxylic acid as white solid (0.12 g, quant); ^{1}H NMR (500 MHz, $CDCl_3$-*d*) δ ppm 7.79-7.71 (m, 2H) 7.51-7.42 (m, 2H) 7.33-7.23 (m, 1H) 6.71 (d, J = 3.4 Hz, 1H) 6.49 (dd, J = 3.4, 1.8 Hz, 1H) 4.94 (br. s, 1H) 3.35-3.21 (m, 2H) 3.10-2.92 (m, 2H) 2.67-2.55 (m, 2H); QTOF ES- MS: (M-H) 334.09; HPLC Ret: 6.24 min.

N-(4-chloro-2-methoxyphenyl)-5,5-difluoro-1-(3-(furan-2-yl)benzoyl)piperidine-3-carboxamide (CCG-258165). Method J followed by Method I starting from tert-butyl 5-((4-chloro-2-methoxyphenyl)carbamoyl)-3,3-difluoropiperidine-1-carboxylate (0.06 g, 0.16 mmol) and 3-(furan-2-yl)benzoic acid (0.03 g, 0.16 mmol) gave N-(4-chloro-2-methoxyphenyl)-5,5-difluoro-1-(3-(furan-2-yl)benzoyl)piperidine-3-carboxamide as yellow solid (0.05 g, 65%); ^{1}H NMR (500 MHz, $CDCl_3$-*d*) δ ppm 8.25 (br.s, 1H) 8.00 (br. s, 1H) 7.79-7.76 (m, 2H) 7.50-7.41 (m, 2H) 7.31 (d, J = 7.7 Hz, 1H) 6.94 (d, 8.7 Hz, 1H) 6.87 (br. s, 1H) 6.70 (d, J = 3.4 Hz, 1H) 6.49 (dd, J = 3.4, 1.8 Hz, 1H) 4.12 (br. s, 2H) 3.89 (br. s, 3H) 3.43-3.24 (m, 1H) 3.10-2.92 (m, 2H) 2.48-2.29 (m, 2H); ^{13}C NMR (500 MHz, $CDCl_3$-*d*) δ ppm 171.12, 168.19, 152.76, 148.63, 142.63, 134.93, 131.44, 129.39, 129.15, 125.88, 125.48, 122.59, 120.84, 120.78, 120.69, 111.84, 110.85, 106.07, 60.38, 55.96, 44.39, 41.40, 35.38, 21.00; QTOF ES+ MS: (M+H) 475.12; HPLC Ret: 7.98 min; 96% pure.

N-(4-chloro-3-methoxyphenyl)-5,5-difluoro-1-(3-(furan-2-yl)benzoyl)piperidine-3-carboxamide (CCG-258166). Method J followed by Method I starting from tert-butyl 5-((4-chloro-3-methoxyphenyl)carbamoyl)-3,3-difluoropiperidine-1-carboxylate (0.05 g, 0.12 mmol) and 3-(furan-2-yl)benzoic acid (0.02 g, 0.12 mmol) gave N-(4-chloro-3-methoxyphenyl)-5,5-difluoro-1-(3-(furan-2-yl)benzoyl)piperidine-3-carboxamide as yellow solid (0.05 g, 88%); ^{1}H NMR (500 MHz, $CDCl_3$-*d*) δ ppm 9.53 (br.s, 1H) 7.78-7.72 (m, 2H) 7.51-7.42 (m, 3H) 7.30 (d, J = 7.6 Hz, 1H) 7.20 (d, 8.5 Hz, 1H) 6.87 (d, J = 8.5 Hz, 1H) 6.68 (d, J = 3.4 Hz, 1H) 6.47 (dd, J = 3.4, 1.8 Hz, 1H) 4.04 (br. s, 2H) 3.83 (br. s, 3H) 3.43 (dd, J = 26.5, 14.0, 1H) 3.22 (t, J = 12.1 Hz, 1H) 2.96 (dq, J = 11.1, 6.3, 5.3 Hz, 1H) 2.52-2.30 (m, 2H); ^{13}C NMR (500 MHz, $CDCl_3$-*d*) δ ppm 171.20, 168.57, 155.03, 152.36, 142.78, 137.88, 134.59, 131.76, 129.85, 125.78, 125.40, 122.17, 118.83, 117.45, 112.31, 111.92, 106.34, 104.36, 60.42, 56.04, 44.49, 40.90, 34.99, 21.05; QTOF ES+ MS: (M+H) 475.12; HPLC Ret: 7.80 min; 98% pure.

N-(3-chloro-4-methoxyphenyl)-5,5-difluoro-1-(3-(furan-2-yl)benzoyl)piperidine-3-carboxamide. (CCG-258704). Method J followed by Method I starting from tert-butyl 5-((3-chloro-4-methoxyphenyl)carbamoyl)-3,3-difluoropiperidine-1-carboxylate (0.07 g, 0.17 mmol) and 3-(furan-2-yl)benzoic acid (0.03 g, 0.16 mmol) gave N-(3-chloro-4-methoxyphenyl)-5,5-difluoro-1-(3-(furan-2-yl)benzoyl)piperidine-3-carboxamide as white solid (0.07 g, 86%); ^{1}H NMR (500 MHz, $CDCl_3$-*d*) δ ppm 9.25 (br.s, 1H) 7.75 (br. s, 2H) 7.54 (br. s, 1H) 7.49-7.42 (m, 2H) 7.32 (dd, 25.3, 8.2 Hz, 2H) 6.79 (d, J = 8.9 Hz, 1H) 6.69 (d, J = 3.4 Hz, 1H) 6.48 (dd, J = 3.3, 1.8 Hz, 1H) 4.84 (s, 1H) 4.02 (br. s, 1H) 3.83 (s, 3H) 3.43 (dd, J = 26.3, 14.0, 1H) 3.22 (t, J = 10.5 Hz, 1H) 2.94 (td, J = 10.7, 5.2 Hz, 1H) 2.55-2.30 (m, 2H); ^{13}C NMR (500 MHz, $CDCl_3$-*d*) δ ppm 168.31, 152.48, 151.88, 142.71, 134.64, 131.67, 129.33, 125.71, 125.49, 122.47, 122.21, 119.64, 118.86, 112.03, 111.87, 106.26, 60.41, 56.31, 44.44, 40.69, 34.92, 21.05; QTOF ES+ MS: (M+H) 475.12; HPLC Ret: 7.67 min; 97% pure.

5,5-difluoro-1-(3-(furan-2-yl)benzoyl)-N-(4-methoxyphenyl)piperidine-3-carboxamide. (CCG-258705). Method J followed by Method I starting from tert-butyl 5-((4-methoxyphenyl)carbamoyl)-3,3-difluoropiperidine-1-carboxylate (0.07 g, 0.18 mmol) and 3-(furan-2-yl)benzoic acid (0.03 g, 0.18 mmol) gave 5,5-difluoro-1-(3-(furan-2-yl)benzoyl)-N-(4-methoxyphenyl)piperidine-3-carboxamide as white solid (0.07 g, 84%); ^{1}H NMR (500 MHz, $CDCl_3$-*d*) δ ppm 8.81 (br.s, 1H) 7.78-7.71 (m, 2H) 7.49-7.39 (m, 4H) 6.69 (d, J = 3.4 Hz, 1H) 6.48 (dd, J = 3.3, 1.7 Hz, 1H) 6.30 (d, J = 7.7 Hz, 1H) 4.81 (s, 1H) 4.01 (br. s, 1H) 3.76 (s, 3H) 3.42 (dd, J = 26.4, 14.0, 1H) 3.24 (br. s, 1H) 2.93 (br. s, 1H) 2.57-2.33 (m, 2H); ^{13}C NMR (500 MHz, $CDCl_3$-*d*) δ ppm 168.15, 156.51, 152.60, 142.67, 131.56, 129.25, 125.68, 125.62, 122.36, 121.74, 114.05, 111.85, 106.19, 60.40, 55.43, 44.45, 40.76, 21.04; QTOF ES+ MS: (M+H) 441.16; HPLC Ret: 7.30 min; 97% pure.

N-(4-chlorophenyl)-5,5-difluoro-1-(3-(furan-2-yl)-5-methoxybenzoyl)piperidine-3-carboxamide (CCG-258524). Method J followed by Method I starting from tert-butyl 5-((4-

chlorophenyl)carbamoyl)-3,3-difluoropiperidine-1-carboxylate (0.08 g, 0.23 mmol) and 3-(furan-2-yl)-5-methoxybenzoic acid (0.05 g, 0.23 mmol) gave N-(4-chlorophenyl)-5,5-difluoro-1-(3-(furan-2-yl)-5-methoxybenzoyl)piperidine-3-carboxamide as white solid (0.09 g, 83%); ^{1}H NMR (500 MHz, $CDCl_3$-*d*) δ ppm 9.26 (br. s, 1H) 7.55-7.45 (m, 3H) 7.32-7.20 (m, 4H) 6.83 (s, 1H) 6.67 (d, J = 3.4 Hz, 1H) 6.48 (dd, J = 3.4, 1.8 Hz, 1H) 4.04 (br. s, 2H) 3.84 (s, 3H) 3.45-3.39 (m, 1H) 3.24 (t, J = 11.9 Hz, 1H) 2.95-2.88 (m, 1H) 2.51-2.30 (m, 2H) ^{13}C NMR (126 MHz, $CDCl_3$-*d*) δ ppm 168.36, 160.20, 152.41, 142.72, 128.93, 126.98, 125.47, 121.14, 120.97, 118.78, 116.62, 114.68, 111.89, 106.51, 104.25, 60.41, 55.81, 44.47, 40.79, 35.60, 21.14; QTOF ES+ MS: (M+H) 475.12; HPLC Ret: 8.00 min; 98% pure.

N-(4-chloro-3-(prop-2-yn-1-yloxy)phenyl)-5,5-difluoro-1-(3-(furan-2-yl)benzoyl)piperidine-3-carboxamide. (CCG-258723). Method J followed by Method I starting from tert-butyl (4-chloro-3-(prop-2-yn-1-yloxy)phenyl)carbamate (0.03 g, 0.11 mmol) and 5,5-difluoro-1-(3-(furan-2-yl)benzoyl)piperidine-3-carboxylic acid (0.03 g, 0.09 mmol) gave N-(4-chloro-3-(prop-2-yn-1-yloxy)phenyl)-5,5-difluoro-1-(3-(furan-2-yl)benzoyl)piperidine-3-carboxamide as white solid (0.02 g, 46%); ^{1}H NMR (500 MHz, $CDCl_3$-*d*) δ ppm 9.53 (br. s, 1H) 7.76 (d, J = 7.8 Hz, 2H) 7.56 (br. s, 1H) 7.46 (dd, J = 9.0, 4.7 Hz, 2H) 7.33-7.20 (m, 2H) 7.04-6.99 (m, 1H) 6.69 (d, J = 3.4 Hz, 1H) 6.48 (dd, J = 3.4, 1.8 Hz, 1H) 4.84 (d, J = 13.4 Hz, 1H) 4.74-4.70 (m, 2H) 4.03 (br. s, 1H) 3.44 (dd, J = 26.5, 13.9 Hz, 1H) 3.23 (t, J = 11.8 Hz, 1H) 2.97 (dt, J = 11.9, 6.4 Hz, 1H) 2.50-2.35 (m, 2H); ^{13}C NMR (500 MHz, $CDCl_3$-*d*) δ ppm 172.37, 168.53, 153.11, 152.38, 142.78, 137.72, 134.56, 131.74, 130.16, 129.35, 125.80, 125.47, 122.21, 118.20, 113.41, 111.91, 109.02, 106.34, 77.77, 76.23, 60.41, 56.80, 44.52, 40.89, 34.95, 21.05; QTOF ES+ MS: (M+H) 499.12; HPLC Ret: 7.83 min; 97% pure.

N-(4-chloro-3-(2-methoxyethoxy)phenyl)-5,5-difluoro-1-(3-(furan-2-yl)benzoyl)piperidine-3-carboxamide. (CCG-258724). Method J followed by Method I starting from tert-butyl (4-chloro-3-(2-methoxyethoxy)phenyl)carbamate (0.03 g, 0.1 mmol) and 5,5-difluoro-1-(3-(furan-2-

yl)benzoyl)piperidine-3-carboxylic acid (0.03 g, 0.1 mmol) gave N-(4-chloro-3-(2-methoxyethoxy)phenyl)-5,5-difluoro-1-(3-(furan-2-yl)benzoyl)piperidine-3-carboxamide as colorless oil (0.02 g, 52%); ^{1}H NMR (500 MHz, $CDCl_3$-*d*) δ ppm 9.45 (br. s, 1H) 7.75 (br. s, 2H) 7.49-7.39 (m, 3H) 7.35-7.18 (m, 2H) 6.95-6.89 (m, 1H) 6.68 (d, J = 3.4 Hz, 1H) 6.48 (dd, J = 3.4, 1.8 Hz, 1H) 4.84 (d, J = 13.2 Hz, 1H) 4.16-4.08 (m, 3H) 4.03 (br. s, 1H) 3.81-3.74 (m, 2H) 3.48-3.41 (m, 5H) 3.21 (t, J = 12.2 Hz, 1H) 2.93 (dt, J = 11.3, 4.2 Hz, 1H) 2.52-2.30 (m, 2H); ^{13}C NMR (500 MHz, $CDCl_3$-*d*) δ ppm 172.20, 168.49, 154.40, 152.40, 142.77, 137.73, 134.56, 131.71, 130.48, 129.35, 125.77, 125.48, 122.21, 118.12, 112.71, 111.90, 108.39, 106.32, 105.77, 70.71, 68.76, 60.41, 59.38, 52.83, 44.52, 40.86, 34.94, 21.05; QTOF ES+ MS: (M+H) 519.15; HPLC Ret: 7.79 min; 97% pure.

N-(4-chloro-2-(prop-2-yn-1-yloxy)phenyl)-5,5-difluoro-1-(3-(furan-2-yl)benzoyl)piperidine-3-carboxamide. (CCG-258741). Method J followed by Method I starting from tert-butyl 5-((4-chloro-2-(prop-2-yn-1-yloxy)phenyl)carbamoyl)-3,3-difluoropiperidine-1-carboxylate (0.055 g, 0.13 mmol) and 3-(furan-2-yl)benzoic acid (0.024 g, 0.13 mmol) gave N-(4-chloro-2-(prop-2-yn-1-yloxy)phenyl)-5,5-difluoro-1-(3-(furan-2-yl)benzoyl)piperidine-3-carboxamide as white solid (0.05 g, 73%); ^{1}H NMR (500 MHz, $CDCl_3$-*d*) δ ppm 8.29 (br. s, 1H) 7.97 (br. s, 1H) 7.79-7.72 (m, 2H) 7.51-7.43 (m, 2H) 7.32 (d, J = 7.6 Hz, 1H) 7.05-6.97 (m, 2H) 6.71 (d, J = 3.4 Hz, 1H) 6.50 (dd, J = 3.4, 1.8 Hz, 1H) 4.93 (br. s, 1H) 4.80 (br. s, 2H) 4.08 (br. s, 1H) 3.40-3.29 (m, 1H) 3.06 (br. s, 1H) 2.94 (br. s, 1H) 2.49-2.32 (m, 2H); ^{13}C NMR (500 MHz, $CDCl_3$-*d*) δ ppm 173.99, 163.45, 155.84, 152.76, 142.63, 137.04, 134.91, 131.45, 129.27, 129.16, 125.51, 122.63, 122.01, 121.17, 120.02, 112.75, 111.84, 106.07, 93.95, 78.01, 60.38, 56.97, 43.61, 41.25, 34.48, 22.82; QTOF ES+ MS: (M+H) 499.12; HPLC Ret: 7.97 min; 98% pure.

N-(4-chloro-2-(2-methoxyethoxy)phenyl)-5,5-difluoro-1-(3-(furan-2-yl)benzoyl)piperidine-3-carboxamide. (CCG-258742). Method J followed by Method I starting from tert-butyl 5-((4-chloro-2-(2-methoxyethoxy)phenyl)carbamoyl)-3,3-difluoropiperidine-1-carboxylate (0.05 g, 0.13

mmol) and 3-(furan-2-yl)benzoic acid (0.03 g, 0.13 mmol) gave N-(4-chloro-2-(2-methoxyethoxy)phenyl)-5,5-difluoro-1-(3-(furan-2-yl)benzoyl)piperidine-3-carboxamide as white solid (0.04 g, 61%); ^{1}H NMR (500 MHz, $CDCl_3$-*d*) δ ppm 8.71 (br. s, 1H) 8.28 (br. s, 1H) 7.78-7.71 (m, 2H) 7.51-7.42 (m, 2H) 7.31 (d, J = 7.6 Hz, 1H) 7.02-6.93 (m, 2H) 6.71 (d, J = 3.4 Hz, 1H) 6.49 (dd, J = 3.4, 1.8 Hz, 1H) 4.95 (br. s, 1H) 4.19-4.00 (m, 3H) 3.79-3.72 (m, 2H) 3.50 (s, 3H) 3.41-3.22 (m, 1H) 2.99 (br. s, 1H) 2.53-2.28 (m, 2H); ^{13}C NMR (500 MHz, $CDCl_3$-*d*) δ ppm 171.47, 167.02, 152.78, 142.61, 131.45, 129.13, 129.04, 125.49, 121.25, 111.82, 106.06, 77.20, 70.62, 60.33, 59.06, 53.02, 44.33, 39.21, 34.87, 21.02; QTOF ES+ MS: (M+H) 519.15; HPLC Ret: 8.02 min; 98% pure.

N-(4-chlorophenyl)-5,5-difluoro-1-(3-(furan-2-yl)-5-(2-methoxyethoxy)benzoyl)piperidine-3-carboxamide. (CCG-258662). Method J followed by Method I starting from tert-butyl 5-((4-chlorophenyl)carbamoyl)-3,3-difluoropiperidine-1-carboxylate (0.04 g, 0.14 mmol) and 3-(furan-2-yl)-5-(2-methoxyethoxy)benzoic acid (0.04 g, 0.14 mmol) gave N-(4-chlorophenyl)-5,5-difluoro-1-(3-(furan-2-yl)-5-(2-methoxyethoxy)benzoyl)piperidine-3-carboxamide as yellow solid (0.06 g, 83%); *Rotomers included* ^{1}H NMR (500 MHz, $CDCl_3$-*d*) δ ppm 9.52 (br. s, 1H) 9.34 (br. s, 0.5H) 7.50-7.40 (m, 3.5H) 7.34-7.29 (m, 2H) 7.24-7.15 (m, 2.5H) 6.88 (br. s, 0.5H) 6.84 (br. s, 1H) 6.65 (d, J = 3.4 Hz, 1H) 6.49-6.44 (m, 1H) 4.90-4.76 (m, 1.5H) 4.09 (ddt, J = 26.7, 9.0, 5.0 Hz, 3.5Hz) 3.94 (br. s, 0.5H) 3.72 (dt, J = 15.8, 4.6 Hz, 3H) 3.44 (s, 3H) 3.37 (s, 1.5H) 3.15 (t, J = 12.3 Hz, 1.5H) 2.92 (tq, J = 13.6, 8.6, 6.4 Hz, 1.5H) 2.52-2.27 (m, 4H); ^{13}C NMR (126 MHz, $CDCl_3$-*d*) δ ppm 171.97, 170.53, 168.50, 168.40, 159.38, 152.30, 142.74, 136.59, 135.74, 133.00, 129.25, 128.83, 123.44, 122.15, 121.23, 120.06, 114.79, 112.01, 111.65, 106.56, 70.81, 70.62, 67.89, 67.61, 59.19, 52.70, 44.42, 40.72, 34.95, 29.68; QTOF ES+ MS: (M+H) 519.15; HPLC Ret: 7.88 min; 97% pure.

N-(4-chlorophenyl)-5,5-difluoro-1-(3-(furan-2-yl)-5-(prop-2-yn-1-yloxy)benzoyl)piperidine-3-carboxamide. (CCG-258744). Method J followed by Method I starting from tert-butyl 5-((4-

chlorophenyl)carbamoyl)-3,3-difluoropiperidine-1-carboxylate (0.07 g, 0.21 mmol) and 3-(furan-2-yl)-5-(prop-2-yn-1-yloxy)benzoic acid (0.05 g, 0.21 mmol) gave N-(4-chlorophenyl)-5,5-difluoro-1-(3-(furan-2-yl)-5-(prop-2-yn-1-yloxy)benzoyl)piperidine-3-carboxamide as white solid (0.05 g, 52%); ^{1}H NMR (500 MHz, $CDCl_3$-*d*) δ ppm 9.19 (br. s, 1H) 7.50-7.43 (m, 3H) 7.36 (d, J = 1.9 Hz, 2H) 7.23 (d, J = 8.2 Hz, 2H) 6.90 (t, J = 1.9 Hz, 1H) 6.68 (d, J = 3.4 Hz, 1H) 6.48 (dd, J = 3.4, 1.8 Hz, 1H) 4.82-4.69 (m, 3H) 4.05 (br. s, 1H) 3.44 (dd, J = 25.1, 14.0, 1H) 3.26 (t, J = 12.1 Hz, 1H) 2.96-2.89 (m, 2H) 2.53 (t, J = 2.4 Hz, 1H) 2.51-2.34 (m, 2H); ^{13}C NMR (500 MHz, $CDCl_3$-*d*) δ ppm 168.35, 157.98, 152.19, 142.84, 133.08, 128.89, 121.17, 115.62, 112.40, 112.13, 111.92, 109.99, 106.69, 77.76, 76.31, 60.40, 56.01, 44.47, 40.77, 21.05; QTOF ES+ MS: (M+H) 499.12; HPLC Ret: 7.99 min; 96% pure.

tert-butyl (2-(2-(3-(5-((4-chlorophenyl)carbamoyl)-3,3-difluoropiperidine-1-carbonyl)-5-(furan-2-yl)phenoxy)ethoxy)ethyl)carbamate. Method J followed by Method I starting from tert-butyl 5-((4-chlorophenyl)carbamoyl)-3,3-difluoropiperidine-1-carboxylate (0.06 g, 0.17 mmol) and 3-(2-(2-((tert-butoxycarbonyl)amino)ethoxy)ethoxy)-5-(furan-2-yl)benzoic acid (0.068 g, 0.17 mmol) gave tert-butyl (2-(2-(3-(5-((4-chlorophenyl)carbamoyl)-3,3-difluoropiperidine-1-carbonyl)-5-(furan-2-yl)phenoxy)ethoxy)ethyl)carbamate as white solid (0.06 g, 52%); *Rototmers included* ^{1}H NMR (500 MHz, $CDCl_3$-*d*) δ ppm 9.43 (br. s, 1H) 7.51-7.44 (m, 3H) 7.31 (br. s, 2H) 7.21 (d, J = 8.3 Hz, 2H) 6.84 (br. s, 1H) 6.67 (d, J = 3.4 Hz, 1H) 6.47 (br. s, 1H) 5.01 (br. s, 1H) 4.84 (d, J = 13.2 Hz, 1H) 4.18-4.01 (m, 3H) 3.85 (t, J = 4.8 Hz, 2H) 3.60 (t, J = 5.5Hz, 2H) 3.47-3.31 (m, 4H) 3.23-3.16 (m, 1H) 3.01-2.93 (m, 1H) 2.51-2.35 (m, 2.5H) 1.43 (s, 9H); ^{13}C NMR (126 MHz, $CDCl_3$-*d*) δ ppm 171.91, 168.55, 159.37, 156.06, 152.35, 142.74, 136.59, 135.80, 132.95, 128.83, 121.25, 118.89, 114.87, 111.92, 106.56, 79.38, 70.45, 69.33, 67.75, 52.77, 44.43, 40.79, 40.37, 35.03, 29.69, 28.40; QTOF ES+ MS: (M+H) 648.23; HPLC Ret: 8.12 min.

1-(3-(2-(2-aminoethoxy)ethoxy)-5-(furan-2-yl)benzoyl)-N-(4-chlorophenyl)-5,5-difluoropiperidine-3-carboxamide, HCl (CCG-262545). Method J starting from tert-butyl (2-(2-

(3-(5-((4-chlorophenyl)carbamoyl)-3,3-difluoropiperidine-1-carbonyl)-5-(furan-2-yl)phenoxy)ethoxy)ethyl)carbamate (0.02 g, 0.03 mmol) gave 1-(3-(2-(2-aminoethoxy)ethoxy)-5-(furan-2-yl)benzoyl)-N-(4-chlorophenyl)-5,5-difluoropiperidine-3-carboxamide, HCl as white oil (0.18 g, quant); ^{1}H NMR (400 MHz, 80 ^{o}C, DMSO-d_6) δ ppm 10.38 (s, 1H) 8.09 (br. s, 3H) 7.71 (dd, J = 1.8, 0.8 Hz, 1H) 7.68-7.60 (m, 2H) 7.42-7.26 (m, 4H) 7.01 (d, J = 3.4 Hz, 1H) 6.89 (dd, J = 2.6, 1.4 Hz, 1H) 6.58 (dd, J = 3.4, 1.8 Hz, 1H) 4.30-4.21 (m, 3H) 3.84 (t, J = 4.7 Hz, 2H) 3.75 (t, J = 4.7 Hz, 2H) 3.53-3.47 (m, 2H) 3.31-3.21 (m, 1H) 3.04-2.96 (m, 3H) 2.55-2.47 (m, 1H) 2.46-2.18 (m, 1H); *Rotomers included* ^{13}C NMR (400 MHz, 80 ^{o}C, DMSO-d_6) δ ppm 169.77, 169.64, 159.47, 152.63, 143.89, 143.54, 138.23, 137.74, 132.62, 129.09, 128.64, 127.79, 121.93, 121.60, 120.26, 115.24, 114.78, 112.83, 112.60, 112.39, 111.92, 111.47, 107.72, 107.36, 69.65, 69.72, 69.19, 68.31, 67.51, 67.28, 67.12, 67.00, 66.88, 66.77, 66.63, 39.16, 35.62, 35.78, 35.05; QTOF ES+ MS: (M+H) 548.18; HPLC Ret: 5.98 min; 92% pure.

58150-Series Drug Development Procedures (Chapter 3):

oxetan-3-ylmethyl methanesulfonate. In a 25 mL round-bottomed flask, oxetan-3-olmethanol (0.1 g, 0.09 mL, 1.14 mmol) was dissolved in 2 mL DCM and cooled to 0 °C. Et_3N (0.29 g, 0.4 mL, 2.8 mmol) was added followed by a slow addition of MsCl (0.16 g, 0.11 mL, 1.4 mmol). The solution was warmed to 25 °C and stirred for 2 hr. The reaction was quenched with sat. $NaHCO_3$ and extracted with DCM (3 x 20 mL). The organic layers were combined, washed with brine, and concentrated in vacuo to produce orange oil. Similar compounds were made in a similar fashion. Yield=quant. ^{1}H NMR (500 MHz, $CDCl_3$-*d*) δ ppm 4.78-4.76 (m, 2H) 4.51-4.44 (m, 4H) 3.45-3.33 (m, 1H) 3.06 (s, 3H).

(3-methyloxetan-3-yl)methyl methanesulfonate. Orange oil. Yield=quant. ^{1}H NMR (500 MHz, $CDCl_3$-*d*) δ ppm 4.52 (d, J = 6.2 Hz, 2H) 4.43 (d, J = 6.2 Hz, 2H) 4.32 (s, 2H) 3.07 (s, 3H) 1.40 (s, 3H).

***cis/trans*-methyl 3-hydroxycyclopentanecarboxylate.** In a 25 mL round-bottomed flask, methyl 3-oxocyclopentanecarboxylate (0.25 g, 0.22 mL, 1.76 mmol) was dissolved in 5 mL MeOH and cooled to 0 °C. $NaBH_4$ (0.07 g, 1.76 mmol) was added and the reaction was stirred at 0 °C for 1 hr. The reaction was quenched with 1 N HCl and the product was extracted with EtOAc (3 x 20 mL). The organic layers were combined, washed with brine, and evaporated in vacuo to produce red oil. Yield = 88%. ^{1}H NMR (500 MHz, $CDCl_3$-*d*) δ ppm 4.46 (tt, J = 5.3, 2.7 Hz, 0.34H) 4.33 (tt, J = 5.5, 3.0 Hz, 1H) 3.71 (s, 3H) 3.68 (s, 1.3H) 3.12-3.05 (m, 0.3H) 2.89 (tdd, J = 9.2, 6.5, 4.5 Hz, 1H) 2.18-1.60 (m, 8H). ~3:1 diastereomer ratio.

***cis/trans*- methyl 3-((methylsulfonyl)oxy)cyclopentanecarboxylate.** In a 25 mL round-bottomed flask, cis/trans-methyl 3-hydroxycyclopentanecarboxylate (0.22 g, 1.5 mmol) and Et_3N (0.39 g, 0.54 mL, 3.9 mmol) were dissolved in 4 mL DCM. The reaction was cooled to 0 °C and methanesulfonyl chloride (0.2 g, 0.14 mL, 1.8 mmol) was added. The reaction was warmed to room temperature where the reaction proceded for 2 hours. The reaction was quenched with $NaHCO_3$, and the product was extracted with DCM (3 x 20 mL). The organic layers were combined, washed with brine, and concentrated in vacuo producing colorless oil. Similar analogs were made in an analogous fashion. Yield = 99%. ^{1}H NMR (500 MHz, $CDCl_3$-*d*) δ ppm 5.29-5.23 (m, 0.32H) 5.16 (tt, J = 5.9, 4.0 Hz, 1H) 3.70 (s, 3H) 3.68 (s, 1.3H) 3.13-3.02 (m, 0.3H) 3.01 (s, 3H) 2.99 (s, 1.2H) 2.90-2.78 (m, 1H) 2.40-1.85 (m, 8H). ~3:1 diastereomer ratio.

***cis/trans*- ethyl 4-((methylsulfonyl)oxy)cyclohexanecarboxylate.** Yellow oil. Yield = quant. ^{1}H NMR (500 MHz, $CDCl_3$-*d*) δ ppm 4.97-4.90 (m, 0.5H) 4.69-4.61 (m, 0.5H) 4.14 (m, 2H) 3.17-3.07 (m, 1H) 3.03 (s, 1.5H) 2.99 (s, 1.5H) 2.43-2.28 (m, 1H) 2.23-1.90 (m, 4H) 1.84-1.56 (m, 5H) 1.44-1.40 (m, 1.5H) 1.29-1.23 (m, 3H). ~1:1 diastereomer ratio.

2,4-dichloro-5-methylbenzoic acid. 1-bromo-2,4-dichloro-5-methylbenzene (0.11 g, 0.46 mmol) was added to a flame dried 100 mL round-bottomed flask charged with a stir bar

containing tetrahydrofuran (2.0 mL). The solution was placed under Ar_2, cooled to -78 °C, and n-butyllithium in hexanes (1.2 M, 0.42 mL) was added dropwise. The reaction proceeded for 5 min at -78 °C, and then was quickly poured over dry ice (10 g) in a 150 mL beaker. The solvents were evaporated *in vacuo* and the subsequent oil was partitioned between H_2O and hexanes. The aqueous was washed with hexanes (3 x 10 mL) and then 1N HCl (7 mL) was added. The product was extracted with EtOAc (3x 20 mL), washed with brine (3x 10 mL), dried over $MgSO_4$, and concentrated *in vacuo* to produce white powder. Similar compounds were made in an analogous fashion. Yield=100%. ^{1}H NMR (500 MHz, $CDCl_3$-*d*) δ ppm 7.90 (s, 1H) 7.50 (s, 1H) 2.39 (s, 3H); HPLC Ret: 6.59 min.

2-chloro-4-(trifluoromethoxy)benzoic acid. Orange solid. Yield=96%. ^{1}H NMR (500 MHz, $CDCl_3$-*d*) δ ppm 8.11 (d, J = 8.7 Hz, 1H) 7.39 (d, J = 1.7 Hz, 1H) 7.22 (dd, J = 8.8, 1.7 Hz, 1H); HPLC Ret: 6.65 min.

2-chloro-4-cyclopropoxybenzoic acid. methyl 2-chloro-4-hydroxybenzoate (0.25 g, 1.34 mmol) was dissolved in 2.0 mL DMA. Bromocyclopropane (0.54 g, 4.42 mmol) along with Cs_2CO_3 (1.4 g, 4.42 mmol) were added and the reaction was stirred at 155 ^{o}C for 24 hr. The reaction was diluted with 10 mL H_2O and washed with EtOAc (3x 10 mL). The aqueous layer was acidified to pH ~1 with 1N HCl and the product was extracted with EtOAc (3x 15 mL). The organic layers were combined, washed with brine, dried with $MgSO_4$, and evaporated. The subsequent oil was subjected to silica gel chromatography eluting with 45% EtOAc: 55% Hex: 0.01% AcOH. The fractions containing product were concentrated in vacuo to produce white solid. Yield=65%. ^{1}H NMR (500 MHz, DMSO-d_6) δ ppm 13.00 (br. s, 1H) 7.84 (d, 8.7 Hz, 1H) 7.20 (d, J = 2.5 Hz, 1H) 6.99 (dd, J = 8.8, 2.5 Hz, 1H) 3.98 (tt, J = 6.1, 2.9 Hz, 1H) 0.87-0.79 (m, 2H) 0.70 (tdd, J = 5.9, 3.0, 1.5, 2H); TOF ES$^+$ MS: (M+H) 213.03; HPLC Ret: 6.33 min.

methyl 2-chloro-4-(2,2,2-trifluoroethoxy)benzoate. In a 50 mL round-bottomed flask methyl 2-chloro-4-hydroxybenzoate (0.3 g, 1.6 mmol) was dissolved in 6 mL anhydrous DMSO. Cs_2CO_3 (0.68 g, 2.09 mmol) and 1, 1, 1-trifluoro-2-iodoethane (0.44 g, 0.21 mL, 2.09 mmol) were added and the reaction was heated at 105 °C for 16 hr. The reaction was cooled, diluted with H_2O, and extracted with EtOAc (3 x 20 mL). The organic layers were combined, washed with brine, and concentrated in vacuo. The yellow residue was subjected to silica gel chromatography eluting with 5% EtOAc Hex. The fractions containing product were concentrated *in vacuo* to produce yellow solid. Similar analogs were made in an analgous fashion. Yield=41%. ^{1}H NMR (500 MHz, $CDCl_3$-*d*) δ ppm 7.91 (d, J = 8.8 Hz, 1H) 7.03 (d, J = 2.6 Hz, 1H) 6.88 (dd, J = 8.8, 2.6 Hz, 1H) 4.39 (q, J = 7.8 Hz, 2H) 3.91 (s, 3H); TOF ES+ MS: (M+H) 269.1; HPLC Ret: 7.50 min.

methyl 2-chloro-4-(oxetan-3-yloxy)benzoate. *8 hr rxn time and 25% EtOAc: 75% Hex to 35%: EtOAc: 65% Hex chromatography. Yellow solid. Yield=70%. ^{1}H NMR (500 MHz, $CDCl_3$-*d*) δ ppm 7.87 (d, J = 8.7 Hz, 1H) 6.76 (d, J = 2.5 Hz, 1H) 6.64 (dd, J = 8.8, 2.5 Hz, 1H) 5.28-5.20 (m, 2H) 5.02-4.95 (m, 2H) 4.78-4.72 (m, 2H) 3.90 (s, 3H); HPLC Ret: 6.39 min.

methyl 2-chloro-4-(oxetan-3-ylmethoxy)benzoate. methyl 2-chloro-4-hydroxybenzoate (0.16 g, 0.88 mmol) was dissolved in 3.0 mL DMF. oxetan-3-ylmethyl methanesulfonate (0.19 g, 1.14 mmol) along with K_2CO_3 (0.16 g, 1.14 mmol) were added and the reaction was stirred at 90 ^{o}C for 1.5 hr. The reaction was diluted with 10 mL brine and extracted with DCM (3x 15 mL). The organic layers were combined, dried with $MgSO_4$, and evaporated. The subsequent oil was subjected to silica gel chromatography eluting with 30% EtOAc Hex. The fractions containing product were concentrated in vacuo to produce yellow oil. Similar analogs were made in an analogous fashion. Yield=83%. ^{1}H NMR (500 MHz, $CDCl_3$-*d*) δ ppm 7.89 (d, J = 8.8 Hz, 1H) 6.99 (d, J = 2.5 Hz, 1H) 6.84 (dd, J = 8.8, 2.5 Hz, 1H) 4.89 (dd, J = 7.8, 6.3 Hz, 2H) 4.56 (t, J = 6.1 Hz, 2H) 4.24 (d, J = 6.7 Hz, 2H) 3.90 (s, 3H) 3.50-3.40 (m, 1H); HPLC Ret: 6.38 min.

methyl 2-chloro-4-(oxetan-3-ylmethoxy)benzoate. Column: 40% EtOAc: 60% Hex. Yellow oil. Yield=92%. ^{1}H NMR (500 MHz, $CDCl_3$-*d*) δ ppm 7.89 (d, J = 8.8 Hz, 1H) 7.02 (d, J = 2.5 Hz, 1H) 6.86 (dd, J = 8.8, 2.5 Hz, 1H) 4.60 (d, J = 6.0 Hz, 2H) 4.47 (d, J = 6.0 Hz, 2H) 4.07 (s, 2H) 3.90 (s, 3H) 1.44 (s, 3H); HPLC Ret: 6.91 min.

tert-butyl 4-bromo-2-chlorobenzoate. In a 50 mL round-bottomed flask, 4-bromo-2-chlorobezoic acid (0.5 g, 2.12 mmol) was dissolved in THF (10 mL). Boc anhydride (0.56 g, 2.55 mmol), DMAP (0.08 g, 0.64 mmol), and Et_3N (0.32 g, 3.2 mmol, 0.44 mL) were added, and reaction was stirred at 25 °C for 16 hr. The reaction was diluted with EtOAc (50 mL), washed with water (2 x 20 mL) and brine, dried with $MgSO_4$, and concentrated in vacuo. The yellow residue was subjected to silica gel chromatography eluting with 2% to 5% EtOAc Hex. The fractions containing product were concentrated *in vacuo* to produce colorless oil. Yield = 58%. ^{1}H NMR (500 MHz, $CDCl_3$-*d*) δ ppm 7.65-7.58 (m, 2H) 7.43 (dd, J = 8.0, 1.9 Hz, 1H) 1.60 (s, 9H) TOF ES+ MS: (M+Na) 315.2; HPLC Ret: 9.10 min.

methyl 4-bromo-2-chlorobenzoate. Method A starting from 4-bromo-2-chlorobenzoic acid (1.0 g, 4.25 mmol) gave methyl 4-bromo-2-chlorobenzoate as yellow oil (0.93 g, 87%); ^{1}H NMR (500 MHz, $CDCl_3$-*d*) δ ppm 7.72 (d, J = 8.4 Hz, 1H) 7.64 (d, J = 1.5 Hz, 1H) 7.46 (dd, J = 8.4, 1.6 Hz, 1H) 3.93 (s, 3H); TOF ES+ MS: (M+H) 248.9; HPLC Ret: 7.71 min.

methyl 3-bromo-2-chlorobenzoate. Method A starting from 3-bromo-2-chlorobenzoic acid (0.5 g, 2.12 mmol) gave methyl 3-bromo-2-chlorobenzoate as colorless oil (0.52 g, 98%); ^{1}H NMR (500 MHz, $CDCl_3$-*d*) δ ppm 7.77 (dd, J = 8.0, 0.8 Hz, 1H) 7.68 (dd, J = 7.7, 0.8, 1H) 7.19 (td, J = 7.9, 0.8 Hz, 1H) 3.94 (s, 3H); TOF ES+ MS: (M+H) 250.9; HPLC Ret: 7.44 min.

methyl 2,6-difluorobenzoate. Method A starting from 2,6-difluorobenzoic acid (0.5 g, 3.16 mmol) gave methyl 2,6-difluorobenzoate as tan oil (0.43 g, 78%); ^{1}H NMR (500 MHz, $CDCl_3$-*d*))

δ 7.42 (ttd, *J* = 8.5, 6.2, 0.8 Hz, 1H), 7.26 (s, 0H), 7.03 – 6.91 (m, 2H), 3.96 (d, *J* = 0.8 Hz, 3H); TOF ES+ MS: (M+Na) 195; HPLC Ret: 6.38 min.

methyl 2-chloro-4-cyclopropoxybenzoate. Method A starting from 2-chloro-4-cyclopropoxybenzoic acid (0.5 g, 3.16 mmol) gave methyl 2-chloro-4-cyclopropoxybenzoate as colorless oil (0.21 g, 66%); ^{1}H NMR (500 MHz, $CDCl_3$-*d*) δ ppm 7.86 (d, 8.5 Hz, 1H) 7.14 (d, J = 2.5 Hz, 1H) 6.94 (dd, J = 8.8, 2.4 Hz, 1H) 3.90 (s, 3H) 3.77 (tt, J = 6.4, 3.0 Hz, 1H) 0.88-0.75 (m, 4H); TOF ES^+ MS: (M+H) 226.14; HPLC Ret: 7.67 min.

methyl 2-chloro-4-iodobenzoate. Method A starting from 2-chloro-4-iodobenzoic acid (1.0 g, 3.54 mmol) gave methyl 2-chloro-4-iodobenzoate as yellow oil (1.02 g, 97%); ^{1}H NMR (500 MHz, $CDCl_3$-*d*) δ ppm 7.85 (d, 1.6 Hz, 1H) 7.67 (dd, J = 8.2, 1.7 Hz, 1H) 7.55 (d, J = 8.2 Hz, 1H) 3.91 (s, 3H); HPLC Ret: 7.88 min.

methyl 2-chloro-4-(trifluoromethoxy)benzoate. Method A starting from 2-chloro-4-(trifluoromethoxy)benzoic acid (0.21 g, 0.87 mmol) gave methyl 2-chloro-4-(trifluoromethoxy)benzoate as white oil (0.05 g, 24%); ^{1}H NMR (500 MHz, $CDCl_3$-*d*) δ ppm 7.92 (d, J = 8.7 Hz, 1H) 7.33 (d, J = 2.3 Hz, 1H) 7.18 (dd, J = 8.7, 2.4 Hz, 1H) 3.94 (s, 3H); HPLC Ret: 7.90 min. *CF3 group may be unstable to refluxing acid.

methyl 4-(2,2,2-trifluoroethoxy)benzoate. Method A starting from 4-(2,2,2-trifluoroethoxy)benzoic acid (0.5 g, 2.3 mmol) gave methyl 4-(2,2,2-trifluoroethoxy)benzoate as yellow oil (0.4 g, 75%); ^{1}H NMR (500 MHz, $CDCl_3$-*d*) δ ppm 8.03 (d, J = 8.6 Hz, 2H) 6.97 (d, J = 8.6 Hz, 2H) 4.41 (q, 8.0 Hz, 2H) 3.90 (s, 3H); HPLC Ret: 7.23 min.

methyl 4-(difluoromethyl)benzoate. Method A starting from 4-(difluoromethyl)benzoic acid (0.5 g, 2.9 mmol) gave methyl 4-(difluoromethyl)benzoate as white solid (0.49 g, 90%); ^{1}H NMR (500 MHz, $CDCl_3$-*d*) δ ppm 8.13 (d, J = 8.0 Hz, 2H) 7.59 (d, J = 8.0 Hz, 2H) 6.69 (t, 56.1 Hz, 1H) 3.95 (s, 3H); HPLC Ret: 6.79 min.

methyl 2-chloro-3-(trifluoromethyl)benzoate. Method A starting from 2-chloro-3-(trifluoromethyl)benzoic acid (0.5 g, 2.2 mmol) gave methyl 2-chloro-3-(trifluoromethyl)benzoate as yellow oil (0.51 g, 95%); ^{1}H NMR (500 MHz, $CDCl_3$-*d*) δ ppm 7.91-7.80 (m, 2H) 7.44 (t, J = 7.9 Hz, 1H) 3.97 (s, 3H); HPLC Ret: 7.47 min.

methyl 4-(difluoromethoxy)benzoate. Method A starting from 4-(difluoromethoxy)benzoic acid (0.3 g, 1.6 mmol) gave methyl 4-(difluoromethoxy)benzoate as colorless oil (0.27 g, 83%); ^{1}H NMR (500 MHz, $CDCl_3$-*d*) δ ppm 8.06 (d, J = 8.4 Hz, 2H) 7.16 (d, J = 8.4 Hz, 2H) 6.59 (t, 73.2 Hz, 1H) 3.92 (s, 3H).

methyl 2-chloro-4-cyclopropylbenzoate. Method K starting from methyl 4-bromo-2-chlorobenzoate (0.27 g, 1.1 mmol) gave methyl 2-chloro-4-cyclopropylbenzoate as yellow oil (0.12 g, 51%); ^{1}H NMR (500 MHz, $CDCl_3$-*d*) δ ppm 7.81-7.70 (m, 1H) 7.15-7.12 (m, 1H) 7.03-6.94 (m, 1H) 3.90 (s, 3H) 1.95-1.84 (m, 1H) 1.11-1.00 (m, 2H) 0.81-0.70 (m, 2H); TOF ES+ MS: (M+H) 211.0; HPLC Ret: 7.29 min.

methyl 2-chloro-3-cyclopropylbenzoate. Method K starting from methyl 3-bromo-2-chlorobenzoate (0.52 g, 2.1 mmol) gave methyl 2-chloro-3-cyclopropylbenzoate as yellow oil (0.43 g, 97%); ^{1}H NMR (500 MHz, $CDCl_3$-*d*) δ ppm 7.51 (dd, J = 7.7, 1.7 Hz, 1H) 7.21 (t, J = 7.7 Hz, 1H) 7.10 (dd, J = 7.8, 1.6 Hz, 1H) 3.94 (s, 3H) 2.29-2.21 (m, 1H) 1.09-0.96 (m, 2H) 0.71-0.66 (m, 2H); TOF ES+ MS: (M+H) 211.0; HPLC Ret: 7.31 min.

methyl 2-chloro-5-cyclopropylbenzoate. Method K starting from methyl 5-bromo-2-chlorobenzoate (0.5 g, 2.0 mmol) gave methyl 2-chloro-5-cyclopropylbenzoate as yellow oil (0.35 g, 83%); ^{1}H NMR (500 MHz, $CDCl_3$-*d*) δ ppm 7.51 (d, J = 1.6 Hz, 1H) 7.33 (d, J = 8.2 Hz, 1H) 7.11 (dd, J = 7.9, 1.5 Hz, 1H) 3.93 (s, 3H) 1.93-1.86 (m, 1H) 1.05-0.98 (m, 2H) 0.73-0.68 (m, 2H); TOF ES+ MS: (M+H) 211.0; HPLC Ret: 7.31 min.

Methyl 3-chloro-[1, 1'-biphenyl]-4-carboxylate. In a 100 mL round bottomed flask, methyl 4-bromo-2-chlorobenzoate (0.5 g, 2.00 mmol), phenyl boronic acid (0.269 g, 2.21 mmol), palladium (II) acetate (0.045 g, 0.2 mmol), triphenylphosphine (0.026 g, 0.1 mmol) and sodium carbonate (0.64 g, 6.01 mmol) were combined in a solution of DMF (10 mL) and H_2O (1 mL). The mixture was stirred under N_2 at 80 ^oC for 1 hr and the catalyst was filtered through a pad of Celite. The solvents were removed in vacuo and the product was diluted with 25 mL H_2O and extracted with DCM (3x 25 mL). The organic layers were combined, washed with brine, dried with $MgSO_4$, and evaporated. The subsequent oil was subjected to silica gel chromatography eluting with 5% EtOAc: 95% Hex. The fractions containing product were concentrated in vacuo to produce white powder. Yield=79%. ^{1}H NMR (500 MHz, $CDCl_3$-*d*) δ ppm 7.93 (d, J = 8.2, 1H) 7.69 (d, J = 1.5 Hz, 1H) 7.62-7.56 (m, 2H) 7.56-7.50 (m, 1H) 7.51-7.44 (m, 2H) 7.45-7.38 (m, 1H) 3.95 (s, 3H); TOF ES+ MS: (M+H) 247.0; HPLC Ret: 8.22 min.

tert-butyl 2-chloro-4-(prop-1-en-2-yl)benzoate. In a 100 mL round-bottomed flask, tert-butyl 4-bromo-2-chlorobenzoate (0.36 g, 1.24 mmol) and 4,4,5,5-tetramethyl-2-(prop-1-en-2-yl)-1,3,2-dioxaborolane (0.22 g, 1.3 mmol) were dissolved in a solution of 1,4-dioxane:H_2O (13 mL:3.25 mL). The solution was degassed and sodium carbonate (0.27 g, 2.53 mmol) and tetrakis (0.14 g, 0.012 mmol) were added. The reaction was stirred under Ar_2 at 90 °C for 16 hr. The volatile solvents were removed in vacuo, and the solution was diluted with water (10 mL). The product was extracted with DCM (3x, 25 mL), washed with brine (20 mL), dried with $MgSO_4$, and concentrated *in vacuo*. The yellow residue was subjected to silica gel chromatography eluting with 2% EtOAc: 98% Hex. The fractions containing product were concentrated *in vacuo* to produce faint yellow oil. Yield=88%. ^{1}H NMR (500 MHz, $CDCl_3$-*d*) δ ppm 7.71 (dd, J = 8.2, 4.2 Hz, 1H) 7.48 (s, 1H) 7.37 (dd, J = 7.9, 1.8 Hz, 1H) 5.43 (s, 1H) 5.18 (s, 1H) 1.61 (s, 9H) 1.55 (s, 3H); TOF ES+ MS: (M+H) 253.1; HPLC Ret: 9.25 min.

methyl 2-chloro-4-(prop-1-en-2-yl)benzoate. In a 25 mL round-bottomed flask, tert-butyl 2-chloro-4-(prop-1-en-2-yl)benzoate (0.14 g, 0.53 mmol) was dissolved in 1.5 mL DCM and 1.5 mL TFA. The reaction was stirred at 25 °C for 1 hr and then concentrated in vacuo. The resulting white solid was taken up in 3 mL MeOH and sulfuric acid (0.07 g, 0.66 mmol, 0.04 mL) was added. The reaction was stirred at 85 °C for 16 hr. The solution was concentrated *in vacuo* and the residue was taken up in DCM (20 mL) and partitioned between water (20 mL). The product was extracted with DCM (3x 20 mL), washed with brine (40 mL), dried with $MgSO_4$, and concentrated in vacuo to obtain yellow oil. The yellow residue was subjected to silica gel chromatography eluting with 5% EtOAc Hex. The fractions containing product were concentrated *in vacuo* to produce colorless oil. Yield=50% (2-steps). ^{1}H NMR (500 MHz, $CDCl_3$-*d*) δ ppm 7.82 (dd, J = 8.2, 1.6 Hz, 1H) 7.53 (s, 1H) 7.39 (dd, J = 8.2, 1.6 Hz, 1H) 5.47 (s, 1H) 5.22 (s, 1H) 3.93 (s, 3H) 2.14 (s, 3H); TOF ES+ MS: (M+H) 211.1; HPLC Ret: 8.00 min.

methyl 2-chloro-4-vinylbenzoate. methyl 4-bromo-2-chlorobenzoate (0.54 g, 2.16 mmol) was dissolved in 8 mL of DMF (degassed) under inert atmosphere. Vinyl n-tributyl tin (1.4 g, 1.3 mL, 4.33 mmol) and Tetrakis (0.25 g, 0.22 mmol) were added, and the mixture was heated at 100 °C for 1 hr under N_2. The mixture was cooled to 25 °C and 10 mL H_2O was added. The product was extracted with EtOAc (3 x 20 mL), washed with brine (20 mL), dried with $MgSO_4$, and concentrated *in vacuo*. The yellow residue was subjected to silica gel chromatography eluting with 2.5% EtOAc: 97.5% Hex. The fractions containing product were concentrated *in vacuo* to produce colorless oil. Yield=82%. ^{1}H NMR (500 MHz, $CDCl_3$-*d*) δ ppm 7.82 (dd, J = 8.1, 1.3 Hz, 1H) 7.47 (d, J = 1.6 Hz, 1H)) 7.32 (dd, J = 8.1, 1.5 Hz, 1H) 6.67 (ddd, J = 17.6, 10.8, 1.2 Hz, 1H) 5.86 (dd, J = 17.5, 1.3 Hz, 1H) 5.42 (dd, 10.9, 1.3 Hz, 1H) 3.93 (s, 3H); TOF ES+ MS: (M+H) 197.0; HPLC Ret: 7.50 min.

methyl 2-chloro-4-ethylbenzoate. In a flamed dried 25 mL round bottomed flask, methyl 2-chloro-4-vinylbenzoate (0.12 g, 0.59 mmol) and 2-nitrobenzene-1-sulfonyl chloride (0.26 g, 1.19

mmol) were dissolved in 3 mL dry MeCN. The solution was cooled to 0 °C and hydrazine hydrate (0.08 g, 0.07 mL, 2.4 mmol) was slowly added. The reaction was warmed to 25 °C and stirred vigorously for 16 hr under N_2. Upon completion, the reaction was quenched with water (15 mL) and the product was extracted with EtOAc (4 x 20 mL). The layers were combined, dried with $MgSO_4$, and concentrated in vacuo. The yellow residue was subjected to silica gel chromatography eluting with 2.5% EtOAc: 97.5% Hex. The fractions containing product were concentrated *in vacuo* to produce yellow oil. Yield=66%. ^{1}H NMR (500 MHz, $CDCl_3$-*d*) δ ppm 7.78 (dd, J = 8.0, 1.0 Hz, 1H) 7.29 (d, J = 1.6 Hz, 1H) 7.13 (dd, J = 8.2, 1.3 Hz, 1H) 3.92 (s, 3H) 2.66 (q, J = 7.6 Hz, 2H) 1.25 (t, J = 7.6 Hz, 3 Hz); TOF ES+ MS: (M+H) 199.1; HPLC Ret: 7.73 min.

methyl 2-chloro-4-propylbenzoate. In a flame dried 25 mL round-bottomed flask, 2-chloro-4-methylbenzoic acid (0.1 g, 0.59 mmol) was dissolved in THF (1.0 mL). The solution was cooled to 0 °C and LDA (0.13 g, 1.2 mmol, 2.5 mL) was added. The reaction was stirred at 0 °C for 10 mins, and then ethyl iodide (0.14 g, 0.88 mmol, 0.07 mL) was added. After stirring at 0 °C for 1 hour, the reaction was quenched with 1N HCl (10 mL). The product was extracted with EtOAc (3 x 20 mL), washed with brine, dried with $MgSO_4$, and concentrated in vacuo. HPLC Ret: 6.87 min. The subsequent oil was taken up in MeOH (3.0 mL), and sulfuric acid (0.07 g, 0.76 mmol, 0.04 mL) was added. The solution was heated to reflux (85 °C) for 16 hr. The MeOH was removed in vacuo, and the product was extracted with EtOAc (3 x 20 mL), washed with brine, dried with $MgSO_4$, and concentrated in vacuo. The yellow residue was subjected to silica gel chromatography eluting with 2% EtOAc: 98% Hex. The fractions containing product were concentrated *in vacuo* to produce colorless oil. Similar derivatives were made in an analogous fashion. Yield=25%. ^{1}H NMR (500 MHz, $CDCl_3$-*d*) δ ppm 7.77 (d, J = 8.0 Hz, 1H) 7.27 (d, J = 1.6 Hz, 1H)) 7.11 (dd, J = 8.1, 1.6 Hz, 1H) 3.92 (s, 3H) 2.59 (t, J = 7.4 Hz, 2H) 1.65 (h, J = 7.4 Hz, 2H) 0.94 (t, J = 7.4 Hz, 3H); TOF ES+ MS: (M+H) 213.1; HPLC Ret: 8.22 min.

methyl 4-butyl-2-chlorobenzoate. (1-bromoproane used as alkylating agent). HPLC Ret (acid): 7.36 min. Colorless oil. Yield = 53%. ^{1}H NMR (500 MHz, $CDCl_3$-*d*) δ ppm 7.77 (d, J = 8.0 Hz, 1H) 7.27 (d, J = 1.6 Hz, 1H) 7.11 (dd, J = 8.0, 1.5 Hz, 1H) 3.92 (s, 3H) 2.62 (t, J = 7.4 Hz, 2H) 1.69-1.53 (m, 2H) 1.35 (h, J = 7.3 Hz, 2H) 0.93 (t, J = 7.4 Hz, 3H); TOF ES+ MS: (M+H) 227.1; HPLC Ret: 8.75 min.

methyl 2-chloro-4-isobutylbenzoate. (2-bromopropane used as alkylating agent). HPLC Ret (acid): 7.26 min. Colorless oil. Yield = 25%. ^{1}H NMR (500 MHz, $CDCl_3$-*d*) δ ppm 7.77 (d, J = 7.9 Hz, 1H) 7.25 (d, J = 1.6 Hz, 1H) 7.09 (dd, J = 8.0, 1.6 Hz, 1H) 3.92 (s, 3H) 2.48 (d, J = 7.2 Hz, 2H) 1.88 (dp, J = 13.5, 6.8 Hz, 1H) 0.91 (d, J = 6.6 Hz, 6H); TOF ES+ MS: (M+H) 227.1; HPLC Ret: 8.63 min.

methyl 4-(2-hydroxypropan-2-yl)benzoate. In a 100 mL round-bottomed flask, methyl 4-iodobenzoate (1.0 g, 3.8 mmol) was dissolved in 10 mL THF and cooled to 0 °C. 2M iPrMgCl in THF (2.0 mL, 4.01 mmol) was added dropwise and the reaction was stirred at -40 °C for 1.5 hr. Acetone (0.33 g, 0.42 mL, 5.7 mmol) was then added and the reaction was stirred at 25 °C for 1 hr. The reaction was quenched with MeOH and then diluted with H_2O. The product was extracted with EtOAc (3 x 15 mL), and the organic layers were combined, washed with brine, dried with $MgSO_4$, and concentrated in vacuo. The subsequent oil was subjected to silica gel chromatography eluting with 20% EtOAc Hex. The fractions containing product were concentrated in vacuo to produce colorless oil. Similar analogs were made in an analogous fashion. Yield=16% *low yield attributed to rxn temp being too low (supposed to be at -20). ^{1}H NMR (500 MHz, $CDCl_3$-*d*) δ ppm 8.00 (d, J = 7.4 Hz, 2H) 7.56 (d, J = 7.4 Hz, 2H) 3.91 (s, 3H) 1.60 (s, 6H); HPLC Ret: 5.60 min.

methyl 2-chloro-4-(2-hydroxypropan-2-yl)benzoate. Column: 30% EtOAc Hex. Colorless oil. Yield=53%. ^{1}H NMR (500 MHz, $CDCl_3$-*d*) δ ppm 7.81 (d, J = 8.2 Hz, 1H) 7.59 (d, J = 1.7 Hz, 1H) 7.41 (dd, J = 8.2, 1.8 Hz, 1H) 3.93 (s, 3H) 1.58 (s, 6H); HPLC Ret: 6.09 min.

methyl 2-chloro-4-(2-fluoropropan-2-yl)benzoate. In a flame dried 25-mL round bottomed flask, methyl 2-chloro-4-(2-hydroxypropan-2-yl)benzoate (0.11 g, 0.48 mmol) was dissolved in DCM (2 mL) and cooled to -78 °C. DAST (0.08 g, 0.06 mL, 0.48 mmol) was added and the solution was stirred at 25 °C for 2 hr. The reaction was diluted with H_2O, and the product was extracted with DCM (3 x 20 mL). The organic layers were combined, washed with brine (2 x 15 mL), dried with $MgSO_4$, and concentrated *in vacuo*. The oil was subjected to silica gel chromatography eluting with 2.5% EtOAc: 97.5% Hex to 5% EtOAc: 95% Hex. The fractions containing product were concentrated to produce colorless oil. Similar derivatives were made in an analogous fashion. Yield=51%. ^{1}H NMR (500 MHz, $CDCl_3$-*d*) δ ppm 7.83 (d, J = 8.2 Hz, 1H) 7.47 (d, J = 1.7 Hz, 1H) 7.30 (dd, J = 8.2, 1.7 Hz, 1H) 3.93 (s, 3H) 1.70 (d, J = 1.5 Hz, 3H) 1.65 (d, J = 1.5 Hz, 3H); ^{19}F NMR (500 MHz, $CDCl_3$-*d*) δ ppm -139.4 (hept., 1H); HPLC Ret: 8.02 min.

methyl 4-(2-fluoropropan-2-yl)benzoate. Colorless oil. Yield=47%. ^{1}H NMR (500 MHz, $CDCl_3$-*d*) δ ppm 8.03 (d, J = 8.4 Hz, 2H) 7.45 (d, J = 8.4 Hz, 2H) 3.92 (s, 3H) 1.72 (d, J = 1.3 Hz, 3H) 1.67 (d, J = 1.3 Hz, 3H); ^{19}F NMR (500 MHz, $CDCl_3$-*d*) δ ppm -138.9 (hept., 1H); HPLC Ret: 7.74 min.

2-chloro-4-methylbenzohydrazide. Method A followed by Method C starting from 2-chloro-4-methylbenzoic acid (1.0 g, 5.9 mmol) gave 2-chloro-4-methylbenzohydrazide as white solid (0.79 g, 73% (2 steps)); ^{1}H NMR (401 MHz, $CDCl_3$-*d*) δ ppm 7.63 (s, 1H) 7.55 (d, J = 7.9 Hz, 1H) 7.22 (d, J = 1.6 Hz, 1H) 7.12 (dd, J = 7.9, 1.6 Hz, 1H) 4.14 (br. s., 2H) 2.36 (s, 3H); HPLC Ret: 3.95 min.

2-chloro-4-fluorobenzohydrazide. Method A followed by Method C starting from 2-chloro-4-fluorobenzoic acid (1.0 g, 5.7 mmol) gave 2-chloro-4-fluorobenzohydrazide as white solid (0.33 g, 73% (2 steps)); ^{1}HNMR (401 MHz, DMSO-d_6) δ ppm 9.58 (s, 1H) 7.54-7.41 (m, 2H) 7.30-7.25 (m, 1H) 4.50 (br. s., 2H); HPLC Ret: 3.43 min.

2,4-dichlorobenzohydrazide. Method A followed by Method C starting from 2,4-dichlorobenzoic acid (3.0 g, 15.7 mmol) gave 2,4-dichlorobenzohydrazide as white solid (0.33 g, 96% (2 steps)); HPLC Ret: 4.20 min.

2,4-dichloro-5-methylbenzohydrazide. Method A followed by Method C starting from 2,4-dichloro-5-methylbenzoic acid (0.09 g, 0.46 mmol) gave 2,4-dichloro-5-methylbenzohydrazide as white solid (0.07 g, 72% (2 steps)); ^{1}H NMR (500 MHz, DMSO-d_6) δ ppm 9.56 (br. s., 1H) 7.63 (s, 1H) 7.40 (s, 1H) 4.49 (br. s., 2H) 2.32 (s, 3H); QTOF ES+ MS: (M+H) 219.0; HPLC Ret: 4.74 min.

2-chloro-4,5-dimethylbenzohydrazide. Method A followed by Method C starting from 2-chloro-4,5-dimethylbenzoic acid (0.25 g, 1.35 mmol) gave 2-chloro-4,5-dimethylbenzohydrazide as white solid (0.24 g, 90% (2 steps)); ^{1}H NMR (501 MHz, DMSO-d_6) δ ppm 9.43 (br. s., 1H) 7.26 (s, 1H) 7.16 (s, 1H) 4.44 (br. s., 2H) 2.23 (s, 3H) 2.19 (s, 3H); QTOF ES+ MS: (M+H) 199.1; HPLC Ret: 4.41 min.

2-chloro-3,4-dimethylbenzohydrazide. Method A followed by Method C starting from 2-chloro-3,4-dimethylbenzoic acid (0.25 g, 1.35 mmol) gave 2-chloro-3,4-dimethylbenzohydrazide as white solid (0.27 g, 100% (2 steps)); ^{1}H NMR (501 MHz, DMSO-d_6) δ ppm 9.42 (br. s., 1H) 7.16 (d, J = 7.7 Hz, 1H) 7.07 (d, J = 7.7 Hz, 1H) 4.43 (br. s., 2H) 2.32 (s, 3H) 2.29 (s, 3H); QTOF ES+ MS: (M+H) 199.1; HPLC Ret: 4.33 min.

2-chloro-4-(trifluoromethyl)benzohydrazide. (DJK-2-73). Method A followed by Method C starting from 2-chloro-4-(trifluoromethyl)benzoic acid (1.1 g, 4.4 mmol) gave 2-chloro-4-

(trifluoromethyl)benzohydrazide as white solid (1.04 g, 98%); ^{1}H NMR (500 MHz, $CDCl_3$-*d*) δ ppm 7.75 (d, J = 8.1, 1H) 7.70 (d, J = 1.7 Hz, 1H) 7.60 (dd, J = 8.0, 1.7 Hz, 1H) 7.50 (br. s., 1H) 3.94 (br. s., 2H); TOF ES+ MS: (M+H) 239.0; HPLC Ret: 4.48 min.

2-chloro-4-cyclopropylbenzohydrazide. Method C starting from methyl 2-chloro-4-cyclopropylbenzoate (0.12 g, 0.55 mmol) gave 2-chloro-4-cyclopropylbenzohydrazide as white solid (0.1 g, 85%); ^{1}H NMR (500 MHz, $CDCl_3$-*d*) δ ppm 7.63-7.52 (m, 1H) 7.09 (s, 1H) 7.02-7.00 (m, 1H) 4.12 (br. s., 2H) 1.93-1.84 (m, 1H) 1.05 (dtd, J = 6.4, 4.8, 1.3 Hz, 2H) 0.74 (dtd, J = 6.4, 4.8, 1.3 Hz, 2H); TOF ES+ MS: (M+H) 211.0; HPLC Ret: 4.64 min.

4-bromo-2-chlorobenzohydrazide. Method C starting from methyl 4-bromo-2-chlorobenzoate (0.29 g, 1.14 mmol) gave 4-bromo-2-chlorobenzohydrazide as white solid (0.28 g, 97%); ^{1}H NMR (400 MHz, DMSO-d_6) δ ppm 7.42 (d, J = 8.2, 1H) 7.31 (s, 1H) 7.19 (dd, J = 8.2, 1.9 Hz, 1H); TOF ES+ MS: (M+H) 249.0; HPLC Ret: 4.48 min.

3-chloro-[1, 1'-biphenyl]-4-carbohydrazide. Method C starting from methyl 3-chloro-[1, 1'-biphenyl]-4-carboxylate (0.39 g, 1.58 mmol) gave 3-chloro-[1, 1'-biphenyl]-4-carbohydrazide as white solid (0.37 g, 94%); ^{1}H NMR (500 MHz, DMSO-d_6) δ ppm 9.62 (d, J = 26.9 Hz, 1H) 7.87-7.61 (m, 3H) 7.57-7.34 (m, 5H) 4.53 (d, J = 24.8 Hz, 2H); TOF ES+ MS: (M+H) 247.0; HPLC Ret: 5.36 min.

2-chloro-4-propylbenzohydrazide. Method C starting from methyl 2-chloro-4-propylbenzoate (0.03 g, 0.15 mmol) gave 2-chloro-4-propylbenzohydrazide as white solid (0.03 g, quant); HPLC Ret: 5.00.

4-butyl-2-chlorobenzohydrazide. Method C starting from methyl 4-butyl-2-chlorobenzoate (0.07 g, 0.31 mmol) gave 4-butyl-2-chlorobenzohydrazide as white solid (0.07 g, quant); HPLC Ret: 5.47.

2-chloro-4-isobutylbenzohydrazide. Method C starting from methyl 2-chloro-4-isobutylbenzoate (0.03 g, 0.13 mmol) gave 2-chloro-4-isobutylbenzohydrazide as white solid (0.03 g, quant); HPLC Ret: 5.40.

2-chloro-3-cyclopropylbenzohydrazide. Method C starting from methyl 2-chloro-3-cyclopropylbenzoate (0.43 g, 2.02 mmol) gave 2-chloro-3-cyclopropylbenzohydrazide as white solid (0.40 g, 95%); ^{1}H NMR (500 MHz, $CDCl_3$-*d*) δ ppm 7.33 (dd, J = 7.3, 1.4 Hz, 1H) 7.24 (t, J = 7.5 Hz, 1H) 7.06 (dd, J = 7.8, 1.6 Hz, 1H) 4.14 (d, J = 4.2 Hz, 2H) 2.20 (tt, J = 8.6, 5.3 Hz, 1H) 1.09-0.96 (m, 2H) 0.74-0.63 (m, 2H); TOF ES+ MS: (M+H) 211.0; HPLC Ret: 4.55 min.

2-chloro-5-cyclopropylbenzohydrazide. Method C starting from methyl 2-chloro-5-cyclopropylbenzoate (0.35 g, 1.64 mmol) gave 2-chloro-5-cyclopropylbenzohydrazide as white solid (0.33 g, 96%); ^{1}H NMR (500 MHz, $CDCl_3$-*d*) δ ppm 7.41 (br. s., 1H) 7.36 (d, J = 2.3 Hz, 1H) 7.28 (dd, J = 8.3, 0.8 Hz, 1H) 7.08 (dd, J = 8.3, 2.3 Hz, 1H) 1.89 (tt, J = 8.6, 5.0 Hz, 1H) 1.08-0.94 (m, 2H) 0.76-0.64 (m, 2H); TOF ES+ MS: (M+H) 211.0; HPLC Ret: 4.59 min.

2-chloro-4-(prop-1-en-2-yl)benzohydrazide. Method C starting from methyl 2-chloro-4-(prop-1-en-2-yl)benzoate (0.05 g, 0.24 mmol) gave 2-chloro-4-(prop-1-en-2-yl)benzohydrazide as white solid (0.05 g, quant); HPLC Ret: 4.76.

2-chloro-4-vinylbenzohydrazide. Method C starting from methyl 2-chloro-4-vinylbenzoate (0.12 g, 0.59 mmol) gave 2-chloro-4-vinylbenzohydrazide as yellow solid (0.09 g, 76%); ^{1}H NMR (500 MHz, $CDCl_3$-*d*) δ ppm 7.65 (dd, J = 8.0, 1.3 Hz, 1H) 7.44 (m, 2H) 7.36 (dd, J = 8.2, 1.3 Hz, 1H) 6.66 (dd, J = 17.5, 10.9 Hz, 1H) 5.84 (d, J = 17.5 Hz, 1H) 5.41 (d, 10.7 Hz, 1H) 4.14 (br. s, 2H); TOF ES+ MS: (M+H) 197.0; HPLC Ret: 4.43 min.

2-chloro-4-ethylbenzohydrazide. Method C starting from methyl 2-chloro-4-ethylbenzoate (0.08 g, 0.39 mmol) gave 2-chloro-4-ethylbenzohydrazide as white solid (0.075 g, 98%); ^{1}H NMR (500 MHz, $CDCl_3$-*d*) δ ppm 7.61 (dd, J = 7.9, 1.1 Hz, 1H) 7.45 (br. s, 1H) 7.26 (d, J = 1.1

Hz, 1H) 7.17 (dd, J = 8.4, 1.4 Hz, 1H) 4.13 (br. s, 2H) 2.66 (q, J = 7.6 Hz, 2H) 1.24 (t, J = 7.6 Hz, 3H); TOF ES+ MS: (M+H) 199.1; HPLC Ret: 4.61 min.

2-(trifluoromethyl)benzohydrazide. Method C starting from methyl 2-(trifluoromethyl)benzoate (0.5 g, 2.45 mmol) gave 2-(trifluoromethyl)benzohydrazide as white solid (0.38 g, 76%); ^{1}H NMR (500 MHz, $CDCl_3$-*d*) δ ppm 7.73 (dd, J = 7.7, 1.3 Hz, 1H) 7.65-7.48 (m, 3H) 6.98 (br. s, 1H) 4.12 (br. s, 2H); TOF ES+ MS: (M+H) 205.1; HPLC Ret: 3.25 min.

2,6-difluorobenzohydrazide. Method C starting from methyl 2,6-difluorobenzoate (0.43 g, 2.48 mmol) gave 2,6-difluorobenzohydrazide as white solid (0.14 g, 33%); ^{1}H NMR (500 MHz, $CDCl_3$-*d*) δ ppm 7.41 (ttd, J = 8.7, 6.7, 0.8 Hz, 1H) 7.01-6.93 (m, 2H) 4.15 (br. s, 2H); TOF ES+ MS: (M+H) 173.1; HPLC Ret: 3.66 min.

2-chloro-4-cyclopropoxybenzohydrazide. Method C starting from methyl 2-chloro-4-cyclopropoxybenzoate (0.21 g, 0.93 mmol) gave 2-chloro-4-cyclopropoxybenzohydrazide as white solid (0.21 g, 98%); ^{1}H NMR (500 MHz, $CDCl_3$-*d*) δ ppm 7.69 (d, 8.7 Hz, 1H) 7.54 (br. s, 1H) 7.09 (d, J = 2.4 Hz, 1H) 6.99 (dd, J = 8.7, 2.4 Hz, 1H) 4.13 (br. s, 2H) 3.80-3.72 (m, 1H) 0.88-0.73 (m, 4H); TOF ES^+ MS: (M+H) 227.06; HPLC Ret: 4.57 min.

2-chloro-4-(2,2,2-trifluoroethoxy)benzohydrazide. Method C starting from methyl 2-chloro-4-(2,2,2-trifluoroethoxy)benzoate (0.18 g, 0.65 mmol) gave 2-chloro-4-(2,2,2-trifluoroethoxy)benzohydrazide as white solid (0.15 g, 87%); ^{1}H NMR (500 MHz, $CDCl_3$-*d*) δ ppm 7.74 (d, 8.7 Hz, 1H) 7.50 (br. s, 1H) 7.01 (d, J = 2.6 Hz, 1H) 6.92 (dd, J = 8.7, 2.6 Hz, 1H) 4.39 (q, J = 7.9 Hz, 2H) 4.13 (d, J = 4.3 Hz, 2H); TOF ES^+ MS: (M+H) 269.03; HPLC Ret: 4.81 min.

2-chloro-4-(oxetan-3-yloxy)benzohydrazide. Method C starting from methyl 2-chloro-4-(oxetan-3-yloxy)benzoate (0.27 g, 1.13 mmol) gave 2-chloro-4-(oxetan-3-yloxy)benzohydrazide as white solid (0.2 g, 72%); ^{1}H NMR (500 MHz, $CDCl_3$-*d*) δ ppm 7.69 (d, 8.7 Hz, 1H) 7.51 (br. s,

1H) 6.74 (d, J = 2.5 Hz, 1H) 6.67 (dd, J = 8.7, 2.5 Hz, 1H) 5.22 (pd, 6.0, 1.0 Hz, 1H) 4.98 (t, J = 7.1 Hz, 2H) 4.74 (dd, J = 7.3, 5.1 Hz, 2H) 4.12 (d, J = 4.1 Hz, 2H); TOF ES^+ MS: (M+H) 243.05; HPLC Ret: 3.10 min.

2-chloro-4-(trifluoromethoxy)benzohydrazide. Method C starting from methyl 2-chloro-4-(trifluoromethoxy)benzoate (0.05 g, 0.21 mmol) gave 2-chloro-4-(trifluoromethoxy)benzohydrazide as white solid (0.04 g, 74%); ^{1}H NMR (500 MHz, $CDCl_3$-*d*) δ ppm 7.73 (d, 8.6 Hz, 1H) 7.39 (br. s, 1H) 7.31 (d, J = 2.1 Hz, 1H) 7.22 (dd, J = 8.8, 2.1 Hz, 1H) 4.15 (br. s, 2H); TOF ES^+ MS: (M+H) 255.01; HPLC Ret: 4.97 min.

2-chloro-4-(oxetan-3-ylmethoxy)benzohydrazide. Method C starting from methyl 2-chloro-4-(oxetan-3-ylmethoxy)benzoate (0.19 g, 0.73 mmol) gave 2-chloro-4-(oxetan-3-ylmethoxy)benzohydrazide as white solid (0.15 g, 80%); ^{1}H NMR (500 MHz, $CDCl_3$-*d*) δ ppm 7.73 (d, 8.6 Hz, 1H) 7.54 (br. s, 1H) 6.96 (d, J = 2.4 Hz, 1H) 6.89 (dd, J = 8.8, 2.4 Hz, 1H) 4.89 (td, 6.1, 3.0 Hz, 2H) 4.56 (td, J = 6.1, 3.0 Hz, 2H) 4.23 (dd, J = 6.7, 3.0 Hz, 2H) 4.13 (br. s, 2H) 3.48-3.41 (m, 1H); TOF ES^+ MS: (M+H) 257.07; HPLC Ret: 3.65 min.

2-chloro-4-((3-methyloxetan-3-yl)methoxy)benzohydrazide. Method C starting from methyl 2-chloro-4-((3-methyloxetan-3-yl)methoxy)benzoate (0.19 g, 0.71 mmol) gave 2-chloro-4-((3-methyloxetan-3-yl)methoxy)benzohydrazide as white solid (0.17 g, 90%); ^{1}H NMR (500 MHz, $CDCl_3$-*d*) δ ppm 7.73 (d, 8.6 Hz, 1H) 7.56 (br. s, 1H) 6.99 (d, J = 2.4 Hz, 1H) 6.91 (dd, J = 8.8, 2.4 Hz, 1H) 4.60 (dd, J = 6.1, 3.3 Hz, 2H) 4.47 (dd, J = 6.1, 3.4 Hz, 2H) 4.13 (br. s, 2H) 4.06 (s, 2H) 1.44 (s, 3H); TOF ES^+ MS: (M+H) 271.08; HPLC Ret: 4.21 min.

4-(2,2,2-trifluoroethoxy)benzohydrazide. Method C starting from methyl 4-(2,2,2-trifluoroethoxy)benzoate (0.4 g, 1.71 mmol) gave 4-(2,2,2-trifluoroethoxy)benzohydrazide as white solid (0.36 g, 89%); ^{1}H NMR (500 MHz, $CDCl_3$-*d*) δ ppm 7.75 (d, 8.8 Hz, 2H) 7.26 (br. s,

1H) 7.00 (d, J = 8.8 Hz, 2H) 4.40 (q, J = 8.0 Hz, 2H) 4.09 (d, J = 3.8 Hz, 2H); TOF ES^+ MS: (M+H) 235.07; HPLC Ret: 4.65 min.

4-(difluoromethyl)benzohydrazide. Method C starting from methyl 4-(difluoromethyl)benzoate (0.49 g, 2.6 mmol) gave 4-(difluoromethyl)benzohydrazide as white solid (0.36 g, 73%); ^{1}H NMR (500 MHz, $CDCl_3$-*d*) δ ppm 7.84 (d, 7.8 Hz, 2H) 7.61 (d, J = 7.8 Hz, 2H) 7.37 (br. s, 1H) 6.69 (t, J = 56.2 Hz, 1H) 4.12 (br. s, 2H); TOF ES^+ MS: (M+H) 187.07; HPLC Ret: 3.84 min.

4-(trifluoromethoxy)benzohydrazide. Method C starting from methyl 4-(trifluoromethoxy)benzoate (0.5 g, 2.3 mmol) gave 4-(trifluoromethoxy)benzohydrazide as white solid (0.5 g, 100%); ^{1}H NMR (500 MHz, $CDCl_3$-*d*) δ ppm 7.80 (d, J = 8.0 Hz, 2H) 7.36 (br. s, 1H) 7.33-7.25 (m, 2H) 4.11 (br.s, 2H); TOF ES^+ MS: (M+H) 221.05; HPLC Ret: 4.71 min.

2-chloro-3-(trifluoromethyl)benzohydrazide. Method C starting from methyl 2-chloro-3-(trifluoromethyl)benzoate (0.5 g, 2.1 mmol) gave 2-chloro-3-(trifluoromethyl)benzohydrazide as white solid (0.47 g, 92%); ^{1}H NMR (500 MHz, $CDCl_3$-*d*) δ ppm 7.80 (d, 8.1 Hz, 1H) 7.69 (d, J = 8.1 Hz, 1H) 7.46 (t, J = 7.7 Hz, 1H) 7.20 (br. s, 1H) 4.16 (br. s, 2H); TOF ES^+ MS: (M+H) 239.02; HPLC Ret: 4.71 min.

2-chloro-4-(2-fluoropropan-2-yl)benzohydrazide. Method C starting from methyl 2-chloro-4-(2-fluoropropan-2-yl)benzoate (0.2 g, 0.82 mmol) gave 2-chloro-4-(2-fluoropropan-2-yl)benzohydrazide as white solid (0.24 g, 96%); ^{1}H NMR (500 MHz, $CDCl_3$-*d*) δ ppm 7.67 (d, 8.1 Hz, 1H) 7.47-7.42 (m, 2H) 7.32 (dd, J = 8.1, 1.7 Hz, 1H) 4.15 (d, J = 4.3 Hz, 2H) 1.69 (s, 3H) 1.65 (s, 3H); TOF ES^+ MS: (M+H) 231.07; HPLC Ret: 4.76 min.

4-(2-fluoropropan-2-yl)benzohydrazide. Method C starting from methyl 4-(2-fluoropropan-2-yl)benzoate (0.06 g, 0.29 mmol) gave 4-(2-fluoropropan-2-yl)benzohydrazide as white solid (0.03 g, 53%); ^{1}H NMR (500 MHz, $CDCl_3$-*d*) δ ppm 7.74 (d, 8.0 Hz, 2H) 7.46 (d, J = 8.0 Hz, 2H)

7.30 (br. s, 1H) 4.10 (br. s, 2H) 1.71 (s, 3H) 1.67 (s, 3H); TOF ES$^+$ MS: (M+H) 197.11; HPLC Ret: 4.51 min.

4-(difluoromethoxy)benzohydrazide. Method C starting from methyl 4-(difluoromethoxy)benzoate (0.27 g, 1.32 mmol) gave 4-(difluoromethoxy)benzohydrazide as white solid (0.23 g, 87%); ^{1}H NMR (400 MHz, $CDCl_3$-*d*) δ ppm 7.77 (d, J = 8.5 Hz, 2H) 7.30 (br. s, 1H) 7.19 (d, J = 8.5 Hz, 2H) 6.58 (t, J = 73.1 Hz, 1H) 4.10 (br. s, 2H); TOF ES$^+$ MS: (M+H) 203.06; HPLC Ret: 4.19 min.

2,6-dichlorobenzohydrazide. In a 100 mL round bottomed flask hydrazine hydrate (0.18 g, 0.18 mL, 2.63 mmol) and Et_3N (0.27 g, 0.37 mL, 2.63 mmol) were dissolved in DCM (10 mL). The solution was cooled to -78 °C and 2,6-dichlorobenzoyl chloride (0.5 g, 0.34 mL, 2.39 mmol) was added. The reaction was stirred at -78 °C for 1 hr and then 25 °C for 2 hr. The reaction was diluted with water (25 mL) and the product was extracted with DCM (3 x 25 mL). The organic layers were combined, washed with brine, dried with $MgSO_4$, and concentrated in vacuo to produce white solid. Yield=98%. ^{1}H NMR (501 MHz, $CDCl_3$-*d*) δ ppm 7.38-7.27 (m, 3H) 6.99 (br. s, 1H) 4.16 (br. s, 2H); TOF ES+ MS: (M+H) 205.0; HPLC Ret: 2.94 min.

5-(2-chloro-4-methylphenyl)-1,3,4-oxadiaole-2-thiol. Method D starting from 2-chloro-4-methylbenzohydrazide (0.3 g, 1.63 mmol) gave 5-(2-chloro-4-methylphenyl)-1,3,4-oxadiaole-2-thiol as white solid (0.29 g, 77%); ^{1}H NMR (401 MHz, DMSO-d_6) δ ppm 7.80 (d, J = 8.0 Hz, 1H) 7.55 (s, 1H) 7.37 (d, J = 8.1 Hz, 1H) 2.39 (s, 3H); HPLC Ret: 6.69 min.

5-(2-chloro-4-fluorophenyl)-1,3,4-oxadiaole-2-thiol. Method D starting from 2-chloro-4-fluorobenzohydrazide (0.3 g, 1.59 mmol) gave 5-(2-chloro-4-fluorophenyl)-1,3,4-oxadiaole-2-thiol as tan solid (0.28 g, 76%); ^{1}HNMR (401 MHz, DMSO-d_6) δ ppm 7.98 (dd, J = 8.9, 6.0 Hz, 1H) 7.76 (dd, J = 8.9, 2.6 Hz, 1H) 7.45 (t, J = 8.0 Hz, 1H); HPLC Ret: 6.42 min.

5-(2,4-dichlorophenyl)-1,3,4-oxadiazole-2-thiol. Method D starting from 2,4-dichlorobenzohydrazide (1.0 g, 4.88 mmol) gave 5-(2,4-dichlorophenyl)-1,3,4-oxadiazole-2-thiol as white solid (0.99 g, 82%); ^{1}H NMR (401 MHz, MeOD-d_4) δ ppm 7.91 (d, 1H) 7.72 (s, 1H) 7.53 (d, 1H); ^{13}C NMR (401 MHz, MeOD-d_4) δ ppm 178.47, 158.18, 138.04, 133.37, 131.24, 130.84, 127.62, 120.63; TOF ES- MS: (M-H) 246.9; HPLC Ret: 6.97 min.

5-(2-chloro-4-cyclopropylphenyl)-1,3,4-oxadiazole-2-thiol. Method D starting from 2-chloro-4-cyclopropylbenzohydrazide (0.1 g, 0.48 mmol) gave 5-(2-chloro-4-cyclopropylphenyl)-1,3,4-oxadiazole-2-thiol as yellow solid (0.08 g, 70%); ^{1}H NMR (500 MHz, $CDCl_3$-d) δ ppm 10.53 (br. s., 1H) 7.81-7.73 (m, 1H) 7.23 (s, 1H) 7.08 (dd, J = 8.2, 1.8 Hz, 1H) 1.96-1.91 (m, 1H) 1.12 (dt, J = 6.8, 4.8, Hz, 2H) 0.81 (dt, J = 6.8, 4.8, Hz, 2H); TOF ES+ MS: (M+H) 253.0; HPLC Ret: 7.14 min.

5-(4-bromo-2-chlorophenyl)-1,3,4-oxadiazole-2-thiol. Method D starting from 4-bromo-2-chlorobenzohydrazide (0.28 g, 1.11 mmol) gave 5-(4-bromo-2-chlorophenyl)-1,3,4-oxadiazole-2-thiol as white solid (0.26 g, 81%); ^{1}H NMR (400 MHz, DMSO-d_6) δ ppm 7.99 (d, J = 8.2 Hz, 1H) 7.84-7.72 (m, 2H); TOF ES+ MS: (M+Na) 292.9; HPLC Ret: 7.06 min.

5-(2-chloro-4-((trifluoromethyl)phenyl)-1,3,4-oxadiazole-2-thiol. Method D starting from 2-chloro-4-((trifluoromethyl)benzohydrazide (1.0 g, 4.19 mmol) gave 5-(2-chloro-4-((trifluoromethyl)phenyl)-1,3,4-oxadiazole-2-thiol as white solid (0.59 g, 59%); ^{1}H NMR (500 MHz, DMSO-d_6) δ ppm 8.16-8.09 (m, 2H) 7.95-7.89 (m, 1H); TOF ES+ MS: (M+H) 280.1 HPLC Ret: 7.14 min.

5-(3-chloro-[1, 1'-biphenyl]-4-yl)-1, 3, 4-oxadiazole-2-thiol. Method D starting from 3-chloro-[1,1'-biphenyl]-4-carbohydrazide (0.37 g, 1.5 mmol) gave 5-(3-chloro-[1, 1'-biphenyl]-4-yl)-1, 3, 4-oxadiazole-2-thiol as white solid (0.38 g, 88%); ^{1}H NMR (400 MHz, DMSO-d_6) δ ppm 8.02-

7.93 (m, 2H) 7.80-7.72 (m, 3H) 7.53-7.40 (m, 3H); TOF ES+ MS: (M+H) 289.0; HPLC Ret: 7.69 min.

5-(2,4-dichloro-5-methylphenyl)-1,3,4-oxadiazole-2-thiol. Method D starting from 2,4-dichloro-5-methylbenzohydrazide (0.07 g, 0.33 mmol) gave 5-(2,4-dichloro-5-methylphenyl)-1,3,4-oxadiazole-2-thiol as yellow solid (0.07 g, 85%); ^{1}H NMR (500 MHz, $CDCl_3$-*d*) δ ppm 10.30 (br. s., 1H) 7.80 (s, 1H) 7.57 (s, 1H) 2.42 (s, 3H); QTOF ES+ MS: (M+H) 261.0; HPLC Ret: 7.23 min.

5-(2-chloro-4,5-dimethylphenyl)-1,3,4-oxadiazole-2-thiol. Method D starting from 2-chloro-4,5-dimethylbenzohydrazide (0.24 g, 1.21 mmol) gave 5-(2-chloro-4,5-dimethylphenyl)-1,3,4-oxadiazole-2-thiol as white solid (0.22 g, 76%); ^{1}H NMR (501 MHz, $CDCl_3$-*d*) δ ppm 11.03 (br. s., 1H) 7.69 (s, 1H) 7.32 (s, 1H) 2.32 (br. s., 6H); QTOF ES+ MS: (M+H) 241.02; HPLC Ret: 7.00 min.

5-(2-chloro-3,4-dimethylphenyl)-1,3,4-oxadiazole-2-thiol. Method D starting from 2-chloro-3,4-dimethylbenzohydrazide (0.27 g, 1.36 mmol) gave 5-(2-chloro-3,4-dimethylphenyl)-1,3,4-oxadiazole-2-thiol as white solid (0.28 g, 86%); ^{1}H NMR (501 MHz, $CDCl_3$-*d*) δ ppm 10.71 (br. s., 1H) 7.62 (d, J = 7.7 Hz, 1H) 7.21 (d, J = 8.0 Hz, 1H) 2.41 (br. s., 6H); QTOF ES+ MS: (M+H) 241.02; HPLC Ret: 6.97 min.

5-(2-chloro-4-propylphenyl)-1,3,4-oxadiazole-2-thiol. Method D starting from 2-chloro-4-propylbenzohydrazide (0.03 g, 0.15 mmol) gave 5-(2-chloro-4-propylphenyl)-1,3,4-oxadiazole-2-thiol as white solid (0.03 g, 71%); *post acidification, product was extracted with EtOAc (3 x 15 mL), washed with brine, dried with $MgSO_4$, concentrated in vacuo; ^{1}H NMR (500 MHz, $CDCl_3$-*d*) δ ppm 10.36 (br. s., 1H) 7.82 (d, J = 8.1 Hz, 1H) 7.37 (d, J = 1.5 Hz, 1H) 7.26 (dd, J = 8.0, 1.5 Hz, 1H) 2.64 (t, J = 7.6 Hz, 2H) 1.66 (h, J = 7.4 Hz, 2H) 0.96 (t, J = 7.5 Hz, 3H); QTOF ES+ MS: (M+H) 255.0; HPLC Ret: 7.63 min.

5-(4-butyl-2-chlorophenyl)-1,3,4-oxadiazole-2-thiol. Method D starting from 4-butyl-2-chlorobenzohydrazide (0.07 g, 0.31 mmol) gave 5-(4-butyl-2-chlorophenyl)-1,3,4-oxadiazole-2-thiol as white solid (0.06 g, 71%); *post acidification, product was extracted with EtOAc (3 x 15 mL), washed with brine, dried with $MgSO_4$, concentrated in vacuo; ^{1}H NMR (500 MHz, $CDCl_3$-*d*) δ ppm 7.81 (d, J = 8.1 Hz, 1H) 7.37 (d, J = 1.4 Hz, 1H) 7.25 (dd, J = 8.1, 1.5 Hz, 1H) 2.66 (t, J = 7.8 Hz, 2H) 1.64 (p, J = 7.4 Hz, 2H) 1.36 (h, J = 7.5 Hz, 2H) 0.94 (t, J = 7.4 Hz, 3H); QTOF ES+ MS: (M+H) 267.1; HPLC Ret: 8.06 min.

5-(2-chloro-4-isobutylphenyl)-1,3,4-oxadiazole-2-thiol. Method D starting from 2-chloro-4-isobutylbenzohydrazide (0.03 g, 0.13 mmol) gave 5-(2-chloro-4-isobutylphenyl)-1,3,4-oxadiazole-2-thiol as white solid (0.03 g, 87%); *post acidification, product was extracted with EtOAc (3 x 15 mL), washed with brine, dried with MgSO4, concentrated in vacuo; ^{1}H NMR (500 MHz, $CDCl_3$-*d*) δ ppm 10.27 (br. s., 1H) 7.82 (d, J = 8.1 Hz, 1H) 7.36 (d, J = 1.5 Hz, 1H) 7.20 (dd, J = 8.0, 1.6 Hz, 1H) 2.53 (d, J = 7.3 Hz, 2H) 1.92 (dp, J = 13.6, 6.9 Hz, 1H) 0.92 (d, J = 7.4 Hz, 6H); QTOF ES+ MS: (M+H) 267.1; HPLC Ret: 7.96 min.

5-(2-chloro-3-cyclopropylphenyl)-1,3,4-oxadiazole-2-thiol. Method D starting from 2-chloro-3-cyclopropylbenzohydrazide (0.2 g, 0.95 mmol) gave 5-(2-chloro-3-cyclopropylphenyl)-1,3,4-oxadiazole-2-thiol as yellow solid (0.13 g, 55%); ^{1}H NMR (500 MHz, $CDCl_3$-*d*) δ ppm 10.56 (br. s., 1H) 7.69 (dd, J = 7.8, 1.6 Hz, 1H) 7.32 (t, J = 7.8 Hz, 1H) 7.19 (dd, J = 7.8, 1.6 Hz, 1H) 2.27 (ddd, J = 13.9, 8.6, 5.4 Hz, 1H) 1.15-1.03 (m, 2H) 0.77-0.65 (m, 2H); TOF ES+ MS: (M+H) 251.0; HPLC Ret: 7.16 min.

5-(2-chloro-5-cyclopropylphenyl)-1,3,4-oxadiazole-2-thiol. Method D starting from 2-chloro-5-cyclopropylbenzohydrazide (0.15 g, 0.71 mmol) gave 5-(2-chloro-5-cyclopropylphenyl)-1,3,4-oxadiazole-2-thiol as white solid (0.15 g, 81%); ^{1}H NMR (500 MHz, $CDCl_3$-*d*) δ ppm 10.58 (br. s., 1H) 7.59 (d, J = 2.3 Hz, 1H) 7.42 (d, J = 8.3 Hz, 1H) 7.18 (dd, J = 8.4, 2.3 Hz, 1H) 1.94 (ddd,

J = 13.4, 8.4, 5.1 Hz, 1H) 1.11-0.99 (m, 2H) 0.79-0.68 (m, 2H); TOF ES+ MS: (M+H) 251.0; HPLC Ret: 7.19 min.

5-(2-chloro-4-(prop-1-en-2-yl)phenyl)-1,3,4-oxadiazole-2-thiol. Method D starting from 2-chloro-4-(prop-1-en-2-yl)benzohydrazide (0.05 g, 0.24 mmol) gave 5-(2-chloro-4-(prop-1-en-2-yl)phenyl)-1,3,4-oxadiazole-2-thiol as yellow solid (0.06 g, 100%); *post acidification, product was extracted with EtOAc (3 x 15 mL), washed with brine, dried with MgSO4, concentrated in vacuo; ^{1}H NMR (500 MHz, $CDCl_3$-*d*) δ ppm 10.21 (br. s., 1H) 7.91-7.86 (m, 1H) 7.62 (d, J = 1.8 Hz, 1H) 7.50 (dd, J = 8.3, 1.8 Hz, 1H) 5.53 (s, 1H) 5.29 (s, 1H) 2.17 (s, 3H); TOF ES+ MS: (M+H) 253.0; HPLC Ret: 7.30 min.

5-(2-chloro-4-vinylphenyl)-1,3,4-oxadiazole-2-thiol. Method D starting from 2-chloro-4-vinylbenzohydrazide (0.09 g, 0.45 mmol) gave 5-(2-chloro-4-vinylphenyl)-1,3,4-oxadiazole-2-thiol as yellow solid (0.09 g, 83%); ^{1}H NMR (500 MHz, $CDCl_3$-*d*) δ ppm 10.34 (br. s, 1H) 7.88 (dd, J = 8.1, 1.1 Hz, 1H) 7.57 (d, J = 1.5 Hz, 1H) 7.43 (dd, J = 8.4, 1.6 Hz, 1H) 6.70 (dd, J = 17.6, 10.9 Hz, 1H) 5.92 (dd, J = 17.6, 1.1 Hz, 1H) 5.49 (dd, 10.9, 1.1 Hz, 1H); TOF ES+ MS: (M+H) 239.1; HPLC Ret: 6.95 min.

5-(2-chloro-4-ethylphenyl)-1,3,4-oxadiazole-2-thiol. Method D starting from 2-chloro-4-ethylbenzohydrazide (0.08 g, 0.38 mmol) gave 5-(2-chloro-4-ethylphenyl)-1,3,4-oxadiazole-2-thiol as white solid (0.08 g, 87%); ^{1}H NMR (500 MHz, $CDCl_3$-*d*) δ ppm 10.44 (br. s, 1H) 7.83 (dd, J = 8.1, 1.5 Hz, 1H) 7.40 (d, J = 1.5 Hz, 1H) 7.25 (dd, J = 8.1, 1.3 Hz, 1H) 2.71 (q, J = 7.6 Hz, 2H) 1.28 (t, J = 7.6 Hz, 3H); HPLC Ret: 7.16 min.

5-(2-(trifluoromethyl)phenyl)-1,3,4-oxadiazole-2-thiol. Method D starting from 2-(trifluoromethyl)benzohydrazide (0.38 g, 1.85 mmol) gave 5-(2-(trifluoromethyl)phenyl)-1,3,4-oxadiazole-2-thiol as white solid (0.41 g, 90%); ^{1}H NMR (500 MHz, $CDCl_3$-*d*) δ ppm 10.64 (br. s, 1H) 7.98-7.85 (m, 2H) 7.77-7.70 (m, 2H); TOF ES+ MS: (M+Na) 271.2; HPLC Ret: 6.49 min.

5-(2-fluorophenyl)-1,3,4-oxadiazole-2-thiol. Method D starting from 2-fluorobenzohydrazide (0.3 g, 1.95 mmol) gave 5-(2-fluorophenyl)-1,3,4-oxadiazole-2-thiol as tan solid (0.30 g, 79%); ^{1}H NMR (500 MHz, $CDCl_3$-*d*) δ ppm 10.78 (br. s, 1H) 7.92 (ddd, J = 7.9, 7.0, 1.8 Hz, 1H) 7.58 (dddd, J = 8.4, 7.5, 5.0, 1.8 Hz, 1H) 7.36-7-23 (m, 2H); TOF ES+ MS: (M+H) 195.1; HPLC Ret: 5.90 min.

5-(2,6-difluorophenyl)-1,3,4-oxadiazole-2-thiol. Method D starting from 2,6-difluorobenzohydrazide (0.14 g, 0.81 mmol) gave 5-(2,6-difluorophenyl)-1,3,4-oxadiazole-2-thiol as white solid (0.15 g, 83%); ^{1}H NMR (500 MHz, $CDCl_3$-*d*) δ ppm 10.73 (br. s, 1H) 7.57 (tt, J = 8.5, 6.1 Hz, 1H) 7.14-7.06 (m, 2H); TOF ES+ MS: (M+H) 215.0; HPLC Ret: 5.88 min.

5-(2,6-dichlorophenyl)-1,3,4-oxadiazole-2-thiol. Method D starting from 2,6-dichlorobenzohydrazide (0.48 g, 2.33 mmol) gave 5-(2,6-dichlorophenyl)-1,3,4-oxadiazole-2-thiol as white solid (0.49 g, 86%); ^{1}H NMR (501 MHz, $CDCl_3$-*d*) δ ppm 10.86 (br. s, 1H) 7.49-7.46 (m, 3H); TOF ES+ MS: (M+H) 246.0; HPLC Ret: 6.56 min.

5-(2-chloro-4-cyclopropoxyphenyl)-1,3,4-oxadiazole-2-thiol. Method D starting from 2-chloro-4-cyclopropoxybenzohydrazide (0.2 g, 0.88 mmol) gave 5-(2-chloro-4-cyclopropoxyphenyl)-1,3,4-oxadiazole-2-thiol as yellow solid (0.18 g, 78%); ^{1}H NMR (500 MHz, $CDCl_3$-*d*) δ ppm 10.36 (br. s, 1H) 7.84 (d, 8.8 Hz, 1H) 7.24 (d, J = 2.5 Hz, 1H) 7.06 (dd, J = 8.8, 2.5 Hz, 1H) 3.85-3.77 (m, 1H) 0.92-0.79 (m, 4H); TOF ES^{+} MS: (M+H) 269.01; HPLC Ret: 7.13 min.

5-(4-(trifluoromethyl)phenyl)-1,3,4-oxadiazole-2-thiol. Method D starting from 4-(trifluoromethyl)benzohydrazide (0.25 g, 1.23 mmol) gave 5-(4-(trifluoromethyl)phenyl)-1,3,4-oxadiazole-2-thiol as white solid (0.26 g, 86%); ^{1}H NMR (500 MHz, $CDCl_3$-*d*) δ ppm 10.66 (br. s, 1H) 8.07 (d, J = 8.1 Hz, 2H) 7.79 (d, J = 8.1 Hz, 2H); HPLC Ret: 6.92 min.

5-(2-chloro-4-(2,2,2-trifluoroethoxy)phenyl)-1,3,4-oxadiazole-2-thiol. Method D starting from 2-chloro-4-(2,2,2-trifluoroethoxy)benzohydrazide (0.15 g, 0.57 mmol) gave 5-(2-chloro-4-(2,2,2-trifluoroethoxy)phenyl)-1,3,4-oxadiazole-2-thiol as white solid (0.15 g, 86%); ^{1}H NMR (500 MHz, $CDCl_3$-*d*) δ ppm 10.46 (br. s, 1H) 7.90 (d, J = 8.9 Hz, 1H) 7.15 (d, J = 1.9 Hz, 1H) 7.00 (dd, J = 8.9, 2.0 Hz, 1H) 4.43 (q, J = 7.8 Hz, 2H); HPLC Ret: 7.01 min.

5-(2-chloro-4-(oxetan-3-yloxy)phenyl)-1,3,4-oxadiazole-2-thiol. Method D starting from 2-chloro-4-(oxetan-3-yloxy)benzohydrazide (0.20 g, 0.81 mmol) gave 5-(2-chloro-4-(oxetan-3-yloxy)phenyl)-1,3,4-oxadiazole-2-thiol as white solid (0.19 g, 81%); ^{1}H NMR (500 MHz, $CDCl_3$-*d*) δ ppm 10.61 (br. s, 1H) 7.85 (d, 8.8 Hz, 1H) 6.87 (d, J = 2.5 Hz, 1H) 6.74 (dd, J = 8.9, 2.6 Hz, 1H) 5.27 (pd, 6.0, 1.0 Hz, 1H) 5.02 (t, J = 7.1 Hz, 2H) 4.78 (dd, J = 7.3, 5.1 Hz, 2H); TOF ES- MS: (M-H) 282.99; HPLC Ret: 6.03 min.

5-(2-chloro-4-(trifluoromethoxy)phenyl)-1,3,4-oxadiazole-2-thiol. Method D starting from 2-chloro-4-(trifluoromethoxy)benzohydrazide (0.04 g, 0.16 mmol) gave 5-(2-chloro-4-(trifluoromethoxy)phenyl)-1,3,4-oxadiazole-2-thiol as white solid (0.03 g, 71%); ^{1}H NMR (500 MHz, $CDCl_3$-*d*) δ ppm 10.33 (br. s, 1H) 7.97 (d, 8.7 Hz, 1H) 7.44 (d, J = 2.1 Hz, 1H) 7.30 (dd, J = 8.7, 2.1 Hz, 1H); TOF ES- MS: (M-H) 294.96; HPLC Ret: 7.30 min.

5-(2-chloro-4-(oxetan-3-ylmethoxy)phenyl)-1,3,4-oxadiazole-2-thiol. Method D starting from 2-chloro-4-(oxetan-3-ylmethoxy)benzohydrazide (0.15 g, 0.58 mmol) gave 5-(2-chloro-4-(oxetan-3-ylmethoxy)phenyl)-1,3,4-oxadiazole-2-thiol as white solid (0.15 g, 88%); ^{1}H NMR (500 MHz, DMSO-d_6) δ ppm 7.83 (d, 8.8 Hz, 1H) 7.32 (d, J = 2.5 Hz, 1H) 7.15 (dd, J = 8.9, 2.5 Hz, 1H) 4.71 (dd, J = 7.9, 6.1 Hz, 2H) 4.43 (t, J = 6.0 Hz, 2H) 4.35 (d, J = 6.7 Hz, 2H) 3.41 (hept., 6.9 Hz, 1H); TOF ES- MS: (M-H) 297.01; HPLC Ret: 6.01 min.

5-(2-chloro-4-((3-methyloxetan-3-yl)methoxy)phenyl)-1,3,4-oxadiazole-2-thiol. Method D starting from 2-chloro-4-((3-methyloxetan-3-yl)methoxy)benzohydrazide (0.17 g, 0.63 mmol)

gave 5-(2-chloro-4-((3-methyloxetan-3-yl)methoxy)phenyl)-1,3,4-oxadiazole-2-thiol as white solid (0.16 g, 79%); ^{1}H NMR (500 MHz, $CDCl_3$-*d*) δ ppm 10.43 (br. s, 1H) 7.86 (d, 8.9 Hz, 1H) 7.12 (d, J = 2.5 Hz, 1H) 6.98 (dd, J = 8.9, 2.5 Hz, 1H) 4.62 (d, J = 6.1 Hz, 2H) 4.50 (d, J = 6.1 Hz, 2H) 4.12 (s, 2H) 1.46 (s, 3H); TOF ES- MS: (M-H) 311.03; HPLC Ret: 6.46 min.

5-(4-(2,2,2-trifluoroethoxy)phenyl)-1,3,4-oxadiazole-2-thiol. Method D starting from 4-(2,2,2-trifluoroethoxy)benzohydrazide (0.36 g, 1.5 mmol) gave 5-(4-(2,2,2-trifluoroethoxy)phenyl)-1,3,4-oxadiazole-2-thiol as white solid (0.37 g, 89%); ^{1}H NMR (500 MHz, $CDCl_3$-*d*) δ ppm 10.24 (br. s, 1H) 7.92 (d, J = 8.9 Hz, 2H) 7.07 (d, J = 8.8 Hz, 2H) 4.43 (q, J = 7.9 Hz, 2H); TOF ES- MS: (M-H) 275.01; HPLC Ret: 6.83 min.

5-(4-(difluoromethyl)phenyl)-1,3,4-oxadiazole-2-thiol. Method D starting from 4-(difluoromethyl)benzohydrazide (0.36 g, 1.9 mmol) gave 5-(4-(difluoromethyl)phenyl)-1,3,4-oxadiazole-2-thiol as white solid (0.31 g, 72%); ^{1}H NMR (500 MHz, $CDCl_3$-*d*) δ ppm 10.55 (br. s, 1H) 8.04 (d, J = 8.0 Hz, 2H) 7.67 (d, J = 8.0 Hz, 2H) 6.71 (t, J = 56.0 Hz, 1H); TOF ES- MS: (M-H) 227.01; HPLC Ret: 6.39 min.

5-(4-(trifluoromethoxy)phenyl)-1,3,4-oxadiazole-2-thiol. Method D starting from 4-(trifluoromethoxy)benzohydrazide (0.3 g, 1.4 mmol) gave 5-(4-(trifluoromethoxy)phenyl)-1,3,4-oxadiazole-2-thiol as white solid (0.32 g, 90%); ^{1}H NMR (500 MHz, $CDCl_3$-*d*) δ ppm 10.48 (br. s, 1H) 7.99 (d, J = 9.0 Hz, 2H) 7.37 (d, J = 9.0 Hz, 2H); TOF ES- MS: (M-H) 260.99; HPLC Ret: 7.05 min.

5-(2-chloro-3-(trifluoromethyl)phenyl)-1,3,4-oxadiazole-2-thiol. Method D starting from 2-chloro-3-(trifluoromethyl)benzohydrazide (0.3 g, 1.26 mmol) gave 5-(2-chloro-3-(trifluoromethyl)phenyl)-1,3,4-oxadiazole-2-thiol as white solid (0.19 g, 55%); ^{1}H NMR (500

MHz, $CDCl_3$-*d*) δ ppm 10.49 (br. s, 1H) 8.08 (d, J = 7.9 Hz, 1H) 7.93 (d, J = 7.9 Hz, 1H) 7.57 (t, J = 7.9 Hz, 1H); TOF ES- MS: (M-H) 278.96; HPLC Ret: 6.96 min.

5-(2-chloro-4-(2-fluoropropan-2-yl)phenyl)-1,3,4-oxadiazole-2-thiol. Method D starting from 2-chloro-4-(2-fluoropropan-2-yl)benzohydrazide (0.24 g, 1.04 mmol) gave 5-(2-chloro-4-(2-fluoropropan-2-yl)phenyl)-1,3,4-oxadiazole-2-thiol as white solid (0.25 g, 88%); ^{1}H NMR (500 MHz, $CDCl_3$-*d*) δ ppm 10.62 (br. s, 1H) 7.91 (d, 8.3 Hz, 1H) 7.59 (d, J = 1.4 Hz, 1H) 7.41 (dd, J = 8.3, 1.4 Hz, 1H) 1.73 (d, J = 1.1 Hz, 3H) 1.68 (d, J = 1.1 Hz, 3H); TOF ES- MS: (M-H) 271.01; HPLC Ret: 7.15 min.

5-(4-(2-fluoropropan-2-yl)phenyl)-1,3,4-oxadiazole-2-thiol. Method D starting from 4-(2-fluoropropan-2-yl)benzohydrazide (0.03 g, 0.15 mmol) gave 5-(4-(2-fluoropropan-2-yl)phenyl)-1,3,4-oxadiazole-2-thiol as white solid (0.04 g, 100%); ^{1}H NMR (500 MHz, $CDCl_3$-*d*) δ ppm 10.38 (br. s, 1H) 7.93 (d, J = 8.8 Hz, 2H) 7.53 (d, J = 8.8 Hz, 2H) 1.73 (d, J = 0.8 Hz, 3H) 1.69 (d, J = 0.8 Hz, 3H); TOF ES- MS: (M-H) 237.05; HPLC Ret: 6.87 min.

5-(4-(difluoromethoxy)phenyl)-1,3,4-oxadiazole-2-thiol. Method D starting from 4-(difluoromethoxy)benzohydrazide (0.23 g, 1.2 mmol) gave 5-(4-(difluoromethoxy)phenyl)-1,3,4-oxadiazole-2-thiol as white solid (0.22 g, 77%); ^{1}H NMR (500 MHz, $CDCl_3$-*d*) δ ppm 10.59 (br. s, 1H) 7.96 (d, J = 8.7 Hz, 2H) 7.26 (d, J = 8.8 Hz, 2H) 6.61 (t, J = 72.7 Hz, 1H); TOF ES- MS: (M-H) 243.00; HPLC Ret: 6.47 min.

***tert*-butyl-3-((5-(2-chloro-4-methylphenyl)-1,3,4-oxadiazol-2-yl)thio)propanoate.** Method E starting from 5-(2-chloro-4-methylphenyl)-1,3,4-oxadiazole-2-thiol (0.25 g, 1.1 mmol) and t-butyl-3-bromopropanoate (0.28 g, 1.3 mmol) gave tert-butyl-3-((5-(2-chloro-4-methylphenyl)-1,3,4-oxadiazol-2-yl)thio)propanoate as white solid (0.27 g, 70%); ^{1}H NMR (401 MHz, DMSO-d_6) δ ppm 7.86 (d, J = 8.1 Hz, 1H) 7.56 (d, J = 1.5 Hz, 1H) 7.37 (d, J = 8.2 Hz, 1H) 3.45 (t, J = 6.8 Hz,

2H) 2.82 (t, J = 6.8 Hz, 2H) 2.40 (s, 3H) 1.41 (s, 9H); TOF ES+ MS: (M+H) 354.0; HPLC Ret: 8.66 min.

***tert*-butyl-3-((5-(2-chloro-4-fluorophenyl)-1,3,4-oxadiazol-2-yl)thio)propanoate.** Method E starting from 5-(2-chloro-4-fluorophenyl)-1,3,4-oxadiazole-2-thiol (0.25 g, 1.1 mmol) and t-butyl-3-bromopropanoate (0.27 g, 1.3 mmol) gave tert-butyl-3-((5-(2-chloro-4-fluorophenyl)-1,3,4-oxadiazol-2-yl)thio)propanoate as yellow oil (0.28 g, 73%); Column: 0% EtOAc: 100% Hex to 30% EtOAc: 70% Hex; ^{1}HNMR (401 MHz, DMSO-d_6) δ ppm 8.05 (dd, J = 8.8, 6.1 Hz, 1H) 7.76 (dd, J = 8.9, 2.6 Hz, 1H) 7.48 (ddd, J = 8.9, 8.1, 2.6 Hz, 1H) 3.46 (t, J = 6.8 Hz, 2H) 2.82 (t, J = 6.8 Hz, 2H) 1.42 (s, 9H); TOF ES+ MS: (M+H) 356.9; HPLC Ret: 8.36 min.

tert-butyl 3-((5-(2,4-dichloro-5-methylphenyl)-1,3,4-oxadiazol-2-yl)thio)propanoate. Method E starting from 5-(2,4-dichloro-5-methylphenyl)-1,3,4-oxadiazole-2-thiol (0.07 g, 0.28 mmol) and t-butyl-3-bromopropanoate (0.07 g, 0.34 mmol) gave tert-butyl 3-((5-(2,4-dichloro-5-methylphenyl)-1,3,4-oxadiazol-2-yl)thio)propanoate as green oil (0.09 g, 82%); Column: 15% EtOAc: 85% Hex; ^{1}H NMR (500 MHz, $CDCl_3$-*d*) δ ppm 7.84 (s, 1H) 7.55 (s, 1H) 3.51 (t, J = 6.8 Hz, 2H) 2.86 (t, J = 6.8 Hz, 2H) 2.42 (s, 3H) 1.47 (s, 9H); QTOF ES+ MS: (M+H) 389.0; HPLC Ret: 8.95 min.

tert-butyl 3-((5-(2-chloro-4,5-dimethylphenyl)-1,3,4-oxadiazol-2-yl)thio)propanoate. Method E starting from 5-(2-chloro-4,5-dimethylphenyl)-1,3,4-oxadiazole-2-thiol (0.11 g, 0.46 mmol) and t-butyl-3-bromopropanoate (0.08 g, 0.55 mmol) gave tert-butyl 3-((5-(2-chloro-4,5-dimethylphenyl)-1,3,4-oxadiazol-2-yl)thio)propanoate as colorless oil (0.13 g, 77%); Column: 10% EtOAc: 90% Hex; ^{1}H NMR (501 MHz, $CDCl_3$-*d*) δ ppm 7.71 (s, 1H) 7.30 (s, 1H) 3.49 (t, J = 6.9 Hz, 2H) 3.32 (s, 3H) 2.86 (t, J = 6.8 Hz, 2H) 2.28 (s, 3H) 1.47 (s, 9H); QTOF ES+ MS: (M+H) 369.1; HPLC Ret: 7.81 min.

tert-butyl 3-((5-(2-chloro-3,4-dimethylphenyl)-1,3,4-oxadiazol-2-yl)thio)propanoate. Method E starting from 5-(2-chloro-3,4-dimethylphenyl)-1,3,4-oxadiazole-2-thiol (0.14 g, 0.56 mmol) and t-butyl-3-bromopropanoate (0.09 g, 0.67 mmol) gave tert-butyl 3-((5-(2-chloro-3,4-dimethylphenyl)-1,3,4-oxadiazol-2-yl)thio)propanoate as colorless oil (0.17 g, 80%); Column: 20% EtOAc: 80% Hex; ^{1}H NMR (501 MHz, $CDCl_3$-*d*) δ ppm 7.61 (d, J = 7.9 Hz, 1H) 7.18 (d, J = 7.9 Hz, 1H) 3.49 (t, J = 6.8 Hz, 2H) 3.42 (s, 3H) 2.86 (t, J = 6.9 Hz, 2H) 2.38 (s, 3H) 1.47 (s, 9H); QTOF ES+ MS: (M+H) 369.1; HPLC Ret: 7.63 min.

tert-butyl 3-((5-(2-chloro-4-cyclopropylphenyl)-1,3,4-oxadiazol-2-yl)thio)propanoate. Method E starting from 5-(2-chloro-4-cyclopropylphenyl)-1,3,4-oxadiazole-2-thiol (0.03 g, 0.12 mmol) and t-butyl-3-bromopropanoate (0.03 g, 0.14 mmol) gave tert-butyl 3-((5-(2-chloro-4-cyclopropylphenyl)-1,3,4-oxadiazol-2-yl)thio)propanoate as colorless oil (0.04 g, 93%); Column: 5% EtOAc: 95% Hex; ^{1}H NMR (500 MHz, $CDCl_3$-*d*) δ ppm 7.81 (d, J = 8.1, 1H) 7.20 (d, J = 1.7 Hz, 1H) 7.05 (dd, J = 8.2, 1.7 Hz, 1H) 3.49 (t, J = 6.8 Hz, 2H) 2.86 (t, J = 6.8 Hz, 2H) 1.92 (ddd, J = 13.4, 8.7, 5.0 Hz, 1H) 1.47 (s, 9H) 1.13-1.04 (m, 2H) 0.79 (dt, J = 6.8, 4.9 Hz, 2H); TOF ES+ MS: (M+H) 381.1; HPLC Ret: 8.98 min.

tert-butyl 3-((5-(2,6-difluorophenyl)-1,3,4-oxadiazol-2-yl)thio)propanoate. Method E starting from 5-(2,6-difluorophenyl)-1,3,4-oxadiazole-2-thiol (0.07 g, 0.33 mmol) and t-butyl-3-bromopropanoate (0.08 g, 0.39 mmol) gave tert-butyl 3-((5-(2,6-difluorophenyl)-1,3,4-oxadiazol-2-yl)thio)propanoate as colorless oil (0.09 g, 83%); Column: 18% EtOAc: 82% Hex; ^{1}H NMR (500 MHz, $CDCl_3$-*d*) δ ppm 7.51 (tt, J = 8.5, 6.1 Hz, 1H) 7.12-7.04 (m, 2H) 3.51 (t, J = 6.8 Hz, 2H) 2.87 (t, J = 6.8 Hz, 2H) 1.47 (s, 9H); TOF ES+ MS: (M+H) 343.1; HPLC Ret: 7.83 min.

tert-butyl 3-((5-(2-(trifluoromethyl)phenyl)-1,3,4-oxadiazol-2-yl)thio)propanoate. Method E starting from 5-(2-(trifluoromethyl)phenyl)-1,3,4-oxadiazole-2-thiol (0.07 g, 0.28 mmol) and t-butyl-3-bromopropanoate (0.07 g, 0.34 mmol) gave tert-butyl 3-((5-(2-(trifluoromethyl)phenyl)-

1,3,4-oxadiazol-2-yl)thio)propanoate as colorless oil (0.09 g, 88%); Column: 18% EtOAc: 82% Hex; ^{1}H NMR (501 MHz, $CDCl_3$-*d*) δ ppm 8.06-8.00 (m, 1H) 7.85 (dd, J = 7.2, 1.8 Hz, 1H) 7.75-7.64 (m, 2H) 3.49 (t, J = 6.9 Hz, 2H) 2.85 (t, J = 6.9 Hz, 2H) 1.47 (s, 9H); TOF ES+ MS: (M+H) 375.1; HPLC Ret: 8.30 min.

tert-butyl 3-((5-(2-fluorophenyl)-1,3,4-oxadiazol-2-yl)thio)propanoate. Method E starting from 5-(2-fluorophenyl)-1,3,4-oxadiazole-2-thiol (0.07 g, 0.36 mmol) and t-butyl-3-bromopropanoate (0.09 g, 0.43 mmol) gave tert-butyl 3-((5-(2-fluorophenyl)-1,3,4-oxadiazol-2-yl)thio)propanoate as colorless oil (0.1 g, 88%); Column: 18% EtOAc: 82% Hex; ^{1}H NMR (501 MHz, $CDCl_3$-*d*) δ ppm 8.04-7.97 (m, 1H) 7.52 (ddddd, J = 8.3, 7.5, 5.0, 1.8, 0.7 Hz, 1H) 7.32-7.20 (m, 2H) 3.51 (t, J = 6.8 Hz, 2H) 2.86 (t, J = 6.8 Hz, 2H) 1.47 (s, 9H); TOF ES+ MS: (M+H) 325.1; HPLC Ret: 7.88 min.

tert-butyl 3-((5-(2,6-dichlorophenyl)-1,3,4-oxadiazol-2-yl)thio)propanoate. Method E starting from 5-(2,6-dichlorophenyl)-1,3,4-oxadiazole-2-thiol (0.07 g, 0.28 mmol) and t-butyl-3-bromopropanoate (0.07 g, 0.34 mmol) gave tert-butyl 3-((5-(2,6-dichlorophenyl)-1,3,4-oxadiazol-2-yl)thio)propanoate as colorless oil (0.09 g, 84%); Column: 15% EtOAc: 85% Hex; ^{1}H NMR (501 MHz, $CDCl_3$-*d*) δ ppm 7.45-7.39 (m, 3H) 3.52 (t, J = 6.5 Hz, 2H) 2.87 (t, J = 6.5 Hz, 2H) 1.48 (s, 9H); TOF ES+ MS: (M+H) 375.0; HPLC Ret: 8.53 min.

t-butyl 4-((5-(4-bromo-2-chlorophenyl)-1,3,4-oxadiazole-2-yl)thio)butanoate. Method E starting from 5-(2-chloro-4-bromophenyl)-1,3,4-oxadiazole-2-thiol (0.26 g, 0.89 mmol) and t-butyl-4-bromobutanoate (0.26 g, 1.2 mmol) gave t-butyl 4-((5-(4-bromo-2-chlorophenyl)-1,3,4-oxadiazole-2-yl)thio)butanoate as colorless oil (0.32 g, 84%); Column: 10% EtOAc: 90% Hex; ^{1}H NMR (500 MHz, $CDCl_3$-*d*) δ ppm 7.83 (d, J = 8.4 Hz, 1H) 7.73 (d, J = 1.9 Hz, 1H) 7.54 (dd, J = 8.4, 1.9 Hz, 2H) 3.36 (t, J = 7.2 Hz, 2H) 2.43 (t, J = 7.2 Hz, 2H) 2.16 (p, J = 7.2 Hz, 2H) 1.45 (s, 9H); TOF ES+ MS: (M+H) 434.9; HPLC Ret: 9.22 min.

methyl-4-((5-(2,4-dichlorophenyl)-1,3,4-oxadiazol-2-yl)thio)butanoate. Method E starting from 5-(2,4-dichlorophenyl)-1,3,4-oxadiazole-2-thiol (0.2 g, 0.81 mmol) and methyl 4-bromobutanoate (0.13 g, 0.97 mmol) gave methyl-4-((5-(2,4-dichlorophenyl)-1,3,4-oxadiazol-2-yl)thio)butanoate as white solid (0.19 g, 66%); Column: 20% EtOAc: 80% Hex; ^{1}H NMR (401 MHz, DMSO-d_6) δ ppm 8.00 (d, J = 8.5 Hz, 1H) 7.92 (d, J = 2.1 Hz, 1H) 7.66 (dd, J = 8.5, 2.1 Hz, 1H) 3.60 (s, 3H) 3.35 (t, J = 7.4 Hz, 2H) 2.50 (t, J = 7.4 Hz, 2H) 2.12-1.97 (m, 2H); TOF ES+ MS: (M+H) 346.9; HPLC Ret: 7.94 min.

methyl 4-((5-(2-chloro-4-methylphenyl)-1,3,4-oxadiazol-2-yl)thio)butanoate. Method E starting from 5-(2-chloro-4-methylphenyl)-1,3,4-oxadiazole-2-thiol (0.02 g, 0.10 mmol) and methyl 4-bromobutanoate (0.01 g, 0.12 mmol) gave methyl 4-((5-(2-chloro-4-methylphenyl)-1,3,4-oxadiazol-2-yl)thio)butanoate as colorless oil (0.02 g, 70%); Column: 20% EtOAc: 80% Hex; ^{1}H NMR (401 MHz, $CDCl_3$-d) δ ppm 7.84 (d, J = 8.0 Hz, 1H) 7.36 (d, J = 1.2 Hz, 1H) 7.18 (dd, J = 8.0, 1.2 Hz, 1H) 3.69 (s, 3H) 3.36 (t, J = 7.1 Hz, 2H) 2.53 (t, J = 7.2 Hz, 2H) 2.41 (s, 3H) 2.22 (p, J = 7.2 Hz, 2H); TOF ES+ MS: (M+H) 327.0; HPLC Ret: 7.62 min.

ethyl 6-((5-(2,4-dichlorophenyl)-1,3,4-oxadiazol-2-yl)thio)hexanoate. Method E starting from 5-(2,4-dichlorophenyl)-1,3,4-oxadiazole-2-thiol (0.25 g, 1.0 mmol) and ethyl 6-bromohexanoate (0.08 g, 1.2 mmol) gave ethyl 6-((5-(2-chloro-4-methylphenyl)-1,3,4-oxadiazol-2-yl)thio)hexanoate as colorless oil (0.33 g, 84%); Column: 15% EtOAc: 85% Hex; ^{1}H NMR (500 MHz, $CDCl_3$-d) δ ppm 7.91 (d, J = 7.3 Hz, 1H) 7.57 (d, J = 1.0 Hz, 1H) 7.38 (dd, J = 7.3, 1.0 Hz, 1H) 4.14 (q, J = 7.2 Hz, 2H) 3.31 (t, J = 7.3 Hz, 2H) 2.34 (t, J = 7.4 Hz, 2H) 1.89 (p, J = 7.5 Hz, 2H) 1.69 (q, J = 7.6 Hz, 2H) 1.52 (q, J = 6.3 Hz, 2H) 1.26 (t, J = 7.1 Hz, 3H); TOF ES+ MS: (M+H) 389.0; HPLC Ret: 8.86 min.

methyl 4-((5-(p-tolyl)-1,3,4-oxadiazol-2-yl)thio)butanoate. Method E starting from 5-(p-tolyl)-1,3,4-oxadiazole-2-thiol (0.25 g, 1.3 mmol) and methyl 4-bromobutanoate (0.28 g, 1.56 mmol)

gave methyl 4-((5-(p-tolyl)-1,3,4-oxadiazol-2-yl)thio)butanoate as white solid (0.29 g, 76%); Column: 20% EtOAc: 80% Hex; ^{1}H NMR (500 MHz, $CDCl_3$-*d*) δ ppm 2.20 (q, J = 7.1 Hz, 2H) 2.42 (s, 3H) 2.53 (t, J = 7.2 Hz, 2H) 3.36 (t, J = 7.1 Hz, 2H) 3.69 (s, 3H) 7.30 (dd, J = 8.2, 3.7 Hz, 2H) 7.92-7.86 (m, 2H); TOF ES+ MS: (M+H) 293.1; HPLC Ret: 7.33 min.

methyl 4-((5-(4-chlorophenyl)-1,3,4-oxadiazol-2-yl)thio)butanoate. Method E starting from 5-(4-chlorophenyl)-1,3,4-oxadiazole-2-thiol (0.25 g, 1.2 mmol) and methyl 4-bromobutanoate (0.26 g, 1.4 mmol) gave methyl 4-((5-(4-chlorophenyl)-1,3,4-oxadiazol-2-yl)thio)butanoate as white solid (0.29 g, 80%); Column: 20% EtOAc: 80% Hex; ^{1}H NMR (500 MHz, $CDCl_3$-*d*) δ ppm 7.98-7.91 (m, 2H) 7.51-7.44 (m, 2H) 3.70 (s, 3H) 3.37 (t, J = 7.2 Hz, 2H) 2.53 (t, J = 7.2 Hz, 2H) 2.20 (q, J = 7.2 Hz, 2H); TOF ES+ MS: (M+H) 313.0; HPLC Ret: 7.54 min.

methyl 7-((5-(2,4-dichlorophenyl)-1,3,4-oxadiazol-2-yl)thio)heptanoate. Method E starting from 5-(2,4-dichlorophenyl)-1,3,4-oxadiazole-2-thiol (0.2 g, 0.81 mmol) and methyl 7-bromoheptanoate (0.22 g, 0.97 mmol) gave methyl 7-((5-(2,4-dichlorophenyl)-1,3,4-oxadiazol-2-yl)thio)heptanoate as colorless oil (0.28 g, 88%); Column: 20% EtOAc: 80% Hex; ^{1}H NMR (500 MHz, $CDCl_3$-*d*) δ ppm 7.91 (d, J = 8.5, 1H) 7.56 (d, J = 2.1 Hz, 1H) 7.39 (dd, J = 8.5, 2.1 Hz, 1H) 3.67 (s, 3H) 3.30 (t, J = 7.3 Hz, 2H) 2.32 (t, J = 7.5 Hz, 2H) 1.91-1.81 (m, 2H) 1.71-1.60 (m, 2H) 1.54-1.44 (m, 2H) 1.40-1.35 (m, 2H); TOF ES+ MS: (M+Na) 411.0; HPLC Ret: 8.85 min.

ethyl 8-((5-(2,4-dichlorophenyl)-1,3,4-oxadiazol-2-yl)thio)octanoate. Method E starting from 5-(2,4-dichlorophenyl)-1,3,4-oxadiazole-2-thiol (0.2 g, 0.81 mmol) and ethyl 8-bromooctanoate (0.24 g, 0.97 mmol) gave ethyl 8-((5-(2,4-dichlorophenyl)-1,3,4-oxadiazol-2-yl)thio)octanoate as colorless oil (0.33 g, 99%); Column: 15% EtOAc: 85% Hex; ^{1}H NMR (500 MHz, $CDCl_3$-*d*) δ ppm 7.91 (d, J = 8.5, 1H) 7.56 (s, 1H) 7.39 (dd, J = 8.5, 1.9 Hz, 1H) 4.13 (q, J= 7.1 Hz, 3H) 3.30 (t, J = 7.0 Hz, 2H) 2.29 (t, J = 7.5 Hz, 2H) 1.85 (p, J= 7.4 Hz, 2H) 1.63 (p, J= 7.5 Hz, 2H) 1.47 (q, J=

7.4 Hz, 2H) 1.42-1.32 (m, 4H) 1.26 (t, J= 7.2 Hz, 3H); TOF ES+ MS: (M+H) 417.0; HPLC Ret: 9.732 min.

methyl 4-((5-(2-chloro-4-cyclopropylphenyl)-1,3,4-oxadiazol-2-yl)thio)butanoate (CCG-263086). Method E starting from 5-(2-chloro-4-cyclopropylphenyl)-1,3,4-oxadiazole-2-thiol (0.08 g, 0.33 mmol) and methyl 4-bromobutanoate (0.07 g, 0.40 mmol) gave methyl 4-((5-(2-chloro-4-cyclopropylphenyl)-1,3,4-oxadiazol-2-yl)thio)butanoate as white oil (0.07 g, 64%); Column: 20% EtOAc: 80% Hex; ^{1}H NMR (500 MHz, $CDCl_3$-*d*) δ ppm 7.81 (d, J = 8.2 Hz, 1H) 7.19 (s, 1H) 7.05 (dd, J = 8.2, 1.7 Hz, 1H) 3.69 (s, 3H) 2.37 (t, J = 7.2 Hz, 2H) 2.58 (t, J = 7.1 Hz, 2H) 2.20 (p, J = 7.2 Hz, 2H) 1.96-1.91 (tt, J = 8.4, 5.0 Hz, 1H) 1.08 (dt, J = 6.9, 4.9 Hz, 2H) 0.78 (dt, J = 6.9, 4.9 Hz, 2H); TOF ES+ MS: (M+H) 353.0; HPLC Ret: 8.01 min; 94% pure.

methyl 4-((5-(2-chloro-4-(trifluoromethyl)phenyl)-1,3,4-oxadiazol-2-yl)thio)butanoate. Method E starting from 5-(2-chloro-4-(trifluoromethyl)phenyl)-1,3,4-oxadiazole-2-thiol (0.25 g, 0.89 mmol) and methyl 4-bromobutanoate (0.21 g, 1.2 mmol) gave methyl 4-((5-(2-chloro-4-(trifluoromethyl)phenyl)-1,3,4-oxadiazol-2-yl)thio)butanoate as colorless oil (0.16 g, 47%); Column: 20% EtOAc: 80% Hex; HPLC Ret: 7.98 min.

Methyl 4-((5-(3-chloro-[1, 1'-biphenyl]-4-yl)-1, 3, 4-oxadiazol-2-yl)thio)butanoate. Method E starting from 5-(3-chloro-[1,1'-biphenyl]-4-yl)-1,3,4-oxadiazole-2-thiol (0.37 g, 1.28 mmol) and methyl 4-bromobutanoate (0.30 g, 1.7 mmol) gave methyl 4-((5-(3-chloro-[1, 1'-biphenyl]-4-yl)-1, 3, 4-oxadiazol-2-yl)thio)butanoate as colorless oil (0.37 g, 75%); Column: 20% EtOAc: 80% Hex; ^{1}H NMR (500 MHz, $CDCl_3$-*d*) δ ppm 8.03 (d, J = 8.2 Hz, 1H) 7.77 (d, J = 1.8 Hz, 1H) 7.64-7.58 (m, 3H) 7.52-7.39 (m, 3H) 3.70 (s, 3H) 3.38 (t, J = 7.1 Hz, 2H) 2.54 (t, J = 7.2 Hz, 2H) 2.22 (p, J = 7.2 Hz, 2H); TOF ES+ MS: (M+H) 389.0; HPLC Ret: 8.00 min.

methyl 4-((5-(2-chloro-4,5-dimethylphenyl)-1,3,4-oxadiazol-2-yl)thio)butanoate. Method E starting from 5-(2-chloro-4,5-dimethylphenyl)-1,3,4-oxadiazole-2-thiol (0.11 g, 0.46 mmol) and

methyl 4-bromobutanoate (0.08 g, 0.55 mmol) gave methyl 4-((5-(2-chloro-4,5-dimethylphenyl)-1,3,4-oxadiazol-2-yl)thio)butanoate as colorless oil (0.11 g, 73%); Column: 20% EtOAc: 80% Hex; ^{1}H NMR (500 MHz, $CDCl_3$-*d*) δ ppm 7.72 (s, 1H) 7.30 (s, 1H) 3.69 (s, 3H) 3.35 (t, J = 7.2 Hz, 2H) 3.32 (s, 3H) 2.53 (t, J = 7.2 Hz, 2H) 2.28 (s, 3H) 2.21 (p, J = 7.2 Hz, 2H); QTOF ES+ MS: (M+H) 341.1; HPLC Ret: 6.76 min.

methyl 4-((5-(2-chloro-3,4-dimethylphenyl)-1,3,4-oxadiazol-2-yl)thio)butanoate. Method E starting from 5-(2-chloro-3,4-dimethylphenyl)-1,3,4-oxadiazole-2-thiol (0.14 g, 0.56 mmol) and methyl 4-bromobutanoate (0.12 g, 0.67 mmol) gave methyl 4-((5-(2-chloro-3,4-dimethylphenyl)-1,3,4-oxadiazol-2-yl)thio)butanoate as colorless oil (0.15 g, 80%); Column: 25% EtOAc: 75% Hex; ^{1}H NMR (500 MHz, $CDCl_3$-*d*) δ ppm 7.61 (d, J = 8.0 Hz, 1H) 7.18 (d, J = 7.9 Hz, 1H) 3.69 (s, 3H) 3.35 (t, J = 7.2 Hz, 2H) 3.42 (s, 3H) 2.53 (t, J = 7.2 Hz, 2H) 2.38 (s, 3H) 2.21 (p, J = 7.2 Hz, 2H); QTOF ES+ MS: (M+H) 341.1; HPLC Ret: 6.67 min.

methyl 4-((5-(2-chloro-4-vinylphenyl)-1,3,4-oxadiazol-2-yl)thio)butanoate. (CCG-262544). Method E starting from 5-(2-chloro-4-vinylphenyl)-1,3,4-oxadiazole-2-thiol (0.08 g, 0.36 mmol) and methyl 4-bromobutanoate (0.06 g, 0.40 mmol) gave methyl 4-((5-(2-chloro-4-vinylphenyl)-1,3,4-oxadiazol-2-yl)thio)butanoate as white powder (0.07 g, 65%); Column: 20% EtOAc: 80% Hex; ^{1}H NMR (500 MHz, $CDCl_3$-*d*) δ ppm 7.92 (d, J = 8.2 Hz, 1H) 7.56 (d, J = 1.6 Hz, 1H) 7.41 (dd, J = 8.2, 1.7 Hz, 1H) 6.69 (dd, J = 17.6, 10.8 Hz, 1H) 5.89 (d, J = 17.5 Hz, 1H) 5.45 (d, 10.9 Hz, 1H) 3.70 (s, 3H) 3.37 (t, J = 7.1 Hz, 2H) 2.54 (t, J = 7.2 Hz, 2H) 2.21 (p, J = 7.2 Hz, 2H); TOF ES+ MS: (M+H) 339.06; HPLC Ret: 7.82 min; 96% pure.

methyl 4-((5-(2,4-dichlorophenyl)-1,3,4-oxadiazol-2-yl)thio)-2,2-dimethylbutanoate. Method E starting from 5-(2,4-dichlorophenyl)-1,3,4-oxadiazole-2-thiol (0.1 g, 0.41 mmol) and methyl 4-bromo-2,2-dimethylbutanoate (0.11 g, 0.53 mmol) gave methyl 4-((5-(2,4-dichlorophenyl)-1,3,4-oxadiazol-2-yl)thio)-2,2-dimethylbutanoate as white oil (0.1 g, 69%); Reaction proceeded for 24

hrs; Column: 10% EtOAc: 90% Hex ^{1}H NMR (500 MHz, $CDCl_3$-*d*) δ ppm 7.91 (d, J = 8.5 Hz, 1H) 7.57 (d, J = 2.1 Hz, 1H) 7.39 (dd, J = 8.6, 2.1 Hz, 1H) 3.70 (s, 3H) 3.29-3.22 (m, 2H) 2.14-2.07 (m, 2H) 1.27 (s, 6H); TOF ES+ MS: (M+H) 375.0; HPLC Ret: 8.80 min.

methyl 4-((5-(2-chloro-4-cyclopropoxyphenyl)-1,3,4-oxadiazol-2-yl)thio)butanoate. Method E starting from 5-(2-chloro-4-cyclopropoxyphenyl)-1,3,4-oxadiazole-2-thiol (0.1 g, 0.37 mmol) and methyl 4-bromobutanoate (0.08 g, 0.45 mmol) gave methyl 4-((5-(2-chloro-4-cyclopropoxyphenyl)-1,3,4-oxadiazol-2-yl)thio)butanoate as colorless oil (0.11 g, 78%); Column: 20% EtOAc: 80% Hex ^{1}H NMR (500 MHz, $CDCl_3$-*d*) δ ppm 7.86 (d, 8.8 Hz, 1H) 7.24 (d, J = 2.5 Hz, 1H) 7.04 (dd, J = 8.8, 2.5 Hz, 1H) 3.83-3.76 (m, 1H) 3.69 (s, 3H) 3.35 (t, J = 7.2 Hz, 2H) 2.53 (t, J = 7.2 Hz, 2H) 2.20 (p, J = 7.2 Hz, 2H) 0.90-0.78 (m, 4H); TOF ES$^+$ MS: (M+H) 368.06; HPLC Ret: 7.94 min.

methyl 4-((5-(2-chloro-4-methoxyphenyl)-1,3,4-oxadiazol-2-yl)thio)butanoate. Method E starting from 5-(2-chloro-4-methoxyphenyl)-1,3,4-oxadiazole-2-thiol (0.1 g, 0.41 mmol) and methyl 4-bromobutanoate (0.09 g, 0.5 mmol) gave methyl 4-((5-(2-chloro-4-methoxyphenyl)-1,3,4-oxadiazol-2-yl)thio)butanoate as colorless oil (0.12 g, 82%); Column: 25% EtOAc: 85% EtOAc to 45% EtOAc: 55% Hex; ^{1}H NMR (500 MHz, $CDCl_3$-*d*) δ ppm 7.88 (d, J = 8.8 Hz, 1H) 7.05 (dd, J = 2.5 Hz, 1H) 6.92 (dd, J = 8.8, 2.5 Hz, 1H) 3.87 (s, 3H) 3.69 (s, 3H) 3.35 (t, J = 7.1 Hz, 2H) 2.53 (t, J = 7.2 Hz, 2H) 2.20 (p, J = 7.2 Hz, 2H); TOF ES$^+$ MS: (M+H) 343.1; HPLC Ret: 7.31 min.

methyl 4-((5-(4-(trifluoromethyl)phenyl)-1,3,4-oxadiazol-2-yl)thio)butanoate. Method E starting from 5-(4-(trifluoromethyl)phenyl)-1,3,4-oxadiazole-2-thiol (0.08 g, 0.31 mmol) and methyl 4-bromobutanoate (0.07 g, 0.4 mmol) gave methyl 4-((5-(4-(trifluoromethyl)phenyl)-1,3,4-oxadiazol-2-yl)thio)butanoate as white solid (0.09 g, 87%); Column: 15% EtOAc: 75% Hex to 20% EtOAc: 80% Hex; ^{1}H NMR (500 MHz, $CDCl_3$-*d*) δ ppm 8.14 (d, J = 8.2 Hz, 2H) 7.77 (d, J =

8.2 Hz, 2H) 3.70 (s, 3H) 3.39 (t, J = 7.2 Hz, 2H) 2.54 (t, J = 7.1 Hz, 2H) 2.22 (p, J = 7.1 Hz, 2H); TOF ES^+ MS: (M+H) 347.07; HPLC Ret: 7.75 min.

methyl 4-((5-(2-chloro-4-(2,2,2-trifluoroethoxy)phenyl)-1,3,4-oxadiazol-2-yl)thio)butanoate. Method E starting from 5-(2-chloro-4-(2,2,2-trifluoroethoxy)phenyl)-1,3,4-oxadiazole-2-thiol (0.08 g, 0.26 mmol) and methyl 4-bromobutanoate (0.06 g, 0.34 mmol) gave methyl 4-((5-(2-chloro-4-(2,2,2-trifluoroethoxy)phenyl)-1,3,4-oxadiazol-2-yl)thio)butanoate as white solid (0.08 g, 75%); Column: 25% EtOAc: 75% Hex to 30% EtOAc: 70% Hex; ^{1}H NMR (500 MHz, $CDCl_3$-*d*) δ ppm 7.94 (d, J = 8.8 Hz, 1H) 7.12 (d, J = 1.1 Hz, 1H) 6.98 (dd, J = 8.8, 1.1 Hz, 1H) 4.42 (q, J = 8.5 Hz, 2H) 3.70 (s, 3H) 3.36 (t, J = 7.1 Hz, 2H) 2.53 (t, J = 7.1 Hz, 2H) 2.21 (p, J = 7.0 Hz, 2H); TOF ES^+ MS: (M+H) 411.04; HPLC Ret: 7.78 min.

methyl 4-((5-(2-chloro-4-(oxetan-3-yloxy)phenyl)-1,3,4-oxadiazol-2-yl)thio)butanoate. Method E starting from 5-(2-chloro-4-(oxetan-3-yloxy)phenyl)-1,3,4-oxadiazole-2-thiol (0.08 g, 0.26 mmol) and methyl 4-bromobutanoate (0.06 g, 0.34 mmol) gave methyl 4-((5-(2-chloro-4-(oxetan-3-yloxy)phenyl)-1,3,4-oxadiazol-2-yl)thio)butanoate as colorless oil (0.07 g, 70%); Column: 40% EtOAc: 60% Hex to 80% EtOAc: 20% Hex; ^{1}H NMR (500 MHz, $CDCl_3$-*d*) δ ppm 7.88 (d, 8.8 Hz, 1H) 6.85 (d, J = 2.6 Hz, 1H) 6.73 (dd, J = 8.8, 2.6 Hz, 1H) 5.26 (pd, 6.0, 1.0 Hz, 1H) 5.01 (t, J = 7.1 Hz, 2H) 4.77 (dd, J = 7.3, 5.1 Hz, 2H) 3.69 (s, 3H) 3.35 (t, J = 7.2 Hz, 2H) 2.53 (t, J = 7.2 Hz, 2H) 2.20 (p, J = 7.2 Hz, 2H); TOF ES+ MS: (M+H) 285.06; HPLC Ret: 6.03 min.

methyl 4-((5-(2-chloro-4-(trifluoromethoxy)phenyl)-1,3,4-oxadiazol-2-yl)thio)butanoate. Method E starting from 5-(2-chloro-4-(trifluoromethoxy)phenyl)-1,3,4-oxadiazole-2-thiol (0.03 g, 0.11 mmol) and methyl 4-bromobutanoate (0.03 g, 0.15 mmol) gave methyl 4-((5-(2-chloro-4-(trifluoromethoxy)phenyl)-1,3,4-oxadiazol-2-yl)thio)butanoate as colorless oil (0.03 g, 70%); Column: 15% EtOAc: 85% Hex. Colorless oil. Yield = 70%. ^{1}H NMR (500 MHz, $CDCl_3$-*d*) δ ppm

8.02 (d, J = 8.7 Hz, 1H) 7.42 (d, J = 2.1 Hz, 1H) 7.27 (dd, J = 8.8, 2.1 Hz, 1H) 3.70 (s, 3H) 3.37 (t, J = 7.1 Hz, 2H) 2.53 (t, J = 7.2 Hz, 2H) 2.22 (p, J = 7.2 Hz, 2H); TOF ES^+ MS: (M+H) 397.02; HPLC Ret: 8.15 min.

methyl 4-((5-(2-chloro-4-(oxetan-3-ylmethoxy)phenyl)-1,3,4-oxadiazol-2-yl)thio)butanoate. Method E starting from 5-(2-chloro-4-(oxetan-3-ylmethoxy)phenyl)-1,3,4-oxadiazole-2-thiol (0.08 g, 0.27 mmol) and methyl 4-bromobutanoate (0.06 g, 0.35 mmol) gave methyl 4-((5-(2-chloro-4-(oxetan-3-ylmethoxy)phenyl)-1,3,4-oxadiazol-2-yl)thio)butanoate as yellow solid (0.07 g, 69%); Column: 60% EtOAc: 40% Hex to 80% EtOAc: 20% Hex; ^{1}H NMR (500 MHz, $CDCl_3$-*d*) δ ppm 7.89 (d, 8.8 Hz, 1H) 7.08 (d, J = 2.6 Hz, 1H) 6.93 (dd, J = 8.8, 2.6 Hz, 1H) 4.90 (dd, J = 7.7, 6.4 Hz, 2H) 4.57 (t, J = 6.0 Hz, 2H) 4.26 (dd, J = 6.6, 1.1 Hz, 2H) 3.69 (s, 3H) 3.47 (hept., 7.2 Hz, 1H) 3.35 (t, J = 7.2 Hz, 2H) 2.53 (t, J = 7.2 Hz, 2H) 2.21 (p, J = 7.2 Hz, 2H); TOF ES+ MS: (M+H) 399.08; HPLC Ret: 6.78 min.

methyl 4-((5-(2-chloro-4-((3-methyloxetan-3-yl)methoxy)phenyl)-1,3,4-oxadiazol-2-yl)thio)butanoate. Method E starting from 5-(2-chloro-4-((3-methyloxetan-3-yl)methoxy)phenyl)-1,3,4-oxadiazole-2-thiol (0.08 g, 0.26 mmol) and methyl 4-bromobutanoate (0.06 g, 0.33 mmol) gave methyl 4-((5-(2-chloro-4-((3-methyloxetan-3-yl)methoxy)phenyl)-1,3,4-oxadiazol-2-yl)thio)butanoate as colorless oil (0.08 g, 80%); Column: 70% EtOAc: 30% Hex; ^{1}H NMR (500 MHz, $CDCl_3$-*d*) δ ppm 7.90 (d, 8.8 Hz, 1H) 7.10 (d, J = 2.6 Hz, 1H) 6.96 (dd, J = 8.8, 2.5 Hz, 1H) 4.64 (d, J = 6.1 Hz, 2H) 4.48 (d, J = 6.1 Hz, 2H) 4.10 (s, 2H) 3.70 (s, 3H) 3.36 (t, J = 7.1 Hz, 2H) 2.53 (t, J = 7.1 Hz, 2H) 2.22 (p, J = 7.1 Hz, 2H) 1.46 (s, 3H); TOF ES+ MS: (M+H) 413.10; HPLC Ret: 7.25 min.

methyl 4-((5-(4-(2,2,2-trifluoroethoxy)phenyl)-1,3,4-oxadiazol-2-yl)thio)butanoate. Method E starting from 5-((4-(2,2,2-trifluoroethoxy)phenyl)-1,3,4-oxadiazole-2-thiol (0.08 g, 0.27 mmol) and methyl 4-bromobutanoate (0.06 g, 0.35 mmol) gave methyl 4-((5-(4-(2,2,2-

trifluoroethoxy)phenyl)-1,3,4-oxadiazol-2-yl)thio)butanoate as white solid (0.08 g, 79%); Column: 30% EtOAc: 70% Hex to 40% EtOAc: 60% Hex; ^{1}H NMR (500 MHz, $CDCl_3$-*d*) δ ppm 7.98 (d, J = 8.0 Hz, 2H) 7.05 (d, J = 8.0 Hz, 2H) 4.42 (q, J = 8.0 Hz, 2H) 3.69 (s, 3H) 3.35 (t, J = 7.1 Hz, 2H) 2.53 (t, J = 7.2 Hz, 2H) 2.20 (p, J = 7.2 Hz, 2H); TOF ES^{+} MS: (M+H) 377.08; HPLC Ret: 7.48 min.

methyl 4-((5-(4-(difluoromethyl)phenyl)-1,3,4-oxadiazol-2-yl)thio)butanoate. Method E starting from 5-(4-(difluoromethyl)phenyl)-1,3,4-oxadiazole-2-thiol (0.08 g, 0.29 mmol) and methyl 4-bromobutanoate (0.07 g, 0.37 mmol) gave methyl 4-((5-(4-(difluoromethyl)phenyl)-1,3,4-oxadiazol-2-yl)thio)butanoate as white solid (0.09 g, 89%); Column: 30% EtOAc: 70% Hex to 35% EtOAc: 65% Hex; ^{1}H NMR (500 MHz, $CDCl_3$-*d*) δ ppm 8.11 (d, J = 8.0 Hz, 2H) 7.65 (d, J = 8.0 Hz, 2H) 6.70 (t, J = 56.2 Hz, 1H) 3.70 (s, 3H) 3.38 (t, J = 7.2 Hz, 2H) 2.54 (t, J = 7.2 Hz, 2H) 2.22 (p, J = 7.2 Hz, 2H); TOF ES^{+} MS: (M+H) 329.08; HPLC Ret: 7.14 min.

methyl 4-((5-(4-(trifluoromethoxy)phenyl)-1,3,4-oxadiazol-2-yl)thio)butanoate. Method E starting from 5-(4-(trifluoromethoxy)phenyl)-1,3,4-oxadiazole-2-thiol (0.08 g, 0.29 mmol) and methyl 4-bromobutanoate (0.07 g, 0.37 mmol) gave methyl 4-((5-(4-(trifluoromethoxy)phenyl)-1,3,4-oxadiazol-2-yl)thio)butanoate as white solid (0.09 g, 89%); Column: 15% EtOAc: 85% Hex to 25% EtOAc: 75% Hex; ^{1}H NMR (500 MHz, $CDCl_3$-*d*) δ ppm 8.06 (d, J = 8.1 Hz, 2H) 7.34 (d, J = 8.1 Hz, 2H) 3.70 (s, 3H) 3.37 (t, J = 7.2 Hz, 2H) 2.53 (t, J = 7.2 Hz, 2H) 2.21 (p, J = 7.2 Hz, 2H); TOF ES^{+} MS: (M+H) 363.06; HPLC Ret: 7.85 min.

methyl 4-((5-(2-chloro-3-(trifluoromethyl)phenyl)-1,3,4-oxadiazol-2-yl)thio)butanoate. Method E starting from 5-(2-chloro-3-(trifluoromethyl)phenyl)-1,3,4-oxadiazole-2-thiol (0.08 g, 0.27 mmol) and methyl 4-bromobutanoate (0.06 g, 0.35 mmol) gave methyl 4-((5-(2-chloro-3-(trifluoromethyl)phenyl)-1,3,4-oxadiazol-2-yl)thio)butanoate as white solid (0.09 g, 85%); Column: 30% EtOAc: 70% Hex to 35% EtOAc: 65% Hex; ^{1}H NMR (500 MHz, $CDCl_3$-*d*) δ ppm

8.10 (d, J = 7.9 Hz, 1H) 7.89 (d, J = 7.9 Hz, 1H) 7.53 (t, J = 8.0 Hz, 1H) 3.70 (s, 3H) 3.39 (t, J = 7.1 Hz, 2H) 2.54 (t, J = 7.2 Hz, 2H) 2.22 (p, J = 7.1 Hz, 2H); TOF ES^+ MS: (M+H) 381.03; HPLC Ret: 7.81 min.

methyl 4-((5-(2-chloro-4-(2-fluoropropan-2-yl)phenyl)-1,3,4-oxadiazol-2-yl)thio)butanoate. Method E starting from 5-(2-chloro-4-(2-fluoropropan-2-yl)phenyl)-1,3,4-oxadiazole-2-thiol (0.08 g, 0.28 mmol) and methyl 4-bromobutanoate (0.07 g, 0.36 mmol) gave methyl 4-((5-(2-chloro-4-(2-fluoropropan-2-yl)phenyl)-1,3,4-oxadiazol-2-yl)thio)butanoate as colorless oil (0.09 g, 86%); Column: 25% EtOAc: 75% Hex to 35% EtOAc: 65% Hex; ^{1}H NMR (500 MHz, $CDCl_3$-*d*) δ ppm 7.94 (d, J = 8.2 Hz, 1H) 7.56 (d, J = 1.7 Hz, 1H) 7.38 (dd, J = 8.3, 1.8 Hz, 1H) 3.70 (s, 3H) 3.37 (t, J = 7.1 Hz, 2H) 2.54 (t, J = 7.2 Hz, 2H) 2.22 (p, J = 7.2 Hz, 2H) 1.72 (s, 3H) 1.68 (s, 3H); TOF ES^+ MS: (M+H) 373.08; HPLC Ret: 7.96 min.

methyl 4-((5-(4-(2-fluoropropan-2-yl)phenyl)-1,3,4-oxadiazol-2-yl)thio)butanoate. Method E starting from 5-(4-(2-fluoropropan-2-yl)phenyl)-1,3,4-oxadiazole-2-thiol (0.04 g, 0.15 mmol) and methyl 4-bromobutanoate (0.04 g, 0.20 mmol) gave methyl 4-((5-(4-(2-fluoropropan-2-yl)phenyl)-1,3,4-oxadiazol-2-yl)thio)butanoate as colorless oil (0.04 g, 69%); Column: 25% EtOAc: 75% Hex to 35% EtOAc: 65% Hex; ^{1}H NMR (500 MHz, $CDCl_3$-*d*) δ ppm 8.00 (d, J = 8.1 Hz, 2H) 7.51 (d, J = 8.2 Hz, 2H) 3.70 (s, 3H) 3.37 (t, J = 7.2 Hz, 2H) 2.54 (t, J = 7.2 Hz, 2H) 2.22 (p, J = 7.2 Hz, 2H) 1.74 (s, 3H) 1.69 (s, 3H); TOF ES^+ MS: (M+H) 339.12; HPLC Ret: 7.65 min.

methyl 4-((5-(4-(difluoromethoxy)phenyl)-1,3,4-oxadiazol-2-yl)thio)butanoate. Method E starting from 5-(4-(difluoromethoxy)phenyl)-1,3,4-oxadiazole-2-thiol (0.08 g, 0.31 mmol) and methyl 4-bromobutanoate (0.07 g, 0.40 mmol) gave methyl 4-((5-(4-(difluoromethoxy)phenyl)-1,3,4-oxadiazol-2-yl)thio)butanoate as white solid (0.08 g, 72%); Column: 30% EtOAc: 70% Hex to 35% EtOAc: 65% Hex; ^{1}H NMR (500 MHz, $CDCl_3$-*d*) δ ppm 8.02 (d, J = 8.8 Hz, 2H) 7.25 (d, J

= 8.8 Hz, 2H) 6.59 (t, J = 73.1 Hz, 1H) 3.69 (s, 3H) 3.36 (t, J = 7.2 Hz, 2H) 2.53 (t, J = 7.2 Hz, 2H) 2.20 (p, J = 7.2 Hz, 2H); TOF ES^+ MS: (M+H) 345.07; HPLC Ret: 7.20 min.

methyl 4-((5-(2-chloro-4-fluorophenyl)-1,3,4-oxadiazol-2-yl)thio)butanoate. Method E starting from 5-(2-chloro-4-fluorophenyl)-1,3,4-oxadiazole-2-thiol (0.02 g, 0.09 mmol) and methyl 4-bromobutanoate (0.02 g, 0.11 mmol) gave methyl 4-((5-(2-chloro-4-fluorophenyl)-1,3,4-oxadiazol-2-yl)thio)butanoate as white solid (0.01 g, 49%); Column: 25% EtOAc: 75% Hex; ^{1}H NMR (500 MHz, $CDCl_3$-*d*) δ ppm 7.96 (ddd, J = 9.4, 6.1, 3.3 Hz, 1H) 7.29 (dt, J = 8.5, 2.8 Hz, 1H) 7.13 (dd, J = 8.8, 2.1 Hz, 1H) 3.69 (s, 3H) 3.36 (t, J = 7.1 Hz, 2H) 2.53 (t, J = 7.2 Hz, 2H) 2.21 (p, J = 7.2 Hz, 2H); TOF ES^+ MS: (M+H) 331.03; HPLC Ret: 7.30 min.

***trans*-methyl 3-((5-(2,4-dichlorophenyl)-1,3,4-oxadiazol-2-yl)thio)cyclobutanecarboxylate & *cis*-methyl 3-((5-(2,4-dichlorophenyl)-1,3,4-oxadiazol-2-yl)thio)cyclobutanecarboxylate.** 5-(2,4-dichlorophenyl)-1,3,4-oxadiazole-2-thiol (0.1 g, 0.41 mmol), cesium carbonate (0.17 g, 0.51 mmol), and sodium iodide (0.006 g, 0.04 mmol) were dissolved in 2 mL DMSO. Methyl 3-chlorocyclobutanecarboxylate (0.09 g, 0.61 mmol, 0.08 mL) was added and the mixture was stirred at 100 °C for 40 hr. The reaction was diluted with EtOAc and H_2O, and product was extracted with EtOAc (3 x 15 mL). The organic layers were combined, washed with brine (2 x 15 mL), and evaporated *in vacuo*. The oil was subjected to silica gel chromatography eluting with 15% EtOAc: 75% Hex. The diastereomers were separated and fractions containing products were concentrated to produce colorless oils. Similar compounds were made in an analogous fashion. *Trans*-isomer yield=11% & *cis*-isomer yield=22%. *Trans:* ^{1}H NMR (500 MHz, $CDCl_3$-*d*) δ ppm 7.91 (d, J = 8.5 Hz, 1H) 7.57 (d, J = 2.0 Hz, 1H) 7.39 (dd, J = 8.5, 2.0 Hz, 1H) 4.48-4.38 (m, 1H) 3.73 (s, 3H) 3.40 (tt, J = 10.4, 5.7 Hz, 1H) 2.94 (tt, J = 8.4, 5.8 Hz, 2H) 2.56 (dtd, J = 13.3, 6.4, 2.4 Hz, 2H); ^{13}C NMR (500 MHz, $CDCl_3$-*d*) δ ppm 174.87, 164.01, 163.34, 138.08, 133.74, 131.58, 131.19, 127.61, 121.39, 52.07, 37.62, 35.22, 32.73; **NOSEY attached; TOF ES+ MS: (M+H) 359.0; HPLC Ret: 8.02 min. *cis:* ^{1}H NMR (500 MHz, $CDCl_3$-*d*) δ ppm 7.90 (d, J

= 8.5 Hz, 1H) 7.57 (d, J = 2.0 Hz, 1H) 7.39 (dd, J = 8.5, 2.0 Hz, 1H) 4.30 (p, J = 8.6 Hz, 1H) 3.71 (s, 3H) 3.17 (p = 8.9 Hz, 1H) 2.95-2.85 (m, 2H) 2.55 (qd, J = 9.7, 2.9 Hz, 2H); ^{13}C NMR (500 MHz, $CDCl_3$-*d*) δ ppm 173.80, 164.17, 163.30, 138.03, 133.72, 131.57, 131.16, 127.59, 121.39, 52.02, 35.45, 34.45, 33.77; **NOSEY attached; TOF ES+ MS: (M+H) 359.0; HPLC Ret: 7.89 min. *NOSEY shows neighboring *cis* protons and does not show *trans* protons.

***cis*-methyl 3-((5-(2-chloro-4-cyclopropylphenyl)-1,3,4-oxadiazol-2-yl)thio)cyclobutanecarboxylate & *trans*-methyl 3-((5-(2-chloro-4-cyclopropylphenyl)-1,3,4-oxadiazol-2-yl)thio)cyclobutanecarboxylate**. Column: 15% EtOAc: 75% Hex. *cis*-isomer yield=50% & *trans*-isomer yield=30%. *cis:* ^{1}H NMR (500 MHz, $CDCl_3$-*d*) δ ppm 7.81 (d, J = 8.2 Hz, 1H) 7.20 (d, J = 1.7 Hz, 1H) 7.05 (dd, J = 8.2, 1.7 Hz, 1H) 4.35-4.23 (m, 1H) 3.71 (s, 3H) 3.23-3.11 (m, 1H) 2.98-2.84 (m, 2H) 2.61-2.49 (m, 2H) 1.98-1.87 (m, 1H) 1.09 (tdd, J = 6.6, 5.6, 3.8 Hz, 2H) 0.79 (tdd, J = 6.4, 4.8, 2.5 Hz, 2H); **NOSEY attached; TOF ES+ MS: (M+H) 365.1; HPLC Ret: 8.26 min. *trans:* ^{1}H NMR (500 MHz, $CDCl_3$-*d*) δ ppm 7.82 (d, J = 7.8 Hz, 1H) 7.20 (d, J = 1.8 Hz, 1H) 7.05 (dd, J = 7.4, 2.0 Hz, 1H) 4.41 (tddd, J = 10.0, 8.5, 5.9, 2.2 Hz, 1H) 3.73 (s, 3H) 3.45-3.34 (m, 1H) 2.99-2.90 (m, 2H) 2.60-2.50 (m, 2H) 1.97-1.87 (m, 1H) 1.09 (tdd, J = 6.6, 3.8, 2.0 Hz, 2H) 0.79 (tdd, J = 6.5, 4.9, 2.4 Hz, 2H); **NOSEY attached; TOF ES+ MS: (M+H) 365.1; HPLC Ret: 8.40 min. *NOSEY shows neighboring *cis* protons and does not show *trans* protons.

***cis*- methyl 3-((5-(2-chloro-4-(trifluoromethyl)phenyl)-1,3,4-oxadiazol-2-yl)thio)cyclobutanecarboxylate & *trans*- methyl 3-((5-(2-chloro-4-(trifluoromethyl)phenyl)-1,3,4-oxadiazol-2-yl)thio)cyclobutanecarboxylate**. Column: 15% EtOAc: 75% Hex. *cis*-isomer yield=34% & *trans*-isomer yield=18%. *cis:* ^{1}H NMR (500 MHz, $CDCl_3$-*d*) δ ppm 8.11 (d, J = 8.2 Hz, 1H) 7.80 (d, J = 1.7 Hz, 1H) 7.66 (dd, J = 8.5, 1.8 Hz, 1H) 4.33 (td, J = 7.7, 1.5 Hz, 1H) 3.71 (s, 3H) 3.25-3.13 (m, 1H) 3.02-2.81 (m, 2H) 2.62-2.50 (m, 2H); **NOSEY attached; TOF ES+ MS: (M+H) 393.0; HPLC Ret: 8.21 min. *trans:* ^{1}H NMR (500 MHz, $CDCl_3$-*d*) δ ppm 8.12 (d, J =

8.2 Hz, 1H) 7.82 (d, J = 1.7 Hz, 1H) 7.67 (dd, J = 8.7, 1.8 Hz, 1H) 4.51-4.41 (m, 1H) 3.74 (s, 3H) 3.45-3.37 (m, 1H) 3.00-2.91 (m, 2H) 2.62-2.51 (m, 2H); **NOSEY attached; TOF ES+ MS: (M+H) 393.0; HPLC Ret: 8.31 min. *NOSEY shows neighboring *cis* protons and does not show *trans* protons.

***cis*- ethyl 4-((5-(2,4-dichlorophenyl)-1,3,4-oxadiazol-2-yl)thio)cyclohexanecarboxylate & *trans*- ethyl 4-((5-(2,4-dichlorophenyl)-1,3,4-oxadiazol-2-yl)thio)cyclohexanecarboxylate**. *Sodium iodide not used and ethyl 4-((methylsulfonyl)oxy)cyclohexanecarboxylate used as alkylating agent. Column: 15% EtOAc: 85% Hex. *cis*-isomer yield=47% & *trans*-isomer yield=25%. *cis:* ^{1}H NMR (500 MHz, $CDCl_3$-*d*) δ ppm 7.91 (d, J = 8.5 Hz, 1H) 7.57 (d, J = 1.9 Hz, 1H) 7.39 (dd, J = 8.5, 1.9 Hz, 1H) 4.21-4.10 (m, 3H) 2.57-2.47 (m, 1H) 2.13-1.95 (m, 6H) 1.90-1.79 (m, 2H) 1.27 (t, J = 7.2 Hz, 3H); ^{13}C NMR (500 MHz, $CDCl_3$-*d*) δ ppm 174.62, 165.01, 163.15, 137.94, 133.70, 131.54, 131.14, 127.57, 121.47, 60.43, 45.63, 40.79, 30.17, 25.51, 14.23; TOF ES+ MS: (M+H) 373.02; TOF ES+ MS: (M+H) 401.05; HPLC Ret: 9.18 min. *trans:* ^{1}H NMR (500 MHz, $CDCl_3$-*d*) δ ppm 7.92 (dd, J = 8.5, 3.6 Hz, 1H) 7.57 (q, J = 2.0 Hz, 1H) 7.39 (dq, J = 8.5, 2.1 Hz, 1H) 4.14 (q, J = 7.1 Hz, 2H) 3.78-3.68 (m, 1H) 2.42-2.31 (m, 3H) 2.18-2.09 (m, 2H) 1.69-1.55 (m, 4H) 1.26 (t, J = 7.1 Hz, 3H); ^{13}C NMR (500 MHz, $CDCl_3$-*d*) δ ppm 174.87, 164.44, 163.23, 138.00, 133.68, 131.56, 131.16, 127.59, 121.44, 60.43, 45.61, 42.04, 32.26, 28.71, 14.19; TOF ES+ MS: (M+H) 401.05; HPLC Ret: 9.33 min. *No conclusive information was deduced from the NOSEYs. No conclusive information was deduced from the predicted MestraNova NMR spectrum. The isomers were assigned based on their physical behaviors. Generally, the trans isomers (4 & 5 membered rings) elute from silica gel column before cis isomers. Also, the trans ester isomers are crystalline post column chromatography. The isomer that had these two characteristics was assigned as the trans isomer. If the isomers have some unexpected activity then I will need to more concretely define these isomers.

***cis*- methyl 3-((5-(2,4-dichlorophenyl)-1,3,4-oxadiazol-2-yl)thio)cyclopentanecarboxylate *trans*- methyl 3-((5-(2,4-dichlorophenyl)-1,3,4-oxadiazol-2-yl)thio)cyclopentanecarboxylate**. In a 50 mL round-bottomed flask, 5-(2,4-dichlorophenyl)-1,3,4-oxadiazole-2-thiol (0.2 g, 0.81 mmol) was dissolved in 2 mL THF. 95% NaH (0.07 g, 0.85 mmol) was added and the reaction proceeded at 25 °C for 30 min. methyl 3-((methylsulfonyl)oxy)cyclopentanecarboxylate (0.33 g, 1.50 mmol) in THF (2 mL) was added dropwise and the solution was stirred at 50 °C for 16 hr. The reaction was partitioned between sat. $NaHCO_3$ and EtOAc, and the product was extracted with EtOAc (3 x 20 mL). The organic layers were combined, dried with $MgSO_4$, and concentrated *in vacuo*. The oil was subjected to silica gel chromatography eluting with 10% EtOAc: 90% Hex to 20% EtOAc: 80% Hex. The diastereomers were separated and fractions containing products were concentrated to produce colorless oils. *cis*-isomer yield=75% & *trans*-isomer yield=25%. *cis:* ^{1}H NMR (500 MHz, $CDCl_3$-*d*) δ ppm 7.91 (d, J = 8.4 Hz, 1H) 7.57 (d, J = 2.1 Hz, 1H) 7.39 (dd, J = 8.5, 2.1 Hz, 1H) 4.27-4.17 (m, 1H) 3.70 (s, 3H) 3.14-3.03 (m, 1H) 2.59-2.55 (m, 1H) 2.50-2.32 (m, 1H) 2.24-2.14 (m, 1H) 2.00-1.95 (m, 1H) 1.91-1.80 (m, 1H); ^{13}C NMR (500 MHz, $CDCl_3$-*d*) δ ppm 175.58, 164.72, 163.24, 138.01, 133.70, 131.57, 131.55, 127.59, 121.41, 51.96, 45.56, 42.45, 37.02, 33.20, 28.84; TOF ES+ MS: (M+H) 373.02; HPLC Ret: 8.50 min. *trans:* ^{1}H NMR (500 MHz, $CDCl_3$-*d*) δ ppm 7.86 (d, J = 8.5 Hz, 1H) 7.58 (d, J = 2.0 Hz, 1H) 7.41 (dd, J = 8.6, 1.5 Hz, 1H) 5.30-5.24 (m, 1H) 3.72 (s, 3H) 3.22 (p, J = 8.0 Hz, 1H) 2.49-2.42 (m, 1H) 2.38-2.10 (m, 3H) 2.12-1.92 (m, 2H); ^{13}C NMR (500 MHz, $CDCl_3$-*d*) δ ppm 175.60, 175.08, 156.30, 138.59, 133.79, 131.50, 130.84, 127.71, 119.86, 59.63, 51.99, 42.44, 34.45, 31.02, 28.65; TOF ES+ MS: (M+H) 373.02; HPLC Ret: 8.69 min. *No conclusive information was deduced from the NOSEYs. However, comparisons between the experimental CNMR chemical shifts to MestreNova predicted CNMR (attached) chemical shifts was used to assign cis and trans isomers; the experimental and predicted shifts were extremely close. Also of note, the cis isomer had a 10% impurity that was

structurally very similar to the desired product; it was deduced that this impurity was the 5-membered ring conformer (see DJK-7-15 for evidence).

tert-butyl 4-((5-(2-chloro-4-propylphenyl)-1,3,4-oxadiazol-2-yl)thio)butanoate. Method E starting from 5-(2-chloro-4-propylphenyl)-1,3,4-oxadiazole-2-thiol (0.03 g, 0.11 mmol) and t-butyl 4-bromobutanoate (0.03 g, 0.13 mmol) gave tert-butyl 4-((5-(2-chloro-4-propylphenyl)-1,3,4-oxadiazol-2-yl)thio)butanoate as colorless oil (0.03 g, 62%); Column: 10% EtOAc: 90% Hex; ^{1}H NMR (500 MHz, $CDCl_3$-*d*) δ ppm 7.85 (dd, J = 8.0, 1.3 Hz, 1H) 7.27 (s, 1H) 7.20 (dd, J = 8.0, 1.5 Hz, 1H) 3.34 (t, J = 7.2 Hz, 2H) 2.63 (t, J = 7.6 Hz, 2H) 2.43 (t, J = 7.3 Hz, 2H) 2.16 (p, J = 7.3 Hz, 2H) 1.68 (h, J = 7.5 Hz, 2H) 1.46 (s, 9H) 0.96 (t, J = 7.5 Hz, 3H); TOF ES+ MS: (M+H) 397.1; HPLC Ret: 9.81 min.

tert-butyl 4-((5-(4-butyl-2-chlorophenyl)-1,3,4-oxadiazol-2-yl)thio)butanoate. Method E starting from 5-(4-butyl-2-chlorophenyl)-1,3,4-oxadiazole-2-thiol (0.06 g, 0.22 mmol) and t-butyl 4-bromobutanoate (0.06 g, 0.26 mmol) gave tert-butyl 4-((5-(4-butyl-2-chlorophenyl)-1,3,4-oxadiazol-2-yl)thio)butanoate as colorless oil (0.05 g, 54%); Column: 15% EtOAc: 85% Hex; ^{1}H NMR (500 MHz, $CDCl_3$-*d*) δ ppm 7.84 (dd, J = 8.0, 1.2 Hz, 1H) 7.35 (s, 1H) 7.19 (dd, J = 8.2, 1.4 Hz, 1H) 3.34 (t, J = 7.2 Hz, 2H) 2.65 (t, J = 7.8 Hz, 2H) 2.43 (t, J = 7.2 Hz, 2H) 2.16 (p, J = 7.3 Hz, 2H) 1.59 (h, J = 7.5 Hz, 2H) 1.45 (s, 9H) 1.37 (p, J = 7.2 Hz, 2H) 0.94 (t, J = 7.3 Hz, 3H); TOF ES+ MS: (M+H) 411.2; HPLC Ret: 10.53 min.

tert-butyl 4-((5-(2-chloro-4-isobutylphenyl)-1,3,4-oxadiazol-2-yl)thio)butanoate. Method E starting from 5-(2-chloro-4-isobutylphenyl)-1,3,4-oxadiazole-2-thiol (0.03 g, 0.11 mmol) and t-butyl 4-bromobutanoate (0.03 g, 0.13 mmol) gave tert-butyl 4-((5-(2-chloro-4-isobutylphenyl)-1,3,4-oxadiazol-2-yl)thio)butanoate as colorless oil (0.03 g, 61%); Column: 15% EtOAc: 85% Hex; ^{1}H NMR (500 MHz, $CDCl_3$-*d*) δ ppm 7.84 (dd, J = 8.0, 1.4 Hz, 1H) 7.34 (s, 1H) 7.18 (dd, J = 8.0, 1.6 Hz, 1H) 3.34 (t, J = 7.2 Hz, 2H) 2.52 (d, J = 7.2 Hz, 2H) 2.43 (t, J = 7.2 Hz, 2H) 2.15

(p, J = 7.2 Hz, 2H) 1.91 (dp, J = 13.6, 6.8 Hz, 1H) 1.45 (s, 9H) 0.93 (d, J = 6.6 Hz, 6H); TOF ES+ MS: (M+H) 411.2; HPLC Ret: 10.33 min.

tert-butyl 4-((5-(2-chloro-3-cyclopropylphenyl)-1,3,4-oxadiazol-2-yl)thio)butanoate. Method E starting from 5-(2-chloro-3-cyclopropylphenyl)-1,3,4-oxadiazole-2-thiol (0.05 g, 0.2 mmol) and t-butyl 4-bromobutanoate (0.05 g, 0.24 mmol) gave tert-butyl 4-((5-(2-chloro-3-cyclopropylphenyl)-1,3,4-oxadiazol-2-yl)thio)butanoate as colorless oil (0.06 g, 82%); Column: 5% EtOAc: 95% Hex; ^{1}H NMR (500 MHz, $CDCl_3$-*d*) δ ppm 7.69 (dd, J = 7.7, 1.6 Hz, 1H) 7.29 (t, J = 7.8 Hz, 1H) 7.15 (dd, J = 7.9, 1.6 Hz, 1H) 3.35 (t, J = 7.2 Hz, 2H) 2.43 (t, J = 7.2 Hz, 2H) 2.26 (tt, J = 8.6, 5.4 Hz, 1H) 2.16 (p, J = 7.2 Hz, 2H) 1.46 (s, 9H) 1.13-1.02 (m, 2H) 0.77-0.66 (m, 2H); TOF ES+ MS: (M+H) 395.1; HPLC Ret: 9.19 min.

tert-butyl 4-((5-(2-chloro-5-cyclopropylphenyl)-1,3,4-oxadiazol-2-yl)thio)butanoate. Method E starting from 5-(2-chloro-5-cyclopropylphenyl)-1,3,4-oxadiazole-2-thiol (0.05 g, 0.2 mmol) and t-butyl 4-bromobutanoate (0.05 g, 0.24 mmol) gave tert-butyl 4-((5-(2-chloro-5-cyclopropylphenyl)-1,3,4-oxadiazol-2-yl)thio)butanoate as colorless oil (0.07 g, 90%); Column: 5% EtOAc: 95% Hex; ^{1}H NMR (500 MHz, $CDCl_3$-*d*) δ ppm 7.63 (d, J = 2.3 Hz, 1H) 7.39 (d, J = 8.4 Hz, 1H) 7.14 (dd, J = 8.3, 2.3 Hz, 1H) 3.35 (t, J = 7.2 Hz, 2H) 2.43 (t, J = 7.2 Hz, 2H) 2.16 (p, J = 7.2 Hz, 2H) 1.93 (ddd, J = 13.5, 8.6, 5.1 Hz, 1H) 1.45 (s, 9H) 1.07-0.98 (m, 2H) 0.75-0.64 (m, 2H); TOF ES+ MS: (M+H) 395.1; HPLC Ret: 9.21 min.

tert-butyl 4-((5-(2-chloro-4-cyclopropylphenyl)-1,3,4-oxadiazol-2-yl)thio)butanoate. Method E starting from 5-(2-chloro-4-cyclopropylphenyl)-1,3,4-oxadiazole-2-thiol (0.08 g, 0.30 mmol) and t-butyl 4-bromobutanoate (0.05 g, 0.36 mmol) gave tert-butyl 4-((5-(2-chloro-4-cyclopropylphenyl)-1,3,4-oxadiazol-2-yl)thio)butanoate as colorless oil (0.1 g, 85%); Column: 5% EtOAc: 95% Hex; ^{1}H NMR (500 MHz, $CDCl_3$-*d*) δ ppm 7.82 (d, J = 8.2, 1H) 7.20 (d, J = 1.7 Hz, 1H) 7.05 (dd, J = 8.2, 1.8 Hz, 1H) 3.34 (t, J = 7.2 Hz, 2H) 2.42 (t, J = 7.2 Hz, 2H) 2.15 (p, J

= 7.2 Hz, 2H) 1.92 (tt, J = 8.4, 5.0 Hz, 1H) 1.45 (s, 9H) 1.14-1.03 (m, 2H) 0.79 (dt, J = 6.8, 4.8 Hz, 2H); TOF ES+ MS: (M+H) 395.1; HPLC Ret: 9.18 min.

tert-butyl 4-((5-(2-chloro-4-(prop-1-en-2-yl)phenyl)-1,3,4-oxadiazol-2-yl)thio)butanoate. Method E starting from 5-(2-chloro-4-(prop-1-en-2-yl)phenyl)-1,3,4-oxadiazole-2-thiol (0.06 g, 0.24 mmol) and t-butyl 4-bromobutanoate (0.06 g, 0.29 mmol) gave tert-butyl 4-((5-(2-chloro-4-(prop-1-en-2-yl)phenyl)-1,3,4-oxadiazol-2-yl)thio)butanoate as white solid (0.07 g, 72%); Column: 12% EtOAc: 88% Hex; ^{1}H NMR (500 MHz, $CDCl_3$-*d*) δ ppm 7.92 (d, J = 8.3, 1H) 7.61 (d, J = 1.9 Hz, 1H) 7.47 (dd, J = 8.1, 1.3 Hz, 1H) 5.51 (s, 1H) 5.25 (s, 1H) 3.36 (t, J = 7.3 Hz, 2H) 2.43 (t, J = 7.2 Hz, 2H) 2.25-2.12 (m, 5H) 1.46 (s, 9H); TOF ES+ MS: (M+H) 395.1; HPLC Ret: 9.54 min.

tert-butyl 4-((5-(2-chloro-4-isopropylphenyl)-1,3,4-oxadiazol-2-yl)thio)butanoate & tert-butyl 4-((5-(4-isopropylphenyl)-1,3,4-oxadiazol-2-yl)thio)butanoate. Method E starting from a mixture of 5-(2-chloro-4-isopropylphenyl)-1,3,4-oxadiazole-2-thiol and 5-(4-isopropylphenyl)-1,3,4-oxadiazole-2-thiol (0.05 g, 0.24 mmol) and t-butyl 4-bromobutanoate (0.05 g, 0.30 mmol) gave a mixture of tert-butyl 4-((5-(2-chloro-4-isopropylphenyl)-1,3,4-oxadiazol-2-yl)thio)butanoate and tert-butyl 4-((5-(4-isopropylphenyl)-1,3,4-oxadiazol-2-yl)thio)butanoate as colorless oil (0.03 g, 56%); Column: 10% EtOAc: 90% Hex; ^{1}H NMR (500 MHz, $CDCl_3$-*d*) δ ppm 7.92 (d, J = 8.3Hz, 2H) 7.86 (d, J = 8.0 Hz, 0.5H) 7.41-7.32 (m, 2.5H) 7.25 (dd, J = 8.0, 1.6 Hz, 0.5H) 3.34 (t, J = 7.2 Hz, 3H) 3.02-2.90 (m, 1.5H) 2.43 (t, J = 7.2 Hz, 3H) 2.15 (p, J = 7.2 Hz, 3H) 1.45 (s, 13.5H) 1.30-1.26 (m, 9H); TOF ES+ MS: (M+H) 397.1 & 363.2; HPLC Ret: 9.70 & 9.40 min.

tert-butyl 4-((5-(2-chloro-4-vinylphenyl)-1,3,4-oxadiazol-2-yl)thio)butanoate. Method E starting from 5-(2-chloro-4-vinylphenyl)-1,3,4-oxadiazole-2-thiol (0.05 g, 0.21 mmol) and t-butyl 4-bromobutanoate (0.06 g, 0.25 mmol) gave tert-butyl 4-((5-(2-chloro-4-vinylphenyl)-1,3,4-

oxadiazol-2-yl)thio)butanoate as colorless oil (0.06 g, 75%); Column: 0% EtOAc: 100% Hex to 15% EtOAc: 85% Hex; ^{1}H NMR (500 MHz, $CDCl_3$-*d*) δ ppm 7.92 (d, J = 8.2 Hz, 1H) 7.55 (d, J = 1.6 Hz, 1H) 7.41 (dd, J = 8.2, 1.6 Hz, 1H) 6.69 (dd, J = 17.5, 10.9 Hz, 1H) 5.89 (d, J = 17.5 Hz, 1H) 5.45 (d, 10.9 Hz, 1H) 3.35 (t, J = 7.2 Hz, 2H) 2.43 (t, J = 7.2 Hz, 2H) 2.16 (p, J = 7.3 Hz, 2H) 1.45 (s, 9H); TOF ES+ MS: (M+Na) 403.1; HPLC Ret: 9.02 min.

tert-butyl 4-((5-(2-chloro-4-ethylphenyl)-1,3,4-oxadiazol-2-yl)thio)butanoate. Method E starting from 5-(2-chloro-4-ethylphenyl)-1,3,4-oxadiazole-2-thiol (0.05 g, 0.21 mmol) and t-butyl 4-bromobutanoate (0.06 g, 0.25 mmol) gave tert-butyl 4-((5-(2-chloro-4-ethylphenyl)-1,3,4-oxadiazol-2-yl)thio)butanoate as colorless oil (0.07 g, 85%); Column: 0% EtOAc: 100% Hex to 15% EtOAc: 85% Hex; ^{1}H NMR (500 MHz, $CDCl_3$-*d*) δ ppm 7.85 (dd, J = 8.0, 1.5 Hz, 1H) 7.37 (d, J = 1.5 Hz, 1H) 7.22 (dd, J = 8.0, 1.6 Hz, 1H) 3.34 (t, J = 7.2 Hz, 2H) 2.70 (q, J = 7.6 Hz, 2H) 2.43 (t, J = 7.2 Hz, 2H) 2.15 (p, J = 7.2 Hz, 2H) 1.45 (s, 9H) 1.27 (t, J = 7.6 Hz, 3H); TOF ES+ MS: (M+Na) 405.1; HPLC Ret: 9.28 min.

tert-butyl 4-((5-(2-(trifluoromethyl)phenyl)-1,3,4-oxadiazol-2-yl)thio)butanoate. Method E starting from 5-(2-(trifluoromethyl)phenyl)-1,3,4-oxadiazole-2-thiol (0.1 g, 0.41 mmol) and t-butyl 4-bromobutanoate (0.08 g, 0.49 mmol) gave tert-butyl 4-((5-(2-(trifluoromethyl)phenyl)-1,3,4-oxadiazol-2-yl)thio)butanoate as colorless oil (0.14 g, 88%); Column: 15% EtOAc: 75% Hex; ^{1}H NMR (500 MHz, $CDCl_3$-*d*) δ ppm 8.06-8.00 (m, 1H) 7.85 (dd, J = 7.1, 1.9 Hz, 1H) 7.74-7.64 (m, 2H) 3.34 (t, J = 7.2 Hz, 2H) 2.43 (t, J = 7.2 Hz, 2H) 2.15 (p, J = 7.2 Hz, 2H) 1.45 (s, 9H); TOF ES+ MS: (M+H) 389.1; HPLC Ret: 8.46 min.

tert-butyl 4-((5-(2-fluorophenyl)-1,3,4-oxadiazol-2-yl)thio)butanoate. Method E starting from 5-(2-fluorophenyl)-1,3,4-oxadiazole-2-thiol (0.1 g, 0.51 mmol) and t-butyl 4-bromobutanoate (0.14 g, 0.61 mmol) gave tert-butyl 4-((5-(2-fluorophenyl)-1,3,4-oxadiazol-2-yl)thio)butanoate as yellow oil (0.16 g, 91%); Column: 15% EtOAc: 75% Hex ^{1}H NMR (500 MHz, $CDCl_3$-*d*) δ ppm

8.02 (td, J = 7.5, 1.8 Hz, 1H) 7.56-7.48 (m, 1H) 7.32-7.20 (m, 2H) 3.36 (t, J = 7.2 Hz, 2H) 2.43 (t, J = 7.2 Hz, 2H) 2.15 (p, J = 7.2 Hz, 2H) 1.46 (s, 9H); TOF ES+ MS: (M+H) 339.1; HPLC Ret: 8.08 min.

tert-butyl 4-((5-(2-chloro-4-ethoxyphenyl)-1,3,4-oxadiazol-2-yl)thio)butanoate. Method L starting from tert-butyl 4-((5-(2-chloro-4-hydroxyphenyl)-1,3,4-oxadiazol-2-yl)thio)butanoate (0.05 g, 0.14 mmol) and ethyl iodide (0.03 g, 0.2 mmol) gave tert-butyl 4-((5-(2-chloro-4-ethoxyphenyl)-1,3,4-oxadiazol-2-yl)thio)butanoate as colorless oil (0.05 g, 97%); ^{1}H NMR (500 MHz, $CDCl_3$-*d*) δ ppm 7.86 (d, 8.8 Hz, 1H) 7.03 (d, J = 2.4 Hz, 1H) 6.89 (dd, J = 8.8, 2.5 Hz, 1H) 4.09 (q, J = 7.0 Hz, 2H) 3.33 (t, J = 7.2 Hz, 2H) 2.42 (t, J = 7.2 Hz, 2H) 2.15 (p, J = 7.2 Hz, 2H) 1.45 (t, J = 7.0 Hz, 3H) 1.45 (s, 9H); TOF ES^+ MS: (M+H) 399.12; HPLC Ret: 7.40 min.

tert-butyl 4-((5-(2-chloro-4-propoxyphenyl)-1,3,4-oxadiazol-2-yl)thio)butanoate. Method L starting from tert-butyl 4-((5-(2-chloro-4-hydroxyphenyl)-1,3,4-oxadiazol-2-yl)thio)butanoate (0.05 g, 0.14 mmol) and 1-bromopropane (0.02 g, 0.2 mmol) gave tert-butyl 4-((5-(2-chloro-4-propoxyphenyl)-1,3,4-oxadiazol-2-yl)thio)butanoate as colorless oil (0.05 g, 94%); Column: 18% EtOAc: 82% Hex; ^{1}H NMR (500 MHz, $CDCl_3$-*d*) δ ppm 7.86 (d, 8.8 Hz, 1H) 7.04 (d, J = 2.4 Hz, 1H) 6.90 (dd, J = 8.5, 2.5 Hz, 1H) 3.98 (t, J = 6.5 Hz, 2H) 3.33 (t, J = 7.2 Hz, 2H) 2.42 (t, J = 7.2 Hz, 2H) 2.15 (p, J = 7.2 Hz, 2H) 1.89-1.78 (m, 2H) 1.45 (s, 9H) 1.05 (t, J = 7.4 Hz, 3H); TOF ES^+ MS: (M+H) 413.13; HPLC Ret: 9.51 min.

tert-butyl 4-((5-(4-butoxy-2-chlorophenyl)-1,3,4-oxadiazol-2-yl)thio)butanoate. Method L starting from tert-butyl 4-((5-(2-chloro-4-hydroxyphenyl)-1,3,4-oxadiazol-2-yl)thio)butanoate (0.05 g, 0.14 mmol) and 1-iodobutane (0.03 g, 0.2 mmol) gave tert-butyl 4-((5-(4-butoxy-2-chlorophenyl)-1,3,4-oxadiazol-2-yl)thio)butanoate as colorless oil (0.05 g, 92%); Column: 18% EtOAc: 82% Hex; ^{1}H NMR (500 MHz, $CDCl_3$-*d*) δ ppm 7.86 (d, 8.8 Hz, 1H) 7.04 (d, J = 2.5 Hz, 1H) 6.90 (dd, J = 8.8, 2.5 Hz, 1H) 4.02 (t, J = 6.5 Hz, 2H) 3.33 (t, J = 7.2 Hz, 2H) 2.42 (t, J = 7.2

Hz, 2H) 2.15 (p, J = 7.2 Hz, 2H) 1.84-1.74 (m, 2H) 1.55-1.43 (m, 11H) 0.99 (t, J = 7.4 Hz, 3H); TOF ES^+ MS: (M+H) 427.15; HPLC Ret: 10.13 min.

tert-butyl 4-((5-(2-chloro-4-(cyclopropylmethoxy)phenyl)-1,3,4-oxadiazol-2-yl)thio)butanoate. Method L starting from tert-butyl 4-((5-(2-chloro-4-hydroxyphenyl)-1,3,4-oxadiazol-2-yl)thio)butanoate (0.05 g, 0.14 mmol) and (bromomethyl)cyclopropane (0.02 g, 0.16 mmol) gave tert-butyl 4-((5-(2-chloro-4-(cyclopropylmethoxy)phenyl)-1,3,4-oxadiazol-2-yl)thio)butanoate as colorless oil (0.05 g, 93%); Column: 20% EtOAc: 80% Hex; ^{1}H NMR (500 MHz, $CDCl_3$-*d*) δ ppm 7.86 (d, 8.8 Hz, 1H) 7.04 (d, J = 2.4 Hz, 1H) 6.90 (dd, J = 8.8, 2.6 Hz, 1H) 3.86 (d, J = 6.9 Hz, 2H) 3.33 (t, J = 7.2 Hz, 2H) 2.42 (t, J = 7.2 Hz, 2H) 2.15 (p, J = 7.2 Hz, 2H) 1.45 (s, 9H) 1.33-1.22 (m. 1H) 0.73-0.63 (m, 2H) 0.43-0.34 (m, 2H); TOF ES^+ MS: (M+H) 425.13; HPLC Ret: 9.24 min.

tert-butyl 4-((5-(2-chloro-4-isopropoxyphenyl)-1,3,4-oxadiazol-2-yl)thio)butanoate. Method L starting from tert-butyl 4-((5-(2-chloro-4-hydroxyphenyl)-1,3,4-oxadiazol-2-yl)thio)butanoate (0.05 g, 0.14 mmol) and 2-bromopropane (0.02 g, 0.16 mmol) gave tert-butyl 4-((5-(2-chloro-4-isopropoxyphenyl)-1,3,4-oxadiazol-2-yl)thio)butanoate as colorless oil (0.05 g, 84%); Column: 18% EtOAc: 82% Hex; ^{1}H NMR (500 MHz, $CDCl_3$-*d*) δ ppm 7.85 (d, 8.8 Hz, 1H) 7.02 (d, J = 2.5 Hz, 1H) 6.87 (dd, J = 8.7, 2.5 Hz, 1H) 4.61 (hept, J = 6.0 Hz, 1H) 3.33 (t, J = 7.2 Hz, 2H) 2.42 (t, J = 7.2 Hz, 2H) 2.15 (p, J = 7.2 Hz, 2H) 1.45 (s, 9H) 1.40-1.35 (m, 6H); TOF ES^+ MS: (M+H) 413.13; HPLC Ret: 9.29 min.

methyl 4-((5-(2-chloro-3-(2,2,2-trifluoroethoxy)phenyl)-1,3,4-oxadiazol-2-yl)thio)butanoate. In a 10 mL round-bottomed flask, methyl 4-((5-(2-chloro-3-hydroxyphenyl)-1,3,4-oxadiazol-2-yl)thio)butanoate (0.04 g, 0.12 mmol) was dissolved in 0.75 mL anhydrous DMSO. Cs_2CO_3 (0.05 g, 0.15 mmol) and 1, 1, 1-trifluoro-2-iodoethane (0.08 g, 0.37 mmol) were added and the reaction was heated at 105 °C for 16 hr. The reaction was cooled, diluted with H_2O, and

extracted with EtOAc (3 x 20 mL). The organic layers were combined, washed with brine, and concentrated in vacuo. The yellow residue was subjected to silica gel chromatography eluting with 35% EtOAc: 65% Hex. The fractions containing product were concentrated in vacuo to produce white solid. Yield=28%. ^{1}H NMR (500 MHz, $CDCl_3$-*d*) δ ppm 7.67 (dt, 7.9, 1.2 Hz, 1H) 7.38 (t, J = 8.1 Hz, 1H) 7.16 (dd, J = 8.3, 1.4 Hz, 1H) 4.51-4.41 (m, 2H) 3.70 (s, 3H) 3.38 (t, J = 7.2 Hz, 2H) 2.54 (t, J = 7.1 Hz, 2H) 2.22 (p, J = 7.0 Hz, 2H); TOF ES^{+} MS: (M+H) 411.04; HPLC Ret: 7.46 min.

3-((5-(2-chloro-4-methylphenyl)-1,3,4-oxadiazol-2-yl)thio)propanoic acid (CCG-232001). Method F starting from tert-butyl 3-((5-(2-chloro-4-methylphenyl)-1,3,4-oxadiazol-2-yl)thio)propanoate (0.27 g, 0.77 mmol) gave 3-((5-(2-chloro-4-methylphenyl)-1,3,4-oxadiazol-2-yl)thio)propanoic acid as white solid (0.13 g, 57%); ^{1}H NMR (401 MHz, DMSO-d_6) δ ppm 12.45 (br. s., 1H) 7.85 (d, J = 8.0 Hz, 1H) 7.55 (s, 1H) 7.37 (d, J = 8.1 Hz, 1H) 3.46 (t, J = 6.8 Hz, 2H) 2.84 (t, J = 6.8 Hz, 2H) 2.40 (s, 3H); ^{13}C NMR (401 MHz, DMSO-d_6) δ ppm 172.88, 164.42, 163.75, 144.35, 131.77, 131.26, 128.98, 119.78, 34.26, 27.99, 21.05; TOF ES+ MS: (M+H) 398.9; HPLC Ret: 6.31 min; 99% pure.

3-((5-(2-chloro-4-fluorophenyl)-1,3,4-oxadiazol-2-yl)thio)propanoic acid (CCG-232002). Method F starting from tert-butyl 3-((5-(2-chloro-4-fluorophenyl)-1,3,4-oxadiazol-2-yl)thio)propanoate (0.28 g, 0.78 mmol) gave 3-((5-(2-chloro-4-fluorophenyl)-1,3,4-oxadiazol-2-yl)thio)propanoic acid as white solid (0.12 g, 50%); ^{1}HNMR (401 MHz, DMSO-d_6) δ ppm 12.53 (br. s., 1H) 8.09-8.02 (m, 1H) 7.76-7.71 (m, 1H) 7.48 (d, J = 8.1 Hz, 1H) 3.46 (t, J = 6.8 Hz, 2H) 2.84 (t, J = 6.8 Hz, 2H); ^{13}CNMR (101 MHz, DMSO-d_6) δ ppm 172.89, 165.13, 164.74, 163.02, 162.60, 133.72, 119.58, 116.08, 115.87, 34.26, 27.99; TOF ES+ MS: (M+H) 302.9; HPLC Ret: 6.08 min; 98% pure.

3-((5-(2,4-dichloro-5-methylphenyl)-1,3,4-oxadiazol-2-yl)thio)propanoic acid. (CCG-258021). Method F starting from tert-butyl 3-((5-(2,4-dichloro-5-methylphenyl)-1,3,4-oxadiazol-2-yl)thio)propanoate (0.09 g, 0.23 mmol) gave 3-((5-(2,4-dichloro-5-methylphenyl)-1,3,4-oxadiazol-2-yl)thio)propanoic acid as white solid (0.4 g, 65%); ^{1}H NMR (500 MHz, $CDCl_3$-*d*) δ ppm 7.83 (s, 1H) 7.54 (s, 1H) 3.55 (t, J = 6.8 Hz, 2H) 3.04 (t, J = 6.8 Hz, 2H) 2.41 (s, 3H); ^{13}C NMR (500 MHz, $CDCl_3$-*d*) δ ppm 175.94, 164.62, 163.72, 138.29, 135.72, 132.36, 131.31, 130.62, 129.34, 120.94, 33.84, 27.05, 19.46; QTOF ES+ MS: (M+H) 330.97; HPLC Ret: 6.81 min; 95% pure.

3-((5-(2-chloro-4,5-dimethylphenyl)-1,3,4-oxadiazol-2-yl)thio)propanoic acid. **(CCG-258041).** Method F starting from tert-butyl 3-((5-(2-chloro-4,5-dimethylphenyl)-1,3,4-oxadiazol-2-yl)thio)propanoate (0.13 g, 0.35 mmol) gave 3-((5-(2-chloro-4,5-dimethylphenyl)-1,3,4-oxadiazol-2-yl)thio)propanoic acid as white solid (0.08 g, 75%); ^{1}H NMR (501 MHz, $CDCl_3$-*d*) δ ppm 11.00 (br. s., 1H) 7.71 (s, 1H) 7.29 (s, 1H) 3.54 (t, J = 6.8 Hz, 2H) 3.32 (s, 3H) 3.04 (t, J = 6.8 Hz, 2H) 2.28 (s, 3H); ^{13}C NMR (126 MHz, $CDCl_3$-*d*) δ ppm 176.49, 164.54, 164.10, 142.24, 135.99, 131.95, 131.52, 129.77, 119.69, 33.99, 27.00, 19.70, 19.06; QTOF ES+ MS: (M-H) 311.03; HPLC Ret: 5.91 min; 99% pure.

3-((5-(2-chloro-3,4-dimethylphenyl)-1,3,4-oxadiazol-2-yl)thio)propanoic acid. **(CCG-258043).** Method F starting from tert-butyl 3-((5-(2-chloro-3,4-dimethylphenyl)-1,3,4-oxadiazol-2-yl)thio)propanoate (0.17 g, 0.45 mmol) gave 3-((5-(2-chloro-3,4-dimethylphenyl)-1,3,4-oxadiazol-2-yl)thio)propanoic acid as white solid (0.11 g, 80%); ^{1}H NMR (500 MHz, $CDCl_3$-*d*) δ ppm 10.59 (br. s., 1H) 7.60 (d, J = 7.9 Hz, 1H) 7.17 (d, J = 7.9 Hz, 1H) 3.53 (t, J = 6.8 Hz, 2H) 3.32 (s, 3H) 3.04 (t, J = 6.8 Hz, 2H) 2.28 (s, 3H); ^{13}C NMR (126 MHz, $CDCl_3$-*d*) δ ppm 176.37, 165.02, 164.19, 142.27, 136.67, 133.15, 128.14, 120.93, 34.00, 26.99, 21.37, 16.72; QTOF ES+ MS: (M-H) 311.03; HPLC Ret: 5.83 min; 95% pure.

3-((5-(2,6-difluorophenyl)-1,3,4-oxadiazol-2-yl)thio)propanoic acid. (CCG-262527). Method F starting from tert-butyl 3-((5-(2,6-difluorophenyl)-1,3,4-oxadiazol-2-yl)thio)propanoate (0.09 g, 0.26 mmol) gave 3-((5-(2,6-difluorophenyl)-1,3,4-oxadiazol-2-yl)thio)propanoic acid as white solid (0.07 g, 94%); ^{1}H NMR (500 MHz, $CDCl_3$-*d*) δ ppm 10.25 (br. s, 1H) 7.53 (tt, J = 8.5, 6.1 Hz, 1H) 7.13-7.05 (m, 2H) 3.55 (t, J = 6.7 Hz, 2H) 2.73 (t, J = 7.0 Hz, 2H); ^{13}C NMR (500 MHz, $CDCl_3$-*d*) δ ppm 176.42, 165.20, 161.53, 159.50, 157.96, 133.59, 112.46, 33.89, 26.99; TOF ES+ MS: (M+H) 287.0; HPLC Ret: 5.57 min; 95% pure.

3-((5-(2-(trifluoromethyl)phenyl)-1,3,4-oxadiazol-2-yl)thio)propanoic acid. (CCG-262528). Method F starting from tert-butyl 3-((5-(2-(trifluoromethyl)phenyl)-1,3,4-oxadiazol-2-yl)thio)propanoate (0.09 g, 0.24 mmol) gave 3-((5-(2-(trifluoromethyl)phenyl)-1,3,4-oxadiazol-2-yl)thio)propanoic acid as colorless oil (0.07 g, 93%); product required 45% EtOAc: 65% Hex: 0.01% AcOH column chromotragraphy; ^{1}H NMR (501 MHz, $CDCl_3$-*d*) δ ppm 10.22 (br. s, 1H) 8.06-7.99 (m, 1H) 7.86 (dd, J = 7.3, 1.9 Hz, 1H) 7.78-7.67 (m, 2H) 3.53 (t, J = 6.8 Hz, 2H) 3.03 (t, J = 6.8 Hz, 2H); ^{13}C NMR (126 MHz, $CDCl_3$-*d*) δ ppm 176.64, 165.31, 164.17, 132.19, 131.66, 128.83, 127.13, 127.04, 124.17, 121.76, 33.97, 26.95; TOF ES+ MS: (M+H) 319.04; HPLC Ret: 6.18 min; 99% pure.

3-((5-(2-fluorophenyl)-1,3,4-oxadiazol-2-yl)thio)propanoic acid. (CCG-262529). Method F starting from tert-butyl 3-((5-(2-fluorophenyl)-1,3,4-oxadiazol-2-yl)thio)propanoate (0.1 g, 0.31 mmol) gave 3-((5-(2-fluorophenyl)-1,3,4-oxadiazol-2-yl)thio)propanoic acid as white solid (0.07 g, 85%); ^{1}H NMR (501 MHz, $CDCl_3$-*d*) δ ppm 10.31 (br. s, 1H) 8.00 (td, J = 7.5, 1.7 Hz, 1H) 7.57-7.49 (m, 1H) 7.36-7.15 (m, 2H) 3.55 (t, J = 6.8 Hz, 2H) 3.03 (t, J = 6.7 Hz, 2H); ^{13}C NMR (126 MHz, $CDCl_3$-*d*) δ ppm 176.28, 164.49, 162.69, 160.85, 158.79, 133.55, 129.49, 124.65, 116.89, 33.93, 27.03; TOF ES+ MS: (M+H) 269.0; HPLC Ret: 5.58 min; 95% pure.

3-((5-(2,6-dichlorophenyl)-1,3,4-oxadiazol-2-yl)thio)propanoic acid. (CCG-262530). Method F starting from tert-butyl 3-((5-(2,6-dichlorophenyl)-1,3,4-oxadiazol-2-yl)thio)propanoate (0.09 g, 0.24 mmol) gave 3-((5-(2,6-dichlorophenyl)-1,3,4-oxadiazol-2-yl)thio)propanoic acid as colorless oil (0.07 g, 90%); product required 45% EtOAc: 65% Hex: 0.01% AcOH column chromotragraphy; ^{1}H NMR (501 MHz, $CDCl_3$-*d*) δ ppm 10.51 (br. s, 1H) 7.36-7.24 (m, 3H) 3.56 (t, J = 6.7 Hz, 2H) 3.05 (t, J = 6.7 Hz, 2H); ^{13}C NMR (126 MHz, $CDCl_3$-*d*) δ ppm 176.79, 165.49, 160.91, 136.51, 133.05, 128.30, 123.75, 33.93, 27.01; TOF ES+ MS: (M+H) 318.97; HPLC Ret: 6.23 min; 99% pure.

4-((5-(2,4-dichlorophenyl)-1,3,4-oxadiazol-2-yl)oxy)butanoic acid. (CCG-257223). Method F starting from tert-butyl 4-((5-(2,4-dichlorophenyl)-1,3,4-oxadiazol-2-yl)oxy)butanoate (0.06 g, 0.16 mmol) gave 4-((5-(2,4-dichlorophenyl)-1,3,4-oxadiazol-2-yl)oxy)butanoic acid as white solid (0.4 g, 89%); ^{1}H NMR (501 MHz, $CDCl_3$-*d*) δ ppm 7.75 (d, J = 8.5 Hz, 1H) 7.59 (br. s., 1H) 7.54 (d, J = 2.1 Hz, 1H) 7.37 (dd, J = 8.5, 2.1 Hz, 1H) 3.93 (t, J = 6.7 Hz, 2H) 2.53 (t, J = 7.2 Hz, 2H) 2.17 (p, J = 7.0 Hz, 2H); ^{13}C NMR (126 MHz, $CDCl_3$-*d*) δ ppm 177.90, 153.08, 150.84, 137.89, 133.40, 131.38, 130.53, 127.56, 121.02, 45.15, 30.61, 23.22; TOF ES+ MS: (M+Na) 338.9; HPLC Ret: 6.52 min; 98% pure.

4-((5-(4-bromo-2-chlorophenyl)-1,3, 4-oxadiazole-2-yl)thio)butanoic acid. (CCG-257389). Method F starting from tert-butyl 4-((5-(4-bromo-4-chlorophenyl)-1,3,4-oxadiazol-2-yl)thio)butanoate (0.05 g, 0.12 mmol) gave 4-((5-(4-bromo-2-chlorophenyl)-1,3, 4-oxadiazole-2-yl)thio)butanoic acid as white solid (0.04 g, 94%); ^{1}H NMR (500 MHz, $CDCl_3$-*d*) δ ppm 7.83 (d, J = 8.4 Hz, 1H) 7.73 (d, J = 1.9 Hz, 1H) 7.54 (dd, J = 8.5, 1.9 Hz, 2H) 3.39 (t, J = 7.2 Hz, 2H) 2.59 (t, J = 7.1 Hz, 2H) 2.22 (p, J = 7.1 Hz, 2H); ^{13}C NMR (500 MHz, $CDCl_3$-*d*) δ ppm 176.35, 164.99, 163.50, 134.00, 133.78, 131.66, 130.54, 126.15, 121.75, 32.23, 31.60, 24.31; TOF ES+ MS: (M+H) 378.9; HPLC Ret: 6.91 min; 95% pure.

4-((5-(2-chloro-3-cyclopropylphenyl)-1,3,4-oxadiazol-2-yl)thio)butanoic acid. (**CCG-259066)** Method F starting from tert-butyl 4-((5-(2-chloro-3-cyclopropylphenyl)-1,3,4-oxadiazol-2-yl)thio)butanoate (0.06 g, 0.15 mmol) gave 4-((5-(2-chloro-3-cyclopropylphenyl)-1,3,4-oxadiazol-2-yl)thio)butanoic acid as white oil (0.02 g, 39%); **post evaporation, 0% to 5% MeOH DCM column performed; ^{1}H NMR (500 MHz, $CDCl_3$-*d*) δ ppm 7.68 (dd, J = 7.7, 1.6 Hz, 1H) 7.29 (t, J = 7.8 Hz, 1H) 7.15 (dd, J = 7.8, 1.6 Hz, 1H) 3.39 (t, J = 7.2 Hz, 2H) 2.59 (t, J = 7.1 Hz, 2H) 2.31-2.18 (m, 3H) 1.13-0.98 (m, 2H) 0.77-0.66 (m, 2H); ^{13}C NMR (500 MHz, $CDCl_3$-*d*) δ ppm 175.45, 164.64, 143.05, 134.30, 129.45, 128.56, 126.72, 123.34, 109.99, 32.30, 31.60, 24.37, 14.02, 8.05; TOF ES+ MS: (M+H) 339.0; HPLC Ret: 6.94 min; 95% pure

4-((5-(2-chloro-5-cyclopropylphenyl)-1,3,4-oxadiazol-2-yl)thio)butanoic acid. (CCG-259067). Method F starting from tert-butyl 4-((5-(2-chloro-5-cyclopropylphenyl)-1,3,4-oxadiazol-2-yl)thio)butanoate (0.07 g, 0.18 mmol) gave 4-((5-(2-chloro-5-cyclopropylphenyl)-1,3,4-oxadiazol-2-yl)thio)butanoic acid as white oil (0.03 g, 55%); **post evaporation, 0% to 5% MeOH DCM column performed; ^{1}H NMR (500 MHz, $CDCl_3$-*d*) δ ppm 8.90 (br. s, 1H) 7.63 (d, J = 2.2 Hz, 1H) 7.39 (d, J = 8.3 Hz, 1H) 7.14 (dd, J = 8.4, 2.3 Hz, 1H) 3.38 (t, J = 7.1 Hz, 2H) 2.59 (t, J = 7.1 Hz, 2H) 2.22 (p, J = 7.1 Hz, 2H) 1.93 (tt, J = 8.4, 5.0 Hz, 1H) 1.08-0.98 (m, 2H) 0.73 (dt, 6.8, 4.9 Hz, 2H); ^{13}C NMR (500 MHz, $CDCl_3$-*d*) δ ppm 177.92, 164.64, 164.35, 143.59, 130.93, 129.86, 129.51, 128.16, 122.37, 32.32, 31.62, 24.35, 14.89, 9.56; TOF ES+ MS: (M+H) 339.1; HPLC Ret: 6.98 min; 97% pure.

3-((5-(2-chloro-4-cyclopropylphenyl)-1,3,4-oxadiazol-2-yl)thio)propanoic acid. (CCG-259068). Method F starting from tert-butyl 4-((5-(2-chloro-4-cyclopropylphenyl)-1,3,4-oxadiazol-2-yl)thio)butanoate (0.04 g, 0.11 mmol) gave 4-((5-(2-chloro-4-cyclopropylphenyl)-1,3,4-oxadiazol-2-yl)thio)butanoic acid as white oil (0.01 g, 41%); **post evaporation, 0% to 5% MeOH DCM column performed; ^{1}H NMR (500 MHz, $CDCl_3$-*d*) δ ppm 7.81 (d, J = 8.2, 1H) 7.20 (d, J = 1.7 Hz, 1H) 7.05 (dd, J = 8.2, 1.8 Hz, 1H) 3.53 (t, J = 6.8 Hz, 2H) 3.03 (t, J = 6.8 Hz, 2H)

1.92 (tt, J = 8.4, 5.0 Hz, 1H) 1.14-1.02 (m, 2H) 0.79 (dt, J = 6.9, 4.8 Hz, 2H); ^{13}C NMR (500 MHz, $CDCl_3$-*d*) δ ppm 176.07, 164.42, 164.12, 150.11, 132.83, 130.66, 128.15, 124.29, 119.45, 33.97, 27.05, 15.41, 10.39; TOF ES+ MS: (M+H) 325.0; HPLC Ret: 6.79 min; 95% pure.

4-((5-(2-chloro-4-ethoxyphenyl)-1,3,4-oxadiazol-2-yl)thio)butanoic acid (CCG-262687). Method F starting from tert-butyl 4-((5-(2-chloro-4-ethoxyphenyl)-1,3,4-oxadiazol-2-yl)thio)butanoate (0.05 g, 0.13 mmol) gave 4-((5-(2-chloro-4-ethoxyphenyl)-1,3,4-oxadiazol-2-yl)thio)butanoic acid as white solid (0.03 g, 70%); ^{1}H NMR (500 MHz, $CDCl_3$-*d*) δ ppm 10.18 (br. s, 1H) 7.86 (d, 8.8 Hz, 1H) 7.03 (d, J = 2.5 Hz, 1H) 6.89 (dd, J = 8.8, 2.5 Hz, 1H) 4.09 (q, J = 7.0 Hz, 2H) 3.37 (t, J = 7.1 Hz, 2H) 2.59 (t, J = 7.1 Hz, 2H) 2.21 (p, J = 7.1 Hz, 2H) 1.44 (t, J = 7.0 Hz, 3H); ^{13}C NMR (500 MHz, $CDCl_3$-*d*) δ ppm 177.97, 163.97, 161.63, 134.07, 131.92, 116.78, 114.90, 113.76, 64.19, 32.29, 31.59, 24.35, 14.54; TOF ES$^+$ MS: (M+H) 343.05; HPLC Ret: 6.78 min; 97% pure.

4-((5-(2-chloro-4-propoxyphenyl)-1,3,4-oxadiazol-2-yl)thio)butanoic acid (CCG-262688). Method F starting from tert-butyl 4-((5-(2-chloro-4-propoxyphenyl)-1,3,4-oxadiazol-2-yl)thio)butanoate (0.05 g, 0.12 mmol) gave 4-((5-(2-chloro-4-propoxyphenyl)-1,3,4-oxadiazol-2-yl)thio)butanoic acid as white solid (0.03 g, 70%); ^{1}H NMR (500 MHz, $CDCl_3$-*d*) δ ppm 10.50 (br. s, 1H) 7.86 (d, 8.8 Hz, 1H) 7.04 (d, J = 2.5 Hz, 1H) 6.90 (dd, J = 8.8, 2.5 Hz, 1H) 3.97 (t, J = 6.5 Hz, 2H) 3.37 (t, J = 7.1 Hz, 2H) 2.59 (t, J = 7.1 Hz, 2H) 2.21 (p, J = 7.2 Hz, 2H) 1.84 (p, J = 7.2 Hz, 2H) 1.05 (t, J = 7.4 Hz, 3H); ^{13}C NMR (500 MHz, $CDCl_3$-*d*) δ ppm 178.06, 164.26, 163.96, 161.83, 134.05, 131.91, 116.81, 114.83, 113.76, 70.10, 32.31, 31.59, 24.34, 22.33, 10.39; TOF ES$^+$ MS: (M+H) 357.07; HPLC Ret: 7.30 min; 99% pure.

4-((5-(4-butoxy-2-chlorophenyl)-1,3,4-oxadiazol-2-yl)thio)butanoic acid (CCG-262689). Method F starting from tert-butyl 4-((5-(4-butoxy-2-chlorophenyl)-1,3,4-oxadiazol-2-yl)thio)butanoate (0.05 g, 0.12 mmol) gave 4-((5-(4-butoxy-2-chlorophenyl)-1,3,4-oxadiazol-2-

yl)thio)butanoic acid as white solid (0.04 g, 81%); ^{1}H NMR (500 MHz, $CDCl_3$-*d*) δ ppm 10.34 (br. s, 1H) 7.85 (d, 8.8 Hz, 1H) 7.03 (d, J = 2.5 Hz, 1H) 6.90 (dd, J = 8.8, 2.5 Hz, 1H) 4.01 (t, J = 6.5 Hz, 2H) 3.37 (t, J = 7.1 Hz, 2H) 2.59 (t, J = 7.1 Hz, 2H) 2.21 (p, J = 7.1 Hz, 2H) 1.84-1.74 (m, 2H) 1.49 (t, J = 7.5 Hz, 2H) 0.99 (t, J = 7.4 Hz, 3H); ^{13}C NMR (500 MHz, $CDCl_3$-*d*) δ ppm 178.02, 164.26, 163.95, 161.84, 134.05, 131.90, 116.80, 114.82, 113.79, 68.34, 32.30, 31.59, 30.97, 24.34, 19.11, 13.76; TOF ES$^+$ MS: (M+H) 371.08; HPLC Ret: 7.76 min; 99% pure.

4-((5-(2-chloro-4-(cyclopropylmethoxy)phenyl)-1,3,4-oxadiazol-2-yl)thio)butanoic acid (CCG-262690). Method F starting from tert-butyl 4-((5-(2-chloro-4-(cyclopropylmethoxy)phenyl)-1,3,4-oxadiazol-2-yl)thio)butanoate (0.05 g, 0.12 mmol) gave 4-((5-(2-chloro-4-(cyclopropylmethoxy)phenyl)-1,3,4-oxadiazol-2-yl)thio)butanoic acid as white solid (0.03 g, 76%); column: 45% EtOAc: 55% Hex: 0.1% AcOH; ^{1}H NMR (500 MHz, $CDCl_3$-*d*) δ ppm 10.24 (br. s, 1H) 7.85 (d, 8.8 Hz, 1H) 7.04 (d, J = 2.4 Hz, 1H) 6.91 (dd, J = 8.9, 2.5 Hz, 1H) 3.86 (t, J = 7.0 Hz, 2H) 3.37 (t, J = 7.1 Hz, 2H) 2.58 (t, J = 7.1 Hz, 2H) 2.21 (p, J = 7.1 Hz, 2H) 1.33-1.22 (m, 1H) 0.73-0.63 (m, 2H) 0.43-0.32 (m, 2H); ^{13}C NMR (500 MHz, $CDCl_3$-*d*) δ ppm 177.98, 164.23, 164.02, 161.68, 134.07, 131.92, 116.88, 114.88, 113.86, 73.34, 32.31, 31.59, 24.34, 9.95, 3.28; TOF ES$^+$ MS: (M+H) 369.07; HPLC Ret: 7.14 min; 97% pure.

4-((5-(2-chloro-4-isopropoxyphenyl)-1,3,4-oxadiazol-2-yl)thio)butanoic acid (CCG-262691). Method F starting from tert-butyl 4-((5-(2-chloro-4-isopropoxyphenyl)-1,3,4-oxadiazol-2-yl)thio)butanoate (0.05 g, 0.11 mmol) gave 4-((5-(2-chloro-4-isopropoxyphenyl)-1,3,4-oxadiazol-2-yl)thio)butanoic acid as white oil (0.03 g, 82%); column: 45% EtOAc: 55% Hex: 0.1% AcOH; ^{1}H NMR (500 MHz, $CDCl_3$-*d*) δ ppm 9.77 (br. s, 1H) 7.85 (d, 8.8 Hz, 1H) 7.02 (d, J = 2.5 Hz, 1H) 6.88 (dd, J = 8.8, 2.5 Hz, 1H) 4.61 (p, J = 6.1 Hz, 1H) 3.37 (t, J = 7.1 Hz, 2H) 2.59 (t, J = 7.1 Hz, 2H) 2.21 (p, J = 7.1 Hz, 2H) 1.37 (d, J = 6.1 Hz, 6H); ^{13}C NMR (500 MHz, $CDCl_3$-*d*) δ ppm 178.00, 164.27, 163.92, 160.73, 134.08, 131.96, 117.80, 114.63, 114.53, 70.76, 32.31, 31.59, 24.35, 21.80; TOF ES$^+$ MS: (M+H) 357.07; HPLC Ret: 7.12 min; 99% pure.

4-((5-(2-chloro-4-propylphenyl)-1,3,4-oxadiazol-2-yl)thio)butanoic acid. (CCG-259001). Method F starting from t-butyl 4-((5-(2-chloro-4-propylphenyl)-1,3,4-oxadiazol-2-yl)thio)butanoate (0.03 g, 0.06 mmol) gave 4-((5-(2-chloro-4-propylphenyl)-1,3,4-oxadiazol-2-yl)thio)butanoic acid as white oil (0.01 g, 47%); product required 2% MeOH:98% DCM:0.01% AcOH silica gel column chromatography followed by semi-prep; ^{1}H NMR (500 MHz, $CDCl_3$-*d*) δ ppm 7.84 (d, J = 8.0, 1H) 7.35 (s, 1H) 7.20 (dd, J = 8.1, 1.6 Hz, 1H) 3.38 (t, J = 7.2 Hz, 2H) 2.64-2.57 (m, 4H) 2.22 (p, J = 7.2 Hz, 2H) 1.68 (h, J = 7.4 Hz, 2H) 0.96 (t, J = 7.5 Hz, 3H); ^{13}C NMR (500 MHz, $CDCl_3$-*d*) δ ppm 177.82, 164.39, 164.31, 148.13, 132.68, 131.10, 131.06, 130.72, 127.35, 120.08, 37.52, 32.27, 31.59, 24.35, 23.95, 13.65; TOF ES+ MS: (M+H) 341.1; HPLC Ret: 7.43 min; 97% pure.

4-((5-(4-butyl-2-chlorophenyl)-1,3,4-oxadiazol-2-yl)thio)butanoic acid. (CCG-259002). Method F starting from t-butyl 4-((5-(4-butyl-2-chlorophenyl)-1,3,4-oxadiazol-2-yl)thio)butanoate (0.05 g, 0.11 mmol) gave 4-((5-(4-butyl-2-chlorophenyl)-1,3,4-oxadiazol-2-yl)thio)butanoic acid as white solid (0.02 g, 52%); ^{1}H NMR (500 MHz, $CDCl_3$-*d*) δ ppm 7.84 (d, J = 8.0 Hz, 1H) 7.35 (d, J = 1.6 Hz, 1H) 7.20 (dd, J = 8.0, 1.6 Hz, 1H) 3.38 (t, J = 7.1 Hz, 2H) 2.65 (t, J = 7.3 Hz, 2H) 2.59 (t, J = 7.1 Hz, 2H) 2.23 (p, J = 7.1 Hz, 2H) 1.63 (p, J = 7.6 Hz, 2H) 1.37 (h, J = 7.4 Hz, 2H) 0.93 (t, J = 7.5 Hz, 3H); ^{13}C NMR (500 MHz, $CDCl_3$-*d*) δ ppm 178.06, 164.41, 164.30, 148.40, 132.67, 131.09, 131.04, 130.73, 127.30, 120.00, 35.22, 32.92, 32.32, 31.59, 24.34, 22.22, 13.84; TOF ES+ MS: (M+H) 355.1; HPLC Ret: 7.90 min; 95% pure.

4-((5-(2-chloro-4-isobutylphenyl)-1,3,4-oxadiazol-2-yl)thio)butanoic acid. (CCG-259003). Method F starting from t-butyl 4-((5-(2-chloro-4-isobutylphenyl)-1,3,4-oxadiazol-2-yl)thio)butanoate (0.03 g, 0.06 mmol) gave 4-((5-(2-chloro-4-isobutylphenyl)-1,3,4-oxadiazol-2-yl)thio)butanoic acid as colorless oil (0.02 g, 79%); product required 2% MeOH:98% DCM:0.01% AcOH silica gel column chromatography followed by semi-prep; ^{1}H NMR (500 MHz, $CDCl_3$-*d*) δ ppm 7.84 (dd, J = 8.1, 1.3 Hz, 1H) 7.32 (d, J = 1.5 Hz, 1H) 7.17 (dd, J = 8.1, 1.3 Hz,

1H) 3.38 (t, J = 7.1 Hz, 2H) 2.59 (t, J = 7.1 Hz, 2H) 2.52 (d, J = 7.2 Hz, 2H) 2.22 (p, J = 7.1 Hz, 2H) 1.91 (hept, J = 6.7 Hz, 1H) 0.93 (d, J = 6.6 Hz, 6H); ^{13}C NMR (500 MHz, $CDCl_3$-*d*) δ ppm 177.74, 164.41, 164.31, 147.21, 132.58, 131.64, 130.59, 127.94, 120.14, 44.87, 32.30, 31.60, 29.99, 24.38, 22.22; TOF ES+ MS: (M+H) 355.1; HPLC Ret: 7.79 min; 93% pure.

4-((5-(2-chloro-4-(prop-1-en-2-yl)phenyl)-1,3,4-oxadiazol-2-yl)thio)butanoic acid. **(CCG-259164).** Method F starting from t-butyl 4-((5-(2-chloro-4-(prop-1-en-2-yl)phenyl)-1,3,4-oxadiazol-2-yl)thio)butanoate (0.02 g, 0.06 mmol) gave 4-((5-(2-chloro-4-(prop-1-en-2-yl)phenyl)-1,3,4-oxadiazol-2-yl)thio)butanoic acid as white oil (0.006 g, 34%); product required 40% EtOAc:60% DCM:0.01% AcOH silica gel column chromatography followed by semi-prep; ^{1}H NMR (500 MHz, MeOH-d_4) δ ppm 7.92 (d, J = 8.2 Hz, 1H) 7.71 (d, J = 1.7 Hz, 1H) 7.61 (dd, J = 8.3, 1.8 Hz, 1H) 5.58 (d, J = 1.3 Hz, 1H) 5.29 (t, J = 1.5 Hz, 1H) 3.38 (t, J = 7.2 Hz, 2H) 2.51 (t, J = 7.2 Hz, 2H) 2.17 (m, 5H); ^{13}C NMR (500 MHz, MeOH-d_4) δ ppm 174.78, 165.21, 163.91, 145.82, 141.17, 132.50, 130.52, 127.70, 124.18, 120.87, 114.90, 47.06, 31.81, 31.34, 24.62, 20.05; TOF ES+ MS: (M+H) 339.1; HPLC Ret: 7.17 min; 96% pure.

4-((5-(4-isopropylphenyl)-1,3,4-oxadiazol-2-yl)thio)butanoic acid. (CCG-262458). Method F starting from t-butyl 4-((5-(2-chloro-4-isopropylphenyl)-1,3,4-oxadiazol-2-yl)thio)butanoate (0.03 g, 0.08 mmol) gave 4-((5-(4-isopropylphenyl)-1,3,4-oxadiazol-2-yl)thio)butanoic acid as white oil (0.008 g, 32%); product required semi-prep (bonus product); ^{1}H NMR (500 MHz, MeOH-d_4) δ ppm 7.86 (d, J = 8.1 Hz, 1H) 7.49 (d, J = 1.7 Hz, 1H) 7.38 (dd, J = 8.1, 1.7 Hz, 1H) 3.38 (t, J = 7.2 Hz, 2H) 2.99 (hept, J = 7.0 Hz, 1H) 2.51 (t, J = 7.2 Hz, 2H) 2.14 (p, J = 7.2 Hz, 2H) 1.29 (d, J = 6.9 Hz, 6H); ^{13}C NMR (500 MHz, MeOH-d_4) δ ppm 174.11, 165.07, 164.11, 154.83, 132.45, 130.74, 128.88, 125.45, 119.83, 33.80, 31.86, 31.34, 24.65, 22.39; TOF ES+ MS: (M+H) 341.1; HPLC Ret: 7.32 min; 99% pure.

4-((5-(2-chloro-4-isopropylphenyl)-1,3,4-oxadiazol-2-yl)thio)butanoic acid. (CCG-259165). Method F starting from t-butyl 4-((5-(2-chloro-4-isopropylphenyl)-1,3,4-oxadiazol-2-yl)thio)butanoate (0.03 g, 0.08 mmol) gave 4-((5-(2-chloro-4-isopropylphenyl)-1,3,4-oxadiazol-2-yl)thio)butanoic acid as white oil (0.009 g, 36%); product required semi-prep; ^{1}H NMR (500 MHz, MeOH-d_4) δ ppm 7.91 (d, J = 8.3 Hz, 2H) 7.42 (d, J = 8.3 Hz, 2H) 3.36 (t, J = 7.2 Hz, 2H) 2.98 (hept, J = 6.9 Hz, 1H) 2.51 (t, J = 7.2 Hz, 2H) 2.13 (q, J = 7.2 Hz, 2H) 1.28 (d, J = 6.9 Hz, 6H); ^{13}C NMR (500 MHz, MeOH-d_4) δ ppm 174.79, 165.97, 164.35, 153.44, 127.04, 126.41, 120.69, 34.07, 31.79, 31.30, 24.60, 22.64; TOF ES+ MS: (M+H) 307.1; HPLC Ret: 7.05 min; 99% pure.

4-((5-(2-chloro-4-ethylphenyl)-1,3,4-oxadiazol-2-yl)thio)butanoic acid. **(CCG-259166).** Method F starting from t-butyl 4-((2-chloro-4-ethylphenyl)-1,3,4-oxadiazol-2-yl)thio)butanoate (0.07 g, 0.18 mmol) gave 4-((5-(2-chloro-4-ethylphenyl)-1,3,4-oxadiazol-2-yl)thio)butanoic acid as white solid (0.05 g, 83%); product required 50% EtOAc 50% Hex 0.01% AcOH silica gel column chromatography; ^{1}H NMR (500 MHz, $CDCl_3$-d) δ ppm 9.52 (br. s, 1H) 7.85 (d, J = 8.0, 1H) 7.37 (d, J = 1.6 Hz, 1H) 7.22 (dd, J = 8.1, 1.6 Hz, 1H) 3.38 (t, J = 7.1 Hz, 2H) 2.70 (q, J = 7.6 Hz, 2H) 2.59 (t, J = 7.1 Hz, 2H) 2.23 (p, J = 7.2 Hz, 2H) 1.27 (t, J = 7.6 Hz, 3H); ^{13}C NMR (500 MHz, $CDCl_3$-d) δ ppm 178.04, 164.39, 164.29, 149.58, 132.76, 130.81, 130.54, 126.78, 120.06, 32.32, 31.60, 28.51, 24.34, 14.87,; TOF ES+ MS: (M+Na) 349.0; HPLC Ret: 6.96 min; 98% pure.

4-((5-(2-(trifluoromethyl)phenyl)-1,3,4-oxadiazol-2-yl)thio)butanoic acid. (CCG-262525). Method F starting from t-butyl 4-((2-(trifluoromethyl)phenyl)-1,3,4-oxadiazol-2-yl)thio)butanoate (0.13 g, 0.34 mmol) gave 4-((5-(2-(trifluoromethyl)phenyl)-1,3,4-oxadiazol-2-yl)thio)butanoic acid as colorless oil (0.1 g, 93%); product required 55% EtOAc 45% Hex 0.01% AcOH silica gel column chromatography; ^{1}H NMR (500 MHz, $CDCl_3$-d) δ ppm 10.45 (br. s, 1H) 8.07-8.00 (m, 1H) 7.85 (dd, J = 7.1, 2.0 Hz, 1H) 7.75-7.65 (m, 2H) 3.37 (t, J = 7.2 Hz, 2H) 2.59 (t, J = 7.1 Hz,

2H) 2.21 (p, J = 7.1 Hz, 2H); ^{13}C NMR (500 MHz, $CDCl_3$-*d*) δ ppm 178.29, 165.45, 164.05, 132.18, 131.65, 128.78, 127.06, 126.98, 124.19, 122.01, 32.28, 31.55, 24.34; TOF ES+ MS: (M+H) 333.1; HPLC Ret: 6.31 min; 97% pure.

4-((5-(2-fluorophenyl)-1,3,4-oxadiazol-2-yl)thio)butanoic acid. (CCG-262526). Method F starting from t-butyl 4-(2-fluorophenyl)-1,3,4-oxadiazol-2-yl)thio)butanoate (0.15 g, 0.44 mmol) gave 4-((5-(2-fluorophenyl)-1,3,4-oxadiazol-2-yl)thio)butanoic acid as white solid (0.11 g, 89%); ^{1}H NMR (500 MHz, $CDCl_3$-*d*) δ ppm 10.76 (br. s, 1H) 8.07-8.00 (td, J = 7.5, 1.7 Hz, 1H) 7.53 (dd, J = 7.6, 1.7 Hz, 1H) 7.31-7.20 (m, 2H) 3.39 (t, J = 7.1 Hz, 2H) 2.59 (t, J = 7.1 Hz, 2H) 2.21 (p, J = 7.1 Hz, 2H); ^{13}C NMR (500 MHz, $CDCl_3$-*d*) δ ppm 178.02, 164.64, 162.49, 158.77, 133.48, 129.47, 124.64, 116.64, 111.93, 32.32, 31.59, 24.30; TOF ES+ MS: (M+H) 283.1; HPLC Ret: 5.75 min; 97% pure.

4-((5-(2,4-dichlorophenyl)-1,3,4-oxadiazol-2-yl)thio)butanoic acid (CCG-232120). Method G starting from methyl 4-((5-(2,4-dichlorophenyl)-1,3,4-oxadiazol-2-yl)thio)butanoate (0.19 g, 0.54 mmol) gave 4-((5-(2,4-dichlorophenyl)-1,3,4-oxadiazol-2-yl)thio)butanoic acid as white solid (0.06 g, 35%); ^{1}H NMR (401 MHz, DMSO-d_6) δ ppm 12.21 (br. s., 1H) 8.00 (d, J = 8.6 Hz, 1H) 7.93 (d, J = 2.1 Hz, 1H) 7.66 (dd, J = 8.6, 2.1 Hz, 1H) 3.34 (t, J = 7.3 Hz, 2H) 2.40 (t, J = 7.3 Hz, 2H) 2.11-1.95 (m, 2H); ^{13}C NMR (401 MHz, DMSO-d_6) δ ppm 174.15, 164.95, 162.95, 137.54, 133.14, 132.75, 131.19, 128.64, 121.70, 32.62, 31.96, 24.96; TOF ES+ MS: (M+H) 332.9; HPLC Ret: 6.82 min; 98% pure.

4-((5-(2-chloro-4-methylphenyl)-1,3,4-oxadiazol-2-yl)thio)butanoic acid (CCG-232922). Method G starting from methyl 4-((5-(2-chloro-4-methylphenyl)-1,3,4-oxadiazol-2-yl)thio)butanoate (0.15 g, 0.46 mmol) gave 4-((5-(2-chloro-4-methylphenyl)-1,3,4-oxadiazol-2-yl)thio)butanoic acid as white solid (0.1 g, 69%); ^{1}H NMR (500 MHz, $CDCl_3$-*d*) δ ppm 8.67 (br. s., 1H) 7.82 (d, J = 8.0 Hz, 1H) 7.35 (s, 1H) 7.19 (d, J = 7.9 Hz, 1H) 3.38 (t, J = 7.1 Hz, 2H) 2.59

(t, J = 7.1 Hz, 2H) 2.40 (s, 3H) 2.21 (q, J = 7.1 Hz, 2H); ^{13}C NMR (500 MHz, $CDCl_3$-*d*) δ ppm 178.02, 164.39, 164.28, 143.42, 132.64, 131.68, 130.67, 127.96, 119.89, 32.31, 31.60, 24.34, 21.24; TOF ES+ MS: (M+H) 313.4; HPLC Ret: 6.53 min; 99% pure.

4-((5-(p-tolyl)-1,3,4-oxadiazol-2-yl)thio)butanoic acid (CCG-232924). Method G starting from methyl 4-((5-(p-tolyl)-1,3,4-oxadiazol-2-yl)thio)butanoate (0.13 g, 0.43 mmol) gave 4-((5-(p-tolyl)-1,3,4-oxadiazol-2-yl)thio)butanoic acid as white solid (0.1 g, 97%); ^{1}H NMR (500 MHz, $CDCl_3$-*d*) δ ppm 7.89 (dd, J = 8.2, 1.5 Hz, 2H) 7.29 (dd, J = 7.8, 1.5 Hz, 2H) 3.38 (t, J = 7.2 Hz, 2H) 2.59 (t, J = 7.2 Hz, 2H) 2.42 (s, 3H) 2.21 (p, J = 7.1 Hz, 2H); ^{13}C NMR (500 MHz, $CDCl_3$-*d*) δ ppm 177.89, 166.00, 163.65, 142.29, 129.74, 126.65, 120.69, 32.30, 31.57, 24.30, 21.63,; TOF ES+ MS: (M+H) 279.4; HPLC Ret: 6.23 min; 99% pure.

4-((5-(4-chlorophenyl)-1,3,4-oxadiazol-2-yl)thio)butanoic acid (CCG-232943). Method G starting from methyl 4-((5-(4-chlorophenyl)-1,3,4-oxadiazol-2-yl)thio)butanoate (0.29 g, 0.93 mmol) gave 4-((5-(4-chlorophenyl)-1,3,4-oxadiazol-2-yl)thio)butanoic acid as white solid (0.18 g, 63%); ^{1}H NMR (500 MHz, $CDCl_3$-*d*) δ ppm 10.67 (br. s., 1H) 7.94 (d, J = 10 Hz, 2H) 7.48 (d, J = 10 Hz, 2H) 3.39 (t, J = 7.2 Hz, 2H) 2.59 (t, J = 7.2 Hz, 2H) 2.22 (p, J = 7.1 Hz, 2H); ^{13}C NMR (500 MHz, $CDCl_3$-*d*) δ ppm 178.05, 165.01, 164.32, 137.98, 129.45, 127.94, 121.95, 32.27, 31.58, 24.24; TOF ES+ MS: (M+H) 299.0; HPLC Ret: 6.46 min; 99% pure.

6-((5-(2,4-dichlorophenyl)-1,3,4-oxadiazol-2-yl)thio)hexanoic acid (CCG-232923). Method G starting from ethyl 6-((5-(2,4-dichlorophenyl)-1,3,4-oxadiazol-2-yl)thio)hexanoate (0.15 g, 0.39 mmol) gave 6-((5-(2,4-dichlorophenyl)-1,3,4-oxadiazol-2-yl)thio)hexanoic acid as white solid (0.08 g, 55%); reaction needed 6 hours to complete; ^{1}H NMR (500 MHz, $CDCl_3$-*d*) δ ppm 10.73 (br. s., 1H) 7.91(d, J = 8.5 Hz, 1H) 7.57 (d, J = 2.1 Hz, 1H) 7.39 (dd, J = 8.5, 2.1 Hz, 1H) 3.31 (t, J = 7.3 Hz, 2H) 2.39 (t, J = 7.3 Hz, 2H) 1.90 (p, J = 7.5 Hz, 2H) 1.70 (q, J = 7.6 Hz, 2H) 1.59-1.49 (m, 2H); ^{13}C NMR (500 MHz, $CDCl_3$-*d*) δ ppm 179.55, 165.47, 163.23, 137.97, 133.70,

131.57, 131.15, 127.59, 121.45, 33.84, 32.49, 29.08, 28.41, 28.20, 24.42; TOF ES+ MS: (M+H) 376.0; HPLC Ret: 7.71 min; 98% pure.

7-((5-(2,4-dichlorophenyl)-1,3,4-oxadiazol-2-yl)thio)heptanoic acid (CCG-232962). Method G starting from methyl 7-((5-(2,4-dichlorophenyl)-1,3,4-oxadiazol-2-yl)thio)heptanoate (0.27 g, 0.69 mmol) gave 7-((5-(2,4-dichlorophenyl)-1,3,4-oxadiazol-2-yl)thio)heptanoic acid as white solid (0.17 g, 65%); ^{1}H NMR (500 MHz, $CDCl_3$-*d*) δ ppm 7.91 (d, J = 8.5, 1H) 7.58-7.54 (m, 1H) 7.39 (dd, J = 8.5, 1.4 Hz, 1H) 3.30 (t, J = 7.3 Hz, 2H) 2.37 (t, J = 7.4 Hz, 2H) 1.87 (p, J = 7.4 Hz, 2H) 1.67 (q, J = 7.6 Hz, 2H) 1.50 (p, J = 7.4 Hz, 2H) 1.42 (q, J = 8.0 Hz, 2H); ^{13}C NMR (500 MHz, $CDCl_3$-*d*) δ ppm 179.55, 165.47, 163.23, 137.97, 133.70, 131.57, 131.15, 127.59, 121.45, 33.84, 32.49, 29.08, 28.41, 28.20, 24.42; TOF ES+ MS: (M+Na) 411.0; HPLC Ret: 8.85 min; 99% pure.

8-((5-(2,4-dichlorophenyl)-1,3,4-oxadiazol-2-yl)thio)octanoic acid (CCG-232963). Method G starting from ethyl 8-((5-(2,4-dichlorophenyl)-1,3,4-oxadiazol-2-yl)thio)octanoate (0.33 g, 0.79 mmol) gave 8-((5-(2,4-dichlorophenyl)-1,3,4-oxadiazol-2-yl)thio)octanoic acid as white solid (0.19 g, 63%); reaction needed 24 hours to complete; ^{1}H NMR (500 MHz, $CDCl_3$-*d*) δ ppm 7.91 (d, J = 8.5, 1H) 7.56 (s, 1H) 7.39 (dd, J = 8.5, 2.0 Hz, 1H) 3.30 (t, J = 7.4 Hz, 2H) 2.36 (t, J = 7.4 Hz, 2H) 1.86 (p, J= 7.4 Hz, 2H) 1.65 (p, J= 7.5 Hz, 2H) 1.49 (q, J= 7.5 Hz, 2H) 1.43-1.34 (m, 4H); ^{13}C NMR (500 MHz, $CDCl_3$-*d*) δ ppm 179.49, 165.53, 163.22, 137.96, 133.70, 131.56, 131.15, 127.58, 121.48, 33.89, 32.56, 29.20, 28.80, 28.62, 28.35, 24.52; TOF ES+ MS: (M+H) 389.0; HPLC Ret: 7.98 min; 99% pure.

4-((5-(2-chloro-4-cyclopropylphenyl)-1,3,4-oxadiazol-2-yl)thio)butanoic acid (CCG-232964). Method G starting from methyl 4-((5-(2-chloro-4-cyclopropylphenyl)-1,3,4-oxadiazol-2-yl)thio)butanoate (0.07 g, 0.21 mmol) gave 4-((5-(2-chloro-4-cyclopropylphenyl)-1,3,4-oxadiazol-2-yl)thio)butanoic acid as white oil (0.07 g, 92%); column: 5% MeOH: 95% DCM: 0.01% AcOH;

^{1}H NMR (500 MHz, $CDCl_3$-*d*) δ ppm 8.11 (br. s., 1H) 7.81 (d, J = 8.2 Hz, 1H) 7.19 (s, 1H) 7.05 (dd, J = 8.2, 1.7 Hz, 1H) 2.58 (t, J = 7.1 Hz, 2H) 2.37 (t, J = 7.2 Hz, 2H) 2.20 (p, J = 7.2 Hz, 2H) 1.96-1.91 (tt, J = 8.4, 5.0 Hz, 1H) 1.08 (dt, J = 6.9, 4.9 Hz, 2H) 0.78 (dt, J = 6.9, 4.9 Hz, 2H); ^{13}C NMR (500 MHz, $CDCl_3$-*d*) δ ppm 177.84, 164.36, 164.26, 150.10, 132.77, 130.66, 128.12, 124.27, 119.43, 32.36, 31.61, 24.37, 15.40, 10.41; TOF ES+ MS: (M+H) 339.0; HPLC Ret: 6.93 min; 97% pure.

4-((5-(2-chloro-4-(trifluoromethyl)phenyl)-1,3,4-oxadiazol-2-yl)thio)butanoic acid (CCG-257390). Method G starting from methyl 4-((5-(2-chloro-4-(trifluoromethyl)phenyl)-1,3,4-oxadiazol-2-yl)thio)butanoate (0.16 g, 0.42 mmol) gave 4-((5-(2-chloro-4-(trifluoromethyl)phenyl)-1,3,4-oxadiazol-2-yl)thio)butanoic acid as white solid (0.12 g, 81%); ^{1}H NMR (500 MHz, $CDCl_3$-*d*) δ ppm 8.12 (d, J = 8.2 Hz, 1H) 7.82 (d, J = 1.6 Hz, 1H) 7.66 (dd, J = 8.3, 1.8 Hz, 1H) 3.41 (t, J = 7.2 Hz, 2H) 2.60 (t, J = 7.1 Hz, 2H) 2.24 (p, J = 7.1 Hz, 2H); ^{19}F NMR (500 MHz, $CDCl_3$-*d*) δ ppm 63.24; ^{13}C NMR (500 MHz, $CDCl_3$-*d*) δ ppm 177.45, 165.54, 163.05, 133.60, 131.35, 128.38, 125.99, 123.94, 123.91, 32.16, 31.62, 24.28; TOF ES+ MS: (M+H) 367.0; HPLC Ret: 6.99 min; 97% pure.

4-((5-(3-chloro-[1, 1'-biphenyl]-4-yl)-1, 3, 4-oxadiazol-2-yl)thio)butanoic acid (CCG-257423). Method G starting from methyl 4-((5-(3-chloro-[1, 1'-biphenyl]-4-yl)-1, 3, 4-oxadiazol-2-yl)thio)butanoate (0.36 g, 3.9 mmol) gave 4-((5-(3-chloro-[1, 1'-biphenyl]-4-yl)-1, 3, 4-oxadiazol-2-yl)thio)butanoic acid as white solid (0.28 g, 82%); ^{1}H NMR (500 MHz, $CDCl_3$-*d*) δ ppm 8.03 (d, J = 8.1 Hz, 1H) 7.77 (d, J = 1.8 Hz, 1H) 7.63-7.60 (m, 3H) 7.52-7.39 (m, 3H) 3.40 (t, J = 7.2 Hz, 2H) 2.60 (t, J = 7.1 Hz, 2H) 2.24 (p, J = 7.1 Hz, 2H); ^{13}C NMR (500 MHz, $CDCl_3$-*d*) δ ppm 177.29, 164.63, 164.11, 145.45, 138.32, 133.28, 131.16, 129.64, 129.10, 128.75, 127.11, 125.64, 121.23, 32.16, 31.63, 24.37; TOF ES+ MS: (M+H) 375.0; HPLC Ret: 7.43 min; 98% pure.

4-((5-(2-chloro-4,5-dimethylphenyl)-1,3,4-oxadiazol-2-yl)thio)butanoic acid. **(CCG-258042).** Method G starting from methyl 4-((5-(2-chloro-4,5-dimethylphenyl)-1,3,4-oxadiazol-2-yl)thio)butanoate (0.11 g, 0.33 mmol) gave 4-((5-(2-chloro-4,5-dimethylphenyl)-1,3,4-oxadiazol-2-yl)thio)butanoic acid as white solid (0.08 g, 71%); ^{1}H NMR (500 MHz, $CDCl_3$-*d*) δ ppm 10.83 (br. s., 1H) 7.71 (s, 1H) 7.29 (s, 1H) 3.38 (t, J = 7.1 Hz, 2H) 3.32 (s, 3H) 2.59 (t, J = 7.1 Hz, 2H) 2.28 (s, 3H) 2.22 (p, J = 7.2 Hz, 2H); ^{13}C NMR (500 MHz, $CDCl_3$-*d*) δ ppm 177.93, 164.41, 164.24, 142.14, 135.96, 131.93, 131.52, 129.74, 119.82, 32.27, 31.60, 24.34, 19.69,19.05; QTOF ES- MS: (M-H) 325.0; HPLC Ret: 5.93 min; 95% pure.

4-((5-(2-chloro-3,4-dimethylphenyl)-1,3,4-oxadiazol-2-yl)thio)butanoic acid. (CCG-258044). Method G starting from methyl 4-((5-(2-chloro-3,4-dimethylphenyl)-1,3,4-oxadiazol-2-yl)thio)butanoate (0.15 g, 0.45 mmol) gave 4-((5-(2-chloro-3,4-dimethylphenyl)-1,3,4-oxadiazol-2-yl)thio)butanoic acid as white solid (0.11 g, 73%); ^{1}H NMR (500 MHz, $CDCl_3$-*d*) δ ppm 10.91 (br. s., 1H) 7.60 (d, J = 7.9 Hz, 1H) 7.17 (d, J = 7.9 Hz, 1H) 3.37 (t, J = 7.2 Hz, 2H) 3.42 (s, 3H) 2.59 (t, J = 7.1 Hz, 2H) 2.38 (s, 3H) 2.23 (p, J = 7.1 Hz, 2H); ^{13}C NMR (500 MHz, $CDCl_3$-*d*) δ ppm 178.00, 164.88, 164.32, 142.18, 136.63, 133.13, 128.30, 128.13, 121.05, 32.30, 31.58, 24.34, 21.36, 16.72; QTOF ES+ MS: (M-H) 325.0; HPLC Ret: 5.89 min; 99% pure.

4-((5-(2-chloro-4-cyclopropoxyphenyl)-1,3,4-oxadiazol-2-yl)thio)butanoic acid (CCG-262762). Method G starting from methyl 4-((5-(2-chloro-4-cyclopropoxyphenyl)-1,3,4-oxadiazol-2-yl)thio)butanoate (0.1 g, 0.27 mmol) gave 4-((5-(2-chloro-4-cyclopropoxyphenyl)-1,3,4-oxadiazol-2-yl)thio)butanoic acid as white solid (0.07 g, 75%); ^{1}H NMR (500 MHz, $CDCl_3$-*d*) δ ppm 11.07 (br. s, 1H) 7.86 (d, J = 8.8 Hz, 1H) 7.22 (d, J = 2.4 Hz, 1H) 7.04 (dd, J = 8.8, 2.5 Hz, 1H) 3.80 (tt, J = 6.2, 3.0 Hz, 1H) 3.37 (t, J = 7.1 Hz, 2H) 2.59 (t, J = 7.1 Hz, 2H) 2.21 (p, J = 7.1 Hz, 2H) 0.92-0.77 (m, 4H); ^{13}C NMR (500 MHz, $CDCl_3$-*d*) δ ppm 177.72, 164.22, 164.01, 133.99, 131.86, 131.78, 117.37, 115.47, 114.41, 51.62, 32.22, 31.60, 24.35, 6.28; TOF ES+ MS: (M+H) 369.07; HPLC Ret: 6.90 min; 98% pure.

4-((5-(2-chloro-4-methoxyphenyl)-1,3,4-oxadiazol-2-yl)thio)butanoic acid. CCG-262827. Method G starting from methyl 4-((5-(2-chloro-4-methoxyphenyl)-1,3,4-oxadiazol-2-yl)thio)butanoate (0.1 g, 0.29 mmol) gave 4-((5-(2-chloro-4-methoxyphenyl)-1,3,4-oxadiazol-2-yl)thio)butanoic acid as white solid (0.09 g, 94%); ^{1}H NMR (500 MHz, $CDCl_3$-*d*) δ ppm 10.78 (br. s, 1H) 7.87 (d, J = 8.8 Hz, 1H) 7.04 (d, J = 2.5 Hz, 1H) 6.91 (dd, J = 8.8, 2.5 Hz, 1H) 3.87 (s, 3H) 3.37 (t, J = 7.2 Hz, 2H) 2.59 (t, J = 7.1 Hz, 2H) 2.21 (p, J = 7.1 Hz, 2H); ^{13}C NMR (500 MHz, $CDCl_3$-*d*) δ ppm 178.05, 164.18, 164.03, 162.21, 134.12, 131.96, 116.34, 115.12, 113.38, 55.76, 32.32, 31.60, 24.34; TOF ES^{+} MS: (M+H) 329.0; HPLC Ret: 6.27 min; 99% pure.

4-((5-(4-(trifluoromethyl)phenyl)-1,3,4-oxadiazol-2-yl)thio)butanoic acid (CCG-263094). Method G starting from methyl 4-((5-(4-(trifluoromethyl)phenyl)-1,3,4-oxadiazol-2-yl)thio)butanoate (0.09 g, 0.27 mmol) gave 4-((5-(4-(trifluoromethyl)phenyl)-1,3,4-oxadiazol-2-yl)thio)butanoic acid as white solid (0.06 g, 68%); ^{1}H NMR (500 MHz, $CDCl_3$-*d*) δ ppm 10.41 (br. s., 1H) 8.14 (d, J = 8.2 Hz, 2H) 7.77 (d, J = 8.2 Hz, 2H) 3.41 (t, J = 7.2 Hz, 2H) 2.60 (t, J = 7.1 Hz, 2H) 2.22 (p, J = 7.1 Hz, 2H); ^{19}F NMR (500 MHz, $CDCl_3$-*d*) δ ppm -63.16 (s, 3H); ^{13}C NMR (500 MHz, $CDCl_3$-*d*) δ ppm 177.97, 165.00, 164.64, 133.41, 126.97, 126.13, 124.59, 121.90, 32.22, 31.57, 24.22; TOF ES+ MS: (M+H) 333.04; HPLC Ret: 6.76 min; 99% pure.

4-((5-(2-chloro-4-(2,2,2-trifluoroethoxy)phenyl)-1,3,4-oxadiazol-2-yl)thio)butanoic acid (CCG-263095). Method G starting from methyl 4-((5-(2-chloro-4-(2,2,2-trifluoroethoxy)phenyl)-1,3,4-oxadiazol-2-yl)thio)butanoate (0.08 g, 0.19 mmol) gave 4-((5-(2-chloro-4-(2,2,2-trifluoroethoxy)phenyl)-1,3,4-oxadiazol-2-yl)thio)butanoic acid as white solid (0.06 g, 77%); ^{1}H NMR (500 MHz, $CDCl_3$-*d*) δ ppm 10.85 (br. s., 1H) 7.93 (d, J = 8.8 Hz, 1H) 7.12 (d, J = 2.5 Hz, 1H) 6.98 (dd, J = 8.9, 2.6 Hz, 1H) 4.42 (q, J = 7.9 Hz, 2H) 3.38 (t, J = 7.1 Hz, 2H) 2.59 (t, J = 7.1 Hz, 2H) 2.22 (p, J = 7.1 Hz, 2H); ^{19}F NMR (500 MHz, $CDCl_3$-*d*) δ ppm -73.76 (t, 3H); ^{13}C NMR (500 MHz, $CDCl_3$-*d*) δ ppm 177.80, 164.41, 163.71, 159.47, 134.41, 132.23, 123.89, 117.40,

117.14, 113.78, 65.58, 32.22, 31.59, 24.30; TOF ES+ MS: (M+H) 397.01; HPLC Ret: 6.88 min; 97% pure.

4-((5-(2-chloro-4-(oxetan-3-yloxy)phenyl)-1,3,4-oxadiazol-2-yl)thio)butanoic acid (CCG-263096). Method G starting from methyl 4-((5-(2-chloro-4-(oxetan-3-yloxy)phenyl)-1,3,4-oxadiazol-2-yl)thio)butanoate (0.07 g, 0.18 mmol) gave 4-((5-(2-chloro-4-(oxetan-3-yloxy)phenyl)-1,3,4-oxadiazol-2-yl)thio)butanoic acid as white solid (0.05 g, 79%); ^{1}H NMR (500 MHz, $CDCl_3$-*d*) δ ppm 7.88 (d, 8.8 Hz, 1H) 6.85 (d, J = 2.5 Hz, 1H) 6.73 (dd, J = 8.8, 2.5 Hz, 1H) 5.27 (p, 6.0 Hz, 1H) 5.02 (t, J = 7.1 Hz, 2H) 4.78 (dd, J = 7.3, 5.1 Hz, 2H) 3.37 (t, J = 7.1 Hz, 2H) 2.58 (t, J = 7.1 Hz, 2H) 2.21 (p, J = 7.1 Hz, 2H); ^{13}C NMR (500 MHz, $CDCl_3$-*d*) δ ppm 177.64, 164.26, 163.89, 159.11, 134.38, 132.27, 117.00, 116.16, 113.67, 77.44, 70.69, 32.25, 31.60, 24.33; TOF ES+ MS: (M+H) 371.03; HPLC Ret: 5.85 min; 98% pure.

4-((5-(2-chloro-4-(trifluoromethoxy)phenyl)-1,3,4-oxadiazol-2-yl)thio)butanoic acid (CCG-263097). Method G starting from methyl 4-((5-(2-chloro-4-(trifluoromethoxy)phenyl)-1,3,4-oxadiazol-2-yl)thio)butanoate (0.03 g, 0.08 mmol) gave 4-((5-(2-chloro-4-(trifluoromethoxy)phenyl)-1,3,4-oxadiazol-2-yl)thio)butanoic acid as white solid (0.01 g, 33%); ^{1}H NMR (500 MHz, $CDCl_3$-*d*) δ ppm 8.02 (d, J = 8.8 Hz, 1H) 7.42 (d, J = 2.3 Hz, 1H) 7.27 (dd, J = 8.8, 2.3 Hz, 1H) 3.39 (t, J = 7.1 Hz, 2H) 2.60 (t, J = 7.1 Hz, 2H) 2.24 (p, J = 7.1 Hz, 2H); ^{19}F NMR (500 MHz, $CDCl_3$-*d*) δ ppm -57.88 (s, 3H); ^{13}C NMR (500 MHz, $CDCl_3$-*d*) δ ppm 177.82, 165.06, 163.15, 151.14, 134.28, 132.15, 123.89, 123.27, 121.36, 119.17, 32.21, 31.60, 24.27; TOF ES+ MS: (M+H) 382.99; HPLC Ret: 7.14 min; 98% pure.

4-((5-(2-chloro-4-(oxetan-3-ylmethoxy)phenyl)-1,3,4-oxadiazol-2-yl)thio)butanoic acid (CCG-263098). Method G starting from methyl 4-((5-(2-chloro-4-(oxetan-3-ylmethoxy)phenyl)-1,3,4-oxadiazol-2-yl)thio)butanoate (0.07 g, 0.19 mmol) gave 4-((5-(2-chloro-4-(oxetan-3-ylmethoxy)phenyl)-1,3,4-oxadiazol-2-yl)thio)butanoic acid as white solid (0.06 g, 81%); ^{1}H NMR

(500 MHz, $CDCl_3$-*d*) δ ppm 7.89 (d, 8.8 Hz, 1H) 7.08 (d, J = 2.5 Hz, 1H) 6.94 (dd, J = 8.8, 2.5 Hz, 1H) 4.91 (p, 6.0 Hz, 1H) 4.59 (t, J = 6.1 Hz, 2H) 4.26 (d, J = 6.6 Hz, 2H) 3.47 (hept., J = 6.6 Hz, 1H) 3.37 (t, J = 7.1 Hz, 2H) 2.58 (t, J = 7.1 Hz, 2H) 2.21 (p, J = 7.1 Hz, 2H); ^{13}C NMR (500 MHz, $CDCl_3$-*d*) δ ppm 177.35, 164.11, 164.07, 161.27, 134.18, 132.02, 116.88, 115.56, 113.70, 73.99, 69.44, 34.28, 32.23, 31.62, 24.37; TOF ES+ MS: (M+H) 385.05; HPLC Ret: 5.83 min; 94% pure.

4-((5-(2-chloro-4-((3-methyloxetan-3-yl)methoxy)phenyl)-1,3,4-oxadiazol-2-yl)thio)butanoic acid (CCG-263099). Method G starting from methyl 4-((5-(2-chloro-4-((3-methyloxetan-3-yl)methoxy)phenyl)-1,3,4-oxadiazol-2-yl)thio)butanoate (0.08 g, 0.2 mmol) gave 4-((5-(2-chloro-4-((3-methyloxetan-3-yl)methoxy)phenyl)-1,3,4-oxadiazol-2-yl)thio)butanoic acid as white solid (0.06 g, 74%); ^{1}H NMR (500 MHz, $CDCl_3$-*d*) δ ppm 7.89 (d, 8.8 Hz, 1H) 7.10 (d, J = 2.5 Hz, 1H) 6.96 (dd, J = 8.8, 2.5 Hz, 1H) 4.63 (d, J = 6.1 Hz, 2H) 4.50 (d, J = 6.0 Hz, 2H) 4.10 (s, 2H) 3.38 (t, J = 7.1 Hz, 2H) 2.59 (t, J = 7.1 Hz, 2H) 2.21 (p, J = 7.1 Hz, 2H) 1.46 (s, 3H); ^{13}C NMR (500 MHz, $CDCl_3$-*d*) δ ppm 177.32, 164.09, 161.50, 134.17, 132.01, 116.94, 115.54, 113.72, 79.54, 73.17, 39.54, 32.22, 31.61, 24.36, 21.12; TOF ES+ MS: (M+H) 399.06; HPLC Ret: 6.24 min; 98% pure.

4-((5-(4-(2,2,2-trifluoroethoxy)phenyl)-1,3,4-oxadiazol-2-yl)thio)butanoic acid (CCG-263100). Method G starting from methyl 4-((5-(4-(2,2,2-trifluoroethoxy)phenyl)-1,3,4-oxadiazol-2-yl)thio)butanoate (0.08 g, 0.22 mmol) gave 4-((5-(4-(2,2,2-trifluoroethoxy)phenyl)-1,3,4-oxadiazol-2-yl)thio)butanoic acid as white solid (0.07 g, 87%); ^{1}H NMR (500 MHz, DMSO-d_6) δ ppm 12.20 (br. s., 1H) 7.96 (d, J = 8.0 Hz, 2H) 7.27 (d, J = 8.0 Hz, 2H) 4.90 (q, J = 7.9 Hz, 2H) 3.32 (t, J = 7.2 Hz, 2H) 2.40 (t, J = 7.3 Hz, 2H) 2.00 (p, J = 7.2 Hz, 2H); ^{19}F NMR (500 MHz, DMSO-d_6) δ ppm -72.55 (t, 3H); ^{13}C NMR (500 MHz, DMSO-d_6) δ ppm 174.15, 165.20, 135.31, 130.88, 128.77, 117.45, 116.15, 113.69, 64.91, 32.61, 31.95, 24.99; TOF ES+ MS: (M+H) 363.06; HPLC Ret: 6.59 min; 99% pure.

4-((5-(4-(difluoromethyl)phenyl)-1,3,4-oxadiazol-2-yl)thio)butanoic acid (CCG-263101). Method G starting from methyl 4-((5-(4-(difluoromethyl)phenyl)-1,3,4-oxadiazol-2-yl)thio)butanoate (0.09 g, 0.27 mmol) gave 4-((5-(4-(difluoromethyl)phenyl)-1,3,4-oxadiazol-2-yl)thio)butanoic acid as white solid (0.07 g, 77%); ^{1}H NMR (500 MHz, $CDCl_3$-*d*) δ ppm 11.13 (br. s., 1H) 8.10 (d, J = 8.0 Hz, 2H) 7.65 (d, J = 8.0 Hz, 2H) 6.70 (t, J = 56.1 Hz, 1H) 3.40 (t, J = 7.1 Hz, 2H) 2.60 (t, J = 7.1 Hz, 2H) 2.23 (p, J = 7.1 Hz, 2H); ^{19}F NMR (500 MHz, $CDCl_3$-*d*) δ ppm -112.20 (d, 2H); ^{13}C NMR (500 MHz, $CDCl_3$-*d*) δ ppm 178.10, 164.99, 164.69, 137.31, 126.97, 126.35, 125.64, 113.86, 111.95, 32.27, 31.57, 24.23; TOF ES+ MS: (M+H) 315.06; HPLC Ret: 6.20 min; 99% pure.

4-((5-(4-(trifluoromethoxy)phenyl)-1,3,4-oxadiazol-2-yl)thio)butanoic acid (CCG-263103). Method G starting from methyl 4-((5-(4-(trifluoromethoxy)phenyl)-1,3,4-oxadiazol-2-yl)thio)butanoate (0.09 g, 0.27 mmol) gave 4-((5-(4-(trifluoromethoxy)phenyl)-1,3,4-oxadiazol-2-yl)thio)butanoic acid as white solid (0.05 g, 58%); ^{1}H NMR (500 MHz, $CDCl_3$-*d*) δ ppm 10.88 (br. s., 1H) 8.06 (d, J = 8.6 Hz, 2H) 7.34 (d, J = 8.4 Hz, 2H) 3.39 (t, J = 7.2 Hz, 2H) 2.60 (t, J = 7.1 Hz, 2H) 2.22 (p, J = 7.1 Hz, 2H); ^{19}F NMR (500 MHz, $CDCl_3$-*d*) δ ppm -57.72 (s, 3H); ^{13}C NMR (500 MHz, $CDCl_3$-*d*) δ ppm 178.08, 164.72, 164.47, 151.51, 128.47, 122.01, 121.23, 119.25, 32.26, 31.57, 24.23; TOF ES+ MS: (M+H) 349.05; HPLC Ret: 6.86 min; 98% pure.

4-((5-(2-chloro-3-(trifluoromethyl)phenyl)-1,3,4-oxadiazol-2-yl)thio)butanoic acid (CCG-263104). Method G starting from methyl 4-((5-(2-chloro-3-(trifluoromethyl)phenyl)-1,3,4-oxadiazol-2-yl)thio)butanoate (0.09 g, 0.23 mmol) gave 4-((5-(2-chloro-3-(trifluoromethyl)phenyl)-1,3,4-oxadiazol-2-yl)thio)butanoic acid as white solid (0.05 g, 60%); ^{1}H NMR (500 MHz, $CDCl_3$-*d*) δ ppm 10.88 (br. s., 1H) 8.10 (dd, J = 7.9, 1.6 Hz, 1H) 7.89 (dd, J = 7.9, 1.6 Hz, 1H) 7.54 (t, J = 7.9 Hz, 1H) 3.41 (t, J = 7.2 Hz, 2H) 2.60 (t, J = 7.1 Hz, 2H) 2.24 (p, J = 7.2 Hz, 2H); ^{19}F NMR (500 MHz, $CDCl_3$-*d*) δ ppm -62.59 (s, 3H); ^{13}C NMR (500 MHz, $CDCl_3$-

d) δ ppm 178.11, 165.46, 163.33, 134.44, 130.31, 130.27, 127.03, 125.65, 123.52, 121.34, 32.26, 31.61, 24.24; TOF ES+ MS: (M+H) 367.01; HPLC Ret: 6.81 min; 98% pure.

4-((5-(2-chloro-4-(2-fluoropropan-2-yl)phenyl)-1,3,4-oxadiazol-2-yl)thio)butanoic acid (CCG-263105). Method G starting from methyl 4-((5-(2-chloro-4-(2-fluoropropan-2-yl)phenyl)-1,3,4-oxadiazol-2-yl)thio)butanoate (0.09 g, 0.24 mmol) gave 4-((5-(2-chloro-4-(2-fluoropropan-2-yl)phenyl)-1,3,4-oxadiazol-2-yl)thio)butanoic acid as colorless oil (0.06 g, 76%); column: 30% EtOAc: 70% Hex to 60% EtOAc: 40% Hex: 0.1% AcOH; ^{1}H NMR (500 MHz, $CDCl_3$-*d*) δ ppm 9.58 (br. s, 1H) 7.94 (d, J = 8.2 Hz, 1H) 7.56 (d, J = 1.7 Hz, 1H) 7.38 (dd, J = 8.3, 1.7 Hz, 1H) 3.39 (t, J = 7.1 Hz, 2H) 2.60 (t, J = 7.1 Hz, 2H) 2.23 (p, J = 7.1 Hz, 2H) 1.72 (s, 3H) 1.68 (s, 3H); ^{19}F NMR (500 MHz, $CDCl_3$-*d*) δ ppm -139.23 (hept, 1H); ^{13}C NMR (500 MHz, $CDCl_3$-*d*) δ ppm 178.08, 164.73, 163.90, 150.88, 133.03, 130.94, 126.80, 122.72, 121.58, 32.30, 31.60, 29.05, 28.85, 24.31; TOF ES+ MS: (M+H) 359.06; HPLC Ret: 6.95 min; 98% pure.

4-((5-(4-(2-fluoropropan-2-yl)phenyl)-1,3,4-oxadiazol-2-yl)thio)butanoic acid (CCG-263106). Method G starting from methyl 4-((5-(4-(2-fluoropropan-2-yl)phenyl)-1,3,4-oxadiazol-2-yl)thio)butanoate (0.04 g, 0.10 mmol) gave 4-((5-(4-(2-fluoropropan-2-yl)phenyl)-1,3,4-oxadiazol-2-yl)thio)butanoic acid as white solid (0.01 g, 33%); ^{1}H NMR (500 MHz, $CDCl_3$-*d*) δ ppm 7.99 (d, J = 8.4 Hz, 2H) 7.51 (d, J = 8.4 Hz, 2H) 3.39 (t, J = 7.1 Hz, 2H) 2.60 (t, J = 7.1 Hz, 2H) 2.22 (p, J = 7.1 Hz, 2H) 1.73 (s, 3H) 1.69 (s, 3H); ^{19}F NMR (500 MHz, $CDCl_3$-*d*) δ ppm -138.73 (hept, 1H); ^{13}C NMR (500 MHz, $CDCl_3$-*d*) δ ppm 177.78, 165.57, 164.03, 149.70, 126.72, 124.48, 122.44, 32.24, 31.57, 29.20, 29.00, 24.28; TOF ES+ MS: (M+H) 325.10; HPLC Ret: 6.64 min; 94% pure.

4-((5-(4-(difluoromethoxy)phenyl)-1,3,4-oxadiazol-2-yl)thio)butanoic acid (CCG-263107). Method G starting from methyl 4-((5-(4-(difluoromethoxy)phenyl)-1,3,4-oxadiazol-2-yl)thio)butanoate (0.08 g, 0.22 mmol) gave 4-((5-(4-(difluoromethoxy)phenyl)-1,3,4-oxadiazol-2-

yl)thio)butanoic acid as white solid (0.06 g, 75%); ^{1}H NMR (500 MHz, $CDCl_3$-*d*) δ ppm 10.81 (br. s., 1H) 8.02 (d, J = 8.5 Hz, 2H) 7.24 (d, J = 8.5 Hz, 2H) 6.60 (t, J = 73.0 Hz, 1H) 3.39 (t, J = 7.2 Hz, 2H) 2.59 (t, J = 7.1 Hz, 2H) 2.22 (p, J = 7.1 Hz, 2H); ^{19}F NMR (500 MHz, $CDCl_3$-*d*) δ ppm -81.70 (d, 2H); ^{13}C NMR (500 MHz, $CDCl_3$-*d*) δ ppm 178.00, 164.97, 164.18, 153.54, 128.53, 120.55, 119.70, 117.43, 115.35, 111.26, 32.26, 31.57, 24.25; TOF ES+ MS: (M+H) 331.06; HPLC Ret: 6.28 min; 99% pure.

4-((5-(2-chloro-3-(2,2,2-trifluoroethoxy)phenyl)-1,3,4-oxadiazol-2-yl)thio)butanoic acid. CCG-263235. Method G starting from methyl 4-((5-(2-chloro-3-(2,2,2-trifluoroethoxy)phenyl)-1,3,4-oxadiazol-2-yl)thio)butanoate (0.01 g, 0.03 mmol) gave 4-((5-(2-chloro-3-(2,2,2-trifluoroethoxy)phenyl)-1,3,4-oxadiazol-2-yl)thio)butanoic acid as colorless oil (0.01 g, 89%); column: 55% EtOAc: 45% Hex to 60% EtOAc: 40% Hex: 0.1% AcOH; ^{1}H NMR (500 MHz, $CDCl_3$-*d*) δ ppm 7.67 (d, 7.9 Hz, 1H) 7.38 (t, J = 8.1 Hz, 1H) 7.16 (d, J = 8.2 Hz, 1H) 4.47 (q, J = 8.0 Hz, 2H) 3.39 (t, J = 7.2 Hz, 2H) 2.59 (t, J = 7.2 Hz, 2H) 2.22 (p, J = 7.2 Hz, 2H); ^{13}C NMR (500 MHz, $CDCl_3$-*d*) δ ppm 177.76, 165.01, 163.76, 154.32, 127.78, 125.13, 124.84, 121.84, 118.05, 67.37 32.27, 31.60, 29.70, 24.33; ^{19}F NMR (500 MHz, $CDCl_3$-*d*) δ ppm -73.84 (t, 3H); TOF ES^{+} MS: (M+H) 397.02; HPLC Ret: 6.56 min; 95% pure.

4-((5-(2-chloro-4-fluorophenyl)-1,3,4-oxadiazol-2-yl)thio)butanoic acid. CCG-263236. Method G starting from methyl 4-((5-(2-chloro-4-fluorophenyl)-1,3,4-oxadiazol-2-yl)thio)butanoate (0.01 g, 0.04 mmol) gave 4-((5-(2-chloro-4-fluorophenyl)-1,3,4-oxadiazol-2-yl)thio)butanoic acid as white solid (0.015 g, 100%); column: 45% EtOAc: 55% Hex. White solid. Yield = 100%. ^{1}H NMR (500 MHz, $CDCl_3$-*d*) δ ppm 7.96 (dd, J = 8.8, 5.9 Hz, 1H) 7.30 (dd, J = 8.4, 2.5 Hz, 1H) 7.13 (ddd, J = 8.7, 7.5, 2.6 Hz, 1H) 3.39 (t, J = 7.2 Hz, 2H) 2.59 (t, J = 7.2 Hz, 2H) 2.23 (p, J = 7.2 Hz, 2H); ^{13}C NMR (500 MHz, $CDCl_3$-*d*) δ ppm 177.89, 164.93, 163.42, 162.89, 134.53, 132.59, 119.35, 118.87, 114.96, 32.25, 31.59, 24.29; ^{19}F NMR (500 MHz, $CDCl_3$-*d*) δ ppm -105.46 (t, 1H) TOF ES^{+} MS: (M+H) 317.02; HPLC Ret: 6.23 min; 100% pure.

4-((5-(2,4-dichlorophenyl)-1,3,4-oxadiazol-2-yl)thio)-2,2-dimethylbutanoic acid (CCG-262707). Method G starting from methyl 4-((5-(2,4-dichlorophenyl)-1,3,4-oxadiazol-2-yl)thio)-2,2-dimethylbutanoate (0.05 g, 0.13 mmol) gave 4-((5-(2,4-dichlorophenyl)-1,3,4-oxadiazol-2-yl)thio)-2,2-dimethylbutanoic acid as white oil (0.02 g, 42%); column: 20% EtOAc: 80% Hex: 0.01% AcOH; ^{1}H NMR (500 MHz, $CDCl_3$-*d*) δ ppm 9.81 (br. s, 1H) 7.90 (d, J = 8.5 Hz, 1H) 7.56 (d, J = 2.1 Hz, 1H) 7.39 (dd, J = 8.5, 2.1 Hz, 1H) 3.35-3.27 (m, 2H) 2.17-2.09 (m, 2H) 1.31 (s, 6H); ^{13}C NMR (500 MHz, $CDCl_3$-*d*) δ ppm 183.13, 165.07, 163.31, 138.02, 133.73, 131.53, 131.17, 127.60, 121.37, 42.23, 39.68, 28.22, 24.90; TOF ES+ MS: (M+H) 361.02; HPLC Ret: 7.64 min; 95% pure.

***trans*-3-((5-(2,4-dichlorophenyl)-1,3,4-oxadiazol-2-yl)thio)cyclobutanecarboxylic acid (CCG-262587).** Method G starting from methyl *trans*-3-((5-(2,4-dichlorophenyl)-1,3,4-oxadiazol-2-yl)thio)cyclobutanoate (0.03 g, 0.09 mmol) gave trans-3-((5-(2,4-dichlorophenyl)-1,3,4-oxadiazol-2-yl)thio)cyclobutanecarboxylic acid as white solid (0.02 g, 57%); column: 40% EtOAc: 60% Hex: 0.01% AcOH; ^{1}H NMR (500 MHz, $CDCl_3$-*d*) δ ppm 9.41 (br. s, 1H) 7.91 (d, J = 8.5 Hz, 1H) 7.57 (d, J = 2.0 Hz, 1H) 7.39 (dd, J = 8.5, 2.0 Hz, 1H) 4.48 (p, J = 7.5 Hz, 1H) 3.44 (tt, J = 9.9, 5.5 Hz, 1H) 2.99 (ddd, J = 13.9, 8.3, 5.8 Hz, 2H) 2.61 (dtd, J = 13.3, 6.6, 2.2 Hz, 2H); ^{13}C NMR (500 MHz, $CDCl_3$-*d*) δ ppm 179.91, 164.00, 163.37, 138.15, 133.76, 131.61, 131.20, 127.63, 121.31, 37.48, 35.22, 32.70, 29.68; **NOSEY attached; TOF ES+ MS: (M+H) 344.99; HPLC Ret: 7.03 min; 95% pure. *NOSEY does not show *trans* protons.

***cis*-3-((5-(2,4-dichlorophenyl)-1,3,4-oxadiazol-2-yl)thio)cyclobutanecarboxylic acid (CCG-262588).** Method G starting from methyl cis-3-((5-(2,4-dichlorophenyl)-1,3,4-oxadiazol-2-yl)thio)cyclobutanoate (0.09 g, 0.25 mmol) gave cis-3-((5-(2,4-dichlorophenyl)-1,3,4-oxadiazol-2-yl)thio)cyclobutanecarboxylic acid as white solid (0.05 g, 61%); ^{1}H NMR (500 MHz, $CDCl_3$-*d*) δ ppm 10.08 (br. s, 1H) 7.90 (d, J = 8.4 Hz, 1H) 7.56 (d, J = 2.1 Hz, 1H) 7.39 (dd, J = 8.3, 2.1 Hz, 1H) 4.32 (p, J = 8.6 Hz, 1H) 3.23 (p, J = 8.9 Hz, 1H) 2.94 (dtt, J = 10.8, 8.1, 4.6 Hz, 2H) 2.60

(qd, J = 9.5, 2.7 Hz, 2H); ^{13}C NMR (500 MHz, $CDCl_3$-*d*) δ ppm 178.94, 164.09, 163.37, 138.13, 133.75, 131.60, 131.18, 127.62, 121.30, 35.35, 34.62, 33.56; **NOSEY attached; TOF ES+ MS: (M+H) 344.99; HPLC Ret: 6.90 min; 95% pure. *NOSEY shows *cis* protons.

***cis*-3-((5-(2-chloro-4-cyclopropylphenyl)-1,3,4-oxadiazol-2-yl)thio)cyclobutanecarboxylic acid (CCG-263087).** Method G starting from methyl cis-3-((5-(2-chloro-4-cyclopropylphenyl)-1,3,4-oxadiazol-2-yl)thio)cyclobutanoate (0.08 g, 0.23 mmol) gave cis-3-((5-(2-chloro-4-cyclopropylphenyl)-1,3,4-oxadiazol-2-yl)thio)cyclobutanecarboxylic acid as white solid (0.05 g, 64%); column: 30% EtOAc: 70% Hex to 35% EtOAc: 65% Hex: 0.1% AcOH followed by trituration with EtOAc/Hex; ^{1}H NMR (500 MHz, $CDCl_3$-*d*) δ ppm 9.96 (br. s, 1H) 7.81 (d, J = 8.2 Hz, 1H) 7.20 (d, J = 1.7 Hz, 1H) 7.05 (dd, J = 8.2, 1.7 Hz, 1H) 4.30 (p, J = 8.7 Hz, 1H) 3.22 (p, J = 8.9 Hz, 1H) 2.99-2.88 (m, 2H) 2.59 (qd, J = 9.5, 2.8 Hz, 2H) 1.92 (tt, J = 8.7, 5.0 Hz, 1H) 1.08 (dt, J = 6.9, 4.9 Hz, 2H) 0.78 (dt, J = 6.7, 4.8 Hz, 2H); ^{13}C NMR (500 MHz, $CDCl_3$-*d*) δ ppm 178.92, 164.24, 163.46, 150.10, 132.79, 130.68, 128.12, 124.27, 119.46, 35.30, 34.66, 32.71, 15.40, 10.40; **NOSEY attached; TOF ES+ MS: (M+H) 351.04; HPLC Ret: 7.00 min; 93% pure with trans-diastereomer impurity; 97% pure without trans-diastereomer impurity. *NOSEY shows *cis* protons.

***trans*-3-((5-(2-chloro-4-cyclopropylphenyl)-1,3,4-oxadiazol-2-yl)thio)cyclobutanecarboxylic acid (CCG-263088).** Method G starting from methyl trans-3-((5-(2-chloro-4-cyclopropylphenyl)-1,3,4-oxadiazol-2-yl)thio)cyclobutanoate (0.05 g, 0.14 mmol) gave trans-3-((5-(2-chloro-4-cyclopropylphenyl)-1,3,4-oxadiazol-2-yl)thio)cyclobutanecarboxylic acid as white solid (0.03 g, 57%); column: 40% EtOAc: 60% Hex: 0.1% AcOH followed by trituration with EtOAc/Hex; ^{1}H NMR (500 MHz, $CDCl_3$-*d*) δ ppm 10.03 (br. s, 1H) 7.82 (d, J = 8.2 Hz, 1H) 7.20 (d, J = 1.7 Hz, 1H) 7.05 (dd, J = 8.2, 1.7 Hz, 1H) 4.46 (p, J = 8.7 Hz, 1H) 3.43 (p, J = 4.8 Hz, 1H) 2.98 (ddd, J = 13.7, 8.1, 5.4 Hz, 2H) 2.60 (ddd, J = 13.4, 9.6, 6.5 Hz, 2H) 1.92 (tt, J = 8.5, 5.4 Hz, 1H) 1.09 (dt, J = 6.9, 4.9 Hz, 2H) 0.79 (dt, J = 6.8, 4.9 Hz, 2H); ^{13}C NMR (500

MHz, $CDCl_3$-*d*) δ ppm 180.08, 164.27, 163.36, 150.12, 132.80, 130.69, 128.14, 124.29, 119.46, 37.43, 35.23, 32.70, 15.41, 10.40; **NOSEY attached; TOF ES+ MS: (M+H) 351.04; HPLC Ret: 7.21 min; 92% pure with cis-diastereomer impurity; 94% pure without cis-diastereomer impurity. *NOSEY does not show *trans* protons.

***cis*-3-((5-(2-chloro-4-(trifluoromethyl)phenyl)-1,3,4-oxadiazol-2-yl)thio)cyclobutanecarboxylic acid (CCG-263089).** Method G starting from methyl cis-3-((5-(2-chloro-4-(trifluoromethyl)phenyl)-1,3,4-oxadiazol-2-yl)thio)cyclobutanoate (0.05 g, 0.12 mmol) gave cis-3-((5-(2-chloro-4-(trifluoromethyl)phenyl)-1,3,4-oxadiazol-2-yl)thio)cyclobutanecarboxylic acid as white solid (0.02 g, 48%); column: 40% EtOAc: 60% Hex: 0.1% AcOH followed by trituration with EtOAc/Hex; ^{1}H NMR (500 MHz, $CDCl_3$-*d*) δ ppm 9.69 (br. s, 1H) 8.12 (d, J = 8.2 Hz, 1H) 7.82 (d, J = 1.7 Hz, 1H) 7.66 (dd, J = 8.3, 1.7 Hz, 1H) 4.34 (p, J = 8.6 Hz, 1H) 3.24 (p, J = 8.9 Hz, 1H) 3.04-2.91 (m, 2H) 2.61 (qd, J = 9.4, 2.8 Hz, 2H); ^{13}C NMR (500 MHz, $CDCl_3$-*d*) δ ppm 178.97, 164.68, 162.99, 134.31, 133.60, 131.60, 128.41, 125.94, 123.95, 121.59, 35.35, 34.63, 33.53; **NOSEY attached; TOF ES+ MS: (M+H) 379.00; HPLC Ret: 7.14 min; 95% pure. *NOSEY shows *cis* protons.

***trans*-3-((5-(2-chloro-4-(trifluoromethyl)phenyl)-1,3,4-oxadiazol-2-yl)thio)cyclobutanecarboxylic acid (CCG-263090).** Method G starting from methyl trans-3-((5-(2-chloro-4-(trifluoromethyl)phenyl)-1,3,4-oxadiazol-2-yl)thio)cyclobutanoate (0.03 g, 0.06 mmol) gave trans-3-((5-(2-chloro-4-(trifluoromethyl)phenyl)-1,3,4-oxadiazol-2-yl)thio)cyclobutanecarboxylic acid as white solid (0.09 g, 37%); column: 40% EtOAc: 60% Hex: 0.1% AcOH followed by trituration with EtOAc/Hex; ^{1}H NMR (500 MHz, $CDCl_3$-*d*) δ ppm 9.43 (br. s, 1H) 8.12 (d, J = 8.2 Hz, 1H) 7.82 (d, J = 1.7 Hz, 1H) 7.66 (dd, J = 8.3, 1.7 Hz, 1H) 4.51 (p, J = 7.5 Hz, 1H) 3.45 (p, J = 5.5 Hz, 1H) 3.01 (ddd, J = 13.7, 8.1, 5.3 Hz, 2H) 2.62 (ddd, J = 13.8, 9.5, 6.5 Hz, 2H); ^{13}C NMR (500 MHz, $CDCl_3$-*d*) δ ppm 180.10, 164.62, 162.98, 134.33,

133.60, 131.38, 128.39, 125.94, 123.93, 121.70, 37.49, 35.26, 32.68; **NOSEY attached; TOF ES+ MS: (M+H) 379.00; HPLC Ret: 7.25 min; 98% pure. *NOSEY does not show *trans* protons.

***cis*-3-((5-(2,4-dichlorophenyl)-1,3,4-oxadiazol-2-yl)thio)cyclopentanecarboxylic acid (CCG-263108).** Method G starting from methyl cis-3-((5-(2,4-dichlorophenyl)-1,3,4-oxadiazol-2-yl)thio) cyclopentanoate (0.14 g, 0.36 mmol) gave cis-3-((5-(2,4-dichlorophenyl)-1,3,4-oxadiazol-2-yl)thio)cyclopentanecarboxylic acid as white solid (0.08 g, 62%); column: 40% EtOAc: 60% Hex: 0.1% AcOH followed by trituration with EtOAc/Hex; ^{1}H NMR (500 MHz, $CDCl_3$-*d*) δ ppm 10.61 (br. s, 1H) 7.92 (d, J = 8.5 Hz, 1H) 7.57 (d, J = 1.7 Hz, 1H) 7.39 (dd, J = 8.5, 1.8 Hz, 1H) 4.28-4.20 (m, 1H) 3.18-3.08 (m, 1H) 2.67-2.57 (m, 1H) 2.51-2.41 (m, 1H) 2.29-1.99 (m, 3H) 1.92-1.83 (m, 1H); ^{13}C NMR (500 MHz, $CDCl_3$-*d*) δ ppm 181.03, 164.71, 163.29, 138.08, 133.73, 131.60, 131.18, 127.62, 121.35, 45.04, 42.42, 36.87, 33.18, 28.77; TOF ES+ MS: (M+H) 358.99; HPLC Ret: 7.33 min. *HNMR, CNMR, MS, & HPLC indicated that a 20% impurity remained after column and crystallization purifications. Based on the NMR and HPLC evidence, this impurity was thought to be the thermodynamically stable conformational isomer so it was further investigated. A high temperature HNMR in DMSO at 90 °C did not resolve the expected peaks; however, the formation of this conformer impurity may require a longer time than the 5 min high temp experiment to resolve the isomers. A high-resolution LC/MS showed that the two compounds in the mixture had the same mass of 359.00, and therefore it was concluded that the impurity was the thermodynamically more stable conformer as no other proposed homolog matched the data obtained. Of note, the trans isomer (CCG-263091) did not contain this conformer impurity—having used the same starting material to make both analogs this further strengthened the hypothesis. 82% pure with conformer impurity; 99% pure without conformer impurity. *Comparisons between the experimental CNMR chemical shifts to MestreNova predicted CNMR chemical shifts was used to assign cis and trans isomers; the experimental and predicted shifts were extremely close.

***trans*-3-((5-(2,4-dichlorophenyl)-1,3,4-oxadiazol-2-yl)thio)cyclopentanecarboxylic acid (CCG-263091).** Method G starting from methyl trans-3-((5-(2,4-dichlorophenyl)-1,3,4-oxadiazol-2-yl)thio) cyclopentanoate (0.05 g, 0.14 mmol) gave trans-3-((5-(2,4-dichlorophenyl)-1,3,4-oxadiazol-2-yl)thio)cyclopentanecarboxylic acid as white solid (0.03 g, 60%); ^{1}H NMR (500 MHz, $CDCl_3$-*d*) δ ppm 11.54 (br. s, 1H) 7.87 (d, J = 8.5 Hz, 1H) 7.58 (d, J = 1.9 Hz, 1H) 7.42 (dd, J = 8.5, 1.9 Hz, 1H) 5.32-5.24 (m, 1H) 3.31-3.23 (m, 1H) 2.53-2.45 (m, 1H) 2.38-2.28 (m, 3H) 2.14-2.00 (m, 2H); ^{13}C NMR (500 MHz, $CDCl_3$-*d*) δ ppm 181.40, 175.08, 156.36, 138.64, 133.80, 131.56, 130.85, 127.73, 119.81, 59.55, 42.40, 34.24, 31.02, 28.56; TOF ES+ MS: (M+H) 358.99; HPLC Ret: 7.58 min; 95% pure. *Comparisons between the experimental CNMR chemical shifts to MestreNova predicted CNMR chemical shifts was used to assign cis and trans isomers; the experimental and predicted shifts were extremely close.

***cis*-4-((5-(2,4-dichlorophenyl)-1,3,4-oxadiazol-2-yl)thio)cyclohexanecarboxylic acid (CCG-263092).** Method G starting from ethyl cis-4-((5-(2,4-dichlorophenyl)-1,3,4-oxadiazol-2-yl)thio)cyclohexanoate (0.07 g, 0.18 mmol) gave cis-4-((5-(2,4-dichlorophenyl)-1,3,4-oxadiazol-2-yl)thio)cyclohexanecarboxylic acid as white solid (0.03 g, 52%); reaction required 24 hr; column: 40% EtOAc: 60% Hex: 0.1% AcOH followed by trituration with EtOH/H_2O; ^{1}H NMR (500 MHz, $CDCl_3$-*d*) δ ppm 10.66 (br. s, 1H) 7.91 (d, J = 8.5 Hz, 1H) 7.56 (d, J = 1.8 Hz, 1H) 7.39 (dd, J = 8.5, 1.6 Hz, 1H) 4.15-4.10 (m, 1H) 2.62-2.55 (m, 1H) 2.11-1.98 (m, 6H) 1.93-1.83 (m, 2H); ^{13}C NMR (500 MHz, $CDCl_3$-*d*) δ ppm 180.77, 164.93, 163.21, 138.01, 133.71, 131.57, 131.16, 127.59, 121.40, 45.46, 40.46, 30.08, 25.32; TOF ES+ MS: (M+H) 373.00; HPLC Ret: 7.40 min; 89% pure with trans-diastereomer impurity; 99% pure without trans-diastereomer impurity. *See ethyl ester homolog for explanation of how assignment was made for cis/trans isomers.

***trans*-4-((5-(2,4-dichlorophenyl)-1,3,4-oxadiazol-2-yl)thio)cyclohexanecarboxylic acid (CCG-263093).** Method G starting from ethyl trans-4-((5-(2,4-dichlorophenyl)-1,3,4-oxadiazol-2-

yl)thio)cyclohexanoate (0.04 g, 0.09 mmol) gave trans-4-((5-(2,4-dichlorophenyl)-1,3,4-oxadiazol-2-yl)thio)cyclohexanecarboxylic acid as white solid (0.02 g, 47%); reaction required 24 hr; column: 40% EtOAc: 60% Hex: 0.1% AcOH followed by trituration with EtOAc/Hex; ^{1}H NMR (500 MHz, $CDCl_3$-*d*) δ ppm 9.67 (br. s, 1H) 7.92 (d, J = 8.5 Hz, 1H) 7.57 (d, J = 2.0 Hz, 1H) 7.39 (dd, J = 8.5, 2.0 Hz, 1H) 3.75-3.69 (m, 1H) 2.44-2.38 (m, 3H) 2.21-2.09 (m, 2H) 1.73-1.57 (m, 4H); ^{13}C NMR (500 MHz, $CDCl_3$-*d*) δ ppm 180.73, 164.43, 163.27, 138.07, 133.70, 131.58, 131.18, 127.62, 121.38, 45.43, 41.70, 32.10, 28.45; TOF ES+ MS: (M+H) 373.00; HPLC Ret: 7.55 min; 98% pure. *See ethyl ester homolog for explanation of how assignment was made for cis/trans isomers.

2-(1-(((5-(2,4-dichlorophenyl)-1,3,4-oxadiazol-2-yl)thio)methyl)cyclopropyl)acetic acid (CCG-262705). 2-(2,4-dichlorophenyl)-5-(methylsulfonyl)-1,3,4-oxadiazole (0.05 g, 0.171 mmol) was dissolved in 2 mL acetone. K_2CO_3 (0.028 g, 0.205 mmol) and 2-(1-(mercaptomethyl)cyclopropyl)acetic acid (0.03 g, 0.21 mmol) were added and the mixture was stirred at 25 °C for 1 hr. The acetone was removed *in vacuo* and the remaining residue was partitioned between water (5 mL) and DCM (5 mL). The product was extracted with DCM (3x 10 mL), washed with brine (10 mL), dried with $MgSO_4$, and concentrated *in vacuo*. The residue was subjected to silica gel chromatography eluting with 45% EtOAc: 55% Hex: 0.01% AcOH to produce white solid. Yield=98%. ^{1}H NMR (500 MHz, $CDCl_3$-*d*) δ ppm 10.88 (br. s, 1H) 7.91 (d, J = 8.5 Hz, 1H) 7.56 (d, J = 2.0 Hz 1H) 7.39 (dd, J = 8.5, 2.0 Hz, 1H) 3.54 (s, 2H) 2.52 (s, 2H) 0.82-0.77 (m, 2H) 0.73-0.68 (m, 2H); ^{13}C NMR (500 MHz, $CDCl_3$-*d*) δ ppm 177.39, 165.35, 163.38, 138.08, 133.73, 131.59, 131.16, 127.61, 121.31, 41.36, 39.86, 17.33, 13.48; TOF ES+ MS: (M+H) 359.0; HPLC Ret: 7.28 min; 99% pure.

4-((5-(2-chloro-4-hydroxyphenyl)-1,3,4-oxadiazol-2-yl)thio)butanoic acid. CCG-263233. 4-((5-(2-chloro-4-(prop-2-yn-1-yloxy)phenyl)-1,3,4-oxadiazol-2-yl)thio)butanoic acid (0.04 g, 0.11 mmol) was dissolved in 2:1 DMF/H_2O solution. Bis(triphenylphosphine)palladium(II) chloride

(0.01 g, 0.01 mmol) and trimethylamine (0.09 g, 0.91 mmol, 0.13 mL) were added and the reaction was stirred under nitrogen at 85 °C for 2 hr. The reaction was quenched with H_2O (5 mL) and acidified to pH ~ 1 with 1N HCl (2 mL). The product was extracted with EtOAc (3 x 15 mL), and the resulting organic layer was washed with brine (20 mL), dried with $MgSO_4$, and evaporated. The oil was subjected to silica gel chromatography eluting with 70% EtOAc: 30% Hex: 0.01% AcOH. The fractions containing product were concentrated in vacuo to produce white powder. Similar compounds were made in an analogous fashion. Yield=25%. ^{1}H NMR (500 MHz, MeOD-*d*$_4$) δ ppm 7.76 (dd, J = 8.7, 1.3 Hz, 1H) 6.99 (dd, J = 2.4, 1.3 Hz, 1H) 6.87 (ddd, J = 8.6, 2.4, 1.3 Hz, 1H) 3.36 (t, J = 7.1 Hz, 2H) 2.50 (t, J = 7.1 Hz, 2H) 2.13 (p, J = 7.1 Hz, 2H); ^{13}C NMR (500 MHz, $CDCl_3$-*d*) δ ppm 174.86, 164.42, 164.38, 161.35, 133.61, 131.97, 117.35, 114.52, 113.08, 31.84, 31.31, 24.65; TOF ES$^+$ MS: (M+H) 315.02; HPLC Ret: 5.31 min; 98% pure.

4-((5-(2-chloro-3-hydroxyphenyl)-1,3,4-oxadiazol-2-yl)thio)butanoic acid. (CCG-263234). *note: 4-((5-(2-chloro-3-(prop-2-yn-1-yloxy)phenyl)-1,3,4-oxadiazol-2-yl)thio)butanoic acid used as starting material; silica gel chromatography eluting with 70% EtOAc: 30% Hex: 0.01% AcOH. White powder. Yield=25%. ^{1}H NMR (500 MHz, MeOD-*d*$_4$) δ ppm 7.37 (dt, 7.8, 1.4 Hz, 1H) 7.29 (dt, J = 8.0, 1.2 Hz, 1H) 7.14 (dt, J = 8.2, 1.4 Hz, 1H) 3.37 (t, J = 7.1 Hz, 2H) 2.51 (d, J = 7.1 Hz, 2H) 2.14 (p, J = 7.1 Hz, 2H); ^{13}C NMR (500 MHz, $CDCl_3$-*d*) δ ppm 174.86, 165.19, 164.34, 154.45, 127.62, 123.52, 121.38, 119.37, 119.19, 31.86, 31.33, 24.63; TOF ES$^+$ MS: (M+H) 315.02; HPLC Ret: 5.05 min; 94% pure.

222740-Series SBDD Procedures:

***cis*-6-oxabicyclo[3.2.1]oct-3-en-7-one.** At 0 ^{o}C in a 250 mL round bottomed flask, a solution of *cis*-cyclohex-3-enecarboxylic acid (5 g, 39.6 mmol), sodium bicarbonate (10 g, 119 mmol), and H_2O (40 mL) was combined with a solution of potassium iodide (33 g, 198 mmol), iodine (10.6 g, 41.6 mmol), and H_2O (40 mL). The mixture was stirred warmed to 25 ^{o}C for 18 hr. The product

was extracted with DCM (3 x 50 mL) and the organic layers were combined, washed with $NaHSO_3$ (2 x 50 mL), brine, dried with $MgSO_4$, and then concentrated in vacuo. The remaining oil was dissolved in THF (80 mL) and DBU (7.8 g, 51.5 mmol, 7.77 mL) was added. The reaction took place at 70 ^oC for 5 hr. The solvent was evaporated in vacuo and the subsequent oil was subjected to silica gel plug eluting with with 90% EtOAc: 10% Hex. The fractions containing product were concentrated in vacuo to produce pale yellow oil. Yield=93%. ^1H NMR (500 MHz, $CDCl_3$-*d*) δ ppm 6.24 (dddd, J = 9.2, 5.4, 2.9, 1.5 Hz, 1H) 5.86 (dddd, J = 9.4, 3.8, 2.6, 1.3 Hz, 1H) 4.77 (t, J = 5.7 Hz, 1H) 2.93-2.91 (m, 1H) 2.56-2.43 (m, 4H) 2.10 (d, J = 11.1 Hz, 1H).

***trans*-5-azidocyclohex-3-enecarboxylic acid.** In a 100 mL round-bottomed flask, *trans*-6-oxabicyclo[3.2.1]oct-3-en-7-one (0.5 g, 4.03 mmol) in H_2O (4 mL) was added to a solution of NaN_3 (0.3 g, 4.43 mmol) in THF (10 mL) and stirred at 50 °C for 48 hr. The volatile organics were evaporated *in vacuo* and 2M NaOH (8 mL) was added. The aqueous was washed with Et_2O (3 x 10 mL) and then acidified with 6N HCl (5 mL) on ice. The product was extracted with DCM (3 x 15 mL), washed with brine (30 mL), dried with $MgSO_4$, and concentrated *in vacuo*. Yield=50%. ^1H NMR (500 MHz, $CDCl_3$-*d*) δ ppm 6.06 (dddd, J = 10.0, 4.9, 2.7, 1.0 Hz, 1H) 5.82 (dddt, J = 9.9, 4.4, 2.7, 1.5 Hz, 1H) 4.06 (t, J = 4.3 Hz, 1H) 2.82 (m, 1H) 2.44 (dt, 8.0, 4.5 Hz, 1H) 2.31-2.23 (m, 1H) 2.17 (dt, 7.5, 2.0 Hz, 1H) 1.91 (ddd, J = 13.8, 11.7, 4.8 z, 1H).

***trans*-3-((tert-butoxycarbonyl)amino)cyclohexanecarboxylic acid.** *trans*-5-azidocyclohex-3-enecarboxylic acid (0.1 g, 0.60 mmol) was dissolved in EtOH (2 mL) and H_2O (0.8 mL), and the solvents were degassed. 5% Pd/C (0.02 g, 0.01 mmol) was added and the reaction was stirred at 25 °C for 24 hr under 1 atm hydrogen. The catalyst was filtered through a pad of Celite and the filtrate was concentrated *in vacuo*. The resulting amino acid was dissolved in 1M NaOH (1.5 mL) and dioxane (1.5 mL). The solution was cooled to 0 °C and Boc_2O (0.16 g, 0.69 mmol) was added in one portion. The reaction was warmed to 25 °C and stirred for 16 hr. The reaction was

concentrated *in vacuo* and then acidified with 1M HCl (5 mL). The product was extracted with EtOAc (3 x 15 mL), washed with brine (30 mL), dried with $MgSO_4$, and concentrated *in vacuo*. White solid. Yield=50% (2 steps). TOF ES+ MS: (M-H) 242.0.

***cis*-3-(methoxycarbonyl)cyclohexanecarboxylic acid**. A solution of DCC (0.6 g, 2.9 mmol) in DCM (5 mL) was added dropwise to *cis*-cyclohexane-1,3-dicarboxylic acid (0.5 g, 2.9 mmol) in DCM (5 mL). The reaction was stirred for 1.5 hr at 25 °C. The dicyclohexylurea side product was filtered and washed with cold DCM (20 mL). The filtrate was concentrated *in vacuo* to provide 3-oxabicyclo[3.3.1]nonane-2,4-dione as a white solid. The resulting intermediate was dissolved in MeOH (10 mL). The solution was stirred for 2 days at 25 °C. The reaction was concentrated *in vacuo* to provide a white solid. Yield = 93% (2 steps). ^{1}H NMR (500 MHz, $CDCl_3$-*d*) δ ppm 3.68 (s, 3H) 2.40-2.22 (m, 1H) 2.05-1.96 (m, 2H) 1.92 (dd, J = 6.0, 3.0 Hz, 1H) 1.57 (q, J = 12.7 Hz, 1H) 1.44-1.27 (m, 4H); TOF ES+ MS: (M-H) 185.0.

***cis*-methyl 3-(((benzyloxy)carbonyl)amino)cyclohexanecarboxylate.** In a 100 mL round bottomed flask *cis*-3-(methoxycarbonyl)cyclohexanecarboxylic acid (0.56 g, 3.01 mmol) was dissolved in toluene (10 mL). Et_3N (0.34 g, 0.46 mL, 3.31 mmol) and diphenyl phosphorazidate (0.91 g, 0.71 mL, 3.31 mmol) was added and the reaction was stirred at 110 °C for 1 hr. The solution was cooled to 70 °C and benzyl alcohol (0.49 g, 0.47 mL, 4.5 mmol) was added. The reaction was stirred at 85 °C for 19 hr. The solution was cooled to 25 °C, poured into EtOAc (20 mL) and H_2O (20 mL). The product was extracted with EtOAc (3 x 20 mL), washed with brine (2 x 20 mL), dried with $MgSO_4$, and concentrated in vacuo. The subsequent oil was subjected to silica gel chromatography eluting with 50% EtOAc: 50% Hex. The fractions containing product were concentrated in vacuo to produce yellow oil. Yield=98%. ^{1}H NMR (500 MHz, $CDCl_3$-*d*) δ ppm 7.40-7.21 (m, 5H) 5.08 (s, 2H) 4.70 (s, 1H) 3.66 (s, 3H) 2.42 (td, J = 12.0, 6.1 Hz, 1H) 2.29-2.21 (m, 2H) 2.02-1.89 (m, 2H) 1.84 (dt, J = 13.2, 3.4 Hz, 1H) 1.44-1.05 (m, 4H); TOF ES+ MS: (M+H) 248.1; HPLC Ret: 7.01 min.

***cis*-3-oxabicyclo[3.2.1]octane-2,4-dione.** In a 2 mL microwave flask, cyclopentane-1,3-dicarboxylic acid (0.12 g, 0.95 mmol) was dissolved in Ac_2O (0.81 g, 0.75 mL, 8.40 mmol). The reaction was stirred at 150 °C for 30 mins. The solvents were concentrated in vacuo, and the product was crystalized from Et_2O to produce white solid. Yield=47%. ^{1}H NMR (500 MHz, DMSO-d_6) δ ppm 3.18 (q, J = 3.9 Hz, 2H) 2.35 (d, J = 12.4 Hz, 1H) 2.15-2.02 (m, 2H) 1.89 (dq, J = 6.8, 2.1 Hz, 2H) 1.68 (dt, J = 12.4, 4.1 Hz, 1H).

***Cis/trans*-cyclopentane-1,3-dicarboxylic acid.** In a 50 mL round bottomed flask, cyclopentane-1,3-dicarboxylic acid (0.25 g, 1.6 mmol) was dissolved in conc. HCl (5 mL). The reaction was stirred at 130 °C for 16 mins. The solution was poured into ice, and the products were extracted with EtOAc (3 x 20 mL). The organic layers were combined, dried with $MgSO_4$, and concentrated in vacuo to produce white solid. Yield=94%. ^{1}H NMR (500 MHz, DMSO-d_6) δ ppm 12.07 (s, 4H) 2.80-2.66 (m, 5H) 2.10 (dt, J = 12.8, 8.1 Hz, 1H) 2.01-1.64 (m, 11H).

5-((tert-butoxycarbonyl)amino)nicotinate, Et_3NH^+. In a 25 mL round bottomed flask 5-aminonicotinic acid (0.2 g, 1.45 mmol) was dissolved in 1, 4-dioxane (4 mL) and H_2O (2 mL). Et_3N (0.22 g, 0.3 mL, 2.17 mmol) followed by Boc_2O (0.47 g, 2.17 mmol) were added and the reaction was stirred at 25 °C for 24 hr. The solvents were evaporated in vacuo and the product was subjected to high vacuum until completely dry. The product was washed with Et_2O (3 x 5 mL) and concentrated to afford yellow solid. Yield=70%. ^{1}H NMR (500 MHz, DMSO-d_6) δ ppm 9.58 (s, 1H) 8.61 (s, 1H) 8.21 (s, 1H) 8.00 (s, 1H) 7.39 (t, J = 2.3 Hz, 1H) 2.73 (q, J = 7.2H, 6H) 1.49 (s, 9H) 1.05 (t, J = 7.2 Hz, 9H); TOF ES+ MS: (M-H) 236.9; HPLC Ret: 4.55 min.

1-(1-chloroethyl) 3-methyl 5,6-dihydropyridine-1,3(2H)-dicarboxylate. Arecoline HBr (1.0 g, 4.24 mmol) and K_2CO_3 (0.88 g, 6.4 mmol) were dissolved in 10 mL H_2O were stirred at 25 °C for 30 min. The product was extracted with Et_2O (4 x 20 mL), the organic layers were combined, dried with $MgSO_4$, and evaporated in vacuo. The crude oil was dissolved in DCE (15 mL) and

cooled to 0 °C. 1-chloroethylchloroformate (0.67 g, 0.5 mL, 4.66 mmol) was added dropwise and the reaction took place at 90 °C for 30 min. The reaction was cooled then concentrated in vacuo. The oil was subjected to silica gel chromatography eluting with 20% EtOAc: 80% Hex. The fractions containing product were concentrated to produce yellow oil. Yield=60% (2 steps). ^{1}H NMR (500 MHz, $CDCl_3$-*d*) δ ppm 7.09 (br. s., 1H) 6.64-6.59 (m, 1H) 4.31-4.12 (m, 2H) 3.77 (s, 3H) 3.63-3.51 (m, 2H) 2.45-2.29 (m, 2H) 1.83 (d, J = 1.7 Hz, 3H).

1,2,5,6-tetrahydropyridine-3-carboxylic acid, HBr. 1-(1-chloroethyl) 3-methyl 5,6-dihydropyridine-1,3(2H)-dicarboxylate (0.62 g, 2.5 mmol) was stirred in MeOH (10 mL) at 85 °C for 2 hr. The reaction was concentrated in vacuo and then dissolved in 48% HBr (15 mL). The reaction was stirred at 85 °C for 2 hr and then concentrated to dryness in vacuo. The product was crystalized out of water as the HBr salt to produce colorless crystals. Yield=61%. ^{1}H NMR (500 MHz, DMSO-d_6) δ ppm 12.91 (br. s., 1H) 8.95 (br. s., 2H) 7.00 (tt, J = 3.9, 1.8 Hz, 1H) 3.73 (s, 2H) 3.18 (t, J = 6.1 Hz, 2H) 2.47 (dp, J = 5.7, 2.7 Hz, 2H).

1-(tert-butoxycarbonyl)-1,2,5,6-tetrahydropyridine-3-carboxylic acid. 1,2,5,6-tetrahydropyridine-3-carboxylic acid, HBr (0.32 g, 1.54 mmol) was dissolved in 4M NaOH (5 mL) and tBuOH (5 mL). Boc_2O (0.5 g, 2.31 mmol) was added and the reaction was stirred at 50 °C for 2 hr. The solution was washed with Hex (2 x 10 mL) and acidified with 6N HCl (10 mL). The product was extracted with EtOAc (3 x 20 mL), washed with brine (3 x 15 mL), dried with $MgSO_4$, and concentrated in vacuo. The product was crystalized with EtOAc/Hex to afford white powder. Yield=36%. ^{1}H NMR (500 MHz, $CDCl_3$-*d*) δ ppm 12.91 (br. s., 1H) 8.95 (br. s, 2H) 7.21 (br. s, 1H) 4.13 (br. s, 2H) 3.50 (t, J = 5.7 Hz, 2H) 2.34 (br. s., 2H) 1.48 (s, 9H).

1-(tert-butoxycarbonyl)-5,5-difluoro-3-methylpiperidine-3-carboxylic acid. In a flame dried 50 mL round bottomed flask, 1-tert-butyl 3-methyl 5,5-difluoropiperidine-1,3-dicarboxylate (0.31 g, 1.11 mmol) was dissolved in 5 mL THF and cooled to -78 °C. 1M LiHMDS in THF (1.22 mL,

1.22 mmol) was added dropwise, and the reaction was stirred at -78 °C for 1 hr. MeI (0.17 g, 0.08 mL, 1.22 mmol) was added, and after 2 hr stirring at -78 °C, the reaction was warmed to 25 °C and stirred for another 2 hr. The reaction was quenched with NH_4Cl, and the product was extracted with EtOAc (3 x 20 mL), the organic layers were combined, dried with $MgSO_4$, and evaporated in vacuo. The subsequent oil was subjected to silica gel chromatography eluting with 10% to 15% EtOAc/Hex. The fractions containing product were concentrated to produce colorless oil. 1-tert-butyl 3-methyl 5,5-difluoro-3-methylpiperidine-1,3-dicarboxylate (0.222 g, 0.76 mmol) was dissolved in 2 mL THF, 2 mL 1M NaOH, and 0.5 mL MeOH. The reaction was stirred for 1 hr at 25 °C, the volatile solvents were removed *in vacuo*, and the aqueous was acidified with 1N HCl. The product was extracted with EtOAc (3 x 15 mL), the organic layers were combined, washed with brine, dried with $MgSO_4$, and evaporated in vacuo to produce white solid Yield=81% (2-steps). ^{1}H NMR (500 MHz, DMSO-d_6) δ ppm 3.75-3.37 (m, 3H) 2.48-2.32 (m, 1H) 2.08-1.96 (m, 1H) 1.40 (s, 9H), 1.15 (s, 3H); ^{19}F NMR (470 MHz, DMSO-d_6) δ ppm -95.22—-99.04 (m, 2H); ^{13C} NMR (126 MHz, DMSO-d_6) δ ppm 175.85, 154.13, 120.26, 109.99, 79.98, 49.47, 42.53, 28.33, 22.23.

ethyl 3,7-dihydro-2H-[1,4]dioxino[2,3-e]indole-8-carboxylate & ethyl 3,6-dihydro-2H-[1,4]dioxino[2,3-f]indole-7-carboxylate. In a 100 mL round bottomed flask, a solution of sodium nitrite (0.91 g, 13.2 mmol) in H_2O (6 mL) was added to a solution of 6-amino-1,4-benzodioxane (2 g, 13.2 mmol) in 18% HCl (16 mL) at 0 °C. The combined solution was stirred at 0 °C for 30 min. A solution of ethyl-2-methyl acetoacetate (1.91 g, 1.93 mL, 13.2 mmol) in iPrOH (16 mL) was quickly added, and then the the colution was cooled to -10 °C. A solution of AcOK (1.3 g, 13.2 mmol) in H_2O (6 mL) was added followed by 10 % NaOH dropwise until pH ~ 6. The reaction was stirred at 0 °C for 3 hr. Upon completion, DCM (100 mL) was added, and the product was extracted with DCM (3 x 100 mL). The organic layers were combined, washed with brine (1 x 100 mL), dried with $MgSO_4$, and concentrated in vacuo. The residue was

dissolved in EtOH (2 mL) and then heated to boiling. The solution was added to a 10% alcoholic HCl solution (10 mL), and then the solution was heated at reflux for 1 hr. The reaction was diluted with water, and the product was extracted with EtOAc (3 x 100 mL). The organic layers were combined, dried with $MgSO_4$, and concentrated in vacuo. The subsequent oil was subjected to silica gel chromatography eluting with 15% to 60% EtOAc: Hex. The fractions containing product were concentrated in vacuo producing yellow and orange oil, respectively. Analogous compounds were made in a similar fashion. Yield: ethyl 3,7-dihydro-2H-[1,4]dioxino[2,3-e]indole-8-carboxylate = 13% & ethyl 3,6-dihydro-2H-[1,4]dioxino[2,3-f]indole-7-carboxylate = 9% (2-steps). ethyl 3,7-dihydro-2H-[1,4]dioxino[2,3-e]indole-8-carboxylate: ^{1}H NMR (500 MHz, DMSO-d_6) δ ppm 11.78 (s, 1H) 6.97 (s, 1H) 6.91 (d, J = 8.8 Hz, 1H) 6.84 (d, 8.8 Hz, 1H) 4.35-4.25 (m, 6H) 1.33 (t, J = 7.1Hz, 3H); TOF ES+ MS: (M+H) 247.0; HPLC Ret: 6.51 min. ethyl 3,6-dihydro-2H-[1,4]dioxino[2,3-f]indole-7-carboxylate: ^{1}H NMR (500 MHz, DMSO-d_6) δ ppm 11.45 (s, 1H) 7.06 (s, 1H) 6.96 (s, 1H) 6.83 (s, 1H) 4.36-4.18 (m, 6H) 1.32 (t, J = 7.1Hz, 3H); TOF ES+ MS: (M+H) 248.09; HPLC Ret: 6.57 min.

ethyl 3,7-dihydro-2H-[1,4]dioxino[2,3-e]indole-8-carboxylate & ethyl 3,6-dihydro-2H-[1,4]dioxino[2,3-f]indole-7-carboxylate. Yield: 12% (2-steps). ^{1}H NMR (500 MHz, $CDCl_3$-d) δ ppm 8.82 (br. s., 1H) 7.93 (s, 1H) 7.20-7.10 (m, 1H) 6.83 (t, J = 8.1 Hz, 1H) 6.50 (d, 8.2 Hz, 1H) 4.43-4.26 (m, 8H) 2.11 (d, J = 1.4 Hz, 3H) 1.43-1.33 (m, 4H); TOF ES+ MS: (M+H) 246.07; HPLC Ret: 6.94 min.

Ethyl 6,7-difluoro-1H-indole-2-carboxylate. In a 50 mL round bottomed flask, (2,3-difluorophenyl)hydrazine (0.25 g, 1.74 mmol) was dissolved in DCM (8 mL). Ethyl pyruvate (0.20 g, 1.74 mmol, 0.19 mL) was added, and the reaction was stirred at 25 °C for 1 hr. The reaction was diluted with H_2O, and then the product was extracted with DCM (3 x 15mL). The organics were combined, washed with 1N HCl (2 x 15 mL), washed with brine, $MgSO_4$, and concentrated in vacuo (HPLC = 7.23 min). This hydrozone product was dissolved in PhMe (8

mL) and pTSA (0.3 g, 1.56 mmol) was added. The reaction was attached to a Dein-Stark trap and stirred at reflux for 24 hr. The reaction was cooled and neutralized with sodium bicarbonate. The product was extracted with EtOAc (3 x 15 mL), the organics were combined, washed with brine, dried with $MgSO_4$, and concentrated in vacuo. The subsequent oil was subjected to silica gel chromatography eluting with 10% EtOAc: Hex. The fractions containing product were concentrated in vacuo producing yellow solid. Yield: 29% (2-steps). ^{1}H NMR (500 MHz, $CDCl_3$-*d*) δ ppm 9.05 (br. s., 1H) 7.36 (dd, J = 8.9, 4.2 Hz, 1H) 7.21 (t, J = 2.7 Hz, 1H) 7.04-6.98 (m, 1H) 4.42 (q, J = 7.2 Hz, 2H) 1.40 (t, J = 7.1 Hz, 3H); TOF ES+ MS: (M+H) 226.01.

3,7-dihydro-2H-[1,4]dioxino[2,3-e]indole-8-carboxylic acid. In a 25 mL round bottomed flask, ethyl 3,7-dihydro-2H-[1,4]dioxino[2,3-e]indole-8-carboxylate (0.1 g, 0.40 mmol) was dissolved in a solution of KOH (0.05 g, 0.81 mmol) in H_2O (2 mL) & EtOH (0.05 mL). The solution was stirred at 100 °C for 4 hr, and then cooled to 25 °C. The solution was diluted with H_2O (~2 mL), and then acidified with 4N HCl until precipitate formation. The product was filtered, washed with water, and dried on the high vacuum to produce tan solid. Analogous compounds were made in a similar fashion. Yield=56%. ^{1}H NMR (500 MHz, DMSO-d_6) δ ppm 12.85 (br. s, 1H) 11.64 (s, 1H) 6.92 (s, 1H) 6.88 (d, J = 8.7 Hz, 1H) 6.81 (d, 8.7 Hz, 1H) 4.36-4.31 (m, 2H) 4.28-4.21 (m, 2H); TOF ES+ MS: (M-H) 218.05; HPLC Ret: 4.99 min.

3,7-dihydro-2H-[1,4]dioxino[2,3-e]indole-8-carboxylic acid. Pink solid. Yield=74%. ^{1}H NMR (500 MHz, DMSO-d_6) δ ppm 12.69 (br. s, 1H) 11.31 (s, 1H) 7.04 (s, 1H) 6.90 (s, 1H) 6.82 (s, 1H) 4.28-4.18 (m, 4H); TOF ES+ MS: (M-H) 218.05; HPLC Ret: 5.10 min.

3,9-dihydro-2H-[1,4]dioxino[2,3-g]indole-8-carboxylic acid. Brown solid. Yield=56%. ^{1}H NMR (500 MHz, DMSO-d_6) δ ppm 12.14 (br. s, 1H) 8.39 (s, 1H) 7.10 (d, 1H) 6.77 (t, J = 8.2 Hz, 1H) 6.45 (d, J = 8.1 Hz, 1H) 4.34-4.24 (m, 4H); HPLC Ret: 5.43 min.

6,7-difluoro-1H-indole-2-carboxylic acid. White solid. Yield=54%. ^{1}H NMR (500 MHz, DMSO-d_6) δ ppm 13.15 (br. s, 1H) 12.46 (s, 1H) 7.47 (br.s, 1H) 7.19 (br. s, 1H) 7.12 (br. s, 1H); HPLC Ret: 5.76 min.

methyl 3-(2-(pyrrolidin-1-yl)ethoxy)benzoate. In a 50mL round bottomed flask, methyl 3-hydroxybenzoate (0.25 g, 1.64 mmol) was dissolved in 5 mL DMF. K_2CO_3 (0.30 g, 2.14 mmol) and 1-(2-chloroethyl)pyrrolidine (0.66 g, 4.93 mmol) were added, and the reaction was stirred at 100 °C for 4 hr. The reaction was cooled and diluted with H_2O, and then the product was extracted with EtOAc (3 x 20 mL). The organics were combined, washed with brine, dried with $MgSO_4$, and concentrated in vacuo. The oil was subjected to silica gel chromatography eluting with 2.5% to 10% MeOH: DCM. The fractions containing product were concentrated in vacuo to produce colorless oil. Analogous compounds were made in a similar fashion. Yield=67%. ^{1}H NMR (500 MHz, $CDCl_3$-*d*) δ ppm 7.63 (d, J = 8.6 Hz, 2H) 7.58 (s, 1H) 7.33 (t, J = 8.0 Hz, 1H) 7.12 (d, J = 8.6 Hz, 1H) 4.17 (t, J = 5.9 Hz, 2H) 3.91 (s, 3H) 2.94 (t, J = 5.9 Hz, 2H) 2.66 (d, J = 5.8 Hz, 4H) 1.83 (t, J = 3.7 Hz, 4H); TOF ES+ MS: (M+H) 250.15; HPLC Ret: 4.38 min.

methyl 4-(2-(pyrrolidin-1-yl)ethoxy)benzoate. Brown oil. Yield=87%. ^{1}H NMR (500 MHz, $CDCl_3$-*d*) δ ppm 7.98 (d, J = 8.1 Hz, 2H) 6.93 (d, J = 8.0 Hz, 2H) 4.16 (t, J = 5.9 Hz, 2H) 3.88 (s, 3H) 2.94 (t, J = 5.9 Hz, 2H) 2.62 (ddt, J = 7.5, 6.0, 2.4 Hz, 4H) 1.81 (q, J = 3.4 Hz, 4H); TOF ES+ MS: (M+H) 250.15; HPLC Ret: 4.00 min.

methyl 3-(3-(pyrrolidin-1-yl)propoxy)benzoate. Yellow oil. Yield=34%. ^{1}H NMR (500 MHz, $CDCl_3$-*d*) δ ppm 7.62 (d, J = 7.6 Hz, 1H) 7.55 (s, 1H) 7.33 (t, J = 7.9 Hz, 1H) 7.09 (d, J = 8.3 Hz, 1H) 4.80 (t, J = 6.2 Hz, 2H) 3.91 (s, 3H) 2.74 (s, 2H) 2.66 (br. s, 4H) 2.10 (q, J = 7.1 Hz, 2H) 1.86 (br. s, 4H); TOF ES+ MS: (M+H) 264.16; HPLC Ret: 5.16 min.

1-(2-(3-carboxyphenoxy)ethyl)pyrrolidin-1-ium, HCl. In a 25 mL round-bottomed flask methyl 3-(2-(pyrrolidin-1-yl)ethoxy)benzoate (0.27 g, 1.08 mmol) was dissolved in THF (2.5 mL). 1 M

NaOH (2.5 mL) was added to the solution and the reaction was stirred at 25 °C for 3 hr. The THF was evaporated *in vacuo* and then the solution was acidified with 1 N HCl (7 mL). The solution was concentrated *in vacuo*, and then MeOH was added and the inorganic solids were filtered. The filtrate was concentrated *in vacuo* to produce pink solid. Analogous compounds were made in a similar fashion. Yield=100%. ^{1}H NMR (500 MHz, DMSO-d_6) δ 13.07 (s, 1H) 11.04 (br. s, 1H) 7.58 (dt, J = 7.7, 1.4 Hz, 1H) 7.51 (dt, J = 2.8, 1.5 Hz, 1H) 7.46 (td, J = 8.0, 1.4 Hz, 1H) 7.27 (ddt, J = 8.2, 2.6, 1.2 Hz, 1H) 4.49-4.35 (m, 2H) 3.64-3.51 (m, 4H) 3.15-3.02 (m, 2H) 2.09-1.84 (m, 4H); TOF ES+ MS: (M+H) 236.12; HPLC Ret: 3.75 min.

4-(2-(pyrrolidin-1-yl)ethoxy)benzoic acid, HCl. White solid. Yield=84%. ^{1}H NMR (500 MHz, DMSO-d_6) δ 12.71 (br. s, 1H) 11.58 (br. s, 1H) 7.91 (d, J = 8.4 Hz, 2H) 7.09 (d, J = 8.4 Hz, 2H) 4.47 (t, J = 5.1 Hz, 2H) 3.64-3.50 (m, 4H) 3.09 (br. s, 2H) 2.04-1.86 (m, 4H); TOF ES+ MS: (M+H) 236.13; HPLC Ret: 2.99 min.

3-(3-(pyrrolidin-1-yl)propoxy)benzoic acid, HCl. White solid. Yield=79%. ^{1}H NMR (500 MHz, DMSO-d_6) δ ppm 13.02 (br. s, 1H) 10.80 (br. s, 1H) 7.55 (d, J = 7.6 Hz, 1H) 7.50-7.39 (m, 2H) 7.20 (d, J = 7.9 Hz, 1H) 4.13 (q, J = 5.7 Hz, 2H) 3.54 (h, J = 5.4 Hz, 2H) 3.28 (dt, J = 10.7. 6.2 Hz, 2H) 3.00 (dq, J = 14.9, 7.5 Hz, 2H) 2.17 (dq, J = 12.3, 6.2 Hz, 2H) 2.00 (q, J = 7.2 Hz, 2H) 1.89 (dd, J = 7.7, 4.9 Hz, 2H); TOF ES+ MS: (M+H) 250.14.

(5-amino-2-chlorophenyl)methanol. In a 50-mL round bottomed flask, (2-chloro-5-nitrophenyl)methanol (0.5 g, 2.67 mmol) was dissolved in a solution of H_2O (5.0 mL) and EtOH (2.5 mL). Iron fillings (1.5 g, 26.7 mmol) and conc. HCl (0.1 mL) were added. The reaction was stirred at 100 °C for 3 hr, and then neutralized to pH ~ 10 with 1M NaOH. EtOH (2.5 mL) was added and the iron was filtered, washing with EtOH. The filtrate was concentrated, water was added, and the product was filtered, washing with water, producing pink crystals. Yield=55%. ^{1}H NMR (500 MHz, DMSO-d_6) δ 6.96 (d, J = 8.4 Hz, 1H) 6.77 (d, J = 2.7 Hz, 1H) 6.42 (dd, J = 8.5,

2.8 Hz, 1H) 5.19 (d, J = 4.7 Hz, 3H) 4.41 (d, J = 5.6 Hz, 2H); TOF ES+ MS: (M+H) 158.04; HPLC Ret: 2.27 min.

3-(((tert-butyldiphenylsilyl)oxy)methyl)-4-chloroaniline. In a 25-mL round bottomed flask, (5-amino-2-chlorophenyl)methanol (0.15 g, 0.95 mmol), imidazole (0.1 g, 1.43 mmol), and TBDPS-Cl (0.29 g, 0.27 mL, 1.05 mmol) was dissolved in DMF (4.0 mL) at 0 °C. The reaction was stirred at 25 °C for 24 hr, and then quench with sat. NH_4Cl. The product was extracted with EtOAc (3 x 30 mL), and the organic layers combined, washed with brine (2 x 15 mL), dried with $MgSO_4$, and concentrated in vacuo. The subsequent oil was subjected to silica gel chromatography eluting with 10% to 40% EtOAc: Hex. The fractions containing product were concentrated in vacuo to produce colorless oil. Analogous compounds were made in a similar fashion. Yield=66%. ^{1}H NMR (500 MHz, $CDCl_3$-*d*) δ 7.70 (d, J = 6.8 Hz, 4H) 7.47-7.32 (m, 7H) 7.09-7.01 (m, 2H) 6.52 (dd, J = 8.4, 2.9 Hz, 1H) 4.76 (s, 2H) 3.70 (br. s, 2H) 1.12 (s, 9H); TOF ES+ MS: (M+H) 396.15; HPLC Ret: 7.79 min.

3-((tert-butyldiphenylsilyl)oxy)-5-chloroaniline. Colorless oil. Yield=24%. ^{1}H NMR (500 MHz, $CDCl_3$-*d*) δ 7.70 (d, J = 6.8 Hz, 4H) 7.47-7.31 (m, 6H) 7.26 (s, 1H) 6.22 (dd, J = 9.5, 1.7 Hz, 1H) 5.92 (s, 1H) 3.49 (s, 2H) 1.07 (s, 9H); TOF ES+ MS: (M+H) 382.1; HPLC Ret: 7.97 min.

3-(((tert-butyldiphenylsilyl)oxy)methyl)-5-chloroaniline. Colorless oil. Yield=73%. ^{1}H NMR (500 MHz, $CDCl_3$-*d*) δ 7.61 (d, J = 6.8 Hz, 4H) 7.40-7.27 (m, 6H) 7.18 (s, 1H) 6.62 (s, 1H) 6.51-6.45 (m, 2H) 4.56 (s, 2H) 3.63 (s, 2H) 1.02 (s, 9H); TOF ES+ MS: (M+H) 396.2; HPLC Ret: 8.12 min.

***trans*-3-((tert-butoxycarbonyl)amino)cyclopentanecarboxylic acid.** Method A starting from *trans*-methyl 3-((tert-butoxycarbonyl)amino)cyclopentanecarboxylate (0.25 g, 1.03 mmol) gave trans-3-((tert-butoxycarbonyl)amino)cyclopentanecarboxylic acid as white solid (0.19 g, 81%); ^{1}H NMR (500 MHz, $CDCl_3$-*d*) δ ppm 4.49 (br. s, 1H) 4.08 (br. s, 1H) 2.93 (p, J = 7.9 Hz, 1H)

2.23 (dt, J = 14.0, 7.1 Hz, 1H) 2.13-2.01 (m, 2H) 1.94-1.83 (m, 1H) 1.79 (dd, J = 14.0, 5.4 Hz, 1H) 1.44 (s, 9H); TOF ES+ MS: (M+H) 230.14.

tert-butyl (*trans*-3-((4-chlorophenyl)carbamoyl)cyclohexyl)carbamate. Method I starting from trans-3-(tert-butoxycarbonyl)cyclohexanecarboxylic acid (0.2 g, 0.82 mmol) and 4-chloroaniline (0.11 g, 0.82 mmol) gave tert-butyl (trans-3-((4-chlorophenyl)carbamoyl)cyclohexyl)carbamate as yellow solid (0.3 g, 100%); TOF ES+ MS: (M+Na) 375.1; HPLC Ret: 7.50 min.

tert-butyl (*trans*-3-((4-chlorophenyl)carbamoyl)cyclopentyl)carbamate. Method I starting from *trans*-3-((tert-butoxycarbonyl)amino)cyclopentanecarboxylic acid (0.19 g, 0.84 mmol) and 4-chloroaniline (0.11 g, 0.84 mmol) gave tert-butyl (trans-3-((4-chlorophenyl)carbamoyl)cyclopentyl)carbamate as white solid (0.18 g, 63%); ^{1}H NMR (500 MHz, $CDCl_3$-*d*) δ ppm 7.47 (d, J = 8.4 Hz, 2H) 7.28 (d, J = 8.4 Hz, 2H) 4.51 (br. s, 1H) 4.11 (br. s, 1H) 2.84 (p, J = 8.0 Hz, 1H) 2.29-2.11 (m, 2H) 2.10-1.86 (m, 2H) 1.55 (dd, J = 16.3, 9.7 Hz, 1H) 1.45 (s, 9H); TOF ES+ MS: (M+H) 339.14; HPLC Ret: 7.22 min.

tert-butyl (*cis*-3-((4-chlorophenyl)carbamoyl)cyclopentyl)carbamate. Method I starting from cis-3-((tert-butoxycarbonyl)amino)cyclopentanecarboxylic acid (0.3 g, 1.31 mmol) and 4-chloroaniline (0.17 g, 1.31 mmol) gave tert-butyl (cis-3-((4-chlorophenyl)carbamoyl)cyclopentyl)carbamate as yellow solid (0.36 g, 81%); ^{1}H NMR (500 MHz, $CDCl_3$-*d*) δ ppm 7.48 (d, J = 8.5 Hz, 2H) 7.38 (s, 1H) 7.28 (d, J = 8.4 Hz, 2H) 4.08 (s, 1H) 2.84-2.74 (m, 1H) 2.20 (dt, J = 13.2, 6.5 Hz, 1H) 2.01 (q, J = 8.2 Hz, 2H) 1.88 (dt, J = 14.1, 6.4 Hz, 2H) 1.78 (dd, J = 12.4, 6.0 Hz, 1H) 1.44 (s, 9H); TOF ES+ MS: (M+H) 339.1; HPLC Ret: 7.15 min.

***cis*-3-((4-chlorophenyl)carbamoyl)cyclopentanecarboxylic acid.** In a 25 mL round bottomed flask, *cis*-3-oxabicyclo[3.2.1]octane-2,4-dione (0.05 g, 0.36 mmol) was dissolved in DMF (2 mL).

4-chloroaniline (0.046 g, 0.36 mmol) was added and the reaction was stirred at 25 °C for 16 hr. The reaction was acidified with 1N HCl, and the product was extracted with EtOAc (3 x 15 mL). The layers were combined, washed with brine (2 x 15 mL), dried with $MgSO_4$, and concentrated in vacuo to produce white solid. Yield=95%. ^{1}H NMR (500 MHz, DMSO-d_6) δ ppm 12.07 (br. s, 1H) 10.01 (s, 1H) 7.63 (d, J = 7.8 Hz, 2H) 7.34 (d, J = 7.9 Hz, 2H) 2.85-2.70 (m, 2H) 2.14 (dt, J = 12.6, 7.7 Hz, 1H) 1.98-1.75 (m, 5H); TOF ES+ MS: (M+Na) 290.06; HPLC Ret: 5.63 min.

***cis*-3-((4-chlorophenyl)carbamoyl)cyclopentanecarboxylic acid, *trans*-3-((4-chlorophenyl)carbamoyl)cyclopentanecarboxylic acid, & *cis*-N1,N3-bis(4-chlorophenyl)cyclopentane-1,3-dicarboxamide (CCG-263871).** Method I starting from cyclopentane-1,3-dicarboxylic acid (0.16 g, 1.01 mmol) and 4-chloroaniline (0.12 g, 1.01 mmol) gave a seperable mixture of cis-3-((4-chlorophenyl)carbamoyl)cyclopentanecarboxylic acid (0.22 g, 82%), trans-3-((4-chlorophenyl)carbamoyl)cyclopentanecarboxylic acid (0.063 g, 95%), & cis-N1,N3-bis(4-chlorophenyl)cyclopentane-1,3-dicarboxamide as white solids (0.06 g, 34%), respectively); column: 30% EtOAc: 60% Hex: 0.01% AcOH; ^{1}H NMR (500 MHz, $CDCl_3$-*d*) δ ppm cis-3-((4-chlorophenyl)carbamoyl)cyclopentanecarboxylic acid: 12.09 (br. s, 1H) 10.01 (s, 1H) 7.63 (d, J = 8.4 Hz, 2H) 7.34 (d, J = 8.3 Hz, 2H) 2.77 (dtt, J = 30.9, 14.7, 7.7 Hz, 2H) 2.12 (tt, J = 19.0, 8.2 Hz, 1H) 2.01-1.73 (m, 5H), trans-3-((4-chlorophenyl)carbamoyl)cyclopentanecarboxylic acid: 12.08 (br. s, 1H) 10.05 (s, 1H) 7.63 (d, J = 8.8 Hz, 2H) 7.33 (d, J = 8.8 Hz, 2H) 2.88 (dp, J = 22.0, 7.4 Hz, 1H) 2.70 (dq, J = 15.3, 7.9, 7.4 Hz, 2H) 2.10 (dt, J = 13.0, 8.2 Hz, 1H) 2.02-1.90 (m, 2H) 1.83-1.67 (m, 2H), and cis-N1,N3-bis(4-chlorophenyl)cyclopentane-1,3-dicarboxamide: 10.09 (s, 2H) 7.65 (d, J = 8.6 Hz, 4H) 7.34 (d, J = 8.5 Hz, 4H) 3.00 (p, J = 7.4 Hz, 2H) 2.09-1.97 (m, 5H) 1.90-1.73 (m, 1H); ^{13}C NMR (500 MHz, DMSO-d_6) δ ppm 174.44, 138.79, 128.98, 126.92, 121.03, 45.49, 34.38, 30.71; TOF ES+ MS: (M-H) cis-acid: 266.06, trans-acid 266.06 (M-H), and (M+Na) bis-amide: 399.06; HPLC Ret: cis-acid: 5.72 min, trans-acid: 5.77 min, and

bis-amide: 7.58 min; 98% pure. Note: stereochemical assignment based on procedure directly above.

***cis*-methyl 3-((4-chlorophenyl)carbamoyl)cyclohexanecarboxylate.** Method I starting from *cis*-3-(methoxycarbonyl)cyclohexanecarboxylic acid (0.1 g, 0.54 mmol) and 4-chloroaniline (0.07 g, 0.54 mmol) gave cis-methyl 3-((4-chlorophenyl)carbamoyl)cyclohexanecarboxylate as white solid (0.15 g, 94%); column: 30% EtOAc: 70% Hex; ^{1}H NMR (500 MHz, DMSO-d_6) δ ppm 9.98 (s, 1H) 7.62 (d, J = 8.5 Hz, 2H) 7.33 (d, J = 8.5 Hz, 2H) 3.60 (s, 3H) 2.39 (tt, J = 12.3, 3.7 Hz, 2H) 2.01 (d, J = 13.0 Hz, 1H) 1.89 (d, J = 12.5 Hz, 1H) 1.82 (d, J = 8.8 Hz, 1H) 1.82 (d, J = 8.8 Hz, 2H) 1.48 (q, J = 12.6 Hz, 1H) 1.37-1.20 (m, 3H); TOF ES+ MS: (M+Na) 318.09; HPLC Ret: 6.94 min.

***trans*-3-((4-chlorophenyl)carbamoyl)cyclohexanecarboxylic acid & *trans*-N1,N3-bis(4-chlorophenyl)cyclohexane-1,3-dicarboxamide (CCG-263874).** Method I starting from *trans*-cyclohexane-1,3-carboxylic acid (0.1 g, 0.58 mmol) and 4-chloroaniline (0.07 g, 0.54 mmol) gave trans-3-((4-chlorophenyl)carbamoyl)cyclohexanecarboxylic acid (0.09 g, 55%) and trans-N1,N3-bis(4-chlorophenyl)cyclohexane-1,3-dicarboxamide as white solid (0.05 g, 22%); column: 40% EtOAc: Hex; ^{1}H NMR (500 MHz, $CDCl_3$-d) δ ppm trans-3-((4-chlorophenyl)carbamoyl)cyclohexanecarboxylic acid: 12.13 (br. s, 1H) 9.98 (s, 1H) 7.63 (d, J = 8.8 Hz, 2H) 7.33 (d, J = 8.8 Hz, 2H) 2.73 (p, J = 4.7 Hz, 1H) 2.60 (tt, J = 9.5, 4.1 Hz, 1H) 2.55-2.49 (m, 1H) 1.90 (dt, J = 13.9, 4.2 Hz, 1H) 1.86-1.70 (m, 2H) 1.61 (q, J = 5.9 Hz, 2H) 1.55-1.39 (m, 2H), trans-N1,N3-bis(4-chlorophenyl)cyclohexane-1,3-dicarboxamide: 9.99 (s, 2H) 7.66 (d, J = 8.8 Hz, 4H) 7.34 (d, J = 8.8 Hz, 4H) 2.86 (q, J = 5.7 Hz, 2H) 1.89 (t, J = 5.9 Hz, 2H) 1.72-1.1.61 (m, 6H); ^{13}C NMR (500 MHz, DMSO-d_6) δ ppm 174.72, 138.89, 128.90, 126.84, 121.13, 39.88, 30.08, 28.81, 21.75; TOF ES+ MS: (M+H) trans-acid: 280.07, (M+Na) bis-amide: 413.08; HPLC Ret: trans-acid: 6.20 min, bis-amide: 7.84 min; 99% pure. Note: stereochemical assignment ascertained on procedure directly above.

tert-butyl 5-((2,3-dihydrobenzo[b][1,4]dioxin-6-yl)carbamoyl)-3,3-difluoropiperidine-1-carboxylate. Method I starting from 1-(tert-butoxycarbonyl)-5,5-difluoropiperidine-3-carboxylic acid (0.05 g, 0.19 mmol) and 2,3-dihydrobenzo[b][1,4]dioxin-6-amine (0.03 g, 0.19 mmol) gave tert-butyl 5-((2,3-dihydrobenzo[b][1,4]dioxin-6-yl)carbamoyl)-3,3-difluoropiperidine-1-carboxylate as yellow solid (0.07 g, 99%); column: 10% to 15% EtOAc: Hex; ^{1}H NMR (500 MHz, $CDCl_3$-*d*) δ ppm 7.79 (br.s, 1H) 7.16 (br. s., 1H) 6.91 (d, J = 8.7 Hz, 1H) 6.80 (d, J = 8.7, 1H) 4.24 (s, 4H) 4.17 (br. s, 2H) 3.30-3.10 (m, 2H) 2.80-2.75 (m, 1H) 2.51-2.30 (m, 2H) 1.48 (s, 9H); TOF ES+ MS: (M+Na) 421.2; HPLC Ret: 7.35 min.

tert-butyl 5-((3,4-dimethoxyphenyl)carbamoyl)-3,3-difluoropiperidine-1-carboxylate. Method I starting from 1-(tert-butoxycarbonyl)-5,5-difluoropiperidine-3-carboxylic acid (0.05 g, 0.19 mmol) and 3,4-dimethoxyaniline (0.03 g, 0.19 mmol) gave tert-butyl 5-((3,4-dimethoxyphenyl)carbamoyl)-3,3-difluoropiperidine-1-carboxylate as yellow solid (0.07 g, 96%); column: 30% to 50% EtOAc: Hex; ^{1}H NMR (500 MHz, $CDCl_3$-*d*) δ ppm 7.91 (br.s., 1H) 7.35 (br.s, 1H) 7.26 (s, 1H) 6.92 (d, J = 8.6 Hz, 1H) 6.81 (d, J = 8.6, 1H) 4.25-4.05 (m, 2H) 3.87 (2d, J = 1.3 Hz, 6H) 3.34-3.30 (m, 2H) 2.81-2.72 (m, 1H) 2.48-2.30 (m, 2H) 1.48 (s, 9H); TOF ES+ MS: (M+Na) 423.2; HPLC Ret: 6.79 min.

(S)-tert-butyl 3-((4-chlorophenyl)carbamoyl)piperidine-1-carboxylate. Method I starting from (S)-1-(tert-butoxycarbonyl)piperidine-3-carboxylic acid (0.08 g, 0.33 mmol) and 4-chloroaniline (0.05 g, 0.36 mmol) gave (S)-tert-butyl 3-((4-chlorophenyl)carbamoyl)piperidine-1-carboxylate as white solid (0.11 g, 97%); column 20% to 30% EtOAc/Hex. ^{1}H NMR (500 MHz, $CDCl_3$-*d*) δ ppm 8.43 (br. s, 1H) 7.55 (d, J = 8.3 Hz, 2H) 7.29 (d, J = 8.3 Hz, 2H) 3.79-3.59 (m, 2H) 3.58-3.42 (m, 2H) 3.40-3.32 (m, 1H) 2.56-2.46 (m, 1H) 2.21-2.15 (m, 1H) 1.93-1.85 (m, 1H) 1.62-1.60 (m, 1H) 1.46 (s, 9H); TOF ES+ MS: (M+Na) 361.13; HPLC Ret: 7.67 min.

(R)-tert-butyl 3-((4-chlorophenyl)carbamoyl)piperidine-1-carboxylate. Method I starting from (R)-1-(tert-butoxycarbonyl)piperidine-3-carboxylic acid (0.08 g, 0.33 mmol) and 4-chloroaniline (0.05 g, 0.36 mmol) gave (R)-tert-butyl 3-((4-chlorophenyl)carbamoyl)piperidine-1-carboxylate as white solid (0.11 g, 96%); column 20% to 30% EtOAc/Hex. ^{1}H NMR (500 MHz, $CDCl_3$-*d*) δ 8.47 (br. s, 1H) 7.55 (d, J = 8.5 Hz, 2H) 7.29 (d, J = 8.3 Hz, 2H) 3.80-3.30 (m, 5H) 2.51 (s, 1H) 2.14 (s, 1H) 1.88 (s, 1H) 1.66 (s, 1H) 1.47 (s, 9H); TOF ES+ MS: (M+Na) 361.13; HPLC Ret: 7.63 min.

tert-butyl 5-((4-chlorobenzyl)carbamoyl)-3,3-difluoropiperidine-1-carboxylate. Method I starting from 1-(tert-butoxycarbonyl)-5,5-difluoropiperidine-3-carboxylic acid (0.07 g, 0.26 mmol) and (4-chlorophenyl)methanamine (0.04 g, 0.26 mmol) gave tert-butyl 5-((4-chlorobenzyl)carbamoyl)-3,3-difluoropiperidine-1-carboxylate as white solid (0.06 g, 57%); column: 30% to 40% EtOAc/Hex; ^{1}H NMR (500 MHz, $CDCl_3$-*d*) δ 7.30 (d, J = 8.0 Hz, 2H) 7.18 (d, J = 8.1 Hz, 2H) 6.63 (br. s, 1H) 4.45-4.31 (m, 2H) 4.05 (d, J = 13.8 Hz, 2H) 3.32-3.19 (m, 2H) 3.13 (dd, J = 13.9, 9.8 Hz, 1H) 2.62 (s, 1H) 2.38 (s, 1H) 2.26 (s, 1H) 1.43 (s, 9H); TOF ES+ MS: (M+Na) 411.13; HPLC Ret: 6.36 min.

tert-butyl 5-((3-chlorophenyl)carbamoyl)-3,3-difluoropiperidine-1-carboxylate. Method I starting from 1-(tert-butoxycarbonyl)-5,5-difluoropiperidine-3-carboxylic acid (0.07 g, 0.26 mmol) and 3-chloroaniline (0.03 g, 0.26 mmol) gave tert-butyl 5-((3-chlorophenyl)carbamoyl)-3,3-difluoropiperidine-1-carboxylate as white solid (0.06 g, 65%); column: 15% to 30% EtOAc/Hex; ^{1}H NMR (500 MHz, $CDCl_3$-*d*) δ 8.15 (br. s, 1H) 7.71 (s, 1H) 7.36 (d, J = 8.0 Hz, 1H) 7.25 (t, J = 8.1Hz, 1H) 7.10 (d, J = 8.0 Hz, 1H) 4.15-4.01 (m, 2H) 3.38 (br. s, 2H) 2.79 (s, 1H) 2.50 (s, 1H) 2.31 (s, 1H) 1.48 (s, 9H); TOF ES+ MS: (M+Na) 397.11; HPLC Ret: 8.01 min.

tert-butyl 5-((3,4-dichlorophenyl)carbamoyl)-3,3-difluoropiperidine-1-carboxylate. Method I starting from 1-(tert-butoxycarbonyl)-5,5-difluoropiperidine-3-carboxylic acid (0.07 g, 0.26 mmol)

and 3,4-dichloroaniline (0.04 g, 0.26 mmol) gave tert-butyl 5-((3,4-dichlorophenyl)carbamoyl)-3,3-difluoropiperidine-1-carboxylate as yellow solid (0.06 g, 57%); column: 15% to 30% EtOAc/Hex; ^{1}H NMR (500 MHz, $CDCl_3$-*d*) δ 8.39 (br. s, 1H) 7.85 (s, 1H) 7.39-7.34 (m, 1H) 7.28-7.25 (m, 1H) 4.00-3.94 (m, 2H) 3.51 (br. s, 2H) 2.80 (s, 1H) 2.55 (s, 1H) 2.28 (s, 1H) 1.48 (s, 9H); TOF ES+ MS: (M+Na) 431.07; HPLC Ret: 8.42 min.

tert-butyl 5-((3-(((tert-butyldiphenylsilyl)oxy)methyl)-4-chlorophenyl)carbamoyl)-3,3-difluoropiperidine-1-carboxylate. Method I starting from 1-(tert-butoxycarbonyl)-5,5-difluoropiperidine-3-carboxylic acid (0.12 g, 0.45 mmol) and 3-(((tert-butyldiphenylsilyl)oxy)methyl)-4-chloroaniline (0.18 g, 0.45 mmol) gave tert-butyl 5-((3-(((tert-butyldiphenylsilyl)oxy)methyl)-4-chlorophenyl)carbamoyl)-3,3-difluoropiperidine-1-carboxylate as white solid (0.19 g, 66%); column: 15% to 20% EtOAc/Hex; ^{1}H NMR (500 MHz, $CDCl_3$-*d*) δ 8.09 (br. s, 1H) 7.73-7.65 (m, 6H) 7.48-7.36 (m, 6H) 7.28-7.21 (m, 2H) 4.79 (s, 2H) 4.25-4.17 (m, 1H) 3.21-3.15 (m, 2H) 2.85-2.78 (m, 1H) 2.40-2.30 (m, 2H) 1.48 (s, 9H) 1.14 (s, 9H); TOF ES+ MS: (M+H) 643.26; HPLC Ret: >13 min.

tert-butyl 3-((4-chlorophenyl)carbamoyl)-5,5-difluoro-3-methylpiperidine-1-carboxylate. Method I starting from 1-(tert-butoxycarbonyl)-5,5-difluoro-3-methylpiperidine-3-carboxylic acid (0.07 g, 0.25 mmol) and 4-chloroaniline (0.03 g, 0.25 mmol) gave tert-butyl 3-((4-chlorophenyl)carbamoyl)-5,5-difluoro-3-methylpiperidine-1-carboxylate as yellow solid (0.07 g, 72%); column: 15% to 20% EtOAc/Hex; ^{1}H NMR (500 MHz, $CDCl_3$-*d*) δ 9.10 (br. s, 1H) 7.62 (d, J = 8.5 Hz, 2H) 7.25 (d, J = 8.1 Hz, 2H) 4.56 (br. s, 1H) 4.27 (br. s, 1H) 3.12 (br. s, 2H) 1.74-1.61 (m, 1H) 1.48 (s, 9H) 1.31 (s, 3H); TOF ES+ MS: (M+Na) 395.15; HPLC Ret: 8.17 min.

tert-butyl 5-((4-chloropyridin-2-yl)carbamoyl)-3,3-difluoropiperidine-1-carboxylate. Method I starting from 1-(tert-butoxycarbonyl)-5,5-difluoropiperidine-3-carboxylic acid (0.06 g, 0.23 mmol) and 4-chloropyridin-2-amine (0.03 g, 0.23 mmol) gave tert-butyl 5-((4-chloropyridin-2-

yl)carbamoyl)-3,3-difluoropiperidine-1-carboxylate as colorless oil (0.04 g, 47%); column: 10% to 25% EtOAc/Hex; reaction done at 85 °C; ^{1}H NMR (500 MHz, $CDCl_3$-*d*) δ 8.47 (br. s, 1H) 8.26 (s, 1H) 8.18 (d, J = 5.4 Hz, 1H) 7.07 (d, J = 5.3 Hz, 1H) 4.39-4.18 (m, 2H) 3.19-2.95 (m, 2H) 2.81 (s, 1H) 2.45-2.21 (s, 2H) 1.48 (s, 9H); TOF ES+ MS: (M+Na) 398.11; HPLC Ret: 7.10 min.

tert-butyl 5-((5-chloropyridin-3-yl)carbamoyl)-3,3-difluoropiperidine-1-carboxylate. Method I starting from 1-(tert-butoxycarbonyl)-5,5-difluoropiperidine-3-carboxylic acid (0.06 g, 0.23 mmol) and 5-chloropyridin-3-amine (0.03 g, 0.23 mmol) gave tert-butyl 5-((5-chloropyridin-3-yl)carbamoyl)-3,3-difluoropiperidine-1-carboxylate as colorless oil (0.04 g, 49%); column: 10% to 35% EtOAc/Hex; reaction done at 55 °C; ^{1}H NMR (500 MHz, $CDCl_3$-*d*) δ 9.05 (br. s, 1H) 8.49 (s, 1H) 8.33 (d, J = 15.2 Hz, 2H) 3.94 (s, 2H) 3.48 (s, 2H) 2.88 (s, 1H) 2.56 (s, 1H) 2.29 (s, 1H) 1.48 (s, 9H); TOF ES+ MS: (M+H) 376.12; HPLC Ret: 7.13 min.

tert-butyl 5-((2-chloropyridin-4-yl)carbamoyl)-3,3-difluoropiperidine-1-carboxylate. Method I starting from 1-(tert-butoxycarbonyl)-5,5-difluoropiperidine-3-carboxylic acid (0.06 g, 0.23 mmol) and 2-chloropyridin-4-amine (0.03 g, 0.23 mmol) gave tert-butyl 5-((2-chloropyridin-4-yl)carbamoyl)-3,3-difluoropiperidine-1-carboxylate as yellow oil (0.01 g, 16%); column: 35% EtOAc/Hex; reaction done at 85 °C; ^{1}H NMR (500 MHz, $CDCl_3$-*d*) δ 9.37 (br. s, 1H) 8.26 (d, J = 5.6 Hz, 1H) 7.71 (s, 1H) 7.41 (dd, J = 5.7, 1.8 Hz, 1H) 3.98 (s, 2H) 3.41 (s, 2H) 2.88 (s, 1H) 2.52 (s, 1H) 2.29 (s, 1H) 1.48 (s, 9H); TOF ES+ MS: (M+H) 376.12; HPLC Ret: 7.26 min.

tert-butyl 5-((6-chloropyridin-2-yl)carbamoyl)-3,3-difluoropiperidine-1-carboxylate. Method I starting from 1-(tert-butoxycarbonyl)-5,5-difluoropiperidine-3-carboxylic acid (0.06 g, 0.23 mmol) and 6-chloropyridin-2-amine (0.03 g, 0.23 mmol) gave tert-butyl 5-((6-chloropyridin-2-yl)carbamoyl)-3,3-difluoropiperidine-1-carboxylate as colorless oil (0.04 g, 44%); column: 10-15% EtOAc/Hex; reaction done at 85 °C; ^{1}H NMR (500 MHz, $CDCl_3$-*d*) δ 8.44 (br. s, 1H) 8.11-

8.05 (m, 1H) 7.72-7.65 (s, 1H) 7.12-7.06 (m, 1H) 4.45-4.18 (m, 2H) 3.09 (s, 2H) 2.80 (s, 1H) 2.39 (s, 1H) 2.32-2.22 (m, 1H) 1.48 (s, 9H); TOF ES+ MS: (M+Na) 398.10; HPLC Ret: 7.71 min.

tert-butyl 5-((4-chloro-3-(prop-2-yn-1-yloxy)phenyl)carbamoyl)-3,3-difluoropiperidine-1-carboxylate. Method J followed by Method I starting from tert-butyl (4-chloro-3-(prop-2-yn-1-yloxy)phenyl)carbamate (0.11 g, 0.40 mmol) and 1-(tert-butoxycarbonyl)-5,5-difluoropiperidine-3-carboxylic acid (0.11 g, 0.40 mmol) gave tert-butyl 5-((4-chloro-3-(prop-2-yn-1-yloxy)phenyl)carbamoyl)-3,3-difluoropiperidine-1-carboxylate (0.1 g, 58%) as white solid; column: 15% to 20% EtOAc/Hex; ^{1}H NMR (500 MHz, $CDCl_3$-*d*) δ ppm 8.40 (br. s, 1H) 7.65-7.60 (m, 1H) 7.29 (d, J = 13.8 Hz, 1H) 7.01 (d, J = 8.6 Hz, 1H) 4.78 (d, J = 2.6 Hz, 2H) 4.11-4.05 (m, 1H) 3.45-3.29 (m, 2H) 2.85-2.79 (m, 1H) 2.57 (d, J = 3.0 Hz, 1H) 2.56-2.30 (m, 2H) 1.49 (s, 9H); HPLC Ret: 7.88 min.

tert-butyl (3-((4-chlorophenyl)carbamoyl)phenyl)carbamate. In a 25 mL round bottomed flask, 3-((tert-butoxycarbonyl)amino)benzoic acid (0.2 g, 0.84 mmol) was dissolved in DMF (4 mL) and HATU (0.39 g, 1.01 mmol), 4-chloroaniline (0.13 g, 1.01 mmol), and DIPEA (0.22 g, 0.3 mL, 1.69 mmol) were added. The reaction was stirred at 25 °C for 1 hr and then heated at 150 °C for 30 min. The reaction was cooled to room temperature and then concentrated in vacuo. The subsequent oil was subjected to silica gel chromatography eluting with 30% EtOAc: 70% Hex. The fractions containing product were concentrated in vacuo to produce white solid. Yield=70%. ^{1}H NMR (500 MHz, $CDCl_3$-*d*) δ ppm 7.95 (t, J = 1.9 Hz, 1H) 7.87 (br. s., 1H) 7.60 (d, J = 8.0 Hz, 2H) 7.56-7.47 (m, 2H) 7.40 (t, J = 7.9 Hz, 1H) 7.33 (d, J = 8.0 Hz, 2H) 6.62 (s, 1H) 1.54 (s, 9H); TOF ES+ MS: (M+H) 247.1; HPLC Ret: 7.74 min.

tert-butyl (5-((4-chlorophenyl)carbamoyl)pyridin-3-yl)carbamate. 5-((tert-butoxycarbonyl)amino)nicotinate, Et_3NH+ (0.34 g, 1.00 mmol) was dissolved in DMF (4 mL) and HATU (0.76 g, 2.00 mmol), 4-chloroaniline (0.14 g, 1.10 mmol), and DIPEA (0.32 g, 0.44 mL,

2.50 mmol) were added. The reaction was stirred at 25 °C for 1 hr and then at 150 °C for 2 hr. Brine (20 mL) was added, the product was extracted with EtOAc (3 x 15 mL), and the organic layers combined, washed with dilute HCl (3 x 15 mL) and $NaHCO_3$ (3 x 15 mL), dried with $MgSO_4$, and concentrated in vacuo. The subsequent oil was subjected to silica gel chromatography eluting with 100% EtOAc. The fractions containing product were concentrated in vacuo to produce colorless oil. Yield=20.2%. ^{1}H NMR (500 MHz, DMSO-d_6) δ ppm 10.55 (s, 1H) 9.82 (s, 1H) 8.73 (dd, J = 15.6, 2.2 Hz, 1H) 8.39 (t, J = 2.2 Hz, 1H) 7.79 (d, J = 10 Hz, 2H) 7.43 (d, J = 10 Hz, 2H) 1.50 (s, 9H); TOF ES+ MS: (M+H) 348.1; HPLC Ret: 6.63 min.

tert-butyl 3-((4-chlorophenyl)carbamoyl)-5,6-dihydropyridine-1(2H)-carboxylate. In a 25 mL round bottomed flask, 1-(tert-butoxycarbonyl)-1,2,5,6-tetrahydropyridine-3-carboxylic acid (0.12 g, 0.53 mmol) was dissolved in THF (2 mL) and EDC (0.15 g, 0.8 mmol), DMAP (0.03 g, 0.26 mmol), 4-chloroaniline (0.08 g, 0.63 mmol), and DIPEA (0.14 g, 0.18 mL, 1.06 mmol) were added. The reaction was stirred at 25 °C for 5 hr and the reaction was concentrated in vacuo. The product was partitioned between H_2O and DCM, extracted with DCM (3 x 20 mL), washed with sat. $NaHCO_3$ (2 x 20 mL), 10% citric acid (2 x 20 mL), and brine (3 x 20 mL), dried with $MgSO_4$, and concentrated in vacuo. The product was crystalized with EtOAc/Hex to afford white powder. Yield=79%. ^{1}H NMR (500 MHz, $CDCl_3$-*d*) δ ppm 7.49 (d, J = 8.5 Hz, 2H) 7.30 (d, J = 8.5 Hz, 2H) 6.69 (br. s, 1H) 4.23 (br. s, 2H) 3.53 (t, J = 5.8 Hz, 2H) 2.34 (br. s., 2H) 1.49 (s, 9H); QTOF ES+ MS: (M+H) 337.13.

tert-butyl (*cis*-3-(4-chlorobenzamido)cyclopentyl)carbamate. Method I starting from *cis*-(t-butyl-3-aminocyclopentyl)carbamate, HCl (0.2 g, 0.85 mmol) and 4-chlorobenzoic acid (0.13 g, 0.85 mmol) gave tert-butyl (cis-3-(4-chlorobenzamido)cyclopentyl)carbamate as white solid (0.23 g, 80%); column: 50% to 60% EtOAc:Hex; ^{1}H NMR (500 MHz, $CDCl_3$-*d*) δ ppm 8.41 (d, J = 7.4 Hz, 1H) 7.85 (d, J = 8.5 Hz, 2H) 7.53 (d, J = 8.4 Hz, 2H) 6.92 (d, J = 7.5 Hz, 1H) 4.20 (h, J = 7.4 Hz, 1H) 3.78 (q, J = 7.4 Hz, 1H) 2.22 (dt, J = 14.3, 7.6 Hz, 1H) 1.87 (dq, J = 12.6, 7.0, 6.4

Hz, 1H) 1.79 (dq, J = 14.3, 7.5, 6.6 Hz, 1H) 1.68-1.50 (m, 2H) 1.43 (dd, J = 13.6, 7.0 Hz, 1H) 1.38 (s, 9H); TOF ES+ MS: (M+H) 339.15; HPLC Ret: 6.88 min.

tert-butyl (*trans*-3-(4-chlorobenzamido)cyclopentyl)carbamate. Method I starting from *trans*-t-butyl-(3-aminocyclopentyl)carbamate (0.08 g, 0.37 mmol) and 4-chlorobenzoic acid (0.06 g, 0.37 mmol) gave tert-butyl (trans-3-(4-chlorobenzamido)cyclopentyl)carbamate as white solid (0.12 g, 97%); column: 40% to 80% EtOAc:Hex; ^{1}H NMR (500 MHz, DMSO-d_6) δ ppm 8.40 (d, J = 7.3 Hz, 1H) 7.86 (d, J = 8.2 Hz, 2H) 7.52 (d, J = 8.1 Hz, 2H) 6.91 (d, J = 7.4 Hz, 1H) 4.33 (h, J = 7.1 Hz, 1H) 3.96 (q, J = 7.0 Hz, 1H) 2.06-1.92 (m, 2H) 1.78 (tt, J = 12.1, 6.8 Hz, 2H) 1.49 (dd, J = 12.1, 7.9 Hz, 1H) 1.43 (dd, J = 17.7, 10.0 Hz, 1H) 1.38 (s, 9H); TOF ES+ MS: (M+Na) 361.13; HPLC Ret: 6.76 min.

tert-butyl (*trans*-3-(4-chlorobenzamido)cyclohexyl)carbamate & tert-butyl (*cis*-3-(4-chlorobenzamido)cyclohexyl)carbamate. Method I starting from tert-butyl (3-aminocyclohexyl)carbamate (0.18 g, 0.82 mmol) and 4-chlorobenzoic acid (0.13 g, 0.82 mmol) gave a mixture tert-butyl (trans-3-(4-chlorobenzamido)cyclohexyl)carbamate (0.06 g, 40%) & tert-butyl (cis-3-(4-chlorobenzamido)cyclohexyl)carbamate (0.04 g, 29%) as white solid; column: 25% to 40% EtOAc:Hex; ^{1}H NMR (500 MHz, $CDCl_3$-*d*) δ ppm trans: 8.20 (d, J = 7.5 Hz, 1H) 7.86 (d, J = 8.2 Hz, 2H) 7.52 (d, J = 8.2 Hz, 2H) 6.86 (d, J = 7.7 Hz, 1H) 4.19-4.06 (m, 1H) 3.80-3.74 (m, 1H) 1.69-1.50 (m, 6H) 1.48-1.37 (m, 11H), cis: 8.34 (d, J = 7.9 Hz, 1H) 7.86 (d, J = 8.2 Hz, 2H) 7.52 (d, J = 8.2 Hz, 2H) 6.84 (d, J = 8.1 Hz, 1H) 3.82-3.73 (m, 1H) 3.35-3.22 (m, 1H) 1.94 (d, J = 11.9 Hz, 1H) 1.74 (t, J = 16.0, 3H) 1.38 (s, 9H) 1.33-1.15 (m, 3H) 1.11-1.03 (m, 1H); TOF ES+ MS: (M+Na) trans: 375.15, (M+Na) cis: 375.15; HPLC Ret: trans: 7.08 min, cis: 6.93 min. Note: Amide coupling was performed with tert-butyl (*cis*-3-aminocyclohexyl)carbamate purchased from vendor to confirm assignment of the mixture.

tert-butyl (3-(4-chlorobenzamido)-4-methylphenyl)carbamate. Method I starting from t-butyl-(3-amino-4-methylphenyl)carbamate (0.07 g, 0.32 mmol) and 4-chlorobenzoic acid (0.05 g, 0.32 mmol) gave tert-butyl (3-(4-chlorobenzamido)-4-methylphenyl)carbamate as white solid (0.09 g, 76%); column: 20% EtOAc: Hex. ^{1}H NMR (500 MHz, $CDCl_3$-*d*) δ ppm 7.99 (d, J = 7.8 Hz, 2H) 7.60 (d, J = 7.8 Hz, 2H) 7.51 (br. s, 1H) 7.21 (dd, J = 8.3, 2.2 Hz, 1H) 7.12 (d, J = 8.4 Hz, 1H) 2.13 (s, 3H) 1.47 (s, 9H); TOF ES+ MS: (M+Na) 383.1; HPLC Ret: 7.66 min.

***cis*-methyl 3-(3-(furan-2-yl)benzamido)cyclohexanecarboxylate.** In a dry 25 mL round bottomed flask *cis*-methyl 3-(((benzyloxy)carbonyl)amino)cyclohexanecarboxylate (0.88 g, 3.00 mmol) was dissolved in MeOH (8 mL) and the solvent was degassed. Pd/C (10%, Degussa) (0.16 g, 0.15 mmol) was added and the reaction proceeded at 25 °C for 12 hr under balloon of H_2. The catalyst was filtered through a pad of Celite and the filtrate was concentrated producing yellow oil. 3-(furan-2-yl)benzoic acid (0.24 g, 1.27 mmol) was dissolved in DMF (4 mL) and *cis*-methyl 3-aminocyclohexanecarboxylate (0.2 g, 1.27 mmol), HATU (0.58 g, 1.53 mmol), and N-methylmorpholine (0.52 g, 0.56 mL, 5.09 mmol) were added. The reaction proceeded at 25 °C for 16 hr. Brine (20 mL) was added and the product was extracted with EtOAc (3 x 20 mL). The combined organic layers were washed with sat. $NaHCO_3$ (2 x 20 mL), dilute HCl (2 x 20 mL), dried with $MgSO_4$, and evaporated in vacuo. The subsequent oil was subjected to silica gel chromatography eluting with 30% EtOAc: 70% Hex. The fractions containing product were concentrated in vacuo to produce colorless oil. Yield=21% (2 steps). ^{1}H NMR (500 MHz, $CDCl_3$-*d*) δ ppm 8.48 (d, J = 8.4 Hz, 1H) 8.15 (s, 1H) 7.93-7.70 (m, 3H) 7.51-7.43 (m, 1H) 7.14 (d, J = 3.4 Hz, 1H) 6.56-6.44 (m, 1H) 4.12-3.94 (m, 1H) 3.68 (s, 3H) 3.47-3.35 (m, 1H) 2.54 (td, J = 11.3, 6.1 Hz, 1H) 2.41-2.27 (m, 2H) 1.94-1.85 (m, 1H) 1.55-1.34 (m, 4H); HPLC Ret: 6.42 min.

***cis*-3-(3-(furan-2-yl)benzamido)cyclohexanecarboxylic acid.** Method G starting from *cis*-methyl 3-(3-(furan-2-yl)benzamido)cyclohexanecarboxylate (0.09 g, 0.27 mmol) gave cis-3-(3-(furan-2-yl)benzamido)cyclohexanecarboxylic acid as white solid (0.04, 48%); ^{1}H NMR (500

MHz, DMSO-d_6) δ ppm 11.98 (br. s., 1H) 8.76-8.71 (m, 1H) 8.48 (d, J = 7.9 Hz, 1H) 8.14 (s, 1H) 7.86-7.70 (m, 2H) 7.54-7.46 (m, 1H) 7.02 (d, J = 3.4 Hz, 1H) 6.63 (d, J = 2.6 Hz, 1H) 2.39-2.31 (m, 1H) 2.09-2.02 (m, 1H) 1.90-1.76 (m, 4H) 1.47-1.14 (m, 4H); TOF ES+ MS: (M+H) 314.1; HPLC Ret: 6.05 min.

***cis* tert-butyl (3-(3-(furan-2-yl)benzamido)cyclohexyl)carbamate.** Method I starting from cis t-butyl-(3-aminocyclohexyl)carbamate (0.1 g, 0.47 mmol) and 3-(furan-2-yl)benzoic acid (0.09 g, 0.47 mmol) gave cis tert-butyl (3-(3-(furan-2-yl)benzamido)cyclohexyl)carbamate as white solid (0.1 g, 53%); column: 2.5% MeOH/DCM then crystalized from DCM/MeOH; ^{1}H NMR (500 MHz, DMSO-d_6) δ ppm 8.38 (d, J = 8.0 Hz, 1H) 8.14 (s, 1H) 7.86-7.77 (m, 2H) 7.74 (d , J = 7.8 Hz, 1H) 7.50 (t, J = 7.8 Hz, 1H) 7.02 (d, J = 3.3 Hz, 1H) 6.86 (d, J = 8.1 Hz, 1H) 6.63 (dt, J = 3.1, 1.4 Hz, 1H) 3.88-3.73 (m, 1H) 3.34-3.24 (m, 1H) 1.97 (d, J = 11.8 Hz, 1H) 1.76 (dd, J = 24.9, 12.2, 3H) 1.38 (s, 9H) 1.37-1.20 (m, 3H) 1.08 (q, J = 12.2 Hz, 1H); TOF ES+ MS: (M+Na) 385.21; HPLC Ret: 7.21 min.

***cis* tert-butyl (3-(2,3-dihydrobenzo[b][1,4]dioxine-6-carboxamido)cyclohexyl)carbamate.** Method I starting from cis t-butyl-(3-aminocyclohexyl)carbamate (0.01 g, 0.47 mmol) and 2,3-dihydrobenzo[b][1,4]dioxine-6-carboxylic acid (0.08 g, 0.47 mmol) gave c cis tert-butyl (3-(2,3-dihydrobenzo[b][1,4]dioxine-6-carboxamido)cyclohexyl)carbamate as white solid (0.1 g, 56%); column: 2.5% MeOH/DCM then crystalized from DCM/MeOH; ^{1}H NMR (500 MHz, DMSO-d_6) δ ppm 8.07 (d, J = 7.9 Hz, 1H) 7.40-7.33 (m, 2H) 6.89 (d , J = 8.4 Hz, 1H) 6.82 (d, J = 8.1 Hz, 1H) 4.27 (q, J = 5.1 Hz, 4H) 3.79-3.71 (m, 1H) 3.32-3.25 (m, 1H) 1.91 (d, J = 11.8 Hz, 1H) 1.71 (d, J = 10.7, 3H) 1.38 (s, 9H) 1.37-1.17 (m, 3H) 1.05 (q, J = 12.1 Hz, 1H); TOF ES+ MS: (M+Na) 377.21; HPLC Ret: 6.40 min. Note: Cis assignment was made based off tert-butyl (cis-3-(4-chlorobenzamido)cyclohexyl)carbamate.

methyl 5-(3-(furan-2-yl)benzamido)-2-methylbenzoate. Method I starting from methyl 5-amino-2-methylbenzoate (0.04 g, 0.27 mmol) and 3-(furan-2-yl)benzoic acid (0.05 g, 0.27 mmol) gave methyl 5-(3-(furan-2-yl)benzamido)-2-methylbenzoate as white solid (0.08 g, 84%); column: 20% to 30% EtOAc: Hex; ^{1}H NMR (500 MHz, $CDCl_3$-*d*) δ ppm 8.18-8.14 (m, 1H) 8.13-8.08 (m, 1H) 7.90-7.82 (m, 3H) 7.75 (dp, J = 7.7, 1.0 Hz, 1H) 7.55-7.48 (m, 2H) 7.30 (d, J = 12.1 Hz, 1H) 6.77 (dt, J = 3.4, 0.9 Hz, 1H) 6.52 (dt, J = 3.1, 1.3 Hz, 1H) 3.91 (s, 3H) 2.60 (s, 3H); TOF ES+ MS: (M+H) 336.1; HPLC Ret: 7.79 min.

methyl 1-(5,6-difluoro-1H-indole-2-carbonyl)-5,5-difluoropiperidine-3-carboxylate. Method J followed by Method I starting from 1-tert-butyl 3-methyl 5,5-difluoropiperidine-1,3-dicarboxylate (0.15 g, 0.65 mmol) and 5,6-difluoro-1H-indole-2-carboxylic acid (0.13 g, 0.65 mmol) gave methyl 1-(5,6-difluoro-1H-indole-2-carbonyl)-5,5-difluoropiperidine-3-carboxylate (0.14 g, 60% (2 steps)) as white solid; column: 40% EtOAc: 60% Hex; ^{1}H NMR (500 MHz, $CDCl_3$-*d*) δ ppm 9.41 (br. s, 1H) 7.40 (dd, J = 10.3, 7.7 Hz, 1H) 7.26 (s, 1H) 7.21 (dd, J = 10.3, 6.6 Hz, 1H) 6.87-6.82 (m, 1H) 4.79-4.65 (m, 2H) 3.79 (s, 3H) 3.49 (dd, J = 27.0, 13.9 Hz, 1H) 3.40-3.19 (m, 1H) 2.98 (tt, J = 10.5, 4.4 Hz, 1H) 2.59 (d, J = 11.7 Hz, 1H) 2.30-2.20 (m, 1H); QTOF ES+ MS: (M+H) 359.20; HPLC Ret: 6.83 min.

methyl 5,5-difluoro-1-(5-(trifluoromethoxy)-1H-indole-2-carbonyl)piperidine-3-carboxylate. Method J followed by Method I starting from 1-tert-butyl 3-methyl 5,5-difluoropiperidine-1,3-dicarboxylate (0.15 g, 0.65 mmol) and 5-(trifluoromethoxy)-1H-indole-2-carboxylic acid (0.16 g, 0.65 mmol) gave methyl 5,5-difluoro-1-(5-(trifluoromethoxy)-1H-indole-2-carbonyl)piperidine-3-carboxylate (0.17 g, 64% (2 steps)) as yellow solid; column: 35% EtOAc: 65% Hex; ^{1}H NMR (500 MHz, $CDCl_3$-*d*) δ ppm 9.39 (br. s, 1H) 7.54 (s, 1H) 7.42 (d, J = 8.9 Hz, 1H) 7.18 (dd, J = 8.9, 2.2 Hz, 1H) 6.92-6.87 (m, 1H) 4.80-4.60 (m, 2H) 3.78 (s, 3H) 3.49 (dd, J = 27.0, 13.9 Hz, 1H) 3.45-3.17 (m, 1H) 2.98 (tt, J = 10.5, 4.5 Hz, 1H) 2.59 (d, J = 11.2 Hz, 1H) 2.30-2.20 (m, 1H); QTOF ES+ MS: (M+H) 307.10; HPLC Ret: 7.39 min.

methyl 5,5-difluoro-1-(3-fluoro-5-(pyridin-4-yl)benzoyl)piperidine-3-carboxylate. Method J followed by Method I starting from 1-tert-butyl 3-methyl 5,5-difluoropiperidine-1,3-dicarboxylate (0.39 g, 1.79 mmol) and 3-fluoro-5-(pyridin-4-yl)benzoic acid (0.39 g, 1.79 mmol) gave methyl 5,5-difluoro-1-(3-fluoro-5-(pyridin-4-yl)benzoyl)piperidine-3-carboxylate (0.65 g, 96% (2 steps)) as yellow solid; column: 80% EtOAc: 20% Hex; ^{1}H NMR (500 MHz, DMSO-d_6) δ ppm 8.80-8.66 (m, 2H) 7.95 (s, 1H) 7.86 (d, J = 9.7 Hz, 1H) 7.84-7.77 (m, 2H) 7.72 (br. s, 1H) 7.45-7.36 (m, 1H) 4.58 (br. s, 1H) 4.26 (br. s, 1H) 3.70 (br. s, 1H) 3.56 (br. s, 2H) 3.02 (br. s, 1H) 2.89 (s, 3H) 2.47-2.30 (m, 1H); QTOF ES+ MS: (M+H) 379.13; HPLC Ret: 4.73 min.

5,5-difluoro-1-(3-fluoro-5-(pyridin-4-yl)benzoyl)piperidine-3-carboxylic acid. Method G starting from methyl 5,5-difluoro-1-(3-fluoro-5-(pyridin-4-yl)benzoyl)piperidine-3-carboxylate (0.7 g, 1.72 mmol) gave 5,5-difluoro-1-(3-fluoro-5-(pyridin-4-yl)benzoyl)piperidine-3-carboxylic acid (0.35 g, 56%); filtered solid that formed after acidification; crystalized with EtOH; ^{1}H NMR (500 MHz, DMSO-d_6) δ ppm 13.50 (br. s, 1H) 8.80-8.66 (m, 2H) 7.95 (s, 1H) 7.86 (d, J = 9.7 Hz, 1H) 7.84-7.77 (m, 2H) 7.72 (br. s, 1H) 7.45-7.36 (m, 1H) 4.58 (br. s, 1H) 4.26 (br. s, 1H) 3.70 (br. s, 1H) 3.56 (br. s, 2H) 3.02 (br. s, 1H) 2.47-2.30 (m, 1H); QTOF ES+ MS: (M+H) 365.1; HPLC Ret: 2.10 min.

1-(3-(furan-2-yl)benzoyl)-1,2,5,6-tetrahydropyridine-3-carboxylic acid. Method M followed by Method N starting from 3-(furan-2-yl)benzoic acid (0.1 g, 0.53 mmol) and 1,2,5,6-tetrahydropyridine-3-carboxylic acid, HBr (0.12, 0.59 mmol) gave 1-(3-(furan-2-yl)benzoyl)-1,2,5,6-tetrahydropyridine-3-carboxylic acid as yellow solid (0.08 g, 47% (2 steps)); column: 2.5% MeOH/DCM; ^{1}H NMR (500 MHz, $CDCl_3$-d) δ ppm 7.73 (d, J = 6.8 Hz, 1H) 7.49-7.42 (m, 2H) 7.32-7.19 (m, 2H) 6.69 (d, J = 3.4 Hz, 1H) 6.48 (dd, J = 3.4, 1.8 Hz, 1H) 4.47 (br. s, 1H) 4.18 (br. s, 1H) 3.85 (br. s, 1H) 3.51 (br. s, H) 2.51-2.35 (m, 2H); QTOF ES- MS: (M-H) 296.09; HPLC Ret: 5.66 min.

1-(3-fluoro-5-(pyridin-4-yl)benzoyl)-1,2,5,6-tetrahydropyridine-3-carboxylic acid. Method M followed by Method N starting from 3-fluoro-5-(pyridin-4-yl)benzoic acid (0.1 g, 0.47 mmol) and 1,2,5,6-tetrahydropyridine-3-carboxylic acid, HBr (0.1, 0.49 mmol) gave 1-(3-fluoro-5-(pyridin-4-yl)benzoyl)-1,2,5,6-tetrahydropyridine-3-carboxylic acid as yellow solid (0.07 g, 45% (2 steps)); column: 8% to 10% MeOH: DCM; ^{1}H NMR (500 MHz, DMSO-d_6) δ ppm 12.65 (br. s, 1H) 8.67 (d, J = 7.8 Hz, 2H) 7.88-7.78 (m, 2H) 7.72 (s, 1H) 7.41 (d, J = 8.3 Hz, 1H) 7.00 (s, 1H) 5.76 (d, J = 1 Hz, 1H) 4.27 (br. s, 1H) 4.05 (br. s, 1H) 3.72 (br. s, 1H) 3.39 (br. s, 1H) 2.42-2.33 (m, 2H); QTOF ES+ MS: (M+H) 327.11; HPLC Ret: 3.90 min.

N-(*trans*-3-((4-chlorophenyl)carbamoyl)cyclohexyl)-3-(furan-2-yl)benzamide. (CCG-257863) Method J followed by Method I starting from tert-butyl (trans-3-((4-chlorophenyl)carbamoyl)cyclohexyl)carbamate (0.14 g, 0.40 mmol) and 3-(furan-2-yl)benzoic acid (0.08 g, 0.4 mmol) gave N-(trans-3-((4-chlorophenyl)carbamoyl)cyclohexyl)-3-(furan-2-yl)benzamide (0.07 g, 44% (2 steps)) as white solid; column: 50% EtOAc: 50% Hex; ^{1}H NMR (500 MHz, DMSO-d_6) δ ppm 9.89 (s, 1H) 8.18-8.12 (m, 2H) 7.87-7.74 (m, 3H) 7.64 (d, J = 8.9 Hz, 2H) 7.51 (t, J = 7.7 Hz, 1H) 7.34 (d, J = 8.8 Hz, 2H) 7.04 (d, J = 3.4 Hz, 1H) 6.64 (dd, J = 3.4, 1.8 Hz, 1H) 4.25-4.19 (m, 1H) 2.82-2.77 (m, 1H) 1.88 (t, 5.8 Hz, 2H) 1.72-1.59 (m, 6H); ^{13}C NMR (500 MHz, DMSO-d_6) δ ppm 174.45, 166.21, 152.95, 143.69, 138.80, 136.16, 130.70, 129.21, 128.94, 126.90, 126.27, 122.76, 121.22, 112.63, 109.98, 107.00, 45.49, 40.42, 33.06, 30.57, 28.65, 20.98; TOF ES+ MS: (M+H) 423.1; HPLC Ret: 7.57 min; 98 % pure.

N-(*cis*-3-((4-chlorophenyl)carbamoyl)cyclopentyl)-3-(furan-2-yl)benzamide. (CCG-257942). Method J followed by Method I starting from tert-butyl (*cis*-3-((4-chlorophenyl)carbamoyl)cyclopentyl)carbamate (0.36 g, 1.05 mmol) and 3-(furan-2-yl)benzoic acid (0.19 g, 1.02 mmol) gave N-(cis-3-((4-chlorophenyl)carbamoyl)cyclopentyl)-3-(furan-2-yl)benzamide (0.29 g, 69% (2 steps)) as white solid; the solid was washed with EtOAc; ^{1}H NMR (500 MHz, DMSO-d_6) δ ppm 10.13 (s, 1H) 8.63 (d, J = 7.5 Hz, 1H) 8.21-8.18 (m, 1H) 7.87-7.74

(m, 3H) 7.68 (d, J = 8.3 Hz, 2H) 7.52 (t, J = 7.6 Hz, 1H) 7.36 (d, J = 8.4 Hz, 2H) 7.03 (d, J = 3.4 Hz, 1H) 6.64 (dd, J = 3.4, 1.8 Hz, 1H) 4.42-4.32 (m, 1H) 2.95 (p, J = 7.7 Hz, 1H) 2.24 (dt, J = 14.1, 7.1 Hz, 1H) 2.09-1.85 (m, 3H) 1.79-1.71 (m, 1H); ^{13}C NMR (500 MHz, DMSO-d_6) δ ppm 174.79, 165.76, 152.95, 143.67, 138.68, 135.67, 130.78, 129.35, 129.01, 127.11, 126.67, 126.28, 122.53, 121.20, 112.61, 106.94, 51.49, 44.00, 36.51, 32.31, 28.02; TOF ES+ MS: (M+H) 409.1; HPLC Ret: 7.75 min; 100 % pure.

N-(*trans*-3-((4-chlorophenyl)carbamoyl)cyclopentyl)-3-(furan-2-yl)benzamide (CCG-258452). Method J followed by Method I starting from tert-butyl (trans-3-((4-chlorophenyl)carbamoyl)cyclopentyl)carbamate (0.18 g, 0.52 mmol) and 3-(furan-2-yl)benzoic acid (0.11 g, 0.52 mmol) gave N-(trans-3-((4-chlorophenyl)carbamoyl)cyclopentyl)-3-(furan-2-yl)benzamide (0.07 g, 29% (2 steps)) as white solid; column: 2% MeOH: 98% DCM; ^{1}H NMR (500 MHz, DMSO-d_6) δ ppm 10.04 (s, 1H) 8.46 (d, J = 6.9 Hz, 1H) 8.15 (t, J = 1.8 Hz, 1H) 7.87-7.78 (m, 2H) 7.76 (dt, J = 7.8, 1.3 Hz, 1H) 7.65 (d, J = 8.4 Hz, 2H) 7.51 (t, J = 7.8 Hz, 1H) 7.35 (d, J = 8.5 Hz, 2H) 7.04 (d, J = 3.3 Hz, 1H) 6.64 (dd, J = 3.4, 1.8 Hz, 1H) 4.39 (h, J = 6.7 Hz, 1H) 3.04 (p, J = 7.8 Hz, 1H) 2.17-2.01 (m, 3H) 1.91 (ddd, J = 13.1, 8.9, 5.8 Hz, 1H) 1.79 (dq, J = 11.7, 7.1 Hz, 1H) 1.70 (ddt, J = 14.0, 11.9, 4.8 Hz, 1H); ^{13}C NMR (500 MHz, DMSO-d_6) δ ppm 174.57, 166.13, 152.93, 143.70, 138.79, 135.87, 130.73, 129.28, 128.99, 126.94, 126.77, 126.30, 122.62, 121.12, 112.64, 107.00, 51.51, 44.01, 36.57, 32.44, 28.88; TOF ES+ MS: (M+H) 409.13; HPLC Ret: 7.30 min; 98 % pure.

N-(*cis*-3-(4-chlorobenzamido)cyclopentyl)-3-(furan-2-yl)benzamide. (CCG-263875). Method J followed by Method I starting from tert-butyl (cis-3-(4-chlorobenzamido)cyclopentyl)carbamate (0.04 g, 0.22 mmol) and 3-(furan-2-yl)benzoic acid (0.04 g, 0.22 mmol) gave N-(cis-3-(4-chlorobenzamido)cyclopentyl)-3-(furan-2-yl)benzamide (0.09 g, 97% (2 steps)) as pink solid; column: 80% to 100% EtOAc: Hex; ^{1}H NMR (500 MHz, DMSO-d_6) δ ppm 8.57 (dd, J = 11.6, 7.0 Hz, 2H) 8.16 (s, 1H) 7.92-7.86 (m, 2H) 7.84 (dd, J = 7.8, 1.6 Hz, 1H) 7.82-7.73 (m, 2H) 7.58-

7.48 (m, 3H) 7.02 (d, J = 3.4 Hz, 1H) 6.64 (dt, J = 3.0, 1.3 Hz, 1H) 4.26 (dp, J = 14.1, 6.9 Hz, 2H) 2.37 (dt, J = 13.0, 7.4 Hz, 1H) 1.97 (dq, J = 13.3, 7.1 Hz, 2H) 1.81 (td, J = 7.1, 6.5, 4.0 Hz, 2H) 1.69 (dt, J = 13.0, 8.0 Hz, 1H); ^{13}C NMR (500 MHz, DMSO-d_6) δ ppm 166.13, 165.35, 152.90, 143.68, 136.30, 135.87, 133.86, 130.75, 129.66, 129.32, 128.71, 126.72, 126.30, 122.57, 112.63, 106.99, 50.03, 49.98, 38.91, 38.68, 30.66, 30.63; TOF ES+ MS: (M+H) 409.13; HPLC Ret: 7.13 min; 98 % pure.

N-(*trans*-3-(4-chlorobenzamido)cyclopentyl)-3-(furan-2-yl)benzamide. (CCG-263877). Method J followed by Method I starting from tert-butyl (trans-3-(4-chlorobenzamido)cyclopentyl)carbamate (0.04 g, 0.22 mmol) and 3-(furan-2-yl)benzoic acid (0.06 g, 0.22 mmol) gave N-(trans-3-(4-chlorobenzamido)cyclopentyl)-3-(furan-2-yl)benzamide (0.05 g, 55% (2 steps)) as orange solid; column: 50% to 100% EtOAc: Hex; ^{1}H NMR (500 MHz, DMSO-d_6) δ ppm 8.52 (dd, J = 11.7, 7.4 Hz, 2H) 8.16 (s, 1H) 7.93-7.75 (m, 5H) 7.57-7.49 (m, 3H) 7.03 (d, J = 3.4 Hz, 1H) 6.64 (dd, J = 3.3, 1.8 Hz, 1H) 4.51 (dp, J = 14.1, 6.9 Hz, 2H) 2.14 (dt, J = 12.9, 7.3 Hz, 2H) 1.97 (t, J = 7.1 Hz, 2H) 1.61 (qd, J = 13.3, 12.9, 7.6 Hz, 2H); ^{13}C NMR (500 MHz, DMSO-d_6) δ ppm 166.03, 165.25, 152.92, 143.64, 136.28, 135.81, 133.82, 130.72, 129.69, 129.28, 128.66, 126.76, 126.29, 122.59, 112.62, 106.96, 50.03, 49.78, 49.71, 39.17, 38.66, 31.50, 31.48; TOF ES+ MS: (M+Na) 431.11; HPLC Ret: 6.99 min; 95 % pure.

N-(*trans*-3-(4-chlorobenzamido)cyclohexyl)-3-(furan-2-yl)benzamide. (CCG-263879). Method J followed by Method I starting from tert-butyl (*trans*-3-(4-chlorobenzamido)cyclohexyl)carbamate (0.06 g, 0.16 mmol) and 3-(furan-2-yl)benzoic acid (0.03 g, 0.16 mmol) gave N-(trans-3-(4-chlorobenzamido)cyclohexyl)-3-(furan-2-yl)benzamide (0.05 g, 77% (2 steps)) as yellow solid; column: 50% to 60% EtOAc: Hex; ^{1}H NMR (500 MHz, DMSO-d_6) δ ppm 8.33 (dd, J = 15.2, 7.4 Hz, 2H) 8.14 (d, J = 1.6 Hz, 1H) 7.92-7.73 (m, 5H) 7.57-7.47 (m, 3H) 7.03 (d, J = 3.4 Hz, 1H) 6.64 (dt, J = 3.3, 1.5 Hz, 1H) 4.38-4.27 (m, 2H) 1.85 (t, J = 5.9 Hz, 2H) 1.79-1.66 (m, 4H) 1.58-1.50 (m, 2H); ^{13}C NMR (500 MHz, DMSO-d_6) δ ppm

166.20, 165.43, 152.95, 143.65, 136.18, 136.14, 134.12, 130.64, 129.88, 129.17, 128.59, 126.92, 126.21, 122.79, 112.60, 106.95, 45.31, 45.19, 36.18, 31.13, 31.01, 20.11; TOF ES+ MS: (M+H) 423.15; HPLC Ret: 7.32 min; 96 % pure.

N-(*cis*-3-(4-chlorobenzamido)cyclohexyl)-3-(furan-2-yl)benzamide. (CCG-263880). Method J followed by Method I starting from tert-butyl (*cis*-3-(4-chlorobenzamido)cyclohexyl)carbamate (0.06 g, 0.16 mmol) and 3-(furan-2-yl)benzoic acid (0.03 g, 0.16 mmol) gave N-(cis-3-(4-chlorobenzamido)cyclohexyl)-3-(furan-2-yl)benzamide (0.04 g, 53% (2 steps)) as white solid; column: 50% EtOAc: Hex to 20% MeOH: DCM; ^{1}H NMR (500 MHz, DMSO-d_6) δ ppm 8.42 (dd, J = 10.0, 7.9 Hz, 2H) 8.14 (t, J = 1.8 Hz, 1H) 7.90-7.72 (m, 5H) 7.57-7.47 (m, 3H) 7.02 (d, J = 3.4 Hz, 1H) 6.63 (dt, J = 3.4, 1.8 Hz, 1H) 3.90 (dqt, J = 11.7, 7.8, 3.5 Hz, 2H) 2.09 (d, J = 11.9 Hz, 1H) 1.89-1.78 (m, 3H) 1.51-1.26 (m, 4H); ^{13}C NMR (500 MHz, DMSO-d_6) δ ppm 165.56, 164.79, 152.92, 143.67, 136.24, 135.96, 133.95, 130.72, 129.68, 129.23, 128.68, 126.74, 126.25, 122.59, 112.61, 106.96, 48.11, 48.02, 39.65, 39.01, 31.81, 23.49; TOF ES+ MS: (M+H) 423.15; HPLC Ret: 7.07 min; 98 % pure.

N-(2,3-dihydrobenzo[b][1,4]dioxin-6-yl)-5,5-difluoro-1-(3-(furan-2-yl)benzoyl)piperidine-3-carboxamide (CCG-263152). Method J followed by Method I starting from tert-butyl 5-((2,3-dihydrobenzo[b][1,4]dioxin-6-yl)carbamoyl)-3,3-difluoropiperidine-1-carboxylate (0.07 g, 0.19 mmol) and 3-(furan-2-yl)benzoic acid (0.04 g, 0.22 mmol) gave N-(2,3-dihydrobenzo[b][1,4]dioxin-6-yl)-5,5-difluoro-1-(3-(furan-2-yl)benzoyl)piperidine-3-carboxamide (0.07 g, 72% (2 steps)) as white solid; column: 35% to 50% EtOac: Hex; ^{1}H NMR (500 MHz, DMSO-d_6) δ ppm 10.13 (br. s, 1H) 9.93 (br. s, 1H) 7.86-7.76 (m, 2H) 7.71 (s, 1H) 7.54 (t, J = 7.8, 1H) 7.35-7.20 (m, 2H) 7.17 (br. s, 1H) 7.07 (s, 1H) 6.79 (br. s, 1H) 6.63 (dd, J = 3.4, 1.8 Hz, 1H) 4.78-4.56 (m, 1H) 4.20 (br. s, 4H) 3.78 (br. s, 2H) 3.49-3.33 (m, 2H) 2.88 (br. s, 1H) 2.44 (br. s, 1H) 2.36-2.22 (m, 1H); ^{13}C NMR (126 MHz, DMSO-d_6) δ 168.81, 158.23, 152.48, 143.89, 143.32, 139.96, 131.09, 129.77, 126.19, 125.24, 122.21, 117.22, 113.00, 112.68, 108.92,

107.34, 64.61, 64.36, 60.20, 39.97, 36.02, 33.54, 21.20, 14.53; QTOF ES+ MS: (M+H) 469.2; HPLC Ret: 7.25 min; 98 % pure.

N-(3,4-dimethoxyphenyl)-5,5-difluoro-1-(3-(furan-2-yl)benzoyl)piperidine-3-carboxamide (CCG-263232). Method J followed by Method I starting from tert-butyl 5-((3,4-dimethoxyphenyl)carbamoyl)-3,3-difluoropiperidine-1-carboxylate (0.07 g, 0.2 mmol) and 3-(furan-2-yl)benzoic acid (0.04 g, 0.2 mmol) gave N-(3,4-dimethoxyphenyl)-5,5-difluoro-1-(3-(furan-2-yl)benzoyl)piperidine-3-carboxamide (0.06 g, 62% (2 steps)) as white solid; column: 50% to 80% EtOac: Hex; precipitate out of EtOAc/Hex; ^{1}H NMR (500 MHz, DMSO-d_6) δ ppm 10.19 (br. s, 1H) 10.01 (br. s, 1H) 7.87-7.78 (m, 2H) 7.74 (s, 1H) 7.55 (t, J = 7.8 Hz, 1H) 7.40-7.30 (m, 2H) 7.16 (br. s, 1H) 7.08 (s, 1H) 6.90 (br. s, 1H) 6.64 (d, J = 3.4 Hz, 1H) 4.80-4.60 (m, 1H) 3.90-3.63 (m, 8H) 3.48 (br. s, 1H) 3.07 (br. s., 1H) 2.91 (br. s, 1H) 2.47 (br. s, 1H) 2.38-2.21 (m, 1H); ^{13}C NMR (126 MHz, DMSO-d_6) δ 168.80, 160.54, 152.49, 145.48, 143.88, 139.91, 131.10, 129.72, 126.17, 125.23, 122.22, 118.49, 112.67, 112.41, 111.72, 107.33, 104.9, 59.02, 56.12, 55.76, 39.96, 36.01, 31.40, 22.50, 14.39; TOF ES+ MS: (M+H) 471.2; HPLC Ret: 6.72 min; 98 % pure.

N-(3-(4-chlorobenzamido)-4-methylphenyl)-3-(furan-2-yl)benzamide (CCG-263154). Method J followed by Method I starting from tert-butyl (3-(4-chlorobenzamido)-4-methylphenyl)carbamate(0.09 g, 0.31 mmol) and 3-(furan-2-yl)benzoic acid (0.06 g, 0.31 mmol) gave N-(3-(4-chlorobenzamido)-4-methylphenyl)-3-(furan-2-yl)benzamide (0.04 g, 30% (2 steps)) as white solid; column: 30% to 40% EtOac: Hex; crashed out of fractions; ^{1}H NMR (500 MHz, DMSO-d_6) δ ppm 10.36 (s, 1H) 10.03 (s, 1H) 8.26 (q, J = 2.0 Hz, 1H) 8.06-7.99 (m, 2H) 7-94-7.80 (m, 4H) 7.66-7.55 (m, 4H) 7.26 (d, J = 8.3 Hz, 1H) 7.08 (d, 3.4 Hz, 1H) 6.65 (dd, J = 3.4, 1.8 Hz, 1H) 2.22 (s, 3H); ^{13}C NMR (500 MHz, DMSO-d_6) δ ppm 165.53, 164.72, 152.78, 143.81, 137.56, 136.84, 136.57, 136.08, 133.67, 130.88, 130.66, 130.03, 129.52, 128.97,

127.02, 126.69, 122.90, 119.17, 118.76, 112.68, 107.21, 17.86; QTOF ES+ MS: (M+H) 431.1; HPLC Ret: 7.84 min; 99 % pure.

N-(4-chlorophenyl)-5,5-difluoro-1-(3-(furan-2-yl)benzoyl)-3-methylpiperidine-3-carboxamide. (CCG-264061). Method J followed by Method I starting from tert-butyl 3-((4-chlorophenyl)carbamoyl)5,5-difluoro-3-methylpiperidine-1-carboxylate (0.07 g, 0.18 mmol) and 3-(furan-2-yl)benzoic acid (0.03 g, 0.18 mmol) gave N-(4-chlorophenyl)-5,5-difluoro-1-(3-(furan-2-yl)benzoyl)-3-methylpiperidine-3-carboxamide (0.07 g, 80% (2 steps)) as yellow solid; column: 40% to 50% EtOac: Hex; ^{1}H NMR (400 MHz, DMSO-d_6, 80 °C) δ ppm 9.37 (br.s 1H) 7.77 (d, J = 8.0 Hz, 1H) 7.69 (d, J = 8.4 Hz, 2H) 7.59 (d, J = 8.4 Hz, 2H) 7.50 (t, J = 7.9 Hz, 1H) 7.36-7.26 (m, 3H) 6.92 (d, J = 3.1 Hz, 1H) 6.58 (dt, J = 3.7, 1.6 Hz, 1H) 3.97 (d, J = 13.7 Hz, 1H) 3.92-3.62 (m, 3H) 2.70 (td, J = 20.0, 17.7, 10.4 Hz, 1H) 2.39-2.24 (m, 1H) 1.30 (s, 3H) 1.28-1.14 (m, 1H); ^{19}F NMR (376 MHz, DMSO-d_6, 80 °C) δ ppm -97.46—-100.35 (m, 2H); QTOF ES+ MS: (M+H) 459.13; HPLC Ret: 8.00 min; 96% pure.

N-(*cis*-3-(4-chlorobenzamido)cyclohexyl)-3-(2-(pyrrolidin-1-yl)ethoxy)benzamide. (CCG-264119). Method J followed by Method I starting from tert-butyl (*cis*-3-(4-chlorobenzamido)cyclohexyl)carbamate (0.05 g, 0.11 mmol) and 3-(2-(pyrrolidin-1-yl)ethoxy)benzoic acid, HCl (0.03 g, 0.11 mmol) gave N-(cis-3-(4-chlorobenzamido)cyclohexyl)-3-(2-(pyrrolidin-1-yl)ethoxy)benzamide (0.03 g, 56% (2 steps)) as white solid; column: 8% to 10% MeOH: DCM; crystalized from DCM:MeOH; ^{1}H NMR (500 MHz, DMSO-d_6) δ ppm 8.43 (d, J = 7.9 Hz, 1H) 8.33 (d, J = 8.0 Hz, 1H) 7.88 (d, J = 8.4 Hz, 2H) 7.53 (d, J = 8.2 Hz, 2H) 7.47-7.40 (m, 2H) 7.36 (t, J = 7.9 Hz, 1H) 7.10 (dd, J = 8.2, 2.5 Hz, 1H) 4.21 (br. s, 2H) 3.87 (dtt, J = 11.8, 7.8, 3.9 Hz, 2H) 3.07 (br. s, 2H) 2.80 (br. s, 4H) 2.04 (d, J = 11.9 Hz, 1H) 1.85-1.76 (m, 7H) 1.49-1.25 (m, 4H); ^{13}C NMR (126 MHz, DMSO-d_6) δ ppm 165.46, 164.75, 158.45, 136.67, 136.23, 133.93, 129.77, 129.69, 128.67, 120.26, 117.66, 113.69, 54.33, 54.15, 48.11, 47.97, 39.91, 39.08, 31.79, 23.50; TOF ES+ MS: (M+H) 470.22; HPLC Ret: 5.14 min; 98 % pure.

N-(*cis*-3-(2,3-dihydrobenzo[b][1,4]dioxine-6-carboxamido)cyclohexyl)-2-(2-(pyrrolidin-1-yl)ethoxy)quinoline-6-carboxamide. (CCG-264120). Method J followed by Method I starting from N-((1R,3S)-3-aminocyclohexyl)-2,3-dihydrobenzo[b][1,4]dioxine-6-carboxamide (0.06 g, 0.15 mmol) and 2-(2-(pyrrolidin-1-yl)ethoxy)quinoline-6-carboxylic acid (0.04 g, 0.15 mmol) gave N-(cis-3-(2,3-dihydrobenzo[b][1,4]dioxine-6-carboxamido)cyclohexyl)-2-(2-(pyrrolidin-1-yl)ethoxy)quinoline-6-carboxamide (0.04 g, 50% (2 steps)) as white solid; column: 8% to 10% MeOH: DCM; crystalized from DCM:MeOH; ^{1}H NMR (500 MHz, DMSO-d_6) δ ppm 8.48 (d, J = 7.8, Hz, 1H) 8.42 (d, J = 2.0 Hz, 1H) 8.33 (d, J = 8.9 Hz, 1H) 8.19-8.09 (m, 2H) 7.80 (d, J = 8.7 Hz, 1H) 7.42-7.35 (m, 2H) 7.09 (d, J = 8.8 Hz, 1H) 6.90 (d, J = 8.3 Hz, 1H) 4.60 (br. s, 2H) 4.27 (q, J = 5.1 Hz, 4H) 3.90 (ddt, J = 25.6, 11.8, 3.9 Hz, 2H) 3.08 (br. s, 2H) 2.78 (br. s, 4H) 2.07 (d, J = 11.8 Hz, 1H) 1.93-1.71 (m, 7H) 1.51-1.26 (m, 4H); ^{13}C NMR (126 MHz, DMSO-d_6) δ ppm 165.37, 164.93, 162.34, 147.48, 146.23, 143.24, 140.79, 131.04, 128.88, 128.24, 128.05, 126.93, 124.57, 121.20, 117.01, 116.76, 114.18, 64.76, 64.44, 54.09, 53.35, 48.16, 47.93, 45.76, 39.91, 39.24, 31.88, 23.56; TOF ES+ MS: (M+H) 545.28; HPLC Ret: 5.05 min; 97% pure.

3-(furan-2-yl)-N-(*cis*-3-(4-(2-(pyrrolidin-1-yl)ethoxy)benzamido)cyclohexyl)benzamide. (CCG-264121). Method J followed by Method I starting from tert-butyl (*cis*-3-(3-furan-2-yl)cyclohexyl)carbamate (0.05 g, 0.13 mmol) and 4-(2-(pyrrolidin-1-yl)ethoxy)benzoic acid (0.03 g, 0.13 mmol) gave 3-(furan-2-yl)-N-(cis-3-(4-(2-(pyrrolidin-1-yl)ethoxy)benzamido)cyclohexyl)benzamide (0.05 g, 72% (2 steps)) as white solid; column: 8% to 10% MeOH: DCM; ^{1}H NMR (500 MHz, DMSO-d_6) δ ppm 8.44 (d, J = 7.9 Hz, 1H) 8.21-8.15 (m, 2H) 7.86-7.72 (m, 5H) 7.50 (t, J = 7.8 Hz, 1H) 7.01 (dd, J = 15.3, 5.8 Hz, 3H) 6.63 (dd, J = 3.3, 1.8 Hz, 1H) 4.16 (br. s, 2H) 3.93-3.84 (m, 2H) 2.93 (br. s, 2H) 2.66 (br. s, 4H) 2.07 (d, J = 11.8 Hz, 1H) 1.89-1.70 (m, 7H) 1.50-1.22 (m, 4H); ^{13}C NMR (126 MHz, DMSO-d_6) δ ppm 165.54, 165.28, 160.92, 152.92, 143.66, 135.96, 130.71, 129.54, 129.28, 127.52, 126.74,

126.24, 122.60, 114.30, 112.61, 109.99, 106.97, 54.41, 48.08, 47.89, 39.90, 39.26, 31.92, 31.84, 23.55, 23.49; TOF ES+ MS: (M+H) 502.27; HPLC Ret: 5.46 min; 99 % pure.

N-(4-chlorophenyl)-1-(2,3-dihydrobenzo[b][1,4]dioxine-6-carbonyl)-5,5-difluoropiperidine-3-carboxamide (CCG-263151). Method J followed by Method I starting from tert-butyl 5-((4-chlorophenyl)carbamoyl)-3,3-difluoropiperidine-1-carboxylate (0.07 g, 0.20 mmol) and 2,3-dihydrobenzo[b][1,4]dioxine-6-carboxylic acid (0.04 g, 0.20 mmol) gave N-(4-chlorophenyl)-1-(2,3-dihydrobenzo[b][1,4]dioxine-6-carbonyl)-5,5-difluoropiperidine-3-carboxamide (0.05 g, 54% (2 steps)) as white solid; column: 40% to 45% EtOAc: Hex; triturated with EtOAc: Hex; ^{1}H NMR (500 MHz, DMSO-d_6) δ ppm 7.71-7.60 (m, 2H) 7.41-7.34 (m, 2H) 6.97-6.87 (m, 3H) 4.28 (dd, J = 7.8, 3.2 Hz, 4H) 4.00-3.89 (m, 2H) 3.18-3.00 (m, 2H) 2.95-2.88 (m, 1H) 2.52-2.41 (m, 1H) 2.36-2.21 (m, 1H); ^{13}C NMR (126 MHz, DMSO-d_6) δ 169.54, 157.88, 153.13, 145.47, 143.61, 138.11, 130.37, 129.10, 127.58, 125.20, 122.36, 122.25, 121.31, 120.96, 119.72, 118.82, 117.55, 116.81, 64.66, 64.50, 60.19, 40.40, 34.68, 27.85, 21.20, 14.53; QTOF ES+ MS: (M+H) 437.1; HPLC Ret: 7.34 min; 94 % pure.

N-(4-chlorophenyl)-1-(3,4-dimethoxybenzoyl)-5,5-difluoropiperidine-3-carboxamide (CCG-263231). Method J followed by Method I starting from tert-butyl 5-((4-chlorophenyl)carbamoyl)-3,3-difluoropiperidine-1-carboxylate (0.07 g, 0.15 mmol) and 3,4-dimethoxybenzoic acid (0.03 g, 0.15 mmol) gave N-(4-chlorophenyl)-1-(3,4-dimethoxybenzoyl)-5,5-difluoropiperidine-3-carboxamide (0.02 g, 23% (2 steps)) as white solid; column: 50% to 80% EtOAc: Hex; triturated with EtOAc: Hex; ^{1}H NMR (500 MHz, DMSO-d_6) δ ppm 10.35 (br. s., 1H) 7.65-7.59 (m, 2H) 7.40-7.31 (m, 2H) 7.04-6.96 (m, 3H) 4.65-4.32 (m, 1H) 3.90-3.50 (m, 7H) 3.25-3.00 (m, 2H) 2.97-2.90 (m, 1H) 2.47-2.38 (m, 1H) 2.35-2.25 (m, 1H); TOF ES+ MS: (M+H) 439.1; HPLC Ret: 6.79 min; 96 % pure.

N-(4-chlorophenyl)-1-(3,9-dihydro-2H-[1,4]dioxino[2,3-g]indole-8-carbonyl)-5,5-difluoropiperidine-3-carboxamide. (CCG-263481). Method J followed by Method I starting from tert-butyl 5-((4-chlorophenyl)carbamoyl)-3,3-difluoropiperidine-1-carboxylate (0.09 g, 0.23 mmol) and 3,9-dihydro-2H-[1,4]dioxino[2,3-g]indole-8-carboxylic acid (0.05 g, 0.23 mmol) gave N-(4-chlorophenyl)-1-(3,9-dihydro-2H-[1,4]dioxino[2,3-g]indole-8-carbonyl)-5,5-difluoropiperidine-3-carboxamide (0.08 g, 77% (2 steps)) as white solid; column: 45% EtOAc: Hex; ^{1}H NMR (500 MHz, DMSO-d_6, 80 °C) δ ppm 10.06 (br. s, 1H) 7.99 (s, 1H) 7.60 (d, J = 8.7 Hz, 2H) 7.33 (d, J = 8.7 Hz, 2H) 6.85 (d, J = 8.0 Hz, 1H) 6.65 (t, J = 8.1 Hz, 1H) 6.37 (d, J = 8.1 Hz, 1H) 4.73-4.56 (m, 2H) 4.30 (dd, J = 5.8, 2.7 Hz, 2H) 4.24 (dd, J = 5.8, 2.7 Hz, 2H) 3.46 (dd, J = 31.1, 13.8 Hz, 1H) 3.19 (t, J = 12.5 Hz, 1H) 3.05-2.91 (m, 1H) 2.51-2.45 (m, 1H) 2.27 (dtd, J = 12.9, 5.4 Hz, 1H); ^{19}F NMR (500 MHz, DMSO-d_6) δ ppm -98.96 (d, 1H), -101.73 (d, 1H); TOF ES+ MS: (M+MeCN) 515.13; HPLC Ret: 7.67 min; 98 % pure.

N-(4-chlorophenyl)-1-(6,7-difluoro-1H-indole-2-carbonyl)-5,5-difluoropiperidine-3-carboxamide. (CCG-263595). Method J followed by Method I starting from tert-butyl 5-((4-chlorophenyl)carbamoyl)-3,3-difluoropiperidine-1-carboxylate (0.09 g, 0.23 mmol) and 6,7-difluoro-1H-indole-2-carboxylic acid (0.05 g, 0.23 mmol) gave N-(4-chlorophenyl)-1-(6,7-difluoro-1H-indole-2-carbonyl)-5,5-difluoropiperidine-3-carboxamide (0.06 g, 62% (2 steps)) as white solid; taken up in hot EtOH and filtered after extraction and evaporation; ^{1}H NMR (400 MHz, DMSO-d_6, 80 °C) δ 12.07 (s, 1H) 10.08 (s, 1H) 7.60 (d, J = 8.4 Hz, 2H) 7.43 (dd, J = 8.9, 4.3 Hz, 1H) 7.33 (d, J = 8.4 Hz, 2H) 7.05 (dt, J = 11.1, 7.6 Hz, 1H) 6.93 (d, J = 3.1 Hz, 1H) 4.63-4.56 (m, 2H) 3.62 (dd, J = 30.4, 13.8 Hz, 1H) 3.34 (t, J = 12.4 Hz, 1H) 3.01 (d, J = 16.5 Hz, 1H) 2.27 (dd, 30.2, 12.8 Hz, 1H); ^{19}F NMR (376 MHz, DMSO-d_6) δ ppm -99.17 (d, J = 240 Hz, 1H) -101.49 (d, J = 238.2 Hz, 1H) -147.29 (ddd, J = 20.2, 11.4, 4.4 Hz, 1H) -158.27 (ddd, J = 20.2, 7.1, 2.9 Hz, 1H); TOF ES+ MS: (M+H) 454.09; HPLC Ret: 7.70 min; 96 % pure.

N-(4-chlorophenyl)-5,5-difluoro-1-(3-(2-(pyrrolidin-1-yl)ethoxy)benzoyl)piperidine-3-carboxamide. (CCG-263596). Method J followed by Method I starting from tert-butyl 5-((4-chlorophenyl)carbamoyl)-3,3-difluoropiperidine-1-carboxylate (0.08 g, 0.18 mmol) and 1-(2-(3-carboxyphenoxy)ethyl)pyrrolidine-1-ium, HCl (0.05 g, 0.18 mmol) gave N-(4-chlorophenyl)-5,5-difluoro-1-(3-(2-(pyrrolidin-1-yl)ethoxy)benzoyl)piperidine-3-carboxamide (0.05 g, 52% (2 steps)) as white solid; column: 5% to 10% MeOH: DCM; ^{1}H NMR (400 MHz, MeOD-d4, 40 °C) δ 7.66 (d, J = 7.8 Hz, 2H) 7.43 (t, J = 8.1 Hz, 1H) 7.29 (d, J = 8.5 Hz, 2H) 7.18-7.11 (m, 1H) 7.10-7.03 (m, 2H) 4.34 (t, J = 5.0 Hz, 2H) 3.40-3.33 (m, 4H) 2.96 (d, J = 14.1 Hz, 1H) 2.52-2.24 (m, 2H) 2.13-2.01 (m, 4H); ^{19}F NMR (376 MHz, MeOD-d4, 40 °C) δ ppm -73.54 (s, 1H) -75.43 (s, 1H); TOF ES+ MS: (M+H) 492.19; HPLC Ret: 5.83 min; 96 % pure.

(S)-N-(4-chlorophenyl)-1-(5-(trifluoromethoxy)-1H-indole-2-carbonyl)piperidine-3-carboxamide. (CCG-263658). Method J followed by Method I starting from (S)-tert-butyl 3-((4-chlorophenyl)carbamoyl)piperidine-1-carboxylate (0.11 g, 0.32 mmol) and 5-(trifluoromethoxy)-1H-indole-2-carboxylic acid (0.08 g, 0.32 mmol) gave (S)-N-(4-chlorophenyl)-1-(5-(trifluoromethoxy)-1H-indole-2-carbonyl)piperidine-3-carboxamide (0.15 g, 99% (2 steps)) as white solid; column: 65% EtOAc: Hex; ^{1}H NMR (400 MHz, DMSO-d_6, 80 °C) δ ppm 11.54 (s, 1H) 9.82 (br. s, 1H) 7.60 (d, J = 7.8 Hz, 2H) 7.53 (d, J = 8.0 Hz, 2H) 7.30 (d, J = 7.9 Hz, 2H) 7.12 (d, J = 9.0 Hz, 1H) 6.84 (d, J = 2.2 Hz, 1H) 4.44 (dd, J = 13.2, 3.9 Hz, 1H) 4.31-4.20 (m, 1H) 3.35 (t, J = 11.8 Hz, 1H) 3.20 (t, J = 12.2 Hz, 1H) 2.64 (dt, J = 11.9, 6.5 Hz, 1H) 2.07 (d, J = 12.5 Hz, 1H) 1.83 (q, J = 11.8 Hz, 2H) 1.56 (d, J = 12.6 Hz, 1H); ^{19}F NMR (376 MHz, DMSO-d_6, 80 °C) δ ppm -56.85 (d, J = 5.5 Hz, 1H) -69.63 (s, 1H) -71.52 (s, 1H); QTOF ES+ MS: (M+H) 466.11; HPLC Ret: 7.89 min; Optical rotation: +67.2872 (0.65 g/L); 99% pure.

(R)-N-(4-chlorophenyl)-1-(5-(trifluoromethoxy)-1H-indole-2-carbonyl)piperidine-3-carboxamide. (CCG-263687). Method J followed by Method I starting from (R)-tert-butyl 3-((4-chlorophenyl)carbamoyl)piperidine-1-carboxylate (0.1 g, 0.3 mmol) and 5-(trifluoromethoxy)-1H-

indole-2-carboxylic acid (0.08 g, 0.31 mmol) gave (R)-N-(4-chlorophenyl)-1-(5-(trifluoromethoxy)-1H-indole-2-carbonyl)piperidine-3-carboxamide (0.14 g, 100% (2 steps)) as white solid; column: 60% EtOAc: Hex; ^{1}H NMR (400 MHz, DMSO-d_6, 80 °C) δ ppm 11.56 (s, 1H) 9.82 (br. s, 1H) 7.59 (d, J = 7.9 Hz, 2H) 7.56-7.46 (m, 2H) 7.30 (d, J = 7.9 Hz, 2H) 7.12 (d, J = 8.9 Hz, 1H) 6.83 (d, J = 2.1 Hz, 1H) 4.43 (dd, J = 13.0, 3.8 Hz, 1H) 4.25 (d, J = 13.3 Hz, 1H) 3.32 (t, J = 11.8 Hz, 1H) 3.18 (t, J = 12.0 Hz, 1H) 2.62 (p, J = 6.3 Hz, 1H) 2.06 (d, J = 12.3 Hz, 1H) 1.83 (td, J = 14.7, 14.2, 4.3 Hz, 2H) 1.56 (d, J = 12.8 Hz, 1H); ^{19}F NMR (376 MHz, DMSO-d_6, 80 °C) δ ppm -56.83 (s, 3H) -69.65 (s, 1H) -71.54 (s, 1H); QTOF ES+ MS: (M+H) 466.11; HPLC Ret: 7.81 min; Optical rotation: -76.6770 (0.646 g/L); 98% pure.

N-(4-chloro-3-(prop-2-yn-1-yloxy)phenyl)-5,5-difluoro-1-(3-fluoro-5-(pyridin-4-yl)benzoyl)piperidine-3-carboxamide. Method J followed by Method I starting from tert-butyl 5-((4-chloro-3-(prop-2-yn-1-yloxy)phenyl)carbamoyl)-3,3-difluoropiperidine-1-carboxylate (0.1 g, 0.23 mmol) and 3-fluoro-5-(pyridin-4-yl)benzoic acid (0.05 g, 0.23 mmol) gave N-(4-chloro-3-(prop-2-yn-1-yloxy)phenyl)-5,5-difluoro-1-(3-fluoro-5-(pyridin-4-yl)benzoyl)piperidine-3-carboxamide (0.09 g, 73% (2 steps)) as white solid; column: 75% to 100% EtOAc: Hex; ^{1}H NMR (500 MHz, $CDCl_3$-d) δ ppm 8.70-8.64 (m, 2H) 7.79-7.68 (m, 3H) 7.65-7.60 (m, 1H) 7.55-7.50 (m, 1H) 7.35-7.28 (m, 2H) 7.22 (d, J = 8.6 Hz, 1H) 4.80 (d, J = 2.6 Hz, 2H) 4.38-4.10 (m, 1H) 3.68-3.50 (m, 1H) 3.42 (t, J = 3.0 Hz, 1H) 3.30-3.21 (m, 1H) 2.94-2.90 (m, 1H) 2.40-2.21 (m, 1H); HPLC Ret: 5.97 min.

N-(4-chlorobenzyl)-5,5-difluoro-1-(3-fluoro-5-(pyridin-4-yl)benzoyl)piperidine-3-carboxamide. (CCG-264058). Method J followed by Method I starting from tert-butyl 5-((4-chlorobenzyl)carbamoyl)-3,3-difluoropiperidine-1-carboxylate (0.06 g, 0.14 mmol) and 3-fluoro-5-(pyridin-4-yl)benzoic acid (0.03 g, 0.14 mmol) gave N-(4-chlorobenzyl)-5,5-difluoro-1-(3-fluoro-5-(pyridin-4-yl)benzoyl)piperidine-3-carboxamide (0.06 g, 87% (2 steps)) as colorless oil; column: 100% EtOAc: Hex; ^{1}H NMR (400 MHz, DMSO-d_6, 80 °C) δ ppm 8.69-8.62 (m, 2H) 8.40

(br. s, 1H) 7.95 (s, 1H) 7.78-7.67 (m, 3H) 7.60 (s, 2H) 7.63-7.58 (m, 5H) 4.26 (d, J = 5.8 Hz, 2H) 4.21-4.11 (m, 2H) 3.52 (dd, J = 30.2, 13.9 Hz, 1H) 3.20 (t, J = 12.1 Hz, 1H) 3.00 (s, 1H) 2.82 (q, J = 9.4 Hz, 1H) 2.39 (br. s, 1H) 2.34-2.13 (m, 1H); ^{19}F NMR (376 MHz, DMSO-d_6, 80 °C) δ ppm -97.46—-104.28 (m, 2H) -111.11 (s, 1H); QTOF ES+ MS: (M+H) 488.13; HPLC Ret: 5.56 min; 96% pure.

N-(3-chlorophenyl)-5,5-difluoro-1-(3-fluoro-5-(pyridin-4-yl)benzoyl)piperidine-3-carboxamide. (CCG-264059). Method J followed by Method I starting from tert-butyl 5-((3-chlorophenyl)carbamoyl)-3,3-difluoropiperidine-1-carboxylate (0.06 g, 0.16 mmol) and 3-fluoro-5-(pyridin-4-yl)benzoic acid (0.04 g, 0.16 mmol) gave N-(3-chlorophenyl)-5,5-difluoro-1-(3-fluoro-5-(pyridin-4-yl)benzoyl)piperidine-3-carboxamide (0.05 g, 59% (2 steps)) as white solid; column: 90% EtOAc: Hex; ^{1}H NMR (400 MHz, DMSO-d_6, 80 °C) δ ppm 10.07 (br.s 1H) 8.66 (d, J = 5.7 Hz, 2H) 7.78-7.67 (m, 4H) 7.62 (d, J = 1.6 Hz, 1H) 7.43 (d, J = 8.3 Hz, 1H) 7.35-7.26 (m, 2H) 7.09 (d, J = 8.1 Hz, 1H) 4.44-4.00 (m, 2H) 3.59 (dd, J = 29.6, 14.1 Hz, 1H) 3.27 (t, J = 12.1 Hz, 1H) 2.96 (br. s, 1H) 2.42-2.24 (m, 1H); ^{19}F NMR (376 MHz, DMSO-d_6, 80 °C) δ ppm -97.46—-102.51 (m, 2H) -111.09 (s, 1H); QTOF ES+ MS: (M+H) 474.11; HPLC Ret: 5.87 min; 99% pure.

N-(3,4-dichlorophenyl)-5,5-difluoro-1-(3-fluoro-5-(pyridin-4-yl)benzoyl)piperidine-3-carboxamide. (CCG-264060). Method J followed by Method I starting from tert-butyl 5-((3,4-dichlorophenyl)carbamoyl)-3,3-difluoropiperidine-1-carboxylate (0.06 g, 0.15 mmol) and 3-fluoro-5-(pyridin-4-yl)benzoic acid (0.03 g, 0.15 mmol) gave N-(3,4-dichlorophenyl)-5,5-difluoro-1-(3-fluoro-5-(pyridin-4-yl)benzoyl)piperidine-3-carboxamide (0.04 g, 40% (2 steps)) as white solid; column: 90% EtOAc: Hex; ^{1}H NMR (400 MHz, DMSO-d_6, 80 °C) δ ppm 10.17 (br.s 1H) 8.66 (d, J = 5.7 Hz, 2H) 7.90 (d, J = 2.3 Hz, 1H) 7.78-7.67 (m, 3H) 7.61 (d, J = 1.7 Hz, 1H) 7.54-7.42 (m, 2H) 7.30 (d, J = 8.1 Hz, 1H) 4.39-4.02 (m, 2H) 3.59 (dd, J = 29.6, 14.0 Hz, 1H) 3.27 (t, J = 12.3 Hz, 1H) 2.96 (br. s, 2H) 2.42-2.21 (m, 1H); ^{19}F NMR (376 MHz, DMSO-d_6, 80 °C) δ

ppm -97.46—-103.79 (m, 2H) -111.08 (s, 1H); QTOF ES+ MS: (M+H) 508.08; HPLC Ret: 6.22 min; 96% pure.

N-(4-chloropyridin-2-yl)-5,5-difluoro-1-(3-fluoro-5-(pyridin-4-yl)benzoyl)piperidine-3-carboxamide. (CCG-264606). Method J followed by Method I starting from tert-butyl 5-((4-chloropyridin-2-yl)carbamoyl)-3,3-difluoropiperidine-1-carboxylate (0.04 g, 0.11 mmol) and 3-fluoro-5-(pyridin-4-yl)benzoic acid (0.02 g, 0.11 mmol) gave N-(4-chloropyridin-2-yl)-5,5-difluoro-1-(3-fluoro-5-(pyridin-4-yl)benzoyl)piperidine-3-carboxamide (0.04 g, 78% (2 steps)) as white solid; column: 65% to 85% EtOAc: Hex; H_2O wash post column needed; ^{1}H NMR (400 MHz, DMSO-d_6, 80 °C) δ ppm 10.72 (br.s 1H) 8.66 (d, J = 4.5 Hz, 2H) 8.28 (d, J = 5.4 Hz, 1H) 8.08 (s, 1H) 7.78-7.68 (m, 3H) 7.62 (t, J = 1.5 Hz, 1H) 7.31 (d, J = 8.8 Hz, 1H) 7.19 (d, J = 8.1 Hz, 1H) 4.35-4.09 (m, 2H) 3.57 (dd, J = 29.2, 13.9 Hz, 1H) 3.30 (t, J = 13.2 Hz, 1H) 2.98 (br. s, 2H) 2.42-2.21 (m, 1H); ^{19}F NMR (376 MHz, DMSO-d_6, 80 °C) δ ppm -98.83—-101.73 (m, 2H) -111.15 (t, J = 9.4 Hz, 1H); QTOF ES+ MS: (M+H) 475.11; HPLC Ret: 5.53 min; 98% pure.

N-(5-chloropyridin-3-yl)-5,5-difluoro-1-(3-fluoro-5-(pyridin-4-yl)benzoyl)piperidine-3-carboxamide. (CCG-264607). Method J followed by Method I starting from tert-butyl 5-((5-chloropyridin-3-yl)carbamoyl)-3,3-difluoropiperidine-1-carboxylate (0.04 g, 0.11 mmol) and 3-fluoro-5-(pyridin-4-yl)benzoic acid (0.02 g, 0.11 mmol) gave N-(5-chloropyridin-3-yl)-5,5-difluoro-1-(3-fluoro-5-(pyridin-4-yl)benzoyl)piperidine-3-carboxamide (0.05 g, 85% (2 steps)) as white solid; column: 85% to 100% EtOAc: Hex; ^{1}H NMR (400 MHz, DMSO-d_6, 80 °C) δ ppm 10.31 (br.s 1H) 8.69-8.59 (m, 3H) 8.29 (s, 1H) 8.15 (s, 1H) 7.77-7.68 (m, 3H) 7.62 (s, 1H) 7.31 (d, J = 9.0 Hz, 1H) 4.37-4.10 (m, 2H) 3.60 (dd, J = 29.5, 14.0 Hz, 1H) 3.29 (t, J = 13.2 Hz, 1H) 2.98 (br. s, 2H) 2.42-2.25 (m, 1H); ^{19}F NMR (376 MHz, DMSO-d_6, 80 °C) δ ppm -97.70—-103.55 (m, 2H) -111.08 (t, J = 9.4 Hz, 1H); QTOF ES+ MS: (M+H) 475.11; HPLC Ret: 5.20 min; 100% pure.

N-(2-chloropyridin-4-yl)-5,5-difluoro-1-(3-fluoro-5-(pyridin-4-yl)benzoyl)piperidine-3-carboxamide. (CCG-264608). Method J followed by Method I starting from tert-butyl 5-((2-chloropyridin-4-yl)carbamoyl)-3,3-difluoropiperidine-1-carboxylate (0.02 g, 0.05 mmol) and 3-fluoro-5-(pyridin-4-yl)benzoic acid (0.01 g, 0.05 mmol) gave N-(2-chloropyridin-4-yl)-5,5-difluoro-1-(3-fluoro-5-(pyridin-4-yl)benzoyl)piperidine-3-carboxamide (0.02 g, 74% (2 steps)) as white solid; column: 80% to 100% EtOAc: Hex; ^{1}H NMR (400 MHz, DMSO-d_6, 80 °C) δ ppm 10.47 (br.s 1H) 8.68-8.62 (m, 3H) 8.23 (d, J = 5.6 Hz, 1H) 7.78-7.66 (m, 4H) 7.61 (s, 1H) 7.44 (d, J = 5.7 Hz, 1H) 7.28 (d, J = 8.5 Hz, 1H) 4.38-4.08 (m, 2H) 3.61 (dd, J = 29.1, 13.8 Hz, 1H) 3.28 (t, J = 13.2 Hz, 1H) 2.98 (br. s, 2H) 2.42-2.21 (m, 1H); ^{19}F NMR (376 MHz, DMSO-d_6, 80 °C) δ ppm -98.42—-103.31 (m, 2H) -111.09 (t, J = 9.3 Hz, 1H); QTOF ES+ MS: (M+H) 475.11; HPLC Ret: 5.20 min; 97% pure.

N-(6-chloropyridin-2-yl)-5,5-difluoro-1-(3-fluoro-5-(pyridin-4-yl)benzoyl)piperidine-3-carboxamide. (CCG-264609). Method J followed by Method I starting from tert-butyl 5-((6-chloropyridin-2-yl)carbamoyl)-3,3-difluoropiperidine-1-carboxylate (0.04 g, 0.1 mmol) and 3-fluoro-5-(pyridin-4-yl)benzoic acid (0.02 g, 0.1 mmol) gave N-(6-chloropyridin-2-yl)-5,5-difluoro-1-(3-fluoro-5-(pyridin-4-yl)benzoyl)piperidine-3-carboxamide (0.02 g, 32% (2 steps)) as white solid; column: 75% to 100% EtOAc: Hex; H_2O wash post column needed; ^{1}H NMR (400 MHz, DMSO-d_6, 80 °C) δ ppm 10.75 (br.s 1H) 8.66 (d, J = 5.2 Hz, 2H) 7.96 (d, J = 8.2 Hz, 1H) 7.83-7.68 (m, 4H) 7.62 (s, 1H) 7.31 (d, J = 5.8 Hz, 1H) 7.15 (d, J = 7.7 Hz, 1H) 4.32-4.10 (m, 2H) 3.55 (dd, J = 29.2, 13.8 Hz, 1H) 3.29 (t, J = 13.2 Hz, 1H) 2.98 (br. s, 2H) 2.39-2.23 (m, 1H); ^{19}F NMR (376 MHz, DMSO-d_6, 80 °C) δ ppm -97.46—-104.04 (m, 2H) -111.16 (t, J = 9.5 Hz, 1H); QTOF ES+ MS: (M+H) 475.11; HPLC Ret: 5.67 min; 98% pure.

1-(5-bromo-2-fluorobenzoyl)-N-(3-chlorophenyl)-5,5-difluoropiperidine-3-carboxamide. (CCG-264464). Method J followed by Method I starting from tert-butyl 5-((3-chlorophenyl)carbamoyl)-3,3-difluoropiperidine-1-carboxylate (0.06 g, 0.2 mmol) and 5-bromo-2-

fluorobenzoic acid (0.04 g, 0.2 mmol) gave 1-(5-bromo-2-fluorobenzoyl)-N-(3-chlorophenyl)-5,5-difluoropiperidine-3-carboxamide (0.07 g, 88% (2 steps)) as yellow solid; column: 20% EtOAc: Hex; ^{1}H NMR (400 MHz, DMSO-d_6, 80 °C) δ ppm 10.07 (br. s, 1H) 7.77-7.65 (m, 2H) 7.54 (br. s, 1H) 7.42 (br. s, 1H) 7.29 (q, J = 9.4, 9.0 Hz, 2H) 7.09 (d, J = 8.0 Hz, 1H) 4.50-4.12 (m, 2H) 3.74-3.38 (m, 2H) 3.37-3.31 (m, 1H) 2.90 (br. s, 1H) 2.38-2.22 (m, 1H); ^{19}F NMR (376 MHz, DMSO-d_6, 80 °C) δ ppm -97.59—-102.14 (m, 2H) -117.67 (s, 1H); QTOF ES+ MS: (M+Na) 498.98; HPLC Ret: 7.78 min; 99% pure.

1-(5-bromo-2-fluorobenzoyl)-N-(3,4-dichlorophenyl)-5,5-difluoropiperidine-3-carboxamide. (CCG-264467). Method J followed by Method I starting from tert-butyl 5-((3,4-dichlorophenyl)carbamoyl)-3,3-difluoropiperidine-1-carboxylate (0.06 g, 0.15 mmol) and 5-bromo-2-fluorobenzoic acid (0.03 g, 0.15 mmol) gave 1-(5-bromo-2-fluorobenzoyl)-N-(3,4-dichlorophenyl)-5,5-difluoropiperidine-3-carboxamide (0.06 g, 87% (2 steps)) as yellow solid; column: 20% EtOAc: Hex; ^{1}H NMR (400 MHz, DMSO-d_6, 80 °C) δ ppm 10.18 (br. s, 1H) 7.90 (br. s, 1H) 7.71-7.67 (m, 1H) 7.56-7.45 (m, 3H) 7.28 (t, J = 9.1 Hz, 1H) 4.65-4.12 (m, 2H) 3.74-3.30 (m, 3H) 2.89 (br. s, 1H) 2.37-2.21 (m, 1H); ^{19}F NMR (376 MHz, DMSO-d_6, 80 °C) δ ppm -95.46—-104.76 (m, 2H) -117.69 (s, 1H); QTOF ES+ MS: (M+Na) 532.94; HPLC Ret: 8.16 min; 99% pure.

N-(3-chlorophenyl)-5,5-difluoro-1-(3-(2-(pyrrolidin-1-yl)ethoxy)benzoyl)piperidine-3-carboxamide. (CCG-264465). Method J followed by Method I starting from tert-butyl 5-((3-chlorophenyl)carbamoyl)-3,3-difluoropiperidine-1-carboxylate (0.06 g, 0.16 mmol) and 3-(2-(pyrrolidine-1-yl)ethoxy)benzoic acid, HCl (0.05 g, 0.18 mmol) gave N-(3-chlorophenyl)-5,5-difluoro-1-(3-(2-(pyrrolidin-1-yl)ethoxy)benzoyl)piperidine-3-carboxamide (0.06 g, 75% (2 steps)) as white solid; column: 5% to 8% MeOH: DCM; ^{1}H NMR (400 MHz, DMSO-d_6, 80 °C) δ ppm 10.07 (br. s, 1H) 7.73 (s, 1H) 7.47-7.35 (m, 2H) 7.31 (t, J = 8.1 Hz, 1H) 7.09 (d, J = 7.4 Hz, 2H) 7.03-6.95 (m, 2H) 4.47-4.02 (m, 2H) 3.35 (dd, J = 30.4, 14.0 Hz, 1H) 3.52-3.47 (m, 2H) 3.20-

2.87 (m, 5H) 2.41-2.14 (m, 1H) 1.84 (br. s, 4H) 1.26 (br. s, 4H); ^{19}F NMR (376 MHz, DMSO-d_6, 80 °C) δ ppm -97.78—-102.24 (m, 2H); QTOF ES+ MS: (M+H) 492.19; HPLC Ret: 5.95 min; 99% pure.

N-(3-chlorophenyl)-5,5-difluoro-1-(3-(3-(pyrrolidin-1-yl)propoxy)benzoyl)piperidine-3-carboxamide. (CCG-264466). Method J followed by Method I starting from tert-butyl 5-((3-chlorophenyl)carbamoyl)-3,3-difluoropiperidine-1-carboxylate (0.06 g, 0.16 mmol) and 3-(3-(pyrrolidine-1-yl)propoxy)benzoic acid, HCl (0.05 g, 0.18 mmol) gave N-(3-chlorophenyl)-5,5-difluoro-1-(3-(3-(pyrrolidin-1-yl)propoxy)benzoyl)piperidine-3-carboxamide (0.05 g, 57% (2 steps)) as white solid; column: 5% to 8% MeOH: DCM; ^{1}H NMR (400 MHz, DMSO-d_6, 80 °C) δ ppm 10.09 (br. s, 1H) 7.74 (s, 1H) 7.47-7.27 (m, 3H) 7.13-7.02 (m, 2H) 7.02-6.92 (m, 2H) 4.27 (br. s, 2H) 3.51 (dd , J = 30.3, 14.1 Hz, 1H) 3.20 (br. s, 7H) 3.01-2.91 (m, 1H) 2.42-2.16 (m, 1H) 2.09 (p, J = 7.3 Hz, 2H) 1.93 (br. s, 4H) 1.25 (br. s, 4H); ^{19}F NMR (376 MHz, DMSO-d_6, 80 °C) δ ppm -98.35—-103.24 (m, 2H); QTOF ES+ MS: (M+H) 506.20; HPLC Ret: 6.07 min; 99% pure.

N-(3,4-dichlorophenyl)-5,5-difluoro-1-(3-(2-(pyrrolidin-1-yl)ethoxy)benzoyl)piperidine-3-carboxamide. (CCG-264468). Method J followed by Method I starting from tert-butyl 5-((3,4-dichlorophenyl)carbamoyl)-3,3-difluoropiperidine-1-carboxylate (0.06 g, 0.16 mmol) and 3-(2-(pyrrolidine-1-yl)ethoxy)benzoic acid, HCl (0.05 g, 0.15 mmol) gave N-(3,4-dichlorophenyl)-5,5-difluoro-1-(3-(2-(pyrrolidin-1-yl)ethoxy)benzoyl)piperidine-3-carboxamide (0.06 g, 75% (2 steps)) as white solid; column: 4% to 6% MeOH: DCM; ^{1}H NMR (400 MHz, DMSO-d_6, 80 °C) δ ppm 10.17 (br. s, 1H) 7.91 (s, 1H) 7.54-7.36 (m, 3H) 7.07 (d, J = 8.4 Hz, 1H) 7.02-6.94 (m, 2H) 4.48-4.00 (m, 2H) 3.51 (dd, J = 30.2, 13.7 Hz, 1H) 3.52-3.47 (m, 1H) 3.15 (br. s, 2H) 2.98-2.89 (m, 4H) 2.38-2.19 (m, 1H) 1.81 (br. s, 4H) 1.24 (br. s, 4H); ^{19}F NMR (376 MHz, DMSO-d_6, 80 °C) δ ppm -97.70—-103.55 (m, 2H); QTOF ES+ MS: (M+H) 526.15; HPLC Ret: 6.32 min; 99% pure.

N-(3,4-dichlorophenyl)-5,5-difluoro-1-(3-(3-(pyrrolidin-1-yl)propoxy)benzoyl)piperidine-3-carboxamide. (CCG-264469). Method J followed by Method I starting from tert-butyl 5-((3,4-dichlorophenyl)carbamoyl)-3,3-difluoropiperidine-1-carboxylate (0.06 g, 0.16 mmol) and 3-(3-(pyrrolidine-1-yl)propoxy)benzoic acid, HCl (0.05 g, 0.16 mmol) gave N-(3,4-dichlorophenyl)-5,5-difluoro-1-(3-(3-(pyrrolidin-1-yl)propoxy)benzoyl)piperidine-3-carboxamide (0.07 g, 91% (2 steps)) as white solid; column: 5% to 8% MeOH: DCM; ^{1}H NMR (400 MHz, DMSO-d_6, 80 °C) δ ppm 10.17 (br. s, 1H) 7.91 (s, 1H) 7.55-7.46 (m, 2H) 7.39 (t, J = 8.0 Hz, 1H) 7.05 (d, J = 8.4 Hz, 1H) 7.01-6.92 (m, 2H) 4.27 (br. s, 2H) 3.51 (dd , J = 30.0, 13.8 Hz, 1H) 3.19 (br. s, 7H) 3.01-2.91 (m, 1H) 2.39-2.21 (m, 1H) 2.10 (p, J = 7.6 Hz, 2H) 1.93 (br. s, 4H) 1.27 (br. s, 4H); ^{19}F NMR (376 MHz, DMSO-d_6, 80 °C) δ ppm -97.39—-103.98 (m, 2H); QTOF ES+ MS: (M+H) 540.16; HPLC Ret: 6.44 min; 99% pure.

N-(3-(((tert-butyldiphenylsilyl)oxy)methyl)-4-chlorophenyl)-5,5-difluoro-1-(3-fluoro-5-(pyridin-4-yl)benzoyl)piperidine-3-carboxamide. In a 25 mL round bottomed flask tert-butyl 5-((3-(((tert-butyldiphenylsilyl)oxy)methyl)-4-chlorophenyl)carbamoyl)-3,3-difluoropiperidine-1-carboxylate (0.19 g, 0.30 mmol) was dissolved in 4 M HCl/Dioxanes (2.0 mL) and the reaction was stirred at 25 °C for 1 hr. The solvents were evaporated in vacuo, and the subsequent solid was taken into the next step without further purification (HPLC = 7.74 min). 3-fluoro-5-(pyridin-4-yl)benzoic acid (0.06 g, 0.29 mmol) was dissolved in DMF (2 mL) and HATU (0.22 g, 0.58 mmol), N-(3-(((tert-butyldiphenylsilyl)oxy)methyl)-4-chlorophenyl)-5,5-difluoropiperidine-3-carboxamide, HCl (0.17 g, 0.29 mmol), and NMM (0.09 g, 0.10 mL, 0.88 mmol) were added. The reaction was stirred at 25 °C for 16 hr and brine (10 mL) was added. The subsequent solid was filtered and dried in vacuo to produce white solid. Yield=84% (2-steps). ^{1}H NMR (500 MHz, DMSO-d_6) δ 10.49 (br. s, 1H) 10.27 (br. s, 1H) 8.68 (br. s, 2H) 8.06 (br. s, 1H) 7.86 (br. s, 1H) 7.79 (d, J = 5.3 Hz, 2H) 7.72-7.58 (m, 6H) 7.54-7.28 (m, 8H) 4.80-4.62 (m, 2H) 3.95-3.74 (m,

1H) 3.58-3.41 (m, 1H) 3.04-2.94 (m, 1H) 2.45-2.21 (m, 1H) 1.06 (s, 9H); TOF ES+ MS: (M+H) 742.25; HPLC Ret: 8.40 min.

N-(4-chlorophenyl)-3-(3-(furan-2-yl)benzamido)benzamide. (CCG-257866). In a 25 mL round bottomed flask tert-butyl (3-((4-chlorophenyl)carbamoyl)phenyl)carbamate (0.2 g, 0.58 mmol) was dissolved in 4N HCl/dioxane solution (2 mL). The reaction was stirred at 25 °C for 3 hr and then concentrated to dryness in vacuo. The remaining white solid was dissolved in DMF (1 mL), and then added to a solution of 3-(furan-2-yl)benzoic acid (0.11 g, 0.58 mmol) and HATU (0.44 g, 1.15 mmol) in DMF (1mL). DIPEA (0.19 g, 0.25 mL, 1.44 mmol) was added and the solution was stirred at 25 °C for 1 hr and then heated at 150 °C for 2 hr. Once cooled to 25 °C the reaction was diluted with brine (30 mL). The product was extracted with EtOAc (3 x 20 mL), washed with dilute HCl (3 x 15 mL) and sat. $NaHCO_3$ (3 x 15 mL), and then concentrated in vacuo. The subsequent oil was subjected to silica gel chromatography eluting with 100% EtOAc. The fractions containing product were concentrated in vacuo to produce colorless oil. The product was crystalized as white powder from the oil using EtOAc/Hex. Similar analogs were made in an analogous fashion. Yield=11%. ^{1}H NMR (500 MHz, DMSO-d_6) δ ppm 10.57 (s, 1H) 10.43 (s, 1H) 8.32 (d, J = 13.0 Hz, 2H) 8.07 (d, J = 8.1 Hz, 1H) 7.92 (dd, J = 13.9, 7.7 Hz, 2H) 7.84 (d, J = 8.3 Hz, 2H) 7.71 (d, J = 7.6 Hz, 1H) 7.61 (t, J = 7.7 Hz, 1H) 7.54 (t, J = 8.0 Hz, 1H) 7.43 (d, J = 8.2 Hz, 2H) 7.12-7.07 (m, 1H) 6.66 (s, 1H); ^{13}C NMR (500 MHz, DMSO-d_6) δ ppm 166.08, 165.82, 152.75, 143.85, 139.76, 138.60, 135.84, 135.80, 130.96, 129.60, 129.17, 129.00, 127.73, 127.09, 126.92, 123.96, 123.19, 122.96, 122.28, 120.45, 112.71, 107.27; TOF ES+ MS: (M+H) 417.1; HPLC Ret: 7.89 min; 99.5 % pure.

N-(4-chlorophenyl)-5-(3-(furan-2-yl)benzamido)nicotinamide. (CCG-257922). Starting from 5-amino-N-(4-chlorophenyl)nicotinamide, HCl. Column: 50% EtOAc: Hex. Crystalized from EtOAc: Hex. White powder. Yield=12.5%. ^{1}H NMR (500 MHz, DMSO-d_6) δ ppm 10.76 (s, 1H) 10.62 (s, 1H) 9.17 (d, J = 2.5 Hz, 1H) 8.89 (s, 1H) 8.70 (s, 1H) 8.32 (s, 1H) 7.94 (dd, J = 20.4,

7.8 Hz, 2H) 7.89-7.80 (m, 3H) 7.63 (t, J = 7.8 Hz, 1H) 7.45 (d, J = 8.4 Hz, 2H) 7.10 (d, J = 3.4 Hz, 1H) 6.66 (s, 1H); ^{13}C NMR (500 MHz, DMSO-d_6) δ ppm 166.21, 164.45, 152.65, 144.84, 143.92, 143.78, 138.25, 136.17, 135.25, 131.05, 130.89, 129.71, 129.09, 128.09, 127.15, 127.06, 123.00, 122.38, 112.74, 107.38; TOF ES+ MS: (M+H) 418.1; HPLC Ret: 6.88 min; 98% pure.

***cis*-N1-(4-chlorophenyl)-N3-(3-(furan-2-yl)phenyl)cyclopentane-1,3-dicarboxamide (CCG-263872).** Method I starting from *cis*-3-((4-chlorophenyl)carbamoyl)cyclopentanecarboxylic acid (0.07 g, 0.27 mmol) and 3-(furan-2-yl)aniline, HCl (0.05 g, 0.27 mmol) gave cis-N1-(4-chlorophenyl)-N3-(3-(furan-2-yl)phenyl)cyclopentane-1,3-dicarboxamide (0.11 g, 98%) as white solid; column: 60% to 80% EtOAc: Hex; ^{1}H NMR (500 MHz, DMSO-d_6) δ ppm 10.05 (s, 1H) 10.00 (s, 1H) 8.03 (d, J = 1.9 Hz, 1H) 7.75 (d, J = 1.7 Hz, 1H) 7.66 (d, J = 8.5 Hz, 2H) 7.52 (d, J = 7.9 Hz, 1H) 7.41-7.32 (m, 4H) 6.87 (d, J = 3.4 Hz, 1H) 6.60 (dd, J = 3.2, 1.8 Hz, 1H) 2.89 (q, J = 9.3 Hz, 2H) 2.19 (dt, J = 12.5, 7.4 Hz, 1H) 2.04 (dt, J = 12.5, 10.3 Hz, 1H) 1.92 (dt, J = 8.1, 5.4 Hz, 4H); ^{13}C NMR (500 MHz, DMSO-d_6) δ ppm 173.93, 173.90, 153.37, 143.34, 140.29, 138.73, 131.12, 129.70, 128.99, 126.98, 121.12, 118.80, 118.66, 114.43, 112.50, 106.27, 46.15, 46.12, 34.58, 30.05; TOF ES+ MS: (M+Na) 431.11; HPLC Ret: 7.71 min; 98 % pure.

***trans*-N1-(4-chlorophenyl)-N3-(3-(furan-2-yl)phenyl)cyclopentane-1,3-dicarboxamide.** Method I starting from trans-3-((4-chlorophenyl)carbamoyl)cyclopentanecarboxylic acid (0.04 g, 0.15 mmol) and 3-(furan-2-yl)aniline, HCl (0.03 g, 0.15 mmol) gave trans-N1-(4-chlorophenyl)-N3-(3-(furan-2-yl)phenyl)cyclopentane-1,3-dicarboxamide (0.02 g, 38%) as white solid; column: 30% to 80% EtOAc: Hex; ^{1}H NMR (500 MHz, DMSO-d_6) δ ppm 10.10 (s, 1H) 10.05 (s, 1H) 8.03 (d, J = 1.5 Hz, 1H) 7.75 (d, J = 1.5 Hz, 1H) 7.66 (d, J = 8.6 Hz, 2H) 7.50 (d, J = 7.7 Hz, 1H) 7.41-7.30 (m, 4H) 6.86 (d, J = 2.7 Hz, 1H) 6.62-6.57 (m, 1H) 3.03 (dt, J = 14.3, 7.5 Hz, 2H) 2.13-1.98 (m, 4H) 1.86-1.76 (m, 2H); ^{13}C NMR (500 MHz, DMSO-d_6) δ ppm 174.49, 153.39, 143.36, 140.36, 138.42, 131.10, 129.68, 128.99, 126.56, 121.03, 118.75, 118.58, 114.39,

112.50, 109.99 106.24, 45.54, 45.50, 34.45, 30.73, 30.70; TOF ES+ MS: (M+H) 409.13; HPLC Ret: 7.62 min; >95 % pure (80% trans: 20% cis).

N-(*cis*-3-((4-chlorophenyl)carbamoyl)cyclohexyl)-3-(furan-2-yl)benzamide. (CCG-257865) Method I starting from *cis*-3-(3-(furan-2-yl)benzamido)cyclohexanecarboxylic acid (0.04 g, 0.13 mmol) and 4-chloroaniline (0.016 g, 0.13 mmol) gave N-(cis-3-((4-chlorophenyl)carbamoyl)cyclohexyl)-3-(furan-2-yl)benzamide (0.02 g, 30%) as brown solid; the product was crystalized from EtOAc/Hex; ^{1}H NMR (500 MHz, DMSO-d_6) δ ppm 10.05 (br. s, 1H) 8.42 (d, J = 8.0 Hz, 1H) 8.15 (br. s, 1H) 7.83 (d, J = 7.9 Hz, 1H) 7.79 (s, 1H) 7.75 (d, J = 7.8 Hz, 1H) 7.64 (d, J = 8.9 Hz, 2H) 7.50 (t, J = 7.7 Hz, 1H) 7.34 (d, J = 8.8 Hz, 2H) 7.02 (d, J = 3.4 Hz, 1H) 6.63 (dd, J = 3.4, 1.8 Hz, 1H) 3.99-3.85 (m, 1H) 3.32 (br. s., 1H) 2.15-1.79 (m, 6H) 1.57 (q, J = 12.2 Hz, 1H) 1.42-1.29 (m, 2H); ^{13}C NMR (500 MHz, DMSO-d_6) δ ppm 173.94, 165.48, 152.93, 143.67, 138.80, 135.85, 130.74, 129.31, 128.98, 126.93, 126.73, 126.28, 122.56, 121.06, 112.62, 106.97, 48.12, 44.48, 35.45, 32.17, 28.74, 24.50; TOF ES+ MS: (M+H) 423.1; HPLC Ret: 7.61 min; 98 % pure.

N-(4-chlorophenyl)-1-(3-(furan-2-yl)benzoyl)-1,2,5,6-tetrahydropyridine-3-carboxamide (CCG-258161). Method I starting from 1-(3-(furan-2-yl)benzoyl)-1,2,5,6-tetrahydropyridine-3-carboxylic acid (0.08 g, 0.25 mmol) and 4-chloroaniline (0.03 g, 0.24 mmol) gave N-(4-chlorophenyl)-1-(3-(furan-2-yl)benzoyl)-1,2,5,6-tetrahydropyridine-3-carboxamide (0.03 g, 27%) as white solid; column: 60% EtOAc: 40% Hex; ^{1}H NMR (500 MHz, DMSO-d_6) δ ppm 10.02 (br. s, 1H) 7.92-7.51 (m, 6H) 7.45-7.29 (m, 3H) 7.08 (br. s, 1H) 6.92 (br. s, 1H) 6.63 (br.s, 1H) 4.40 (br. s, 1H) 4.18 (br. s, 1H) 3.77 (br. s, 1H) 3.45 (br. s, 1H) 2.38 (br. s, 2H); ^{13}C NMR (500 MHz, DMSO-d_6) δ ppm 169.28, 165.12, 152.65, 143.80, 137.20, 131.82, 131.00, 129.64, 128.90, 127.52, 124.733, 122.11, 112.66, 107.24, 84.55, 68.83, 46.65, 43.65, 25.85; QTOF ES+ MS: (M+H) 407.12; HPLC Ret: 7.41 min; 93 % pure.

N-(3-chlorophenyl)-1-(3-fluoro-5-(pyridin-4-yl)benzoyl)-1,2,5,6-tetrahydropyridine-3-carboxamide (CCG-264643). Method I starting from 1-(3-(furan-2-yl)benzoyl)-1,2,5,6-tetrahydropyridine-3-carboxylic acid (0.04 g, 0.12 mmol) and 3-chloroaniline (0.02 g, 0.12 mmol) gave N-(3-chlorophenyl)-1-(3-fluoro-5-(pyridin-4-yl)benzoyl)-1,2,5,6-tetrahydropyridine-3-carboxamide (0.03 g, 62%) as white solid; column: 100% EtOAc; ^{1}H NMR (400 MHz, DMSO-d_6) δ ppm 9.75 (br. s, 1H) 8.65 (d, J = 8.0 Hz, 2H) 7.80-7.60 (m, 3H) 7.56 (d, J = 8.3 Hz, 1H) 7.38-7.22 (m, 2H) 7.08 (d, J = 8.0 Hz, 1H) 6.91 (br. s, 1H) 5.93 (s, 1H) 4.31 (br. s, 2H) 3.60 (br. s, 2H) 2.38 (br. s, 2H); ^{19}F NMR (376 MHz, DMSO-d_6) δ ppm -111.36 (t, J = 9.4 Hz, 1H); TOF ES+ MS: (M+H) 436.12; HPLC Ret: 5.51 min; 85 % pure. 15% impurity is conformational isomer; verified via HPLC/MS & hi-temp HNMR/FNMR.

5,5-difluoro-1-(3-fluoro-5-(pyridin-4-yl)benzoyl)-N-(m-tolyl)piperidine-3-carboxamide. (CCG-264321). Method I starting from 5,5-difluoro-1-(3-fluoro-5-(pyridin-4-yl)benzoyl)piperidine-3-carboxylic acid (0.05 g, 0.12 mmol) and m-toluidine (0.02 g, 0.15 mmol) gave 5,5-difluoro-1-(3-fluoro-5-(pyridin-4-yl)benzoyl)-N-(m-tolyl)piperidine-3-carboxamide (0.05 g, 96%) as white solid; column: 70% to 80% EtOAc: Hex; ^{1}H NMR (400 MHz, DMSO-d_6, 80 °C) δ ppm 9.78 (s, 1H) 8.66 (d, J = 5.0 Hz, 2H) 7.77-7.67 (m, 3H) 7.61 (q, 1.4 Hz, 1H) 7.39-7.28 (m, 3H) 7.15 (t, J = 7.8 Hz, 1H) 6.87 (d, J = 7.5 Hz, 1H) 4.26 (br. s, 2H) 3.56 (dd, J = 30.0, 13.7 Hz, 1H) 3.27 (t, J = 9.9 Hz, 1H) 2.96 (s, 2H) 2.26 (s, 3H) 2.46-2.34 (m, 1H); ^{19}F NMR (376 MHz, DMSO-d_6, 80 °C) δ ppm -98.42—-102.51 (m, 2H) -111.09 (t, J = 9.3 Hz, 1H); QTOF ES+ MS: (M+H) 454.17; HPLC Ret: 5.70 min; 98% pure.

N-(3-ethylphenyl)-5,5-difluoro-1-(3-fluoro-5-(pyridin-4-yl)benzoyl)piperidine-3-carboxamide. (CCG-264322). Method I starting from 5,5-difluoro-1-(3-fluoro-5-(pyridin-4-yl)benzoyl)piperidine-3-carboxylic acid (0.05 g, 0.12 mmol) and 3-ethylaniline (0.02 g, 0.15 mmol) gave N-(3-ethylphenyl)-5,5-difluoro-1-(3-fluoro-5-(pyridin-4-yl)benzoyl)piperidine-3-carboxamide (0.05 g, 88%) as white solid; column: 65% to 80% EtOAc: Hex; ^{1}H NMR (400

MHz, DMSO-d_6, 80 °C) δ ppm 9.83 (s, 1H) 8.66 (d, J = 4.9 Hz, 2H) 7.78-7.67 (m, 3H) 7.62 (s, 1H) 7.42-7.27 (m, 3H) 7.18 (t, J = 7.8 Hz, 1H) 6.90 (d, J = 7.5 Hz, 1H) 4.20 (br. s, 2H) 3.56 (dd, J = 29.9, 14.0 Hz, 1H) 3.26 (t, J = 9.9 Hz, 1H) 2.98 (br. s, 2H) 2.54 (q, J = 7.6 Hz, 2H) 2.30 (dd, J = 19.2, 13.2 Hz, 1H) 1.17 (t, J = 7.6 Hz, 3H); ^{19}F NMR (376 MHz, DMSO-d_6, 80 °C) δ ppm -97.30—-102.57 (m, 2H) -111.09 (t, J = 9.3 Hz, 1H); QTOF ES+ MS: (M+H) 468.19; HPLC Ret: 5.99 min; 98% pure.

5,5-difluoro-1-(3-fluoro-5-(pyridin-4-yl)benzoyl)-N-(3-isopropylphenyl)piperidine-3-carboxamide. (CCG-264323). Method I starting from 5,5-difluoro-1-(3-fluoro-5-(pyridin-4-yl)benzoyl)piperidine-3-carboxylic acid (0.05 g, 0.12 mmol) and 3-isopropylaniline (0.02 g, 0.15 mmol) gave 5,5-difluoro-1-(3-fluoro-5-(pyridin-4-yl)benzoyl)-N-(3-isopropylphenyl)piperidine-3-carboxamide (0.05 g, 86%) as white solid; column: 65% to 80% EtOAc: Hex; ^{1}H NMR (400 MHz, DMSO-d_6, 80 °C) δ ppm 9.82 (s, 1H) 8.66 (d, J = 4.9 Hz, 2H) 7.77-7.67 (m, 3H) 7.62 (s, 1H) 7.45-7.28 (m, 3H) 7.18 (t, J = 7.9 Hz, 1H) 6.93 (d, J = 7.7 Hz, 1H) 4.20 (br. s, 2H) 3.56 (dd, J = 30.0, 13.9 Hz, 1H) 3.26 (t, J = 12.1 Hz, 1H) 2.98 (br. s, 2H) 2.84 (p, J = 6.9 Hz, 1H) 2.37-2.19 (m, 1H) 1.22-1.13 (m, 6H); ^{19}F NMR (376 MHz, DMSO-d_6, 80 °C) δ ppm -96.90—-104.28 (m, 2H) -111.09 (t, J = 9.4 Hz, 1H); QTOF ES+ MS: (M+H) 482.21; HPLC Ret: 6.23 min; 99% pure.

N-(3-cyclopropylphenyl)-5,5-difluoro-1-(3-fluoro-5-(pyridin-4-yl)benzoyl)piperidine-3-carboxamide. (CCG-264324). Method I starting from 5,5-difluoro-1-(3-fluoro-5-(pyridin-4-yl)benzoyl)piperidine-3-carboxylic acid (0.05 g, 0.12 mmol) and 3-cyclopropylaniline (0.02 g, 0.15 mmol) gave N-(3-cyclopropylphenyl)-5,5-difluoro-1-(3-fluoro-5-(pyridin-4-yl)benzoyl)piperidine-3-carboxamide (0.06 g, 100%) as purple solid; column: 70% to 80% EtOAc: Hex; ^{1}H NMR (400 MHz, DMSO-d_6, 80 °C) δ ppm 9.78 (s, 1H) 8.66 (d, J = 4.9 Hz, 2H) 7.77-7.67 (m, 3H) 7.61 (s, 1H) 7.37-7.23 (m, 3H) 7.14 (t, J = 7.9 Hz, 1H) 6.79 (d, J = 7.6 Hz, 1H) 4.20 (br. s, 2H) 3.56 (dd, J = 30.0, 14.0 Hz, 1H) 3.25 (t, J = 12.5 Hz, 1H) 2.98 (br. s, 2H) 2.39-

2.20 (m, 1H) 1.92-1.81 (m, 1H) 0.96-0.82 (m, 2H) 0.61-0.58 (m, 2H); ^{19}F NMR (376 MHz, DMSO-d_6, 80 °C) δ ppm -96.90—-101.35 (m, 2H) -111.09 (t, J = 9.4 Hz, 1H); QTOF ES+ MS: (M+H) 480.19; HPLC Ret: 5.98 min; 99% pure.

5,5-difluoro-1-(3-fluoro-5-(pyridin-4-yl)benzoyl)-N-(3-(trifluoromethyl)phenyl)piperidine-3-carboxamide. (CCG-264325). Method I starting from 5,5-difluoro-1-(3-fluoro-5-(pyridin-4-yl)benzoyl)piperidine-3-carboxylic acid (0.05 g, 0.12 mmol) and 3-(trifluoromethyl)aniline (0.02 g, 0.15 mmol) gave 5,5-difluoro-1-(3-fluoro-5-(pyridin-4-yl)benzoyl)-N-(3-(trifluoromethyl)phenyl)piperidine-3-carboxamide (0.05 g, 78%) as white solid; column: 70% EtOAc: Hex; ^{1}H NMR (400 MHz, DMSO-d_6, 80 °C) δ ppm 10.22 (br. s, 1H) 8.66 (d, J = 4.9 Hz, 2H) 8.01 (s, 1H) 7.80-7.67 (m, 4H) 7.62 (s, 1H) 7.52 (t, J = 8.0 Hz, 1H) 7.40-7.28 (m, 2H) 4.40-4.12 (m, 2H) 3.59 (dd, J = 29.6, 14.0 Hz, 1H) 3.28 (t, J = 12.5 Hz, 1H) 2.98 (br. s, 2H) 2.42-2.22 (m, 1H); ^{19}F NMR (376 MHz, DMSO-d_6, 80 °C) δ ppm -61.54 (s, 3H) -96.90—-101.35 (m, 2H) -111.10 (t, J = 9.4 Hz, 1H); QTOF ES+ MS: (M+H) 508.15; HPLC Ret: 6.12 min; 97% pure.

5,5-difluoro-1-(3-fluoro-5-(pyridin-4-yl)benzoyl)-N-(3-(trifluoromethoxy)phenyl)piperidine-3-carboxamide. (CCG-264326). Method I starting from 5,5-difluoro-1-(3-fluoro-5-(pyridin-4-yl)benzoyl)piperidine-3-carboxylic acid (0.05 g, 0.12 mmol) and 3-(trifluoromethoxy)aniline (0.03 g, 0.15 mmol) gave 5,5-difluoro-1-(3-fluoro-5-(pyridin-4-yl)benzoyl)-N-(3-(trifluoromethoxy)phenyl)piperidine-3-carboxamide (0.06 g, 85%) as white solid; column: 65% EtOAc: Hex; ^{1}H NMR (400 MHz, DMSO-d_6, 80 °C) δ ppm 10.17 (br. s, 1H) 8.66 (d, J = 4.9 Hz, 2H) 7.78-7.59 (m, 5H) 7.48 (d, J = 8.1 Hz, 1H) 7.40 (t, J = 8.1 Hz, 1H) 7.28 (d, J = 8.4 Hz, 1H) 7.00 (d, J = 8.2 Hz, 1H) 4.38-4.08 (m, 2H) 3.58 (dd, J = 29.8, 13.9 Hz, 1H) 3.27 (t, J = 12.5 Hz, 1H) 2.98 (br. s, 2H) 2.42-2.25 (m, 1H); ^{19}F NMR (376 MHz, DMSO-d_6, 80 °C) δ ppm -56.61 (s, 3H) -96.90—-101.35 (m, 2H) -111.10 (t, J = 9.4 Hz, 1H); QTOF ES+ MS: (M+H) 524.14; HPLC Ret: 6.23 min; 99% pure.

N-(2-chlorophenyl)-5,5-difluoro-1-(3-fluoro-5-(pyridin-4-yl)benzoyl)piperidine-3-carboxamide. (CCG-264327). Method I starting from 5,5-difluoro-1-(3-fluoro-5-(pyridin-4-yl)benzoyl)piperidine-3-carboxylic acid (0.05 g, 0.12 mmol) and 2-chloroaniline (0.02 g, 0.15 mmol) gave N-(2-chlorophenyl)-5,5-difluoro-1-(3-fluoro-5-(pyridin-4-yl)benzoyl)piperidine-3-carboxamide (0.03 g, 43%) as white solid; column: 70% EtOAc: Hex; ^{1}H NMR (400 MHz, DMSO-d_6, 80 °C) δ ppm 9.54 (br. s, 1H) 8.66 (d, J = 4.9 Hz, 2H) 7.79-7.68 (m, 3H) 7.66-7.57 (m, 2H) 7.45 (d, J = 8.1 Hz, 1H) 7.36-7.25 (m, 2H) 7.19 (t, J = 8.5 Hz, 1H) 4.24 (m, 2H) 3.56 (dd, J = 30.0, 14.0 Hz, 1H) 3.27 (t, J = 12.5 Hz, 1H) 3.13 (br. s, 1H) 3.00 (s, 1H) 2.42-2.26 (m, 1H); ^{19}F NMR (376 MHz, DMSO-d_6, 80 °C) δ ppm -95.94—-104.76 (m, 2H) -111.10 (t, J = 9.5 Hz, 1H); QTOF ES+ MS: (M+H) 474.12; HPLC Ret: 5.55 min; 95% pure.

N-(3-cyanophenyl)-5,5-difluoro-1-(3-fluoro-5-(pyridin-4-yl)benzoyl)piperidine-3-carboxamide. (CCG-264604). Method I starting from 5,5-difluoro-1-(3-fluoro-5-(pyridin-4-yl)benzoyl)piperidine-3-carboxylic acid (0.05 g, 0.14 mmol) and 3-aminobenzonitrile (0.02 g, 0.14 mmol) gave N-(3-cyanophenyl)-5,5-difluoro-1-(3-fluoro-5-(pyridin-4-yl)benzoyl)piperidine-3-carboxamide (0.01 g, 19%) as white solid; column: 80% EtOAc: Hex; ^{1}H NMR (400 MHz, DMSO-d_6, 80 °C) δ ppm 10.21 (br. s, 1H) 8.67 (t, J = 5.8 Hz, 2H) 8.01 (d, J = 6.3 Hz, 1H) 7.83-7.67 (m, 4H) 7.63 (d, J = 8.0 Hz, 1H) 7.49 (dq, J = 13.7, 7.4 Hz, 2H) 7.30 (t, J = 7.9 Hz, 1H) 4.37-4.08 (m, 2H) 3.60 (dd, J = 31.2, 14.2 Hz, 1H) 3.35-3.21 (m, 1H) 2.98 (br. s, 2H) 2.42-2.19 (m, 1H); ^{19}F NMR (376 MHz, DMSO-d_6, 80 °C) δ ppm -97.94—-103.31 (m, 2H) -111.08 (t, J = 9.4 Hz, 1H); QTOF ES+ MS: (M+H) 465.15; HPLC Ret: 5.45 min; 100% pure.

N-(3-ethynylphenyl)-5,5-difluoro-1-(3-fluoro-5-(pyridin-4-yl)benzoyl)piperidine-3-carboxamide. (CCG-264605). Method I starting from 5,5-difluoro-1-(3-fluoro-5-(pyridin-4-yl)benzoyl)piperidine-3-carboxylic acid (0.05 g, 0.14 mmol) and 3-ethynylaniline (0.02 g, 0.14 mmol) gave N-(3-ethynylphenyl)-5,5-difluoro-1-(3-fluoro-5-(pyridin-4-yl)benzoyl)piperidine-3-carboxamide (0.03 g, 52%) as white solid; column: 80% EtOAc: Hex; ^{1}H NMR (400 MHz,

DMSO-d_6, 80 °C) δ ppm 9.97 (br. s, 1H) 8.70-8.62 (m, 2H) 7.77-7.67 (m, 4H) 7.62 (d, J = 1.7 Hz, 1H) 7.53 (d, J = 8.3 Hz, 1H) 7.29 (td, J = 8.0, 2.0 Hz, 2H) 7.16 (d, J = 8.2 Hz, 1H) 4.38-4.10 (m, 2H) 3.92 (s, 1H) 3.58 (dd, J = 29.6, 13.9 Hz, 1H) 3.27 (t, J = 12.2 Hz, 1H) 2.98 (br. s, 2H) 2.42-2.22 (m, 1H); ^{19}F NMR (376 MHz, DMSO-d_6, 80 °C) δ ppm -98.91—-101.74 (m, 2H) -111.08 (t, J = 9.4 Hz, 1H); QTOF ES+ MS: (M+H) 464.16; HPLC Ret: 5.74 min; 99% pure.

(4-chloro-1H-indazol-1-yl)(5,5-difluoro-1-(3-fluoro-5-(pyridin-4-yl)benzoyl)piperidin-3-yl)methanone. (CCG-264641). Method I starting from 5,5-difluoro-1-(3-fluoro-5-(pyridin-4-yl)benzoyl)piperidine-3-carboxylic acid (0.05 g, 0.14 mmol) and 4-chloro-1H-indazole (0.02 g, 0.14 mmol) gave (4-chloro-1H-indazol-1-yl)(5,5-difluoro-1-(3-fluoro-5-(pyridin-4-yl)benzoyl)piperidin-3-yl)methanone (0.03 g, 45%) as white solid; column: 65% EtOAc: Hex; ^{1}H NMR (400 MHz, DMSO-d_6, 80 °C) δ ppm 8.70-8.58 (m, 2H) 8.23 (d, J = 8.3 Hz, 1H) 7.79-7.70 (m, 3H) 7.70-7.51 (m, 3H) 7.47 (d, J = 7.7 Hz, 1H) 7.37 (td, J = 8.7, 2.5 Hz, 1H) 4.55-4.21 (m, 2H) 3.65 (dd, J = 28.3, 14.0 Hz, 1H) 3.46 (t, J = 12.0 Hz, 1H) 2.98 (br. s, 2H) 2.63-2.48 (m, 1H); ^{19}F NMR (376 MHz, DMSO-d_6, 80 °C) δ ppm -97.94—-102.03 (m, 2H) -111.26 (t, J = 9.4 Hz, 1H); QTOF ES+ MS: (M+H) 499.12; HPLC Ret: 6.27 min; 90% pure (10% impurity is fluoro elimination product).

N-(3-chlorobenzyl)-5,5-difluoro-1-(3-fluoro-5-(pyridin-4-yl)benzoyl)piperidine-3-carboxamide. (CCG-264642). Method I starting from 5,5-difluoro-1-(3-fluoro-5-(pyridin-4-yl)benzoyl)piperidine-3-carboxylic acid (0.05 g, 0.14 mmol) and (3-chlorophenyl)methanamine (0.02 g, 0.14 mmol) gave N-(3-chlorobenzyl)-5,5-difluoro-1-(3-fluoro-5-(pyridin-4-yl)benzoyl)piperidine-3-carboxamide (0.03 g, 49%) as tan solid; column: 80% to 100% EtOAc: Hex; washed with water post-column to remove remaining PF_6 salt; ^{1}H NMR (400 MHz, DMSO-d_6, 80 °C) δ ppm 8.65 (d, J = 8 Hz, 2H) 8.42 (s, 1H) 7.82-7.67 (m, 3H) 7.60 (s, 1H) 7.34-7.25 (m, 4H) 7.17 (d, J = 7.5 Hz, 1H) 4.27 (d, J = 5.8 Hz, 2H) 4.25-4.13 (m, 2H) 3.52 (dd, J = 30.0, 13.9 Hz, 1H) 3.22 (t, J = 12.1 Hz, 1H) 2.98 (br. s, 2H) 2.34-2.16 (m, 1H); ^{19}F NMR (376 MHz, DMSO-

d_6, 80 °C) δ ppm -96.66—-102.51 (m, 2H) -111.11 (t, J = 9.3 Hz, 1H); QTOF ES+ MS: (M+H) 488.14; HPLC Ret: 5.53 min; 98% pure.

N-(3,5-dichlorophenyl)-5,5-difluoro-1-(3-fluoro-5-(pyridin-4-yl)benzoyl)piperidine-3-carboxamide. (CCG-265067). Method I starting from 5,5-difluoro-1-(3-fluoro-5-(pyridin-4-yl)benzoyl)piperidine-3-carboxylic acid (0.03 g, 0.08 mmol) and 3,5-dichloroaniline (0.01 g, 0.08 mmol) gave N-(3,5-dichlorophenyl)-5,5-difluoro-1-(3-fluoro-5-(pyridin-4-yl)benzoyl)piperidine-3-carboxamide (0.01 g, 19%) as white solid; reaction done at 85 °C; column: 65% to 80% EtOAc: Hex; washed with water post-column to remove remaining PF_6 salt; ^{1}H NMR (400 MHz, DMSO-d_6, 80 °C) δ ppm 10.22 (br. s, 1H) 8.66 (d, J = 8.0 Hz, 2H) 7.78-7.67 (m, 3H) 7.67-7.60 (m, 3H) 7.30 (d, J = 8.5Hz, 1H) 7.20 (s, 1H) 4.38-4.10 (m, 2H) 3.60 (dd, J = 29.3, 14.0 Hz, 1H) 3.26 (s, 1H) 2.93 (br. s, 2H) 2.46-2.20 (m, 1H); ^{19}F NMR (376 MHz, DMSO-d_6, 80 °C) δ ppm -97.22—-106.44 (m, 2H) -111.08 (t, J = 9.5 Hz, 1H); QTOF ES+ MS: (M+H) 508.1; HPLC Ret: 6.49 min; 95% pure.

N-(3-bromo-5-chlorophenyl)-5,5-difluoro-1-(3-fluoro-5-(pyridin-4-yl)benzoyl)piperidine-3-carboxamide. (CCG-265068). Method I starting from 5,5-difluoro-1-(3-fluoro-5-(pyridin-4-yl)benzoyl)piperidine-3-carboxylic acid (0.03 g, 0.08 mmol) and 3-bromo-5-chloroaniline (0.02 g, 0.08 mmol) gave N-(3-bromo-5-chlorophenyl)-5,5-difluoro-1-(3-fluoro-5-(pyridin-4-yl)benzoyl)piperidine-3-carboxamide (0.01 g, 22%) as white solid; reaction done at 85 °C; column: 65% to 75% EtOAc: Hex; washed with water post-column to remove remaining PF_6 salt; ^{1}H NMR (400 MHz, DMSO-d_6, 80 °C) δ ppm 10.27 (br. s, 1H) 8.74 (d, J = 8.0 Hz, 2H) 7.86-7.67 (m, 6H) 7.43-7.34 (m, 2H) 4.40-4.11 (m, 2H) 3.68 (dd, J = 29.5, 14.0 Hz, 1H) 3.25 (s, 1H) 3.00 (br. s, 2H) 2.51-2.29 (m, 1H); ^{19}F NMR (376 MHz, DMSO-d_6, 80 °C) δ ppm -97.56—-103.44 (m, 2H) -111.08 (t, J = 9.5 Hz, 1H); QTOF ES+ MS: (M+H) 554.0; HPLC Ret: 6.54 min; 95% pure.

N-(3-chloro-5-methylphenyl)-5,5-difluoro-1-(3-fluoro-5-(pyridin-4-yl)benzoyl)piperidine-3-carboxamide. (CCG-265069). Method I starting from 5,5-difluoro-1-(3-fluoro-5-(pyridin-4-yl)benzoyl)piperidine-3-carboxylic acid (0.03 g, 0.08 mmol) and 3-chloro-5-methylaniline (0.01 g, 0.08 mmol) gave N-(3-chloro-5-methylphenyl)-5,5-difluoro-1-(3-fluoro-5-(pyridin-4-yl)benzoyl)piperidine-3-carboxamide (0.02 g, 50%) as white solid; reaction done at 80 °C; column: 65% to 75% EtOAc: Hex; washed with water post-column to remove remaining PF_6 salt; ^{1}H NMR (400 MHz, DMSO-d_6, 80 °C) δ ppm 9.97 (br. s, 1H) 8.66 (d, J = 8.0 Hz, 2H) 7.77-7.67 (m, 3H) 7.62 (s, 1H) 7.52 (s, 1H) 7.30 (ddt, J = 8.7, 2.4, 1.1 Hz, 1H) 7.26 (s, 1H) 6.93 (s, 1H) 4.35-4.09 (m, 2H) 3.58 (dd, J = 29.7, 14.0 Hz, 1H) 3.26 (t, J = 12.2 Hz, 1H) 2.97 (br. s, 2H) 2.41-2.29 (m, 1H) 2.27 (s, 3H); ^{19}F NMR (376 MHz, DMSO-d_6, 80 °C) δ ppm -96.90—-102.27 (m, 2H) -111.09 (t, J = 9.3 Hz, 1H); QTOF ES+ MS: (M+H) 488.1; HPLC Ret: 6.20 min; 99% pure.

N-(3-chloro-5-methoxyphenyl)-5,5-difluoro-1-(3-fluoro-5-(pyridin-4-yl)benzoyl)piperidine-3-carboxamide. (CCG-265070). Method I starting from 5,5-difluoro-1-(3-fluoro-5-(pyridin-4-yl)benzoyl)piperidine-3-carboxylic acid (0.03 g, 0.08 mmol) and 3-chloro-5-methoxyaniline (0.01 g, 0.08 mmol) gave N-(3-chloro-5-methoxyphenyl)-5,5-difluoro-1-(3-fluoro-5-(pyridin-4-yl)benzoyl)piperidine-3-carboxamide (0.01 g, 24%) as white solid; reaction done at 80 °C; column: 65% to 75% EtOAc: Hex; washed with water post-column to remove remaining PF6 salt; ^{1}H NMR (400 MHz, DMSO-d_6, 80 °C) δ ppm 10.01 (br. s, 1H) 8.66 (d, J = 8.0 Hz, 2H) 7.78-7.67 (m, 3H) 7.61 (s, 1H) 7.34-7.25 (m, 2H) 7.12 (s, 1H) 6.69 (s, 1H) 4.35-4.08 (m, 2H) 3.75 (s, 3H) 3.58 (dd, J = 29.6, 14.0 Hz, 1H) 3.28 (t, J = 12.2 Hz, 1H) 2.96 (br. s, 2H) 2.43-2.19 (m, 1H); ^{19}F NMR (376 MHz, DMSO-d_6, 80 °C) δ ppm -99.07—-101.76 (m, 2H) -111.09 (t, J = 9.4 Hz, 1H); QTOF ES+ MS: (M+H) 504.1; HPLC Ret: 6.06 min; 98% pure.

N-(3-chloro-5-hydroxyphenyl)-5,5-difluoro-1-(3-fluoro-5-(pyridin-4-yl)benzoyl)piperidine-3-carboxamide. (CCG-265071). Method I starting from 5,5-difluoro-1-(3-fluoro-5-(pyridin-4-

yl)benzoyl)piperidine-3-carboxylic acid (0.04 g, 0.11 mmol) and 3-((tert-butyldiphenylsilyl)oxy)-5-chloroaniline (0.04 g, 0.11 mmol) gave N-(3-chloro-5-hydroxyphenyl)-5,5-difluoro-1-(3-fluoro-5-(pyridin-4-yl)benzoyl)piperidine-3-carboxamide (0.02 g, 41% (2 steps)) as white solid; reaction done at 75 °C; column: 75% to 90% EtOAc: Hex; ^{1}H NMR (400 MHz, DMSO-d_6, 80 °C) δ ppm 9.90 (br. s, 1H) 9.55 (br. s, 1H) 8.66 (d, J = 5.2 Hz, 2H) 7.77-7.67 (m, 3H) 7.61 (s, 1H) 7.30 (d, J = 8.7 Hz, 1H) 7.12 (s, 1H) 6.99 (s, 1H) 6.50 (s, 1H) 4.37-4.09 (m, 2H) 3.57 (dd, J = 29.7, 13.8 Hz, 1H) 3.24 (t, J = 14.6 Hz, 1H) 2.97 (br. s, 2H) 2.41-2.17 (m, 1H); ^{19}F NMR (376 MHz, DMSO-d_6, 80 °C) δ ppm -97.22—-103.07 (m, 2H) -111.09 (t, J = 9.3 Hz, 1H); QTOF ES+ MS: (M+H) 490.1; HPLC Ret: 5.37 min; 95% pure.

N-(3-(((tert-butyldiphenylsilyl)oxy)methyl)-5-chlorophenyl)-5,5-difluoro-1-(3-fluoro-5-(pyridin-4-yl)benzoyl)piperidine-3-carboxamide. Method I starting from 5,5-difluoro-1-(3-fluoro-5-(pyridin-4-yl)benzoyl)piperidine-3-carboxylic acid (0.04 g, 0.11 mmol) and 3-(((tert-butyldiphenylsilyl)oxy)methyl)-5-chloroaniline (0.04 g, 0.11 mmol) gave N-(3-(((tert-butyldiphenylsilyl)oxy)methyl)-5-chlorophenyl)-5,5-difluoro-1-(3-fluoro-5-(pyridin-4-yl)benzoyl)piperidine-3-carboxamide (0.02 g, 49%) as white solid; reaction done at 75 °C; column: 55% to 65% EtOAc: Hex; ^{1}H NMR (500 MHz, DMSO-d_6, 80 °C) δ ppm 10.51 (br. s, 1H) 8.68 (br. s, 2H) 7.86 (br. s, 1H) 7.79 (d, J = 5.1 Hz, 2H) 7.64 (br. s, 7H) 7.45 (br. s, 7H) 7.06 (s, 1H) 4.79-4.68 (m, 2H) 4.03 (qd, J = 7.0 Hz, 1H) 3.81 (br. s, 2H) 3.48 (br. s, 1H) 3.25-2.92 (m, 2H) 2.42-2.27 (m, 1H) 1.05 (br. s, 9H); QTOF ES+ MS: (M+H) 742.2; HPLC Ret: 8.62 min.

N-(3-chloro-5-cyanophenyl)-5,5-difluoro-1-(3-fluoro-5-(pyridin-4-yl)benzoyl)piperidine-3-carboxamide. (CCG-265171). Method I starting from 5,5-difluoro-1-(3-fluoro-5-(pyridin-4-yl)benzoyl)piperidine-3-carboxylic acid (0.03 g, 0.08 mmol) and 3-amino-5-chlorobenzonitrile (0.01 g, 0.09 mmol) gave N-(3-chloro-5-cyanophenyl)-5,5-difluoro-1-(3-fluoro-5-(pyridin-4-yl)benzoyl)piperidine-3-carboxamide (0.01 g, 32%) as yellow solid; reaction done at 75 °C; column: 65% to 75% EtOAc: Hex; ^{1}H NMR (400 MHz, DMSO-d_6, 80 °C) δ ppm 10.37 (br. s, 1H)

8.66 (d, J = 5.3 Hz, 2H) 7.94 (s, 1H) 7.88 (s, 1H) 7.78-7.67 (m, 3H) 7.61 (d, J = 7.0 Hz, 2H) 7.30 (d, J = 8.8 Hz, 1H) 4.36-4.09 (m, 2H) 3.61 (dd, J = 29.5, 13.9 Hz, 1H) 3.27 (s, 1H) 2.96 (br. s, 2H) 2.47-2.21 (m, 1H); ^{19}F NMR (376 MHz, DMSO-d_6, 80 °C) δ ppm -97.22—-101.90 (m, 2H) -111.08 (t, J = 9.3 Hz, 1H); QTOF ES+ MS: (M+H) 499.1; HPLC Ret: 5.83 min; 96% pure.

N-(3-chloro-5-(trifluoromethyl)phenyl)-5,5-difluoro-1-(3-fluoro-5-(pyridin-4-yl)benzoyl)piperidine-3-carboxamide. (CCG-265173). Method I starting from 5,5-difluoro-1-(3-fluoro-5-(pyridin-4-yl)benzoyl)piperidine-3-carboxylic acid (0.03 g, 0.08 mmol) and 3-chloro-5-(trifluoromethyl)aniline (0.02 g, 0.12 mmol) gave N-(3-chloro-5-(trifluoromethyl)phenyl)-5,5-difluoro-1-(3-fluoro-5-(pyridin-4-yl)benzoyl)piperidine-3-carboxamide (0.02 g, 38%) as yellow solid; reaction done at 85 °C; column: 60% EtOAc: Hex; washed with water post-column to remove remaining PF_6 salt; ^{1}H NMR (400 MHz, DMSO-d_6, 80 °C) δ ppm 10.35 (br. s, 1H) 8.65 (d, J = 5.5 Hz, 2H) 7.90 (d, J = 19.9 Hz, 2H) 7.77-7.66 (m, 3H) 7.61 (s, 1H) 7.43 (s, 1H) 7.30 (d, J = 8.6 Hz, 1H) 4.38-4.09 (m, 2H) 3.60 (dd, J = 29.2, 13.8 Hz, 1H) 3.27 (s, 1H) 2.96 (br. s, 2H) 2.45-2.22 (m, 1H); ^{19}F NMR (376 MHz, DMSO-d_6, 80 °C) δ ppm -61.83 (s, 3H) -99.16—-101.82 (m, 2H) -111.10 (t, J = 9.0 Hz, 1H); QTOF ES+ MS: (M+H) 542.1; HPLC Ret: 6.48 min; 99% pure.

N-(3-chloro-5-(trifluoromethoxy)phenyl)-5,5-difluoro-1-(3-fluoro-5-(pyridin-4-yl)benzoyl)piperidine-3-carboxamide. (CCG-265174). Method I starting from 5,5-difluoro-1-(3-fluoro-5-(pyridin-4-yl)benzoyl)piperidine-3-carboxylic acid (0.03 g, 0.08 mmol) and 3-chloro-5-(trifluoromethoxy)aniline (0.03 g, 0.12 mmol) gave N-(3-chloro-5-(trifluoromethoxy)phenyl)-5,5-difluoro-1-(3-fluoro-5-(pyridin-4-yl)benzoyl)piperidine-3-carboxamide (0.02 g, 33%) as yellow solid; reaction done at 85 °C; column: 60% EtOAc: Hex; washed with water post-column to remove remaining PF_6 salt; ^{1}H NMR (400 MHz, DMSO-d_6, 80 °C) δ ppm 10.31 (br. s, 1H) 8.65 (d, J = 5.6 Hz, 2H) 7.78-7.67 (m, 3H) 7.69-7.55 (m, 3H) 7.30 (d, J = 8.5 Hz, 1H) 7.12 (s, 1H) 4.40-4.10 (m, 2H) 3.60 (dd, J = 29.4, 13.9 Hz, 1H) 3.29 (s, 1H) 2.97 (br. s, 2H) 2.45-2.14 (m,

1H); ^{19}F NMR (376 MHz, DMSO-d_6, 80 °C) δ ppm -56.82 (s, 3H) -99.08—-101.85 (m, 2H) -111.10 (t, J = 9.3 Hz, 1H); QTOF ES+ MS: (M+H) 558.1; HPLC Ret: 6.58 min; 99% pure.

5,5-difluoro-1-(3-(furan-2-yl)benzoyl)-N-phenethylpiperidine-3-carboxamide. (CCG-265187). Method I starting from 5,5-difluoro-1-(3-(furan-2-yl)benzoyl)piperidine-3-carboxylic acid (0.03 g, 0.09 mmol) and 2-phenylethanamine (0.01 g, 0.1 mmol) gave 5,5-difluoro-1-(3-(furan-2-yl)benzoyl)-N-phenethylpiperidine-3-carboxamide (0.01 g, 31%) as white solid; column: 30% EtOAc: Hex; ^{1}H NMR (400 MHz, DMSO-d_6, 80 °C) δ ppm 7.90-7.81 (br. s, 1H) 7.78 (d, J = 8.0 Hz, 1H) 7.71 (s, 1H) 7.65 (s, 1H) 7.58-7.46 (m, 1H) 7.30-7.17 (m, 3H) 7.18-7.12 (m, 3H) 6.95 (d, J = 3.4 Hz, 1H) 6.58 (dt, J = 3.0, 1.2 Hz, 1H) 4.33-4.05 (m, 2H) 3.43 (dd, J = 30.8, 13.8 Hz, 1H) 3.35-3.25 (m, 2H) 3.07 (t, J = 12.4 Hz, 1H) 2.74-2.64 (m, 2H) 2.27-2.05 (m, 3H); ^{19}F NMR (376 MHz, DMSO-d_6, 80 °C) δ ppm -97.36—-103.39 (m, 2H); QTOF ES+ MS: (M+H) 439.2; HPLC Ret: 7.21 min; 99% pure.

N-(2-chlorophenethyl)-5,5-difluoro-1-(3-(furan-2-yl)benzoyl)piperidine-3-carboxamide. (CCG-265188). Method I starting from 5,5-difluoro-1-(3-(furan-2-yl)benzoyl)piperidine-3-carboxylic acid (0.03 g, 0.09 mmol) and 2-(2-chlorophenyl)ethanamine (0.02 g, 0.1 mmol) gave N-(2-chlorophenethyl)-5,5-difluoro-1-(3-(furan-2-yl)benzoyl)piperidine-3-carboxamide (0.01 g, 28%) as white solid; column: 25% EtOAc: Hex; ^{1}H NMR (400 MHz, DMSO-d_6, 80 °C) δ ppm 7.95-7.85 (br. s, 1H) 7.79 (d, J = 8.0 Hz, 1H) 7.71 (s, 1H) 7.65 (s, 1H) 7.57-7.46 (m, 1H) 7.38-7.30 (m, 1H) 7.31-7.14 (m, 5H) 6.96 (d, J = 2.7 Hz, 1H) 6.58 (dt, J = 3.8, 1.8 Hz, 1H) 4.28-4.05 (m, 2H) 3.50-3.27 (m, 3H) 3.07 (t, J = 12.4 Hz, 1H) 2.85 (br. s, 1H) 2.71-2.61 (m, 1H) 2.29-2.07 (m, 3H); ^{19}F NMR (376 MHz, DMSO-d_6, 80 °C) δ ppm -98.77—-102.18 (m, 2H); QTOF ES+ MS: (M+H) 473.1; HPLC Ret: 7.50 min; 99% pure.

5,5-difluoro-1-(3-(furan-2-yl)benzoyl)-N-(2-(pyridin-4-yl)ethyl)piperidine-3-carboxamide. (CCG-265189). Method I starting from 5,5-difluoro-1-(3-(furan-2-yl)benzoyl)piperidine-3-

carboxylic acid (0.03 g, 0.09 mmol) and 2-(pyridin-4-yl)ethanamine (0.01 g, 0.1 mmol) gave 5,5-difluoro-1-(3-(furan-2-yl)benzoyl)-N-(2-(pyridin-4-yl)ethyl)piperidine-3-carboxamide (0.01 g, 31%) as white solid; column: 95% EtOAc: Hex; ^{1}H NMR (400 MHz, DMSO-d_6, 80 °C) δ ppm 8.39 (d, J = 5.4 Hz, 2H) 7.93 (br. s, 1H) 7.79 (d, J = 7.9 Hz, 1H) 7.71 (s, 1H) 7.65 (s, 1H) 7.50 (t, J = 7.8 Hz, 1H) 7.27 (d, J = 7.7 Hz, 1H) 7.14 (d, J = 4.9 Hz, 2H) 6.95 (d, J = 3.4 Hz, 1H) 6.58 (d, J = 2.9 Hz, 1H) 4.27-4.05 (m, 2H) 3.50-3.30 (m, 3H) 3.05 (t, J = 12.2 Hz, 1H) 2.77-2.60 (m, 3H) 2.40-2.00 (m, 1H); ^{19}F NMR (376 MHz, DMSO-d_6, 80 °C) δ ppm -98.83—-102.13 (m, 2H); QTOF ES+ MS: (M+H) 440.2; HPLC Ret: 5.14 min; 96% pure.

N-(3-(1H-imidazol-1-yl)propyl)-5,5-difluoro-1-(3-(furan-2-yl)benzoyl)piperidine-3-carboxamide. (CCG-265190). Method I starting from 5,5-difluoro-1-(3-(furan-2-yl)benzoyl)piperidine-3-carboxylic acid (0.03 g, 0.09 mmol) and 3-(1H-imidazol-1-yl)propan-1-amine (0.01 g, 0.1 mmol) gave N-(3-(1H-imidazol-1-yl)propyl)-5,5-difluoro-1-(3-(furan-2-yl)benzoyl)piperidine-3-carboxamide (0.01 g, 35%) as white solid; column: 5% MeOH: DCM; washed with water post-column to remove remaining PF_6 salt; ^{1}H NMR (400 MHz, DMSO-d_6, 80 °C) δ ppm 7.89 (br. s, 1H) 7.77 (d, J = 8.1 Hz, 1H) 7.73-7.63 (m, 2H) 7.56-7.46 (m, 2H) 7.28 (d, J = 7.5 Hz, 1H) 7.07 (s, 1H) 6.95 (d, J = 3.4 Hz, 1H) 6.86 (s, 1H) 6.58 (dd, J = 3.4, 2.0 Hz, 1H) 4.28-4.05 (m, 2H) 3.94 (t, J = 7.1 Hz, 2H) 3.47 (dd, J = 30.7, 14.1 Hz, 1H) 3.14 (t, J = 12.1 Hz, 1H) 3.04 (br. s, 2H) 2.37-2.07 (m, 1H) 1.85 (t, J = 7.6 Hz, 2H); ^{19}F NMR (376 MHz, DMSO-d_6, 80 °C) δ ppm -98.89—-102.13 (m, 2H); QTOF ES+ MS: (M+H) 443.2; HPLC Ret: 5.19 min; 95% pure.

N-(2-(1H-imidazol-4-yl)ethyl)-5,5-difluoro-1-(3-(furan-2-yl)benzoyl)piperidine-3-carboxamide. (CCG-265191). Method I starting from 5,5-difluoro-1-(3-(furan-2-yl)benzoyl)piperidine-3-carboxylic acid (0.03 g, 0.09 mmol) and 2-(1H-imidazol-4-yl)ethanamine (0.01 g, 0.1 mmol) gave N-(2-(1H-imidazol-4-yl)ethyl)-5,5-difluoro-1-(3-(furan-2-yl)benzoyl)piperidine-3-carboxamide (0.02 g, 57%) as white solid; column: 2.5% MeOH: DCM;

^{1}H NMR (400 MHz, DMSO-d_6, 80 °C) δ ppm 11.52 (br. s, 1H) 7.87 (br. s, 1H) 7.78 (d, J = 8.0 Hz, 1H) 7.71 (s, 1H) 7.66 (s, 1H) 7.50 (t, J = 7.7 Hz, 1H) 7.42 (s, 1H) 7.27 (d, J = 7.6 Hz, 1H) 6.95 (d, J = 3.4 Hz, 1H) 6.71 (s, 1H) 6.58 (dd, J = 3.4, 2.0 Hz, 1H) 4.27-4.07 (m, 2H) 3.45 (dd, J = 30.1, 14.0 Hz, 1H) 3.34-3.25 (m, 2H) 3.09 (t, J = 12.1 Hz, 1H) 2.71-2.60 (m, 2H) 2.36-2.02 (m, 1H); ^{19}F NMR (376 MHz, DMSO-d_6, 80 °C) δ ppm -98.82—-102.17 (m, 2H); QTOF ES+ MS: (M+H) 429.2; HPLC Ret: 5.11 min; 93% pure.

5,5-difluoro-1-(3-(furan-2-yl)benzoyl)-N-((R)-2-hydroxy-2-phenylethyl)piperidine-3-carboxamide. (CCG-265192). Method I starting from 5,5-difluoro-1-(3-(furan-2-yl)benzoyl)piperidine-3-carboxylic acid (0.03 g, 0.09 mmol) and (R)-2-amino-1-phenylethanol (0.01 g, 0.1 mmol) gave 5,5-difluoro-1-(3-(furan-2-yl)benzoyl)-N-((R)-2-hydroxy-2-phenylethyl)piperidine-3-carboxamide (0.01 g, 30%) as white solid; column: 50% to 65% EtOAc: Hex; ^{1}H NMR (400 MHz, DMSO-d_6, 80 °C) δ ppm 7.86 (br. s, 1H) 7.79 (d, J = 7.7 Hz, 1H) 7.71 (s, 1H) 7.65 (s, 1H) 7.51 (t, J = 7.8 Hz, 1H) 7.35-7.21 (m, 6H) 6.96 (d, J = 3.4 Hz, 1H) 6.58 (dd, J = 3.4, 2.0 Hz, 1H) 5.10 (br. s, 1H) 4.61 (br. s, 1H) 4.33-4.00 (m, 2H) 3.43 (dd, J = 30.1, 14.0 Hz, 1H) 3.30-3.20 (m, 2H) 3.00 (t, J = 12.1 Hz, 1H) 2.75-2.68 (m, 2H) 2.30-2.07 (m, 1H); ^{19}F NMR (376 MHz, DMSO-d_6, 80 °C) δ ppm -98.57—-102.17 (m, 2H); QTOF ES+ MS: (M+H) 455.2; HPLC Ret: 6.47 min; 97% pure.

5,5-difluoro-1-(3-(furan-2-yl)benzoyl)-N-((S)-2-hydroxy-2-phenylethyl)piperidine-3-carboxamide. (CCG-265193). Method I starting from 5,5-difluoro-1-(3-(furan-2-yl)benzoyl)piperidine-3-carboxylic acid (0.03 g, 0.09 mmol) and (S)-2-amino-1-phenylethanol (0.01 g, 0.1 mmol) gave 5,5-difluoro-1-(3-(furan-2-yl)benzoyl)-N-((S)-2-hydroxy-2-phenylethyl)piperidine-3-carboxamide (0.02 g, 54%) as white solid; column: 50% to 60% EtOAc: Hex; ^{1}H NMR (400 MHz, DMSO-d_6, 80 °C) δ ppm 7.87 (br. s, 1H) 7.79 (d, J = 7.9 Hz, 1H) 7.72 (s, 1H) 7.65 (s, 1H) 7.51 (t, J = 7.7 Hz, 1H) 7.35-7.16 (m, 6H) 6.96 (d, J = 3.4 Hz, 1H) 6.59 (dd, J = 3.4, 2.0 Hz, 1H) 5.11 (br. s, 1H) 4.61 (br. s, 1H) 4.29-4.00 (m, 2H) 3.49-3.19 (m, 3H) 3.06 (t,

J = 12.1 Hz, 1H) 2.78-2.69 (m, 2H) 2.31-2.07 (m, 1H); ^{19}F NMR (376 MHz, DMSO-d_6, 80 °C) δ ppm -98.72—-102.57 (m, 2H); QTOF ES+ MS: (M+H) 455.2; HPLC Ret: 6.48 min; 96% pure.

5,5-difluoro-1-(3-(furan-2-yl)benzoyl)-N-(1-methyl-1H-pyrazol-4-yl)piperidine-3-carboxamide. (CCG-265194). Method I starting from 5,5-difluoro-1-(3-(furan-2-yl)benzoyl)piperidine-3-carboxylic acid (0.03 g, 0.09 mmol) and 1-methyl-1H-pyrazol-4-amine (0.01 g, 0.1 mmol) gave 5,5-difluoro-1-(3-(furan-2-yl)benzoyl)-N-(1-methyl-1H-pyrazol-4-yl)piperidine-3-carboxamide (0.02 g, 62%) as white solid; column: 70% to 80% EtOAc: Hex; ^{1}H NMR (400 MHz, DMSO-d_6, 80 °C) δ ppm 9.86 (br. s, 1H) 7.81-7.64 (m, 4H) 7.50 (t, J = 7.7 Hz, 1H) 7.37 (s, 1H) 7.29 (d, J = 7.8 Hz, 1H) 6.95 (d, J = 3.5 Hz, 1H) 6.58 (dt, J = 3.6, 1.8 Hz, 1H) 4.31-4.10 (m, 2H) 3.75 (s, 3H) 3.51 (dd, J = 30.4, 13.8 Hz, 1H) 3.18 (t, J = 12.3 Hz, 1H) 2.88-2.80 (m, 2H) 2.30-2.19 (m, 1H); ^{19}F NMR (376 MHz, DMSO-d_6, 80 °C) δ ppm -98.14—-102.75 (m, 2H); QTOF ES+ MS: (M+H) 415.2; HPLC Ret: 6.06 min; 99% pure.

N-(3-ethyl-1H-pyrazol-5-yl)-5,5-difluoro-1-(3-(furan-2-yl)benzoyl)piperidine-3-carboxamide. (CCG-265195). Method I starting from 5,5-difluoro-1-(3-(furan-2-yl)benzoyl)piperidine-3-carboxylic acid (0.03 g, 0.09 mmol) and 3-ethyl-1H-pyrazol-5-amine (0.01 g, 0.1 mmol) gave N-(3-ethyl-1H-pyrazol-5-yl)-5,5-difluoro-1-(3-(furan-2-yl)benzoyl)piperidine-3-carboxamide (0.01 g, 26%) as white solid; column: 20% EtOAc: Hex; ^{1}H NMR (400 MHz, DMSO-d_6, 80 °C) δ ppm 7.78 (d, J = 7.9 Hz, 1H) 7.75-7.69 (m, 2H) 7.51 (t, J = 7.7 Hz, 1H) 7.32 (d, J = 7.8 Hz, 1H) 6.96 (d, J = 3.4 Hz, 1H) 6.58 (dt, J = 3.6, 1.8 Hz, 1H) 6.31 (br. s, 2H) 4.40-4.00 (m, 2H) 4.05-3.77 (m, 2H) 3.52 (dd, J = 30.4, 13.8 Hz, 1H) 3.31 (t, J = 12.2 Hz, 1H) 2.90-2.80 (m, 2H) 2.32-2.22 (m, 1H); ^{19}F NMR (376 MHz, DMSO-d_6, 80 °C) δ ppm -99.54—-104.37 (m, 2H); QTOF ES+ MS: (M+H) 429.2; HPLC Ret: 7.41 min; 90% pure.

5,5-difluoro-1-(3-(furan-2-yl)benzoyl)-N-(quinolin-3-yl)piperidine-3-carboxamide. (CCG-265196). Method I starting from 5,5-difluoro-1-(3-(furan-2-yl)benzoyl)piperidine-3-carboxylic acid

(0.03 g, 0.09 mmol) and quinolin-3-amine (0.01 g, 0.1 mmol) gave 5,5-difluoro-1-(3-(furan-2-yl)benzoyl)-N-(quinolin-3-yl)piperidine-3-carboxamide (0.01 g, 32%) as white solid; column: 50% to 60% EtOAc: Hex; washed with water post-column to remove remaining PF_6 salt; ^{1}H NMR (400 MHz, DMSO-d_6, 80 °C) δ ppm 8.92 (s, 1H) 8.56 (s, 1H) 7.94 (d, J = 8.6 Hz, 1H) 7.86 (d, J = 8.1 Hz, 1H) 7.78 (d, J = 8.0 Hz, 1H) 7.72-7.68 (m, 2H) 7.67-7.47 (m, 4H) 7.32 (d, J = 7.7 Hz, 1H) 6.95 (d, J = 3.4 Hz, 1H) 6.58 (dt, J = 3.6, 1.8 Hz, 1H) 4.41-4.05 (m, 2H) 3.57 (dd, J = 30.4, 13.8 Hz, 1H) 3.27 (t, J = 12.0 Hz, 1H) 3.09-3.00 (m, 2H) 2.42-2.24 (m, 1H); ^{19}F NMR (376 MHz, DMSO-d_6, 80 °C) δ ppm -99.04—-102.05 (m, 2H); QTOF ES+ MS: (M+H) 462.2; HPLC Ret: 6.19 min; 94% pure.

5,5-difluoro-1-(3-(furan-2-yl)benzoyl)-N-(1H-pyrazolo[3,4-b]pyridin-3-yl)piperidine-3-carboxamide. (CCG-265197). Method I starting from 5,5-difluoro-1-(3-(furan-2-yl)benzoyl)piperidine-3-carboxylic acid (0.03 g, 0.09 mmol) and 1H-pyrazolo[3,4-b]pyridin-3-amine (0.01 g, 0.1 mmol) gave 5,5-difluoro-1-(3-(furan-2-yl)benzoyl)-N-(1H-pyrazolo[3,4-b]pyridin-3-yl)piperidine-3-carboxamide (0.01 g, 27%) as white solid; column: 75% to 80% EtOAc: Hex; ^{1}H NMR (400 MHz, DMSO-d_6, 80 °C) δ ppm 8.55 (d, J = 4.8 Hz, 1H) 8.28 (d, J = 7.8 Hz, 1H) 7.74 (d, J = 7.8 Hz, 1H) 7.72-7.59 (m, 3H) 7.48 (t, J = 7.7 Hz, 1H) 7.38-7.27 (m, 2H) 6.93 (d, J = 3.4 Hz, 1H) 6.57 (dt, J = 3.2, 1.6 Hz, 1H) 6.26 (br. s, 2 Hz) 4.43-4.20 (m, 2H) 3.56 (dd, J = 29.9, 13.7 Hz, 1H) 3.35 (t, J = 12.0 Hz, 1H) 3.00-2.97 (m, 2H) 2.41-2.26 (m, 1H); ^{19}F NMR (376 MHz, DMSO-d_6, 80 °C) δ ppm -98.75—-101.91 (m, 2H); QTOF ES+ MS: (M+H) 452.2; HPLC Ret: 6.16 min; 90% pure.

N-([1,2,4]triazolo[4,3-a]pyridin-3-yl)-5,5-difluoro-1-(3-(furan-2-yl)benzoyl)piperidine-3-carboxamide. (CCG-265198). Method I starting from 5,5-difluoro-1-(3-(furan-2-yl)benzoyl)piperidine-3-carboxylic acid (0.03 g, 0.09 mmol) and [1,2,4]triazolo[4,3-a]pyridin-3-amine (0.01 g, 0.1 mmol) gave N-([1,2,4]triazolo[4,3-a]pyridin-3-yl)-5,5-difluoro-1-(3-(furan-2-yl)benzoyl)piperidine-3-carboxamide (0.01 g, 22%) as white solid; column: 100% EtOAc to 5%

MeOH: DCM; ^{1}H NMR (400 MHz, DMSO-d_6, 80 °C) δ ppm 7.97 (d, J = 7.1 Hz, 1H) 7.78 (d, J = 8.1 Hz, 1H) 7.72-7.65 (m, 4H) 7.51 (t, J = 7.9 Hz, 1H) 7.38-7.28 (m, 3H) 6.98-6.89 (m, 3H) 6.58 (dt, J = 3.5, 1.9 Hz, 1H) 4.48-4.15 (m, 2H) 3.57 (dd, J = 30.0, 13.9 Hz, 1H) 3.33 (t, J = 12.0 Hz, 1H) 3.14 (br. s, 2H) 2.41-2.23 (m, 1H); ^{19}F NMR (376 MHz, DMSO-d_6, 80 °C) δ ppm -99.09—-103.32 (m, 2H); QTOF ES+ MS: (M+H) 452.2; HPLC Ret: 5.67 min; 93% pure.

5,5-difluoro-1-(3-(furan-2-yl)benzoyl)-N-(imidazo[1,2-a]pyridin-3-yl)piperidine-3-carboxamide. (CCG-265199). Method I starting from 5,5-difluoro-1-(3-(furan-2-yl)benzoyl)piperidine-3-carboxylic acid (0.03 g, 0.09 mmol) and imidazo[1,2-a]pyridin-3-amine (0.01 g, 0.1 mmol) gave 5,5-difluoro-1-(3-(furan-2-yl)benzoyl)-N-(imidazo[1,2-a]pyridin-3-yl)piperidine-3-carboxamide (0.02 g, 40%) as white solid; column: 2.5% MeOH: DCM; ^{1}H NMR (400 MHz, DMSO-d_6, 80 °C) δ ppm 10.05 (br. s, 1H) 8.03 (d, J = 7.0 Hz, 1H) 7.79 (d, J = 7.9 Hz, 1H) 7.73-7.69 (m, 2H) 7.55-7.42 (m, 3H) 7.32 (d, J = 7.4 Hz, 1H) 7.21 (t, J = 7.9 Hz, 1H) 6.96 (d, J = 3.0 Hz, 1H) 6.89 (t, J = 6.8 Hz, 1H) 6.58 (dt, J = 3.6, 1.8 Hz, 1H) 4.45-4.17 (m, 2H) 3.57 (dd, J = 29.3, 14.4 Hz, 1H) 3.30 (t, J = 12.3 Hz, 1H) 3.09 (br. s, 2H) 2.42-2.29 (m, 1H); ^{19}F NMR (376 MHz, DMSO-d_6, 80 °C) δ ppm -99.72—-103.48 (m, 2H); QTOF ES+ MS: (M+H) 451.2; HPLC Ret: 5.46 min; 99% pure.

***cis*-N1-(4-chlorophenyl)-N3-(3-(furan-2-yl)phenyl)cyclohexane-1,3-dicarboxamide. (CCG-263876).** Method G followed by Method I starting from *cis*-methyl 3-((4-chlorophenyl)carbamoyl)cyclohexanecarboxylate (0.10 g, 0.34 mmol) and 3-(furan-2-yl)aniline, HCl (0.06 g, 0.22 mmol) gave cis-N1-(4-chlorophenyl)-N3-(3-(furan-2-yl)phenyl)cyclohexane-1,3-dicarboxamide (0.04 g, 50% (2 steps)) as white solid; column: 50% to 80% EtOAc: Hex; ^{1}H NMR (500 MHz, DMSO-d_6) δ ppm 9.99 (s, 1H) 9.93 (s, 1H) 8.01 (s, 1H) 7.75 (s, 1H) 7.64 (d, J = 8.5 Hz, 2H) 7.51 (d, J = 8.0 Hz, 1H) 7.37-7.31 (m, 4H) 6.86 (d, J = 3.4 Hz, 1H) 6.62-6.57 (m, 1H) 2.49-2.35 (m, 2H) 2.06-1.87 (m, 4H) 1.68 (q, J = 12.5 Hz, 1H) 1.42-1.36 (m, 3H); ^{13}C NMR (500 MHz, DMSO-d_6) δ ppm 174.28, 153.37, 143.35, 140.33, 138.76, 131.10, 129.69, 128.98,

126.95, 121.10, 118.78, 118.65, 114.40, 112.50, 106.26, 44.60, 44.57, 31.67, 29.15, 25.17; TOF ES+ MS: (M+Na) 445.13; HPLC Ret: 7.53 min; 95% pure.

***trans*-N1-(4-chlorophenyl)-N3-(3-(furan-2-yl)phenyl)cyclohexane-1,3-dicarboxamide. CCG-263878.** Method G followed by Method I starting from trans-methyl 3-((4-chlorophenyl)carbamoyl)cyclohexanecarboxylate (0.05 g, 0.18 mmol) and 3-(furan-2-yl)aniline, HCl (0.04 g, 0.18 mmol) gave trans-N1-(4-chlorophenyl)-N3-(3-(furan-2-yl)phenyl)cyclohexane-1,3-dicarboxamide (0.06 g, 73% (2 steps)) as white solid; column: 30% to 60% EtOAc: Hex; ^{1}H NMR (500 MHz, DMSO-d_6) δ ppm 10.04-9.93 (m, 2H) 8.10 (d, J = 2.7 Hz, 1H) 7.75 (d, J = 1.7 Hz, 1H) 7.67 (d, J = 8.6 Hz, 1H) 7.54-7.47 (m, 1H) 7.39-7.30 (m, 3H) 6.85 (d, J = 3.3 Hz, 1H) 6.59 (dd, J = 3.4, 1.7 Hz, 1H) 2.91 (dt, J = 13.5, 6.0 Hz, 2H) 1.92 (dt, J = 12.6, 6.3 Hz, 2H) 1.75-1.66 (m, 6H); ^{13}C NMR (500 MHz, DMSO-d_6) δ ppm 174.81, 174.79, 174.75, 153.45, 143.32, 140.50, 140.48, 138.91, 131.05, 129.60, 128.91, 126.83, 121.13, 118.67, 114.46, 112.49, 106.19, 40.09, 40.05, 30.22, 30.16, 28.91, 28.80, 21.79; HPLC/TOF ES+ MS: (M+H) Peak 1: 423.15, HPLC/TOF ES+ MS: (M+MeOH+H) Peak 2: 455.20; HPLC Ret Peak 1: 7.94 min, HPLC Ret Peak 2: 8.05 min; 98 % pure. Note: HNMR, CNMR, & MS all looked good, but HPLC had two neighboring peaks. High temp HNMR on 400 caused amide N-H's to coallese to two broad peaks and HPLC/MS showed both peaks had desirable masses for desired product. I think this compound can cross energy barrier between the two trans chair conformations.

N-(4-chlorophenyl)-5-(3-(furan-2-yl)benzamido)-2-methylbenzamide. (CCG-263153) (DJK-7-42). Method G followed by Method I starting from methyl 5-(3-(furan-2-yl)benzamido)-2-methylbenzoate (0.08 g, 0.22 mmol) and 4-chloroaniline (0.03 g, 0.22 mmol) gave N-(4-chlorophenyl)-5-(3-(furan-2-yl)benzamido)-2-methylbenzamide (0.04 g, 41% (2 steps)); column: 30% to 40% EtOAc: Hex; ^{1}H NMR (500 MHz, DMSO-d_6) δ ppm 10.51 (s, 1H) 10.45 (s, 1H) 8.28 (s, 1H) 7.92 (dt, J = 4.5, 1.7 Hz, 2H) 7.89-7.77 (m, 5H) 7.60 (t, J = 7.8, 1H) 7.45-7.38 (m, 2H) 7.32 (d, J = 8.3 Hz, 1H) 7.08 (d, 3.3 Hz, 1H) 6.65 (dd, J = 3.4, 1.8 Hz, 1H) 2.36 (s, 3H); ^{13}C NMR

(500 MHz, DMSO-d_6) δ ppm 166.17, 165.62, 152.74, 143.85, 138.61, 137.27, 135.86, 131.29, 130.94, 130.75, 129.59, 129.10, 127.60, 127.01, 126.85, 122.85, 121.93, 121.55, 119.49, 112.70, 109.99, 107.25, 19.15; QTOF ES+ MS: (M+H) 431.1; HPLC Ret: 8.10 min; 98 % pure.

1-(5,6-difluoro-1H-indole-2-carbonyl)-5,5-difluoro-N-(4-(2-(pyrrolidin-1-yl)ethoxy)phenyl)piperidine-3-carboxamide. (CCG-263678). Method G followed by Method I starting from methyl 1-(5,6-difluoro-1H-indole-2-carbonyl)-5,5-difluoropiperidine-3-carboxylate (0.14 g, 0.39 mmol) and 4-(2-(pyrrolidin-1-yl)ethoxy)aniline (0.03 g, 0.13 mmol) gave 1-(5,6-difluoro-1H-indole-2-carbonyl)-5,5-difluoro-N-(4-(2-(pyrrolidin-1-yl)ethoxy)phenyl)piperidine-3-carboxamide (0.06 g, 84% (2 steps)) as yellow solid; column: 10% MeOH: DCM; crystalized at 0 °C and washed with hexanes post column; ^{1}H NMR (400 MHz, DMSO-d_6, 80 °C) δ ppm 11.58 (s, 1H) 9.84 (br. s, 1H) 7.62-7.47 (m, 2H) 7.39-7.32 (m, 1H) 6.96 (d, J = 8.8 Hz, 2H) 6.90-6.87 (m, 1H) 6.74 (d, J = 8.3 Hz, 2H) 6.56 (d, J = 8.3 Hz, 2H) 4.72-4.55 (m, 2H) 4.26 (t, J = 5.3 Hz, 2H) 4.14 (t, J = 5.1 Hz, 2H) 3.50 (dt, J = 16.2, 5.1 Hz, 2H) 3.42-3.25 (m, 3H) 3.09-2.84 (m, 4H) 2.05-1.90 (m, 4H); ^{19}F NMR (376 MHz, DMSO-d_6, 80 °C) δ ppm -69.66 (s, 1H) -71.55 (s, 1H) -141.58 (ddd, 20.2, 7.1, 2.9 Hz, 1H) -147.10 (ddd, 20.2, 11.4, 4.4 Hz, 1H); QTOF ES+ MS: (M+H) 533.22; HPLC Ret: 5.61 min; 95% pure.

N-(6-chloropyridin-3-yl)-1-(5,6-difluoro-1H-indole-2-carbonyl)-5,5-difluoropiperidine-3-carboxamide. (CCG-263679). Method G followed by Method I starting from methyl 1-(5,6-difluoro-1H-indole-2-carbonyl)-5,5-difluoropiperidine-3-carboxylate (0.02 g, 0.23 mmol) and 6-chloropyridine-3-amine (0.04 g, 0.13 mmol) gave N-(6-chloropyridin-3-yl)-1-(5,6-difluoro-1H-indole-2-carbonyl)-5,5-difluoropiperidine-3-carboxamide (0.03 g, 49% (2 steps)) as white solid; crystallized from EtOH; ^{1}H NMR (400 MHz, DMSO-d_6, 80 °C) δ ppm 11.58 (s, 1H) 10.29 (br. s, 1H) 8.58 (d, J = 2.7 Hz, 1H) 8.03 (dd, J = 8.6, 2.7 Hz, 1H) 7.57 (dd, J = 11.1, 8.1 Hz, 1H) 7.42 (d, J = 8.7 Hz, 1H) 7.35 (dd, J = 11.0, 7.1 Hz, 1H) 6.92-6.88 (m, 1H) 4.68-4.55 (m, 2H) 3.63 (dd, J = 30.4, 13.8 Hz, 1H) 3.34 (t, J = 12.3 Hz, 1H) 2.46-2.25 (m, 1H); ^{19}F NMR (376 MHz, DMSO-

d_6, 80 °C) δ ppm -99.22 (s, 1H) -101.23 (s, 1H) -141.57 (ddd, 20.2, 7.1, 2.9 Hz, 1H) -147.10 (ddd, 20.2, 11.4, 4.4 Hz, 1H); QTOF ES+ MS: (M+H) 455.09; HPLC Ret: 7.09 min; 95% pure.

N-(5-chloropyridin-2-yl)-1-(5,6-difluoro-1H-indole-2-carbonyl)-5,5-difluoropiperidine-3-carboxamide. (CCG-263739). Method G followed by Method I starting from methyl 1-(5,6-difluoro-1H-indole-2-carbonyl)-5,5-difluoropiperidine-3-carboxylate (0.04 g, 0.13 mmol) and 5-chloropyridine-2-amine (0.02 g, 0.13 mmol) gave N-(5-chloropyridin-2-yl)-1-(5,6-difluoro-1H-indole-2-carbonyl)-5,5-difluoropiperidine-3-carboxamide (0.02 g, 35% (2 steps)) as white solid; reaction performed at 55 °C; column: 35% to 60% EtOAc: Hex; ^{1}H NMR (400 MHz, DMSO-d_6, 80 °C) δ ppm 11.59 (s, 1H) 10.70 (s, 1H) 8.32 (d, J = 2.6 Hz, 1H) 8.05 (d, J = 8.9 Hz, 1H) 7.85 (dd, J = 8.9, 2.6 Hz, 1H) 7.56 (dd, J = 11.1, 8.0 Hz, 1H) 7.34 (dd, J = 11.0, 7.1 Hz, 1H) 6.90 (d, J = 2.0 Hz, 1H) 4.60 (d, J = 12.6 Hz, 2H) 3.59 (dd, J = 30.0, 14.0 Hz, 1H) 3.35 (t, J = 12.1 Hz, 1H) 3.19-3.05 (m, 1H) 2.40-2.28 (m, 1H); ^{19}F NMR (376 MHz, DMSO-d_6, 80 °C) δ ppm -97.30—-103.15 (m, 2H) -141.66 (ddd, 21.2, 11.1, 8.0 Hz, 1H) -147.15 (ddd, 21.0, 11.1, 7.1 Hz, 1H); QTOF ES+ MS: (M+H) 455.09; HPLC Ret: 7.41 min; 96% pure.

5,5-difluoro-N-(4-(2-(pyrrolidin-1-yl)ethoxy)phenyl)-1-(5-(trifluoromethoxy)-1H-indole-2-carbonyl)piperidine-3-carboxamide. (CCG-263680). Method G followed by Method I starting from methyl 1-(5-(trifluoromethoxy)-1H-indole-2-carbonyl)-5,5-difluoropiperidine-3-carboxylate (0.05 g, 0.13 mmol) and 4-(2-(pyrrolidin-1-yl)ethoxy)aniline (0.03 g, 0.13 mmol) gave 5,5-difluoro-N-(4-(2-(pyrrolidin-1-yl)ethoxy)phenyl)-1-(5-(trifluoromethoxy)-1H-indole-2-carbonyl)piperidine-3-carboxamide (0.02 g, 30% (2 steps)) as yellow solid; crystallized from EtOH; ^{1}H NMR (400 MHz, DMSO-d_6, 80 °C) δ ppm 11.68 (s, 1H) 9.77 (br. s, 1H) 7.61-7.48 (m, 2H) 7.45 (d, J = 8.5 Hz, 2H) 7.14 (d, J = 9.1 Hz, 1H) 6.93 (br. s, 1H) 6.86 (d, J = 8.6 Hz, 2H) 4.65-4.55 (m, 2H) 4.03 (t, J = 6.0 Hz, 2H) 3.61 (dd, J = 30.6, 14.0 Hz, 1H) 3.32 (t, J = 12.1 Hz, 2H) 2.78 (t, J = 6.0 Hz, 2H) 2.59-2.50 (m, 4H) 2.50-2.45 (m, 2H) 1.74-1.63 (m, 4H); ^{19}F NMR

(376 MHz, DMSO-d_6, 80 °C) δ ppm -56.81 (s, 3H) -98.37—-102.40 (m, 1H); QTOF ES+ MS: (M+H) 581.22; HPLC Ret: 6.24 min; 95% pure.

N-(6-chloropyridin-3-yl)-5,5-difluoro-1-(5-(trifluoromethoxy)-1H-indole-2-carbonyl)piperidine-3-carboxamide. (CCG-263681). Method G followed by Method I starting from methyl 1-(5-(trifluoromethoxy)-1H-indole-2-carbonyl)-5,5-difluoropiperidine-3-carboxylate (0.05 g, 0.13 mmol) and 6-chloropyridine-3-amine (0.02 g, 0.13 mmol) gave N-(6-chloropyridin-3-yl)-5,5-difluoro-1-(5-(trifluoromethoxy)-1H-indole-2-carbonyl)piperidine-3-carboxamide (0.05 g, 53% (2 steps)) as whtie solid; column: 40% to 60% EtOAc: Hex; ^{1}H NMR (400 MHz, DMSO-d_6, 80 °C) δ ppm 11.66 (s, 1H) 10.26 (br. s, 1H) 8.58 (d, J = 2.7 Hz, 1H) 8.03 (dd, J = 8.7, 2.7 Hz, 1H) 7.60-7.49 (m, 2H) 7.41 (d, J = 8.7 Hz, 1H) 7.14 (d, J = 9.0 Hz, 1H) 6.94-6.90 (m, 1H) 4.66-4.58 (m, 2H) 3.64 (dd, J = 30.2, 13.8 Hz, 1H) 3.36 (t, J = 12.3 Hz, 1H) 3.08-2.99 (m, 1H) 2.45-2.26 (m, 1H); ^{19}F NMR (376 MHz, DMSO-d_6, 80 °C) δ ppm -56.81 (s, 3H) -98.33—-102.06 (m, 2H); QTOF ES+ MS: (M+H) 503.09; HPLC Ret: 7.35 min; 96% pure.

N-(5-chloropyridin-2-yl)-5,5-difluoro-1-(5-(trifluoromethoxy)-1H-indole-2-carbonyl)piperidine-3-carboxamide. (CCG-263740). Method G followed by Method I starting from methyl 1-(5-(trifluoromethoxy)-1H-indole-2-carbonyl)-5,5-difluoropiperidine-3-carboxylate (0.05 g, 0.13 mmol) and 5-chloropyridine-2-amine (0.02 g, 0.13 mmol) gave N-(5-chloropyridin-2-yl)-5,5-difluoro-1-(5-(trifluoromethoxy)-1H-indole-2-carbonyl)piperidine-3-carboxamide (0.03 g, 47% (2 steps)) as whtie solid; column: 30% to 60% EtOAc: Hex; reaction performed at 55 °C; ^{1}H NMR (400 MHz, DMSO-d_6, 80 °C) δ ppm 11.67 (s, 1H) 10.68 (s, 1H) 8.31 (d, J = 2.5 Hz, 1H) 8.04 (d, J = 8.9 Hz, 1H) 7.84 (dd, J = 8.9, 2.6 Hz, 1H) 7.59-7.48 (m, 2H) 7.14 (d, J = 8.9 Hz, 1H) 6.94 (d, J = 2.1 Hz, 1H) 4.61 (d, J = 10.2 Hz, 2H) 3.60 (dd, J = 30.2, 14.1 Hz, 1H) 3.37 (t, J = 12.2 Hz, 1H) 3.20-3.15 (m, 1H) 2.44-2.22 (m, 1H); ^{19}F NMR (376 MHz, DMSO-d_6, 80 °C) δ ppm -56.81 (s, 3H) -98.96 (d, J = 239.4 Hz, 1H) -101.34 (d, J = 236.5 Hz, 1H); QTOF ES+ MS: (M+H) 503.09; HPLC Ret: 7.85 min; 97% pure.

N-(3-chloro-5-fluorophenyl)-5,5-difluoro-1-(3-fluoro-5-(pyridin-4-yl)benzoyl)piperidine-3-carboxamide. (CCG-265172). 5,5-difluoro-1-(3-fluoro-5-(pyridin-4-yl)benzoyl)piperidine-3-carboxylic acid (0.03 g, 0.08 mmol) was dissolved in DMF (1.0 mL), and EDC (0.02, 0.1 mmol) DMAP (0.01 g, 0.08 mmol), 3-chloro-5-fluoroaniline (0.02 g, 0.12 mmol), and DIPEA (0.03 g, 0.04 mL, 0.25 mmol) were added. The reaction was stirred at 25 °C for 16 hr and brine (10 mL) was added. The product was extracted with EtOAc (3 x 15 mL), dried with $MgSO_4$, and concentrated in vacuo. The subsequent oil was subjected to silica gel chromatography eluting with 70% to 80% EtOAc: Hex to produce white solid. Yield=30% (2-steps). ^{1}H NMR (400 MHz, DMSO-d_6, 80 °C) δ ppm 10.24 (br. s, 1H) 8.66 (d, J = 5.7 Hz, 2H) 7.77-7.67 (m, 3H) 7.62 (s, 1H) 7.48 (s, 1H) 7.40 (d, J = 11.1 Hz, 1H) 7.30 (d, J = 8.2 Hz, 1H) 7.01 (d, J = 8.7 Hz, 1H) 4.37-4.10 (m, 2H) 3.60 (dd, J = 29.2, 14.0 Hz, 1H) 3.25 (s, 1H) 2.98 (br. s, 2H) 2.41-2.23 (m, 1H); ^{19}F NMR (376 MHz, DMSO-d_6, 80 °C) δ ppm -98.93—-101.84 (m, 2H) -109.91— -110.56 (m, 1H) -111.09 (t, J = 9.4 Hz, 1H); QTOF ES+ MS: (M+H) 492.1; HPLC Ret: 6.02 min; 97% pure.

N-(4-chlorophenyl)-1-(4,5-difluoro-1H-indole-2-carbonyl)-5,5-difluoropiperidine-3-carboxamide. (CCG-263412). Method M followed by Method N starting from 4,5-difluoro-1H-indole-2-carboxylic acid (0.03 g, 0.13 mmol) and N-(4-chlorophenyl)-5,5-difluoropiperidine-3-carboxamide (0.03 g, 0.13 mmol) gave N-(4-chlorophenyl)-1-(4,5-difluoro-1H-indole-2-carbonyl)-5,5-difluoropiperidine-3-carboxamide as white solid (0.02 g, 37% (2 steps)); column: 35% to 65% EtOAc:Hex; ^{1}H NMR (500 MHz, DMSO-d_6) δ ppm 12.13 (br. s., 1H) 10.36 (br. s., 1H) 7.63 (d, J = 8.4 Hz, 2H) 7.38 (d, J = 8.3 Hz, 2H) 7.25 (d, J = 5.8 Hz, 2H) 7.06-7.02 (m, 1H) 4.65-4.60 (m, 1H) 3.35-3.15 (m, 2H) 2.99-2.92 (m, 1H) 2.44-2.31 (m, 2H); ^{19}F NMR (470 MHz, DMSO-d_6) δ ppm -99.39 (d, 1H), -101.78 (d, 1H), -148.03 (s, 1H), -151.95 (s, 1H); TOF ES+ MS: (M-H) 452.08; HPLC Ret: 7.70 min; 98 % pure.

N-(4-chlorophenyl)-1-(3,7-dihydro-2H-[1,4]dioxino[2,3-e]indole-8-carbonyl)-5,5-difluoropiperidine-3-carboxamide. (CCG-263413). Method M followed by Method N starting

from 3,7-dihydro-2H-[1,4]dioxino[2,3-e]indole-8-carboxylic acid (0.03 g, 0.11 mmol) and N-(4-chlorophenyl)-5,5-difluoropiperidine-3-carboxamide (0.03 g, 0.11 mmol) gave N-(4-chlorophenyl)-1-(3,7-dihydro-2H-[1,4]dioxino[2,3-e]indole-8-carbonyl)-5,5-difluoropiperidine-3-carboxamide as tan solid (0.02 g, 35% (2 steps)); column: 40% EtOAc:Hex; ^{1}H NMR (500 MHz, DMSO-d_6) δ ppm 11.37 (br. s., 1H) 10.34 (br. s., 1H) 10.07 (s, 1H) 7.63 (d, J = 8.4 Hz, 2H) 7.49 (d, J = 1.7 Hz, 1H) 7.37 (d, J = 8.3 Hz, 2H) 6.91 (br. s., 1H) 4.68-4.30 (m, 5H) 3.80-3.45 (m, 2H) 2.97-2.91 (m, 1H) 2.44-2.29 (m, 2H); ^{19}F NMR (500 MHz, DMSO-d_6) δ ppm -99.56 (d, 1H), -101.88 (d, 1H); TOF ES+ MS: (M-H) 474.10; HPLC Ret: 7.39 min; 97 % pure.

N-(4-chlorophenyl)-1-(3,6-dihydro-2H-[1,4]dioxino[2,3-f]indole-7-carbonyl)-5,5-difluoropiperidine-3-carboxamide. (CCG-263414). Method M followed by Method N starting from 3,6-dihydro-2H-[1,4]dioxino[2,3-f]indole-7-carboxylic acid (0.03 g, 0.11 mmol) and N-(4-chlorophenyl)-5,5-difluoropiperidine-3-carboxamide (0.03 g, 0.11 mmol) gave N-(4-chlorophenyl)-1-(3,6-dihydro-2H-[1,4]dioxino[2,3-f]indole-7-carbonyl)-5,5-difluoropiperidine-3-carboxamide as yellow solid (0.02 g, 39% (2 steps)); column: 40% to 80% EtOAc:Hex; ^{1}H NMR (500 MHz, DMSO-d_6) δ ppm 11.26 (br. s., 1H) 10.37 (s, 1H) 7.63 (d, J = 8.5 Hz, 2H) 7.38 (d, J = 8.8 Hz, 2H) 7.04 (s, 1H) 6.84 (s, 1H) 6.75 (br. s., 1H) 4.73-4.60 (m, 2H) 4.27-4.17 (m, 4H) 3.61-3.30 (m, 2H) 2.94 (t, J = 12.2 Hz, 1H) 2.42-2.23 (m, 2H); ^{19}F NMR (500 MHz, DMSO-d_6) δ ppm -99.56 (d, 1H), -101.79 (d, 1H); TOF ES+ MS: (M+H) 476.12; HPLC Ret: 7.31 min; 98 % pure.

N-(4-chlorophenyl)-5,5-difluoro-1-(6-fluoro-1-methyl-1H-indole-2-carbonyl)piperidine-3-carboxamide. (CCG-263415). Method M followed by Method N starting from 6-fluoro-1-methyl-1H-indole-2-carboxylic acid (0.03 g, 0.11 mmol) and N-(4-chlorophenyl)-5,5-difluoropiperidine-3-carboxamide (0.03 g, 0.11 mmol) gave N-(4-chlorophenyl)-5,5-difluoro-1-(6-fluoro-1-methyl-1H-indole-2-carbonyl)piperidine-3-carboxamide as white solid (0.06 g, 96% (2 steps)); column: 25% EtOAc:Hex; ^{1}H NMR (500 MHz, DMSO-d_6) δ ppm 10.36 (br. s., 1H) 7.68-7.60 (m, 3H) 7.46-7.40 (m, 1H) 7.37 (d, J = 8.4 Hz, 2H) 6.98 (td, J = 9.2, 2.3 Hz, 1H) 6.79 (br. s., 1H) 4.82-4.19 (m, 3H)

3.74 (s, 3H) 3.00-2.91 (m, 1H) 2.42-2.26 (m, 2H); ^{19}F NMR (500 MHz, DMSO-d_6) δ ppm -99.69 (d, 1H), -102.32 (d, 1H) -118.18 (s, 1H); TOF ES+ MS: (M+H) 450.12; HPLC Ret: 7.91 min; 99% pure.

N-(3-(((tert-butyldiphenylsilyl)oxy)methyl)-4-chlorophenyl)-5,5-difluoro-1-(3-fluoro-5-(pyridin-4-yl)benzoyl)piperidine-3-carboxamide (CCG-263741). In a 25 mL round-bottomed flask methyl N-(3-(((tert-butyldiphenylsilyl)oxy)methyl)-4-chlorophenyl)-5,5-difluoro-1-(3-fluoro-5-(pyridin-4-yl)benzoyl)piperidine-3-carboxamide (0.075 g, 0.10 mmol) was dissolved in THF (1.0 mL). 1M TBAF (in THF) (0.20 mL, 0.20 mmol) was added and the mixture was stirred under nitrogen at 25 °C for 1 hr. The reaction was quenched with water (20 mL) and the product was extracted with EtOAc (3x 15 mL). The organic layer was washed with NH_4Cl (3 x 15 mL), brine (2 x 15 mL), dried with magnesium sulfate, and evaporated. The residue was subjected to silica gel chromatography eluting with 5% MeOH: 95% DCM. The fractions containing product were concentrated in vacuo to produce white solid. Yield=55% (2-steps). ^{1}H NMR (400 MHz, DMSO-d_6, 80 °C) δ 10.02 (br. s, 1H) 8.69-8.62 (m, 2H) 7.78-7.67 (m, 4H) 7.61 (d, J = 1.7 Hz, 1H) 7.51 (dd, J = 8.4, 2.6 Hz, 1H) 7.35-7.25 (m, 2H) 5.06 (br. s, 1H) 4.53 (d, J = 5.4 Hz, 2H) 4.38-4.10 (m, 2H) 3.57 (dd, J = 29.8, 13.8 Hz, 1H) 3.28 (t, J = 13.0 Hz, 1H) 3.03-2.93 (m, 2H) 2.40-2.20 (m, 1H); ^{19}F NMR (376 MHz, DMSO-d_6, 80 °C) δ ppm -99.52—-102.20 (m, 2H) -111.08 (s, 1H); QTOF ES+ MS: (M+H) 504.13; HPLC Ret: 5.51 min; 97% pure.

N-(4-chloro-3-hydroxyphenyl)-5,5-difluoro-1-(3-fluoro-5-(pyridin-4-yl)benzoyl)piperidine-3-carboxamide. (CCG-263482). N-(4-chloro-3-(prop-2-yn-1-yloxy)phenyl)-5,5-difluoro-1-(3-fluoro-5-(pyridin-4-yl)benzoyl)piperidine-3-carboxamide (0.09 g, 0.17 mmol) was dissolved in 2:1 DMF/H_2O solution (1.5 mL). Bis(triphenylphosphine)palladium(II) chloride (0.01 g, 0.02 mmol) and triethylamine (0.14 g, 0.40 mmol, 0.19 mL) were added and the reaction was stirred under nitrogen at 85 °C for 1 hr. The reaction was quenched with H_2O (5 mL) and acidified to pH ~ 1 with 1N HCl (2 mL). The product was extracted with EtOAc (3 x 20 mL), and the resulting

organic layer was washed with brine (20 mL), dried with MgSO4, and evaporated. The oil was subjected to silica gel chromatography eluting with 80% EtOAc: 100% Hex. The fractions containing product were concentrated in vacuo to produce white solid. Yield=62%. ^{1}H NMR (400 MHz, DMSO-d_6, 80 °C) δ ppm 9.93 (s, 1H) 9.81 (br. s, 1H) 7.79-7.48 (m, 7H) 7.38 (d, J = 2.4 Hz, 1H) 7.31 (d, J = 8.6 Hz, 1H) 7.19 (d, J = 8.7 Hz, 1H) 6.97 (d, J = 8.7 Hz, 1H) 4.39-4.15 (m, 2H) 3.58 (dd, J = 30.0, 14.0 Hz, 1H) 3.26 (t, J = 12.5 Hz, 1H) 3.10-2.90 (m, 2H) 2.41-2.20 (m, 1H); ^{19}F NMR (400 MHz, DMSO-d_6) δ ppm -100.37 (dd, 2H), -111.05 (s, 1H); TOF ES+ MS: (M+H) 490.11; HPLC Ret: 5.30 min; 94% pure.

N-(3-chlorophenyl)-5,5-difluoro-1-(2-fluoro-5-(pyridin-4-yl)benzoyl)piperidine-3-carboxamide. (CCG-264470). In a 10 mL round-bottomed flask, 1-(5-bromo-2-fluorobenzoyl)-N-(3-chlorophenyl)-5,5-difluoropiperidine-3-carboxamide (0.034 g, 0.071 mmol) and pyridin-4-ylboronic acid (0.01 g, 0.075 mmol) were dissolved in a solution of toluene:EtOH (0.5 mL:0.5 mL). The solution was degassed and sodium carbonate (0.02 g, 0.21 mmol) and Tetrakis (0.003 g, 0.05 mmol) were added. The reaction was stirred under N_2 at 90 °C for 16 hr. The reaction was cooled to RT, and the solution was diluted with water (10 mL). The product was extracted with EtOAc (3 x 15 mL), washed with brine (20 mL), dried with $MgSO_4$, and concentrated *in vacuo*. The yellow residue was subjected to silica gel chromatography eluting with 3% MeOH: 97% DCM. The fractions containing product were concentrated *in vacuo* to produce faint yellow solid. Similar compounds were made in an analogous fashion. Yield=83%. ^{1}H NMR (400 MHz, DMSO-d_6, 80 °C) δ ppm 10.05 (br. s, 1H) 8.68-8.60 (m, 2H) 7.91 (br. s, 1H) 7.79-7.69 (m, 2H) 7.70-7.50 (m, 4H) 7.43 (t, J = 8.8 Hz, 2H) 7.30 (t, J = 8.2 Hz, 1H) 7.08 (d, J = 7.5 Hz, 1H) 4.66-4.13 (m, 2H) 3.71-3.19 (m, 3H) 2.89 (br. s, 1H) 2.41-2.25 (m, 1H); ^{19}F NMR (376 MHz, DMSO-d_6, 80 °C) δ ppm -96.18—-104.76 (m, 2H) -115.80 (s, 1H); QTOF ES+ MS: (M+Na) 496.10; HPLC Ret: 5.85 min; 98% pure.

N-(3,4-dichlorophenyl)-5,5-difluoro-1-(2-fluoro-5-(pyridin-4-yl)benzoyl)piperidine-3-carboxamide. (CCG-264471). Yellow solid. Yield=94%. ^{1}H NMR (400 MHz, DMSO-d_6, 80 °C) δ ppm 10.19 (br. s, 1H) 8.63 (dt, J = 4.9, 1.6 Hz, 2H) 7.91 (br. s, 1H) 7.79-7.71 (m, 1H) 7.69-7.55 (m, 3H) 7.56-7.39 (m, 3H) 4.70-4.15 (m, 2H) 3.75-3.18 (m, 3H) 2.96-2.90 (m, 1H) 2.42-2.21 (m, 1H); ^{19}F NMR (376 MHz, DMSO-d_6, 80 °C) δ ppm -96.90—-104.52 (m, 2H) -115.85 (s, 1H); QTOF ES+ MS: (M+Na) 579.16; HPLC Ret: 6.22 min; 99% pure.

1-(3-bromobenzyl)piperidin-2-one. In a 25-mL round bottomed flask, NaH (0.067 g, 2.77 mmol) was dissolved in THF (2.0 mL) and cooled to 0 °C. piperidin-2-one (0.25 g, 2.52 mmol) dissolved in THF (8 mL) was added, and the reaction was warmed to 25 °C for 2 hr. 1-bromo-3-(bromomethyl)benzene (0.67 g, 2.70 mmol) was added, and the reaction was stirred at 25 °C for 4 hr. The reaction was quenched with H_2O, and the product was extracted with EtOAc (3 x 15 mL), washed with brine, dried with $MgSO_4$, and concentrated in vacuo. The subsequent oil was subjected to silica gel chromatography eluting with 50% to 60% EtOAc/Hex. The fractions containing product were concentrated in vacuo to produce colorless oil. Yield=89%. ^{1}H NMR (500 MHz, $CDCl_3$-*d*) δ 7.41-7.37 (m, 2H) 7.23-7.17 (m, 2H) 4.56 (s, 2H) 3.20 (t, J = 5.6 Hz, 2H) 2.47 (t, J = 6.2 Hz, 2H) 1.85-1.76 (m, 4H); TOF ES+ MS: (M+H) 268.03; HPLC Ret: 6.26 min.

benzyl 1-(3-bromobenzyl)-2-oxopiperidine-3-carboxylate. In a 50-mL round bottomed flask, 1-(3-bromobenzyl)piperidin-2-one (0.3 g, 1.12 mmol) was dissolved in THF (3.0 mL) and cooled to -78 °C. 1M LiHMDS in THF (2.3 mL, 2.35 mmol) was added dropwise, and the reaction was stirred at -78 °C for 10 mins. Benzyl chloroformate (0.19 g, 0.16 mL, 1.12 mmol) was added, and the reaction was stirred at -78 °C for 1 hr. The reaction was quenched with NH_4Cl, and the product was extracted with EtOAc (3 x 15 mL), washed with brine, dried with $MgSO_4$, and concentrated in vacuo. The subsequent oil was subjected to silica gel chromatography eluting with 30% to 40% EtOAc/Hex. The fractions containing product were concentrated in vacuo to produce colorless oil. Yield=78%. ^{1}H NMR (500 MHz, $CDCl_3$-*d*) δ 7.44-7.28 (m, 7H) 7.19 (d, J =

7.6 Hz, 1H) 7.13 (t, J = 7.7 Hz, 1H) 5.23 (s, 2H) 4.71 (d, J = 14.8 Hz, 1H) 4.45 (d, J = 14.9 Hz, 1H) 3.56 (t, J = 6.9 Hz, 1H) 3.23 (ddq, J = 24.0, 12.1, 6.5, 5.9 Hz, 2H) 2.21-2.02 (m, 2H) 1.90 (dddd, J = 13.5, 11.6, 5.7, 3.8 Hz, 1H) 1.80-1.68 (m, 1H); TOF ES+ MS: (M+Na) 326.05; HPLC Ret: 7.69 min.

1-(3-(furan-2-yl)benzyl)-2-oxopiperidine-3-carboxylic acid. In a 25 mL round bottomed flask, benzyl 1-(3-bromobenzyl)-2-oxopiperidine-3-carboxylate (0.2 g, 0.5 mmol), furan-2-ylboronic acid (0.07 g, 0.6 mmol), Tetrakis® (0.03 g, 0.03 mmol), and Na_2CO_3 (0.13 g, 1.24 mmol) were dissolved in DME (3 mL) and H_2O (3 mL). The solution was degassed and heated at 100 °C for 16 hr under Ar_2. The solution was filtered through a pad of Celite® to remove particulates. The filtrate was acidified with 1N HCl (15 mL) and the product was extracted with EtOAc (3 x 15 mL), washed with brine, dried with $MgSO_4$, and concentrated *in vacuo* to produce yellow solid. Yield=94%. ^{1}H NMR (500 MHz, DMSO-d_6) δ 12.63 (br. s, 1H) 7.75 (d, J = 1.7 Hz, 1H) 7.61-7.59 (m, 2H) 7.39 (t, J = 8.1 Hz, 1H) 7.16 (d, J = 7.7 Hz, 1H) 6.94 (d, J = 3.3 Hz, 1H) 6.59 (dd, J = 3.4, 1.8 Hz, 1H) 4.68 (d, J = 15.0 Hz, 1H) 4.44 (d, J = 15.0 Hz, 1H) 3.38 (t, J = 6.4 Hz, 1H) 3.24 (t, J = 6.1 Hz, 2H) 2.09-1.91 (m, 2H) 1.86-1.70 (m, 2H); HPLC Ret: 6.12 min.

N-(4-chlorophenyl)-1-(3-(furan-2-yl)benzyl)-2-oxopiperidine-3-carboxamide. (CCG-264644). Method I starting from 1-(3-(furan-2-yl)benzyl)-2-oxopiperidine-3-carboxylic acid (0.05 g, 0.17 mmol) and 4-chloroaniline (0.02 g, 0.17 mmol) gave N-(4-chlorophenyl)-1-(3-(furan-2-yl)benzyl)-2-oxopiperidine-3-carboxamide (0.06 g, 85%); column: 40% EtOAc/Hex; ^{1}H NMR (500 MHz, DMSO-d_6) δ 10.34 (br. s, 1H) 7.76 (d, J = 1.9 Hz, 1H) 7.67 (d, J = 8.7 Hz, 2H) 7.64-7.58 (m, 2H) 7.44-7.36 (m, 3H) 7.19 (d, J = 7.6 Hz, 1H) 6.97 (d, J = 3.4 Hz, 1H) 6.61 (dd, J = 3.4, 1.8 Hz, 1H) 4.64 (d, J = 15.0 Hz, 1H) 4.53 (d, J = 15.0 Hz, 1H) 3.51 (t, J = 7.4 Hz, 1H) 3.29 (h, J = 6.6 Hz, 2H) 2.10-2.01 (m, 2H) 2.02-1.92 (m, 1H) 1.72 (tdd, J = 13.1, 8.5, 5.2 Hz, 1H); ^{13}C NMR (500 MHz, $CDCl_3$-*d*) δ ppm 169.80, 166.85, 153.34, 143.41, 138.43, 130.97, 129.56,

129.10, 127.29, 126.86, 122.80, 122.63, 121.07, 112.52, 106.45, 50.36, 49.82, 47.68, 25.44, 21.18; QTOF ES+ MS: (M+H) 409.13; HPLC Ret: 7.84 min; 99% pure.

N-(3-chlorophenyl)-1-(3-(furan-2-yl)benzyl)-2-oxopiperidine-3-carboxamide. (CCG-264645). Method I starting from 1-(3-(furan-2-yl)benzyl)-2-oxopiperidine-3-carboxylic acid (0.05 g, 0.17 mmol) and 3-chloroaniline (0.02 g, 0.17 mmol) gave N-(3-chlorophenyl)-1-(3-(furan-2-yl)benzyl)-2-oxopiperidine-3-carboxamide (0.06 g, 82%); column: 40% EtOAc/Hex; ^{1}H NMR (500 MHz, DMSO-d_6) δ 10.40 (br. s, 1H) 7.90 (d, J = 2.1 Hz, 1H) 7.76 (t, J = 2.1 Hz, 1H) 7.68-7.58 (m, 2H) 7.50-7.32 (m, 3H) 7.19 (d, J = 7.6 Hz, 1H) 7.13 (d, J = 7.6 Hz, 1H) 6.99 (d, J = 3.0 Hz, 1H) 6.61 (dd, J = 3.4, 2.1 Hz, 1H) 4.67 (d, J = 15.0 Hz, 1H) 4.51 (d, J = 15.1 Hz, 1H) 3.52 (t, J = 7.4 Hz, 1H) 3.30 (h, J = 4.3 Hz, 2H) 2.11-2.02 (m, 2H) 2.02-1.92 (m, 1H) 1.73 (dt, J = 14.3, 6.2 Hz, 1H); ^{13}C NMR (500 MHz, $CDCl_3$-*d*) δ ppm 170.11, 166.76, 153.36, 143.40, 140.89, 138.42, 133.54, 130.98, 130.91, 129.56, 126.86, 123.49, 122.78, 122.61, 119.01, 117.93, 112.49, 106.45, 50.39, 49.82, 47.68, 25.42, 21.12; QTOF ES+ MS: (M+H) 409.13; HPLC Ret: 7.90 min; 97% pure.

N-(3-chloro-5-(hydroxymethyl)phenyl)-5,5-difluoro-1-(3-fluoro-5-(pyridin-4-yl)benzoyl)piperidine-3-carboxamide (CCG-265072). In a 10 mL round-bottomed flask, N-(3-(((tert-butyldiphenylsilyl)oxy)methyl)-5-chlorophenyl)-5,5-difluoro-1-(3-fluoro-5-(pyridin-4-yl)benzoyl)piperidine-3-carboxamide (0.04 g, 0.05 mmol) was dissolved in THF (0.5 mL). 1 M TBAF in THF (0.11 mL, 0.11 mmol) was added and the mixture was stirred under nitrogen at 25 °C for 1 hr. The reaction was quenched with water (20 mL) and the product was extracted with EtOAc (3x 15 mL). The organic layer was washed with brine, dried with magnesium sulfate, and evaporated, providing yellow oil. The residue was subjected to silica gel chromatography eluting with 85% EtOAc: 100% Hex. The fractions containing product were concentrated in vacuo to produce white solid. Yield=70%. ^{1}H NMR (400 MHz, DMSO-d_6, 80 °C) δ ppm 10.04 (br. s, 1H) 8.66 (d, J = 5.3 Hz, 2H) 7.77-7.67 (m, 3H) 7.61 (d, J = 7.0 Hz, 2H) 7.40 (s, 1H) 7.31 (d, J = 8.6

Hz, 1H) 7.04 (s, 1H) 5.00 (t, J = 5.5 Hz, 1H) 4.46 (d, J = 5.5 Hz, 2H) 4.34-4.09 (m, 2H) 3.58 (dd, J = 29.5, 13.7 Hz, 1H) 3.25 (t, J = 8.0 Hz, 1H) 2.96 (br. s, 2H) 2.45-2.20 (m, 1H); ^{19}F NMR (376 MHz, DMSO-d_6, 80 °C) δ ppm -99.00—-101.91 (m, 2H) -111.09 (t, J = 9.4 Hz, 1H); QTOF ES+ MS: (M+H) 504.1; HPLC Ret: 5.19 min; 99% pure.

Bibliography:

1 Rockey, D. C., Bell, P. D. & Hill, J. A. Fibrosis--a common pathway to organ injury and failure. *N Engl J Med* **372**, 1138-1149, doi:10.1056/NEJMra1300575 (2015).

2 Costner, M. I. & Jacobe, H. Dermatopathology of connective tissue diseases. *Adv Dermatol* **16**, 323-359; discussion 360 (2000).

3 Rosenbloom, J., Castro, S. V. & Jimenez, S. A. Narrative review: fibrotic diseases: cellular and molecular mechanisms and novel therapies. *Ann Intern Med* **152**, 159-166, doi:10.7326/0003-4819-152-3-201002020-00007 (2010).

4 Wynn, T. A. Common and unique mechanisms regulate fibrosis in various fibroproliferative diseases. *J Clin Invest* **117**, 524-529, doi:10.1172/JCI31487 (2007).

5 Wynn, T. A. Cellular and molecular mechanisms of fibrosis. *J Pathol* **214**, 199-210, doi:10.1002/path.2277 (2008).

6 Allanore, Y. *et al.* Systemic sclerosis. *Nature Reviews Disease Primers* **1**, doi:Artn 15002 10.1038/Nrdp.2015.2 (2015).

7 Fala, L. Ofev (Nintedanib): First Tyrosine Kinase Inhibitor Approved for the Treatment of Patients with Idiopathic Pulmonary Fibrosis. *Am Health Drug Benefits* **8**, 101-104 (2015).

8 Piera-Velazquez, S., Mendoza, F. A. & Jimenez, S. A. Endothelial to Mesenchymal Transition (EndoMT) in the Pathogenesis of Human Fibrotic Diseases. *J Clin Med* **5**, doi:10.3390/jcm5040045 (2016).

9 Thannickal, V. J. *et al.* Matrix biology of idiopathic pulmonary fibrosis: a workshop report of the national heart, lung, and blood institute. *Am J Pathol* **184**, 1643-1651, doi:10.1016/j.ajpath.2014.02.003 (2014).

10 Nanthakumar, C. B. *et al.* Dissecting fibrosis: therapeutic insights from the small-molecule toolbox. *Nature reviews. Drug discovery* **14**, 693-720, doi:10.1038/nrd4592 (2015).

11 Wick, G. *et al.* The immunology of fibrosis. *Annu Rev Immunol* **31**, 107-135, doi:10.1146/annurev-immunol-032712-095937 (2013).

12 Li, X., Zhu, L., Wang, B., Yuan, M. & Zhu, R. Drugs and Targets in Fibrosis. *Front Pharmacol* **8**, 855, doi:10.3389/fphar.2017.00855 (2017).

13 Lundvig, D. M., Immenschuh, S. & Wagener, F. A. Heme oxygenase, inflammation, and fibrosis: the good, the bad, and the ugly? *Front Pharmacol* **3**, 81, doi:10.3389/fphar.2012.00081 (2012).

14 Hinz, B. *et al.* Recent developments in myofibroblast biology: paradigms for connective tissue remodeling. *Am J Pathol* **180**, 1340-1355, doi:10.1016/j.ajpath.2012.02.004 (2012).

15 Follonier, L., Schaub, S., Meister, J. J. & Hinz, B. Myofibroblast communication is controlled by intercellular mechanical coupling. *J Cell Sci* **121**, 3305-3316, doi:10.1242/jcs.024521 (2008).

16 Hinz, B., Celetta, G., Tomasek, J. J., Gabbiani, G. & Chaponnier, C. Alpha-smooth muscle actin expression upregulates fibroblast contractile activity. *Mol Biol Cell* **12**, 2730-2741 (2001).
17 Tomasek, J. J., Gabbiani, G., Hinz, B., Chaponnier, C. & Brown, R. A. Myofibroblasts and mechano-regulation of connective tissue remodelling. *Nat Rev Mol Cell Bio* **3**, 349-363, doi:10.1038/nrm809 (2002).
18 Wipff, P. J., Rifkin, D. B., Meister, J. J. & Hinz, B. Myofibroblast contraction activates latent TGF-beta1 from the extracellular matrix. *J Cell Biol* **179**, 1311-1323, doi:10.1083/jcb.200704042 (2007).
19 Darby, I. A., Laverdet, B., Bonte, F. & Desmouliere, A. Fibroblasts and myofibroblasts in wound healing. *Clin Cosmet Investig Dermatol* **7**, 301-311, doi:10.2147/CCID.S50046 (2014).
20 Anders, H. J. & Schaefer, L. Beyond Tissue Injury-Damage-Associated Molecular Patterns, Toll-Like Receptors, and Inflammasomes Also Drive Regeneration and Fibrosis. *J Am Soc Nephrol* **25**, 1387-1400, doi:10.1681/Asn.2014010117 (2014).
21 Ellson, C. D., Dunmore, R., Hogaboam, C. M., Sleeman, M. A. & Murray, L. A. Danger-Associated Molecular Patterns and Danger Signals in Idiopathic Pulmonary Fibrosis. *Am J Resp Cell Mol* **51**, 163-168, doi:10.1165/rcmb.2013-0366TR (2014).
22 Ouyang, X. S., Ghani, A. & Mehal, W. Z. Inflammasome biology in fibrogenesis. *Bba-Mol Basis Dis* **1832**, 979-988, doi:10.1016/j.bbadis.2013.03.020 (2013).
23 Huebener, P. & Schwabe, R. F. Regulation of wound healing and organ fibrosis by toll-like receptors. *Biochim Biophys Acta* **1832**, 1005-1017, doi:10.1016/j.bbadis.2012.11.017 (2013).
24 Lee, S., Suh, G. Y., Ryter, S. W. & Choi, A. M. K. Regulation and Function of the Nucleotide Binding Domain Leucine-Rich Repeat-Containing Receptor, Pyrin Domain-Containing-3 Inflammasome in Lung Disease. *Am J Resp Cell Mol* **54**, 151-160, doi:10.1165/rcmb.2015-0231TR (2016).
25 Terlizzi, M. *et al.* Activation of the Absent in Melanoma 2 Inflammasome in Peripheral Blood Mononuclear Cells From Idiopathic Pulmonary Fibrosis Patients Leads to the Release of Pro-Fibrotic Mediators. *Front Immunol* **9**, doi:ARTN 670 10.3389/fimmu.2018.00670 (2018).
26 Xiang, M. & Fan, J. Pattern Recognition Receptor-Dependent Mechanisms of Acute Lung Injury. *Mol Med* **16**, 69-82, doi:10.2119/molmed.2009.00097 (2010).
27 Bergsbaken, T., Fink, S. L. & Cookson, B. T. Pyroptosis: host cell death and inflammation. *Nat Rev Microbiol* **7**, 99-109, doi:10.1038/nrmicro2070 (2009).
28 Desai, O., Winkler, J., Minasyan, M. & Herzog, E. L. The Role of Immune and Inflammatory Cells in Idiopathic Pulmonary Fibrosis. *Front Med* **5**, doi:ARTN 43 10.3389/fmed.2018.00043 (2018).
29 Mack, M. Inflammation and fibrosis. *Matrix Biol* **68-69**, 106-121, doi:10.1016/j.matbio.2017.11.010 (2018).
30 White, E. S. & Mantovani, A. R. Inflammation, wound repair, and fibrosis: reassessing the spectrum of tissue injury and resolution. *J Pathol* **229**, 141-144, doi:10.1002/path.4126 (2013).
31 Amulic, B., Cazalet, C., Hayes, G. L., Metzler, K. D. & Zychlinsky, A. Neutrophil Function: From Mechanisms to Disease. *Annual Review of Immunology, Vol 30* **30**, 459-489, doi:10.1146/annurev-immunol-020711-074942 (2012).
32 Wynn, T. A. Integrating mechanisms of pulmonary fibrosis. *J Exp Med* **208**, 1339-1350, doi:10.1084/jem.20110551 (2011).

33 Van Linthout, S., Miteva, K. & Tschope, C. Crosstalk between fibroblasts and inflammatory cells. *Cardiovasc Res* **102**, 258-269, doi:10.1093/cvr/cvu062 (2014).
34 Braga, T. T., Agudelo, J. S. H. & Camara, N. O. S. Macrophages During the Fibrotic Process: M2 as Friend and Foe. *Front Immunol* **6**, doi:ARTN 602 10.3389/fimmu.2015.00602 (2015).

35 Lech, M. & Anders, H. J. Macrophages and fibrosis: How resident and infiltrating mononuclear phagocytes orchestrate all phases of tissue injury and repair. *Bba-Mol Basis Dis* **1832**, 989-997, doi:10.1016/j.bbadis.2012.12.001 (2013).
36 Wynn, T. A. & Vannella, K. M. Macrophages in Tissue Repair, Regeneration, and Fibrosis. *Immunity* **44**, 450-462, doi:10.1016/j.immuni.2016.02.015 (2016).
37 Zhang, L. *et al.* Macrophages: friend or foe in idiopathic pulmonary fibrosis? *Resp Res* **19**, doi:ARTN 170 10.1186/s12931-018-0864-2 (2018).

38 Klein, T. & Bischoff, R. Physiology and pathophysiology of matrix metalloproteases. *Amino Acids* **41**, 271-290, doi:10.1007/s00726-010-0689-x (2011).
39 Page-McCaw, A., Ewald, A. J. & Werb, Z. Matrix metalloproteinases and the regulation of tissue remodelling. *Nat Rev Mol Cell Bio* **8**, 221-233, doi:10.1038/nrm2125 (2007).
40 Craig, V. J., Zhang, L., Hagood, J. S. & Owen, C. A. Matrix Metalloproteinases as Therapeutic Targets for Idiopathic Pulmonary Fibrosis. *Am J Resp Cell Mol* **53**, 585-600, doi:10.1165/rcmb.2015-0020TR (2015).
41 Giannandrea, M. & Parks, W. C. Diverse functions of matrix metalloproteinases during fibrosis. *Dis Model Mech* **7**, 193-203, doi:10.1242/dmm.012062 (2014).
42 Arpino, V., Brock, M. & Gill, S. E. The role of TIMPs in regulation of extracellular matrix proteolysis. *Matrix Biol* **44-46**, 247-254, doi:10.1016/j.matbio.2015.03.005 (2015).
43 Pardo, A., Cabrera, S., Maldonado, M. & Selman, M. Role of matrix metalloproteinases in the pathogenesis of idiopathic pulmonary fibrosis. *Resp Res* **17**, doi:ARTN 23 10.1186/s12931-016-0343-6 (2016).

44 Lacraz, S. *et al.* Suppression of metalloproteinase biosynthesis in human alveolar macrophages by interleukin-4. *J Clin Invest* **90**, 382-388, doi:10.1172/JCI115872 (1992).
45 Shapiro, S. D., Campbell, E. J., Kobayashi, D. K. & Welgus, H. G. Immune Modulation of Metalloproteinase Production in Human Macrophages - Selective Pretranslational Suppression of Interstitial Collagenase and Stromelysin Biosynthesis by Interferon-Gamma. *Journal of Clinical Investigation* **86**, 1204-1210, doi:Doi 10.1172/Jci114826 (1990).
46 Bradding, P. & Pejler, G. The controversial role of mast cells in fibrosis. *Immunol Rev* **282**, 198-231, doi:10.1111/imr.12626 (2018).
47 Hugle, T. Beyond allergy: the role of mast cells in fibrosis. *Swiss Med Wkly* **144**, doi:ARTN w13999 10.4414/smw.2014.13999 (2014).

48 Overed-Sayer, C., Rapley, L., Mustelin, T. & Clarke, D. L. Are mast cells instrumental for fibrotic diseases? *Frontiers in Pharmacology* **4**, doi:ARTN 174 10.3389/fphar.2013.00174 (2014).

49 Beghdadi, W. *et al.* Mast cell chymase protects against renal fibrosis in murine unilateral ureteral obstruction. *Kidney Int* **84**, 317-326, doi:10.1038/ki.2013.98 (2013).
50 Levi-Schaffer, F. & Piliponsky, A. M. Tryptase, a novel link between allergic inflammation and fibrosis. *Trends Immunol* **24**, 158-161, doi:10.1016/S14714906(03)00058-9 (2003).
51 Masubuchi, S. *et al.* Chymase inhibitor ameliorates hepatic steatosis and fibrosis on established non-alcoholic steatohepatitis in hamsters fed a methionine- and choline-deficient diet. *Hepatol Res* **43**, 970-978, doi:10.1111/hepr.12042 (2013).

52 Dell'Italia, L. J., Collawn, J. F. & Ferrario, C. M. Multifunctional Role of Chymase in Acute and Chronic Tissue Injury and Remodeling. *Circ Res* **122**, 319-336, doi:10.1161/Circresaha.117.310978 (2018).
53 Bot, I., Shi, G. P. & Kovanen, P. T. Mast Cells as Effectors in Atherosclerosis. *Arterioscl Throm Vas* **35**, 265-271, doi:10.1161/Atvbaha.114.303570 (2015).
54 Marshall, B. G. & Shaw, R. J. T cells and fibrosis. *Chem Immunol* **78**, 148-158 (2000).
55 Postlethwaite, A. E. Role of T cells and cytokines in effecting fibrosis. *Int Rev Immunol* **12**, 247-258 (1995).
56 Borthwick, L. A., Wynn, T. A. & Fisher, A. J. Cytokine mediated tissue fibrosis. *Bba-Mol Basis Dis* **1832**, 1049-1060, doi:10.1016/j.bbadis.2012.09.014 (2013).
57 Sahin, H. & Wasmuth, H. E. Chemokines in tissue fibrosis. *Bba-Mol Basis Dis* **1832**, 1041-1048, doi:10.1016/j.bbadis.2012.11.004 (2013).
58 Sziksz, E. *et al.* Fibrosis Related Inflammatory Mediators: Role of the IL-10 Cytokine Family. *Mediat Inflamm*, doi:Artn 764641 10.1155/2015/764641 (2015).

59 Biernacka, A., Dobaczewski, M. & Frangogiannis, N. G. TGF-beta signaling in fibrosis. *Growth Factors* **29**, 196-202, doi:10.3109/08977194.2011.595714 (2011).
60 Kim, K. K., Sheppard, D. & Chapman, H. A. TGF-beta 1 Signaling and Tissue Fibrosis. *Csh Perspect Biol* **10**, doi:ARTN a022293 10.1101/cshperspect.a022293 (2018).

61 Meng, X. M., Nikolic-Paterson, D. J. & Lan, H. Y. TGF-beta: the master regulator of fibrosis. *Nat Rev Nephrol* **12**, 325-338, doi:10.1038/nrneph.2016.48 (2016).
62 Meng, X. M., Tang, P. M. K., Li, J. & Lan, H. Y. TGF-beta/Smad signaling in renal fibrosis. *Front Physiol* **6**, doi:ARTN 82 10.3389/fphys.2015.00082 (2015).

63 Pakshir, P. & Hinz, B. The big five in fibrosis: Macrophages, myofibroblasts, matrix, mechanics, and miscommunication. *Matrix Biol* **68-69**, 81-93, doi:10.1016/j.matbio.2018.01.019 (2018).
64 Bochaton-Piallat, M. L., Gabbiani, G. & Hinz, B. The myofibroblast in wound healing and fibrosis: answered and unanswered questions. *F1000Res* **5**, doi:10.12688/f1000research.8190.1 (2016).
65 Klingberg, F., Hinz, B. & White, E. S. The myofibroblast matrix: implications for tissue repair and fibrosis. *J Pathol* **229**, 298-309, doi:10.1002/path.4104 (2013).
66 Hinz, B. Formation and function of the myofibroblast during tissue repair. *J Invest Dermatol* **127**, 526-537, doi:10.1038/sj.jid.5700613 (2007).
67 Baum, J. & Duffy, H. S. Fibroblasts and Myofibroblasts: What Are We Talking About? *J Cardiovasc Pharm* **57**, 376-379, doi:10.1097/FJC.0b013e3182116e39 (2011).
68 Micallef, L. *et al.* The myofibroblast, multiple origins for major roles in normal and pathological tissue repair. *Fibrogenesis Tissue Repair* **5**, S5, doi:10.1186/1755-1536-5-S1-S5 (2012).
69 Stone, R. C. *et al.* Epithelial-mesenchymal transition in tissue repair and fibrosis. *Cell and Tissue Research* **365**, 495-506, doi:10.1007/s00441-016-2464-0 (2016).
70 Piera-Velazquez, S., Li, Z. D. & Jimenez, S. A. Role of Endothelial-Mesenchymal Transition (EndoMT) in the Pathogenesis of Fibrotic Disorders. *Am J Pathol* **179**, 1074-1080, doi:10.1016/j.ajpath.2011.06.001 (2011).
71 Darby, I. A. & Hewitson, T. D. Fibroblast differentiation in wound healing and fibrosis. *Int Rev Cytol* **257**, 143-+, doi:10.1016/S0074-7696(07)57004-X (2007).
72 Kalluri, R. & Weinberg, R. A. The basics of epithelial-mesenchytnal transition (vol 119, pg 1420, 2009). *Journal of Clinical Investigation* **120**, 1786-1786, doi:10.1172/Jci39104c1 (2010).

73 O'Connor, J. W. & Gomez, E. W. Biomechanics of TGFbeta-induced epithelial-mesenchymal transition: implications for fibrosis and cancer. *Clin Transl Med* **3**, 23, doi:10.1186/2001-1326-3-23 (2014).
74 El Agha, E. *et al.* Mesenchymal Stem Cells in Fibrotic Disease. *Cell Stem Cell* **21**, 166-177, doi:10.1016/j.stem.2017.07.011 (2017).
75 Kendall, R. T. & Feghali-Bostwick, C. A. Fibroblasts in fibrosis: novel roles and mediators. *Frontiers in Pharmacology* **5**, doi:ARTN 123 10.3389/fphar.2014.00123 (2014).
76 Cox, T. R. *et al.* LOX-Mediated Collagen Crosslinking Is Responsible for Fibrosis-Enhanced Metastasis. *Cancer Res* **73**, 1721-1732, doi:10.1158/0008-5472.Can-12-2233 (2013).
77 Phan, S. H. Biology of fibroblasts and myofibroblasts. *Proc Am Thorac Soc* **5**, 334-337, doi:10.1513/pats.200708-146DR (2008).
78 Guo, Y., Xiao, L., Sun, L. & Liu, F. Wnt/beta-Catenin Signaling: a Promising New Target for Fibrosis Diseases. *Physiol Res* **61**, 337-346 (2012).
79 Kavian, N., Servettaz, A., Weill, B. & Batteux, F. New Insights into the Mechanism of Notch Signalling in Fibrosis. *The Open Rheumatology Journal* **6**, 96-102, doi:10.2174/1874312901206010096 (2012).
80 Ding, H. *et al.* Sonic Hedgehog Signaling Mediates Epithelial-Mesenchymal Communication and Promotes Renal Fibrosis. *J Am Soc Nephrol* **23**, 801-813, doi:10.1681/Asn.2011060614 (2012).
81 Hu, L. P., Lin, X. Y., Lu, H., Chen, B. C. & Bai, Y. H. An Overview of Hedgehog Signaling in Fibrosis. *Mol Pharmacol* **87**, 174-182, doi:10.1124/mol.114.095141 (2015).
82 Carthy, J. M. TGFbeta signaling and the control of myofibroblast differentiation: Implications for chronic inflammatory disorders. *J Cell Physiol* **233**, 98-106, doi:10.1002/jcp.25879 (2018).
83 Harvey, K. A., Paranavitana, C. N., Zaloga, G. P. & Siddiqui, R. A. Diverse signaling pathways regulate fibroblast differentiation and transformation through Rho kinase activation. *J Cell Physiol* **211**, 353-363, doi:10.1002/jcp.20939 (2007).
84 Glasser, S. W. *et al.* Mechanisms of Lung Fibrosis Resolution. *Am J Pathol* **186**, 1066-1077, doi:10.1016/j.ajpath.2016.01.018 (2016).
85 Snowdon, V. K. & Fallowfield, J. A. Models and Mechanisms of Fibrosis Resolution. *Alcohol Clin Exp Res* **35**, 794-799, doi:10.1111/j.1530-0277.2010.01400.x (2011).
86 Yang, X. H., Chen, B., Liu, T. & Chen, X. H. Reversal of myofibroblast differentiation: A review. *Eur J Pharmacol* **734**, 83-90, doi:10.1016/j.ejphar.2014.04.007 (2014).
87 Kosla, J., Dvorakova, M., Dvorak, M. & Cermak, V. Effective myofibroblast dedifferentiation by concomitant inhibition of TGF-beta signaling and perturbation of MAPK signaling. *Eur J Cell Biol* **92**, 363-373, doi:10.1016/j.ejcb.2013.10.013 (2013).
88 Gibbons, M. A. *et al.* Ly6C(hi) Monocytes Direct Alternatively Activated Profibrotic Macrophage Regulation of Lung Fibrosis. *Am J Resp Crit Care* **184**, 569-581, doi:10.1164/rccm.201010-1719OC (2011).
89 Sennello, J. A. *et al.* Lrp5/beta-Catenin Signaling Controls Lung Macrophage Differentiation and Inhibits Resolution of Fibrosis. *Am J Resp Cell Mol* **56**, 191-201, doi:10.1165/rcmb.2016-0147OC (2017).
90 Duffield, J. S. *et al.* Selective depletion of macrophages reveals distinct, opposing roles during liver injury and repair. *Journal of Clinical Investigation* **115**, 56-65, doi:10.1172/Jci200522675 (2005).
91 Ramachandran, P. & Iredale, J. P. Liver fibrosis: a bidirectional model of fibrogenesis and resolution. *Qjm-Int J Med* **105**, 813-817, doi:10.1093/qjmed/hcs069 (2012).

92 Kuilman, T., Michaloglou, C., Mooi, W. J. & Peeper, D. S. The essence of senescence. *Gene Dev* **24**, 2463-2479, doi:10.1101/gad.1971610 (2010).
93 Schafer, M. J., Haak, A. J., Tschumperlin, D. J. & LeBrasseur, N. K. Targeting Senescent Cells in Fibrosis: Pathology, Paradox, and Practical Considerations. *Curr Rheumatol Rep* **20**, doi:ARTN 3 10.1007/s11926-018-0712-x (2018).

94 Schafer, M. J. *et al.* Cellular senescence mediates fibrotic pulmonary disease. *Nat Commun* **8**, doi:ARTN 14532 10.1038/ncomms14532 (2017).

95 Murphy, A. M., Wong, A. L. & Bezuhly, M. Modulation of angiotensin II signaling in the prevention of fibrosis. *Fibrogenesis Tissue* **8**, doi:UNSP 7 10.1186/s13069-015-0023-z (2015).

96 Talele, N. P., Fradette, J., Davies, J. E., Kapus, A. & Hinz, B. Expression of alpha-Smooth Muscle Actin Determines the Fate of Mesenchymal Stromal Cells. *Stem Cell Rep* **4**, 1016-1030, doi:10.1016/j.stemcr.2015.05.004 (2015).
97 Deng, X. L. *et al.* Transcriptional regulation of increased CCL2 expression in pulmonary fibrosis involves nuclear factor-kappa B and activator protein-1. *Int J Biochem Cell B* **45**, 1366-1376, doi:10.1016/j.biocel.2013.04.003 (2013).
98 Lipson, K. E., Wong, C., Teng, Y. & Spong, S. CTGF is a central mediator of tissue remodeling and fibrosis and its inhibition can reverse the process of fibrosis. *Fibrogenesis Tissue Repair* **5**, S24, doi:10.1186/1755-1536-5-S1-S24 (2012).
99 Rodriguez-Pascual, F., Busnadiego, O. & Gonzalez-Santamaria, J. The profibrotic role of endothelin-1: Is the door still open for the treatment of fibrotic diseases? *Life Sci* **118**, 156-164, doi:10.1016/j.lfs.2013.12.024 (2014).
100 Kim, K. K., Sisson, T. H. & Horowitz, J. C. Fibroblast growth factors and pulmonary fibrosis: it's more complex than it sounds. *J Pathol* **241**, 6-9, doi:10.1002/path.4825 (2017).
101 Maddaluno, L., Urwyler, C. & Werner, S. Fibroblast growth factors: key players in regeneration and tissue repair. *Development* **144**, 4047-4060, doi:10.1242/dev.152587 (2017).
102 To, W. S. & Midwood, K. S. Plasma and cellular fibronectin: distinct and independent functions during tissue repair. *Fibrogenesis Tissue Repair* **4**, 21, doi:10.1186/1755-1536-4-21 (2011).
103 Panula, P. *et al.* International Union of Basic and Clinical Pharmacology. XCVIII. Histamine Receptors. *Pharmacol Rev* **67**, 601-655, doi:10.1124/pr.114.010249 (2015).
104 Iwakiri, Y. Nitric oxide in liver fibrosis: The role of inducible nitric oxide synthase. *Clin Mol Hepatol* **21**, 319-325, doi:10.3350/cmh.2015.21.4.319 (2015).
105 Segel, M. J. *et al.* Role of interferon-gamma in the evolution of murine bleomycin lung fibrosis. *Am J Physiol-Lung C* **285**, L1255-L1262, doi:10.1152/ajplung.00303.2002 (2003).
106 Borthwick, L. A. The IL-1 cytokine family and its role in inflammation and fibrosis in the lung. *Semin Immunopathol* **38**, 517-534, doi:10.1007/s00281-016-0559-z (2016).
107 Agarwal, S. K. Integrins and cadherins as therapeutic targets in fibrosis. *Frontiers in Pharmacology* **5**, doi:ARTN 131 10.3389/fphar.2014.00131 (2014).

108 Huaux, F. *et al.* A profibrotic function of IL-12p40 in experimental pulmonary fibrosis. *J Immunol* **169**, 2653-2661, doi:DOI 10.4049/jimmunol.169.5.2653 (2002).
109 Passalacqua, G. *et al.* IL-13 and idiopathic pulmonary fibrosis: Possible links and new therapeutic strategies. *Pulm Pharmacol Ther* **45**, 95-100, doi:10.1016/j.pupt.2017.05.007 (2017).

110 Park, M. J. *et al.* IL-1-IL-17 Signaling Axis Contributes to Fibrosis and Inflammation in Two Different Murine Models of Systemic Sclerosis. *Front Immunol* **9**, doi:ARTN 1611 10.3389/fimmu.2018.01611 (2018).

111 Rancoule, C. *et al.* Lysophosphatidic acid (LPA) as a pro-fibrotic and pro-oncogenic factor: a pivotal target to improve the radiotherapy therapeutic index. *Oncotarget* **8**, 43543-43554, doi:10.18632/oncotarget.16672 (2017).

112 Klinkhammer, B. M., Floege, J. & Boor, P. PDGF in organ fibrosis. *Mol Aspects Med* **62**, 44-62, doi:10.1016/j.mam.2017.11.008 (2018).

113 Bozyk, P. D. & Moore, B. B. Prostaglandin E-2 and the Pathogenesis of Pulmonary Fibrosis. *Am J Resp Cell Mol* **45**, 445-452, doi:10.1165/rcmb.2011-0025RT (2011).

114 Richter, K. & Kietzmann, T. Reactive oxygen species and fibrosis: further evidence of a significant liaison. *Cell Tissue Res* **365**, 591-605, doi:10.1007/s00441-016-2445-3 (2016).

115 Distler, J. H. W., Schett, G., Gay, S. & Distler, O. The controversial role of tumor necrosis factor alpha in fibrotic diseases. *Arthritis Rheum* **58**, 2228-2235, doi:10.1002/art.23645 (2008).

116 Barratt, S. L., Flower, V. A., Pauling, J. D. & Millar, A. B. VEGF (Vascular Endothelial Growth Factor) and Fibrotic Lung Disease. *Int J Mol Sci* **19**, doi:ARTN 1269 10.3390/ijms19051269 (2018).

117 Yan, Z., Kui, Z. & Ping, Z. Reviews and prospectives of signaling pathway analysis in idiopathic pulmonary fibrosis. *Autoimmun Rev* **13**, 1020-1025, doi:10.1016/j.autrev.2014.08.028 (2014).

118 Hosseinzadeh, A. *et al.* Idiopathic pulmonary fibrosis (IPF) signaling pathways and protective roles of melatonin. *Life Sci* **201**, 17-29, doi:10.1016/j.lfs.2018.03.032 (2018).

119 Knipe, R. S., Tager, A. M. & Liao, J. K. The Rho Kinases: Critical Mediators of Multiple Profibrotic Processes and Rational Targets for New Therapies for Pulmonary Fibrosis. *Pharmacol Rev* **67**, 103-117, doi:10.1124/pr.114.009381 (2015).

120 Piersma, B., Bank, R. A. & Boersema, M. Signaling in fibrosis: TGF-beta, wNT, and YAP/TAZ converge. *Front Med* **2**, doi:ARTN 59 10.3389/fmed.2015.00059 (2015).

121 Tsou, P. S., Haak, A. J., Khanna, D. & Neubig, R. R. Cellular Mechanisms of Tissue Fibrosis. 8. Current and future drug targets in fibrosis: focus on Rho GTPase-regulated gene transcription. *Am J Physiol-Cell Ph* **307**, C2-C13, doi:10.1152/ajpcell.00060.2014 (2014).

122 Rosenbloom, J., Mendoza, F. A. & Jimenez, S. A. Strategies for anti-fibrotic therapies. *Bba-Mol Basis Dis* **1832**, 1088-1103, doi:10.1016/j.bbadis.2012.12.007 (2013).

123 Bonner, J. C. Regulation of PDGF and its receptors in fibrotic diseases. *Cytokine Growth F R* **15**, 255-273, doi:10.1016/j.cytogfr.2004.03.006 (2004).

124 Mercer, P. F. *et al.* Exploration of a potent PI3 kinase/mTOR inhibitor as a novel anti-fibrotic agent in IPF. *Thorax* **71**, 701-711, doi:10.1136/thoraxjnl-2015-207429 (2016).

125 Hu, M. *et al.* Therapeutic Targeting of Src Kinase in Myofibroblast Differentiation and Pulmonary Fibrosis. *J Pharmacol Exp Ther* **351**, 87-95, doi:10.1124/jpet.114.216044 (2014).

126 Hsu, H. S. *et al.* Involvement of ER stress, PI3K/AKT activation, and lung fibroblast proliferation in bleomycin-induced pulmonary fibrosis. *Sci Rep-Uk* **7**, doi:ARTN 14272 10.1038/s41598-017-14612-5 (2017).

127 Han, Q., Lin, L. J., Zhao, B. L., Wang, N. P. & Liu, X. M. Inhibition of mTOR ameliorates bleomycin-induced pulmonary fibrosis by regulating epithelial-mesenchymal transition. *Biochem Bioph Res Co* **500**, 839-845, doi:10.1016/j.bbrc.2018.04.148 (2018).

128 Zhao, X. K. *et al.* Focal Adhesion Kinase Regulates Fibroblast Migration via Integrin beta-1 and Plays a Central Role in Fibrosis. *Sci Rep-Uk* **6**, doi:ARTN 19276 10.1038/srep19276 (2016).

129 Burgy, O. & Konigshoff, M. The WNT signaling pathways in wound healing and fibrosis. *Matrix Biol* **68-69**, 67-80, doi:10.1016/j.matbio.2018.03.017 (2018).

130 Koike, K. *et al.* Protective role of JAK/STAT signaling against renal fibrosis in mice with unilateral ureteral obstruction. *Clin Immunol* **150**, 78-87, doi:10.1016/j.clim.2013.11.003 (2014).

131 Case, A. H. & Johnson, P. Clinical use of nintedanib in patients with idiopathic pulmonary fibrosis. *Bmj Open Respir Res* **4**, doi:UNSP e000192 10.1136/bmjresp-2017-000192 (2017).

132 Raghu, G. & Selman, M. Nintedanib and pirfenidone. New antifibrotic treatments indicated for idiopathic pulmonary fibrosis offer hopes and raises questions. *Am J Respir Crit Care Med* **191**, 252-254, doi:10.1164/rccm.201411-2044ED (2015).

133 Scelfo, C., Caminati, A. & Harari, S. Recent advances in managing idiopathic pulmonary fibrosis. *F1000Res* **6**, 2052, doi:10.12688/f1000research.10720.1 (2017).

134 Tepede, A. & Yogaratnam, D. Nintedanib for Idiopathic Pulmonary Fibrosis. *J Pharm Pract*, 897190017735242, doi:10.1177/0897190017735242 (2017).

135 Rafii, R., Juarez, M. M., Albertson, T. E. & Chan, A. L. A review of current and novel therapies for idiopathic pulmonary fibrosis. *J Thorac Dis* **5**, 48-73, doi:10.3978/j.issn.2072-1439.2012.12.07 (2013).

136 Lim, R., Ricardo, S. D. & Sievert, W. Cell-Based Therapies for Tissue Fibrosis. *Frontiers in Pharmacology* **8**, doi:ARTN 633 10.3389/fphar.2017.00633 (2017).

137 Gyorfi, A. H., Matei, A. E. & Distler, J. H. W. Targeting TGF-beta signaling for the treatment of fibrosis. *Matrix Biol* **68-69**, 8-27, doi:10.1016/j.matbio.2017.12.016 (2018).

138 Wollin, L. *et al.* Mode of action of nintedanib in the treatment of idiopathic pulmonary fibrosis. *Eur Respir J* **45**, 1434-1445, doi:10.1183/09031936.00174914 (2015).

139 Tzouvelekis, A. *et al.* Mesenchymal Stem Cells for the Treatment of Idiopathic Pulmonary Fibrosis. *Front Med* **5**, doi:ARTN 142 10.3389/fmed.2018.00142 (2018).

140 Friedman, S. L., Sheppard, D., Duffield, J. S. & Violette, S. Therapy for Fibrotic Diseases: Nearing the Starting Line. *Sci Transl Med* **5**, doi:ARTN 167sr1 10.1126/scitranslmed.3004700 (2013).

141 McVicker, B. L. & Bennett, R. G. Novel Anti-fibrotic Therapies. *Frontiers in Pharmacology* **8**, doi:ARTN 318 10.3389/fphar.2017.00318 (2017).

142 Mora, A. L., Rojas, M., Pardo, A. & Selman, M. Emerging therapies for idiopathic pulmonary fibrosis, a progressive age-related disease. *Nat Rev Drug Discov* **16**, 755-772, doi:10.1038/nrd.2017.170 (2017).

143 Tanase, C. P., Ogrezeanu, I. & Badiu, C. MicroRNAs. *Elsev Insight*, 91-96, doi:10.1016/B978-0-12-415830-6.00008-1 (2012).

144 Thum, T. *et al.* MicroRNA-21 contributes to myocardial disease by stimulating MAP kinase signalling in fibroblasts. *Nature* **456**, 980-U983, doi:10.1038/nature07511 (2008).

145 van Rooij, E. *et al.* Dysregulation of microRNAs after myocardial infarction reveals a role of miR-29 in cardiac fibrosis. *Proc Natl Acad Sci U S A* **105**, 13027-13032, doi:10.1073/pnas.0805038105 (2008).

146 Grygiel-Gorniak, B. Peroxisome proliferator-activated receptors and their ligands: nutritional and clinical implications - a review. *Nutr J* **13**, doi:Artn 17 10.1186/1475-2891-13-17 (2014).

147 Wright, M. B., Bortolini, M., Tadayyon, M. & Bopst, M. Minireview: Challenges and opportunities in development of PPAR agonists. *Mol Endocrinol* **28**, 1756-1768, doi:10.1210/me.2013-1427 (2014).

148 Mangoni, M. *et al.* A PPAR-gamma agonist attenuates pulmonary injury induced by irradiation in a murine model. *Lung Cancer* **90**, 405-409, doi:10.1016/j.lungcan.2015.11.005 (2015).

149 Wu, M. H. *et al.* Rosiglitazone Abrogates Bleomycin-Induced Scleroderma and Blocks Profibrotic Responses Through Peroxisome Proliferator-Activated Receptor-gamma. *Am J Pathol* **174**, 519-533, doi:10.2353/ajpath.2009.080574 (2009).

150 Sandbo, N. *et al.* Control of myofibroblast differentiation by microtubule dynamics through a regulated localization of mDia2. *J Biol Chem* **288**, 15466-15473, doi:10.1074/jbc.M113.464461 (2013).

151 Tomasek, J. J. *et al.* Contraction of myofibroblasts in granulation tissue is dependent on Rho/Rho kinase/myosin light chain phosphatase activity. *Wound Repair Regen* **14**, 313-320, doi:10.1111/j.1743-6109.2006.00126.x (2006).

152 Zhou, Y. *et al.* Inhibition of mechanosensitive signaling in myofibroblasts ameliorates experimental pulmonary fibrosis. *J Clin Invest* **123**, 1096-1108, doi:10.1172/JCI66700 (2013).

153 Sandbo, N. & Dulin, N. Actin cytoskeleton in myofibroblast differentiation: ultrastructure defining form and driving function. *Transl Res* **158**, 181-196, doi:10.1016/j.trsl.2011.05.004 (2011).

154 Small, E. M. The actin-MRTF-SRF gene regulatory axis and myofibroblast differentiation. *J Cardiovasc Transl Res* **5**, 794-804, doi:10.1007/s12265-012-9397-0 (2012).

155 Scharenberg, M. A. *et al.* TGF-beta-induced differentiation into myofibroblasts involves specific regulation of two MKL1 isoforms. *J Cell Sci* **127**, 1079-1091, doi:10.1242/jcs.142075 (2014).

156 Huang, X. *et al.* Matrix stiffness-induced myofibroblast differentiation is mediated by intrinsic mechanotransduction. *Am J Respir Cell Mol Biol* **47**, 340-348, doi:10.1165/rcmb.2012-0050OC (2012).

157 Sandbo, N. *et al.* Delayed stress fiber formation mediates pulmonary myofibroblast differentiation in response to TGF-beta. *Am J Physiol Lung Cell Mol Physiol* **301**, L656-666, doi:10.1152/ajplung.00166.2011 (2011).

158 Johnson, L. A. *et al.* Novel Rho/MRTF/SRF inhibitors block matrix-stiffness and TGF-beta-induced fibrogenesis in human colonic myofibroblasts. *Inflamm Bowel Dis* **20**, 154-165, doi:10.1097/01.MIB.0000437615.98881.31 (2014).

159 Haak, A. J. *et al.* Targeting the Myofibroblast Genetic Switch: Inhibitors of Myocardin-Related Transcription Factor/Serum Response Factor-Regulated Gene Transcription Prevent Fibrosis in a Murine Model of Skin Injury. *J Pharmacol Exp Ther* **349**, 480-486, doi:10.1124/jpet.114.213520 (2014).

160 Yu, O. M., Miyamoto, S. & Brown, J. H. Myocardin-Related Transcription Factor A and Yes-Associated Protein Exert Dual Control in G Protein-Coupled Receptor- and RhoA-Mediated Transcriptional Regulation and Cell Proliferation. *Mol Cell Biol* **36**, 39-49, doi:10.1128/MCB.00772-15 (2016).

161 Li, C. *et al.* RhoA determines lineage fate of mesenchymal stem cells by modulating CTGF-VEGF complex in extracellular matrix. *Nat Commun* **7**, 11455, doi:10.1038/ncomms11455 (2016).

162 Masszi, A. *et al.* Central role for Rho in TGF-beta1-induced alpha-smooth muscle actin expression during epithelial-mesenchymal transition. *Am J Physiol Renal Physiol* **284**, F911-924, doi:10.1152/ajprenal.00183.2002 (2003).
163 Evelyn, C. R. *et al.* CCG-1423: a small-molecule inhibitor of RhoA transcriptional signaling. *Mol Cancer Ther* **6**, 2249-2260, doi:10.1158/1535-7163.Mct-06-0782 (2007).
164 Prencipe, M. *et al.* Identification of transcription factors associated with castration-resistance: is the serum responsive factor a potential therapeutic target? *Prostate* **73**, 743-753, doi:10.1002/pros.22618 (2013).
165 Mae, S. *et al.* Combination of small molecules enhances differentiation of mouse embryonic stem cells into intermediate mesoderm through BMP7-positive cells. *Biochem Biophys Res Commun* **393**, 877-882, doi:10.1016/j.bbrc.2010.02.111 (2010).
166 Sakai, N. *et al.* LPA(1)-induced cytoskeleton reorganization drives fibrosis through CTGF-dependent fibroblast proliferation. *Faseb J* **27**, 1830-1846, doi:10.1096/fj.12-219378 (2013).
167 Bell, J. L. *et al.* Optimization of novel nipecotic bis(amide) inhibitors of the Rho/MKL1/SRF transcriptional pathway as potential anti-metastasis agents. *Bioorganic & Medicinal Chemistry Letters* **23**, 3826-3832, doi:10.1016/j.bmcl.2013.04.080 (2013).
168 Hutchings, K. M. *et al.* Pharmacokinetic optimitzation of CCG-203971: Novel inhibitors of the Rho/MRTF/SRF transcriptional pathway as potential antifibrotic therapeutics for systemic scleroderma. *Bioorganic & Medicinal Chemistry Letters* **27**, 1744-1749, doi:https://doi.org/10.1016/j.bmcl.2017.02.070 (2017).
169 Sisson, T. H. *et al.* Inhibition of Myocardin-Related Transcription Factor/Serum Response Factor Signaling Decreases Lung Fibrosis and Promotes Mesenchymal Cell Apoptosis. *Am J Pathol* **185**, 969-986, doi:10.1016/j.ajpath.2014.12.005 (2015).
170 Evelyn, C. R. *et al.* Design, synthesis and prostate cancer cell-based studies of analogs of the Rho/MKL1 transcriptional pathway inhibitor, CCG-1423. *Bioorganic & Medicinal Chemistry Letters* **20**, 665-672, doi:10.1016/j.bmcl.2009.11.056 (2010).
171 Haak, A. J. *et al.* Pharmacological Inhibition of Myocardin-related Transcription Factor Pathway Blocks Lung Metastases of RhoC-Overexpressing Melanoma. *Mol Cancer Ther* **16**, 193-204, doi:10.1158/1535-7163.Mct-16-0482 (2017).
172 Jin, W. Z. *et al.* Increased SRF transcriptional activity in human and mouse skeletal muscle is a signature of insulin resistance. *Journal of Clinical Investigation* **121**, 918-929, doi:10.1172/Jci41940 (2011).
173 Yu-Wai-Man, C. *et al.* Local delivery of novel MRTF/SRF inhibitors prevents scar tissue formation in a preclinical model of fibrosis. *Sci Rep-Uk* **7**, doi:ARTN 518 10.1038/s41598-017-00212-w (2017).

174 Agopian, A. *et al.* A new generation of peptide-based inhibitors targeting HIV-1 reverse transcriptase conformational flexibility. *J Biol Chem* **284**, 254-264, doi:10.1074/jbc.M802199200 (2009).
175 Lomenick, B., Olsen, R. W. & Huang, J. Identification of Direct Protein Targets of Small Molecules. *Acs Chem Biol* **6**, 34-46, doi:10.1021/cb100294v (2011).
176 Sato, S., Murata, A., Shirakawa, T. & Uesugi, M. Biochemical Target Isolation for Novices: Affinity-Based Strategies. *Chem Biol* **17**, 616-623, doi:10.1016/j.chembiol.2010.05.015 (2010).
177 Mackinnon, A. L. & Taunton, J. Target Identification by Diazirine Photo-Cross-linking and Click Chemistry. *Curr Protoc Chem Biol* **1**, 55-73, doi:10.1002/9780470559277.ch090167 (2009).
178 Smith, E. & Collins, I. Photoaffinity labeling in target- and binding-site identification. *Future Med Chem* **7**, 159-183, doi:10.4155/Fmc.14.152 (2015).

179 Vendrell, M., Zhai, D. T., Er, J. C. & Chang, Y. T. Combinatorial Strategies in Fluorescent Probe Development. *Chemical Reviews* **112**, 4391-4420, doi:10.1021/cr200355j (2012).
180 Chan, J. N., Nislow, C. & Emili, A. Recent advances and method development for drug target identification. *Trends Pharmacol Sci* **31**, 82-88, doi:10.1016/j.tips.2009.11.002 (2010).
181 Hughes, J. P., Rees, S., Kalindjian, S. B. & Philpott, K. L. Principles of early drug discovery. *Brit J Pharmacol* **162**, 1239-1249, doi:10.1111/j.1476-5381.2010.01127.x (2011).
182 Jones, L. H. An industry perspective on drug target validation. *Expert Opin Drug Dis* **11**, 623-625, doi:10.1080/17460441.2016.1182484 (2016).
183 Schenone, M., Dancik, V., Wagner, B. K. & Clemons, P. A. Target identification and mechanism of action in chemical biology and drug discovery. *Nature Chemical Biology* **9**, 232-240, doi:10.1038/Nchembio.1199 (2013).
184 Wang, S. *et al.* Advanced Activity-Based Protein Profiling Application Strategies for Drug Development. *Frontiers in Pharmacology* **9**, doi:ARTN 353 10.3389/fphar.2018.00353 (2018).

185 Ong, S. E., Li, X. Y., Schenone, M., Schreiber, S. L. & Carr, S. A. Identifying Cellular Targets of Small-Molecule Probes and Drugs with Biochemical Enrichment and SILAC. *Methods Mol Biol* **803**, 129-140, doi:10.1007/978-1-61779-364-6_9 (2012).
186 Lomenick, B. *et al.* Target identification using drug affinity responsive target stability (DARTS). *P Natl Acad Sci USA* **106**, 21984-21989, doi:10.1073/pnas.0910040106 (2009).
187 Roelofs, K. G., Wang, J. X., Sintim, H. O. & Lee, V. T. Differential radial capillary action of ligand assay for high-throughput detection of protein-metabolite interactions. *P Natl Acad Sci USA* **108**, 15528-15533, doi:10.1073/pnas.1018949108 (2011).
188 McFedries, A., Schwaid, A. & Saghatelian, A. Methods for the Elucidation of Protein-Small Molecule Interactions. *Chem Biol* **20**, 667-673, doi:10.1016/j.chembiol.2013.04.008 (2013).
189 Rix, U. & Superti-Furga, G. Target profiling of small molecules by chemical proteomics. *Nature Chemical Biology* **5**, 616-624, doi:10.1038/nchembio.216 (2009).
190 Wyatt, P. G., Gilbert, I. H., Read, K. D. & Fairlamb, A. H. Target Validation: Linking Target and Chemical Properties to Desired Product Profile. *Curr Top Med Chem* **11**, 1275-1283 (2011).
191 Sugimoto, O., Arakaki, T., Kamio, H. & Tanji, K. The use of a Mitsunobu reagent for the formation of heterocycles: a simple method for the preparation of 3-alkyl-5-aryl-1,3,4-oxadiazol-2(3H)-ones from carboxylic acids. *Chem Commun* **50**, 7314-7317, doi:10.1039/c4cc01971g (2014).
192 Toda, N., Asano, S. & Barbas, C. F. Rapid, Stable, Chemoselective Labeling of Thiols with Julia-Kocienski-like Reagents: A Serum-Stable Alternative to Maleimide-Based Protein Conjugation. *Angew Chem Int Edit* **52**, 12592-12596, doi:10.1002/anie.201306241 (2013).
193 Wet-Osot, S., Phakhodee, W. & Pattarawarapan, M. Application of N-Acylbenzotriazoles in the Synthesis of 5-Substituted 2-Ethoxy-1,3,4-oxadiazoles as Building Blocks toward 3,5-Disubstituted 1,3,4-Oxadiazol-2(3H)-ones. *J Org Chem* **82**, 9923-9929, doi:10.1021/acs.joc.7b01863 (2017).
194 Yan, X. *et al.* Propylene oxide assisted one-pot, tandem synthesis of substituted-1,3,4-oxadiazole-2(3H)-ones in water. *Tetrahedron* **68**, 7978-7983, doi:10.1016/j.tet.2012.07.004 (2012).

195 Hill, J. R. & Robertson, A. A. B. Fishing for Drug Targets: A Focus on Diazirine Photoaffinity Probe Synthesis. *Journal of Medicinal Chemistry* **61**, 6945-6963, doi:10.1021/acs.jmedchem.7b01561 (2018).
196 Reddy, A. S., Kumar, M. S. & Reddy, G. R. A convenient method for the preparation of hydroxamic acids. *Tetrahedron Lett* **41**, 6285-6288, doi:Doi 10.1016/S0040-4039(00)01058-3 (2000).
197 Sun, J. *et al.* Oxadiazole derivatives containing 1,4-benzodioxan as potential immunosuppressive agents against RAW264.7 cells. *Bioorg Med Chem* **19**, 4895-4902, doi:10.1016/j.bmc.2011.06.061 (2011).
198 Karabanovich, G. *et al.* Development of 3,5-Dinitrobenzylsulfanyl-1,3,4-oxadiazoles and Thiadiazoles as Selective Antitubercular Agents Active Against Replicating and Nonreplicating Mycobacterium tuberculosis. *Journal of Medicinal Chemistry* **59**, 2362-2380, doi:10.1021/acs.jmedchem.5b00608 (2016).
199 Hutchinson, J. H. *et al.* Thiopyrano[2,3,4-c,d]indoles as inhibitors of leukotriene biosynthesis. EP518426A1 (1992).
200 Mimero, P., Saluzzo, C. & Amouroux, R. Regioselective Cleavage of Tetrahydrofurans Bearing Proximate Functional-Groups with Acid Iodides. *Synthetic Commun* **25**, 613-627, doi:Doi 10.1080/00397919508011398 (1995).
201 Schlosser, M., Heiss, C., Marzi, E. & Scopelliti, R. Proton mobility in 2-substituted 1,3-dichlorobenzenes: "ortho" or "meta" metalation? *Eur J Org Chem*, 4398-4404, doi:10.1002/ejoc.200600350 (2006).
202 Ram, V. J. & Pandey, H. N. Synthesis of Mannich Bases and Sulfides Derived from 5-(Para-)-Chlorophenyl 1,3,4-Oxadiazol-2-Thione. *Agr Biol Chem Tokyo* **37**, 1465-1469 (1973).
203 Young, R. W. & Wood, K. H. The Cyclization of 3-Acyldithiocarbazate Esters. *J Am Chem Soc* **77**, 400-403, doi:Doi 10.1021/Ja01607a051 (1955).
204 Jorge, S. D. *et al.* Novel benzofuroxan derivatives against multidrug-resistant Staphylococcus aureus strains: Design using Topliss' decision tree, synthesis and biological assay. *Bioorg Med Chem* **19**, 5031-5038, doi:10.1016/j.bmc.2011.06.034 (2011).
205 Suman, S. P. & Bahel, S. C. Fungicidal Activity of Oxadiazolyl Sulfides. *Agr Biol Chem Tokyo* **43**, 1339-1341 (1979).
206 Requena, C. E., Perez-Moreno, G., Ruiz-Perez, L. M., Vidal, A. E. & Gonzalez-Pacanowska, D. The NTP pyrophosphatase DCTPP1 contributes to the homoeostasis and cleansing of the dNTP pool in human cells. *Biochem J* **459**, 171-180, doi:10.1042/Bj20130894 (2014).
207 Song, F. F. *et al.* Human dCTP pyrophosphatase 1 promotes breast cancer cell growth and stemness through the modulation on 5-methyl-dCTP metabolism and global hypomethylation. *Oncogenesis* **4**, e159, doi:10.1038/oncsis.2015.10 (2015).
208 Zhang, Y. *et al.* dCTP pyrophosphohydrase exhibits nucleic accumulation in multiple carcinomas. *Eur J Histochem* **57**, 185-191, doi:10.4081/ejh.2013.e29 (2013).
209 Morisaki, T. *et al.* Comparative Proteomics Analysis of Gastric Cancer Stem Cells. *PLoS One* **9**, doi:ARTN e110736 10.1371/journal.pone.0110736 (2014).
210 Llona-Minguez, S. *et al.* Discovery of the First Potent and Selective Inhibitors of Human dCTP Pyrophosphatase 1. *J Med Chem* **59**, 1140-1148, doi:10.1021/acs.jmedchem.5b01741 (2016).
211 Feng, J. *et al.* An improved malachite green assay of phosphate: mechanism and application. *Anal Biochem* **409**, 144-149, doi:10.1016/j.ab.2010.10.025 (2011).

212 Freyer, M. W. & Lewis, E. A. Isothermal titration calorimetry: experimental design, data analysis, and probing macromolecule/ligand binding and kinetic interactions. *Methods Cell Biol* **84**, 79-113, doi:10.1016/S0091-679X(07)84004-0 (2008).
213 Nusgen, N. *et al.* Inter-locus as well as intra-locus heterogeneity in LINE-1 promoter methylation in common human cancers suggests selective demethylation pressure at specific CpGs. *Clin Epigenetics* **7**, doi:ARTN 17 10.1186/s13148-015-0051-y (2015).

214 International Human Genome Sequencing, C. *et al.* Initial sequencing and analysis of the human genome. *Nature* **409**, 860, doi:10.1038/35057062 https://www.nature.com/articles/35057062#supplementary-information (2001).

215 Altorok, N., Tsou, P. S., Coit, P., Khanna, D. & Sawalha, A. H. Genome-wide DNA methylation analysis in dermal fibroblasts from patients with diffuse and limited systemic sclerosis reveals common and subset-specific DNA methylation aberrancies. *Ann Rheum Dis* **74**, 1612-1620, doi:10.1136/annrheumdis-2014-205303 (2015).
216 Satpathy, S., Nabbi, A. & Riabowol, K. RegulatING chromatin regulators: post-translational modification of the ING family of epigenetic regulators. *Biochemical Journal* **450**, 433-442, doi:10.1042/Bj20121632 (2013).
217 Morrison, J. F. The Slow-Binding and Slow, Tight-Binding Inhibition of Enzyme-Catalyzed Reactions. *Trends Biochem Sci* **7**, 102-105, doi:Doi 10.1016/0968-0004(82)90157-8 (1982).
218 Waley, S. G. The kinetics of slow-binding and slow, tight-binding inhibition: the effects of substrate depletion. *Biochem J* **294 (Pt 1)**, 195-200 (1993).
219 Walkup, G. K. *et al.* Translating slow-binding inhibition kinetics into cellular and in vivo effects. *Nat Chem Biol* **11**, 416-423, doi:10.1038/nchembio.1796 (2015).
220 Hayashi, K. i., Watanabe, B., Nakagawa, Y., Minami, S. & Morita, T. RPEL Proteins Are the Molecular Targets for CCG-1423, an Inhibitor of Rho Signaling. *PLOS ONE* **9**, e89016, doi:10.1371/journal.pone.0089016 (2014).
221 Evelyn, C. R. *et al.* Small-Molecule Inhibition of Rho/MKL/SRF Transcription in Prostate Cancer Cells: Modulation of Cell Cycle, ER Stress, and Metastasis Gene Networks. *Microarrays (Basel).* **5(2).** E13. doi: 10.3390/microarrays5020013. (2016).
222 Lundquist, M. R. *et al.* Redox modification of nuclear actin by MICAL-2 regulates SRF signaling. *Cell* **156**, 563-576, doi:10.1016/j.cell.2013.12.035 (2014).
223 Adeniran, C. & Hamelberg, D. Redox-Specific Allosteric Modulation of the Conformational Dynamics of kappa B DNA by Pirin in the NF-kappa B Supramolecular Complex. *Biochemistry-Us* **56**, 5002-5010, doi:10.1021/acs.biochem.7b00528 (2017).
224 Bell, J. L. *et al.* Design and synthesis of tag-free photoprobes for the identification of the molecular target for CCG-1423, a novel inhibitor of the Rho/MKL1/SRF signaling pathway. *Beilstein J Org Chem* **9**, 966-973, doi:10.3762/bjoc.9.111 (2013).
225 Belanger, D. B. *et al.* Preparation of aminomethyl-biaryl derivatives as complement alternative pathway modulators for treatment of opthalmic and other diseases. WO2015009977A1 (2015).
226 Feutrill, J., Leriche, C. & Middlemiss, D. Preparation of aniline derivatives as EP2 agonists useful in treating glaucoma. WO2013037705A2 (2013).
227 Davenport, A. J. *et al.* 1,3-Thiazol-2-ylbenzamides as P2X purinoceptor antagonists and their preparation. WO2016091776A1 (2016).
228 Lercher, L., McGouran, J. F., Kessler, B. M., Schofield, C. J. & Davis, B. G. DNA Modification under Mild Conditions by Suzuki-Miyaura Cross-Coupling for the Generation of Functional Probes. *Angew Chem Int Edit* **52**, 10553-10558, doi:10.1002/anie.201304038 (2013).

229 Davda, D. *et al.* Profiling targets of the irreversible palmitoylation inhibitor 2-bromopalmitate. *ACS Chem Biol.* **8**, 1912-1917. doi: 1910.1021/cb400380s. Epub 402013 Jul 400325. (2013).
230 Wendler, W. M. F., Kremmer, E., Forster, R. & Winnacker, E. L. Identification of Pirin, a novel highly conserved nuclear protein. *J Biol Chem* **272**, 8482-8489, doi:DOI 10.1074/jbc.272.13.8482 (1997).
231 Dechend, R. *et al.* The Bcl-3 oncoprotein acts as a bridging factor between NF-kappaB/Rel and nuclear co-regulators. *Oncogene.* **18**, 3316-3323. doi: 3310.1038/sj.onc.1202717. (1999).
232 Liu, F. *et al.* Pirin is an iron-dependent redox regulator of NF-kappaB. *Proc Natl Acad Sci U S A.* **110**, 9722-9727. doi: 9710.1073/pnas.1221743110. Epub 1221742013 May 1221743128. (2013).
233 Miyazaki, I., Simizu, S., Okumura, H., Takagi, S. & Osada, H. A small-molecule inhibitor shows that pirin regulates migration of melanoma cells. *Nat Chem Biol* **6**, 667-673, doi:10.1038/nchembio.423 (2010).
234 Brzoska, K., Stepkowski, T. M. & Kruszewski, M. Basal PIR expression in HeLa cells is driven by NRF2 via evolutionary conserved antioxidant response element. *Mol Cell Biochem.* **389**, 99-111. doi: 110.1007/s11010-11013-11931-11010. Epub 12014 Jan 11015. (2014).
235 Licciulli, S. *et al.* Pirin Inhibits Cellular Senescence in Melanocytic Cells. *Am J Pathol* **178**, 2397-2406, doi:10.1016/j.ajpath.2011.01.019 (2011).
236 Qiao, Z. J., Wang, D., Hahn, J., Ai, J. K. & Wang, Z. Pirin Down-Regulates the EAF2/U19 Protein and Alleviates its Growth Inhibition in Prostate Cancer Cells. *Prostate* **74**, 113-120, doi:10.1002/pros.22729 (2014).
237 Yamaoka, H. *et al.* A novel small compound accelerates dermal wound healing by modifying infiltration, proliferation and migration of distinct cellular components in mice. *J Dermatol Sci* **74**, 204-213, doi:10.1016/j.jdermsci.2014.03.002 (2014).
238 Komai, K., Niwa, Y., Sasazawa, Y. & Simizu, S. Pirin regulates epithelial to mesenchymal transition independently of Bcl3-Slug signaling. *Febs Lett* **589**, 738-743, doi:10.1016/j.febslet.2015.01.040 (2015).
239 Marcucci, F., Stassi, G. & De Maria, R. Epithelial-mesenchymal transition: a new target in anticancer drug discovery. *Nature Reviews Drug Discovery* **15**, 311-325, doi:10.1038/nrd.2015.13 (2016).
240 Cheeseman, M. D. *et al.* Discovery of a Chemical Probe Bisamide (CCT251236): An Orally Bioavailable Efficacious Pirin Ligand from a Heat Shock Transcription Factor 1 (HSF1) Phenotypic Screen. *J Med Chem* **60**, 180-201, doi:10.1021/acs.jmedchem.6b01055 (2017).
241 Kufareva, I. & Abagyan, R. Methods of protein structure comparison. *Methods in molecular biology (Clifton, N.J.)* **857**, 231-257, doi:10.1007/978-1-61779-588-6_10 (2012).
242 Foster, C. T., Gualdrini, F. & Treisman, R. Mutual dependence of the MRTF-SRF and YAP-TEAD pathways in cancer-associated fibroblasts is indirect and mediated by cytoskeletal dynamics. *Genes Dev.* **31**, 2361-2375. doi: 2310.1101/gad.304501.304117. Epub 302018 Jan 304509. (2017).
243 Crider, B. J., Risinger, G. M., Jr., Haaksma, C. J., Howard, E. W. & Tomasek, J. J. Myocardin-related transcription factors A and B are key regulators of TGF-beta1-induced fibroblast to myofibroblast differentiation. *J Invest Dermatol.* **131**, 2378-2385. doi: 2310.1038/jid.2011.2219. Epub 2011 Jul 2321. (2011).
244 Speight, P., Kofler, M., Szaszi, K. & Kapus, A. Context-dependent switch in chemo/mechanotransduction via multilevel crosstalk among cytoskeleton-regulated

MRTF and TAZ and TGFbeta-regulated Smad3. *Nat Commun.* **7:11642.**, 10.1038/ncomms11642. (2016).

245 Medjkane, S., Perez-Sanchez, C., Gaggioli, C., Sahai, E. & Treisman, R. Myocardin-related transcription factors and SRF are required for cytoskeletal dynamics and experimental metastasis. *Nat Cell Biol* **11**, 257-268, doi:ncb1833 [pii] 10.1038/ncb1833 (2009).

246 Licciulli, S. *et al.* Pirin delocalization in melanoma progression identified by high content immuno-detection based approaches. *BMC Cell Biol.* **11:5.**, 10.1186/1471-2121-1111-1185. (2010).

247 ALBRECHT BRIAN K (US), A. J. E. U., GAGNON ALEXANDRE (CA), HARMANGE JEAN-CHRISTOPHE (US), NAVESCHUK CHRISTOPHER G (US). MODULATORS OF METHYL MODIFYING ENZYMES, COMPOSITIONS AND USES THEREOF. (2013).

248 SHEN, D.-M. E. L. A., Rahway, New Jersey, 07065, US), SINZ, Christopher J. (126 East Lincoln Avenue, Rahway, New Jersey, 07065, US), CRESPO, Alexander (126 East Lincoln Avenue, Rahway, New Jersey, 07065, US), WILSON, Jonathan E. (126 East Lincoln Avenue, Rahway, 07065, US), MCCRACKEN, Troy (126 East Lincoln Avenue, Rahway, New Jersey, 07065, US), XU, Shimin (6 Tai-He Road, BDA, Beijing 6, 100176, CN), LI, Haitang (6 Tai-He Road, BDA, Beijing 6, 100176, CN). TRIAZOLYL PYRIMIDINONE COMPOUNDS AS PDE2 INHIBITORS. (2016).

249 Allen, J. R., Hitchcock, S. A., Turner, W. W., Jr. & Liu, B. Preparation of indanylamide derivatives as muscarinic M1 agonists. WO2004094363A1 (2004).

250 Wu, G. G., Itoh, T., McLaughlin, M., Liu, Z. & Qian, G. Process for the preparation of 3-amino-4-cyclobutyl-2-hydroxybutanamide derivatives. WO2013066734A1 (2013).

251 Kocis, P., Tolar, M. & Hey, J. Preparation of cyclopentane and pyrrolidine derivatives for treating and preventing neurodegenerative disorders. WO2017027582A1 (2017).

252 Suzuki, N., Hajicek, N. & Kozasa, T. Regulation and Physiological Functions of G12/13-Mediated Signaling Pathways. *Neurosignals* **17**, 55-70, doi:10.1159/000186690 (2009).

253 Liang, M. R. *et al.* A modified murine model of systemic sclerosis: bleomycin given by pump infusion induced skin and pulmonary inflammation and fibrosis. *Lab Invest* **95**, 342-350, doi:10.1038/labinvest.2014.145 (2015).

254 Batteux, F., Kavian, N. & Servettaz, A. New insights on chemically induced animal models of systemic sclerosis. *Curr Opin Rheumatol* **23**, 511-518, doi:10.1097/BOR.0b013e32834b1606 (2011).

255 Srivastava, A. K., Khare, P., Nagar, H. K., Raghuwanshi, N. & Srivastava, R. Hydroxyproline: A Potential Biochemical Marker and Its Role in the Pathogenesis of Different Diseases. *Curr Protein Pept Sc* **17**, 596-602, doi:10.2174/1389203717666151201192247 (2016).

256 Tala, A. *et al.* Pirin: A novel redox-sensitive modulator of primary and secondary metabolism in Streptomyces. *Metab Eng* **48**, 254-268, doi:10.1016/j.ymben.2018.06.008 (2018).

257 Yao, X. Q., Momin, M. & Hamelberg, D. Elucidating Allosteric Communications in Proteins with Difference Contact Network Analysis. *J Chem Inf Model* **58**, 1325-1330, doi:10.1021/acs.jcim.8b00250 (2018).

258 Song, S., Zhu, S. F., Pu, L. Y. & Zhou, Q. L. Iridium-Catalyzed Enantioselective Hydrogenation of Unsaturated Heterocyclic Acids. *Angew Chem Int Edit* **52**, 6072-6075, doi:10.1002/anie.201301341 (2013).

259 Partsvaniya, D. A. *et al.* Indole-Derivatives .128. Synthesis and Properties of 5,6-Ethylendioxyindoles and 4,5-Ethylendioxyindoles-Ethylene Dioxyindoles. *Khim Geterotsikl*+, 1624-1628 (1986).

260 Bentley, J. M. *et al.* Preparation of 1,2,3,4,10,10a-hexahydro-1H-pyrazino[1,2-a]indoles and analogs and 5-HT receptor agonists for treatment of CNS diseases, cardiovascular disorders, gastrointestinal disorders, and obesity. WO2002010169A1 (2002).
261 Geyer, R., Nordemann, U., Strasser, A., Wittmann, H. J. & Buschauer, A. Conformational Restriction and Enantioseparation Increase Potency and Selectivity of Cyanoguanidine-Type Histamine H4 Receptor Agonists. *J Med Chem* **59**, 3452-3470, doi:10.1021/acs.jmedchem.6b00120 (2016).
262 Argese, E. *et al.* Assessment of chloroaniline toxicity by the submitochondrial particle assay. *Environ Toxicol Chem* **20**, 826-832 (2001).
263 Chhabra, R. S., Huff, J. E., Haseman, J. K., Elwell, M. R. & Peters, A. C. Carcinogenicity of p-chloroaniline in rats and mice. *Food Chem Toxicol* **29**, 119-124 (1991).
264 Skipper, P. L., Kim, M. Y., Sun, H. L., Wogan, G. N. & Tannenbaum, S. R. Monocyclic aromatic amines as potential human carcinogens: old is new again. *Carcinogenesis* **31**, 50-58, doi:10.1093/carcin/bgp267 (2010).
265 Valentovic, M. A. *et al.* In Vitro toxicity of 2- and 4-chloroaniline: comparisons with 4-amino-3-chlorophenol, 2-amino-5-chlorophenol and aminophenols. *Toxicol In Vitro* **10**, 713-720 (1996).
266 Beaulieu, P. L. *et al.* Aza follow-ups to BI 207524, a thumb pocket 1 HCV NS5B polymerase inhibitor. Part 1: Mitigating the genotoxic liability of an aniline metabolite. *Bioorg Med Chem Lett* **25**, 1135-1139, doi:10.1016/j.bmcl.2014.12.028 (2015).
267 Benigni, R. & Bossa, C. Mechanisms of chemical carcinogenicity and mutagenicity: a review with implications for predictive toxicology. *Chem Rev* **111**, 2507-2536, doi:10.1021/cr100222q (2011).
268 Shamovsky, I. *et al.* Explanation for main features of structure-genotoxicity relationships of aromatic amines by theoretical studies of their activation pathways in CYP1A2. *J Am Chem Soc* **133**, 16168-16185, doi:10.1021/ja206427u (2011).
269 Birch, A. M. *et al.* Rationally Designing Safer Anilines: The Challenging Case of 4-Aminobiphenyls. *Journal of Medicinal Chemistry* **55**, 3923-3933, doi:10.1021/jm3001295 (2012).
270 O'Neill, P. M. *et al.* Synthesis, Antimalarial Activity, and Preclinical Pharmacology of a Novel Series of 4 '-Fluoro and 4 '-Chloro Analogues of Amodiaquine. Identification of a Suitable "Back-Up" Compound for N-tert-Butyl Isoquine. *Journal of Medicinal Chemistry* **52**, 1828-1844, doi:10.1021/jm8012757 (2009).
271 Moody, C. L., Franckevicius, V., Drouhin, P., Klein, J. E. M. N. & Taylor, R. J. K. Copper-catalysed approach to spirocyclic oxindoles via a direct C-H, Ar-H functionalisation. *Tetrahedron Lett* **53**, 1897-1899, doi:10.1016/j.tetlet.2012.01.120 (2012).
272 Zeng, Q. *et al.* Purification, crystallization and preliminary X-ray analysis of human pirin. *Acta Crystallogr D* **59**, 1496-1498, doi:10.1107/S0907444903012289 (2003).